PEPTOPLEXES AS ARTIFICIAL VIRUSES FOR NUCLEIC ACID VACCINE DELIVERY

DISSERTATION
ZUR ERLANGUNG DES GRADES
"DOKTOR DER NATURWISSENSCHAFTEN"
IM PROMOTIONSFACH CHEMIE

am Institut für Organische Chemie
Fachbereich 09: Chemie, Pharmazie und Geowissenschaften
Johannes Gutenberg-Universität

vorgelegt von

Philipp Heller

geboren in Wiesbaden

Mainz, März 2017

Philipp Heller: *PeptoPlexes as Artificial Viruses for Nucleic Acid Vaccine Delivery,* PhD Thesis,
© März 2017

This thesis was carried out at the Johannes Gutenberg-Universität Mainz from September 2013 to March 2017.
D77 (Dissertation Johannes Gutenberg-Universität Mainz)

Dean of the Faculty	
1st report	
2nd report	
Submitted	29.03.2017
Oral examination	12.05.2017

Our knowledge can only be finite, while our ignorance must necessarily be infinite.

— Karl R. Popper

ABSTRACT

Nucleic acid vaccines encode subunit antigens on DNA or mRNA level which, following transfection of target cells, can be expressed and processed like conventional peptide antigens. Based on the current state of knowledge, this class of vaccines seems especially promising in the context of tumor immunotherapy. The present work describes the establishment of a novel class of non-viral vectors which are based on polypept(o)ides as underlying material and are capable to deliver nucleic acid vaccines into dendritic cells. In the context of medical application, polypept(o)ides hold great promise as a source material for the formation of biocompatible nanoparticles, since they combine high stability in aqueous solution, unique secondary structures and the intrinsic multifunctionality of the amino acids with enzymatic degradability. In order to bring nuceic acids into an intravenous administration form, the polypept(o)ides developed in this work are designed to condense pDNA or mRNA into polyplexes with core-shell architecture (PeptoPlexes).

Introducing nucleic acids into non-dividing cells like dendritic cells is a challenging procedure. Thus, throughout the PhD thesis, polypept(o)ides and PeptoPlexes were constantly refined and functionality of the systems was increased successively. Methods applied for the development of PeptoPlexes involved organic and polymer synthesis, physicochemical characterization, biochemistry, microscopy studies, cell biology and animal studies. Eventually, the latest generation of PeptoPlexes succeeded in the transfection of dendritic cells by mimicking key functions of viruses, namely, targeted cellular uptake, stimuli-responsive disassembly, endosomal escape and nuclear import of the genetic code. Preliminary *in vivo* experiments indicate a favorable biodistribution of PeptoPlexes...

KURZDARSTELLUNG

Nukleinsäure-basierte Impfstoffe codieren spezifische Antigene auf DNA- oder mRNA-Ebene, welche nach der Transfektion entsprechender Zielzellen exprimiert und wie ein konventionelles Peptidantigen prozessiert werden können. Nach gegenwärtigem Forschungsstand ergeben sich für diesen Vakzin-Typ besonders im Bereich der Tumorimmuntherapie vielversprechende Anwendungsmöglichkeiten. In der vorliegenden Arbeit wird eine neue Klasse non-viraler Vektoren etabliert, die auf Polypept(o)iden als zugrundeliegendem Material basieren und in der Lage sind, Nukleinsäure-Vakzine in dendritische Zellen zu transportieren. Im Hinblick auf die medizinische Anwendung bilden Polypept(o)ide ein sehr gut geeignetes Ausgangsmaterial für die Herstellung von biokompatiblen Nanopartikeln, da sie hohe Stabilität in wässriger Lösung, einzigartige Sekundärstrukturen und die intrinsische Multifunktionalität der Aminosäuren mit enzymatischer Abbaubarkeit vereinen. Um Nukleinsäuren in eine für die intravenöse Gabe geeignete Darreichungsform zu bringen, sind die in dieser Arbeit entwickelten Polypept(o)ide darauf ausgelegt, mRNA oder pDNA zu kondensieren und Polyplexe mit Kern-Schale-Struktur auszubilden (PeptoPlexe).

Nukleinsäuren in teilungsinaktive Zellen, wie es dendritische Zellen sind, einzubringen, stellt eine große Herausforderung dar. Daher mussten die Polypept(o)ide und PeptoPlexe während der Doktorarbeit permanent weiterentwickelt und ihre Funktionalität schrittweise erhöht werden. Im Zuge der PeptoPlex-Entwicklung kamen Methoden aus dem Bereich der

organischen Synthese und Polymersynthese, Methoden zur physikochemischen Charakterisierung, biochemische Methoden, Mikroskopie-Studien, Zellbiologie sowie Tierstudien zum Einsatz. Schließlich konnte mit der neuesten Generation an PeptoPlexen eine erfolgreiche Transfektion von dendritischen Zellen erreicht werden. Die Effizienz der PeptoPlexe kommt dabei durch die Nachahmung viraler Schlüsselfunktionen, d.h. zielgerichtete zelluläre Aufnahme, stimuliresponsive Disassemblierung, aktive endosomale Freisetzung und aktiver Transport der genetischen Information in den Zellkern, zustande. Vorläufige Experimente *in vivo* deuten auf eine vorteilhafte Biodistribution der PeptoPlexe hin...

PUBLICATIONS

List of publications written or contributed to during the PhD thesis. Parts of the thesis have been published in the papers indicated.

- P. Heller, D. Hobernik, B. Weber, M.Schinnerer, M. Bros, M. Barz, 2017, to be submitted → Chapter 12
- P. Heller, D. Hobernik, U. Lächelt, M.Schinnerer, B. Weber, M. Schmidt, E. Wagner, M. Bros, M. Barz, *J. Control. Release*, **2017**, submitted. → Chapter 10
- P. Heller, J. Zhou, B. Weber, D. Hobernik, M. Bros, F. Schmid, M. Barz, *Small*, **2017**. → Chapter 9
- R. Holm, B. Weber, P. Heller, K. Klinker, D. Westmeier, D. Docter, R.H. Stauber, M. Barz, *Macromol. Biosci.*, **2017**.
- M. Scherer, C. Kappel, N. Mohr, K. Fischer, P. Heller, R. Forst, F. Depoix, M. Bros, R. Zentel, *Biomacromolecules*, **2016**, 17, 3305-3317.
- K. Klinker, R. Holm, P. Heller, M. Barz, *Polym. Chem.*, **2015**, 6, 4612-4623.
- P. Heller, N. Mohr, A. Birke, B. Weber, A. Reske-Kunz, M. Bros and M. Barz, *Macromol. Biosci.*, **2015**, 15, 63-73. → Chapter 7
- P. Heller, B. Weber, A. Birke and M. Barz, *Macromol. Rapid Commun.*, **2015**, 36, 38-44. → Chapter 8
- P. Heller, A. Birke, D. Huesmann, B. Weber, K. Fischer, A. Reske-Kunz, M. Bros and M. Barz, *Macromol. Biosci.*, **2014**, 14, 1380-1395. → Chapter 5
- P. Heller, D. Huesmann, M. Scherer and M. Barz, in *Molecular Vaccines: From Prophylaxis to Therapy*, ed. M. Giese, Springer, Vienna/New York, **2013**. → Chapter 3

CONTENTS

Part I

INTRODUCTION

1 OBJECTIVES AND OVERVIEW

The following work is the result of around three years of research and involves the systematic development of polypept(o)ide-based non-viral vectors conceptualized for the delivery of nucleic acid vaccines in the context of cancer immunotherapy. Evolution of these systems started with simple diblock copolymer structures and eventually led to the generation of artificial viruses, which are able to transfect primary dendritic cells.

Polypept(o)ides are hybrid polymers with polypeptide and polypeptoid blocks. They combine high stability in aqueous solution, unique secondary structures and the intrinsic multifunctionality of the amino acids with enzymatic degradability. Thus, polypept(o)ides depict a very promising source material for a novel class of biocompatible nanoparticles designed for medical application.

Apart from recombinant and solid phase synthesis, polypeptides as well as polypeptoids are accessible by the ring-opening polymerization (ROP) of α-amino acid *N*-carboxyanhydrides (NCAs). NCA polymerization allows a fast and cost efficient large scale production of polypeptides/polypeptoids with yet low dispersities (<1.2). Although it does not provide precise control over the peptide primary structure it still gives access to polypeptide architectures with defined block sequence and is the method of choice whenever the latter is sufficient, as for example in the case of block copolymer synthesis. Covering the most important recent literature on polypeptides and polypeptoids, Chapter 2 provides a comprehensive overview of the synthetic aspects of this class of polymers as well as their application in nucleic acid delivery, theranostics and vaccination.

Nanoparticles, in general, allow an entirely new strategy in vaccination. Opposed to the classic administration of attenuated whole pathogens or fragments thereof, sequence-defined subunit antigens can now be combined with appropiate adjuvants on a single particle and then co-delivered to target cells. Chapter 3 describes recent developments in this novel field of nanoparticulate vaccine delivery.

Instead of administration in peptide form, subunit antigens can also be encoded on plasmid DNA (pDNA) or messenger RNA (mRNA), forming a class of nucleic acid-based vaccines. Professional antigen-presenting cells (APCs), notably dendritic cells (DCs), transfected with these vaccines produce the encoded antigen *in situ* after transcription/translation of the genetic information. Subsequently, the generated peptide can be processed along MHC pathways like any other peptide antigen.[1] Yet, what sets nucleic acid vaccines apart from conventional peptide-based formulations is efficient presentation of antigens via MHC I to CD8$^+$ T cells by all subpopulations of DCs, since nucleic acid-encoded transgenes are expressed like endogenous genes. Especially in anti-cancer vaccination, a CD8$^+$ T cell-based immune response as induced by MHC I presentation is important for killing of tumor cells and thus desirable. In contrast, with the exception of cross-presentation, exogenous peptide antigens internalized by dendritic cells are predominantly presented via MHC II and might thus be less suited for activation of CD8$^+$ T cells. In the particular case of pDNA, a DC-specific promotor like the fascin gene promotor promises an additional level of specifity, preventing antigen expression/presentation in non-target cells and reducing side effects, as, for example, immune tolerance.

Recently, BioNTech, as first company worldwide, has successfully translated a mRNA-based individualized cancer vaccine from bench into clinics using a systemically injectable nanoparticulate lipid formulation.[2, 3] Multiple other companys are now on the brink of entering clinical studies with individualized nucleic acid-based vaccines.[4] This trend clearly demonstrates the demand for innovative nucleic acid delivery concepts like the one proposed in this work.

In vivo delivery of nucleic acids requires vectors, which protect their cargo during blood circulation while mediating efficient transfection of target cells. Viruses and virus like particles for gene therapy have been researched extensively and reached a level of great sophistication. Nevertheless, they still face several issues and concerns such as immunogenicity, restricted loading capacity, undesired cell tropism and challenging analytics and production.[5] Non-viral vectors, on the other hand, often suffer from poor transfection efficiency or low stability during blood circulation. The aim of this PhD thesis is to establish polypept(o)ides as novel non-viral vectors for the delivery of nucleic acid vaccines to dendritic cells (DCs) and to develop appropiate strategies to overcome the aforementioned obstacles of non-viral vectors.

Efforts started with the synthesis of diblock copolypept(o)ides combining a cationic polylysine (PLys) block for complexation of pDNA and a hydrophilic polysarcosine (PSar) segment for shielding. As described in Chapter 5, various PLys-b-PSar polymers of different block lenghts were investigated for the formation of polyplexes (in the following termed PeptoPlexes) and transfection efficiency in HEK 293T cells was assessed to elucidate basic structure-property relationships. In Chapter 6 the question of how many pDNA molecules are located within a single PeptoPlex is addressed by means of TIRF microscopy.

Quickly it became clear, that a simple diblock system with cationic and shielding block, although being quite efficient in transfecting HEK 293T cells, was insufficient for nucleic acid delivery to DCs. In a side project addressing cellular uptake as the first step of cell transfection, mannose was investigated for its suitability to function as DC-targeting ligand (Chapter 7). First, a mannose initiator was applied to generate amphiphilic polypept(o)ides with a polysarcosine and a poly(glutamic acid γ-benzyl ester) (PGlu(OBn)) block. Second, micelles were prepared from the obtained polymers and analyzed for their binding to DCs. These studies laid the groundwork for the later functionalization of PeptoPlexes with mannose and other targeting ligands.

After cellular uptake, the endosomal escape of any nanoparticle is the next main hurdle for efficienct intracellular delivery. In order to address this issue and to increase transfection efficiency of PeptoPlexes, a third functionality in form of endosomolytic moieties is eminently important. One way to incorporate this functionality into the PeptoPlexes is to extend the underlying polymers with a third block. Hence, PLys(Boc)-b-PLys(TFA)-b-PSar triblock copolypept(o)ides with orthogonally deprotectable PLys segments were established forming the basis for all following developments (Chapter 8). The main idea behind this system is that the PLys(TFA) segment can be deprotected without affecting the PLys(Boc) block, making the ε-amines available for polymer analogous reactions and further functionalization.

Histidine is a well-known endosomolytic agent[6] which acts through its pH buffering capacity between pH 4 and 6, eventually triggering the so-called proton sponge effect during endosomal acidification.[7] Thus, the PLys-b-PSar diblock copolypept(o)ides developed in Chapters 5 and the middle segment of the triblock copolypept(o)ides developed in Chapter 8 were modified with histidine to increase their transfection efficiency. Chapter 9 outlines how the polymer microstructure of the corresponding histidinylated copolypept(o)ides, i.e. statistical distribution of histidine along the polymer chain versus defined triblock architecture, influences physicochemical and biological properties of derived polyplexes. The comparative study was supported by simulations of polymer-pDNA interactions (bead spring model) as well as by experimental data.

In comparison to randomly histidine-modified diblock copolymers the triblock structure turned out to be superior for pDNA complexation, yielding PeptoPlexes of favorable physicochemical and biological properties. Consequently, this architecture was further adapted for the next step in PeptoPlex development (Chapter 10). This time, instead of histidine, succinimidyl 3-(2-pyridyldithio)propionate (SPDP) was utilized to install the middle block with activated thiol groups. Subsequently, these groups could be combined with thiol-containing cross-linkers to bioreversibly stabilize PeptoPlexes via disulfide bonds and to enhance their transfection efficiency. The cross-linkers are designed to be bifunctional: in addition to thiols for disulfide formation, they also contain pH buffering secondary amines similar to histidine, rendering them endosomolytic. Furthermore, combining one triblock copolypept(o)ide with various different cross-linkers enabled the quick generation of a PeptoPlex library. This modular approach finally yielded a PeptoPlex fomulation, which was able to transfect a model dendritic cell line (DC2.4) with a model pDNA vaccine.

Following the development of triblock copolypept(o)ide-based PeptoPlexes, a side project was devoted to image endosomal escape of histidine-modified as well as cross-linkable PeptoPlexes by means of spinning disc confocal microscopy (Chapter 11). Visualization of endosomal escape was achieved by employing galectin-8 as intracellular marker for the staining of damaged endosomal compartments. The approach allowed a qualitative comparison between different PeptoPlex forumulations.

Finally, as last step of PeptoPlex improvement presented in this work, a PeptoPlex-based artificial virus was created in which the cross-linkable triblock copolypept(o)ides function as a framework for the attachment of several virus-inspired components: I) For enhanced DC targeting mannose, trimannose or aDEC205 can be installed on the PeptoPlex surface by click reaction. II) Cross-linking of PeptoPlexes is conducted with a cystein-containing fusogenic peptide (LAH4-L1),[8] which is released in the endosome upon cellular uptake and catalyzes endosomal escape by membrane interaction. III) In case of pDNA delivery a nuclear localization signal (NLS) is attached to the plasmid via intercalation, which mediates the import of the pDNA into the cell nucleus.

The virus-mimicking PeptoPlexes were evaluated for pDNA and mRNA delivery to murine bone marrow-derived dendritic cells (BMDCs) and human dendritic cells (Chapter 12 and 13). Dendritic cells were successfully transfected with these systems, as proven by reporter gene readout as well as a functional T cell proliferation assay. Moreover, first *in vivo* experiments in mice were performed to investigate biodistribution of the final PeptoPlexes after systemic injection (Chapter 14).

2 MATERIAL ASPECTS OF POLYPEPTIDES

Taken in part from: P. Heller, C. Scholz, M. Barz, “Material Aspects of Polypeptides”, *to be submitted*

2.1 SYNTHESIS AND CHARACTERIZATION OF POLYPEPTIDES/POLYPEPTOIDS/POLY(AMINO ACID)S USED IN MATERIAL APPLICATIONS

2.1.1 Polymerization Techniques

The ring-opening polymerization of *N*-carboxy-α-amino acid anhydrides (NCA) is the most widely used synthetic method to access poly(amino acid)-containing materials, allowing production of high molecular weight polypeptides in large scale and without detectable racemization.[9]

The synthesis of NCAs and their polymerization were first described by Hermann Leuchs at the beginning of the 20th century.[10–12] Today, the common synthetic route for NCA formation is the Fuchs-Farthing method,[13, 14] nevertheless, Leuchs method is still being used for synthesis of NCAs which are not directly accessible by phosgenation.[15, 16] Starting from 1921, NCA polymerization for the directed synthesis of polypeptides was for the first time applied by Theodor Curtius and Fritz Wessely.[17–21] Since the pioneering work of Deming in 1997 establishing a transition metal-mediated version of NCA polymerization,[22, 23] a variety of further methods and advancements enabling living/controlled NCA polymerization have been published and detailed in excellent reviews.[24, 25] The most common principle behind these methods is to replace the activated monomer mechanism (AMM) of NCA polymerization with other more favorable chain growth polymerization mechanisms, as the former in general produces high molecular weight polymers of large polydispersities and without any control over chain length or end-group functionality. Because AMM is induced through initiation by bases and basic impurities, its suppression on the one hand can be achieved with sophisticated initiators[22, 23, 26, 27] substituting the more traditional amine initiators. On the other hand, AMM may also be prevented by employing extremely pure and dry reagents and solvents (most frequently THF and DMF), optionally combined with high vacuum techniques (HVT),[28] polymerization at low temperatures[29] or both,[30] all allowing application of conventional amine initiators (normal amine mechanism, NAM) while still suppressing AMM.

Apart from shifting reaction mechanism, there are other critical points during NCA polymerization which also have been subject to optimization efforts. Only lately, an organocatalysis-based methodology for NCA polymerization exploiting a thiourea derivative was reported by the group of Hadjichristidis.[31] Through hydrogen bonding, *N,N'*-bis[3,5-bis(trifluoromethyl)phenyl]thiourea (TU-S) tackles several reaction steps within the NCA polymerization process at the same time. It simultaneously provides activation of NCA monomers, reversible deactivation of polymer chain ends and silencing of tertiary amines. In this way, well-defined linear (PDI 1.02-1.05) and multi-arm polypeptides could be obtained. In a different work, thiourea had already been utilized for its chaotropic properties to suppress secondary structure formation of the growing polypeptide chain during polymerization.[32]

Further more recently described strategies for optimizing NCA polymerization involve the application of N_2 flow to accelerate the polymerization reaction by CO_2 removal[33] or initiation by ammonium tetrafluoroborate salt,[34] which depicts an advancement from the original ammonium chloride initiator reported by Dimitrov and Schlaad.[27]

Cameron and co-workers discussed a simplified approach to NCA polymerization deliberately avoiding the more elaborate methods[25] proposed by other groups. Conventional primary amine initiation in combination with rigorously purified educts and THF as solvent led to defined homopolypeptides, although in general polydispersities were higher than those obtained with other methods.[35]

In summary, all the described novel developments in NCA polymerization from of the last two decades now enable the synthesis of well-defined polypeptide materials with high complexity and functionality.

In our own studies involving polypeptide synthesis by NCA polymerization we observed that for an average degree of polymerization up to 100 clean polymerization conditions and reduced temperatures readily yielded well-defined polymers.[36, 37] From our experience we can thus conclude that in this polymer size regime highly pure monomers, solvents and initiators in combination with inert polymerization conditions are sufficient to afford polypeptides of narrow molecular weight distribution. For higher chain lengths, additional measures as reported by other groups and described above are necessary.

2.1.1.1 *Initiators*

To promote NCA polymerization in a living/controlled fashion initiators should exhibit high nucleophilicity, particularly with respect to the propagating chain, but weak basicity. Only under this condition polymerization can proceed along favorable mechanisms like NAM instead of the AMM. Suitable nucleophilic initiators which have been employed successfully therefore include transition metal complexes,[38] silazanes/trimethylsilyl (TMS) amines,[26, 39] primary amines or their corresponding salts,[27, 34] alcohols,[31, 40] thiols,[41] amidines[42] and *N*-heterocyclic carbenes[43–45]. Heise and co-workers lately introduced photopolymerization of NCAs through *in situ* generation of a cyclohexylamine initiator by UV-induced breakdown of photoamine generators.[46]

Initiators can also bear additional chemical functionalities to create polypeptides with distinct α-chain end groups. For example, dual initiators can combine NCA polymerization with atom transfer radical polymerization (ATRP),[47] reversible addition-fragmentation chain-transfer (RAFT),[48] or nitroxide-mediated polymerization (NMP)[49] creating a polypeptide macroinitiator as intermediate product, respectively. Polypeptides deployable for click chemistry can be generated with azido and alkyne or dibenzocyclooctyne containing initiators, allowing the combination of the polypeptide with other polymer blocks,[50–53] poly- saccharides,[54, 55] polypeptides,[56, 57] lipophiles,[58] targeting ligands[59] or nanoparticles[60].

Holm *et al*. recently introduced another example for a bifunctional initiator.[61] Mono-Boc-cystamine was applied for the successive polymerization of sarcosine (Sar) NCA and γ-benzyl-L-glutamate (Glu(OBn)) NCA after intermediate capping and deprotection steps. The synthetic procedure yielded amphiphilic polymers with a disulfide linkage between both blocks.

Finally, amine end group-containing macroinitiators, e.g. PEG-NH_2[62–65] or polysarcosine (PSar)[66] can be applied in NCA polymerization to generate block copolymers and copolymer hybrids, while initiators with multiple amine groups such as PAMAM G4[67] provide access to more complex architectures like dendrimer or star-shaped polymers.[68–71]

In addition to soluble initiators, suitable surface-bound nucleophilic moieties like primary amine groups can also be used to induce polymerization of NCAs.[72–74] Thus derived polypeptide layers may provide multifunctional biocompatible interfaces. Exemplary studies will be covered in the "Grafted Polypeptides" section.

2.1.2 Linear and Cyclic Homopolymers

The most simple polymers which can be obtained by NCA polymerization are homopolypeptides. Historically, homopolypeptides produced by NCA polymerization were used as models for natural polypeptides and proteins to elucidate relationships between primary and secondary structure.[24] In this way, amino acids could be categorized according to their conversion to α-helix, β-sheet or random coil-forming polypeptides.[75, 76]

These different secondary structures, which can be adopted by (homo)polypeptides, may interfere with standard polymer analytics such as GPC, leading to artifacts, as pointed out by Huesmann *et al*. for the example of poly-L-lysine (PLys).[36] The group investigated poly(*N*-ε-benzyloxycarbonyl-L-lysine) (PLys(Z)) and poly(*N*-ε-trifluoroacetyl-L-lysine) (PLys(TFA)) of chain lengths between 20 and 200. Counterintuitively, GPC traces were bimodal for smaller polymers, but monomodal for larger ones. Moreover, it was found that during polymerization a growing PLys(Z) chain undergoes a transition from monomodal to bimodal and back to monomodal distribution. The observations could be explained by the co-occurrence of random coil and α-helix conformation in a certain chain length range, as determined by circular dichroism spectroscopy. The effects on GPC traces thereby derived from a 1.6-fold increase in the hydrodynamic volume of the polymers at the coil-helix transition.

Polyglutamic acid (PGA) and its derivatives probably are the most widely studied homopolypeptides. At physiological pH, PGA has a negative net charge and adopts a random coil conformation, while undergoing a transition to α-helical structure with decreasing pH.[77, 78] Protected precursor polymers of PGA are easily accessible by NCA polymerization with dispersities as low as 1.10.[79] Moreover, PGA is highly hydrophilic and biocompatible. Together with the side chain carboxylate groups allowing various modifications and derivatizations,[80, 81] these properties make it a very interesting material for biomedical applications.

Known under the name Paclitaxel Polyglumex (Opaxio), PGA is employed as carrier for the cytostatic drug paclitaxel of the taxane family.[82, 83] The drug is conjugated by ester linkage to the γ-carboxylic acid side chains of the PGA backbone. The proposed mechanism of action is intracellular release of active paclitaxel after endocytosis and cleavage by lysosomal enzymes.[84] PGA-paclitaxel conjugate has been tested in clinical trials for the treatment of several cancer types.[85] Currently, it is evaluated as maintenance therapy for ovarian cancer in a phase 3 study. Further PGA-based drug formulations investigated are PGA-doxycycline[86] for the treatment of rare amyloidotic disease and conjugates of PGA and an anti-apoptodic peptide to reduce inflammation in kidney cells.[87] Another concept for PGA-conjugates envisages to exploit its hydrophilicity and biocompatibility for the masking, delivery and stimuli-responsive unmasking of therapeutic proteins.[88]

The α-helix conformation which in principal can be adopted by homopolypeptides such as PGA is an interesting motif within the biomedical application context as it emulates the three-dimensional structure of natural peptides and proteins. Yet, as pointed out above, at physiological pH PGA exists as random coil rather than as α-helix because electrostatic repulsion of the side chains destabilizes the latter. Consequently, it is not surprising that in recent years, significant effort has been undertaken to establish PGA derivatives with increased α-helical content and stability. In this regard, using HMDS initiator Cheng and co-workers synthesized an array of side chain-modified PGA derivatives, which differed in the hydrophobicity and the length of an alkyl spacer within the modified side chain (grafting efficiency 95%).[79] The alkyl spacer was introduced by post polymerization esterification of the γ-carboxylate groups and contained a primary amine at the opposite end. Longer and more hydrophobic spacers correlated with a higher α-helical content and increased helix stability of the respective PGA derivatives, as determined by circular dichroism spectroscopy. These results can be explained by hydrophobic stabilization and the separation of the charged primary amines from the polypeptide backbone, which is paralleled by less electrostatic repulsion interfering with the α-helical structure. The work culminated in the synthesis of γ-(4-vinylbenzyl)-L-glutamate (VBLG) NCA and its polymerization yielding poly(γ-(4-vinylbenzyl)-L-glutamate) (PVBLG) of low dispersity (<1.1, DP up to 267).

In several studies, the groups of Jianjun Cheng and Paula T. Hammond extended the research on α-helical PGA derivatives. Thereby, PVBLG, poly(γ-propargyl l-glutamate) (PPLG)[80] and other structures formed the starting material for further polymer analogous reactions (in case of PVBLG: ozonolysis and reductive amination, for PPLG: click reactions) affording ionic polypeptides with stable α-helix conformation, which were utilized for nucleic acid delivery (e.g. PVBLG-8/PPABLG as the most effective PVBLG derivative)[89, 90] or as antimicrobial substances[91, 92]. The stable α-helical structure plays a crucial role in both applications as it facilitates membrane destabilization and pore formation thereby mimicking natural α-helical cell penetrating peptides (CPPs).[90] For instance, racemic PVBLG derivatives with random coil structure exhibited far inferior transfection efficiencies.[89]

Another application of PGA-derived α-helical polypeptides reported by Hammond and co-workers is the use as backbone material in hydrogel scaffolds, which can be employed for tissue engineering. Mimicking natural extracellular matrix proteins, the α-helical structure again has a crucial impact in dictating stiffness and nanoscale organization of the derived hydrogels.[93, 94]

As the reactive side chain carboxylate group of glutamic acid NCA has to be protected during polymerization - most commonly via a benzyl ester - it is not surprising that the protected precursor polymer of PGA, poly(γ-benzyl-L-glutamate) (PBG), enjoys considerable popularity as hydrophobic PGA-derivative. For instance, Donghui and co-workers recently studied a series of pyrenyl-terminated PBGs (PDI 1.17-1.55, M_n up to 14.8 kDa for [M]:[I] 100:1), obtained from initiation with 1-pyrenemethylamine hydrochloride, for their interaction with single-walled carbon nanotubes (SWCNTs) in solution and solid state.[95]

The group of Deming lately reported on phosphorylcholine derivatives of poly(homoserine).[96] Precursor polymers with PDI around 1.20 and DP up to 130 could be readily obtained by polymerization of corresponding NCAs with $Co(PMe_3)_4$ initiator. A one-step post polymerization reaction involving nucleophilic substitution of bromide and removal of the benzyl protective groups at the phosphate side chain yielded poly(L-phosphorylcholine homoserine). In contrast, the synthetic procedure was not suitable for poly(L-phosphorylcholine serine) due to β-elimination of the serine, followed by chain degradation.

The Deming group has also extensively studied thioether-containing polypeptides for their applicability as stimuli-responsive systems.[97–101] Using cobalt-based initiators in THF, homopolymers from methionine NCA or various derivatives of cysteine and homocysteine NCAs with low dispersities (<1.2) were successfully synthesized. The thioether motif in all these polymers allows redox-responsive (oxidation to sulfoxide/sulfone)[97, 102] or even multistimuli-responsive (oxidation, alkylation, temperature)[100] transition from α-helix to random coil structure. As a second feature, chemoselective alkylation reactions at the

thioether group permit various post polymerization derivatizations of the precursor polymer.[98, 101]
Dong and co-workers synthesized L-PCys(*S*-(*o*-nitrobenzyl) (PDI 1.46, M_n 2.7 kDa) and D,L-PCys(*S*-(*o*-nitrobenzyl) (PDI 1.46, M_n 6.4 kDa) as another class of stimuli-responsive PCys derivatives.[103] Here, the *o*-nitrobenzyl groups can be cleaved by UV radiation, thereby increasing hydrophilicity of the polymer segment[104] and making the freed thiol groups accessible for disulfide cross-linking or side chain modifications like grafting-onto of PEG480.[103, 105]

Also aiming for redox-responsive homopolypeptides, Schäfer *et al.* just recently reported on the polymerization of *S*-alkylsulfonyl-L-cysteine NCA to obtain PCys(SO_2Et)$_{13\text{-}28}$ (PDI 1.13-1.15, M_n up to 11.6 kDa) or PCys(SO_2iPr)$_{15\text{-}23}$ (PDI 1.15-1.17, M_n up to 9.5 kDa) for chemoselective asymmetric disulfide formation.[106] The two novel protective groups are stable during NCA polymerization or peptide coupling conditions while reacting with thiols within minutes.

Complementary to thiol-containing poly(amino acids), poly(histidine) (PHis) depicts another stimuli-responsive, i.e. pH-responsive homopolypeptide. The imidazole ring with its unsaturated nitrogen atom can be protonated at pKa $\sim$ 6.5, rendering PHis soluble at lower pH ($\sim$6.3) and insoluble at physiological pH (7.4).[107] As for other amino acids with reactive side chains, the imidazole nitrogen has to be protected during polypeptide synthesis to prevent interference with the polymerization reaction. Iatrou and co-workers developed a novel N^{im}-trityl-protected histidine NCA to obtain well-defined polyhistidine (PHis) using high vacuum techniques and dimethylamine as initiator (PDI 1.12-1.23, M_n up to 36.3 kDa).[108] The polymerization followed first order kinetics and proceeded without termination reactions, although slower than for other common NCAs. The trityl group could be easily removed with TFA in dichloromethane. According to circular dichroism spectroscopy, PHis switched conformation from random coil to β-sheet with increasing pH. Moreover, the pK_a of the polymers depended on the molecular weight and could be tuned by randomly adding leucine or γ-benzyl glutamate into the PHis chain.

Defined poly(*O*-benzyl-L-threonine) PBnT (PDI 1.16-1.40, M_n up to 30.9 kDa for [M]:[I] 150) was synthesized for the first time by Gibson and Cameron employing the above described simplified NCA polymerization approach.[35] The polymerization displayed first-order kinetics and led to monomodal weight distribution and predictable M_n. PBnT was also successfully incorporated into diblock copolymers.

Other NCA-polymerized homopolypeptides which have been investigated and recently reported in literature include polyalanine,[109] poly(aspartic acid) (PAsp)[110] and poly(proline) (PPro). Among these, the latter is particularly interesting because of its unique α-helical secondary structure. PPro either adopts the poly(proline) II helix (PPII), for example found in collagen,[111] or less frequently the poly(proline) I helix (PPI). Because of the helix conformation, PPro like PGA is a reasonable backbone material for artificial cell penetrating agents.[112] Due to the cyclic structure of proline and the resulting conformational restrictions, the corresponding NCA cannot be synthesized with classic Leuchs or Fuchs-Farthing procedure, as the *N*-carbamoyl intermediate does not cyclize spontaneously. Recently reported methods to overcome this issue involve the application of polymer-supported bases[113] or Boc-protected proline instead of the free amino acid[114]. The group of Hadjichristidis and Iatrou harnessed this methodology to obtain well-defined PPro hompolymers (PDI 1.23-1.26, M_n up to 13.0 kDa).[114, 115]

In an attempt to generate a more lipophilic and stable analogue of PPro, Martin *et al.* synthesized D- and L-poly(silaproline) (polySip), a silicon-containing derivative. Interestingly, they used a secondary amine in the form of *O*-benzyl-protected proline instead of a more conventional primary amine as initiator. In case of proline this should not be disadvantageous, as the *N*-substitution prevents the occurrence of AMM. Unfortunately, no characterization of the obtained polymers by SEC was provided. According to circular dichroism spectra, polySip adopted a PPII conformation like PPro, albeit with increased thermal stability.[116]

Apart from homopolypeptides, homopolypeptoids - their *N*-substituted analogs - have been studied by several groups, although the same variety of NCAs as for polypeptides is not yet established. Similar to proline, the *N*-substitution within the underlying NCA monomers (NNCAs) prevents reaction via the AMM, facilitating a controlled polymerization.[109, 117, 118] Though, with the exception of PSar, polypeptoids have been rediscovered only recently.[43, 119, 120] Luxenhofer and co-workers detailed the preparation and characterization of various hydrophilic, hydrophobic and amphiphilic homopolypeptoids bearing C1-C4 side chains, which could be obtained with Poisson distribution (PDI 1.14-1.31 depending on NCA, M_n up to 5.4 kDa for PSar with [M]:[I] 100:1).[121] The syntheses were initiated with benzylamine and carried out in benzonitrile or *N*-methyl-2-pyrrolidinone (NMP). Polymerizations followed first-order kinetics. The polymerization rates for PSar were examined more closely and showed dependencies of solvent, acid content of the reaction solution and pressure. In a follow-up publication the group extended the research on this polymer class, this time investigating the thermal properties of homopolypeptoids with C1-C5 side chains.[122]

Aside from linear homopolypeptides and homopolypeptoids, their cyclic analogues can also be derived from NCA polymerization. In fact, cyclic polypeptides were confirmed as side products of NCA polymerization in nucleophilic solvents such as DMSO, DMF and NMP.[123, 124] Directed synthesis of various cyclic polypeptides was achieved by thermal NCA polymerization[125] or by using pyridine or *N*-ethyldiisopropylamine as catalysts[126]. However, all these methods do not allow the synthesis of defined products. In contrast, for cyclic polypeptoids controlled polymerization is possible with the already mentioned amidine[42] and *N*-heterocyclic carbene[43, 44] initiators, as demonstrated for the first time by Zhang and co-workers. In this case the cyclization reaction occurs as the last step of a zwitterionic ring-opening polymerization between oppositely charged chain ends. The Zhang group employed this methodology to obtain cyclic poly(*N*-Bu-glycine) from initiation with bis(2,6-diisopropylphenyl)imidazol-2-ylidene in THF and compared it with its linear analogue.[43] Good control over the molecular weight and PDI (1.04-1.12) was maintained even for higher [M]:[I] ratios up to 400:1, indicating a living polymerization with minimal inter- or intrachain transfer. Interestingly, when the solvent of the polymerization was changed from THF to DMF, i.e. to a solvent that can better stabilize zwitterionic species, control of the polymerization was significantly compromised. In a subsequent study, the group synthesized a series of linear and cyclic polypeptoids bearing various linear or branched alkyl side chains for investigations on crystallization and melting behavior.[127]

A synthetic route towards defined cyclic homopolypeptides by post polymerization cyclization was proposed by Politakos *et al*. The group compared linear and cyclic benzyl-protected poly(L-tyrosine) obtained by ROP of the corresponding NCA with hexamethylenediamine under high vacuum conditions and subsequent cyclization with phosgene.[128] As expected, both polymers virtually exhibited the same molecular weight and polydispersity in GPC (PDI 1.06, Mn 2.6 kDa for linear and cyclic species). With regard to secondary structure, linear poly(L-tyrosine) adopted β-sheet conformation whereas cyclic poly(L-tyrosine) existed as a mixture of α-helix, β-sheet and random coil. These conformational differences i.a. were reflected in smaller particle size, less aggregation and smaller polydispersity for cyclic poly(L-tyrosine), as determined by DLS.

2.1.3 Copolymers

Copolypeptides result from the combination of different polypeptides with each other or with other polymer classes. While one polypeptide component may introduce multifunctionalitiy (functional groups, secondary structure, stimuli-responsiveness, degradability etc.) present on the assortment of amino acids, the other component (be it peptidic or non-peptidic) may provide solubility, processability, nonfouling properties, etc., leading to sophisticated materials with higher complexity than their single elements.

Since NCA polymerization can be conducted with simultaneous or sequential feeding of different NCA monomers, random and block copolypeptides can be generated in a one pot approach.[24, 129] Furthermore, the combination of NCA polymerization with other polymerization techniques, for example through the use of macroinitiators, provides convenient access to hybrid polymers.[9] In both cases, post polymerization joining of individual blocks depicts a valuable supplementary methodology. Finally, grafting-from and grafting-onto techniques enable more elaborate copolymer architectures like star-shape and bottle brushes. Considering this toolbox of various synthetic methods, it is no surprise that a plethora of fully copolypeptide as well as polypeptide hybrid materials have been established in recent years, which can only be sketched in this chapter.

2.1.3.1 *Block Copolymers*

Block copolypeptides and hybrids can be generated either by polymerizing from a (homopolypeptide) macroinitiator or by multi-step feeding of different NCA monomers without intermediate workup. Early studies on block copolypeptides through amine initiation already reported on both methods.[130–132] Likewise, in the first publication on transition metal-mediated NCA polymerization by Deming, the synthesis of di- and triblock copolypeptides was already covered.[22] While nowadays especially in the biomedical field AB diblock copolypeptides are the most frequently used materials, other more complex architectures like triblock, tetrablock and pentablock copolypeptides have been synthesized,[129] proving that the livingness of NCA polymerization can be retained over multiple feeding steps.

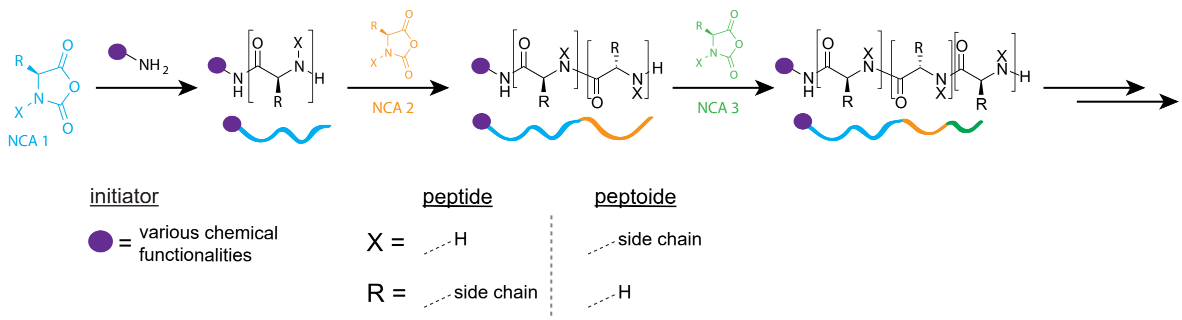

Figure 2.1: Synthetic route towards block copolypeptides/peptoids by successive polymerization of (N)NCAs.

Investigating the extent of block sequence control in NCA polymerization, Heise and coworkers were able to push limits to octablock copolypeptides with short alternating PBG and poly(*tert*-butyl-L-glutamate) (PTG) blocks.[133] $(PBG_5\text{-b-}PTG_5)_4$ of low dispersity (PDI 1.12, M_n 9.5 kDa) could be prepared by initiation with *n*-hexylamine in DMF and rotational feeding of the two respective monomers. Selective deprotection of the PTG blocks and subsequent grafting with PEG500-NH_2 rendered the octablock copolymers water-soluble.

Among the synthetically accessible polypeptides, amphiliphilic block copolypeptides are of particular interest, as in a block-selective solvent this property gives rise to the formation of superstructures through hierarchical self-assembly. In the special case of peptides self-assembly is additionally directed by secondary structures. Thus, it is not surprising that most synthetic efforts aim at the creation of amphiphilic block copolyeptides and hybrid polymers. Commonly deployed hydrophilic blocks include PLys,[64, 134, 135] PGA[136] and derivatives thereof[59] for fully peptidic materials, plus PEG,[137] polyoxazolines (POx),[138, 139] PSar,[37] polysaccharides[54, 55, 140] and Poly(*N*-(2-hydroxypropyl)methacrylamide) (PHPMA)[141, 142] for hybrid materials. Popular hydrophobic components are hydrophobic PLys and PGA derivatives (e.g. PLys(Z), PBG) on the one hand and naturally hydrophobic amino acids like alanine and leucine on the other. In most cases, synthesis is started with the more soluble (hydrophilic) block (PLys/PGA derivatives, PEG, PSar etc.) which keeps the second, less soluble block in solution and ensures low dispersities.[24, 129]

PGA-b-PLys(Z) as prepared by Cameron and co-workers is an example for an all-peptide amphiphilic AB diblock where PGA forms the hydrophilic component.[136] In this study, several precursor polymers with varying block lengths were synthesized by initiation with *N*-benzyl-TMS amine in DMF (PDI 1.17-1.28, M_n up to 30.5 kDa for PBG_{50}-b-$PLys(Z)_{50}$). Selective deprotection of the PBG block with KOH in water/THF yielded amphiphilic, micelle-forming block copolypeptides.

In a series of publications Deming and co-workers investigated amphiphilic block copolypeptides containing PLys as hydrophilic component for their hydrogel forming behavior. Initial efforts involved the preparation of diblock architectures (PDI 1.1-1.3 depending on NCA, M_n up to 52.1 kDa) incorporating leucine (Leu) or valine (Val) as α-helix or β-sheet adopting hydrophobic components.[143] Later work expanded polymer synthesis to $PLys_{180}$-b-$PLeu_{40}$-b-$PLys_{180}$ triblocks[144] and even pentablock copolypeptides of $PLys_{60}$-b-$PLeu_{20}$-b-$PLys_x$-b-$PLeu_{20}$-b-$PLys_{60}$ sequence, where x was varied from 10 to 200.[145] In case of the latter PDIs of 1.19-1.27 and M_n of around 16 kDa were determined for the first block, but no SEC data for the final pentablocks were provided. Further research led to the synthesis of various narrowly distributed diblock copolypeptides with $PLys_{180}$-b-X_n architecture, where X depicts the hydrophobic, α-helix forming blocks like PAla, PLeu, poly(phenylalanine) (PPhe) or P(Ala-co-Leu) (PDI 1.05-1.09 depending on NCA and block length, Mn around 47 kDa).[146] Differing in amino acid composition and block lengths, this diblock copolypeptide library allows the fine-tuning of stiffness and viscosity of derived hydrogels, which were applied for the local delivery of hydrophobic cargo to the central nervous system.

The Deming group also investigated amphiphilic methionine-containing block copolypeptides of $PMet_{65}$-b-$P(Leu_{0.5}$-co-$Phe_{0.5})_{20}$ architecture (Mn 8.65 kDa, no PDI provided), where PMet upon oxidation in water to the corresponding sulfoxide depicts the hydrophilic component. Self-assembly of these polymers afforded stimuli-responsive vesicles.[102]

Han *et al*. followed a similar approach to Deming in working on amphiphilic diblock copolypeptides of the PLys-b-PLeu type (M_w 17.37 kDa for $PLys_{55}$-b-$PLeu_{24}$).[59] In this case, after polymerization with propargyl amine as bifunctional initiator, the positive net charge of the PLys segment was converted to a negative net charge by post polymerization amidation with 2,3-dimethylmaleic anhydride and in aqueous solution the final polymers formed micelles.

As alternative to the prevailing amphiphilic diblock copolypeptides, Iatrou *et al*. utilized HVT to gain well-defined, amphiphilic ABA-type triblock copolypeptides of PLys-b-PBG-b-PLys composition (PDI around 1.15, M_n up to 91.0 kDa for $PLys_{131}$-b-PBG_{137}-b-$PLys_{131}$) designated for drug and gene loading after polymersome formation.[64, 134] Synthesis was conducted by outward polymerization of two PBG blocks from a diamino initiator, followed by addition of Lys(Boc) NCA and deprotection. In another series of publications, the group detailed the generation of various PPro-containing block copolypeptides. Employing HVT, well-defined PBG-b-PPro (M_n up to 45.0 kDa)[114, 115] and PLys-b-PPro (PDI 1.10, M_n up to 239.1 kDa)[114, 147] block copolypeptides as well as PEG-b-PPro (PDI 1.10, M_n up to 36.8 kDa) and PPro-b-PEG-b-PPro (PDI 1.10, M_n up to 19.3 kDa) hybrids[114] could be obtained.

As already mentioned, apart from purely peptidic systems, hybrid polymers with a functional peptide block and a non-peptidic hydrophilic block enjoy considerable popularity. Arguably, PEG is the most frequently used hydrophilic component to form amphiphilic copolypeptide hybrids. As pointed out earlier, it can simply be introduced through a PEG-NH_2 macroinitiator. For instance, the group of Kataoka employs α-methoxy ω-amino PEG (mPEG-NH_2, 2-20 kDa) for polymerization of various peptidic blocks like PGA, PAsp, PLys or respective derivatives thereof.[62, 148] The obtained AB-type hybrid polymers show narrow molecular weight distribution (PDI < 1.2), while the polymerization degree of the peptide segment can be adjusted up to 100.[137]

Kudo *et al*. polymerized ornithine(Z) NCA from a mPEG-NH_2 (12 kDa) macroinitiator in DMF, generating PEG-b-Porn$(Z)_{30}$ (PDI 1.09). Over multiple reaction steps the poly-ornithine(Z) block was converted to polyarginine (PArg), and the resulting polycatiomer was used to form polyion complex (PIC) micelles with hyaluronic acid or chondroitin sulfate.[149]

Other recent examples for PEG-NH_2 initiated diblock copolypeptides include studies from Hammond and co-workers[150] and the Cheng group[151]. In the former case mPEG-NH_2 (5 kDa or 10 kDa) and γ-propargyl L-glutamate NCA yielded PEG(5)-b-$PPPLG_{53}$ or PEG(10)-b-$PPPLG_{45}$ with PDIs from 1.11-1.15. Subsequent derivatization by click chemistry afforded pH-responsive polymers self-assembling into polymersomes, which were loaded with doxorubicin.[150] The latter case is a follow-up study of the already mentioned PVBLG-derivatives (PPABLG)[89, 90] for nucleic acid delivery (see Subsection 2.1.2). In an effort to augment these α-helical homopolypeptides with a hydrophilic (shielding) segment, PEG_{113}-NH_2 was combined with a PVBLG-derived block leading to PEG_{113}-b-$PVBLG_{76}$ (PDI 1.21, M_n 20.7 kDa) and PEG_{113}-b-$PVBLG_{287}$ (PDI 1.29, M_n 75.3 kDa). Both polymers were further modified and evaluated for gene delivery.[151]

Scholz and co-workers exploited the PEG macroinitiator approach to build ABC-type PEG_{114}-b-$PBG_{20\text{-}24}$-b-$PLeu_{10\text{-}23}$, PEG_{114}-b-$PLeu_{12\text{-}23}$-b-$PBG_{22\text{-}24}$ and A(B/C)-type PEG_{114}-b-P($BG_{23\text{-}26}$-co-$Leu_{12\text{-}23}$) architectures, as controlled by NCA feeding sequence and ratio, which were investigated for their self-assembly behavior.[63] Polymerization was initiated with $mPEG_{114}$-NH_2 (5 kDa) and conducted in the presence of 0.2 M urea in DMF to suppress hydrogen bond formation between nascent peptide chains. Observed PDIs ranged from 1.04-1.09 for triblocks and from 1.11-1.15 for PEG-b-(PBG-co-PLeu) diblocks. In a previous study, the same synthetic strategy was applied to afford PEG_{114}-b-$PGA_{57\text{-}108}$-b-$PCys_{7\text{-}14}$ (PDI 1.14-1.17) and PEG_{114}-b-($PGA_{50\text{-}102}$-co-$PCys_{7\text{-}19}$) (PDI 1.26-1.34) hybrids. The polycysteine (PCys) block worked as anchor to graft these polymers onto gold surfaces and gold nanoparticles.[152]

Recently, Schlaad and co-workers also reported on ABC-type hybrid copolypeptides derived from a PEG macroinitiator.[153] PEG_{42}-b-$PLys_{61}$-b-PGA_{62} was prepared by sequential polymerization of Lys(Z) NCA and Glu(OBn) NCA in DMF (PDI 1.07, M_n 30.6 kDa), followed by removal of protective groups. The polymer was analyzed for its pH-dependent aggregation behavior induced by the helix-coil transition of the two peptidic blocks. Slightly different architectures of PEG_{188}-b-PBG_{36}-b-$PLys_{36}$ composition (PDI 1.10, M_n 24.9 kDa) with polymersome forming capability were previously described by Iatrou *et al*.[64]

Despite the dominance of PEG as hydrophilic component in amphiphilic systems, other hydrophilic materials have been explored for the combination with polypeptides. Lately, the polypeptoid PSar has gained increased attention as a substitute for PEG in block copolymer architectures (block copolypept(o)ides).[37, 154] Obviously, in contrast to the latter, incorporation of PSar is not only feasible through macroinitiation, but can also be achieved by sequential polymerization of the respective (N)NCAs, similar to the synthesis of classic block copolypeptides. Using amine initiators in DMF, Barz and co-worker recently adopted this strategy to obtain amphiphilic PSar-b-PBG, PSar-b-PCys(SO_2Et) or cationic PSar-b-PLys hybrid polymers for drug or gene delivery applications, either starting with the PSar or the polypeptide block. Besides, different post polymerization ligation techniques were evaluated as an alternative route to PSar-containing block copolymers.[57] Eventually, over several studies, various narrowly distributed block copolypept(o)ides (PDI < 1.2) with diblock[61, 155–157] and triblock[158, 159] architectures were obtained. DP as determined by ^{1}H-NMR could be adjusted from 44-600 for the PSar block, from 22-117 for PBG and from 13-111 for PLys(PG). In addition, a recent publication of the Barz group introduced $PSar_{94\text{-}407}$-b-$PCys(SO_2Et)_{13\text{-}28}$ block copolypept(o)ides (PDI 1.25-1.38, M_n up to 32.1 kDa) which can self-assemble into core-cross-linkable micelles. Hereby, the self-assembly conditions and the nature of cross-linkers allow independent control of micelle shape and polarity.

Already in the 1990s, the group of Shunsaku Kimura had begun to research on amphiphilic PSar-based diblock copolymers, with PGA(OMe),[160, 161] PLys(Z)[160] or PAla[160, 162] as hydrophobic component. Polymers were synthesized by sequential NCA polymerization with *n*-hexylamine in DMF and investigated for their self-assembly properties. However, in these old studies, the PSar block was kept rather short with a DP below 30 and SEC plots supplementary to M_n values were not provided. In later works, $(\text{Leu-2-aminoisobutyric acid})_6$ ($(\text{Leu-Aib})_6$) or poly-L-lactic acid (PLLA) replaced the previous polypeptide blocks as hydrophobic component. In case of the former, $(\text{Leu-Aib})_6$ obtained by liquid phase method was applied as macroinitiator for the polymerization of PSar in DMF/$CHCl_3$ 1:1 (DP up to 60, no quantitative SEC data provided).[163, 164] For synthesis of the latter, the PLLA block was polymerized at first from a mono-protected diamino initiator (1,2-ethylenediamine) (DP 16-30, PDI 1.05-1.14).[165, 166] Subsequently, the second amino group was deprotected to initiate the polymerization of the PSar block in DMF (DP 22-150, no SEC data of final polymers provided). In a follow-up study, the synthetic protocol was refined with more complex initiators to obtain A_2B-type $(PSar_{26})_2$-b-$PLLA_{33}$ and A_3B-type $(PSar_{23})_3$-b-$PLLA_{30}$ (no SEC data provided).[167]

Other efforts to find PEG alternatives for the combination with a hydrophobic polypeptide block led to the development of PBG-b-polysaccharide hybrids, as reported by Lecommandoux and co-workers.[54, 55, 140] Obviously, these polymers cannot be obtained directly by polymerizing one block onto the other, as the hydroxyl groups within the polysaccharide block would interfere with NCA polymerization. Instead, PBG_{23} (PDI 1.1, M_n 5 kDa) or PBG_{59} (PDI 1.16, M_n to 18.2 kDa) was first synthesized using a bifunctional azide-containing amine initiator and subsequently joined to an alkyne-terminated hyaluronan or dextran block via click chemistry. The resulting amphiphilic block copolymers self-assembled into polymersomes, which were loaded with doxorubicin.

An elegant straightforward methodology towards materials combining carbohydrate and polypeptide components are glycopolypeptides derived from polymerization of sugar-modified NCAs[97] or post polymerization glycosylation[168] of the polypeptide backbone. These have been described and reviewed elsewhere.[169, 170]

Another synthetic strategy for combination of polysaccharide and polypeptide blocks, where successive polymerization of both components is possible, was proposed by Dong *et al*.[171, 172] Here, ATRP polymerization of a lactose-based glycomonomer generated a diamino-terminated polyacrylate with acetyl-protected carbohydrate side chains. In a following step, the amino termini were exploited for the ROP of γ-benzyl glutamic acid or alanine NCA, yielding ABA-type $PGA_{20\text{-}100}$-b-PAEL-b-$PGA_{20\text{-}100}$ (PDI 1.19-1.42, M_n up to

77.7 kDa) and PAla$_{9-93}$-b-PAEL-b-PAla$_{9-93}$ (PDI 1.06-1.41, M_n up to 31.9 kDa) after several deprotection reactions.

Combinations of a hydrophobic polypeptide with a hydrophilic polyacrylate segment generated through ATRP was also reported by Agut *et al*.[50] as well as Huang and Chang[173]. In the first example, an azide-terminated PDMAEMA block and an alkyne-terminated PBG block were synthesized separately and subsequently linked together via click chemistry to obtain PDMAEMA$_{85}$-b-PGA$_{37-186}$ (PDI 1.20-1.25, M_n up to 37.3 kDa). Polymers were characterized for their pH- and thermoresponsive self-assembly behavior.[50] In the second example, polymer synthesis was performed via a heterofunctional initiator starting with the polymerization of NIPAm, followed by deprotection to afford an amine hydrochloride-terminated PNIPAm macroinitiator. The latter was applied for the polymerization of Lys(Z) or Glu(OBn) NCA in DMF, yielding PNIPAm$_{90}$-b-PLys(Z)$_{38-71}$ (PDI 1.19-1.26, M_n up to 28.1 kDa) and PNIPAm$_{90}$-b-PBG$_{37-55}$ (PDI 1.39-1.43, M_n up to 13.0 kDa).[173]

Similar to ATRP, combination of NCA polymerization with RAFT as performed by the groups of Jing and Liu were also exploited to obtain PNIPAm-b-polypeptide hybrid polymers. In all cases, amino-terminated PNIPAm was applied as macroinitiator for the polymerization of the polypeptide block. Within two quickly succeeding publications Jing and co-workers employed PNIPam$_{32}$-NH_2 in its hydrochloride form to afford PNIPAm$_{32}$-b-PBG$_{21-54}$ (PDI 1.20-1.48, M_n up to 27.8 kDa)[174] or PNIPAm$_{32}$-b-PLys(Z)$_{26-61}$ (PDI 1.09-1.25, M_n up to 30.0 kDa) copolymers[175]. Interestingly, polymerization of the former was conducted in DMSO, while the latter were generated in DMF. Both types of polymers were (partially) deproctected and investigated for pH- and temperature-dependent phase transition and self-assembly behavior. Liu and co-workers chose dichloromethane as yet another solvent for the synthesis of PNIPAm$_{65}$-b-PBG$_{110}$ (PDI 1.29, M_n up to 35.1 kDa), which, after deprotection, was studied for micellization properties.[176]

In contrast to the aforementioned groups, Tappertzhofen *et al*. followed the reverse reaction procedure for the synthesis of polypeptide-b-polyacrylate polymers. First, PLys(Z)$_{30}$ (PDI 1.11, M_n 12.6 kDa) was obtained from amine-initiated NCA polymerization in DMF. Afterwards, it was coupled to a chain transfer agent (cta) to generate a polypeptide macro cta for the polymerization of PFPMA. Subsequent conversion of the PPFPMA block to hydrophilic PHPMA yielded PLys(Z)$_{30}$-b-PHPMA$_{200}$ (PDI 1.47, M_n 38.5 kDa). After deprotection of the PLys(Z) block, the final PLys-b-PHPMA polymer was evaluated as pDNA transfection reagent.[141] In a follow-up study the same synthetic strategy was adopted to build a macro cta bearing a disulfide group between the PLys(Z) block and the cta functionality (PDI 1.13, Mn 11.0 kDa). Succeeding reaction steps afforded PLys(Z)$_{30}$-S-S-b-PHPMA$_{230-430}$ (PDI 1.43-1.52, M_n up to 65.0 kDa), which, upon cleavage of the protective group, were used to form redox-responsive polyplexes.[142]

Complementary to block copolypeptides, block copolymer architectures built exclusively of polypeptoids as underlying material have been described and reviewed in detail.[120] It is interesting to note that a first proof of principle regarding their controlled synthesis by NNCA polymerization was given by Zhang and co-workers with the example of cyclic PSar$_{50}$-b-P(*N*-Bu-gly)$_{25}$ (PDI 1.03, M_n 6.5 kDa). For comparison, also linear PSar-b-P(*N*-bu-gly) was prepared, but unfortunately no SEC data was provided.[43] In a successive study, Lee *et al*. compared linear PSar$_{100}$-b-P(*N*-dec-gly)$_{10}$ (PDI 1.05, M_n 12.5), initiated with benzylamine, and cyclic PSar$_{100}$-b-P(*N*-dec-gly)$_{10}$ (PDI 1.21, M_n 14.7), synthesized with a *N*-heterocyclic carbene initiator, for their gelation properties.[177] The Zhang group further diversified the pool of available NNCAs. For example, linear amphiphilic block copolypeptoids forming core cross-linkable micelles were obtained by the sequential polymerization of *N*-ethyl glycine NCA (substituting sarcosine NCA as hydrophilic component), *N*-decyl glycine NCA and *N*-propargyl glycine NCA. Reaction was carried out in THF with benzylamine as initiator, yielding P(*N*-et-gly)$_{134\text{-}204}$-b-P((*N*-pg-gly)$_{13\text{-}62}$-co-(*N*-dec-gly)$_{15\text{-}49}$) (PDI 1.02-1.06, M_n up to 40.8 kDa). Derived micelles could be reversibly stabilized with a disulfide containing cross-linker introduced by click chemistry and were evaluated for delivery of doxorubicin.[178] Finally, the group reported on ABC-type triblock copolypeptoids for hydrogel formation. Sequential benzylamine initiated ROP was conducted with sarcosine NCA, *N*-methoxyethyl glycine NCA or *N*-methoxyethoxyethyl glycine NCA for the hydrophilic segment, *N*-butyl/octyl/decyl glycine NCA for the hydrophobic segment and *N*-allyl glycine NCA to introduce a thermoresponsive element. Various well-defined polymers of P(*N*-allyl-gly)$_{23\text{-}98}$-b-PSar$_{25\text{-}158}$-b-P(*N*-decyl-gly)$_{5\text{-}18}$ composition (PDI 1.03-1.15, M_n up to 41.4 kDa) were obtained and examined for sol-gel transition and micellization.[179]

Parallel to the group of Zhang, Luxenhofer and co-workers introduced well-defined AB-type block copolypeptoids in an initial study.[121] Polymers were synthesized in benzonitrile with benzylamine as initiator. Their compositions as calculated from $[M]_0/[I]_0$ included PSar$_{50}$-b-P(*N*-pr-gly)$_{25}$ (PDI 1.13, M_n 5.7 kDa), PSar$_{50}$-b-P(*N*-bu-gly)$_{25}$ (PDI 1.16, M_n 6.8 kDa) and PSar$_{50}$-b-P(*N*-*i*bu-gly)$_{25}$ (PDI 1.09, M_n 5.6 kDa). That followed, Fetsch and Luxenhofer reported on the controlled sequential polymerization of a pentablock copolypeptoid with a target sequence of PSar$_5$-b-P(*N*-et-gly)$_5$-b-P(*N*-pr-gly)$_5$-b-P(N-pen-gly)$_5$-b-P(*N*-bu-gly)$_5$ as adjusted by $[M]_0/[I]_0$ ratio (PDI 1.18, M_n 2.6 kDa).[66] The group could further demonstrate the generation of a pentablock copolypeptoid aimed for PSar$_{10}$-b-P(*N*-et-gly)$_{10}$-b-PSar$_{10}$-b- P(*N*-et-gly)$_{10}$-b-PSar$_{10}$ composition from solid support in NMP supplemented with 10% HBF_4 (PDI 1.34).[180] The comparatively increased PDI was attributed to a misbalance between high polymerization rate and slow monomer diffusion into the gel. Finally, in two quickly succeeding publications, Fetsch *et al.* explored the aqueous self-assembly of block copolypeptoids with PSar as hydrophilic component, systematically varying hydrophilic:hydrophobic block length ratio (60:5-21:24) and side chain composition of the hydrophobic blocks (C2-C5, benzyl, phenylethyl).[181, 182] Polymers were prepared in benzonitrile either from a PSar$_{50}$ macroinitiator (PDI 1.07-1.12 depending on block ratio and NNCA, M_n up to 9.6 kDa) or by sequential NNCA polymerization with various amine initiators (PDI 1.07-1.18 depending on block ratio and NNCA, M_n up to 6.2 kDa). Observed superstructures included polymersomes, micelles, worms and oligo-lamellar morphologies.

2.1.3.2 *Random Copolymers*

Although synthetic random copolypeptides of multiple amino acids may come the closest to natural proteins, they are far less covered in recent literature than block copolypeptides.

While traditionally being synthesized via copolymerization of two or more different NCAs,[24, 25] random copolypeptides can also be obtained from partial/statistical modification (e.g. deprotection) of the amino acid side chain within one polypeptide block, as for example demonstrated by Higuchi *et al*.[183, 184] and others[103, 105, 185]. Arguably, the first method is complicated by the inability to properly monitor and govern kinetics of individual amino acid NCA monomers during copolymerization, resulting in poor control over the latter. For instance, copolymerization of NCAs with strongly diverging side chains, especially with respect to steric hindrance or secondary structure formation, may suffer from varying NCA reactivity and polymerization speed, shifting the final copolymer architecture from ideal random to rather gradient or multiblock. Consequently, differences in NCA reactivity are a logical root for slightly higher PDIs of some random copolypeptides when compared to homopolypeptides of only one amino acid or the corresponding block copolymers with the same amino acid composition. SEC data substantiating this tendency can be found in several publications[108, 133, 152, 186] and was for example discussed by Scholz and co-workers.[63]

These points have to be taken into account, when studying random polypeptides. As it is unlikely that most NCA mixtures lead to ideal random copolypeptides each case should be investigated carefully. Not surprisingly, early works on random copolypeptides therefore focused on the elucidation of NCA reactivity ratios and resulting amino acid sequences as well as the correlation between polymer composition and secondary structure.[24, 25] Tackling the issue of the varying NCA reactivities and polymerization kinetics, Zelzer and Heise recently proposed a new methodology to monitor NCA consumption in a binary mixture copolymerization with Glu(OBn) and Lys(Z) NCA as two model monomers.[186] Applying a HPLC setup calibrated for both NCAs, they were able to track the respective monomer concentrations over the course of copolymerization. Regardless of initial monomer ratio, Glu(OBn) NCA reacted faster than Lys(Z) NCA, resulting in an incessantly increasing mole fraction of Lys(Z) NCA and a composition drift of the copolymer sequence. Matching HPLC data with copolypeptide composition obtained from ^{1}H-NMR analysis at low-conversion time points, the authors concluded that the first 30% of the final copolypeptide chain are richer in Glu(OBn), whereas the last 70% loosely reflect the initial monomer ratio. Hence, the copolypeptides in this system deviate slightly from an ideal random copolymer and rather resemble a gradient polymer instead.

While most reported copolypeptides are composed of two amino acids, a recent example for random terpolypeptides with three different amino acids was given by Dmitrovic *et al*.[187] P($BG_{11\text{-}28}$-co-Lys(Z)$_{9\text{-}25}$-co-$Ala_{7\text{-}18}$) (PDI 1.20-1.61, M_n up to 10.4 kDa) was obtained from ROP of corresponding NCAs at varying ratios in DMF with benzylamine as initiator. After deprotection of BG and Lys(Z) units, the terpolypeptides were used as additives in $CaCO_3$ mineralization. Going beyond that, Chen *et al*. first copolymerized three NCAs at 1:1:1 ratio resulting in Poly(Orn(Z)-co-Gly-co-Asp(OBn)) (PDI 1.08, M_n 25.8 kDa), which after deprotection and random guanidization was converted to the tetrapolymer Poly(Orn-co-Arg-co-Gly-co-Asp(OBn)) (PDI 1.19, M_n 5.0 kDa). The copolymer was evaluated for vascular and tissue permeabilization *in vivo*.[188]

Furthermore, the drug Glatiramer acetate (Copaxone®) is produced through copolymerization of NCAs from four amino acids - alanine, lysine, glutamic acid and tyrosine - at defined molar ratio with a DP between 40 and 100 (average M_n 6.4 kDa).[189] It is also the first example for an approved random copolypeptide with therapeutic application and has been successfully established for the treatment of multiple sclerosis grossing annual sales of around 4 billion USD.

In several recently published studies, random copolypeptides are not deployed as a standalone polymer, but just form one segment embedded within a greater block copolymer architecture (also see Block Copolymer Section). For instance, copolymerized hydrophobic amino acids at varying ratios can be used to fine-tune overall hydrophobicity of the resulting random block,[63, 146] or to control block flexibility[102]. In a study by Iatrou *et al*., His(Trt) NCA was copolymerized with Glu(OBn) NCA or Leu NCA at different ratios under HVT conditions from a PEG macroinitiator to obtain PEG-b-P(His-co-BG) (PDI 1.10-1.14, M_n up to 15.9 kDa) and PEG-b-P(His-co-Leu) (PDI 1.09-1.17, M_n up to 16.0 kDa).[108] The group observed that in contrast to homopolymerization of PHis, the copolymerizations did not become heterogeneous. From this observation it was inferred that Glu(OBn) as well as Leu units were distributed randomly along the PHis block and suppressed secondary structure formation of the latter. Moreover, pK_a and degree of protonation of the PHis block as well as the swelling behavior of PEG-b-P(His-co-PLeu(BG)) could be adjusted by the amount of incorporated hydrophobic amino acids. Blocks from copolymerization can also be feasible, when a certain additional functionality for further modifications is supposed to be distributed randomly along one block. In this way, Li *et al*. incorporated *N*-propargyl glycine into a hydrophobic *N*-decyl glycine block to make it amenable for click reactions,[178] while Scholz and co-workers exploited the thiol groups of PEG-b-(PGA-co-PCys) to decorate gold surfaces[152] (for both also see Block Copolymer Section).

The group of Cheng copolymerized the earlier mentioned VBLG NCA together with 4,5-dimethoxy-2-nitrobenzyl-glutamate (DMNBLG) NCA at various ratios to obtain $PDMNBLG_{19\text{-}76}$-co-PVBLG-$8_{114\text{-}175}$ (PDI 1.02-1.06, M_n up to 57.2 kDa).[190] The randomly distributed DMNBLG groups rendered the polymers responsive to a photonic stimulus, upon which a masked negative charge would be exposed, destabilizing the α-helical conformation and reducing the overall cationic net charge of the copolymer. When treated with UV radiation, polyplexes of PDMNBLG-co-PVBLG-8 showed higher transfection efficiency and diminished cytotoxicity as compared to PVBLG-8 alone.

Kramer and Deming randomly distributed methionine units along a PLys chain by copolymerizing both NCAs with a cobalt initiator in THF.[99] The resulting P(Lys$(TFA)_{0.8}$-co-$Met_{0.2})_{32}$ (PDI 1.21, Mn 6.5 kDa) and P(Lys$(TFA)_{0.8}$-co-$Met_{0.2})_{135}$ (PDI 1.21, Mn 27.7 kDa) were deprotected and subjected to further post polymerization reactions utilizing the methionine side chain.

Schlaad and co-workers prepared P(BG-co-$allylgly)_{50}$ with varying amounts of either L-, D-, or DL-allylglycine (PDI around 1.10, M_n up to 9.7 kDa).[168] Copolypeptides were deprotected and reacted with 1-thio-β-D-glucopyranose via the allyl side chain to obtain random glycopolypeptides which were investigated for their secondary structure in dependence of solution pH. In a follow-up study, the same sort of copolypeptides, i.e. P(BG-co-allylgly) with DP between 53-170 and varying amounts of incorporated L-, or DL-allylglycine (PDI around 1.18-1.28, M_n up to 31.9 kDa), was employed as starting material to build organogels.[191] The physical network of the organogels could be preserved by crosslinking the allylglycine moieties using 1,9- nonanedithiol and benzophenone. Upon deprotection of the BG groups, the cross-linked organogels could then be transformed into hydrogels.

The group of Zhang prepared clickable, non-ionic random copolypeptides by copolymerizing γ-propargyl-Glu NCA and *N*-ε-2-[2-(2-methoxyethoxy)ethoxy]acetyl-L-lysine (EG_2-Lys) NCA at varying ratios in DMF with benzylamine initiator.[192] Because of the EG_2-Lys units the obtained P($PG_{14\text{-}70}$-co-$(EG_2\text{-}Lys)_{18\text{-}72}$) polymers (PDI 1.23-1.39, M_n up to 35.4 kDa) were readily water-soluble up to 50 mol% PG content and mainly adopted α-helical conformation. Copolypeptides were successfully employed in click reactions, i.a. with the cell adhesion inducing pentapeptide GRGDS. Complementary to that, Zhang and co-workers also reported on clickable copolypeptoids. They exploited zwitterionic ring-opening copolymerization of *N*-propargyl glycine and *N*-butyl glycine in THF, induced by a carbene initiator to obtain cyclic P((N-pg-gly$)_{39\text{-}159}$-co-(N-bu-gly$)_{30\text{-}173}$) (PDI 1.11-1.30, M_n 56.0 kDa).[45] In a successive step, the propargyl groups of the cyclic copolypeptoid were reacted with azide-terminated PEG550 or PEG2k to afford PEG-decorated bottlebrush polymers with random copolypeptoid backbone. The group performed a similar study, switching the initiator from carbene to 1,8-diazabicycloundec-7-ene (DBU). Thereby, cyclic P((N-pg-gly$)_{177}$-co-(N-bu-gly$)_{41}$) (PDI 1.45, M_n 75 kDa) was generated from polymerization in THF.[42] As in the former case, subsequent click reaction with azide-terminated PEG550 yielded a PEG-decorated bottlebrush polymer with random polypeptoid backbone. In another attempt towards bottlebrush copolymers, random copolypeptoids were explored as macromonomers for ring-opening metathesis polymerization (ROMP).[193] For this, *N*-et-gly NCA and *N*-but-gly NCA were first copolymerized at varying ratios in toluene with 5-norbornene-2-methylamine as initiator. The resulting Nor-P((N-et-gly$)_{27\text{-}40}$-co-(N-but-gly$)_{9\text{-}21}$) macromonomers (PDI around 1.05, M_n up to 10.4 kDa) were subsequently converted by ROMP using the Grubb's 2nd generation catalyst, yielding amphiphilic thermoresponsive bottlebrush polymers with PNor backbone at a target DP from 25-200 (PDI 1.39-3.04, M_n up to 526 kDa). Similar to the linear macromonomers, the bottlebrush copolypeptoids showed a cloud point transition in aqueous solution, albeit being strongly dependent on the thermal history of the solution. In another study of the Zhang group, the class of P((*N*-et-gly)-co-(*N*-but-gly)) copolypeptoids was also investigated for its performance in kinetic gas hydrate inhibition: Reyes *et al*. therefore synthesized P((*N*-et-gly)$_{16}$-co-(*N*-but-gly)$_6$) and P((*N*-et-gly)$_{17}$-co-(*N*-*i*but-gly)$_5$) (no PDIs provided, M_n 2.1 kDa for both polymers) with benzylamine initiator in THF.[194]

2.1.3.3 *Grafted Copolymers*

In the following section, recent examples are given, where either polypept(o)ides form the backbone for grafting reactions - or, conversely, where polypept(o)ides are utilized as grafting material. The term grafting is considered as describing a process during which multiple (co)polymer chains are attached onto a surface or a (co)polymer substrate, either by means of polymerization (grafting-from) or by post polymerization reactions (grafting-onto). Comparing both methods from a very general perspective, polymerization from a substrate (grafting-from) can afford dense, homogeneous functionalization but may suffer from poor control over molecular weight and dispersity of the grafted polymers, owing to the increased complexity of the initiator (multidenticity) or its immobilization in the case of surface-grafting. The grafting-onto approach allows better synthetic control and detailed characterization of the preformed polymer chains but requires additional reaction steps to attach it to the substrate. Steric hindrance and impaired diffusion of the polymers may result in heterogeneous, low density grafting.

Decorating surfaces with polypeptide/polypeptoid films by using grafting methodologies holds great promises, as it gives access to the design of biocompatible, multifunctional interfaces. NCA polymerization from amino-functionalized SiO_2 surfaces has been reported as early as 1974.[195] Following efforts on polypeptide surface grafting explored different reaction conditions and grafting techniques on various types of surfaces.[74] Since then the field has expanded rapidly and is subject to more specific recent reviews,[72–74] which is why it is only covered thoroughly in this section.

Recently, Klok and co-workers reported on non-fouling peptide films created by the grafting-from approach.[196] Oligo(ethyleneglycol) modified L-lysine NCA was polymerized from aminosilanized (APTMS or APDES) silicon, quartz and glass substrates at 50 °C (48-72 h) in a THF/DMF (5:1) solvent mixture. Depending on monomer and reaction time, APTMS afforded brushes of 14-38 Å thickness, while APDES produced layers of 2.9-5 Å, as determined by ellipsometry. According to circular dichroism measurements, the brushes adopted stable α-helical conformations from pH 4-9. Confirming the low-fouling properties of PLys(OEG), a significant reduction of bovine serum albumin (BSA) and fibrinogen adsorption was observed for coated surfaces. Moreover, degree of adsorption reduction correlated with the length of the oligo(ethyleneglycol) side chains. In another study, replacing PLys(OEG) with PGA(OEG), the group investigated vapor deposition surface-initiated ring-opening polymerization (SI-ROP) of γ-di- or tri(ethylene glycol)-modified L-or D-glutamic acid NCAs on APS-functionalized silicon and quartz surfaces.[197] PGA(EG_2) brushes with up to 80 nm thickness could be successfully prepared, while PGA(EG_3) afforded less than 30 nm, possibly due to the longer OEG side chain associated with larger steric hindrance. The brushes preserved α-helix structure between 10 and 70 °C. QCM-D experiments revealed significant dehydration of PGA(EG_2) brushes upon heating from 10 to 40 °C without significant variations in film thickness according to AFM and ellipsometry, inidicating that mainly hydration and dehydration of the OEG side chains contributed to the thermoresponsiveness of the brushes.

In several studies, the group of Luxenhofer investigated polypeptoid brushes from surface-initiated NNCA polymerization. Schneider *et al*. conducted initiation from self-assembled APTMS monolayers on SiO_2 surfaces in benzonitrile to create homo and amphiphilic diblock copolypeptoid brushes based on PSar and P(*N*-bu-gly).[198] As determined by ellipsometry, PSar brushes of up to 40 nm thickness (indicating DP of 111 in case of fully stretched backbone), could be obtained by direct as well as stepwise polymerization. For P(*N*-bu-gly) brushes, an average height of 12 nm was attained. Amphiphilic brushes were synthesized with P(*N*-bu-gly)-b-PSar as well as with PSar-b-P(*N*-bu-gly) sequence, producing layers of 21 nm and 42 nm thickness, respectively. In another study, the group could also demonstrate the polymerization of pentablock copolypept(o)ides from solid support (also see Block Copolymer Section).[180] Following efforts led to the transfer of the synthetic methodology to gold surfaces and combination with microcontact printing and UV-lithography to obtain patterned PSar brushes.[199] AFM scans revealed polymer heights of 40 nm for SiO_2 and 28 nm for gold substrates.

In addition to flat surfaces, grafting reactions are also conducted on curved substrates. For instance, Lu *et al*. polymerized P(*N*-allyl gly)-based nanorods in THF from isolated APTES coated silica mesospheres, which were prepared within a octadecyltrichlorosilane (OTS) film using particle lithography.[200] According to AFM, average length of the polymer chains was 6 nm which corresponds to a DP of 14, assuming a fully stretched polymer backbone.

Kar *et al*. grafted alkyne-terminated polyarginine (PArg) onto azide decorated mesoporous silica nanoparticles via copper click reaction to afford pDNA delivery vehicles.[60] In advance, $PArg_9$ (PDI 1.11) and $PArg_{18}$ (PDI 1.06) were derived from ROP in DMF with propargylamine as initiator.

Working with gold nanoparticles, the groups of Scholz and Dong used a grafting-onto approach to coat the latter with PEG-b-PGA-b-PCys, PEG-b-(PGA-co-PCys)[152] or PCys-g-PEG,[105] respectively, via the thiol groups (also see Homopolymer and Block Copolymer Sections).

Fokina *et al*. functionalized heterotelechelic DBCO-$PSar_{198}$ (PDI 1.2, M_n 26.1 kDa) with different lipoic acid-based anchor groups through strain-promoted azide-alkyne cycloaddition and used it for the grafting onto quantum dots via ligand exchange. The procedure yielded stable, water-soluble quantum dots.[201]

In a grafting-from approach, Gkikas *et al*. performed NCA polymerization from single and multiwall carbon nanotubes as yet another type of substrate.[202] First, primary amines were attached onto the carbon nanotube surface via Diels-Alder cycloaddition. The following surface initiated ROP of proline NCA in THF under HVT conditions yielded SWNT-g-PPro and MWNT-g-PPro, which readily dissolved in organic solvents and were well dispersed due to the repulsive force of the PPro helices.

Of course, grafting of polypeptides is not only limited to surfaces, but can also be conducted from polymeric substrates. In this way, star and bottle brush architectures are accessible. For example, Cameron and co-workers reported on the generation of star-shaped block copolymers with a PEG core grafted with a PAla shell.[65] In this study, four-arm amine-terminated PEG was applied as macroinitiator for the ROP of varying amounts of Ala NCA in 1,4 dioxane, affording $(PAla_{4\text{-}100})_4$-g-StarPEG (no SEC data provided). The star copolymers were utilized to self-assemble to physical hydrogels which were, due to the PAla shell, selectively degradable by elastase.

Pan *et al.* obtained PAMAM-g-$PLys_{2.1\text{-}6}$ (M_n up to 62.5 kDa) from polymerization of Lys(Z) NCA with a PAMAM G4 macroinitiator in DMF followed by deprotection and tested it for gene delivery.[67] Barz and co-workers utilized a disulfide containing three amine initiator for the synthesis of three-arm polypept(o)ide star polymers consisting of a hydrophobic PLys(Boc) core and a hydrophilic PSar shell, yielding S-S($PLys(Boc)_{25}$-b-$PSar_{100})_3$ (PDI 1.12-1.13, M_n up to 54.2 kDa). The grafting-from (core-first) approach enabled a direct control of size and resulted in well-defined core cross-linked star-shaped nanoparticles with an additional intrinsic stimuli-responsiveness at elevated glutathione levels. The particles were well tolerated by HeLa, HEK 293T and DC 2.4 cells.[71]

Hoertz *et al.* obtained bottle brush polymers with PSar or PLys(TFA)-b-PSar side chains from NCA polymerization with a poly[*N*-(6-aminohexyl)methacrylamide] (PDI 1.64) or a PLys macroinitiator.[203] PSar-containing brushes (PDI 1.72-1.74) displayed a hydrodynamic radius of 40.4 and 63.5 nm, respectively. The PLys(TFA)-b-PSar-containing brush polymers were deprotected and subsequently deployed for siRNA complexation and delivery to AML-12 hepatocytes.

Combining ROMP and NCA polymerization, Zhang *et al.* prepared amphiphilic polypeptide-containing hybrid dual bottle brush block copolymers. Synthetic sequence started with the sequential polymerization of a norbonyl-PEG macromonomer and copolymerization of amine-containing *N*-(2-((trimethylsilyl)amino)ethyl)-5-norbornene-endo-2,3-dicarboximide and another norbornene monomer. The resulting ROMP block copolymer was applied as macroinitiator for the grafting-from polymerization of Glu(OBn) NCA or Lys(Z) NCA in DMF, producing amphiphilic brush block copolymers of (P-g-PEG)-b-(P-g-$PBG_{20\text{-}40}$) (PDI 1.04-1.09, M_n up to 38.7 kDa) and (P-g-PEG)-b-(P-g-$PLys(Z)_{20}$) (PDI 1.09, M_n 13.3 kDa) composition. Polylactide nanoparticles coated with the brush block copolymers exhibited significantly improved stability in PBS solution compared to those coated with amphiphilic linear block copolymers such as PEG-b-polylactide and PEG-b-polypeptide.

Bottlebrush polymers are also accessible by the grafting-to approach. For instance, Jing and co-workers prepared PGA-g-PNIPAM hybrid graft copolymers by coupling NHS-activated PGA with amino-semitelechelic PNIPAM (no SEC data provided, grafting efficiency 70-84%).[204] Phase-transition and aggregation behavior of the graft copolymers were investigated by turbidity measurements and dynamic laser scattering, showing dependencies of temperature and pH.

The group of Zhang exploited click chemistry to graft azide-terminated PEG550 or PEG2k onto cyclic P((*N*-pg-gly) and random P((*N*-pg-gly)-co-(*N*-bu-gly)) polypeptoids (also see Random Copolymer Section).[42, 45] Grafting efficiency turned out to be low (<19%) in case of the P((N-pg-gly) homopolypeptoids, possibly owing to aggregate formation in the organic solvent of the click reaction, restricting the access of the PEG chains to the propargyl groups. It was significantly increased (up to 93%) in case of the P((N-pg-gly)-co-(N-bu-gly)) copolymers, due to the reduced aggregation tendency. According to AFM, the resulting bottle brush polymers showed diameters between 250 and 500 nm.

In a follow-up study of the linear PEG-b-PVBLG-8 diblock copolymers mentioned before (see Block Copolymer Section), Cheng and co-workers expanded the available copolymer architectures for this system, i.a. by grafting from and grafting onto techniques.[205] PEG_{113}-g-$(PPABLG_{91})_8$ star copolymers (PDI 1.31, M_n 23.0 kDa) were obtained by NCA polymerization from an 8-arm amine-terminated PEG macroinitiator in a mixture of DMF and nitrobenzene, followed by ozonolysis and reductive amination of the glutamate side chains. In addition, grafting $mPEG_{12}$-NH_2 onto a $PVBLG_{120}$ backbone in DMF via the same post polymerization reactions yielded $(PVBLG\text{-g-}PEG_{12})_{15}$-co-$PPABLG_{105}$ with bottle brush architecture (PDI 1.21, M_n 2.94 kDa).

2.2 POLYPEPTIDE-BASED POLYPLEXES FOR DELIVERY OF NUCLEIC ACIDS

In the last decades, polypeptide based polyelectrolytes have attained great interest for application as non-viral vectors for delivery of therapeutic nucleic acids like pDNA, mRNA, siRNA and other short oligonucleotides.[206] While each of these nucleic acid classes has its own delivery challenges,[207] a common characteristic is the anionic net charge providing a template for complexation through a cationic counterpart, driven by electrostatic interaction and entropy gain (release of counterions).[208] As the basic canonical amino acids lysine and arginine are a natural constituent in domains of DNA binding proteins such as histones[209] or protamine,[210] it is a rational approach to employ their polymeric form for nucleic acid complexation and delivery. Apart from that, polypeptides from cationic derivatives of other amino acids also depict possible candidates for non-viral vectors.[5, 90]

pDNA was the first type of nucleic acid researched with a therapeutic intend and PLys was one of the first non-viral vectors investigated,[211] with DNA binding and transfection studies conducted as early as in the 1960s[212] and 1980s,[213] respectively. Years later, Wagner and co-workers evaluated PLys-transferrin conjugates as non-viral vectors.[214–216] Besides PLys for pDNA complexation, these early systems already contained key elements for efficient transfection such as targeting ligands (transferrin) and endosomolytic moieties (virus-derived fusogenic peptides).[217]

With PEG-b-PLys diblock copolymers Kataoka and co-workers introduced a neutral, shielding component to PLys-based transfection systems in the 1990s.[218] They observed, that these hybrid polymers formed core-shell segmented polyplexes of around 50 nm with oligonucleotides[219] as well as pDNA[220] and were able to protect their cargo from nuclease attack.[221] On functional level, PEG-b-PLys polyplexes were successfully employed to transfect HepG2 and HEK 293 cells in the presence of serum *in vitro*.[222, 223] After intravenous injection, blood circulation correlated positively with PLys chain length, however, sustained reporter gene expression was limited to the liver.[222] In addition to polyplex formation, PEG-b-PLys was also utilized as coating material for retroviral vectors, improving transduction efficiency 3- to 7-fold without increasing cytotoxicity.[224]

Next to PEG, other hydrophilic polymers have been explored as shielding material for PLys-based polyplexes. Heller *et al.* introduced the PSar-b-PLys system as fully peptidic alternative to PEG-b-PLys. Derived polyplexes achieved 30-50% of jetPEI efficiency in HEK 293T cell luciferase readout while causing no detectable cytotoxicity at relevant concentrations. Besides, a clear structure-property relationship between molar block ratio and transfection efficiency as well as cytotoxicity was revealed.[156]

Tappertzhofen *et al.* combined PLys with PHPMA as shell material. PHPMA-b-PLys polyplexes mediated transfection of HEK 293T cells and were well tolerated without detectable cytotoxicity, as determined by MTT assay and Annexin V/7-AAD staining in FACS.[141] In a follow-up study, a disulfide linker was installed between PLys and PHPMA segment to create stimuli-responsive polyplexes which can eject their shell in reductive milieu, i.e. intracellular space, upon disulfide cleavage. Performance of these polyplexes, as assessed by eGFP expression in FACS, reached jetPEI level.[142]

Hadjichristidis and co-workers developed amphiphilic PLys-b-PBG-b-PLys triblock copolypeptides to complex or encapsulate pDNA into vesicular structures. However, no transfection experiments were conducted.[134]

PLys, albeit being a good complexation agent, lacks any pH buffering or other endosomolytic acting groups, thus transfection efficiency is intrinsically limited.[211] Consequently, apart from adding shielding segments, various other efforts were undertaken in the last two decades to optimize *in vitro* and *in vivo* performance of PLys-based systems. For instance, Midoux and co-workers reported mannosylation of PLys to target macrophages,[225] or coupled the lysine side chains with histidine as pH buffering component to augment transfection efficiency via proton sponge effect.[226, 227] PLys with 38% histidinylation degree showed more than 1000-fold increase in luciferase gene expression compared to non-modified control.

In a follow-up study on the above mentioned PLys-b-PSar system,[156] Barz and co-workers compared two different architectures of histidinylated block copolypept(o)ides on simulation and experimental level.[159] It turned out that a defined triblock microstructure with PLys-b-PLys(His)-b-PSar block sequence is more efficient in compacting pDNA than a diblock architecture with histidine randomly distributed along the PLys segment, possibly owing to differences in charge density. Triblock systems thus formed smaller polyplexes, enhanced stability against degradation by DNase I and provided better transfection performance.

As an alternative approach to histidinylation, Meyer *et al.* coupled PLys with the fusogenic peptide melittin, enhancing siRNA as well as pDNA delivery.[211]

Several groups devoted their research to alternative architectures of PLys (dendritic/branched instead of linear) as means to enhance transfection efficiency.[67, 228–231] Klok and co-workers explored hyperbranched PLys as non-viral vector. This architecture was more effective than linear or dendritic PLys of comparable molecular weight[231] and also afforded similar or higher gene expression than PEI and FuGENE HD.[229] On the other hand, dendritic and branched PLys exhibited higher cytotoxicity than the linear analog, possibly due to impaired enzymatic degradation.[230]

Okuda *et al.* tried to augment transfection efficiency of dendritic PLys by substituting the terminal amino acids with arginine and histidine.[228] Modification with arginine provided 3-12-fold increased gene expression in several cell lines. In contrast, histidinylation, due to the altered protonation status and charge density of modified dendrimers, had a negative effect which could be reversed when polyplexes were formed under acidic conditions.

Attempting to augment stability of PEG-b-PLys polyplexes through covalent cross-linking, Kataoka and co-workers incorporated thiols into the polymer backbone via modification of the lysine side chains with *N*-succinimidyl 3-(2- pyridyldithio)propionate (SPDP) or 2-iminothiolane and subsequent reduction.[232, 233] After polyplex formation, reoxidation of the thiols leads to disulfide formation granting covalent stabilization, while cleavage of the disulfide bonds by glutathione upon cellular uptake allows dissociation of the polyplexes and release of cargo. Luciferase readout in HEK 293T cells revealed a 50-fold higher *in vitro* transfection efficiency of 28% thiolated/cross-linked polyplexes compared to non-cross-linked ones.[233] *In vivo*, systemically injected 15% cross-linked polyplexes decorated with RGD peptides as targeting motive induced significant growth inhibition of pancreatic adenocarcinoma, mediated through the therapeutic effect of sFlt-1 coding pDNA. Additionally, blood circulation was prolonged through cross-linking indicating enhanced stability.[234, 235]

Heller *et al.* adopted and modified the cross-linking strategy of Kataoka and co-workers. In this case, PLys-b-PLys(PDP)-b-PSar triblock copolymers derived from modification of the middle lysine block with SPDP were applied for polyplex formation with pDNA. After the complexation step, thiol-bearing cross-linkers were added to the polyplexes reacting with the PDP groups within the polymers. Apart from thiols, the bifunctional cross-linkers also contained endosomolytic groups. Cross-linked polyplexes exhibited superior stability in serum and increased transfection efficiency in HEK 293T cells. Furthermore, the modular approach allowed screening of different cross-linkers and facile generation of a polyplex library. A lead formulation was successfully deployed for transfection of dendritic cells with a model pDNA vaccine.

In various recent publications, PEG-b-PLys block copolymers were also evaluated for *in vitro* and *in vivo* siRNA delivery.[236] Due to the much smaller size of siRNA compared to pDNA, which implicates weaker electrostatic interaction, additional stabilization of polyplexes to prolong blood circulation might be an even more important issue.[207] This was achieved by disulfide cross-linking alone (same synthetic strategy as for pDNA polyplexes, >2-fold increase of circulation half-life compared to naked siRNA),[237, 238] disulfide cross-linking in combination with cholesterol coupled siRNA for hydrophobic stabilization (significantly longer blood retention time than for cross-linking only)[239] or grafting onto gold particles[240]. In all cases, active tumor targeting was realized by modification of polyplexes with cRGD peptides.

Next to the naturally cationic polypeptides PLys and PArg,[60] derivatives of polyaspartic acid (PAsp(X)), which are generated post polymerization by side-chain aminolysis reaction with oligoamines (e.g. oligo(ethyleneimines)), are another important polypeptidic material for nucleic acid delivery. As an advantage to PLys, PAsp(X) are intrinsically endosomolytic because of the pH buffering secondary amines introduced by the aminolysis reaction. $PAsp(DET)_{52}$ was recently applied for *ex vivo* transfection of mesenchymal stem cell with brain-derived neurotrophic factor-coding pDNA, exhibiting one order of magnitude better performance than the commercial transfection reagent FuGENE HD. Transfected cells were then transplanted into mice for treatment of pre-induced spinal cord injury.[110]

Like PLys, PAsp(X) usually is also combined with PEG as hydrophilic block. PEG-b-PAsp(DPT) was first applied for siRNA delivery *in vitro*, achieving significant luciferase gene knockdown in HEK 293T and HuH-7 cells.[241] In the following, the concept was expanded to pDNA delivery via PEG-b-PAsp(DET).[242] Over a wide range of N/P ratios, combined components formed polyplexes of around 80 nm diameter. Transfection rates in murine primary osteoblasts were similar to those of linear PEI, while polyplexes showed no notable cytotoxicity, although being applied at very high N/P ratios. As inferred from comparison of different oligoamine side chains, incorporation of secondary amines turned out to be the key element for efficient transfection. *In vivo*, PEG-b-PAsp(DET) polyplexes were evaluated on the basis of the same pancreatic cancer model as the PEG-b-PLys system[234] mentioned above. For targeting, PEG-b-PAsp(DET) was modified with cRGD peptide at the distal end of the PEG segment, while additional hydrophobic stabilization of derived polyplexes was realized by attaching cholesterol to the ω-terminus of the PAsp(DET) block.[243] Systemically injected polyplexes delivering sFlt-1 coding pDNA promoted marked tumor growth inhibition, especially when equipped with targeting ligands, while a positive correlation was found between blood circulation time and PEG chain length. A follow-up study on the same system focused on the influence of free excess polymer on *in vitro* as well as *in vivo* performance and investigated how to avoid abundance of unbound polymer.[244]

Aside from siRNA and pDNA delivery, in a series of recent publications PAsp(X) was also explored for mRNA transfection. As mRNA in general is more prone to nuclease-mediated degradation than pDNA, protection against nuclease attack is of great importance. *In vitro* screening of different PAsp(X) derivatives revealed, that a higher number of aminoethylene repeats in the side chain had a positive impact on mRNA integrity in serum[245] and translation efficiency[246]. This observation possibly is due to differences in pK_a values and protonation status of the oligoamines, with a higher protonation degree offering increased complex stability[245] and preservative binding of translation factors[246].

Subsequently, PEG-b-PAsp(DET) and PEG-b-PAsp(TET) where utilized for mRNA therapy in a mouse model of osteoarthritis, successfully suppressing disease progression.[247] PEG-PAsp(TEP)-Chol carrying sFlt-1 coding mRNA was evaluated for treatment of pancreatic cancer in mice, showing similar positive results like the pDNA-based therapy (see above).[245] Furthermore, mRNA encoding the amyloid-beta degrading protein neprilysin was formulated with PEG-b-Asp(DET) and monitored for *in vivo* activity in a murine Alzheimers's disease model after intracerebroventricular infusion, demonstrating effective reduction of the amyloid-beta load in the mouse brain.[248]

Finally, in a layer-by-layer approach for delivery of siRNA or pDNA, the two polypeptides PLys and PAsp(X) have also been co-formulated. In the first example, PAsp(X) was combined with PEG-b-PLys.[249] Initially, siRNA was mixed with azide-terminated, thiolated PEG-b-PLys to create cross-linked complexes. In a subsequent click reaction DBCO-functionalized PAsp(DET) with amines masked by an acid-labile moiety, was coated onto the complex surface yielding dual stimuli-responsive polyplexes sensitive to acidic tumor environment plus the reductive intracellular milieu. The PAsp(x) coating led to significantly increased gene silencing capacity *in vitro*. In the second example, the inverse approach was conducted for generation of dual stimuli-responsive pDNA polyplexes. Here, pDNA was first complexes by thiolated PLys. Negatively charged PEG-b-PAsp(DET-Aco), where similar as in the first example amines are masked by an acid-labile moiety, was then coated onto the cross-linked binary polyplexes by means of electrostatic interaction, resulting in enhanced gene transfection efficiency in cultured cells (Huh-7 and HUVEC) without associated cytotoxicity.[250]

An entirely different class of polypeptidic non-viral vectors for pDNA and siRNA delivery, based on derivatives of PVBLG, was developed by Cheng and co-workers (also see Subsection 2.1.2).[79, 89] Effficacy of these systems, like for many CPPs, relies on amphiphilicity and the stable α-helical conformation of the polypeptide backbone, which promotes interaction with cellular membranes and their destabilization, thereby fostering cellular uptake and endosomal escape.[90] Initially, a library of various amine side chains introduced to the PVBLG backbone via ozonolysis and reductive amination was screened through luciferase assay for transfection efficiency in COS-7 cells, with PVBLG-8 (PPABLG) showing the best results and surpassing PEI by a factor of 12.[89] Besides the library screening approach, the effects of different side chain functionalities on *in vitro* performance of cationic, helical PGA derivatives were explored more systematically. The collective effects of guanidine groups and hydrophobic content within the side chains, plus α-helical structure of the polypeptide backbone were revealed to be decisive for high membrane activity and transfection efficiency.[251]

In several follow-up publications, the PVBLG-8 system was further developed (also see Subsection 2.1.3). A PEG block was attached to the PVBLG-8 segment to improve biocompatibility. Polyplexes derived from the diblock copolymers were evaluated in IMR-90 cells and human embryonic stem cells, exhibiting reduced cytotoxicity while still preserving high transfection efficiency, which outperformed Lipofectamine 2000.[151] In another study, different copolymer architectures (diblock, triblock, bottle brush and star-shaped) for combination of PEG and PVBLG-8 blocks were compared *in vitro*.[205] Linear Diblock and triblock copolymers were less cytotoxic while delivering pDNA equally efficient like the non-PEGylated control. Highest transfection efficiency was found for the star-shaped architecture (3-5-fold increase compared to PVBLG-8 alone, 3-134-fold compared to Lipofectamine 2000). In contrast, the bottle brush architecture was least efficient.

In addition to PEGylation, PVBLG-8 was also functionalized with 4,5-dimethoxy-2-nitrobenzyl-glutamate (DMNBLG) to render derived polyplexes light-responsive.[190] Exposure to light caused unmasking of negatively charged groups along the polypeptide backbone, decreasing cationic charge density and α-helical conformation. This resulted in reduced cytotoxicity, facilitated pDNA release and elevated transfection levels in HeLa cells. For siRNA delivery with its demand for additional stabilization, disulfide cross-linked polyplexes were generated from partially thiolated PVBLG-8 by oxidizing randomly distributed thiol groups after complex formation. Cross-linked polyplexes had a 50% smaller size than non-cross-linked ones and mediated 60% gene knockdown in HeLa cells compared to 40% knockdown for non-cross-linked control.[185] Finally, PVBLG-8 was employed for intravenous administration and *in vivo* delivery of TNF-α siRNA to macrophages, achieving effective systemic TNF-α knockdown and establishing an anti-inflammatory effect which rescued mice from LPS/D-GalN-induced hepatic sepsis.[252] In this case, as alternative for cross-linking, PVBLG-8 and siRNA were co-formulated with a polyanionic PGA derivative to enhance polyplex stability.

2.3 POLYPEPTIDE-BASED NANOPARTICLES FOR DIAGNOSTIC/THERANOSTIC APPLICATIONS

It is now widely accepted that the accumulation level and intratumoral distributions of nanoparticles vary notably for different types of cancers but also among individual patients,[253] i.a. depending on the presence or absence of the EPR effect.[254] Approaches to address this heterogenicity involve the application of diagnostic nanoparticles for screening of patients before and during treatment with therapeutic nanoparticles, or the combination of diagnostic and therapeutic functions in one nanoparticle. Both strategies are part of a wider concept described by the term theranostics, which aims towards individualized therapies.[255, 256] In this regard, besides many other materials, polypeptides have been explored for the combination with diagnostic (imaging) agents. The group of Kataoka developed several nanoparticles for *in vivo* MRI application with a gadolinium[257–261] or iron oxide[262–265] core, either coated with a PEG-b-PGA,[257] PEG-b-PAsp[259, 260, 262–264] or PEG-b-PAsp(DET)[258] shell. In some cases, platinum complexes[257, 258] or calcium phosphate (CaP)[259, 260] were additionally incorporated into the core to create theranostic and organic-inorganic hybrid nanoparticles, respectively. Complementary to the coating method, cRGD-modified PICsomes obtained from PEG-b-PAsp and P([5-aminopentyl]-α,β-aspartamide) were loaded with iron oxide and utilized for targeted MRI in an orthotopic glioblastoma model.[265] Moreover, in one study the imaging agents (indium for SPECT and gadolinium for MRI) were not included into the core, but simultaneously attached to the shell of DOTA-PEG-b-PBG based micelles.[261]

The above mentioned system with PEG-b-PAsp shell and diethylenetriaminepentaacetic acid gadolinium (III) (Gd-DTPA)/CaP core were evaluated for noninvasive diagnosis of solid tumors (T1-weighted imaging).[259] The particles with a z-average hydrodynamic diameter of about 80 nm were prepared in a two-step process, involving self-assembly of the components followed by hydrothermal treatment. After intravenous administration, the hybrid nanoparticles achieved substantial contrast enhancement in an EPR-active, C-26 subcutaneous murine tumor model with encapsulated Gd-DTPA exhibiting 6-fold increase in relaxivity compared to the free form.

Theranostic nanoparticles based on PEG-b-PGA were simultaneously loaded with DACHPt and Gd-DTPA through reversible complex formation between both agents.[257] Here, the longitudinal relaxivity of incorporated Gd-DTPA increased 24 times compared to the free form. The micelles afforded strong tumor contrast enhancement in a murine orthotopic pancreatic cancer model, as successfully visualized in real-time manner by MRI. Moreover, they permitted non-invasive monitoring of tumor volume during treatment.

Recently, several other groups have proposed theranostic concepts based on (partially) polypeptidic nanoparticles, aiming to combine NIR imaging with drug delivery[52, 105] and photodynamic/photothermal[53, 105] therapy. However, these concepts are still in early phase and have not evolved from *in vitro* stage yet: Fu *et al.* used galactose-targeted POEGMA-b-P(Lys-co-Asp) as a platform for linkage of a NIR dye (via terminal amine) and doxorubicine (via hydrazone spacer to Asp units). Derived micelles were evaluated for drug release in HepG2 and NIH3T3 cells.[52] Dong and co-workers investigated gold nanoparticles decorated with PCys-g-PEG for NIR radiation induced release of doxorubicin and photothermal therapy in HeLa cells.[105] Liu *et al.* entrapped the photosensitizer BODIPY-Br_2 in POEGMA-b-PAsp(DIPEA) based micelles. *In vitro* tests on HepG2 cells revealed a cell suppression rate of >40% after exposure to NIR light. At the same time, the internalization of the nanoparticles by cells could be traced by NIRF imaging.[53]

2.4 POLYPEPTIDE-BASED NANOPARTICLES FOR VACCINE DELIVERY

Synthetic subunit antigen vaccines provide many advantages over traditional vaccines derived from live attenuated, killed, or inactivated pathogens.[266] However, synthetic vaccines often lack the immunogenicity to evoke a strong immune response or may even induce immune tolerance. The co-administration of adjuvants allows to overcome this issue by amplifying and directing immune responses.[267] Facilitating the simultaneous delivery of subunit antigens and adjuvants into antigen-presenting cells represents the main opportunity of nanoparticle-mediated vaccination.

Although recent years have seen considerable efforts in developing nanoparticulate vaccine formulations,[268, 269] the literature on polypeptide-based nanoparticle vaccines is still rather limited.

Jiskoot and co-workers loaded polymersomes based on PBG_{50}-K (where K is a hydrophilic peptide with G(KIAALKE)$_3$-NH_2 amino acid sequence) with HA subunit antigens and evaluated their immunogenicity in mice.[270] In this approach the intrinsic adjuvant properties of PBG_{50}-K were exploited, leading to an elevated systemic immune response compared to HA alone.

Weber *et al.* utilized polymersomes from amphiphilic PSar-b-PGlu(OBn) polymers for the simultaneous encapsulation of the subunit antigen SIINFEKL and the adjuvant CpG. The polymersomes displayed a hydrodynamic radius of 39.2 nm and were successfully deployed for co-delivery of antigen and adjuvant into dendritic cells. The authors observed dendritic cell activation involving upregulation of CD80, CD86 and MHC II. Furthermore, activated dendritic cells could induce antigen-specific T cell proliferation.

As an alternative to polymersomes, Schinnerer *et al.* employed bottle brush polymers for the co-delivery of ovalbumin as model antigen and CpG as immune activator. The polymers were constituted by a PLys backbone and PSar side chains with terminal azide groups. The azide groups allowed covalent attachment of antigen and adjuvant to the nanocarrier through click reaction, representing a complementary approach to the encapsulation strategies described above. Click reaction was also utilized to decorate the bottle brush polymers with anti-DEC205 antibodies. The bottle brush polymers displayed low unspecific cellular uptake and stable circulation in mice (78% remaining brushes after 24h).

3 NANOPARTICULATE VACCINE FORMULATIONS

Taken in part from: P. Heller, D. Huesmann, M. Scherer, M. Barz, "From polymers to nanomedicines: New materials for future vaccines", in "Molecular Vaccines - From Prophylaxis to Therapy", *Springer International Publishing*, 2014, pp. 643

3.1 ADVANTAGES OF PARTICLE-BASED VACCINES

The next years will see an increasing use of synthetic subunit antigen vaccines because they provide many advantages over traditional vaccines derived from live attenuated, killed, or inactivated pathogens.[266] However, it is a well-known fact that synthetic peptides often lack the immunogenicity to induce a strong immune response. Therefore, efficient vaccination requires the use of adjuvants.[271] In the field of tumor immunotherapy, adjuvants are especially important to reverse tumor immunosuppression mediated, for example, by regulatory T cells or myeloid-derived suppressor cells. Adjuvants, among other things, promote the maturation of antigen-presenting cells by interaction with receptors of the innate immune system, e.g., dendritic cells. Only mature dendritic cells are able to generate co-stimulatory signals, which together with the presented antigen lead to the desired effector T cell responses. Thus, it is important that antigen and adjuvant act on dendritic cells concomitantly. Most of today's human vaccine formulations use aluminum-based compounds as adjuvants. However, as recent years have seen intense research for more potent and specific alternatives,[272] new means of co-delivery are required.

Another problem of subunit antigen vaccines is their susceptibility to enzymatic degradation. To increase their lifetime and biological activity, protective carrier molecules are needed. Nanoparticles have become of great interest as an instrument to protect antigens and adjuvants against blood serum proteins and to ensure their safe and simultaneous delivery to dendritic cells.

Alongside their capability for protection[273] and co-delivery of antigen and adjuvant, nanoparticles show several other advantages:

- They can deliver an antigen together with combinations of adjuvants overcoming immune suppression by regulatory T cells.[274–276]
- They trap their cargo, thus preventing systemic distribution and toxicity.[277]
- They can be used as a platform to present multiple copies of an antigen on their surface which especially improves B cell activation.[278]
- They can promote the cytosolic accumulation of antigens in dendritic cells. This is important for cross-presentation, the key mechanism for $CD8^+$ T cell activation.
- Modification of nanoparticles with inert substances like poly(ethylene glycol) that mediate stealth properties[279] can minimize protein absorption and lower their immunogenicity. This increases their blood circulation time.[280]
- Surface functionalization of nanoparticles with receptor ligands or antibodies enables specific tissue or cellular targeting.[280] Thereby, antigen and adjuvant are retained at

the site of action so that unspecific distribution is reduced, lower doses are needed, and adverse reactions to vaccination are minimized.

- Nanoparticles provide a sustained release of adjuvants and thus a prolonged exposure to the immune system which is essential for a proper activation of dendritic cells.[281]

3.2 APPROACHES

Big potential for nanoparticulate vaccine formulations most likely lies in cancer immunotherapy. In addition to this, applications for vaccination against various infectious diseases are investigated. These include, for example, nanoparticle-based vaccines against influenza,[282] West Nile encephalitis,[283] and malaria.[284]

The components of a typical nanoparticulate vaccine formulation combine an antigen (T cell and/or B cell epitopes), adjuvant, and targeting moiety on one particle.[277] A wide variety of antigens such as peptides/proteins,[285] lipoproteins,[286] glycopeptides,[287] tumor-associated carbohydrate antigens (TACA),[288] and carbohydrate mimetic peptides[289] are tested in combination with nanoparticulate carriers.

Two basic concepts can be distinguished for targeting dendritic cells with antigens: *ex vivo* pulsing and subsequent administration of matured dendritic cells or direct *in vivo* targeting of immature dendritic cells. Nanoparticles are especially evaluated for *in vivo* strategies.[290]

The group of adjuvants mainly studied in the context of nanoparticulate vaccines are several Toll-like receptor ligands. LPS, the major component of the outer membrane of Gram-negative bacteria, is a pathogen-derived TLR 4 ligand. While being far too toxic for systemic application as an immune potentiator for classic vaccines, LPS shows promising results *in vitro* and in mouse models, when administered within PLGA nanoparticles.[291] 7-acyl lipid A, a component of LPS, is also investigated in mice as an additive for PLGA-based vaccines.[292] In addition to pathogen-derived TLR ligands, synthetic molecules mimicking pathogen-associated molecular patterns (PAMPs) are evaluated. Representatives of this group are CpG oligodeoxynucleotides (CpG ODN), binding to TLR 9, and polyribosinic:polyribocytidic acid (Poly I:C), a TLR 3 ligand.[274] Alongside the general activation of dendritic cells, the application of certain TLR ligands like CpG oligodeoxynucleotides and LPS together with nanoparticulate carriers might be of special interest as they, contrary to alum, elicit a Th1-biased immune response.[293] Demento *et al.* developed PLGA nanoparticles loaded with a recombinant envelope protein antigen from the West Nile virus and surface functionalized with CpG ODN. In several experiments they compared this system with unmodified nanoparticles and an aluminum hydroxide vaccine formulation. In mice, CpG ODN modified nanoparticles produced a Th1 immune response biased antibody profile in contrast to a Th2 profile elicited by aluminum hydroxide. Moreover, immunization of mice with modified nanoparticles induced a higher number of circulating effector T cells and an enhanced antigen-specific IL-2 and IFN-γ production compared to control groups. In a mouse model of West Nile encephalitis, modified nanoparticles showed a superior protection in comparison to aluminum hydroxide.[283]

Studies suggest that some nanoparticles, probably by binding to Toll-like receptors, can act as adjuvants themselves.[294] This has been shown for high molecular weight γ-PGA particles,[295] PLGA nano- and microparticles,[296] poly(anhydride) nanoparticles,[297] liposomes,[298] polystyrene nano- and microparticles,[299] and acid-degradable cationic polyacrylamide nanoparticles.[300] Though, particle size and concentration seem to be critical for activation of dendritic cells as in other experiments, PLGA particles failed to induce dendritic cell maturation.[301]

In one experiment, mucosal immunization of mice against highly pathogenic influenza A H5N1 virus was carried out. The vaccine consisted of recombinant influenza hemagglutinin (rHA) antigen and γ-PGA/chitosan nanoparticles. This system was compared to two other formulations: inactivated virus with γ-PGA/chitosan nanoparticles and cholera toxin with recombinant influenza hemagglutinin antigen. The γ-PGA/ chitosan nanoparticles in combination with rHA antigen led to potent virus-specific humoral and cellular immune responses. Compared to cholera toxin the adjuvant properties of the γ-PGA/chitosan nanoparticles were equally good. Immunized mice were protected against challenge with a lethal dose of highly pathogenic influenza A H5N1 virus.[302]

A different concept for nanoparticle-based vaccines investigated in multiple studies[303, 304] involves the delivery of nucleic acids (mRNA or pDNA) encoding a defined antigen into dendritic cells. In contrast to peptide antigens, mRNA and pDNA have to remain intact and functional all along the endocytic route until they have reached the cytosol or the nucleus, respectively. After being endocytosed, nanoparticles functionalized with buffering groups or cell penetrating peptides can protect nucleic acids against hydrolytic enzymes and foster endosomal escape.[305] Once nucleic acids have reached their destination inside the cell, expression of the encoded peptide antigen can start.

One advantage of pDNA is that it can encode for various peptide antigens. Thus, one nanoparticulate system that is able to transport pDNA can be used for a broad range of vaccinations. Further, pDNA can function as an immunostimulant because it contains CpG sequences recognized by TLR 9.[306]

Sudowe *et al.* investigated the potential of in vivo pDNA vaccination to generate an immune response against β-Gal as model antigen. Plasmids encoding β-Gal under the control of DC-specific, keratinocyte-specific, or unspecific promoters were adsorbed on gold nanoparticles and applied to the skin of mice via gene gun. As a result, Th1-biased immune responses were observed. Moreover, with regard to $CD8^+$ T cell priming, it was shown that the presentation of endogenous antigen produced by transfected skin dendritic cells is equally effective as the cross-presentation of exogenous antigen.[1]

As mentioned above, the surface of nanocarriers can be functionalized with a multitude of different ligands, including proteins, peptides, antibodies, antibody fragments, aptamers, and small molecules.[280] By targeting defined cell surface structures with receptor ligands or antibodies attached to nanoparticles, an increased and/or more specific cellular uptake might be achieved. Considering vaccine formulations in particular, the configuration of the carrier system with ligands for pattern recognition receptors, e.g., Toll-like receptors or C-type lectin receptors, might augment its immunogenicity and contribute to dendritic cell activation.[304] Different targeting concepts have been realized with various particulate carriers and have shown stronger immune responses compared to nontargeted carriers.[307] Mannose is a ligand for a C-type lectin receptor expressed on dendritic cells. Multiple research projects have examined its performance for targeting dendritic cells and macrophages.[308–315] In experiments comparing mannose-decorated PLGA particles with plain PLGA particles, it was shown that mannose only causes a slight increase in cellular uptake. Presumably, because depending on the experimental conditions, nonspecific uptake usually predominates specific uptake.[316] However, in another study it was demonstrated that mannan, a natural polymannose derived from the cell wall of Saccharomyces Cerevisiae, when conjugated to PLGA particles leads to increased antigen-specific $CD4^+$ and $CD8^+$ T cell responses.[317] Other methods for addressing dendritic cells reported in literature are the deployment of Fc receptor ligands or anti-DEC-205 antibodies. Raghuwanshi *et al.* evaluated a two component vaccine formulation, one element being biotinylated

PLGA nanoparticles loaded with ovalbumin as model antigen and the other a bifunctional fusion protein consistent of truncated core-streptavidin and an anti-DEC-205 single-chain antibody. They observed a twofold increase in receptor-mediated uptake of functionalized nanoparticles compared to nontargeted nanoparticles. OVA-specific IgG responses of mice immunized with anti-DEC-205-modified nanoparticles in connection with αCD40 as adjuvant were considerably higher than those of control groups.[318]

To trigger an antibody response, an antigen has to be recognized and processed not only by dendritic cells but also by B cells. Consequently, alongside T cell epitopes, the inclusion of B cell epitopes into a vaccine formulation is a central approach. As mentioned before, nanoparticles can be used to present multiple copies of epitopes on their surface.[278] This enables the induction of T cell-independent type I antibody responses as has been shown for virus-like particles.[319] T cell-independent type II antibody responses can be realized through co-delivery of adjuvants suited for B cell activation.[320]

Especially in tumor immunotherapy, the delivery of B cell epitopes derived from glycopeptides, TACA, or carbohydrate mimetic peptides is of great interest. In several studies Kunz *et al.* investigated the B cell activating potential of different synthetic tumor-associated MUC1 glycopeptides which contain the Thomsen-Friedenreich antigen, its precursor or its sialylated derivatives. They chemically linked the glycopeptides to bovine serum albumin (BSA) or tetanus toxoid as carrier molecules. These vaccine systems were applied to Balb/c mice. In the case of the BSA formulations, complete Freud's adjuvant was co-administered. For all vaccines strong specific antibody responses against the MUC1 antigens were observed.[321–323]

Brinãs *et al.* used gold nanoparticles to co-deliver MUC4 glycopeptides containing the Thomsen-Friedenreich antigen together with a peptide derived from the complement protein C3d as B cell activating adjuvant. Mice immunized with these nanoparticles showed statistically significant immune responses.[320]

4 CHARACTERIZATION METHODS AND THEORETICAL BACKGROUD

4.1 PHYSICOCHEMICAL CHARACTERIZATION OF PEPTOPLEXES

4.1.1 Light Scattering

4.1.1.1 *Principle of Light Scattering*[324]

Light scattering is one of the most common methods used for the characterization of solute polymers and nanoparticles. When regarded as an electromagnetic wave of the length λ, propagating in space (x) and time (t), light can be described by the wave equation:

$$E(x,t) = E_0 \left(sin\left(\frac{2\pi x}{\lambda}\right) + sin\left(\frac{2\pi \frac{c}{\lambda}}{t}\right)\right) \tag{4.1}$$

Scattering of light derives from the fundamental interactions of electromagnetic radiation and matter: When an incoming electromagnetic wave encounters any given particle, the spatial charge distribution within the particle gets remodeled according to the time-modulation of the wave. The molecule thus behaves as an oscillating dipole emitting electromagnetic radiation of the same wavelength as the incoming wave (elastic scattering). The emission proceeds isotropically in all directions perpendicular to the axis of oscillation (Fig. 4.1).

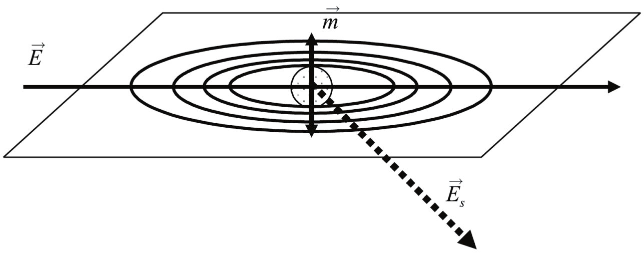

Figure 4.1: Schematic illustration of light scattering. An oscillating dipole is generated by an incident light wave and emits light isotropically.[324]

For any particle larger than $20/\lambda$ interaction with light leads to the simultaneous induction of several oscillating dipoles, resulting in a phase difference and nonisotropic interference between the emitted light waves (Fig. 4.2). Consequently, the scatttering intensity I for such particles depends on the angle or scattering vector q from which the emitted light beam is observed with respect to the incident light beam. Apart from the angle dependency, the interference pattern of intraparticular scattered light (known as particle form factor, P) is influenced by size and shape of the particle, which is exploited for characterization by static light scattering.

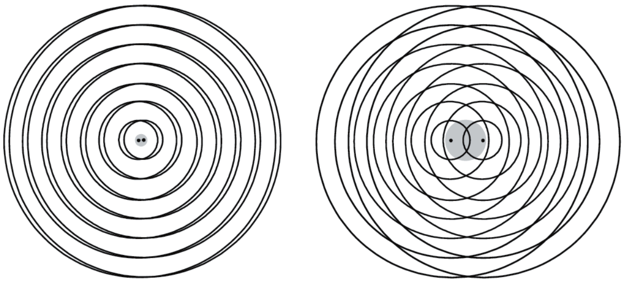

Figure 4.2: Interference pattern of intraparticular scattered light from small (left) and large (right) particles.[324]

4.1.1.2 *Dynamic Light Scattering[324]*

Interference pattern and scattering intensity of particles in solution also undergo temporal variation resulting from changing interparticle positions as a consequence of the Brownian motion of particles (Fig. 4.3).

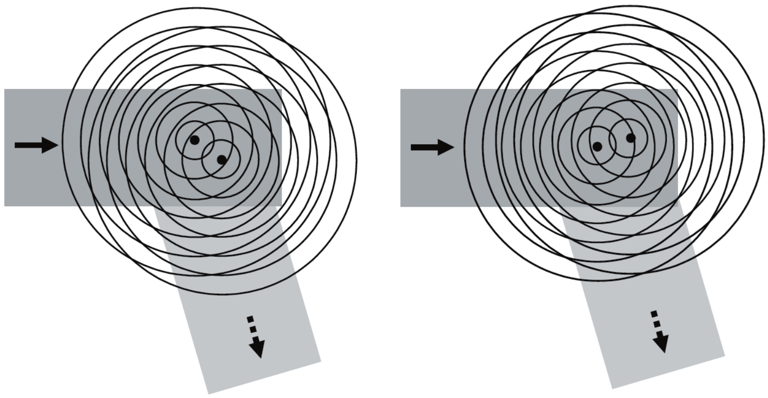

Figure 4.3: Temporal variation of interference pattern and scattering intensity resulting from Brownian motion of solute particles.[324]

The fluctuation of scattering intensity in time is utilized in dynamic light scattering (DLS), providing a quantitative measure for mobility of particles and determination of their selfdiffusion coefficient.

For quantitative analysis, scattering intensity fluctuation measured at a fixed scattering vector q over a distinct time interval t is expressed as autocorrelation function $\langle I(q,t)I(q,t+\tau)\rangle$ and plotted against the correlation time τ (Fig. 4.4).

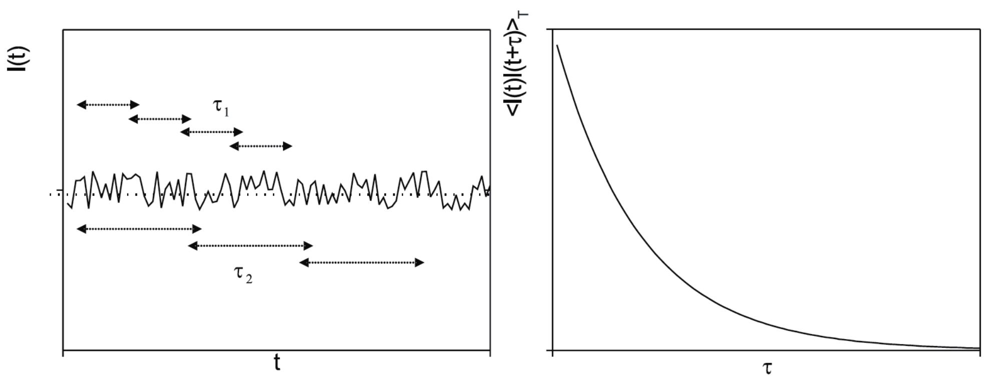

Figure 4.4: Measurement of temporal intensity fluctuations and plotting of the derived autocorrelation function against correlation time τ.[324]

The main quantity determined by this procedure is the dynamic structure factor F_s, alternatively denoted as g_1, containing the information about the mobility of scattering particles. F_s and the intensity autocorrelation function are linked through the Siegert relation:

$$F_s(q,\tau) = \exp(-D_s q^2 \tau) = \langle E_s(q,t) E_s * (q,t+\tau) \rangle = \sqrt{\frac{\langle I(q,t) I(q,t+\tau) \rangle}{\langle I(q,t)^2 \rangle} - 1} \tag{4.2}$$

Calculation of F_s for a certain q gives direct access to the selfdiffusion coefficient D_s of the scattering particle. Applying the Stokes-Einstein-equation,

$$D_s = \frac{kT}{f} = \frac{kT}{6\pi\eta R_H} \tag{4.3}$$

the corresponding hydrodynamic radius R_H can be obtained. In this case, regardless of particle shape R_H always corresponds to the radius of an equally sized, solid sphere.

For polydisperse particles the scattering intensity of each particle species i depends on the species' number density (n_i), particle mass (M_i), and particle form factor $P_i(q)$: $I \sim n_i \cdot M_i^2 \cdot P_i(q)$. Consequently, F_s cannot be described by a single exponential function but by a superposition of several correlation functions weighted by a distribution function $P(D_s)$ for the selfdiffusion coefficient.

$$F_s(q,\tau) = \int_0^\infty P(D_s) \exp(-q^2 D_s \tau) dD_s \tag{4.4}$$

For samples of small polydispersities ($\Delta R_H / \langle R_H \rangle \leq 0.2$), $F_s(q,\tau)$ can be approximated by a cumulant analysis based on a series expansion.

$$\ln F_s(q,\tau) = -\kappa_1 \tau + \frac{1}{2!}\kappa_2 \tau^2 - \frac{1}{3!}\kappa_3 \tau^3 + \ldots \tag{4.5}$$

The average selfdiffusion coefficient is thereby derived from the first cumulant $\kappa_1 = \langle D_s \rangle q^2$, while the second cumulant gives quantitative information about the polydispersity of the selfdiffusion coefficient.

As already mentioned, for particles larger $20/\lambda$, scattering intensity and therefore also D_s is angle or q-dependent. The apparent selfdiffusion coefficient D_{app} of a sample at a certain q is correlated to single species properties by

$$D_{app}(q) = \frac{\sum n_i \cdot M_i^2 \cdot P_i(q) \cdot D_i}{\sum n_i \cdot M_i^2 \cdot P_i(q)} \tag{4.6}$$

To exclude contributions from particle form factor P and nondiffusional processes like rotation to D_s, the actual z-average selfdiffusion coefficient $\langle D_s \rangle_z$ of a particle sample has to be obtained by from $D_{app}(q)$. According to

$$P(q) = 1 - \frac{1}{3} s^2 q^2 + \ldots \tag{4.7}$$

for $q = 0$, $P_i(q)$ gets 1 and does not contribute to D_s as depicted in eq. 4.6. Therefore, by plotting D_{app} against q and extrapolating the fit, which for small particles (R_H = 10 - 100 nm) is given as

$$D_{app}(q) = \langle D_s \rangle_z \left(1 + K \left\langle R_g^2 \right\rangle_z q^2\right) \tag{4.8}$$

against zero, $\langle D_s \rangle_z$ is obtained as y-axis intercept. Finally, the z-average hydrodynamic radius $\left\langle R_H^{-1} \right\rangle_z$ of a particle sample can then be calculated from the Stokes-Einstein-equation (eq. 4.3).

4.1.1.3 *Light Scattering in Plasma*

Light scattering measurement performed in blood plasma as solvent is a powerful methodology to check if a particle sample induces aggregation of proteins.[325, 326] If this is the case, aggregated proteins are detected as an additional species that can be discriminated from native proteins and the particle fraction. The dynamic structure factor of native blood proteins in pure plasma ($g_{1,s}$) can be fitted by a triexponential correlation function according to eq. 4.4.

$$g_{1,s}(\tau) = \alpha_{1,s} \cdot \exp\left(-D_{1,s} q^2 \tau\right) + \alpha_{2,s} \cdot \exp\left(-D_{2,s} q^2 \tau\right) + \alpha_{3,s} \cdot \exp\left(-D_{3,s} q^2 \tau\right) \tag{4.9}$$

In contrast, the dynamic structure factor of nanoparticles ($g_{1,np}$) is commonly fitted by a biexponential correlation function. If both components are mixed and do not interact or interact only marginally, the correlation function of the mixture $g_{1,m}$ is constituted by the sum of the individual correlation functions.

$$g_{1,m}(\tau) = f_s g_{1,s}(\tau) + f_{np} g_{1,np}(\tau) \tag{4.10}$$

Therefore, if no aggregation occurs, the experimental data obtained for the mixture should be perfectly fittable by this function, as for example in the case presented in Fig. 4.5.

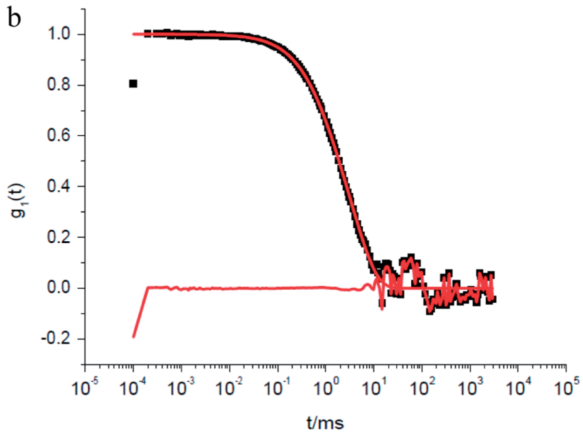

Figure 4.5: Autocorrelation function of PLL-*g*-PEO$_{20}$ in human serum as an example for the absence of aggregation. Red line: fit with eq. 4.10 and the resulting residue, ■ experimental data. Example obtained from Rausch *et. al*.[325]

If, on the other hand, significant interaction between nanoparticles and blood proteins arises and aggregation is induced, the experimental data cannot be fitted by eq. 4.10 anymore. Instead, another exponential term has to be added to the correlation function to take the emerging aggregates into account.

$$g_{1,m}(\tau) = f_s g_{1,s}(\tau) + f_{np} g_{1,np}(\tau) + f_{agg} g_{1,agg}(\tau) \tag{4.11}$$

Only such a modified correlation function gives a realistic extrapolation for the measured data. Fig. 4.6 shows a case, in which aggregation between nanoparticles and blood proteins occurs. It is clearly visible that only the correlation function which takes aggregation into account (red line) is in line with the measured data points.

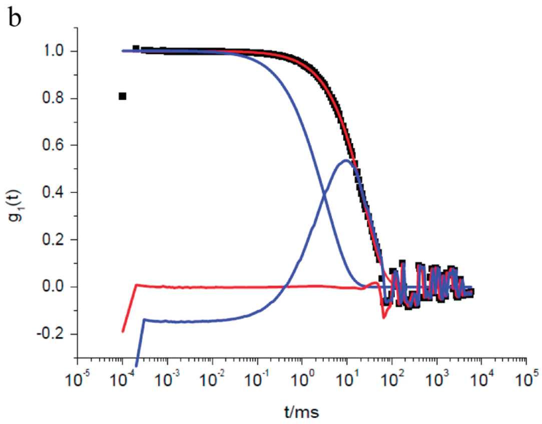

Figure 4.6: Autocorrelation function of PLL-*g*-PEO_8 in human serum as an example for the occurence of aggregation. Blue line: fit with eq. 4.10 and the resulting residue, red line: fit with eq. 4.11 and the resulting residue, ■ experimental data. Example obtained from Rausch *et. al.*[325]

The additionally introduced term $f_{agg}g_{1,agg}(\tau)$ allows the calculation of the selfdiffusion coefficient and hence hydrodynamic radius of the aggregates according to

$$g_{1,agg}(\tau) = \alpha_{1,agg} \cdot \exp\left(-D_{1,agg}q^2\tau\right) \tag{4.12}$$

Eventually, presence or absence of protein aggregation induced by nanoparticles as well as the aggregate size can be easily monitored by applying the above outlined procedure and comparing experimental and theoretically predicted data. Thus light scattering measurements in plasma represents a valuable routine control to check the *in vivo* applicability of nanoparticles.

4.1.2 Molecular Dynamics Simulation - Bead Spring Model

Molecular dynamics simulation is a computational method to calculate the time-dependent physical movement of atoms or molecules. It is commonly applied for modeling dynamics and thermodynamics of macromolecules within the nanosecond or microsecond regime although millisecond time scales have been reported.[327] Macromolecules like synthetic polymers, proteins or nucleic acids can be simulated using the bead-spring model[328] originally proposed by P. E. Rouse.[329] In this model, a polymer is constituted by N +1 beads which are connected by N massless springs. A bead represents one or more repeat units, whereas the springs form the covalent bonds in between. The potential energy of a bead spring chain is given by

$$H_l(\{l_i\}) = C_l\sum_{i=1}^{N}(l_i - l_0)^2/2 = C_l\sum_{i=1}^{N}(|R_i - R_{i-1}| - l_0)^2/2 \tag{4.13}$$

with R_i as the position of each bead in space and l_i as the relative distance between the beads. Beads can be indicated with further attributes such as hydrophilicity/hydrophobicity or charge. Such properties are adjusted by setting the Lenard-Jones interaction between two beads accordingly.

When applied for computing the complexation process between nucleic acids and cationic polymers, molecular dynamics simulation with bead spring model enables a theoretical prediction of the structure and composition of the resulting polyplexes.

4.1.3 Cryogenic Transmission Electron Microscopy

In contrast to conventional light microscopy, transmission electron microscopy (TEM) exploits electrons instead of photons for imaging. A TEM image is created from information about density, phase and periodicity of transmitted electrons following their interaction with the specimen's atoms.

In microscopy, the relation between resolution d, wavelength λ, refractive index n and the angle α at which radiation enters the lense is given by

$$d = \frac{\lambda}{2n \sin \alpha} \tag{4.14}$$

Due to the much smaller de Broglie wavelenght of electrons compared to photons, the resolution of TEM is substantially higher than in light microscopy. For imaging, electrons are emanated by thermionic emission or field electron emission into a vacuum and accelerated along an electric potential. The electron beam is then focused onto the sample through electrostatic and electromagnetic lenses. Eventually, the resulting image is projected on an imaging device, for example a fluorescent screen. Fig. 4.7 shows the basic setup for TEM.

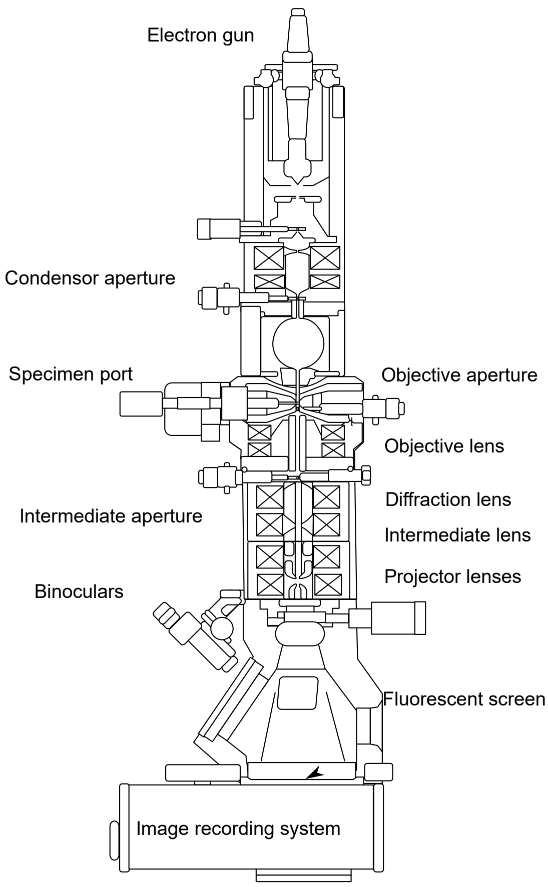

Figure 4.7: Basic components of TEM.[1]

Cryo-electron microscopy is a special form of TEM which allows the observation of vitrified specimens. It is commonly applied for the analysis of biological samples in their physiological environment, i.e. aqueous solution. Additional manipulations such as staining or fixation are not required. Moreover, radiation damage of samples is reduced because of the low temperature during imaging. Cryo-TEM is a valuable method for realistic imaging of

1 Image adopted from https://en.wikipedia.org/wiki/Transmission_electron_microscopy.

synthetic nanoparticles intended for biomedical application, which like biological macromolecules, are usually dispersed in water or buffer. As samples are embedded in vitreous ice and remain hydrated throughout analysis, collapse, aggregation or surface adsorption of the sample, which might occur in other imaging techniques, are prevented. Thus, the natural size and shape of nanoparticles in solution can be investigated.

Before analysis, vitrification of sample solutions is the key step to prevent formation of ice crystals that would otherwise damage the molecular structure of the specimen. The rapid freezing required for vitrification of water can be achieved by cryofixation. Samples are therefore immersed in liquid ethane or propane cooled by liquid nitrogen, providing the necessary cooling rates.

4.1.4 Gel Electrophoresis

Gel electrophoresis is a quick and easy method to analyze size and conformation of nucleic acids by exploiting their negative net charge. Moreover, complexation of nucleic acids by cationic molecules in relation to charge ratio can be visualized. The gel matrix is constituted of the polysaccharide agarose which forms pores of variable size depending on the applied concentration. Implementation of an electric field causes migration of nucleic acids along the voltage gradient towards the positive pole. Smaller molecules thereby migrate faster than larger ones, leading to a separation according to hydrodynamic diameter. In contrast to free nucleic acid, polyplexes with a large enough N/P ratio remain stuck in the gel pockets. Hence, both species and the intermediate steps from one to the other can be discriminated. To stain nucleic acids, the gel matrix is spiked with intercalating dyes such as ethidium bromide or GelRed$^{\text{TM}}$

Gel electrophoresis also allows assessment of polyplex stability and their capability to protect nucleic acid against nuclease attack. For instance incubating polyplexes with negatively charged heparin might displace nucleic acid from the complex which can then be detected as free species in subsequent gel electrophoresis.

4.1.5 Total Internal Reflection Fluorescence Microscopy

Total internal reflection fluorescence microscopy (TIRFM) is a form of fluorescence microscopy which allows the selective observation of surface-bound fluorescent molecules within a sample. In contrast to conventional fluorescence microscopy, in TIRFM non-bound fluorophores in the surrounding volume are not excited due to total internal reflection of the incident light beam. Hence, background fluorescence is significantly diminished. Total internal reflection is only possible at interfaces where the refractive index n drops from the first medium to the second medium. When incoming light encounters such a medium boundary at a sufficiently high angle it is completely reflected back into the first medium. The critical angle Θ_c for total internal reflection can be calculated from Snell's Law

$$n_1 \cdot \sin \Theta_1 = n_{:2} \cdot \sin \Theta_2 \tag{4.15}$$

yielding $\Theta_c = \sin^{-1}(\frac{n_2}{n_1})$. In the second medium, an evanescent wave is created adjacent to the interface. In TIRFM, this evanescent wave is applied for imaging, only exciting the fluorophores in a small region vicinale to the glass-water interface between coverslip and specimen (Fig. 4.8). As the electromagnetic field of the evanescent wave decays exponentially from the interface, the penetration depth into the specimen is only around 100 nm and therefore excitation of fluorophores is restricted.

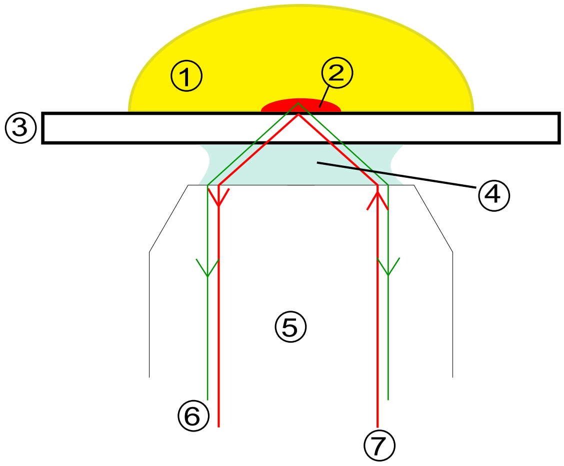

Figure 4.8: Optical path in TIRFM.[2]

Apart from cell imaging, TIRFM can be applied for single molecule analysis of surface-bound particles. For example, quantitative comparison of fluorescence for different particle species allows conclusions on particle composition.

4.2 BIOLOGICAL EVALUATION OF POLYPLEXES

4.2.1 Confocal Microscopy

In fluorescence microscopy, imaging of biological specimen is often impaired by light from out-of-focus planes interfering with the fluorescence signal of structures of interest. Confocal microscopes are designed to overcome this problem by filtering the signal of interest from out-of-focus emission while keeping it strong enough for detection at the same time.

A confocal microscope is a special form of fluorescence microscope operating with two aperture pinholes, one downstream from the light source and one in front of the detector. The two pinholes and the point of illumination in the specimen are confocal to each other (Fig. 4.9). As a consequence of the setup, only a small volume within the sample is illuminated by the incoming light and, additionally, out-of-focus signal from the specimen is eliminated.

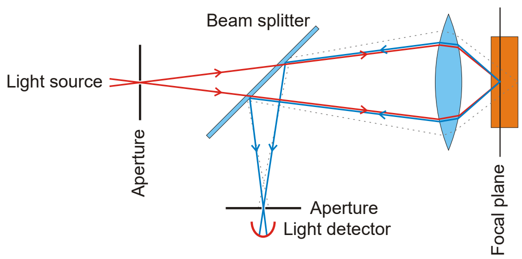

Figure 4.9: Optical path in confocal microscopy.[3]

2 Image adopted from https://en.wikipedia.org/wiki/Total_internal_reflection_fluorescence_microscope.

3 Image adopted from https://en.wikipedia.org/wiki/Confocal_microscopy.

Thus, compared to conventional wide-field microscopes background fluorescence from the surrounding volume is diminished and the optical resolution is significantly increased. Since a large part of the sample fluorescence is blocked, confocal microscopes are equipped with light sources of high excitation power like lasers.
A confocal laser scanning microscope (CLSM) generates a 2D image through point-by-point raster scanning across a sample in the horizontal plane. In addition, 3D images can be obtained by screening multiple planes along the z-axis. CLSM enable optical sectioning of a sample in extremely thin planes and detection of structures burried deep within a specimen. However, the raster scanning technique requires long imaging times for 2D and all the more for 3D images. Slow imaging of samples together with high-intensity excitation induce photo-toxicity and are also rather incompatible with investigations of dynamic processes as for example in living cells. Thus, CLSM are best suited for imaging of fixed samples where high optical resolution and thin sectioning are desired in particular.

As an alternative to CLSM, spinning disc confocal microscopes are provided with a rotating disc containing an array of pinholes arranged in a spiral. Compared to CLSM, this setup allows much more light throughput at the cost of diminished confocality and thicker optical sectioning. Because multiple pinholes are used in parallel, scanning of a sample proceeds much faster than in case of CLSM especially allowing imaging of dynamic processes in living samples. Moreover, each pinhole can focus on a specific specimen region for a longer time. Thus, lower excitation energy is required for illumination, reducing photo-toxicity and sample bleaching. Spinning disc confocal microscopes are therefore particularly suited for live cell imaging and imaging of moving objects over longer time courses.

4.2.2 Flow Cytometry

Flow cytometry is a widely used spectroscopic method to analyze properties of cell populations on single cell level. During measurement of a sample, individual cells are consecutively conveyed past a laser. In the process, forward and sideward scattered light as well as cell-associated fluorescence are collected by different detectors (Fig. 4.10).

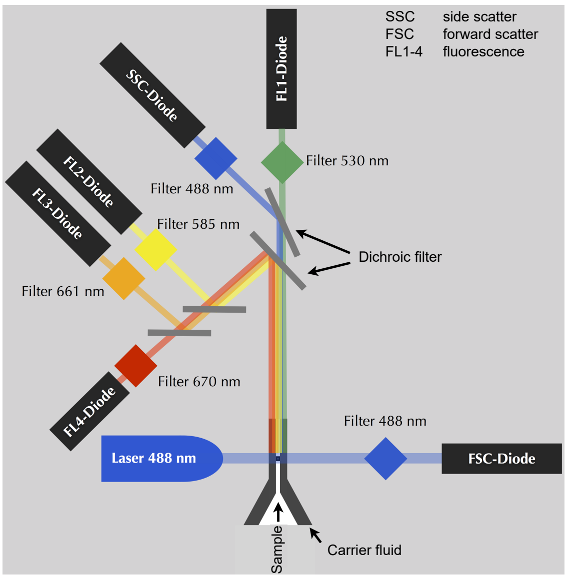

Figure 4.10: Setup of a flow cytometry system.[4]

4 Image adopted from `https://de.wikipedia.org/wiki/Durchflusszytometrie`.

Forward scattered light (FSC) is correlated with the cell volume, while sideward scattered light (SSC) provides information about cell granularity. These parameters can already be used to distinguish certain cell populations. The fluorescence detectors further enable quantitative measurement of cell-associated fluorophores. For instance, by staining cells with fluorescently labeled antibodies, which bind to cell type-specific intracellular molecules or surface structures, a more detailed analysis of different cell populations becomes possible. The data acquired individually for each cell within a sample is presented in form of histogramms or dotplots.

4.2.3 Luciferase Assay

The luciferase assay is a straightforward quantitative method for determination of a reagent's transfection efficiency, which allows fast screening approaches due to its simplicity. It is based on transfection with reporter genes encoding the luciferase enzymes from *Renilla reniformis* (sea pansy) or *Photinus pyralis* (firefly). Firefly luciferase catalyzes the oxidative decarboxylation of D-luciferin to oxyluciferin to (Fig 4.11).[330] Bioluminescence created during the reaction (λ = 480 nm) can be quanitified with a luminometer. It is directly correlated with the amount of luciferase produced by transfected cells, and therefore with the transfection efficiency of the tested reagent.

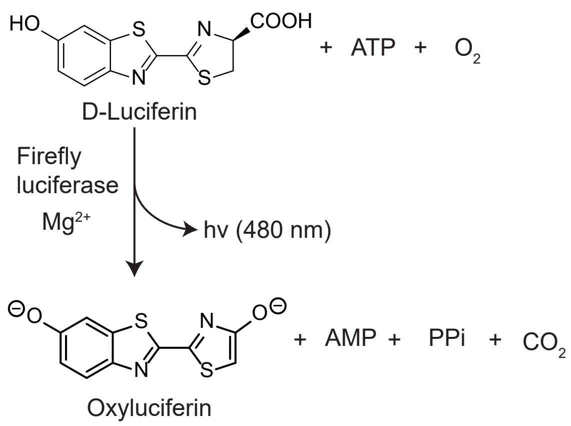

Figure 4.11: Oxidative decarboxylation of D-luciferin and associated emission of light.

4.2.4 Cell viability Assay

MTT and XTT assay are colorimetric tests to assess cell viability. MTT (3-(4,5-dimethylthiazol-2-yl)-2,5-diphenyltetrazolium bromide) is a yellow, membrane crossing tetrazolium salt, XTT (2,3-bis-(2-methoxy-4-nitro-5-sulfophenyl)-2H-tetrazolium-5-carboxanilide) is another, closely related reagent. In viable, metabolically active cells MTT or XTT are reduced to water insoluble formazan by NADH and NADPH (Fig. 4.12). After cell lysis and solubilization of the formazan crystalls, formazan-associated absorbance is measured at 570 nm (for MTT) or 450 nm (for XTT) with a spectrophotometer. MTT/XTT assays, thus, enable quantitative measurement of metabolic acitivity and thereby indirect assessment of cell viability.[331]

Figure 4.12: Reduction of MTT by NADH/NADPH.

4.2.5 Enzyme-linked immunosorbent assay (ELISA)

ELISA is a biochemical assay which relies on the combination of antibody binding and enzymatic reactions for quantitative spectrophotometric detection of a certain substance in a sample. In a sandwich ELISA (Fig. 4.13)a surface is coated with antibodies specific for the substance in the sample to be analyzed. In the first step, the sample is added onto the surface and any present substance binds as antigen to the surface antibody. Following a washing step, a second substance-specific antibody which binds to another site of the antigen is applied. This primary antibody is either directly linked to an enzyme or a secondary, enzyme-linked antibody, which binds specifically to the Fc region of the primary antibody, is added after a washing step. Subsequently, another washing step is carried out. Afterwards, a substrate is added that can be converted by the enzyme yielding a colored product for absorption or fluorescence measurement. Eventually, the spectrophotometric readout provides information about the concentration of the antigen in the analyzed sample.

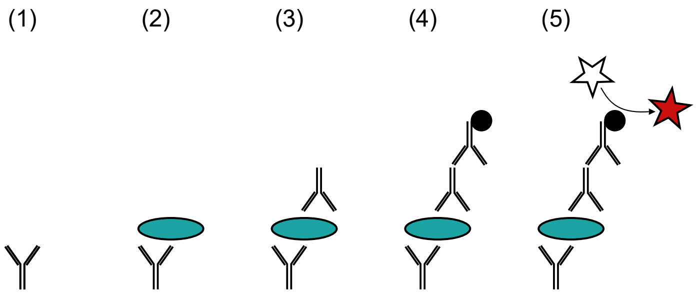

Figure 4.13: Principle of sandwich ELISA. Blue: antigen, black: enzyme linked to secondary antibody.[5]

4.2.6 T Cell Proliferation Assay

A T cell proliferation assay can be utilized as a functional readout for the transfection efficiency of the PeptoPlexes developed in this work. In other words, it gives feedback of their suitability to function as carriers for a pDNA vaccine.

The assay consists of several steps. In general, antigen-presenting cells, i.e. dendritic cells (DCs), are first pulsed with any given antigen. In the special case of this work, the cells are transfected with PeptoPlexes carrying a model pDNA antigen encoding ovalbumin. Cell lines applied are DC2.4 cells (a murine model for native DCs) and native bone marrow-derived dendritic cells (BMDCs, generated from murine bone-marrow progenitor cells). After 24 hours of transfection and accumulation of antigen, cells are stimulated with an adjuvant such as lipopolysaccharides (LPS) or CpG oligodeoxynucleotides to induce

5 Image adopted from `https://en.wikipedia.org/wiki/ELISA`.

maturation and antigen (ovalbumin) presentation. Subsequently, matured dendritic cells are co-cultured with $CD4^+$ or $CD8^+$ T cells. In the context of this work, $CD8^+$ T cells are isolated from OT I mice, while $CD4^+$ T cells are obtained from OT II mice. The monoclonal T cells of these mouse strains exclusively express transgenic T cell receptors (TCR) recognizing ovalbumin residues 257-264 presented on MHC I (in case of $CD8^+$/OT I) and ovalbumin residues 323-339 presented on MHC II (in case of $CD4^+$/OT II), respectively. Consequently, during co-culture, clonal expansion of the T cells is only initiated if the DCs applied present fragments of ovalbumin via MHC I/MHC II. The ovalbumin presentation, however, depends on the successful transfection of the dendritic cells in the first step. Therefore, the degree of T cell proliferation directly correlates with the functionality (transfection efficiency) of the applied PeptoPlexes.

T cell proliferation is measured via a ^{3}H-thymidine proliferation assay. As cells are cultured in the presence of the radioactive nucleoside ^{3}H-thymidine, it is incorporated into new strands of chromosomal DNA during mitotic cell division. The extend of ^{3}H-thymidine incorporation and thus cell proliferation is determined by a scintillation beta-counter measuring the tritium-associated radioactivity in DNA recovered from the cells.

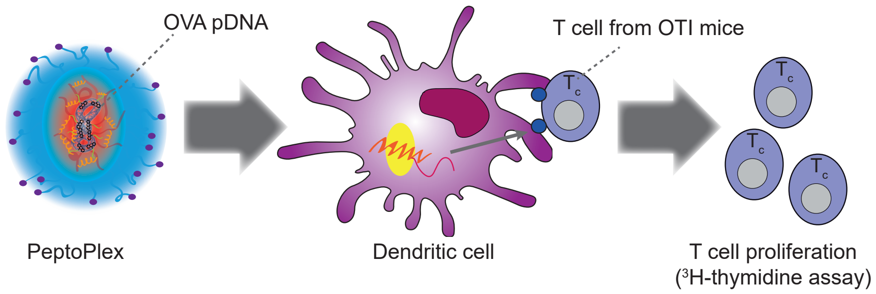

Figure 4.14: Procedure for T cell proliferation assay as performed in this work.

Part II

PEPTOPLEXES FROM DIBLOCK COPOLYPEPT(O)IDES

The PhD thesis started with the synthesis of PLys-b-PSar diblock copolymers which combine the most fundamental components for the formation of core-shell type polyplexes: A cationic segment (PLys) binding the negatively charged nucleic acid and a neutral, hydrophilic segment (PSar) constituting the shell material. The first generation of PeptoPlexes could be obtained through the combination of these diblock copolymers and pDNA. The PeptoPlexes were characterized for their physicochemical properties and compared to free pDNA. Moreover, first structure-property relationships between polymer block lenght, transfection efficiency and cytotoxicity in HEK 293T cells were investigated.

5 INTRODUCING PEPTOPLEXES: POLYLYSINE-BLOCK-POLYSARCOSINE BASED POLYPLEXES FOR TRANSFECTION OF HEK 293T CELLS

P. Heller, A. Birke, D. Huesmann, B. Weber, K. Fischer, A. Reske-Kunz, M. Bros, M. Barz, *Macromolecular Bioscience*, 2014, **14**, 1380-1395

ABSTRACT

A series ofwell-defined polypeptide-polypeptoid block copolymers based on the body's own amino acids sarcosine and lysine are prepared by ring opening polymerization of *N*-carboxyanhydrides. Block lengths were varied between 200-300 for the shielding polysarcosine block and 20-70 for the complexing polylysine block. Dispersity indexes ranged from 1.05 to 1.18. Polylysine is polymerized with benzyloxycarbonyl as well as trifluoroacetyl protecting groups at the ε-amine group and optimized deprotection protocols for both groups are reported. The obtained block ionomers are used to complex pDNA resulting in the formation of polyplexes (PeptoPlexes). The PeptoPlexes can be successfully applied in the transfection of HEK 293T cells and are able to transfect up to 50% of cells in vitro (FACS assay), while causing no detectable toxicity in an Annexin V assay. These findings are a first indication that PeptoPlexes may be a suitable alternative to PEG based non-viral transfection systems.

5.1 INTRODUCTION

Despite a number of challenges gene therapy holds great potential for the treatment of a plethora of diseases.[332–335] For example, genetic modification of blood stem cells by retroviral vectors has rescued children affected by severe combined immunodeficiency.[336] In general, therapies in which only a small number of cells need to be genetically reprogrammed may hold the greatest potential for a successful use of gene delivery systems. In connection with this, the transcriptional targeting and stimulation of dendritic cells (DC) may offer new perspectives in cancer immunotherapy,[337, 338] as only a small number of dendritic cells need to be activated to induce a potent immune response against an antigen.[339] In accordance, as few as approximately 10^2 DCs transfected with an antigen-encoding plasmid DNA (pDNA) were reported to induce a profound antigen-specific immune response in recipient mice.[340] DNA-based vaccines are particularly attractive because they hold several advantages over conventional peptide/protein vaccines.[341] For example, they are able to elicit both, $CD4^+$ and $CD8^+$ T cell responses.[1, 342] In addition, antigen and immune adjuvant can be combined with a DC-specific promotor on one plasmid. Nonetheless, both extracellular and intracellular degradation of pDNA, are major limitations of pDNA-based immunotherapy. One possibility to protect pDNA against degradation and mediate its delivery is the use of polymeric carriers. Aside from protecting their cargo, polymeric carriers designed for *in vivo* delivery of DNA vaccines should exhibit good transfection efficiency and especially minimal cytotoxicity.

Accordingly, the development of pDNA carriers itself is often limited by low efficiency,[343] significant toxicity,[344, 345] high polymer dispersity and therefore broad size distribution of polyplexes. In contrast, efficient viral vectors bear various risks (immune response, lack of control, etc.) leading to major concerns of clinical safety.[346] Consequently, the material used for transfection is of great importance.

Polymeric transfection systems have been under development for two decades and especially with a view to *in vivo* application some common design principles can be derived from the outstanding contributions of Wagner *et al*. and Kataoka and co-workers.[214, 347, 348] In general, block copolymer-based core-shell structures seem to be the most suitable systems for intravenous applications. In this case a hydrophilic, nonionic block is combined with a polycationic block. While complexation of oligonucleotides (pDNA, mRNA, siRNA, etc.) is performed by the polycationic block (polydimethylaminoethyl methacrylate (PDMEAMA),[349] poly- or oligoethylene imine (PEI),[350, 351] poly-L-lysine (PLys),[352] polyarginine or derivatives thereof[353]), the non-ionic block forms a hydrophilic corona around the polyplex. The polymer corona can reduce or completely suppress unspecific interactions with serum proteins caused by hydrophobic or electrostatic interactions, thereby circulation times are elongated and coagulation is reduced.[350, 354]

Most of the above described polymer systems are based on polyethylene glycol (PEG),[355, 356] acrylates with oligo ethylene glycol side chains (POEGMA)[357] or polyoxazolines[358] as shielding block. The common feature of these systems is that they are not degradable *in vivo*. Many groups are currently investigating degradable and non-degradable alternatives to the gold standard PEG.[359] Gu *et. al*, for example, used naturally occurring hyaluronic acid as hydrophilic component.[360] Another highly desirable alternative are block copolypeptides. However, the published work on non-ionic, water soluble and protein resistant polypeptide-based transfection systems is almost exclusively limited to PEGylated derivatives of polylysine.[196, 220] The naturally occurring amino acid sarcosine - *N*-methylglycine - does also provide stealth-like properties but surprisingly the work on polysarcosine and polysarcosine-based block copolymers is highly restricted.[109, 117, 118, 121] The fact that polysarcosine (PSar) is almost completely overlooked when it comes to stealth-like polymers is much of a surprise with respect to the fact, that PSar combines properties of polypeptides with the stealth-like properties of PEG as already demonstrated by the groups of Langer and Whitesides, who investigated PSar as coating for protein resistant surfaces.[361, 362] Kimura and co-workers have studied PSar-b-PAla and PSar-b-PLA copolymers.[162, 166, 363] Aditionally, Zuckermann and co-workers have performed excellent work on solid phase synthesis of PSar.[364] But in all these reports sarcosine was kept at a low degree of polymerization of 20-30. This appears insufficient concerning the work of Kissel and co-workers who reported that in the case of PEG a low molecular weight polymer block is not able to effectively shield polyplexes from unspecific aggregation with erythrocytes.[365] Recently, Birke *et al*. have demonstrated the successful synthesis of PSar-based polypeptoid-polypeptide hybrids with Xn = 200-400 by controlled ring opening polymerization of the corresponding NCAs.[155] To derive PSar blocks of this chain length, the ROP of sarcosine NCAs appears to be the most practical method, since it is relatively simple to perform in a living manner and easily scalable to multigram or kilogram.

While the ROP of the sarcosine NCA proceeds under living conditions, the polymerization of α-amino acid-*N*-carboxy anhydrides needs to be controlled. During the last decades various techniques have been introduced to control the polymerization of NCAs. These are transition metal catalysts,[366] hexamethyldisilazane,[26] ammonium salts,[27] low polymerization temperature[29] and high vacuum techniques[28]. For the synthesis of well-defined polypeptides with a polymerization degree up to 100 highly pure reaction conditions are sufficient - as reported by Huesmann *et al*.[36] and Birke *et al*.[155]. Therefore, we have applied the same conditions to the synthesis of PLys-block-PSar copolymers.

In the following article, we would like to introduce the synthesis of PLys-block-PSar copolymers with respect to protecting group chemistry and describe the formation of polyplexes of this novel class of polypeptide-polypeptoid block copolymers with pDNA (pRLEF1α, pEGFP-N1). In order to avoid complex nomenclature we named these systems PeptoPlexes. Furthermore, we provide first structure-property relationships on transfection efficiency and cellular toxicity of PeptoPlexes.

5.2 RESULTS AND DISCUSSION

5.2.1 Polymer Synthesis

The synthesis of PLys-b-PSar copolymers was performed by sequential ring opening polymerization of corresponding NCAs followed by deprotection of the poly-L-lysine block (Fig. 5.1). PLys-b-PSar copolymers cannot be directly synthesized by polymerization of the corresponding NCAs, because the ε-amine of lysine interferes during polymerization and thus needs to be protected during NCA synthesis and polymerization. Therefore, either acid or base labile protecting groups can be applied. In this work, we have explored both methodologies using benzyloxycarbonyl (Z) and trifluoroacetyl (TFA) to protect the ε-amine group in the lysine side chain, because like PEG, PSar is not indefinitely stable under harsh deprotection conditions.

Formation of the corresponding NCA monomers was performed according to the Fuchs-Farthing method.[367] Monomers were purified by recrystallization until the melting point was 101 °C for lysine(Z) NCA and 103 °C for lysine(TFA) NCA. The absence of chloride ions was monitored by the silver nitrate test. The synthesis of sarcosine NCA was carried out according to Luxenhofer and co-workers[121] The crude product could be easily purified by sublimation at 80-85 °C and <1 x 10^{-2} mbar. Sarcosine NCA had a melting point of 102-104 °C, which is in agreement to literature (103-105 °C).[15, 368]

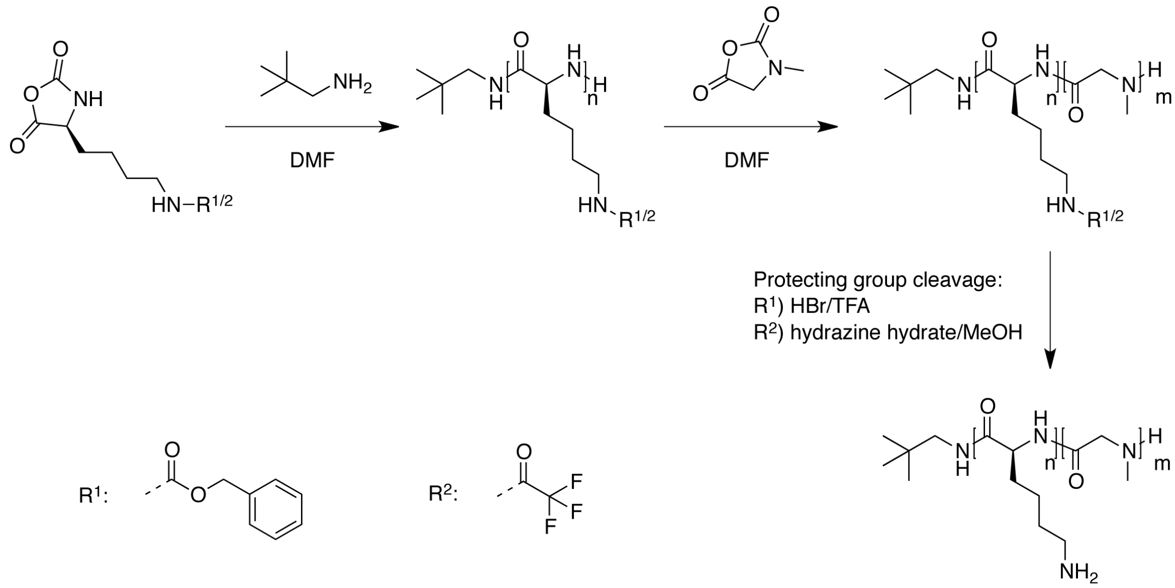

Figure 5.1: Synthetic pathway to PLys-b-PSar copolymers by sequential ring opening polymerization of sarcosine and *N*-ε-benzyloxycarbonyl-L-lysine/ *N*-ε-trifluoroacetyl-L-lysine α-*N*-carboxy anhydrides.

The ring opening polymerization of NCAs was performed in absolute dimethylformamide (DMF) using neopentylamine as initiator according to Birke *et al*.[155] In this work we first synthesized polylysine blocks with degrees of polymerization varying between 20 and 70. The synthesis of PLys(Z) as well as of PLys(TFA) was carried out at ambient temperature of 20 °C. As known from solid phase synthesis, the TFA protecting groups at ε-position are not affected by the free amine present at the propagating chain end or the initiator at ambient temperature. PLys(Z) and PLys(TFA) homopolymers were used in the next step to initiate the polymerization of sarcosine NCAs, again at ambient temperature. The degree of polymerization of the PSar block was varied from about 200 to 300. The final block copolymers displayed a dispersity (*Đ*) index of around 1.1. The GPC analysis showed clear shifts in the GPC traces from homopolymers used as macroinitiators to block copolymers. This indicates chain extension and thus successful formation of block copolymers (Fig. 5.2). The absence of homopolymers was also verified by DOSY NMR experiments (SI, Fig. 5.16).

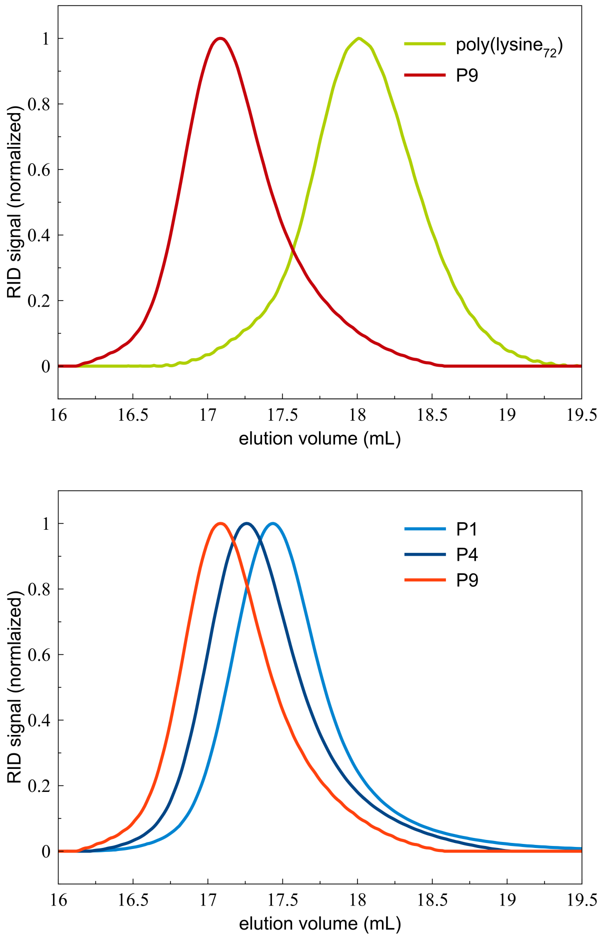

Figure 5.2: GPC plots of homo- and block copolymers with varying block lengths in HFIP.

In summary, the synthesis of PLys(Z)-b-PSar as well as PLys(TFA)-b-PSar copolymers can be performed under controlled conditions at scales from 100 mg to several grams yielding narrowly distributed block polymers with dispersities of around 1.1.

To yield the desired block ionomers PLys(Z)-b-PSar and PLys(TFA)-b-PSar copolymers have to be deprotected. As already mentioned in the introduction, different protecting groups were applied to protect the ε-amine of lysine. This was done to study the influence of basic as well as acidic deprotection conditions on the novel class of polypeptide-polypeptoid hybrids.

First, the deprotection of PLys(Z)-b-PSar polymers under acidic conditions with a mixture of hydrobromic acid/trifluoracetic acid (HBr/TFA) was investigated. Under such conditions polyethers (e.g., PEG) can be cleaved (inverse Williamson ether synthesis). On the other hand, HBr/TFA and HBr/glacial acid are standard conditions for the removal of Z and Bn protecting groups.[369] Thus, we applied these deprotection conditions to the PLys(Z)-block-PSar copolymers for different reaction times. Additionally, different molar ratios of HBr to Z groups of the polymer were investigated since HBr acts as cleaving agent.

Results showed that the amount of HBr plays an essential role and needs to be precisely controlled (Fig. 5.3). To study the influence of deprotection conditions on PSar integrity we compared the ^{1}H-NMR signal intensity of PSar from 3 to 2.6 ppm with the benzyl protons using the methyl groups of the initiator (neopentylamine) as internal standard. The use of 1.5 eq of HBr over a period of 6 hours already leads to a reduction in PSar integrity of around 20%. Higher amounts of HBr enhance degradation leading to a reduction of 25-30% in PSar integrity. By the use of 1.05 eq of HBr in TFA and a reaction time of 12 hours at 20 °C we were able to obtain quantitative deprotection of PLys(Z)-block-PSar copolymers without detectable polymer degradation within the accuracy of ¹H-NMR. Notably, we did not see an effect of lysine block length on the deprotection efficiency.

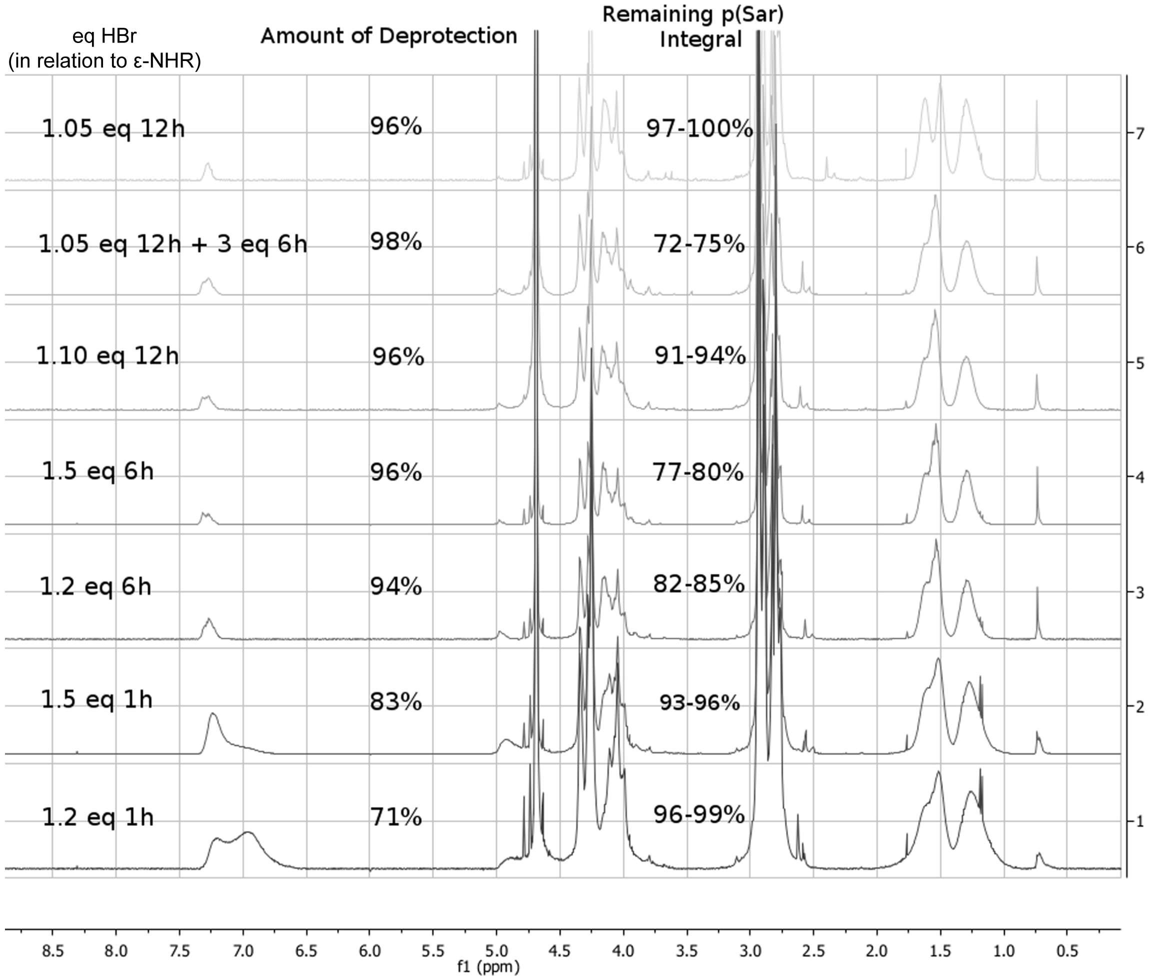

Figure 5.3: Effect of deprotection condition with respect to protecting group cleavage and polymer integrity using acidic mixture of HBr/ TFA. Polymer integrity was calculated from remaining PSar integral after dialysis.

Deprotection conditions could be adjusted to PLys(Z)-b-PSar copolymers in a way that quantitative deprotection was achieved without detectable degradation of the PSar backbone. Nevertheless, it has to be concluded that acidic deprotection conditions are not ideal for the synthesis of PLys-b-PSar copolymers. Thus, in the next step block copolypeptides with TFA protecting group on the ε-amine of lysine were investigated. In this case, deprotection can be achieved under basic conditions, for example, NaOH/methanol[370] or KOH/THF[371]. However, we utilized deprotection with hydrazine hydrate as an alternative methodology, since this approach proceeds under mild conditions with respect to basicity. Reaction times as well as ratios of hydrazine hydrate to trifluoroacetyl groups were varied. The deprotection reactions were performed for 12 up to 72 hours and ratios of hydrazine hydrate to Lys(TFA) were set between 1.25:1 and 50:1.

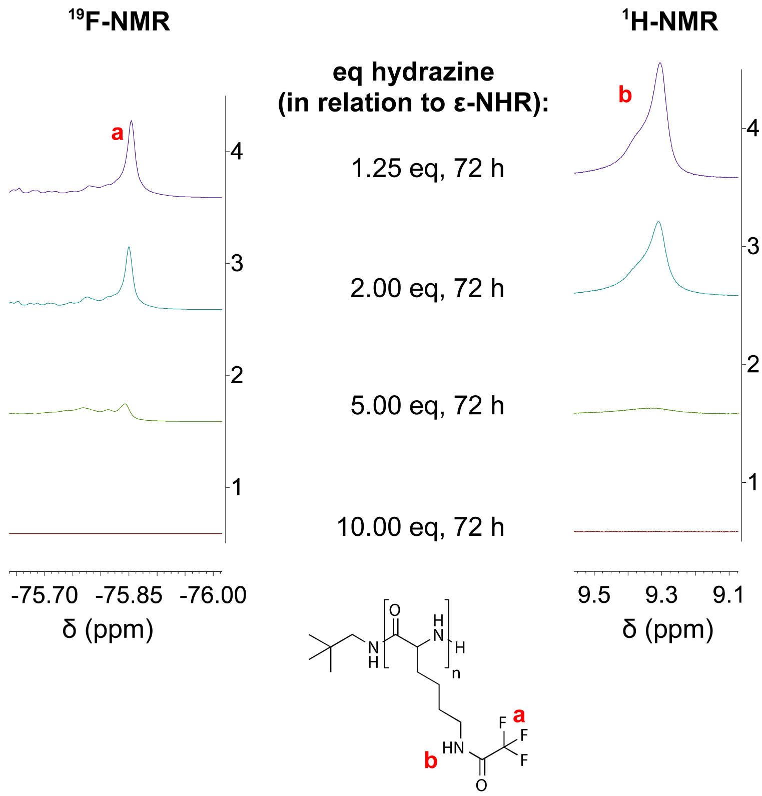

Figure 5.4: Effect of deprotection conditions with respect to protecting group cleavage using hydrazine hydrate in MeOH.

Complete deprotection could be achieved using 10 eq of hydrazine hydrate in methanol and 72 hours reaction time (Fig. 5.4). In this case, the TFA amide associated signal in ^{19}F NMR as well as the amide proton attributed signal in ^{1}H NMR vanish completely. In contrast, lower amounts of hydrazine hydrate did not completely deprotect the samples. Notably, we did not observe degradation or racemization of polymers even at 1000 times excess of hydrazine hydrate.

As reported before, the acidic deprotection of Z groups can be accomplished as well, but it is much more difficult to control the reaction parameters. Thus, we can conclude that the use of TFA protecting groups with subsequent deprotection using hydrazine hydrate is the method of choice for the synthesis of PLys-b-PSar copolymers.

Taking into account these findings, we have synthesized a variety of different PLys-b-PSar copolymers in order to investigate structure property relationships of this novel class of block ionomers, regarding polyplex formation and stability as well as transfection efficiency and cytotoxicity. The characteristics of the utilized polypeptide-block-polypeptoid copolymers are displayed in Table 5.1.

Table 5.1: Characteristics of PLys-block-PSar copolymers.

	LYSINE:SARCOSINE UNIT RATIO[A]	M_N[B]	Đ[B]	LYSINE CONTENT (m_{PLys}/m_{total})
P1	22:225	26.8	1.13	15%
P2	22:334	30.1	1.12	11%
P3	32:171	27.8	1.14	25%
P4	32:255	28.6	1.18	18%
P5	41:142	26.0	1.17	34%
P6	41:242	30.3	1.11	23%
P7	53:213	27.1	1.07	31%
P8	53:271	30.9	1.11	26%
P9	72:263	30.9	1.05	33%

[A] as determined by 1H NMR spectroscopy after deprotection
[B] kg/mol, as determined by GPC with HFIP as solvent and PMMA standards

5.2.2 PeptoPlex Formation and Characterization

PeptoPlexes were formed by addition of PLys-b-PSar copolymers to pDNA. The mixture was allowed to equilibrate overnight (14 hours). To evaluate the stability of formed PeptoPlexes, they were subjected to gel electrophoresis and examined for their capability to complex pDNA (Fig. 5.5). In general, PeptoPlexes became more stable with increasing polymer excess. At $m_{\text{polymer}}/m_{\text{pDNA}}$ ratio of 14:1 all polymers investigated were able to induce full pDNA retardation. Furthermore, it became apparent that particularly at low $m_{\text{polymer}}/m_{\text{pDNA}}$ ratios PeptoPlexes of P1 ($PLys_{22}$ block) are not as stable as PeptoPlexes of PLys-b-PSar systems with higher lysine content. This discrepancy was still obvious at tenfold polymer excess (indicated by red arrows). However, limited complexation capacity of P1 could be compensated by applying the latter in greater excess (full pDNA retardation at 14-fold excess).

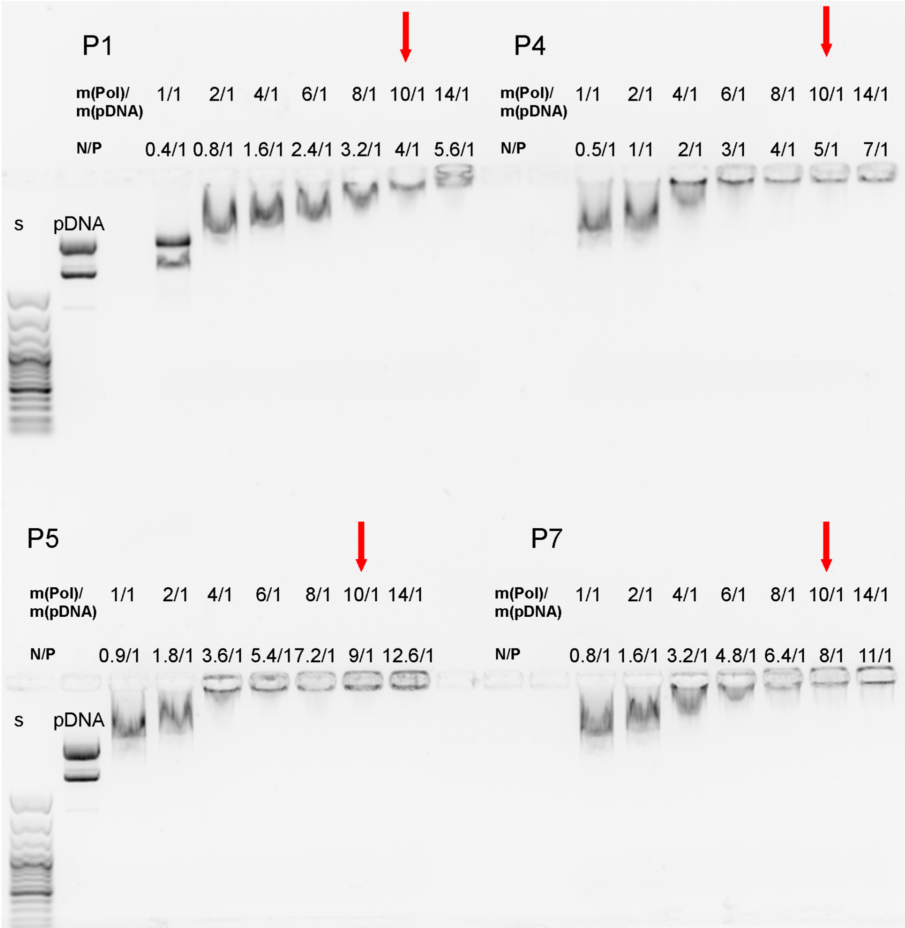

Figure 5.5: Gel electrophoresis at varying $\mathrm{m_{polymer}/m_{pDNA}}$ ratios, showing the transition of free pDNA to stable PeptoPlexes. s = GeneRuler^{TM} 100 bp DNA ladder. Red arrows indicate $m_{\mathrm{polymer}}/m_{\mathrm{pDNA}}$ ratios also used in luciferase assay. Gel concentration: 0.7%.

Of course, the application of $m_{\mathrm{polymer}}/m_{\mathrm{pDNA}}$ ratios does not consider the variation of lysine content between different polypeptides. This has to be kept in mind when comparing complexation capacity, transfection efficiency or cytotoxicity of the block copolypeptides. A valuable method to incorporate differences in lysine content is the usage of N/P ratios - or $m_{\mathrm{PLys}}/m_{\mathrm{pDNA}}$ ratios (with m_{PLys} being the net weight of the lysine blocks) which directly correspond to N/P ratios. The translation from $m_{\mathrm{PLys}}/m_{\mathrm{pDNA}}$ to N/P can be performed as follows:

$$\frac{N}{P} = \frac{m_{PLys}}{m_{pDNA}} \cdot \frac{1}{M_{Lys(monomer)} \cdot n_{phosphate}} \tag{5.1}$$

$\mathrm{n_{phosphate}}$ (amount of phosphate groups in 1 µg pDNA) = $3.07 \cdot 10^{-9} \frac{\mathrm{mol}}{\mathrm{\mu g}}$

Comparison of calculated N/P ratios shows that all investigated block copolypeptides formed stable PeptoPlexes at N/P 4:1-5:1.

Using these N/P ratios, multi angle DLS experiments were carried out in Tris buffer (10 mM). Applying the Stoke-Einstein equation we observed hydrodynamic radii of around 40 nm for the PeptoPlexes with slight angle dependency, which indicates spherical structures with narrow size distribution (SI, Subsection 5.5.2). In detail, the hydrodynamic radii of PeptoPlexes were hardly affected by the length of the PLys or PSar block. The PeptoPlexes based on $\mathrm{PLys_{32}}$-b-$\mathrm{PSar_{171}}$ (**P3**: $\langle R_h \rangle = 40.0\,\mathrm{nm}$), $\mathrm{PLys_{32}}$-b-$\mathrm{PSar_{255}}$ (**P4**: $\langle R_h \rangle = 40.7\,\mathrm{nm}$), $\mathrm{PLys_{41}}$-b-$\mathrm{PSar_{142}}$ (**P5**: $\langle R_h \rangle = 40.5\,\mathrm{nm}$) and $\mathrm{PLys_{41}}$-b-$\mathrm{PSar_{242}}$ (**P6**: $\langle R_h \rangle = 42.7\,\mathrm{nm}$) differed only marginally in radious indicating that the plasmid itself determines the hydrodynamic radius and diameter of PeptoPlexes.

However, more detailed light scattering studies on formation kinetics of PeptoPlexes and their structural dependency on polymer and pDNA properties are warranted and currently ongoing.

5.2.3 Transfection Studies Using Luciferase Assays

As a first step of biological evaluation of PeptoPlexes luciferase assays were carried out with all synthesized polymers. This screening gave a quantitative overview over the transfection efficiencies of the PLys-b-PSar systems compared to jetPEI (linear PEI, mean molecular weight of 22 kDa;[372] Fig. 5.6).

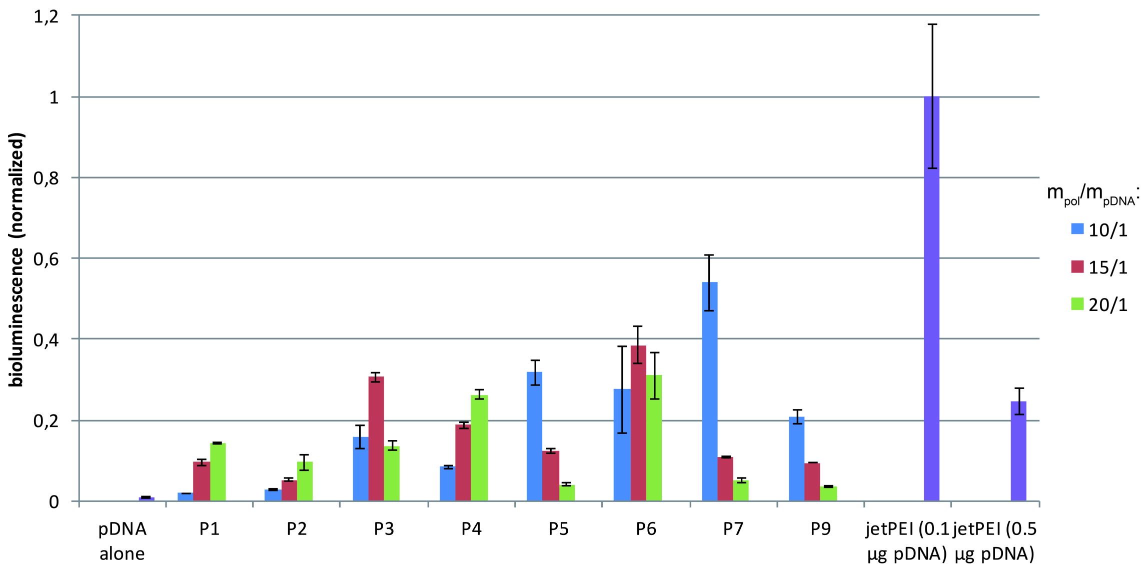

Figure 5.6: Normalized bioluminescence measured from cell lysates of HEK 293T cells after 24 hour incubation with PeptoPlexes of different PLys-block-PSar systems. $m_{\text{polymer}}/m_{\text{pDNA}}$ ratios were varied while keeping m_{pDNA} constant at 0.5 µg per well. JetPEI was applied according to manufacturer's protocol. Plain pDNA and jetPEI function as controls, $n = 3$.

In general, there are two important requirements for good transfection efficiency[345, 373]: First, the reagent should provide stable complexation of pDNA to prohibit degradation and facilitate cellular uptake while allowing endosomal translocation and intracellular release. Second, transfection reagents should induce minimal cytotoxicity at effective concentrations, especially with regard to *in vivo* applications.

Highest transfection efficiencies (around 30 - 50% in relation to jetPEI) were achieved by polymers with lysine chain lengths of 30 up to 50 units. This result was expected because on the one hand systems with less lysine content are not capable to form stable complexes with pDNA - at least at low polymer excess - as discussed above (Fig. 5.5). On the other hand, polymers with longer lysine blocks as well as jetPEI (with 0,5 µg pDNA) exhibit high cytotoxicity because of membrane disruptive effects and other apoptotic mechanisms, limiting transfection efficiency.[344, 345] Another finding is also allegeable by considering stable complexation and cytotoxicity as the limiting parameters for transfection efficiency: Polymers with high lysine content ($M_{\text{PLys}}/M_{\text{total}}$ ratio) showed lower transfection efficiency at higher polymer excess (cytotoxicity) whereas systems with low lysine content showed higher transfection efficiency at higher polymer excess (sufficient complexation).

Insufficient complexation and cytotoxicity as limiting parameters for transfection efficiency were confirmed by gel electrophoresis (Fig. 5.5) and MTT assays (SI, Fig. 5.22).

5.2.4 Cytotoxicity Studies Using MTT Assay

MTT assay was carried out to expose the relation between cytotoxicity and transfection efficiency of PLys-block-PSar systems. For this purpose, polymers with the highest lysine content were applied using constant $m_{\mathrm{PLys}}/m_{\mathrm{pDNA}}$ ratios instead of $m_{\mathrm{polymer}}/m_{\mathrm{pDNA}}$ ratios. Hereby, the influence of lysine block length could be taken into account (see Subsection 5.2.2). The clear negative correlation between lysine block length and cell viability indicates that low transfection levels observable at high polymer excess or long lysine blocks (in case of PLys$_{72}$-b-PSar$_{263}$), indeed can be attributed to block ionomer cytotoxicity. Nevertheless, all PLys-b-PSar systems except for PLys$_{72}$-b-PSar$_{263}$ showed only little cytotoxicity at the concentration needed for effective transfection compared to jetPEI (SI, Fig. 5.22), thereby meeting an important requirement for future *in vivo* applications.

5.2.5 FACS Analysis

The initial screening of PLys-b-PSar systems by luciferase assay, gel electrophoresis and MTT assay followed a more detailed examination of their *in vitro* performance on single-cell level by various FACS assays: Cellular uptake of PeptoPlexes was screened by applying FITC-labeled polymers and confirmed by confocal microscopy. Transfection ability of polymers could be monitored through detection of eGFP positive cells. In addition, by utilizing Annexin V to stain apoptotic cells, cytotoxicity measurement via FACS offered a potent alternative to MTT assays.

A general advantage of FACS analysis over luciferase and MTT assays is the possibility to screen exactly the same number of cells for every sample. This reduces random errors deriving from variation of cell densities in culture plates. Furthermore, assessing transfection efficiency by FACS allows the determination of the actual percentage of transfected cells in combination with cell-specific protein (eGFP) expression levels. In contrast, measurement of transfection levels by luciferase assay lacks the differentiation between high copy transfection of a few cells or low copy transfection of many cells.

5.2.5.1 *Cellular Uptake of PeptoPlexes*

The cell membrane is the first barrier for *in vitro* transfection. Consequently, the uptake of PeptoPlexes by HEK 293T cells was investigated by using FITC-labeled PeptoPlexes. Cells were incubated with PeptoPlexes for various times. A considerable shift of cell-associated fluorescence can be observed when comparing untreated cells with PeptoPlex-treated ones (Fig. 5.7). Hence, most cells are associated with PeptoPlexes. In addition, confocal laser scanning microscopy revealed intracellular localization of PeptoPlexes after 2 hours of incubation. These findings demonstrate that PeptoPlexes are taken up by cells (Fig. figure 5.7). This suggests that the above mentioned fluorescence shift derives from cellular uptake of PeptoPlexes by HEK 293T cells.

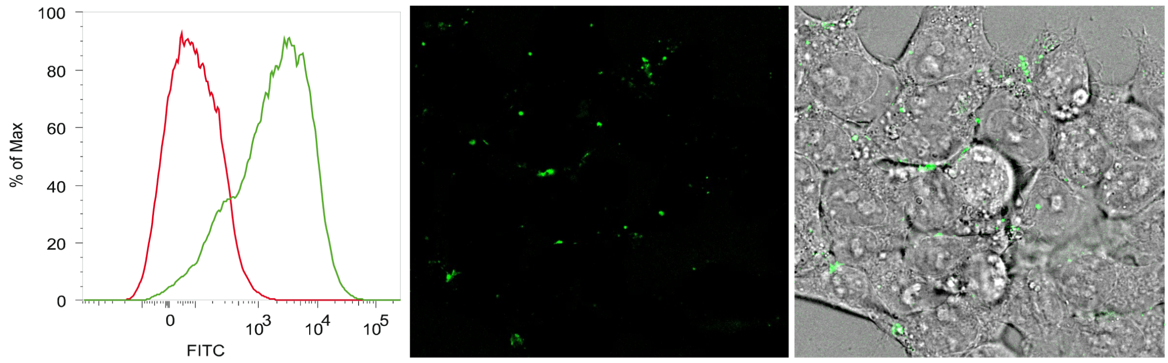

Figure 5.7: Cellular uptake of PetoPlexes. Left: Histograms of HEK 293T cells after 24 hour incubation with PeptoPlexes of FITC-labeled PLys$_{41}$-b-PSar$_{242}$ (green) and of untreated control (red). PeptoPlexes were applied using constant $m_{\text{polymer}}/m_{\text{pDNA}}$ ratio of 15/1 and 5 µg pDNA per well. Right: Representative confocal microscopy images confirming intracellular localization of PeptoPlexes.

5.2.5.2 *Transfection Studies Using FACS-Based Methods*

Assessing transfection efficiency by FACS allows the determination of the actual percentage of transfected cells in combination with cell-specific protein (eGFP) expression levels. For FACS analysis, HEK 293T cells were transfected with different PeptoPlexes (Fig. 5.8). To reveal the actual influence of lysine and sarcosine block length on transfection efficiency, all polymers were applied with similar $m_{\text{PLys}}/m_{\text{pDNA}}$ ratios, as already done in the MTT assays. In general, best transfection levels were achieved when applying $\text{m}_{\text{PLys}}/\text{m}_{\text{pDNA}}$ ratios of 2.5 (N/P = 6). A maximum in transfection efficiency was noticed for **P3** with **P1** following closely behind.

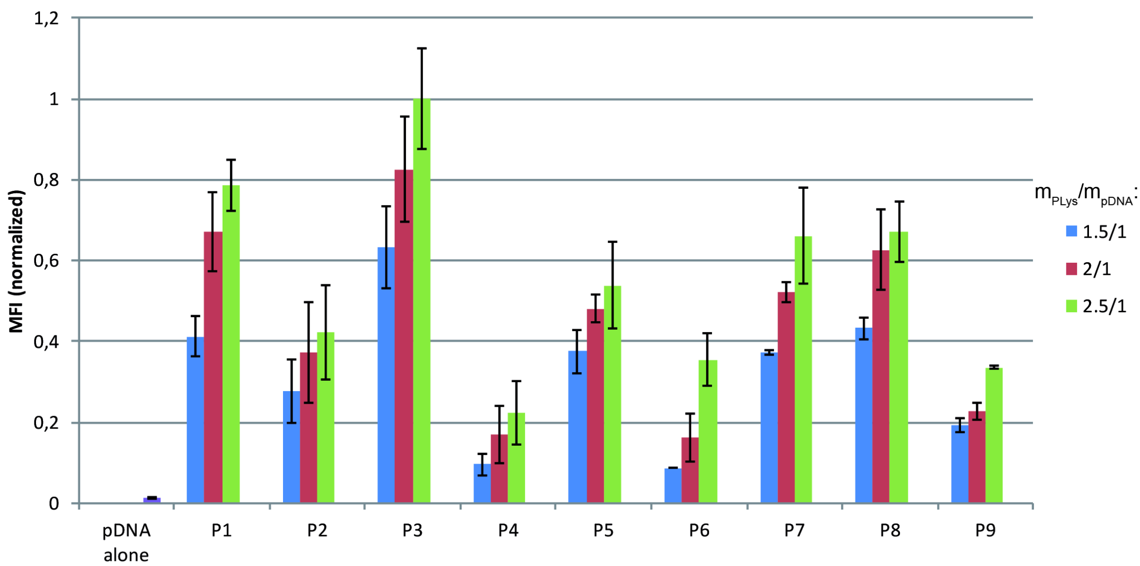

Figure 5.8: Normalized MFIs after 24 h incubation of HEK 293T cells with PeptoPlexes of different PLys-b-PSar systems and cultivation for 48 hours. $m_{\text{PLys}}/m_{\text{pDNA}}$ ratios were varied while keeping m_{pDNA} constant at 5 µg per well. Plain pDNA functions as control, n = 3.

The precise FACS assay enables the determination of detailed structure-property relationships. Polymers with longer PSar block showed a remarkable decline of transfection efficiency compared to their counterparts with shorter PSar blocks but same lysine block length. Apparently, this clear correlation is produced by the shielding properties of PSar, most likely reducing unspecific interactions of the PLys blocks with lipid membranes or proteins. In contrast to other pairs, the transfection efficiencies of **P7** and **P8** approximately reached the same height. In this case, the increase of sarcosine block length from 213 to 271 (i. e. decrease of lysine content) may be not big enough to cause a significant diminishment of transfection efficiency.

With regard to the influence of PLys block length on transfection efficiency, only slight differences were observable for block lengths between 20 and 50 units. The good performance of **P1** contrasts the outcome of luciferase assay (Fig. figure 5.6). This can be explained by the above mentioned shortcomings of the luciferase assay. Accordingly, the low transfection efficiency of **P1** in luciferase assay may not really be attributed to the short PLys block per se. On the other hand, the poor transfection performance of **P9** in FACS (Fig. figure 5.8) is in close analogy to its low efficiency in luciferase assay and can directly be attributed to the length of the lysine block and the accompanying cytotoxicity. For all other PeptoPlexes, the transfection efficiencies determined by luciferase assay and FACS assay correlated well.

Table 5.2: Percentage of eGFP positive HEK 293T cells after 24 hours incubation with PeptoPlexes of different PLys-b-PSar systems ($m_{\text{PLys}}/m_{\text{pDNA}}$=2.5/1) and cultivation for 48 hours.

TRANSFECTION REAGENT	M_{PDNA}/µg	EGFP POSITIVE CELLS/%
pDNA (negative control)	5	2.70
jetPEI (positive control)	5	69.35
P1	5	28.77
P2	5	12.65
P3	5	34.56
P4	5	8.81
P5	5	25.77
P5	7.5	33.01
P5	10	48.64
P6	5	12.88
P7	5	27.28
P8	5	26.56
P9	5	15.22

As already mentioned above the performed FACS assay with eGFP enables the determination of the actual percentage of transfected cells. When looking at the percentage of eGFP positive HEK 293T cells after transfection (Table 5.2), virtually the same trend compared to MFIs is recognizable: PeptoPlexes of **P3** transfected around 35% of the cell population, other polymers with short PSar block, respectively, lay in close reach. The analogues with long sarcosine block transfected considerably fewer cells, as did P9.

In another experiment we tested if transfection efficiency of **P5** - as a representative for PLys-b-PSar systems - could be enhanced by increasing the total amount of PeptoPlexes per well. The percentage of eGFP positive cells could be boosted to around 50% when using PeptoPlexes with 10 µg of pDNA per well (Table 5.2). In addition, further experiments with the same representative polypeptide showed that eGFP expression level of transfected cells was considerably higher after 72 hours than after 24 hours (SI, Fig. 5.25). This underlines the capability of PLys-b-PSar systems to maintain high transfection rates over longer periods of time.

In summary, a PLys block of about 30 units in combination with a PSar block with a degree of polymerization of around 200 leads to the highest levels of eGFP expression (MFI) in combination with the highest amount of transfected cells. Surprisingly, the PeptoPlexes based on **P3** were not much less effective than the commercial agent jetPEI, which does not contain a shielding block. Thus, transfection efficiencies of PeptoPlexes based on polymers **P3** and **P5** may be high enough to make these systems attractive for future *in vivo* applications.

5.2.5.3 *Cytotoxicity Studies Using FACS-Based Methods*

A potent alternative to MTT assay is the staining of apoptotic and necrotic cells by Annexin V. Annexin V binds to phosphatidylserine located on the outer surface of apoptotic or necrotic cells. Due to this binding Annexin V can already label cells in their early apoptotic phase and it therefore is a very useful marker to tag these cell populations.[374] Assessment of cytotoxicity by Annexin V staining is much more accurate than MTT assays because the latter is not indicative for apoptosis and therefore on the one hand may not cover all apoptotic effects of polymers.[345] Instead, MTT assay measures the metabolic activity of cells which on the other hand can be influenced by a number of factors nonrelated to polymer exposure.[344] By examining HEK 293T cells after 72 hour incubation with PeptoPlexes (same conditions as applied for determination of transfection efficiency), we ensured the absence of apoptotic effects of PeptoPlexes. Cellular toxicities of the polymer with the highest transfection efficiency and the one with the highest lysine content - **P3** and **P5** - were monitored by this method in a concentration dependent manner.

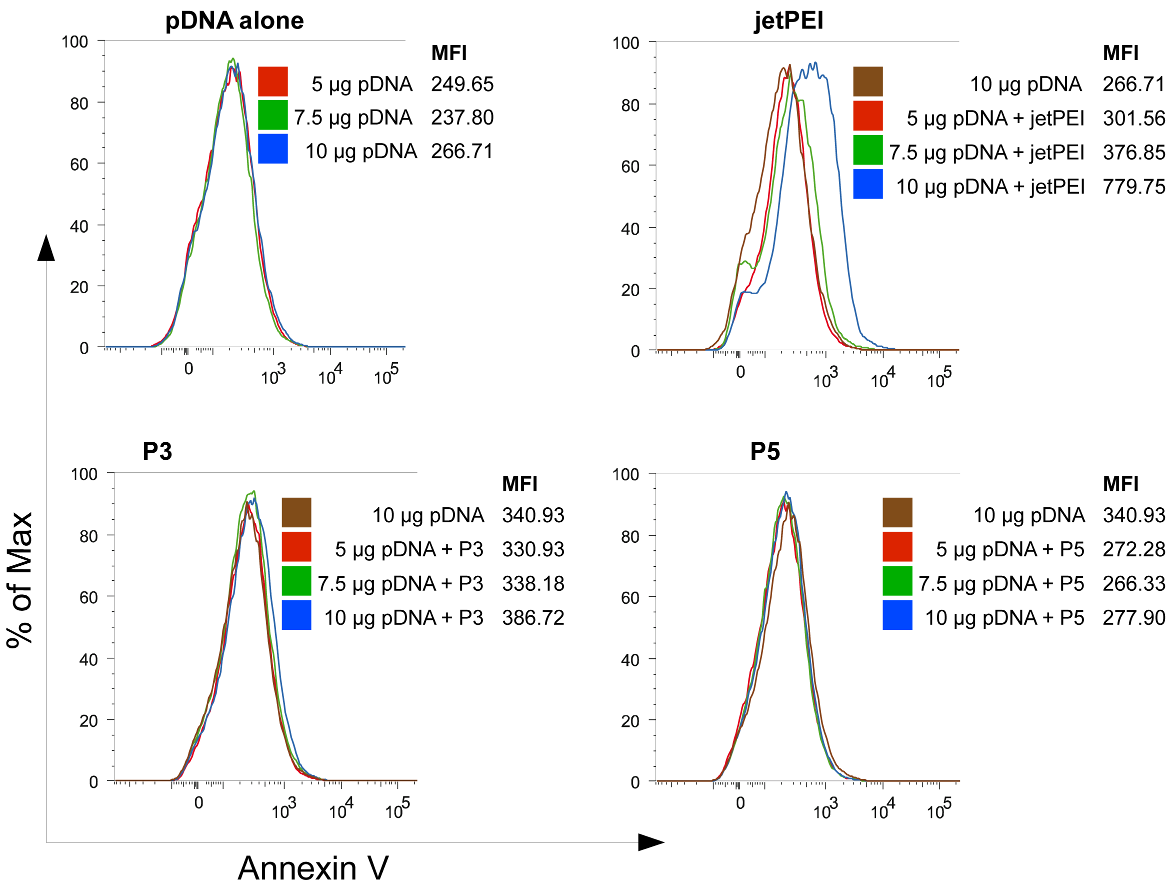

Figure 5.9: Representative histogramms of Annexin V-stained HEK 293T cells after 24 hours incubation with PeptoPlexes of **P3** or **P5**, polyplexes of jetPEI or plain pDNA and cultivation for another 48 h. Total amounts of pDNA and polymers were varied while keeping $m_{\text{PLys}}/m_{\text{pDNA}}$ ratios constant at 2.5:1. JetPEI was applied according to manufacturer's protocol.

Histogramms of Annexin V-stained HEK 293T cells incubated with varying amounts of PeptoPlexes show no observable shifts in fluorescence intensity even at highest amounts applied (Fig. figure 5.9). This means that cytotoxicity of PeptoPlexes does not increase when applying them in higher amounts but stays at the same low level as for untreated cells. In conclusion, increasing the total amount of PeptoPlexes does not compromise cell viability.

Table 5.3: Percentage of Annexin V positive HEK 293T cells after 24 hours incubation with PeptoPlexes of different PLys-block-PSar systems (m_{PLys}/m_{pDNA}=2.5/1) and cultivation for 48 hours.

TRANSFECTION REAGENT	M_{PDNA}/µg	ANNEXIN V POSITIVE CELLS/%
pDNA (negative control)	5	7.13
jetPEI (positive control)	5	9.42
jetPEI	7.5	18.43
jetPEI	10	34.88
P3	5	6.04
P3	7.5	6.87
P3	10	7.50
P5	5	6.53
P5	7.5	6.39
P5	10	7.39

Peptoplexes based on polymers **P3** and **P5** did not lead to a higher amount of Annexin V positive cells compared to the negative control. In contrast, jetPEI lead to detectable toxicity already at the lowest polyplex concentration. From 7.5 µg pDNA per well, jetPEI causes severe cellular toxicity. Consequently, in cases where biocompatibility of a transfection reagent has higher priority than sheer transfection efficiency PLys-b-PSar systems offer a potent alternative to reagents like jetPEI.

5.3 CONCLUSION

In this study, PLys-b-PSar systems with narrow molecular weight distributions and varying block lengths were synthesized. Both, carboxybenzyl and trifluoroacetate were successfully used as protecting groups for lysine. However, it was observed that TFA protecting groups are better compatible with block copolypeptide synthesis and deprotection. Depending on PLys block lengths, polypeptides were capable to form PeptoPlexes with pDNA, which we named PeptoPlexes.

PeptoPlexes could be successfully used for transfection of HEK 293T cells, as proven by luciferase as well as FACS-based assays. In general, transfection efficiencies determined by luciferase and FACS assays correlated well for most systems. Variations may be due to the limitations of the luciferase assay. The most effective PeptoPlexes were able to transfect around 35% of HEK 293T cells. In contrast to jetPEI, no cytotoxicity was detected at relevant PeptoPlex concentrations. These results are a promising first step with regard to future *in vivo* applications of PeptoPlexes in the context of gene therapy or DNA vaccines.

5.4 EXPERIMENTAL SECTION

5.4.1 Materials

DMF was purchased from VWR, dried over BaO and subsequently distilled *in vacuo* onto pre-dried molecular sieves (3Å). THF and hexane were purchased from Sigma-Aldrich and distilled from Na/K. Diethylether was distilled prior to use to remove the stabilizer. Other solvents were used as received. Diphosgene was purchased from Alfa Aesar and used as provided. Neopentylamine was purchased from TCI Europe, dried over NaOH and fractionally distilled. Sarcosine was purchased from Sigma-Aldrich, while all protected amino acids were purchased from ORPEGEN. Fluorescein isothiocyanate (FITC) was purchased from Sigma-Aldrich and purified by HPLC. EGFP coding DNA (pEGFP-N1) was purchased from Clontech (Mountain View, USA) and duplicated in *Escherichia Coli* Top 10 (Invitrogen). JetPEI transfection reagent was purchased from Polyplus-Transfection SA (Illkirch, France). Alexa Fluor 647-conjugated Annexin V was purchased from BioLegend (San Diego, USA). CellTiter 96 Non-Radioactive Cell Proliferation Assay kit (for MTT assay) was purchased from Promega (Madison, USA). Coelenterazine h (for luciferase assay) was purchased from Biotrend (Germany).

5.4.2 Instrumentation

5.4.2.1 *Polymer Characterization*

300 MHz ^{1}H-NMR spectra were recorded on a Bruker AC 300, 400 MHz ^{1}H-NMR spectra were recorded on a Bruker Avance-II 400. All spectra were recorded at room temperature and analyzed with ACDLabs 6.0 software. Degrees of polymerization as well as molecular weights were calculated by comparing the integral of the neopentylamine initiator peak either with the integrals of benzylic methylene protons of the protecting group (for PLys(Z)), with the integrals of the ε-protons (for PLys(TFA)), or with the average of integrals of methyl group and α-protons (for PSar) in the 400 MHz ^{1}H-NMR spectra. Attenuated total reflectance Fourier transformed infrared (ATR-FTIR) spectroscopy was performed on a FT/IR-4100 (JASCO Corporation) with an ATR sampling accessory (MIRacleTM, Pike Technologies). IR Spectra were analyzed using Spectra Manager 2.0 (JASCO Corporation).

Melting points were determined using a METTLER FP62 (METTLER WAAGEN GMBH).

Hexafluoroisopropanol (HFIP) gel permeation chromatography (GPC) was performed with HFIP containing 3 g/L potassium trifluoroacetate as eluent at 40 °C and a flow rate of 0.8 mL $\cdot$ min^{-1}. The columns were packed with modified silica (PFG columns; particle size: 7 µm, porosity: 100 & 1000 Å). Polymers were detected with a refractive index detector (G 1362A RID, JASCO) and a UV/Vis Detector (UV-2075 Plus, JASCO). Molecular weights were calculated using a calibration performed with PMMA standards (Polymer Standards Services GmbH) and toluene as internal standard. Elution diagrams were analyzed using the WinGPC UniChrome 8.00 (Build 994) software from Polymer Standards Services.

5.4.2.2 *Biological Experiments*

(3-(4,5-Dimethylthiazol-2-yl)-2,5-diphenyltetrazolium bromide (MTT) assay measurements were performed using a Dynex MRX TC Revelation microtiter plate reader (Dynex Technologies, Chantilly, VA).

Luciferase assay was carried out with a 96 well plate chemoluminescence reader (Centro LB 960; Berthold Technologies, Bad Wildbad, Germany) using Mikrowin 2000 software.

FACS experiments were executed on a FACS Canto II flow cytometer equipped with BD FACS Diva software (both from BD Biosciences, San Diego, CA). Data were analyzed using FlowJo software (FLOWJO, Ashland, OR).

Live cell images were acquired on an inverted confocal microscope TCS SP5 (Leica, Wetzlar, Germany) equiped with an oil-immersion objective (63 magnification; NA 1.4) and a laser set capable of 405 nm/488 nm/561 nm excitation. Images were recorded at 512 x

512 8-bit-pixel resolution with a pinhole of 130 μm and confocal plane depth of 1.0 μm, resulting in a total image size width and height of 246 μm.

Fluorescence images for visualization of eGFP expression were acquired on an inverted fluorescence microscope BX50 (Olympus, Hamburg, Germany) equipped with an oil-immersion objective (UPlanFl 60x/1.25 Oil Iris Ph3) and a mercury lamp with a filter set capable of excitation in red/green and UV range. Images were recorded at 2080 x 1544 3x12 bit resolution (ColorView II Camera; Soft Imaging System, Münster, Germany).

5.4.3 Methods and Protocols - Preparation of PeptoPlexes

5.4.3.1 *Synthesis of N-ε-Benzyloxycarbonyl-L-Lysine N-Carboxyanhydride*

The Synthesis was adapted from literature and modified.[375] In a three necked flask equipped with a reflux condenser and a septum, 15 g (53.5 mmol) of *N*-ε-Z-protected lysine were suspended in 300 mL of absolute THF under dry nitrogen atmosphere. The condenser outlet was connected to two gas washing bottles filled with aqueous NaOH, removing excess HCl and phosgene. Afterwards, 5.2 mL (42.8 mmol) of diphosgene were added slowly via syringe and the nitrogen stream was reduced. The solution was mildly refluxed yielding a yellowish clear solution after 2 hours of stirring. Overnight, a steady flow of dry nitrogen was lead through the solution into the gas washing bottles. The solvent was evaporated under reduced pressure and absolute THF was added to completely dissolve the crude reaction product. The solution was precipitated with absolute hexane and stored at 4 °C for 1 hour. The solid was collected by filtration under dry nitrogen atmosphere and washed with hexane. The crude reaction product was then recrystallized twice with absolute THF/Hexane. 14.3 g of purified reaction product (46.7 mmol; 87% yield; colorless needles) were transferred into a Schlenk tube and stored at -80 °C. Melting point: 101 °C (lit. 101 °C).[15]
^{1}H-NMR (300 MHz, DMSO-d$_6$): δ [ppm] = 9.09 (1H, s, -**NH**-CO-O-CO-), 7.40-7.25 (6H, m, -**C_6H_5** and -N**H**-CH_2), 5.01 (2H, s, -O-**CH_2**-C_6H_5), 4.43 (1H, t, ^{3}J H,H = 6.0 Hz, -CO-**CH**-CH_2-), 2.99 (2H, q, ^{3}J $_{H,H}$ = 6.3 Hz, -**CH_2**-NH-), 1.74-1.31 (6H, m, -CH-**CH_2-CH_2-CH_2**-CH_2-NH-).

5.4.3.2 *Synthesis of N-ε-Trifluoroacetyl-L-Lysine N-Carboxyanhydride*

12.5 g (51.6 mmol) of *N*-ε-trifluoroacetyl protected lysine and 300 mL of absolute THF were added into a three necked flask equipped with a reflux condenser and a septum under a steady flow of dry nitrogen. The condenser outlet was connected to two gas washing bottles filled with aqueous NaOH, removing excess HCl and phosgene. Then, 5.50 mL (45.6 mmol) of diphosgene were added slowly via syringe and the nitrogen stream was reduced. The colorless suspension was mildly refluxed for 2 hours, yielding a cloudy solution. After this, a steady flow of dry nitrogen was lead through the solution overnight. The solution was filtered under dry nitrogen atmosphere. The solvent was evaporated under reduced pressure and absolute THF was added to completely dissolve the crude reaction product. Excess absolute hexane was added to the solution. After 1 hour storage at 4 °C, the solid was collected by filtration under dry nitrogen atmosphere and washed with hexane. The crude product was recrystallized twice with absolute THF/Hexane. 10.43 g of the purified product (39,0 mmol; 75% yield; colorless needles, melting point: 101 °C (lit: 92 - 93 °C)[376]) were obtained and stored in a Schlenk tube at -80 °C.
^{1}H-NMR (300 MHz, DMSO-d$_6$): δ [ppm] = 9.40 (1H, s, -**NH**-CO-CF_3), 9.09 (1H, s, -**NH**-CO-O-CO-), 4.43 (1H, t, ^{3}J H,H = 6.3 Hz, -CO-**CH**-CH_2-), 3.17 (2H, q, ^{3}J H,H = 6.3 Hz, -**CH_2**-NH-), 1.79-1.61 (2H, m, -C$_H$-**CH_2**-CH_2-CH_2-CH_2-NH-), 1.53-1.46 (2H, quin, ^{3}J $_{H,H}$ = 7.13 Hz, -CH-CH_2-CH_2-**CH2**-CH_2-NH-), 1.42-1.24 (2H, m, -CH-CH_2-**CH_2**-CH_2-CH_2-NH-).

5.4.3.3 *Synthesis of Sarcosine N-Carboxyanhydride*

The Synthesis of sarcosine NCA was adapted from literature and modified.[121] 14.92 g (167.4 mmol) of sarcosine were weighed into a three neck flask and dried in vacuo for 1 hour. 300 mL of absolute THF were added under a steady flow of dry nitrogen and 16.2 mL (134 mmol) of diphosgene were added slowly via syringe and the nitrogen stream was reduced. The colorless suspension was mildly refluxed for 3 hours yielding a clear solution. Overnight, a steady flow of dry nitrogen was lead through the solution into two gas washing bottles filled with aqueous NaOH solution. The solvent was evaporated under reduced pressure, yielding a brownish oil as crude reaction product. The oil was heated to 50 °C and dried under reduced pressure (20 mbar, then <10^{-2} mbar for 2 h) to obtain an amorphous solid, free of phosgene and HCl. The crude product was redissolved in 40 mL of absoute THF and precipitated with 300 mL of dry hexane. The solution was cooled to -18 °C overnight to complete precipitation. The solid was filtered under dry nitrogen atmosphere and dried under a stream of dry nitrogen for 60 - 90 minutes and afterwards in high vacuum for 2 hours in a sublimation apparatus. The crude product was sublimated at 80 - 85 °C and <$1\text{x}10^{-2}$ mbar. The product was collected from the sublimation apparatus in a glove box on the same day. The 12.64 g of purified product (110 mmol, 65% yield, colorless crystallites) were stored in a Schlenk tube at -80 °C, only handled in a glove box and used up quickly. Melting point: 102 - 104 °C (lit: 102 - 105 °C).[15, 368]
^{1}H-NMR (300 MHz, $CDCl_3$): δ [ppm] = 4.22 (2H, s, –N(CH_3)-**CH_2**-CO-), 2.86 (3H, s, -CH_3).

5.4.3.4 *Synthesis of Poly(N-ε-Benzyloxycarbonyl-L-Lysine$_n$)*

Under nitrogen counter flow, n eq of lysine(Z) NCA were transferred into a pre-dried Schlenk tube equipped with a stir bar and dried in high vacuum for 1 hour. Then, lysine(Z) NCA was dissolved in absolute DMF. 2 eq of neopentylamine were added to 2 mL of dry DMF in a glass vial flooded with nitrogen and mixed. For initiation, 1 mL of the prepared stock solution was directly added to the Schlenk tube via syringe (yielding a reaction solution with 100 mg/mL monomer concentration). The solution was stirred at room temperature and kept at a constant pressure of 0.25 bar of dry nitrogen via the Schlenk line to prevent impurities from entering the reaction vessel while allowing CO_2 to escape. Completion of the reaction was confirmed by IR spectroscopy (disappearance of the NCA peaks (1853 and 1786 cm^{-1})). Directly after completion of the reaction the polymer was precipitated to cold ether and centrifuged (4500 rpm at 4 °C for 15 min). After discarding the liquid fraction, new ether was added and the polymer was resuspended using a sonic bath. The suspension was centrifuged again and the procedure was repeated. After DMF removal by the resuspension steps, the polymer was dissolved in dioxane and lyophilized, obtaining a stiff, porous mass of polymer. For different chain lengths yields ranged from 73 to 82%.
^{1}H-NMR of PLys(Z)$_{32}$ (400 MHz, DMSO–d_6): δ [ppm] = 8.50-7.70 (23H (1n), br, -**NH**-CO-CH-), 7.50-7.00 (184H (5n), br, -C_6H_5), 5.20-4.70 (63H (2n), br, -O-**CH_2**-C_6H_5), 4.35-3.60 (28H (1n), br, -CO-**CH**-NH), 3.20-2.70 (63H (2n), br, -**CH_2**-NH-), 2.30-0.90 (182H (6n), br, -CH-**CH_2-CH_2-CH_2**-CH_2-NH_2), 0.82 (9H, d, $^3J_{H,H}$ =12.5 Hz, (**CH_3**)$_3$-C-).

5.4.3.5 *Synthesis of Poly(N-ε-Trifluoroacetyl-L-Lysine$_n$)*

The synthesis of PLys(TFA) homopolymers was carried out similar to PLys(Z). However, as PLys(TFA) precipitates slowly in ether, the precipitation step was done overnight at 4°C. After centrifugation the liquid fraction was discarded and the precipitate dissolved in MeOH, diluted 1:5 with Millipore water and instantly lyophilized, obtaining a fluffy colorless powder. Yields ranged from 62 to 81%.

^{1}H-NMR of PLys(TFA)$_{29}$ (400 MHz, DMSO-d$_6$): δ [ppm] = 9.65-9.15 (29H (1n), br, -**NH**-CO-CF$_3$), 8.84-7.11 (27H (1n), br, -**NH**-CO-CH-), 4.48-3.55 (28H (1n), br, -CO-**CH**-NH-), 3.22-2.99 (58H (2n), br, -**CH$_2$**-NH-), 2.19 -1.01 (172H (6n), br, -CH-**CH$_2$-CH$_2$-CH$_2$**-CH$_2$-NH-) 0.83 (9H (1n), d, $^3J_{H,H}$ =8.4 Hz, (**CH$_3$**)$_3$-C-).

5.4.3.6 *Synthesis of Poly(N-ε-Benzyloxycarbonyl-L-Lysine$_n$-block-Sarcosine$_m$)*

1 eq of previously prepared PLys(Z) was transferred into a pre-dried Schlenk tube equipped with a stir bar, dried in high vacuum for 1 hour and then dissolved in abs. DMF. After 1 hour, m eq of sarcosine NCA were dissolved in absolute DMF and added to PLys(Z) via syringe (yielding a reaction solution with 100 mg/mL monomer concentration). The solution was stirred at room temperature and kept at a constant pressure of 0.25 bar of dry nitrogen via the Schlenk line to prevent impurities from entering the reaction vessel while allowing CO_2 to escape. Completion of the reaction was confirmed by IR spectroscopy (disappearance of the NCA peaks (1853 and 1786 cm^{-1})). Directly after completion of the reaction, the polymer was precipitated to cold ether and centrifuged (4500 rpm at 4°C for 15 min). After discarding the liquid fraction, new ether was added and the polymer was resuspended using a sonic bath. The suspension was centrifuged again and the procedure was repeated. After DMF was removed by the resuspension steps the polymer was dissolved in Millipore water and lyophilized, obtaining a fluffy powder. For different chain lengths and scales (100 - 1000 mg), yields ranged from 70 to 95%.
^{1}H-NMR of PLys(Z)$_{32}$-block-PSar$_{171}$ (400 MHz, DMSO-d$_6$): δ [ppm] = 8.40-7.64 (8H, br, -**NH**-CO-CH-), 7.60-6.63 (174H (6m), br, -C$_6$H$_5$ and -CH$_2$-**NH**-CO-O-), 5.08-4.83 (57H (2m), br, -O-**CH$_2$**-C$_6$H$_5$), 4.66-3.60 (354H (1m+2n), br, -CO-**CH**-NH and –N(CH$_3$)-**CH$_2$**-CO-), 3.14-2.57 (567H (3n+2m), br, -NCH$_3$ and -**CH$_2$**-NH-), 2.16-0.94 (160H (6m), br, -CH-**CH$_2$-CH$_2$-CH$_2$**-CH$_2$-NH-), 0.82 (9H, d, $^3J_{H,H}$ =12.86 Hz (**CH$_3$**)$_3$-C-).

5.4.3.7 *Synthesis of Poly(N-ε-Trifluoroacteyl-L-Lysine$_n$-block-Sarcosine$_m$)*

The synthesis of PLys(TFA)-block-PSar was carried out under the same conditions reported for PLys(Z)-b-PSar.
^{1}H-NMR of PLys(TFA)$_{49}$-block-PSar$_{212}$ (400 MHz, DMSO-d$_6$): δ [ppm] = 9.60-9.10 (50H (1n), br, -**NH**-CO-CF$_3$), 8.75-7.10 (44H (1n), br, -**NH**-CO-CH2-), 4.65-3.60 (468H (1n+2m), br, -CO-**CH**-NH and -NCH$_3$-**CH$_2$**-CO-), 3.22-3.05 (98H (2n), br, -**CH$_2$**-NH-CO-CF$_3$), 3.02-2.65 (648H (3m), br, -NCH$_3$), 2.15-1.02 (278H (6n), br, -CH-**CH$_2$-CH$_2$-CH$_2$**-CH$_2$-NH-), 0.83 (9 H, br, (**CH$_3$**)$_3$-C-).

5.4.3.8 *Deprotection of Poly(N-ε-Benzyloxycarbonyl-L-Lysine$_n$-block-Sarcosine$_m$) with HBr/ TFA*

In a round bottomed flask, the polymer was dissolved in TFA at a concentration of 30 mg/mL and the desired amount of eq (1.05 to 4.0 fold excess with regard to the (Z)-group) of HBr in acetic acid (33% w/w) were added with an Eppendorf pipette. The solution was stirred for 12 hours, diluted with Millipore water and neutralized with $NaHCO_3$. The solution was dialyzed with a Spectra/Por (Roth) membrane with a nominal molecular weight cut-off (NMWCO) of 3500 g/mol for 3 - 5 days with regular substitution of water and then lyophilized to yield the deprotected polymer as a fluffy, colorless powder. Yields ranged from 32% (4 eq) - 90% (1.05 eq). ^{1}H-NMR is provided for PLys(Z)$_{32}$-block-PSar$_{171}$ deprotected with 1.05 eq of HBr for 12 hours.
^{1}H-NMR (400 MHz, D$_2$O) δ [ppm] = 7.40-7.08 (26H (6n), br, -C$_6$H$_5$), 5.05-4.85 (8H (2n), br, -O-**CH$_2$**-C$_6$H$_5$), 4.60-3.73 (364H (1n+2m), br, -CO-**CH**-NH and -NCH$_3$-**CH$_2$**-CO-), 3.22-2.46

(578H (2n+3m), br, -**CH**$_2$-NH$_2$, NCH$_3$), 1.85-0.95 (202H (6n), br, -CH-**CH$_2$-CH$_2$-CH$_2$**-CH$_2$-NH-), 0.75 (9 H, br, (**CH$_3$**)$_3$-C-).

5.4.3.9 *Deprotection of Poly(N-ε-Trifluoroacteyl-L-Lysine$_n$-block-Sarcosine$_m$)*

In a round bottomed flask, the polymer was dissolved in MeOH at a concentration of 30-50 mg/mL and 10 eq of Hydrazine-hydrate (with regard to the (TFA)-group) were added with an Eppendorf pipette. The solution was stirred for 72 hours and diluted with Millipore water. Afterwards, the solution was dialyzed with a Spectra/Por (Roth) membrane with a nominal molecular weight cut-off (NMWCO) of 3500 g/mol for 3-5 days with regular substitution of water and then lyophilized to yield the deprotected polymer as a fluffy, colorless powder. Yields ranged from 75-87%. ^{1}H-NMR is provided for PLys$_{61}$-block-PSar$_{282}$.
^{1}H-NMR (400 MHz, D$_2$O) δ [ppm] = 4.45-3.90 (550H (1n+2m), br, -CO-**CH**-NH- and -NCH$_3$-**CH$_2$**-CO-), 3.15-2.55 (870H (2n+3m), br, -**CH$_2$**-NH$_2$ and NCH$_3$), 1.85-1.00 (306H (6n), br, -CH-**CH$_2$-CH$_2$-CH$_2$**-CH$_2$-NH), 0.73 (9H, s, (**CH$_3$**)$_3$-C-).

5.4.3.10 *Labeling of Block Copolypeptides with Fluorescein Isothiocyanate*

10.0 mg of polymer were dissolved in 1.5 mL DMSO and 3 eq (with regard to the terminal amino group) of fluorescein isothiocyanate (FITC) were added. The solution was stirred for 72 h at 80 °C. Afterwards, labeled block copolypeptides were separated from excess dye by SEC using water as eluent.

5.4.3.11 *Formation of PeptoPlexes*

Block copolymers were dissolved in sterile water to obtain solutions with final concentrations of 1 µg/µL. PeptoPlex solutions were prepared by dilution of the desired amount of plasmid DNA in 10 mM TRIS HCl buffer and subsequent addition of polymer at amounts indicated. The obtained PeptoPlex solutions were mixed by frequent pipetting and were allowed to stand overnight at room temperature. The final volume of the PeptoPlex solutions totaled up to 12 µL for gel electrophoresis, 20 µL for luciferase and MTT assay and 200 µL for FACS analysis. Polyplex solutions of jetPEI (Polyplus-transfection SA, Illkirch, France) and plasmid DNA were prepared according to manufacturer's protocol.

5.4.4 Methods and Protocols - Physicochemical Characterization of PeptoPlexes

5.4.4.1 *Characterization of PeptoPlexes by Agarose Gel Electrophoresis*

Gel electrophoresis was performed to monitor polyplex formation. For this, 500 ng of plasmid DNA and the desired amount of polymer were premixed as indicated above and were loaded into slots of 0.7% agarose gels (90 V, 150 mA). GelRed was used for pDNA and PeptoPlex staining.

5.4.4.2 *Characterization of PeptoPlexes by Dynamic Light Scattering Experiment*

Solutions of PeptoPlexes with 10 µg pDNA and varying amounts of polymer (depending on applied polymer and m_{PLys}/m_{pDNA} ratio) in TRIS HCl buffer were prepared. After transfer to a dust free flow box, all samples were filtered (Millex HV 0.45µm) into dust free cylindrical scattering cells (Suprasil, 20 mm diameter, Hellma, Mühlheim, Germany). Dynamic light scattering measurements (DLS) were performed using a Uniphase He/Ne Laser (l=632.8 nm, 22 mW), a ALV-SP125 Goniometer, a ALV/High QE APD-Avalanche photo-diode with fibre optical detection, a ALV 5000/E/PCI-correlator and a Lauda RC-6 thermostat unit at 20 °C. Angular dependent measurements of typically 15° steps were carried out in the range $30° \leq q \leq 150°$. For data evaluation experimental intensity correlation functions were transformed into amplitude correlation functions applying the Siegert relation extended to include negative values after baseline subtraction by calculation $g_1(t) = SIGN(G2(t)) \cdot SQRT(ABS((G2(t) - A)/A)$. All field correlation functions usually showed monomodal decay and were fitted by a sum of two exponentials $g1(t) = a \cdot exp(-t/b) + c \cdot exp(-t/d)$ to take polydispersity into account. Average apparent diffusion coefficients D_{app} were calculated by applying $q^2 \cdot D_{app} = (a \cdot b - 1 + c \cdot d - 1)/(a + c)$ resulting in an angular-dependent diffusion coefficient D_{app} or reciprocal hydrodynamic radius $\langle 1/R_h \rangle_{app}$, according to formal application of Stokes Einstein law. By extrapolation of $\langle 1/R_h \rangle_{app}$ to $q = 0$ z-average hydrodynamic radii $R_h = \langle 1/R_h \rangle_{z^{-1}}$ were obtained (uncorrected for *c*-dependency).

5.4.5 Methods and Protocols - Biological Characterization of PeptoPlexes

5.4.5.1 *Cell Culture*

HEK 293T cells were grown in DMEM, supplemented with 10% FBS, 4 mM L-glutamine, 0.1 µM 2-mercaptoethanol, 100 units x mL^{-1} penicillin, and 100 µg x mL^{-1} streptomycin. Cells were maintained in a 37 °C humidified atmosphere with 5% CO_2 and were handled under sterile conditions.

5.4.5.2 *Determination of Cellular Toxicity of PeptoPlexes in HEK 293T Cells by MTT Assay*

Cytotoxicity of PeptoPlexes was assessed by MTT assay using the "CellTiter 96® Non-Radioactive Cell Proliferation Assay" kit (Promega, Madison, USA) according to manufacturer's protocol. On day 1, HEK 293T cells were seeded onto 96-well culture plates at a concentration of 1.5 x 10^4 cells per 100 µL per well. Medium was changed after 3 hours. On the following day, cells were incubated in triplicates with plain pDNA (0.5 µg per well) or PeptoPlexes (formed with 0.5 µg pDNA and the desired amounts of polymers, respectively) as indicated. On day 3, 30 µL of MTT substrate solution were added to each well, and cells were cultured for another 4 h. Subsequently, 100 µL of mixed solubilization/stop solution were added to each well. After 1 h, the absorbance at 570 nm was measured.

5.4.5.3 *Determination of Cellular Toxicity of PeptoPlexes in HEK 293T Cells by Flow Cytometry*

To assess apoptotic effects on single cell level, HEK 293T cells were seeded onto wells of 12 well cell culture plates (each 1.5 x 10^5 cells in 1 mL). On the following day, pDNA (5 µg per well) or PeptoPlexes (formed with 5 µg pDNA and the desired amounts of polymers, respectively) were added as indicated. After another 3 days, cells were harvested (PBS/2mM EDTA). Cells were resuspended in HBSS buffer and were coincubated with Alexa Fluor 647-conjugated Annexin V to identify apoptotic cells, and 7-AAD to gate out necrotic cells. Both agents were purchased from BioLegend (San Diego, CA). Samples were analyzed by flow cytometry using a FACS Canto II flow cytometer equipped with BD FACS Diva software (both from BD Biosciences, San Diego, CA). Data were analyzed using FlowJo software (FLOWJO, Ashland, OR).

5.4.5.4 *Quantitative Assessment of Transfection Efficiencies in HEK 293T Cells*

For quantiative detection of transfection efficiencies, a reporter vector encoding *Renilla reniformis* luciferase under control of the human EF1a gene promoter (pRL-EF1a; Bros *et al.*,

2003) was used. HEK 293T cells were seeded onto wells of a 96 well cell culture plate (each 1.5 x 10^4 cells in 100 µL). Medium was changed after 3 hours. On the following day, cells were incubated in triplicates with naked pDNA (0.5 µg per well) or PeptoPlexes (formed with 0.5 µg pDNA and the desired amounts of polymers, respectively) as indicated. Medium was changed the next day. 24 h after the onset of transfection, medium was removed and cells were lyzed (Renilla luciferase assay lysis buffer; Promega, Heidelberg, Germany). Lysates were assayed for *Renilla* luciferase activities. Bioluminescence was determined according to the following procedure: addition of 100 µL substrate solution per well, 3 s equilibration, 10 s measurement.

5.4.5.5 *Determination of Transfection Efficiency of PeptoPlexes in HEK 293T Cells by Flow Cytometry*

To assess transfection efficiencies on single cell level, an eGFP-coding reporter vector (pEGFP-N1; Clontech, Mountain View, CA) was used. For this, HEK 293T cells were seeded onto wells of 12 well cell culture plates (each 1.5 x 10^5 cells in 1 mL). One day later, culture medium was changed and cells were incubated with naked pDNA (5 µg per well) or PeptoPlexes (formed with 5 µg pDNA and the desired amounts of polymers, respectively) as indicated. The following day, medium was replenished. Three days after the onset of transfection, cells were harvested (PBS/2 mM EDTA), and samples were analyzed by flow cytometry (see above) for frequencies of eGFP positive cells.

5.4.5.6 *Confocal Microscopy Studies in HEK 293T Cells*

Cells were seeded on µ-slide (chambered coverslip) with 8 wells from Ibidi at a density of 2 x 10^5 cell/mL. After 24 h of incubation at 37 °C, the medium was removed, replaced with OptiMEM and cells were treated with PeptoPlex solution. Afterwards the 8-well plate was moved to the confocal microscope equipped with a live cell unit. Images were captured with a confocal Leica microscope.

ACKNOWLEDGEMENTS

The authors would like to thank Prof. Rudolf Zentel and Prof. Manfred Schmidt for stimulating discussions and scientific advice. Furthermore, the authors would like to thank Dr. Jiajia Zhou and Prof. Friederike Schmid for VMD simulations and theoretical insights. Support by the Microscopy Core Facility of the Institute of Molecular Biology (IMB) Mainz is gratefully acknowledged. Furthermore, the authors would like to acknowledge funding from DFG 1066-1, COMATT and the NMFZ Mainz.

5.5 SUPPORTING INFORMATION

5.5.1 NMR Spectra

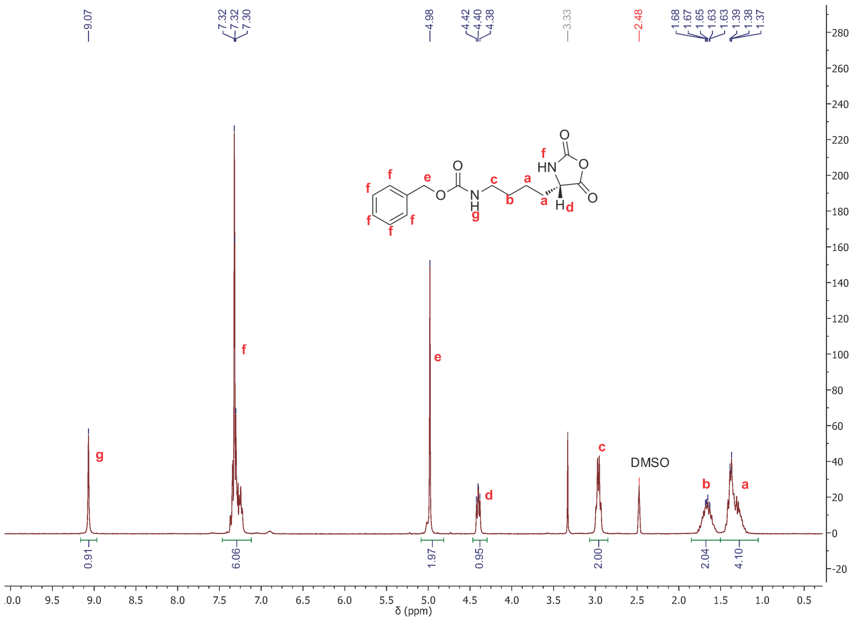

Figure 5.10: ^{1}H-NMR spectrum of *N*-ε-benzyloxycarbonyl-L-lysine *N*-carboxyanhydride.

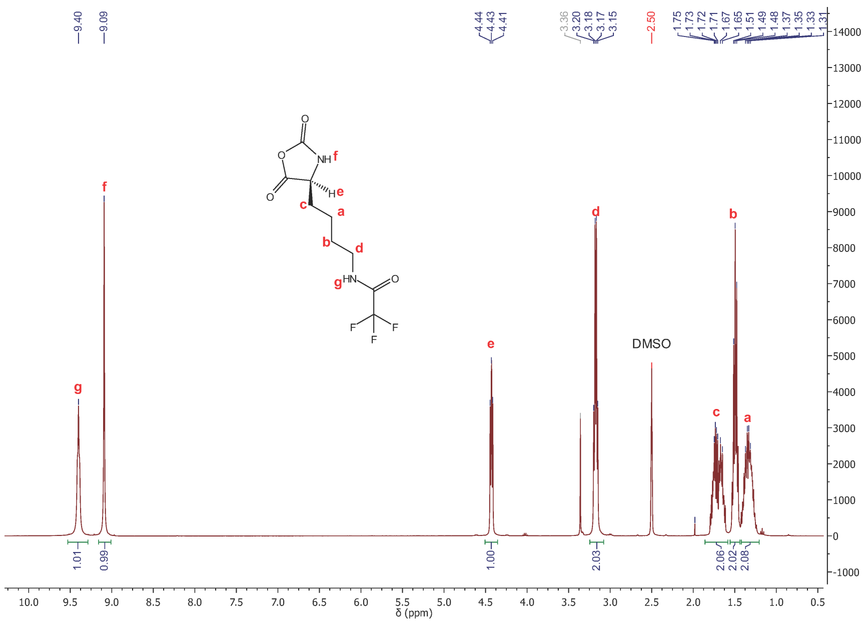

Figure 5.11: ^{1}H-NMR spectrum of *N*-ε-trifluoroacetyl-L-lysine *N*-carboxyanhydride.

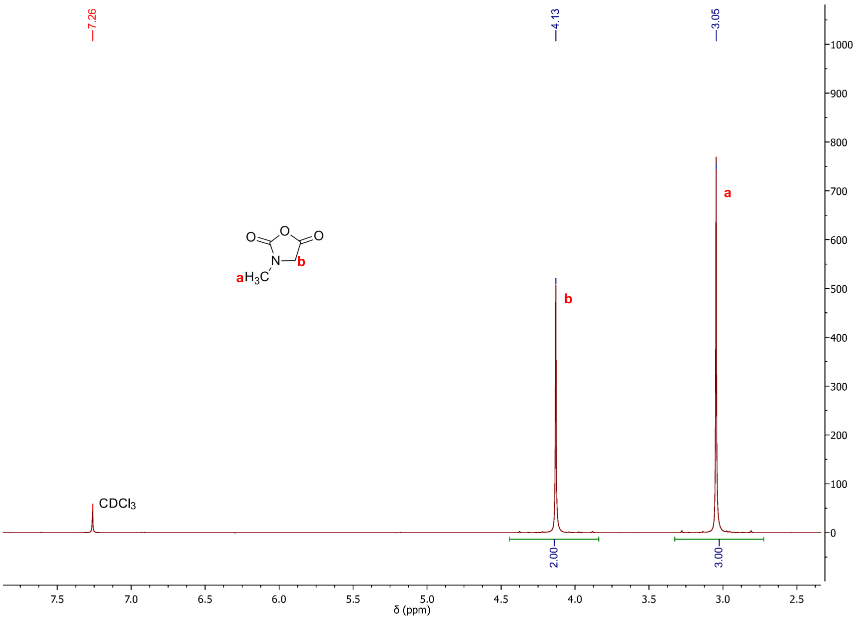

Figure 5.12: ^{1}H-NMR spectrum of sarcosine *N*-carboxyanhydride.

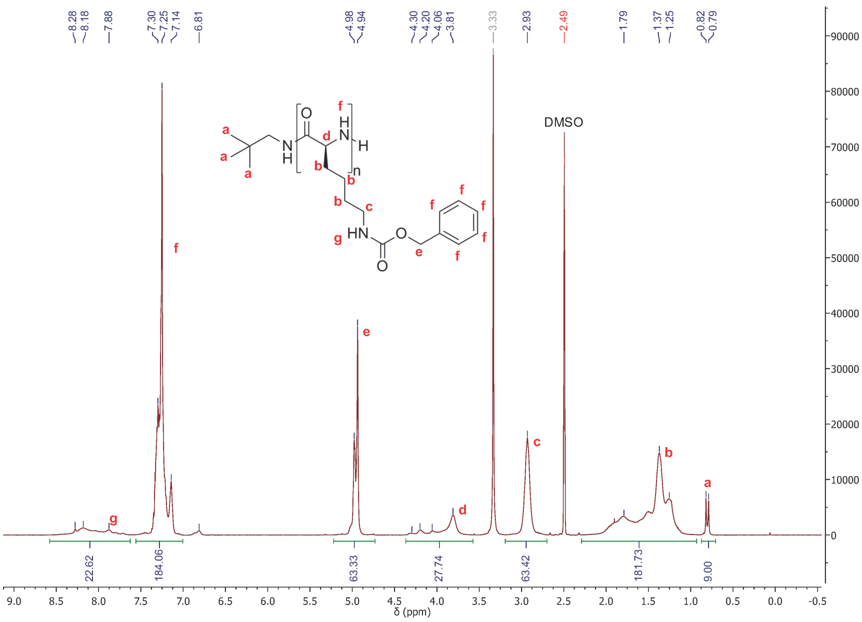

Figure 5.13: ^{1}H-NMR spectrum of PLys(Z)$_n$.

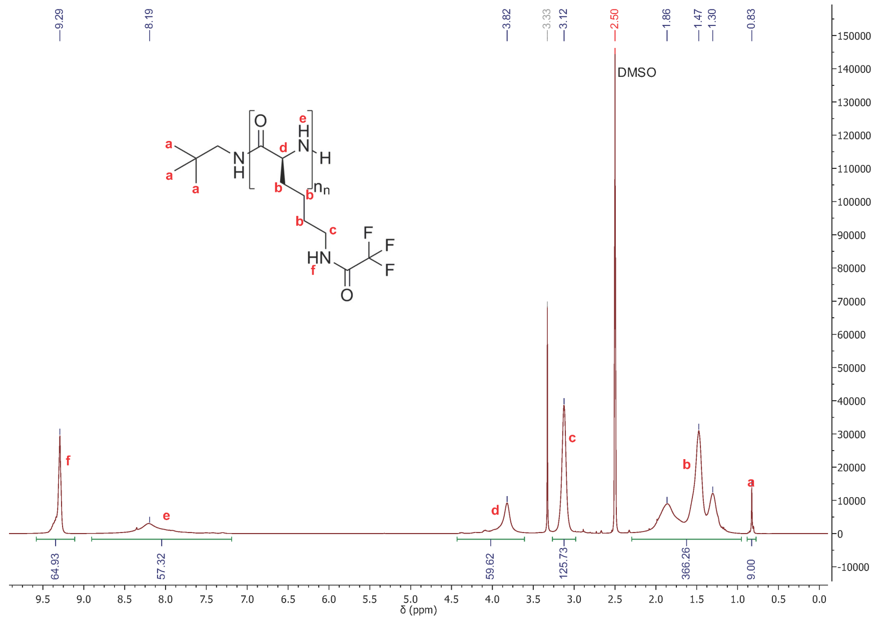

Figure 5.14: ^{1}H-NMR spectrum of PLys(TFA)$_n$.

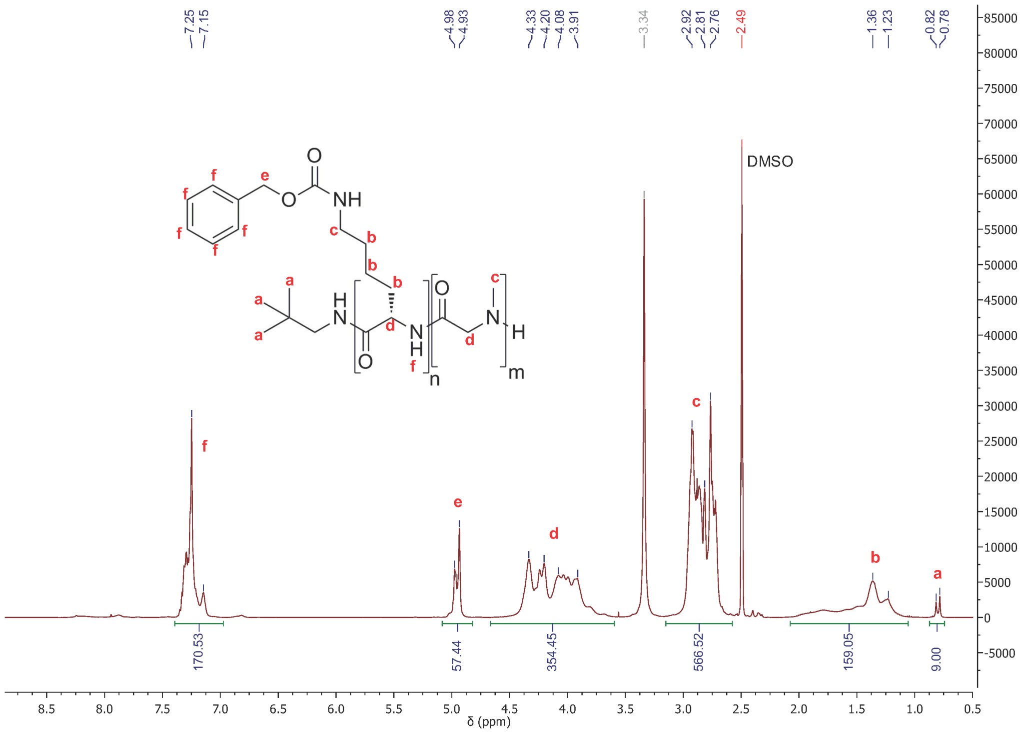

Figure 5.15: ^{1}H-NMR spectrum of PLys(Z)$_n$-b-PSar$_m$.

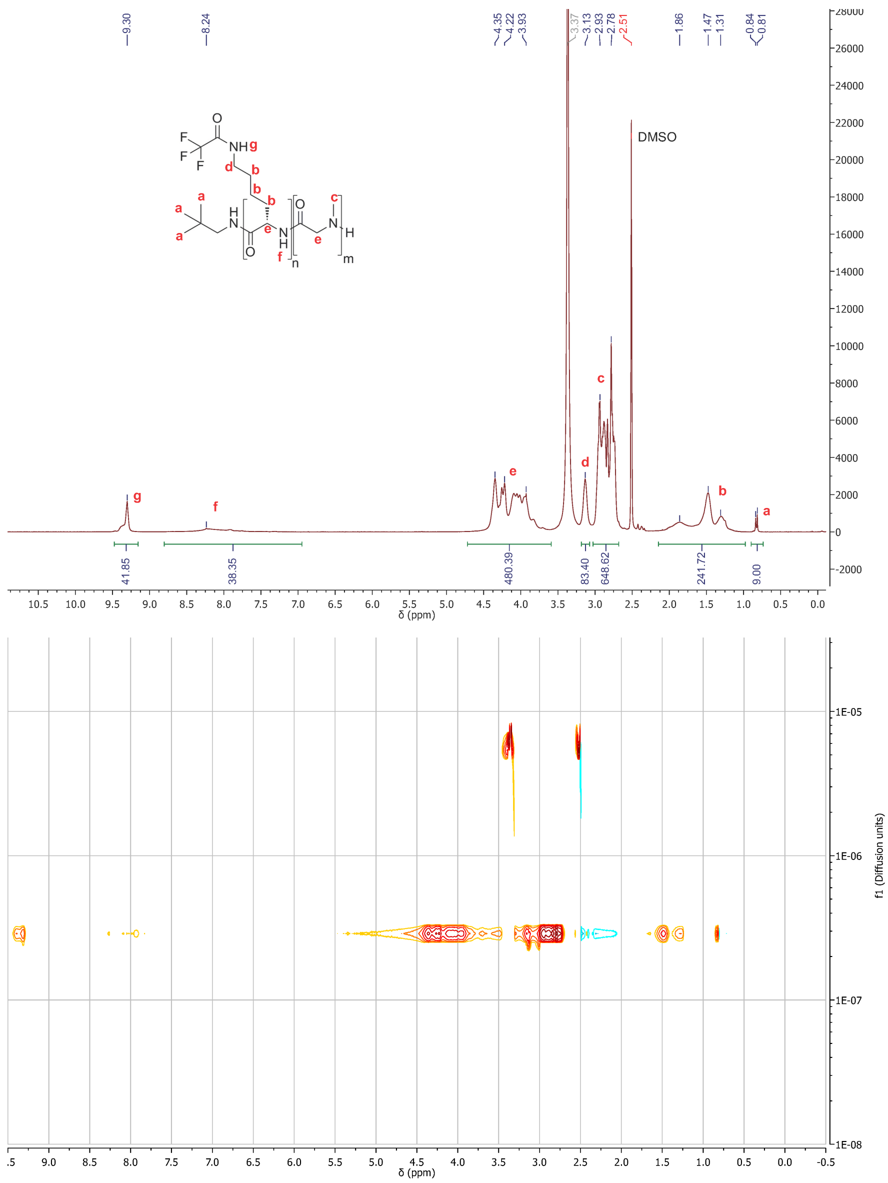

Figure 5.16: ^{1}H-NMR and DOSY NMR spectra of $PLys(TFA)_n$-b-$PSar_m$.

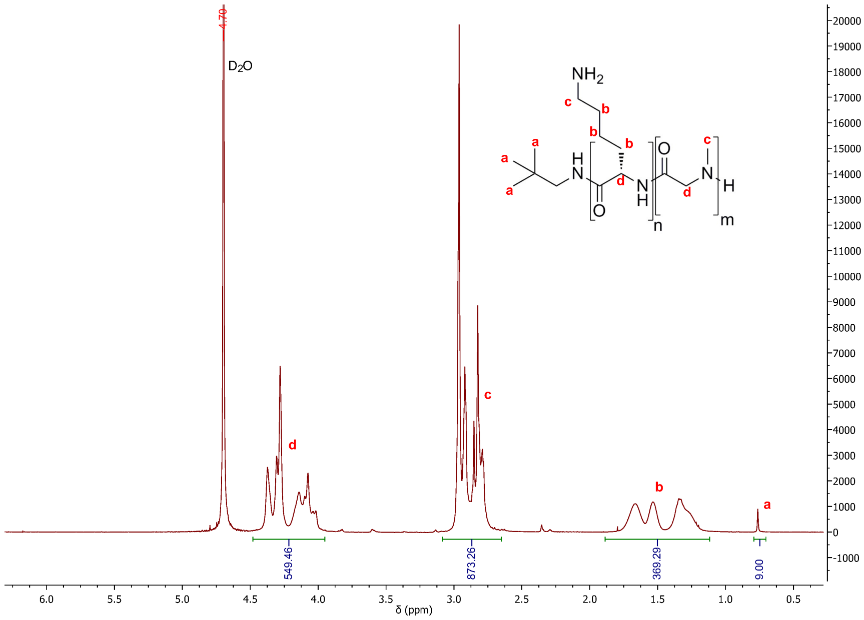

Figure 5.17: ^{1}H-NMR spectrum of $PLys_n$-b-$PSar_m$.

5.5.2 Multi Angle Dynamic Light Scattering

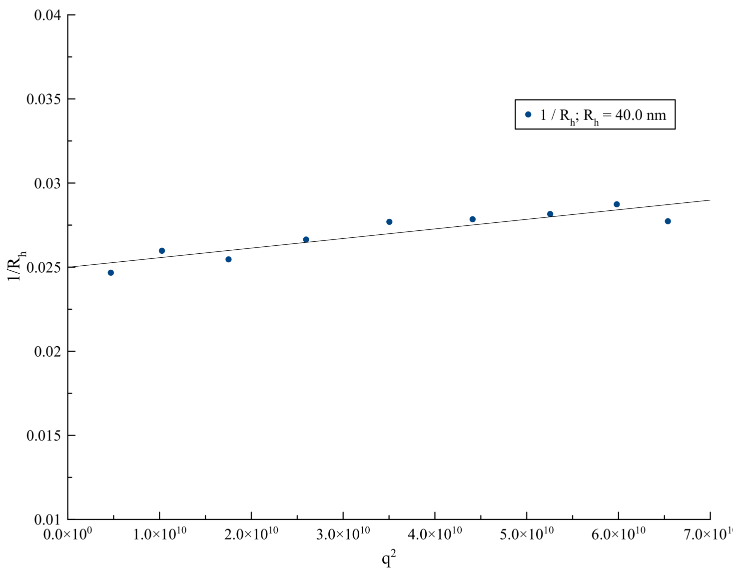

Figure 5.18: DLS angle dependency of $\langle R_h \rangle$ (raw data points and coresponding linear fit) of PeptoPlexes based on eGFP-N1 and P3. PeptoPlexes were applied using constant m_{PLys}/m_{pDNA} ratio of 2.5/1 and 10 µg pDNA in 3 mL of 10 mM Tris buffer.

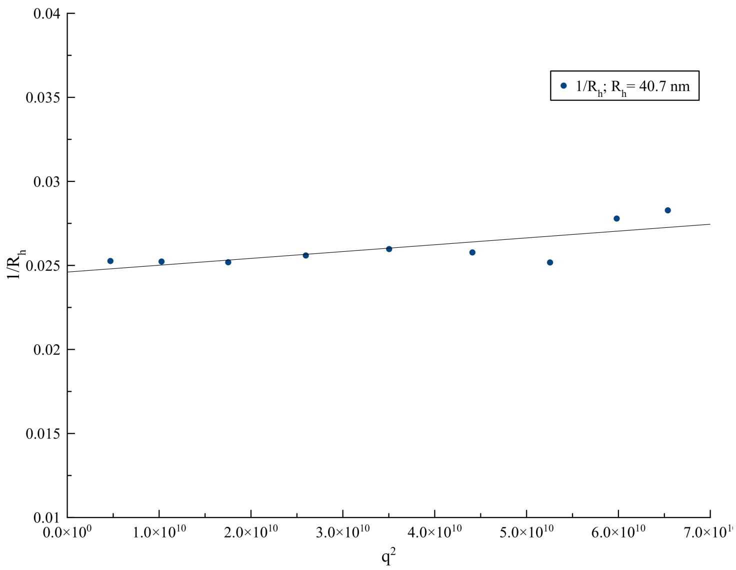

Figure 5.19: DLS angle dependency of $\langle R_h \rangle$ (raw data points and coresponding linear fit) of PeptoPlexes based on eGFP-N1 and P4. PeptoPlexes were applied using constant m_{PLys}/m_{pDNA} ratio of 2.5/1 and 10 µg pDNA in 3 mL of 10 mM Tris buffer.

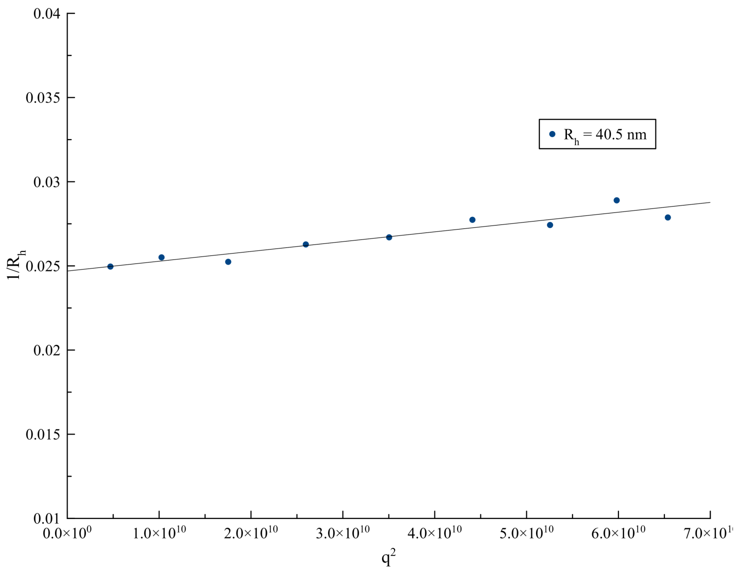

Figure 5.20: DLS angle dependency of $\langle R_h \rangle$ (raw data points and coresponding linear fit) of PeptoPlexes based on eGFP-N1 and P5. PeptoPlexes were applied using constant m_{PLys}/m_{pDNA} ratio of 2.5/1 and 10 µg pDNA in 3 mL of 10 mM Tris buffer.

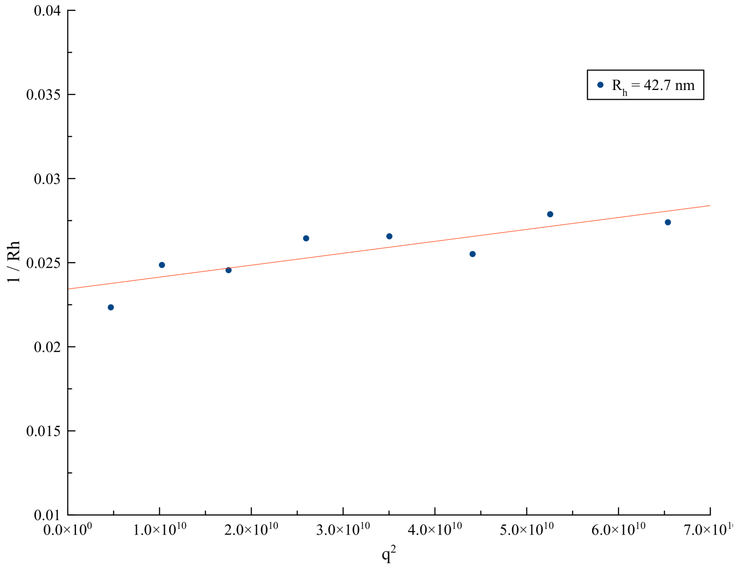

Figure 5.21: DLS angle dependency of $\langle R_h \rangle$ (raw data points and coresponding linear fit) of PeptoPlexes based on eGFP-N1 and P6. PeptoPlexes were applied using constant m_{PLys}/m_{pDNA} ratio of 2.5/1 and 10 µg pDNA in 3 mL of 10 mM Tris buffer.

5.5.3 MTT Assay

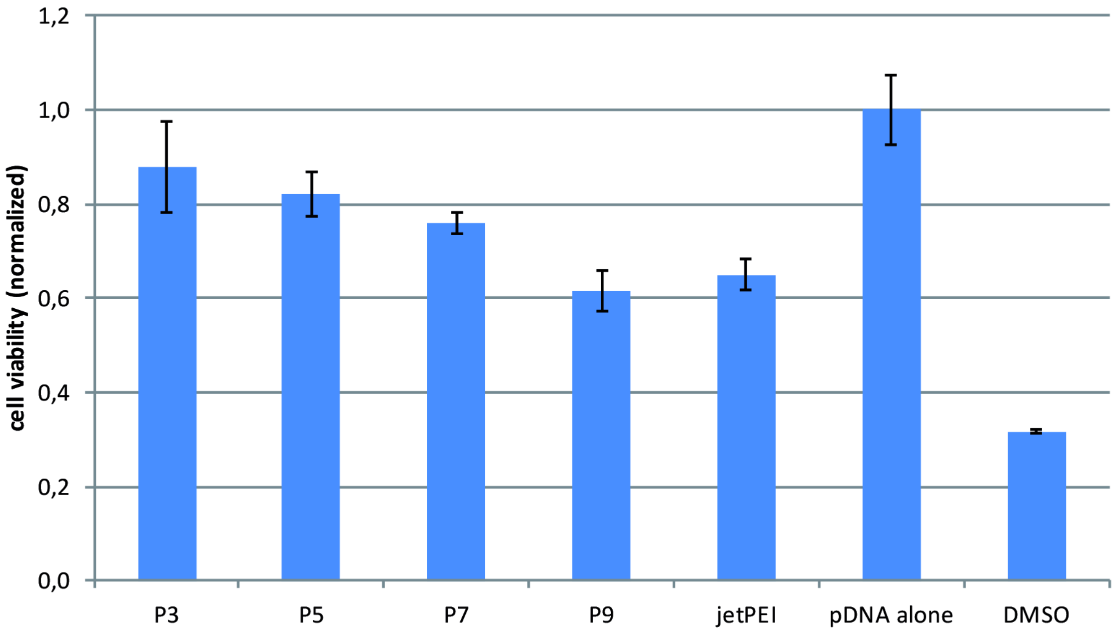

Figure 5.22: Normalized viability of HEK 293T cells after 24 hours incubation with Peptoplexes of different PLys-block-PSar systems. All peptoplexes were applied using constant m_{PLys}/m_{pDNA} ratio of 2.5/1 and 0.5 µg pDNA per well. JetPEI was used according to manufacturer's protocol. DMSO and plain pDNA function as controls, n = 3.

5.5.4 FACS

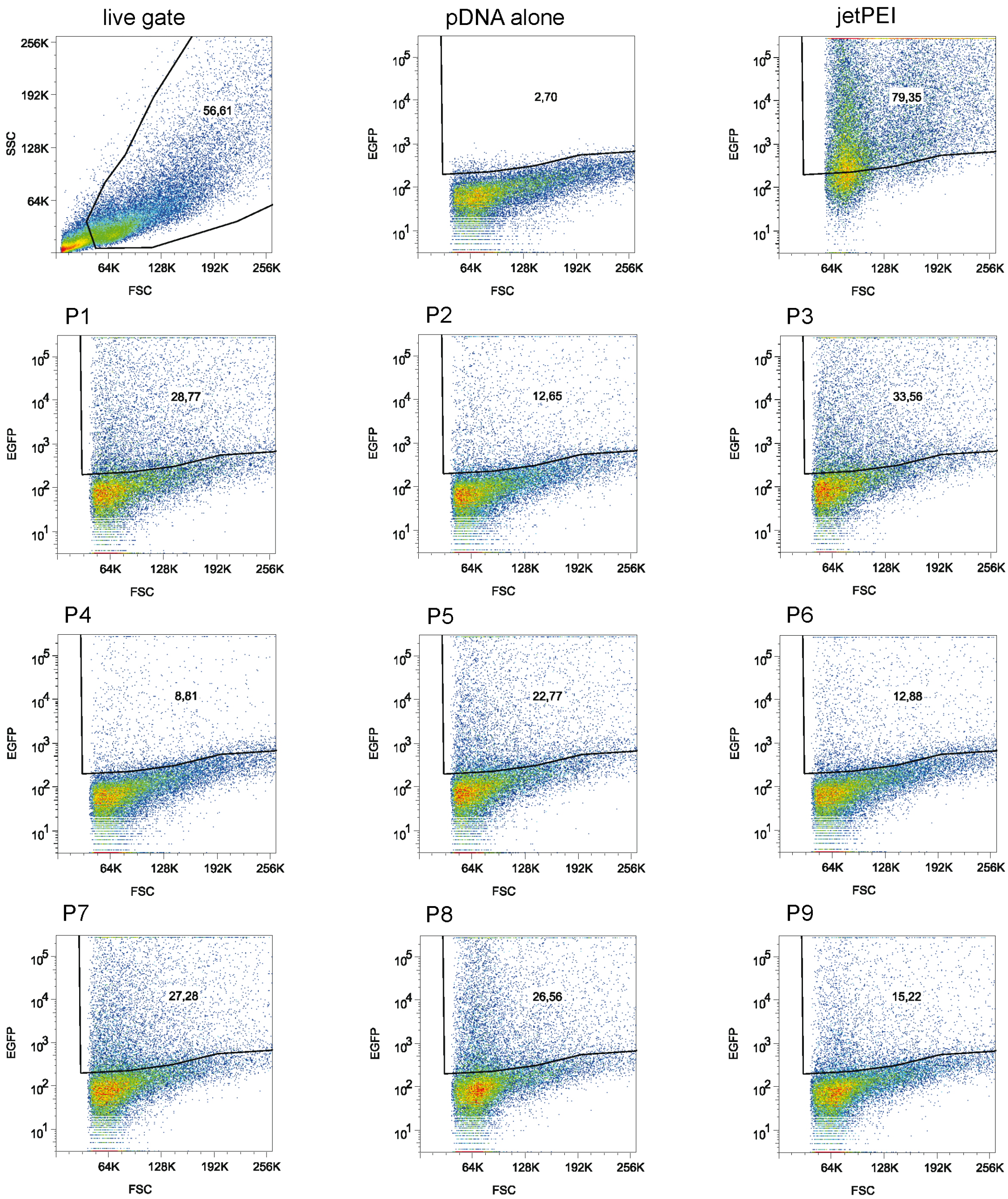

Figure 5.23: Dotplots showing HEK 293T cells after 24 h incubation with PeptoPlexes of different PLys-block-PSar systems and cultivation for 48 h. m_{PLys}/m_{pDNA} ratios were set at 2.5/1, mpDNA was kept at 5 µg per well. Plain pDNA functions as control.

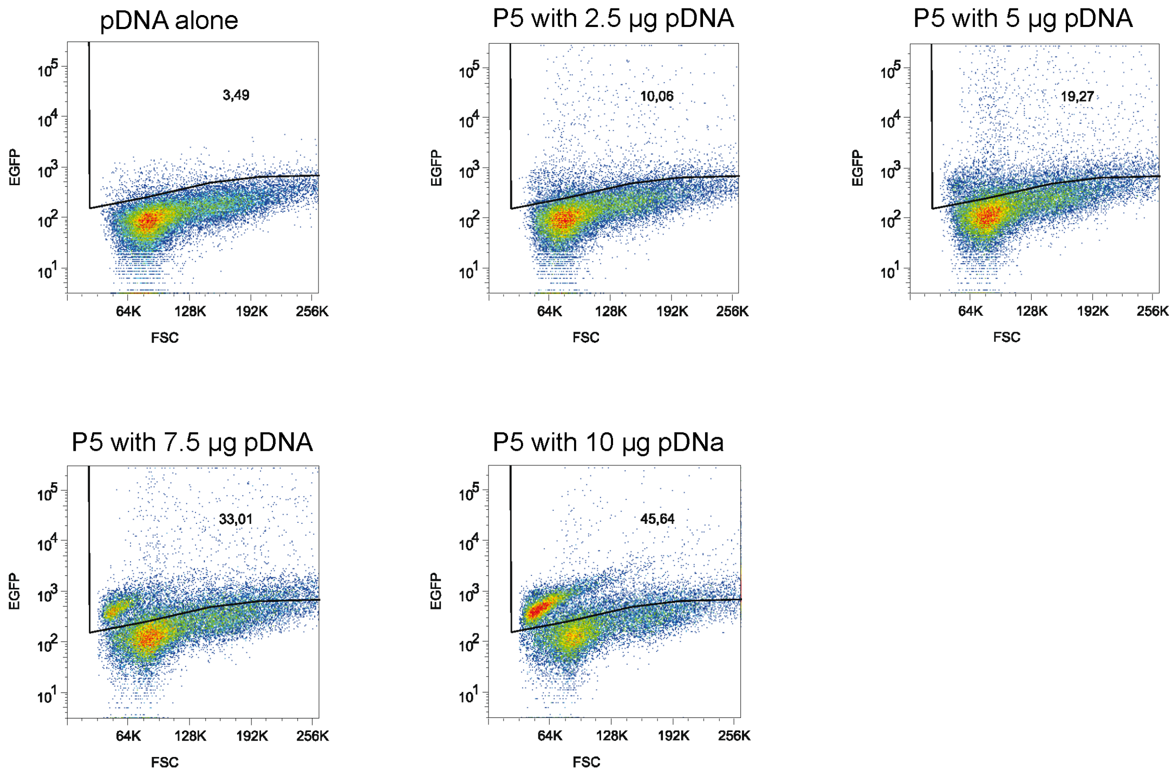

Figure 5.24: Dotplots showing HEK 293T cells after 24 h incubation with PeptoPlexes of P5 and cultivation for 48 h. m_{PLys}/m_{pDNA} ratios were set at 2.5/1, m_{pDNA} was increased from 2.5 µg to 10 µg per well. Plain pDNA functions as control.

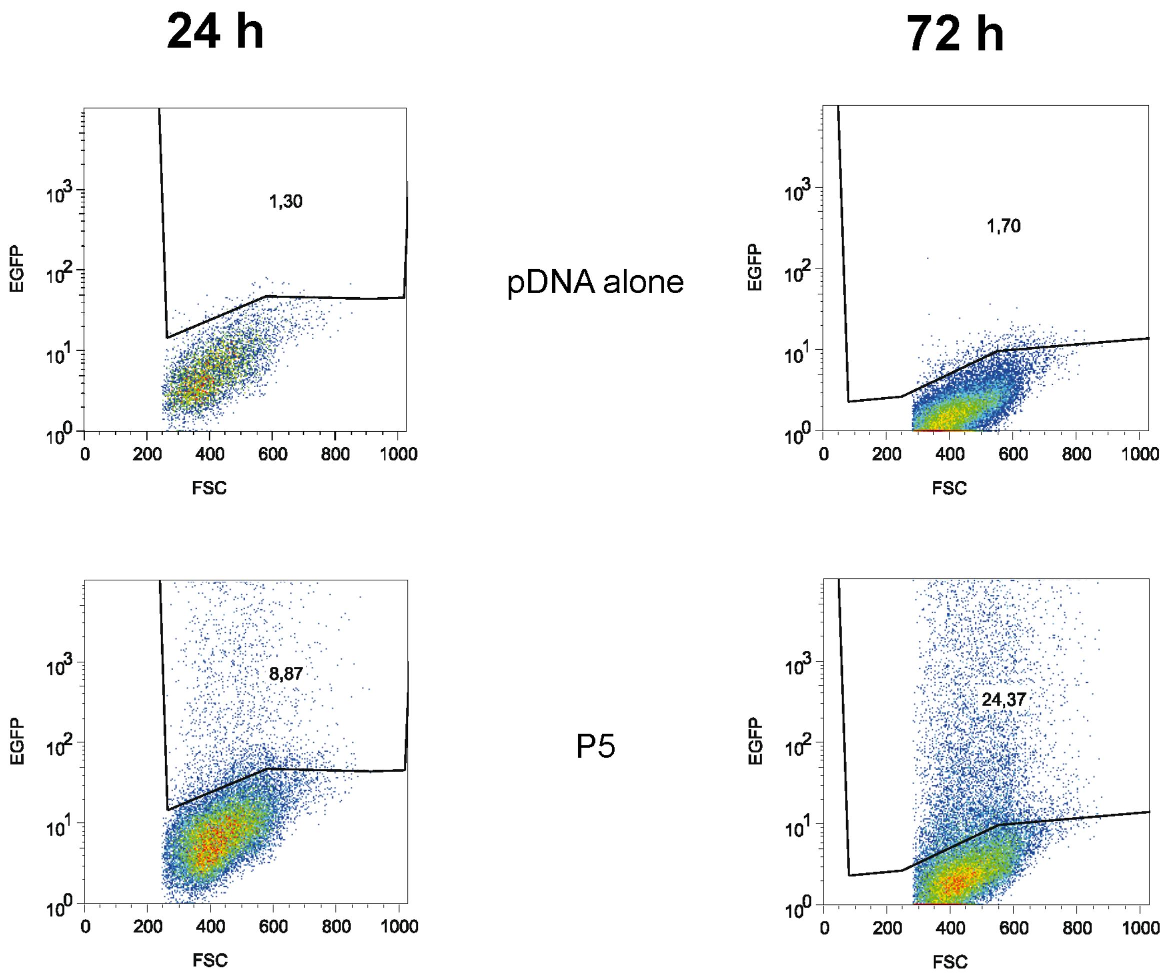

Figure 5.25: Dotplots showing HEK 293T cells after 24 h incubation with PeptoPlexes of P5 (left) or 24 h incubation with further cultivation for 48 h (right). m_{PLys}/m_{pDNA} ratios were set at 2.5/1, mpDNA was kept at 5 µg per well. Plain pDNA functions as control.

5.5.5 Fluorescence Microscopy

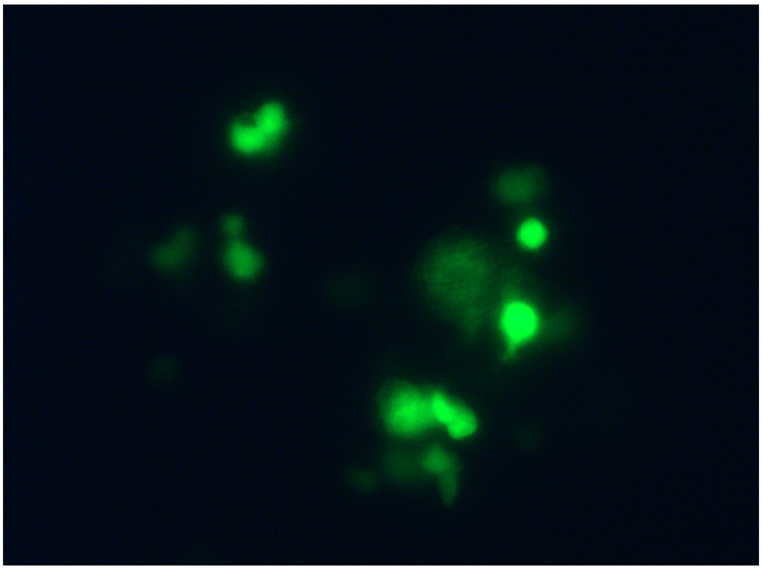

Figure 5.26: Representative fluorescence image showing eGFP expression in HEK 293T cells after 24 h incubation with PeptoPlexes of P1 and cultivation for 24 h. m_{PLys}/m_{pDNA} ratios were set at 2.5/1, mpDNA was kept at 5 µg per well.

6 QUANTIFICATION OF PDNA MOLECULES PER PEPTOPLEX BY TIRF MICROSCOPY

6.1 INTRODUCTION

Knowing the composition of polyplexes, i.e. the number of pDNA molecules within one complex, is of fundamental interest, since it helps to understand the complexation behavior of different types of polymers or polymer architectures. In a more practical context, it allows calculation of the amount of polyplexes a defined amount of pDNA will yield after comlexation and thus provides the basis for a realistic estimation of the absolute number of particles (polyplexes) applied in a certain *in vitro* or *in vivo* experiment.

With respect to solely cationic homopolymers, such as polyethyleneimine (PEI) or PLys, Lai and Zanten demonstrated that the rapid formation of primary single-pDNA polyplexes was followed by aggregation into larger secondary multi-pDNA structures over time.[377] The obvious explanation for this lies in the fact that without interference by a non-charged segment, polycationic compounds may induce bridging of multiple pDNA molecules. Considering block copolymers with a cationic and a neutral shielding segment, like the PLys-b-PSar system introduced in this work, on the other hand, it is reasonable to expect the formation of stable, single-pDNA complexes with core-shell architecture. In this case the shielding block should prevent the bridging of multiple pDNA copies by the cationic block. Consequently, aggregation of primary complexes into multi-pDNA structures is blocked.

6.2 RESULTS AND DISCUSSION

The fact that according to DLS PeptoPlexes are smaller in size than the corresponding free pDNA (~40 nm vs ~90 nm, see Chapter 5) indeed suggests that on average one PeptoPlex contains one plasmid. Nevertheless, to substantiate this assumption, quantitative fluorescence spectroscopy provides a complementary method. More specifically, total reflection fluorescence (TIRF) microscopy was applied to image single molecules of DAPI-labeled pDNA or single PeptoPlexes containing DAPI-labeled pDNA. DAPI is an intercalating dye commonly used for DNA staining in fluorescence microscopy. When quantified and compared for free pDNA and PeptoPlexes, the DAPI-associated fluorescence intensity provides a measure for the number of pDNA copies per PeptoPlex. To vary the investigated pDNA in size, experiments were conducted with the pUC19 cloning vector (2686 bp) as well as with pEGFP-N1 DNA (4733 bp). In both cases, a PLys-b-PSar diblock copolymer was applied at N/P 4 for polyplex formation. As first step of the experimental procedure, pDNA or polyplexes were incubated with DAPI. Subsequently, the stained samples were flushed onto specifically prepared coverslips using a microfluidic system. After a washing step, the remaining surface-bound pDNA or PeptoPlexes were imaged with a costum-built TIRF microscope.

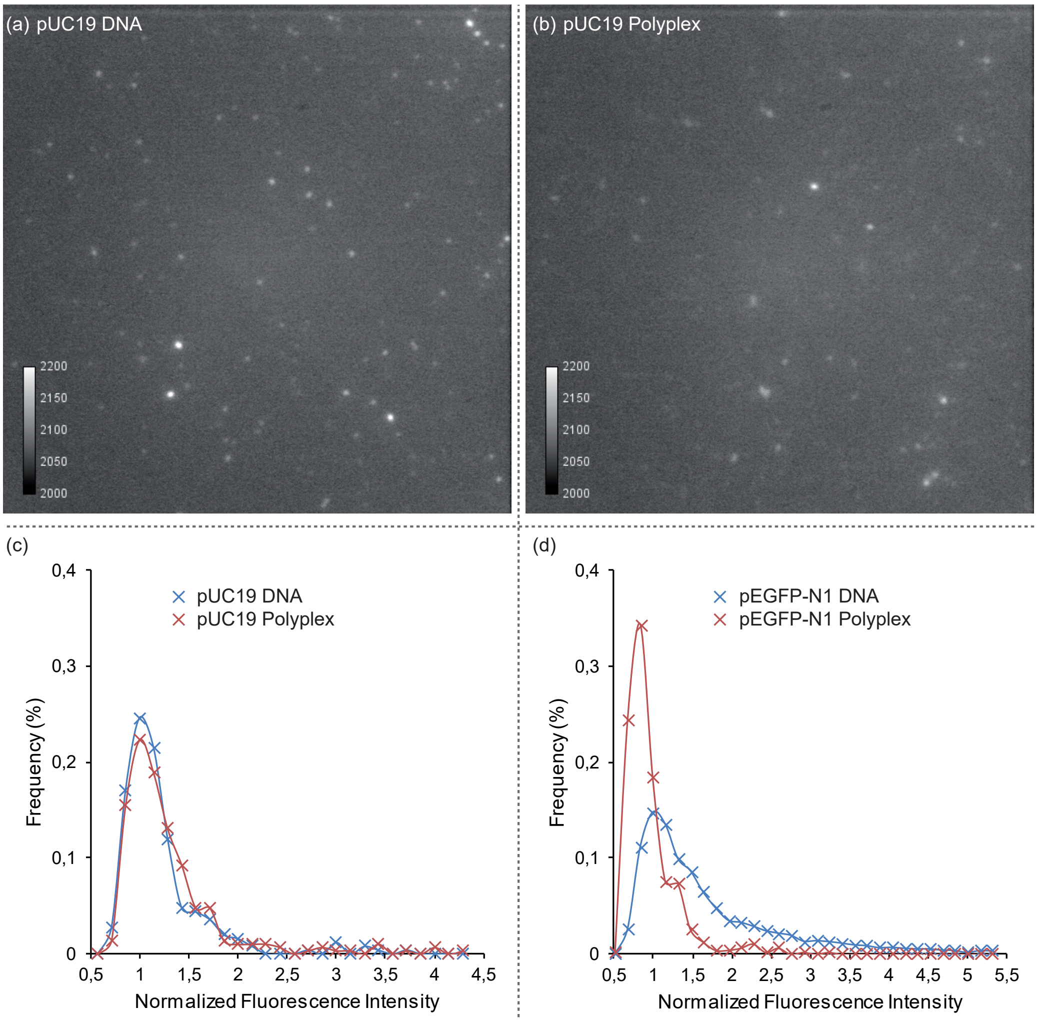

Figure 6.1: TIRF microscopy for quantitative fluorescence detection. (a) Representative fluorescence image of single pUC19 DNA molecules. (b) Representative fluorescence image of single pUC19 DNA containing polyplexes. (c) Fluorescence intensity distribution for pUC19 DNA (blue) and pUC19 DNA containing PeptoPlexes (red). (c) Fluorescence intensity distribution for pEGFP-N1 DNA (blue) and pEGFP-N1 DNA containing polyplexes (red).

In Fig. 6.1 (a) and (b) each fluorescing point corresponds to a single pDNA molecule or PeptoPlex, respectively. The qualitative data already indicates a comparable fluorescence intensity for both species. For quantification, the raw fluorescence intensity of each point was analyzed with mathlab software drawing on algorithms written in the group of Prof. Kirchhausen. As a result, free pDNA and polyplex showed a similar fluorescence intensity distribution with the respective maxima lying in the same range, indicating one copy of pDNA per PeptoPlex on average.

Of course, some limitations of the method have to be considered. pDNA located within a polyplex is in a more condensed state than free pDNA. Thus, in case of complexed pDNA, the DNA-bound DAPI molecules are closer to each other and quenching of the DAPI-associated fluorescence may occur. On the other hand intercalation of DAPI into pDNA might be impaired per se in case of polyplexes because the complexed pDNA is less accessible than free pDNA. Fluorescence quenching or impaired intercalation might explain the slight shift of the fluorescence maximum between free pEGFP-N1 and the corresponding polyplex (Fig. 6.1 (d)). Nevertheless, it is unlikely that these effects are large enough to alter the measured fluorescence intensity substantially. For instance, in case of pUC19, intensity distribution of free pDNA and polyplex are well aligned.

In summary, results from TIRF microscopy support the suggestion from DLS experiments, i.e. formation of single-pDNA polyplexes. Within the context of this work, single-pDNA polyplexes, as experimentally confirmed by two independent methods to this point, are an important prerequisite for the validity of the simulations described in Chapter 9. In future experiments, static light scattering, another complementary method, will further elucidate PeptoPlex composition, also providing an estimation for the number of polymers per polyplex.

Part III

MANNOSE-MODIFIED PEPTOMICELLES

Active targeting of cells can increase transfection efficiency of non-viral vectors. Thus, in a side project within the PhD thesis mannose was investigated as a targeting ligand for dendritic cells. In order to assess the effect of mannose functionalization on cellular uptake, micelles derived from amphiphilic Mannose-PSar-b-PGlu(OBn) diblock copolymers were utilized as a model system. The studies conducted in this part provided the groundwork for the later functionalization of PeptoPlexes with mannose.

7 DIRECTED INTERACTIONS OF BLOCK COPOLYPEPT(O)IDES WITH MANNOSE-BINDING RECEPTORS: PEPTOMICELLES TARGETED TO CELLS OF THE INNATE IMMUNE SYSTEM

P. Heller, N. Mohr, A. Birke, B. Weber, A. Reske-Kunz, M. Bros, M. Barz, *Macromolecular Bioscience*, 2015, **15**, 63-73

ABSTRACT

Core-shell structures based on polypept(o)ides combine stealth-like properties of the corona material polysarcosine with adjustable functionalities of the polypeptidic core. Mannose-bearing block copolypept(o)ides (PSar-b-PGlu(OBn)) have been synthesized using 11-amino-3,6,9-trioxa-undecyl-2,3,4,6-tetra-O-acetyl-O-α-D-mannopyranoside as initiator in the sequential ring-opening polymerization of α-amino acid *N*-carboxyanhydrides. These amphiphilic block copolypept(o)ides self-assemble into multivalent PeptoMicelles and bind to mannose-binding receptors as expressed by dendritic cells. Mannosylated micelles showed enhanced cell uptake in DC 2.4 cells and in bone marrow-derived dendritic cells (BMDCs) and therefore appear to be a suitable platform for immune modulation.

7.1 INTRODUCTION

In nature, glycoproteins are involved in a multitude of essential biological processes, which range from phagocytosis and inflammation to cell-cell interactions and signal transduction.[169, 378] Many researchers have investigated multivalent binding of carbohydrates presented on polymers, polymeric micelles, polymersomes or inorganic nanoparticles to cytosolic, extracellular or trans-membrane proteins.[379–385] In general, the interaction between a single carbohydrate moiety and its receptor is comparatively weak (*nM* to *mM* affinities). Thus, to enhance the binding strength of carbohydrates for directed interaction (drug targeting) multivalence turned out to be of particular importance. This phenomenon is known as the cluster glycoside effect[386] and has been studied in depth for decades.

Besides binding to model proteins like concavalin A[383] or inhibition of hemagglutination (HIA),[379, 380] glycoside functionalization of nanoparticles can be used to direct their binding to transmembrane proteins and to trigger specific internalization; prominent examples involve the targeting of the transferrin receptor[387, 388] and mannose-binding receptors (e.g., MMR family, DC-SIGN).[389] Activation of cellular uptake pathways like clathrin-mediated endocytosis by targeting transmembrane proteins is of major interest to enhance internalization and to alter intracellular distribution, as clearly demonstrated in studies on uptake kinetics, pathway specificity and intracellular distribution of viruses.[390, 391]

In this context, mannose-functionalized nanoparticles have been investigated to target dendritic cells (DCs) as well as macrophages.[389, 392] Both cell types play important roles in the first line of immune defence and are interesting cellular targets to induce/alter immune responses. In case of DCs, especially vaccination with mannose-modified carriers against various model antigens or diseases has been studied.[317, 393–395] Macrophages, on the other hand, are potential targets for the delivery of drugs, e.g., against tuberculosis[396] or leishmaniasis[397, 398]. While after i.v. injection ending up in macrophages is likely to be the fate of mannosylated nanoparticles, subcutaneous administration has already demonstrated that macrophage uptake can be minimized because transfer to the lymphatic system occurs rapidly and therefore exposes particles almost exclusively to dendritic cells.[290]

Nearly all targeted delivery systems have a common feature: a directed interaction of a recognition structure on the particle corona with a cellular transmembrane protein. Therefore, the recognition structure needs to be exposed on the particle surface. The self-assembly of amphiphilic block copolymers in a block-selective solvent offers a versatile route to the formation of core-shell structures. Provided that the amphiphilic polymers already contain the recognition structure, micelles that present these structures on the corona can be directly obtained through this process.[399] Therefore, the targeting moiety - for example, peptide or glycoside - needs to be attached to the hydrophilic block by conjugation to the side chain or the end group. BIND Therapeutics is currently investigating the concept of end group modification for block copolymer-based nanoparticles containing the chemotherapeutic docetaxel in clinical trials. These nanoparticles are decorated with a small molecule ligand (ACUPA) targeting a prostate cancer specific antigen as expressed specifically by prostate cancer cells.[400]

While functionalization of the polymer side chains can be achieved by polymer-analogous reactions,[401, 402] functional end groups are accessible by the use of appropriate initiators for polymerization. The ring-opening polymerization of *N*-substituted α-amino acid *N*-carboxyanhydrides, e.g., sarcosine NCA, leads to polymers with high end group integrity in one step. Thus, the use of bioactive initiators represents a straight forward approach for the synthesis of end group-functionalized polypept(o)ides such as glycosylated polypept(o)ides presented in this work. Other strategies for the synthesis of glycopolypeptides involve the polymerization of glycosylated NCAs or postpolymerization glycosylation.[169, 385, 403–406]

Almost 40 years after the first report on the living polymerization of the polypeptoide polysarcosine (PSar),[117] scientists have rediscovered this type of polymer as a very interesting material being - amongst others[359]- a potential alternative to PEG for biomedical applications. Polysarcosine is a typical example for a material, which behaves accordingly to the Whitesides rules for protein-resistant surfaces,[362, 407] since it is non-ionic, hydrophilic and a weak hydrogen bond acceptor. Therefore, it is not much of a surprise, that PSar has already demonstrated protein-resistant properties[361, 362] as well as non-immunogenic properties[164] and thus meets the requirements for biocompatibility. While Guo and Zhang used PSar for the synthesis of cyclic polypeptoides,[44] the group of Luxenhofer applied it for the synthesis of block copolypeptoides.[121] Sun and Zuckerman derived monodisperse PSar by solid phase synthesis.[364] Surprisingly, so far only the groups of Kimura and Barz used PSar as substitute of PEG in amphiphilic di-[155] and tri-block[158] copolymers designed for biomedical applications: for example Lactosomes,[166, 167] microspheres,[162] Nanosheets,[164] PeptoMicelles[155] and PeptoPlexes[156].

7.2 RESULTS AND DISCUSSION

As mentioned above, PSar as well as various other polypept(o)ides are accessible by nucleophilic ring-opening polymerization of α-amino acid *N*-carboxyanhydrides (NCAs) as well as *N*-Thiocarboxyanhydrides (NTAs). In this approach functional amines can be employed as long as they do not interfere with the polymerization itself. Therefore, we have synthesized an acetylated mannose derivative, in which a primary amine is linked with a glycol spacer to the cyclic hexose moiety by an α-glycosidic bond. The α-glycosidic linkage is known to be of major importance for any biorecognition process.[408] During synthesis, the neigboring group effect ensures the formation of the α-glycosidic linkage, which can be clearly seen in the coupled HSQC measurement (SI, Fig. 7.15). In the next step, the primary amine of the mannose derivative was used to initiate the sequential polymerization of sarcosine (Sar), lysine(TFA) (Lys(TFA)) and glutamic acid(OBn) (Glu(OBn)) NCAs (Fig. 7.1).

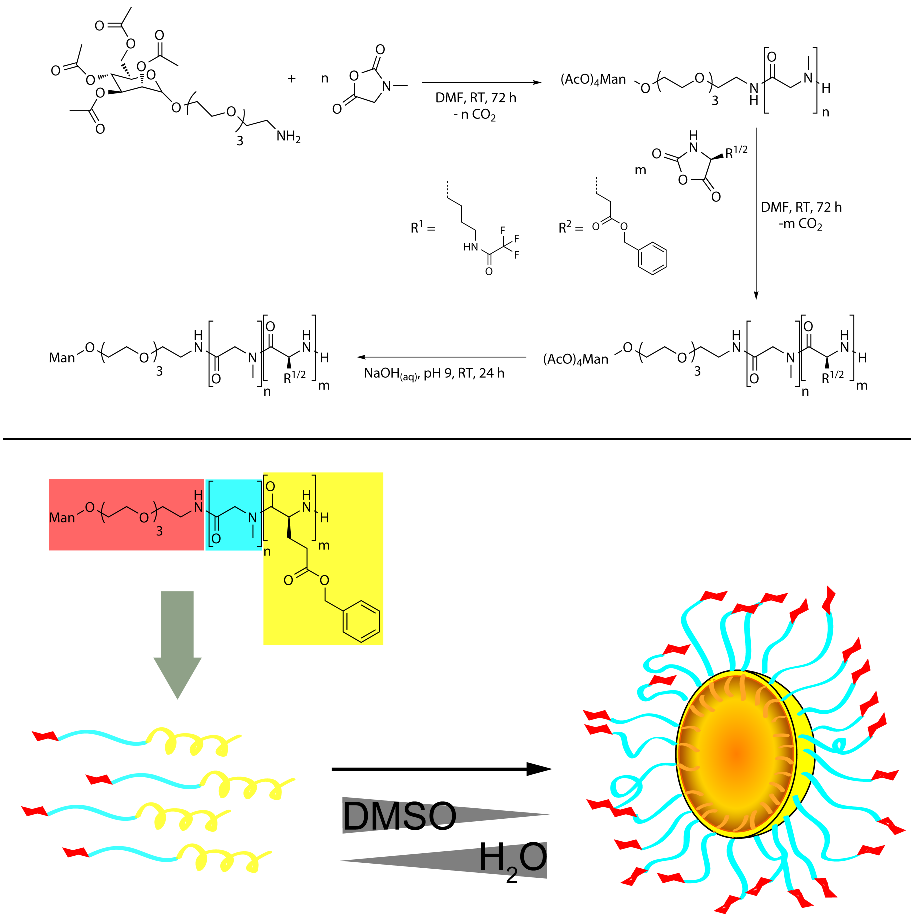

Figure 7.1: Synthesis of mannose-functionalized PSar-block-PGlu(OBn) or PSar-block-PLys(TFA) block copolypept(o)ides, selective deprotection of mannose end groups and self-assembly of Man-PSar-block-PGlu(OBn) coplymers into PeptoMicelles targeting mannose-binding receptors.

The polymerizations proceeded in a well-controlled manner yielding block copolypept(o)ides with narrow monomodal molecular weight distributions and low dispersities between 1.13-1.17 (Table 7.1).

Table 7.1: Characteristics of synthesized block copolymers and micelles.

	POLYMER	CALCULATED BLOCK RATIO	BLOCK RATIO^{A}	M_N^{B}	Đ^{B}	R_H^{C}	μ_2^{C}
P1	Man-PSar-b-PGlu(OBn)	300:30	277:28	46.2	1.13	63.7	0.13
P2	PSar-b-PGlu(OBn)	300:30	309:25	40.7	1.12	72.8	0.15
P3	Man-PSar-b-PLys(TFA)	300:30	319:29	49.4	1.17	nd	nd

^{A} as determined by ^{1}H-NMR spectroscopy in DMSO-d6
^{B} kg/mol, as determined by GPC with HFIP as solvent and PMMA standards
^{C} nm, as determined by DLS in PBS buffer, c = 0.0667 g/L

The ^{1}H-NMR signal of the acetyl protecting groups can be easily integrated and related to the polysarcosine backbone protons enabling precise determination of the degree of polymerization.

Diffusion-ordered spectroscopy (DOSY) NMR experiments displayed only one diffusing species, which reflects the absence of free initiators or low molecular weight polymers (Fig. 7.2).

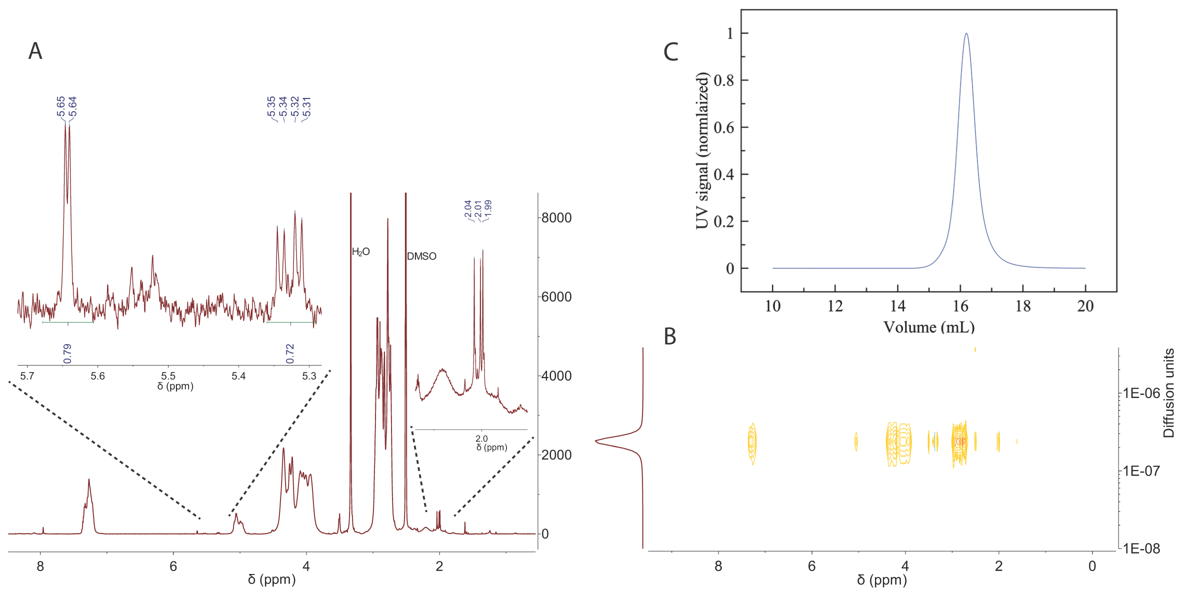

Figure 7.2: Characterization of mannose-containing block copolypept(o)ides. (A) 400 MHz ^{1}H-NMR of Man-PSar$_{277}$-block-PGlu(OBn)$_{28}$ (**P1**) showing mannose end group-derived signals, (B) DOSY NMR of Man-PSar$_{277}$-block-PGlu(OBn)$_{28}$ proving the linkage between mannose end group and polymer, (C) GPC plot of Man-PSar$_{277}$-block-PGlu(OBn)$_{28}$ showing unimodal weight distribution.

Polymer-analogous reactions such as labelling of polymers with dyes (see Subsection 7.4.4) are easy to conduct by using the terminal amino groups of the protected polypeptide blocks. In case of Man-PSar-b-PGlu(OBn), the chosen protecting groups enable the stepwise deprotection of glycoside and polymer using $NaOH_{(aq)}$, pH 9. Specificity of these deprotection conditions was verified by relating the benzyl ester-derived ^{1}H NMR signals before and after deprotection of the mannose end group (SI, Fig. 7.18 and 7.20). In case of Man-PSar-b-PLys(TFA) the simultaneous deprotection of glycoside and polymer is feasible by using hydrazine hydrate (SI, Fig. 7.19 and 7.21). Therefore, this versatile synthetic pathway can be used for the generation of labeled mannose-functionalized PeptoMicelles as well as of PeptoPlexes.

For preparation of PeptoMicelles labeled block copolymers **P1** or **P2** were diluted in DMSO and the solvent was gradually switched to H_2O (Fig. 7.1). Characterization of micelles by dynamic light scattering in both cases revealed a minor angle-dependency which is most likely related to dispersity of the micelles (Fig 7.3). Hydrodynamic radii were 63.7 nm for **P1** and 75.8 nm for **P2**. These particle sizes are still likely to allow entering cells by clathrin-mediated endocytosis.[409]

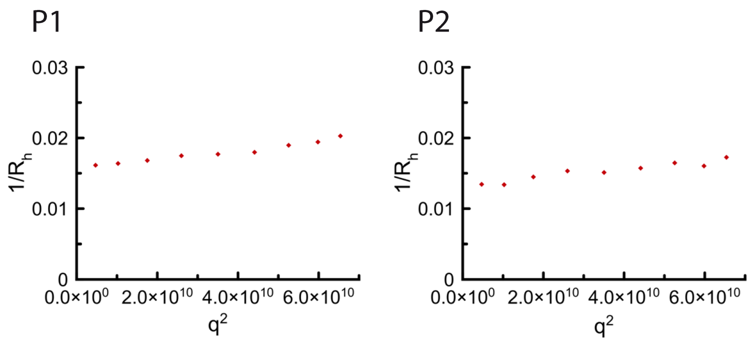

Figure 7.3: Dynamic light scattering of PeptoMicelles **P1** (R_h = 63.7 nm) and **P2** (R_h = 75.8 nm).

After DLS measurements PeptoMicelles were subjected to biological evaluation. Initially, the cellular uptake of mannose-functionalized PeptoMicelles was investigated using DC 2.4 cells. This cell line is well established as model for DCs and is known to express mannose-binding receptors (MRs).[410] Consequently, it has been utilized for uptake studies with mannose-modified nanoparticles in many publications.[410–414]

MTT assay performed with DC 2.4 cells did not display any decrease in cell viability related to the presence of PeptoMicelles at concentrations up to 0.5 mg/mL (SI, Fig. 7.27), which appears well above suitable concentrations for modulation of DC-function *in vivo*. MR binding of mannose-functionalized PeptoMicelles and subsequent MR-mediated endocytosis were verified with a dual strategy. DC 2.4 cells were preincubated with mannan to saturate MRs and therefore intercept binding and endocytosis of functionalized PeptoMicelles on receptor level. To interrupt endocytosis on a more downstream level, cells were preincubated with dynasore-OH which does not interfere with MR binding of PeptoMicelles but prevents scission of endocytic vesicles by targeting dynamin-1 and dynamin-2.[415] Experiments for cells pretreated in this manner were conducted with mannosylated PeptoMicelles (**P1**) and with ovalbumin (OVA) as model protein for MR-mediated uptake[416] (Fig. 7.4 (A) and SI, Fig. 7.25). Blocking with mannan led to a slight decrease of binding/uptake for OVA (approx. 25%), while binding/uptake of **P1** was lowered to around 50% of starting level. The still existing binding/uptake of OVA and **P1** may be related to incomplete saturation of MRs, mannan-triggered recruitment/recycling[417, 418] of additional MRs to the cell surface and action of alternative uptake pathways like macropinocytosis and phagocytosis. In line, binding/uptake of OVA and **P1** was not reduced any further by higher mannan concentrations but increased again (data not shown), also suggesting recruitment of additional MRs. After preincubation of cells with dynasore-OH, the uptake of OVA and **P1** was diminished by 80% and 60%, respectively. This finding confirms that **P1** - like OVA - is mainly taken up via clathrin-mediated endocytosis which is known to be the endocytic mechanism behind MR-driven uptake.[417] As in case of mannan, the still existing uptake of OVA and **P1** after pretreatment of cells with dynasore-OH may be attributable to alternative uptake routes.

After confirmation of MR-governed uptake of **P1** we investigated its performance in relation to non-mannosylated PeptoMicelles (**P2**). In addition to DC 2.4 cells, bone marrow-derived dendritic cells (BMDCs) were used as representative of MR-expressing DCs derived from primary progenitors. As expected, **P1** showed a significantly higher cellular interaction compared to **P2** in case of DC 2.4 cells (Fig. 7.4 (B)) and BMDCs (Fig. 7.4 (C)). In both cell types the binding/uptake of **P1** exceeded the binding/uptake of **P2** by approx. 70%. Furthermore, the uptake ratio between **P1** and **P2** was comparable to that between **P1** with and **P1** without mannan/dynasore-OH preincubation.

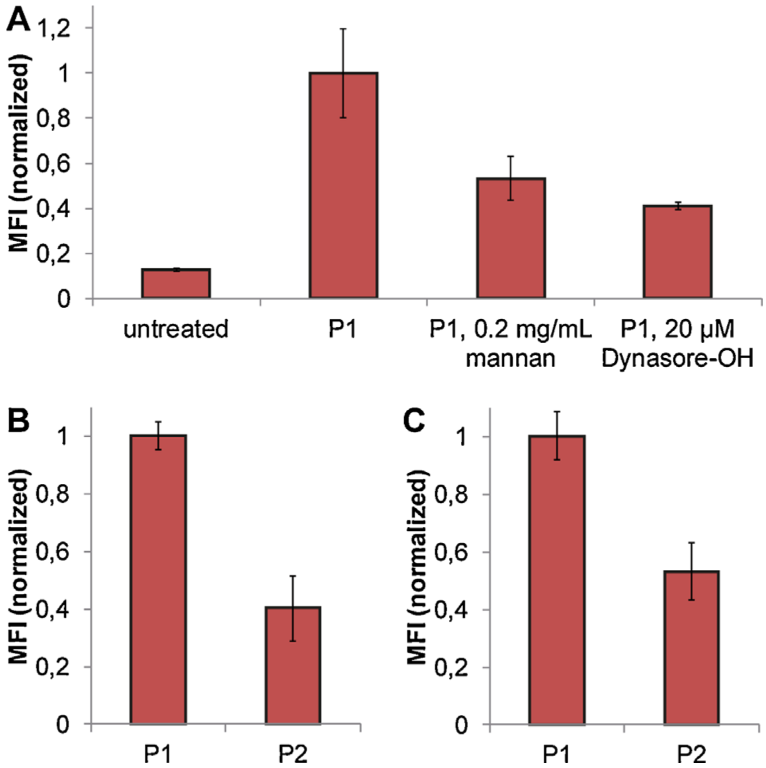

Figure 7.4: Uptake studies with **P1** and **P2**. (A) Blocking experiment with DC 2.4 cells. (B) Comparison of uptake efficiency with DC 2.4 cells. (C) Comparison of uptake efficiency with bone marrow-derived dendritic cells (BMDCs). (n = 3)

All these findings point to an enhancement of uptake of **P1** by interaction with MRs in comparison with **P2**. Unspecific mechanisms such as macropinocytosis contribute considerably to the uptake of PeptoMicelles, irrespective of their mannosylation. These results are in line to reports of other groups which also describe mannosylation-related increase in uptake of - in this case - PLGA or dextran particles yet also observing unspecific uptake.[316, 412] Though, mannosylation of PeptoMicelles induces a substantial increase in cellular uptake, which may enable targeting of MR-expressing cells like DCs or macrophages.

7.3 CONCLUSION

In this work we demonstrated a versatile synthetic pathway to block copolypept(o)ides with bioactive end groups. The derived block copolymers possess low dispersity indices around 1.1 ensuring well-controlled polymerization. The reported pathway enables the synthesis of amphiphilic block copolymers or block ionomers with mannose end groups using different protecting groups (orthogonally or simultaneously cleavable). These polymers can self-assemble into polymeric core-shell structures, e.g., micelles, which were successfully used to enhance cellular uptake in DC 2.4 as well as BMDCs. Our findings provide first evidence that mannosylated PeptoMicelles possess the potential to target MRs on cells of the innate immune system.

7.4 EXPERIMENTAL SECTION

7.4.1 Materials

DMF was purchased from VWR, dried over BaO and subsequently distilled *in vacuo* onto pre-dried molecular sieves (3 Å). THF and hexane were purchased from Sigma-Aldrich and distilled from Na/K. Diethylether was distilled prior to use to remove the stabilizer. Other solvents were used as received. Diphosgene was purchased from Alfa Aesar and used as provided. Neopentylamine was purchased from TCI Europe, dried over NaOH and fractionally distilled. Sarcosine was purchased from Sigma-Aldrich, all protected amino Acids were purchased from ORPEGEN. Oregon Green 488-X, Succinimidyl Ester, 6-isomer was purchased from Life Technologies. Cell culture media were bought from Lonza. CellTiter 96 Non-Radioactive Cell Proliferation Assay kit (for MTT assay) was purchased from Promega (Madison, USA). Mannan from *Saccharomyces Cerevisiae* was purchased from Sigma-Aldrich. Dynasore-OH was kindly provided by Prof. T. Kirchhausen from Harvard Medical School, Boston.

7.4.2 Instrumentation

7.4.2.1 *Polymer Characterization*

400 MHz ^{1}H-NMR spectra were recorded on a Bruker Avance II 400. HSQC and DOSY NMR measurements were performed on a Bruker Avance III HD 400. All spectra were recorded at room temperature and analyzed with MestReNova software. Degrees of polymerization as well as molecular weights were calculated by comparing the integrals of the neopentylamine initiator peak or the mannose initiator acetyl peaks either with the integrals of the side chain amide protons (for PLys(TFA)), with the protective group protons (for PGlu(OBn)) or with the average of integrals of methyl group and α-protons (for PSar) in the 400 MHz ^{1}H-NMR spectra.

Attenuated total reflectance Fourier transformed infrared (ATR-FTIR) spectroscopy was performed on an FT/IR-4100 (JASCO) with an ATR sampling accessory (MIRacleTM, Pike Technologies). IR Spectra were analyzed using Spectra Manager 2.0 (JASCO).

Melting points were determined using a METTLER FP62 (METTLER WAAGEN GMBH).

Hexafluoroisopropanol (HFIP) gel permeation chromatography (GPC) was performed with HFIP containing 3 g/L potassium trifluoroacetate as eluent at 40 °C and a flow rate of 0.8 mL/min. The columns were packed with modified silica (PFG columns; particle size: 7 mm, porosity: 100 and 1000 Å). Polymer was detected with a refractive index detector (G 1362A RID, JASCO) and a UV/Vis Detector (UV-2075 Plus, JASCO). Molecular weights were calculated using a calibration performed with PMMA standards (Polymer Standards Services GmbH) and toluene as internal standard. Elution diagrams were analyzed using WinGPC UniChrome 8.00 (Build 994) software from Polymer Standards Services.

Preparative reverse phase-HPLC was performed with a Knauer HPLC-System (Berlin, Germany), consisting of two HPLC pumps (Smartline 1000), an UV/Vis-detector (Smartline 2500), a RI-detector (Smartline 2400) and a Phenomenex (Torrance, U.S.A.) Luna-column (10 µm, C18(2), 100 A, 250 × 30 mm^2) run at a flow of 10.0 mL/min and loaded with a 2 mL injection loop. The system was operated and samples analyzed with D-7000 HPLC-System-Manager software (version 4.1). For the preparative runs a mixture of THF and Millipore water with a gradient from 40/60 to 90/10 (THF/water) over 50 min was utilized. The UV/Vis-detector was set to a wavelength of 488 nm.

Labeling efficiency for polymers was determined by measuring the Oregon Green 488-related absorbance at 488 nm with a Nanodrop® ND-1000.

7.4.2.2 *Biological Experiments*

(3-(4,5-Dimethylthiazol-2-yl)-2,5-diphenyltetrazolium bromide (MTT) assay measurements were performed using a Dynex MRX TC Revelation microtiter plate reader (Dynex Technologies, Chantilly, VA).

FACS experiments were executed on a FACS Canto II flow cytometer equipped with BD FACS Diva software (both from BD Biosciences, San Diego, CA). Data were analyzed using FlowJo software (FLOWJO, Ashland, OR).

7.4.3 Methods and Protocols - Preparation of Mannose Initiator

7.4.3.1 *Tetraethylene Glycol Monotosylate*

To a mixture of 4.11 g (103 mmol) sodium hydroxide in 23 mL of water and 23 mL THF tetraethylene glycol was added. The solution was cooled to 0 °C and a mixture of 12.15 g (65 mmol) *p*-toluenesulfonic acid in 100 mL THF was added dropwise. The reaction mixture was stirred for 2 hours at 0 °C. After stirring 2 hours at room temperature the mixture was poured into ice-cold water and extracted with dichloromethane (4 x 150 mL). The organic layers were washed with water (275 mL) and dried over magnesium sulfate. Rotary evaporation gave a pale yellow oil which was used in the next reaction step without further purification. Yield: 22 g (63 mmol, 97%), Lit.: 90%[419]. R_f = 0.24 (cyclohexane/EtOAc 1:4).
^{1}H NMR (300 MHz, $CDCl_3$): δ [ppm] = 7.77 (2H, d, J = 8.5 Hz, -SO_2-*o*-Ar-H), 7.32 (2H, d, J = 8.5 Hz, -SO_2-*m*-Ar-H), 4.14 (2H, t, J = 4.5 Hz, -CH_2-OTos), 3.71-3.51 (14H, m, -CH_2-CH_2-O-), 2.42 (3H, s, -CH_3).
ESI-MS: (m/z) = 371.13 ([M + Na]$^+$, calc.: 371.11). $C_{15}H_{24}O_7S$ (348.41 g · mol^{-1})

7.4.3.2 *N-(11-hydroxy-3,6,9-trioxaundecyl)phthalimide*

A mixture of 22 g (63 mmol) of tetraethylene glycol monotosylate, 14 g (76 mmol) potassiumphthalimide and 3 g molecular sieve (3 Å) in 160 mL dimethylformamide was stirred for 10 hours at 150 °C and 8 hours at room temperature. The suspension was filtered through Celite and washed with DMF. The solvent was evaporated using high vacuum. The crude product was co-distilled with toluene (470 mL) and purified by column chromatography (eluent: EtOAc) to obtain a pale yellow oil. Yield: 18.2 g (56 mmol, 89%), Lit.: 57%[419]. R_f = 0.34 (EtOAc).
^{1}H NMR (300 MHz, $CDCl_3$): δ [ppm] = 7.85-7.81 (2H, m, Ar-H), 7.72-7.68 (2H, m, Ar-H), 3.88 (2H, d, J = 5.5 Hz, NPhth-CH_2-CH_2-O-), 3.73 (2H, t, J = 5.8 Hz, NPhth-CH_2-CH_2-O-), 3.75-3.52 (12H, m, -CH_2-CH_2-O-).
ESI-MS: (m/z) = 346.14 ([M + Na]$^+$, calc.: 346.13). $C_{16}H_{21}NO_6$ (348.41 g · mol^{-1})

7.4.3.3 *1-Amino-11-hydroxy-3,6,9-trioxaundecan*

To a solution of 18.2 g (56 mmol) *N*-(11-hydroxy-3,6,9-trioxaundecyl) phthalimide in 100 mL ethanol 3.5 mL (110 mmol) hydrazine hydrate was added and stirred for 2.5 h at 80 °C. A colorless solid precipitates and after cooling to room temperature 1.0 M HCl was

added until pH = 1 was achieved. The solvent was evaporated under vacuum and the residue was taken up in 200 mL of water. After filtration through Celite sodium hydroxide solution was added until a pH of 11 was reached. The basic filtrate was stirred for 20 min at room temperature and the water was removed by rotary evaporation. The crude product was dissolved in 300 mL chloroform, dried over $MgSO_4$ and filtrated through Celite. The solvent was removed by rotary evaporation to obtain an orange oil, which was used in the next reaction step without further purification. Yield: 7.8 g (40 mmol, 71%).
^{1}H NMR (300 MHz, $CDCl_3$): δ [ppm] = 3.71-3.50 (14H, m, -CH_2-CH_2-O-), 2.87-2.84 (2H, t, J = 4.2 Hz, -CH_2-NH_2).
ESI-MS: (m/z) = 195.14 ($[M + H]^+$, calc.: 194.14). $C_8H_{19}NO_4$ (193.24 g . mol^{-1})

7.4.3.4 *1-(Benzoyloxycarbonylamino-11-hydroxy-3,6,9- trioxa) undecan*[369]

To a solution of 7.8 g (40 mmol) 1-amino-11-hydroxy-3,6,9-trioxaundecan in 270 mL water 6.7 g (80 mmol) $NaHCO_3$ was dissolved and the mixture was stirred at 0 °C. 8.6 mL (60 mmol) of benzyl chloroformate were dissolved in 50 mL dioxan at 5 °C and added dropwise to the reaction mixture. The solution was stirred for 2 hours at 0 °C and overnight at room temperature. 50 mL water was added and the water phase was extracted with ethyl acetate (2 x 150 mL). The organic layers were collected and extracted with saturated $NaHCO_3$ solution (2 x 150 mL).The aqueous layers were acidified by 1.0 M HCl to pH = 1 and extracted with ethyl acetate (3 x 100 mL). The organic layers were collected, dried over $MgSO_4$, filtrated, and the solvent was removed by rotary evaporation. The yellow oil was purified by column chromatography (eluent: EtOAc). Yield: 8.5 g (26 mmol, 65%). R_f = 0.29 (EtOAc).
^{1}H NMR (300 MHz, $CDCl_3$): δ [ppm] = 7.35-7.29 (5H, m, Ar-H), 5.10 (2H, s, -O-CH_2-Ar), 3.66-3.53 (14H, m, -CH_2-CH_2-O-), 3.35 (2H, t, J = 9.5 Hz, -NH-CH_2-CH_2-O-).
ESI-MS: (m/z) = 350.17 ($[M + Na]^+$, calc.: 350.22). $C_{16}H_{25}NO_6$ (327.24 g . mol^{-1})

7.4.3.5 *1,2,3,4,6-Penta-O-acetyl-*D*-mannopyranoside*

To a solution of 5 g (27.7 mmol) D-mannose in 200 mL pyridine 39 mL (415 mmol) acetic anhydride was added and stirring was continued overnight at room temperature. After co-evaporation with toluene (3 x 40 mL), the residue was taken up in 200 mL ethyl acetate, washed with 2 n HCl (3 x 50 mL), water (1 x 40 mL), saturated sodium bicarbonate (3 x 50 mL), and brine (1 x 40 mL). The organic layers were dried with Na_2SO_4 and rotary evaporation gave an α,β mixture as a pale yellow oil, which was used in the next reaction without further purification. Yield 10 g (25.6 mmol, 92%). Lit.: 100%.[420] R_f = 0.57 (n-hexane/EtOAc 1:1).
^{1}H NMR (300 MHz, $CDCl_3$): δ [ppm] = 6.06 (1H, d, J = 1.8 Hz, 1α), 5.84 (1H, d, J = 1.2 Hz, 1β), 5.46 (1H, dd, J = 1.1 Hz, 3.3 Hz, 2β), 5.24-5.34 (3H, m, 2α, 3α, 4α), 5.12 (1H, dd, J = 3.3 Hz, 9.9 Hz, 3β), 4.23-4.32 (2H, m, 4β, 5α), 4.12-4.02 (4H, m, 6αα, 6βα, 6αβ, 6ββ), 3.78 (1H, ddd, J = 2.4 Hz, 5.3 Hz, 9.8 Hz, 5β), 2.19-1.94 (5s, 15H, -CH_3).
ESI-MS: (m/z) = 413.52 ($[M + Na]^+$, calc.: 413.11), 803.242 ($[M + Na]^+$, calc.: 803.23). $C_{16}H_{22}O_{11}$ (390.12 g . mol^{-1})

7.4.3.6 *2,3,4,6-Tetra-O-acteyl-*D*-mannopyranosyl bromide*

10 g (25.6 mmol) 1,2,3,4,6-Penta-*O*-acetyl-D-mannopyranoside was dissolved in 25 mL dichloromethane and stirred at room temperature under argon. 20 mL of 33% HBr/acetic acid was added via syringe and the reaction was stirred at room temperature for 2 hours. 100 mL of dichloromethane was added and the reaction mixture was extracted with ice-cold water (3 x 200 mL). The organic layer was neutralized by a saturated sodium bicarbonate

solution, washed with brine, dried over sodium sulfate and concentrated under reduced pressure to give a yellow oil which was used in the next reaction without further purification. Yield 9.8 g (24 mmol, 93%). Lit.: 81%.[420] R_f = 0.30 (*n*-hexane/EtOAc 6:4).
^{1}H NMR (300 MHz, $CDCl_3$): δ [ppm] = 6.26 (1H, d, J = 1.1 Hz, 1), 5.67 (1H, dd, J = 3.4 Hz, 10.2 Hz, 3), 5.40 (1H, dd, J = 1.6 Hz, 3.4 Hz, 2), 5.31 (1H, t, J = 10.1 Hz, 4), 4.29 (1H, dd, J = 4.8 Hz, 12.4 Hz, 5), 4.18 (1H, ddd, J = 1.9 Hz, 4.9 Hz, 10.1 Hz, 6a), 4.09 (1H, dd, J = 2.1 Hz, 12.4 Hz, 6b), 2.23-2.03 (12H, 4s, $-CH_3$).
ESI-MS: (*m/z*) = 412.16 ($[M + H]^+$, calc.: 412.20). $C_{14}H_{19}O_5Br$ (411.20 g · mol^{-1})

7.4.3.7 *1-Benzyloxycarbonylamino-3,6,9-trioxaundecan-2,3,4,6-tetra-O-acetyl-β-D-mannopyranoside*

2.4 g (5.9 mmol) 1,2,3,4,6-Penta-*O*-acetyl-D-mannopyranosyl bromide and 2.9 g (8.9 mmol) 1-(benzoyloxycarbonylamino-11-hydroxy-3,6,9-trioxa) undecan were dissolved in 100 mL dichloromethane. 3 g molecular sieve (3 Å) was added and the reaction mixture was stirred for 30 min at -20 °C and under argon atmosphere in the absence of light. 1.9 g (7.5 mmol) silver trifluoromethane sulfonate was added and the reaction was stirred at room temperature overnight. After neutralizing with triethylamine (pH = 8) the mixture was filtered through Celite, washed with dichloromethane, and dried over $MgSO_4$. The solvent was removed by rotary evaporation and the crude product was purified by column chromatography to obtain a pale yellow oil. Yield 2.7 g (4.1 mmol, 70%). R_f = 0.60 (EtOAc).
^{1}H NMR (300 MHz, $CDCl_3$): δ [ppm] = 7.34 (5H, m, Ar-H), 5.34 (1H, dd, J = 3.2 Hz,10 Hz, 4), 5.28 (1H, d, J = 9.6 Hz, 3), 5.25 (1H, t, J = 1.6 Hz, 2), 5.08 (2H, s, $-O-CH_2-Ar$), 4.85 (1H, d, J = 1.6, 1), 4.28 (1H, dd, J = 5.2 Hz, 12 Hz, 5), 4.18 (1H, t, J = 4.4 Hz, 6a), 4.06 (1H, m, 6b), 3.63-3.53 (14H, m, $-CH_2-CH_2-O-$), 3.38 (2H, q, J = 5.2 Hz, $-CH_2$-O-man), 2.13 (3H, s, $-CH_3$), 2.08 (3H, s, $-CH_3$), 2.02 (3H, s, $-CH_3$), 1.97 (3H, s, $-CH_3$).
ESI-MS: (*m/z*) = 680.28 ($[M + Na]^+$, calc.: 680.64). $C_{30}H_{43}NO_{15}$ (657.66 g · mol^{-1})

7.4.3.8 *11-Amino-3,6,9-trioxa-undecyl-2,3,4,6-tetra-O-acetyl-O-α-D-mannopyranoside*

0.5 g (0.76mmol) 1-Benzyloxycarbonylamino-3,6,9-trioxaundecan- 2,3,4,6-tetra-*O*-acetyl-β-D-mannopyranoside was dissolved in 10 mL methanol. Acetic acid was added until a pH of 4-5 was reached and the reaction mixture was degassed by a slight vacuum. The reaction vessel was flushed with argon and approximately 0.5 g of $Pd(OH)_2/C$ (20%) as catalystwere added in counterflow. After degassing with a slight vacuum the reaction vessel was flooded with H_2 and the mixture was stirred at room temperature overnight. The H_2 atmosphere was changed into an argon atmosphere and the catalyst was removed by filtration. The mixture was neutralized by saturated $NaHCO_3$ solution until a pH value of 8. The solution was concentrated by rotary evaporation. Water was added and lyophilization yielded a pale yellow oil. Yield: 0.4 g (0.76mmol, 100%). R_f = 0.20 (cyclohexane/EtOH/TEA 2:3:0.15).
^{1}H NMR (400 MHz, $CDCl_3$): δ [ppm] = 6.61 (br, $-NH_2$), 5.34 (1H, dd, J = 3.2 Hz, 10 Hz, 4), 5.28 (1H, d, J = 9.6 Hz, 3), 5.25 (1H, t, J = 1.6 Hz, 2), 4.87 (1H, d, J = 1.6, 1), 4.28 (1H, dd, J = 5.2 Hz, 12 Hz, 5), 4.22 (1H, t, J = 4.4 Hz, 6a), 4.10 (1H, m, 6b), 3.63-3.53 (14H, m, CH_2-CH_2-O-), 3.05 (2H, m, $-CH_2-NH_2$), 2.15 (3H, s, $-CH_3$), 2.09 (3H,s, $-CH_3$), 2.03 (3H, s, $-CH_3$), 1.98 (3H,s, $-CH_3$).
ESI-MS: (*m/z*) = 524.65 ($[M + H]^+$, calc.: 524.23), 546.20 ($[M + Na]^+$, calc.: 546.21). $C_{22}H_{37}NO_{13}$ (523.23 g · mol^{-1})

7.4.4 Methods and Protocols - Preparation of Micelles

7.4.4.1 *Synthesis of Sarcosine N-Carboxyanhydride*

The Synthesis of sarcosine NCA was adapted from literature and modified.[121] 14.92 g (167.4 mmol) of sarcosine were weighed into a three neck flask and dried in vacuo for 1 hour. 300 mL of absolute THF were added under a steady flow of dry nitrogen and 16.2 mL (134 mmol) of diphosgene were added slowly via syringe and the nitrogen stream was reduced. The colorless suspension was mildly refluxed for 3 hours yielding a clear solution. Overnight, a steady flow of dry nitrogen was lead through the solution into two gas washing bottles filled with aqueous NaOH solution. The solvent was evaporated under reduced pressure, yielding a brownish oil as crude reaction product. The oil was heated to 50 °C and dried under reduced pressure (20 mbar, then $<10^{-2}$ mbar for 2 h) to obtain an amorphous solid, free of phosgene and HCl. The crude product was redissolved in 40 mL of absoute THF and precipitated with 300 mL of dry hexane. The solution was cooled to -18 °C overnight to complete precipitation. The solid was filtered under dry nitrogen atmosphere and dried under a stream of dry nitrogen for 60 - 90 minutes and afterwards in high vacuum for 2 hours in a sublimation apparatus. The crude product was sublimated at 80 - 85 °C and $<1\text{x}10^{-2}$ mbar. The product was collected from the sublimation apparatus in a glove box on the same day. The 12.64 g of purified product (110 mmol, 65% yield, colorless crystallites) were stored in a Schlenk tube at -80 °C, only handled in a glove box and used up quickly. Melting point: 102 - 104 °C (lit: 102 - 105 °C).[15, 368]
^{1}H-NMR (300 MHz, $CDCl_3$): δ [ppm] = 4.22 (2H, s, –N(CH_3)-**CH_2**-CO-), 2.86 (3H, s, -CH_3).

7.4.4.2 *Synthesis of N-ε-Trifluoroacetyl-L-Lysine N-Carboxyanhydride*

12.5 g (51.6 mmol) of *N*-ε-trifluoroacetyl protected lysine and 300 mL of absolute THF were added into a three necked flask equipped with a reflux condenser and a septum under a steady flow of dry nitrogen. The condenser outlet was connected to two gas washing bottles filled with aqueous NaOH, removing excess HCl and phosgene. Then, 5.50 mL (45.6 mmol) of diphosgene were added slowly via syringe and the nitrogen stream was reduced. The colorless suspension was mildly refluxed for 2 hours, yielding a cloudy solution. After this, a steady flow of dry nitrogen was lead through the solution overnight. The solution was filtered under dry nitrogen atmosphere. The solvent was evaporated under reduced pressure and absolute THF was added to completely dissolve the crude reaction product. Excess absolute hexane was added to the solution. After 1 hour storage at 4 °C, the solid was collected by filtration under dry nitrogen atmosphere and washed with hexane. The crude product was recrystallized twice with absolute THF/Hexane. 10.43 g of the purified product (39,0 mmol; 75% yield; colorless needles, melting point: 101 °C (lit: 92 - 93 °C)[376]) were obtained and stored in a Schlenk tube at -80 °C.
^{1}H-NMR (300 MHz, DMSO-d_6): δ [ppm] = 9.40 (1H, s, -**NH**-CO-CF_3), 9.09 (1H, s, -**NH**-CO-O-CO-), 4.43 (1H, t, ^{3}J H,H = 6.3 Hz, -CO-**CH**-CH_2-), 3.17 (2H, q, ^{3}J H,H = 6.3 Hz, -**CH_2**-NH-), 1.79-1.61 (2H, m, -C_H-**CH_2**-CH_2-CH_2-CH_2-NH-), 1.53-1.46 (2H, quin, ^{3}J $_{H,H}$ = 7.13 Hz, -CH-CH_2-CH_2-**CH2**-CH_2-NH-), 1.42-1.24 (2H, m, -CH-CH_2-**CH_2**-CH_2-CH_2-NH-).

7.4.4.3 *Synthesis of γ-Benzyl-L-Glutamate N-Carboxyanhydride*

The synthesis was adapted from literature and modified.[367] 10.01 g (42.1 mmol) of benzyl-ester protected glutamine were weighed into a three-neck flask and dried under vacuum for 1 hour. The solid was suspended in 200 mL of absolute THF under a steady flow of nitrogen. Then 4.07 mL (33.7 mmol) of diphosgene were added slowly via syringe and the nitrogen stream was reduced. The colorless suspension was mildly refluxed for 1.5 h, yielding a yellowish solution. After the last particles were dissolved a steady flow of dry nitrogen was lead throw the solution for 3 h. The condenser outlet was connected to two gas washing bottles filled with aqueous NaOH, removing excess HCl and phosgene.

The remaining solvent was evaporated under reduced pressure and absolute THF was added to completely dissolve the reaction product. Excess absolute hexane was added to the solution and the latter kept at 4 °C overnight to crystallize. The solid was filtered under dry nitrogen atmosphere and the crude product was recrystallized from THF/hexane twice, washed with hexane, dried in a dry nitrogen flow, and finally in high vacuum. A total of 10.52 g of the purified product (40 mmol; 95% yield; colorless needles; melting point: 93 – 94 °C (lit: 93 – 94 °C)[15]) was obtained and stored in a Schlenk tube at -80 °C.
^{1}H-NMR (300 MHz, CDCl3): δ [ppm] = 9.11 (1H, s, -NH-), 7.42-7.20 (5H, m, -C_6H_5), 5.10 (2H, s, -**CH_2**-C_6H_5), 4.52-4.42 (1H, dd, $^3J_{H,H}$ = 7.9), 5.5 Hz, -CO-**CH**-NH-), 2.52-2.48 (2H, t, $^3J_{H,H}$ = 7.9 Hz, BnO-CO-**CH_2**-), 2.15-1.85 (2H, m, -**CH_2**-CH-).

7.4.4.4 *Synthesis of (Man)-PSar$_n$*

N eq of PSar NCA were weighed into a Schlenk tube, dried under vacuum for 1 hour and dissolved in absolute DMF. A stock solution of either mannose initiator or neopentylamine in absolute DMF was prepared in a separate Schlenk tube. Both solutions were joined via syringe to yield a final monomer concentration of 0.1 g/mL. The polymerization solution was stirred at room temperature for 3 days and kept at a constant pressure of 1.25 bar of dry nitrogen via the Schlenk line to prevent impurities from entering the reaction vessel while allowing CO_2 to escape. Completion of the reaction was confirmed by IR spectroscopy (disappearance of the NCA peaks (1853 and 1786 cm^{-1})). Directly after completion of the reaction the polymer was precipitated into cold diethyl ether and centrifuged (4500 rpm at 4 °C for 15 min). After discarding the liquid fraction, new ether was added and the polymer was resuspended using a sonic bath. The suspension was centrifuged again and the procedure was repeated. After DMF removal by the resuspension steps, the polymer was dissolved in water and lyophilized to obtain a stiff, porous, colorless solid. Yield: 88.9%.
^{1}H-NMR of Man-PSar$_n$ (400 MHz, D_2O): δ [ppm] = 5.65 (1H, d, $^3J_{H-H}$ = 2.29 Hz, man.ini), 5.35 (1H, dd, $^3J_{H-H}$ = 4.17 Hz, $^3J_{H-H}$ = 5.87 Hz, man.ini), 5.10 (1H, t, $^3J_{H-H}$ = 10.16 Hz, man.ini), 4.52-3.95 (2nH, br, -NCH_3-**CH_2**-CO-), 3.70-3.47 (14H, br, man.ini), 3.19-2.60 ((3n+2)H, br, -NCH_3- and man.ini), 2.10-1.95 (12H, br, -CO-CH_3 of man.ini).

7.4.4.5 *Synthesis of (Man)-PSar$_n$-b-PGlu(OBn)$_m$*

1 eq of previously prepared homopolymer was weighed into a Schlenk tube, dried under vacuum for 1 h and dissolved in absolute DMF (0.1 g/mL). In a separate Schlenk tube m eq of Glu(OBn)NCA were dried under vacuum and dissolved in absolute DMF (0.1 g/mL). Both solutions were joined via syringe. Polymerization was carried out for 3 d at 0 °C under dry nitrogen atmosphere. Completion of the reaction was monitored by IR spectroscopy (disappearance of the NCA peaks (1853 and 1786 cm^{-1})). Directly after completion of the reaction the polymer was precipitated into cold diethyl ether and centrifuged (4500 rpm at 4 °C for 15 min). After discarding the liquid fraction, new ether was added and the polymer was resuspended using a sonic bath. The suspension was centrifuged again and the procedure was repeated. After DMF removal by the resuspension steps, the polymer was suspended in water and lyophilized to obtain a stiff, porous, colorless solid. Yield: 93.7%.
^{1}H-NMR of Man-PSar$_n$-b-PGlu(OBn)$_m$ (400 MHz, DMSO-d_6): δ [ppm] = 7.41-7.07 (5mH, br, -C_6H_5), 5.65 (1H, d, $^3J_{H-H}$ = 2.31 Hz, man.ini), 5.34 (1H, dd, $^3J_{H-H}$ = 3.90 Hz, $^3J_{H-H}$ = 6.11 Hz,

man.ini), 5.16-4.85 ((2m+1)H, br, -$\mathbf{CH_2}$-C_6H_5 and man.ini), 4.60-3.65 ((2n+1m)H, br, –NCH_3-$\mathbf{CH_2}$-CO- and -CO-**CH**-NH-), 3.54-3.47 (14H, br, man.ini), 3.17-2.62 ((3n+2)H, br, -NCH_3- and man.ini), 2.31-1.66 ((4m+12)H, br, -$\mathbf{CH_2}$-$\mathbf{CH_2}$-COOBn and -CO-$\mathbf{CH_3}$ of man.ini).

7.4.4.6 *Synthesis of (Man)-PSar$_n$-b-PLys(TFA)$_m$*

(Man)-PSar$_n$-b-PLys(TFA)$_m$ was prepared similarly to the synthesis of (Man)-PSar$_n$-b-PGlu(OBn)$_m$ by using Lys(TFA) NCA instead of Glu(OBn) NCA. Yield: 90.0%.
^{1}H-NMR of Man-PSar$_n$-b-PLys(TFA)$_m$ (400 MHz, DMSO-d_6): δ [ppm] = 9.49-9.21 (1mH, br, -**NH**-CO-CF_3), 5.65 (1H, d, $^3J_{H\text{-}H}$ = 2.29 Hz, man.ini), 5.35 (1H, dd, $^3J_{H\text{-}H}$ = 3.94 Hz, $^3J_{H\text{-}H}$ = 6.07 Hz, man.ini), 5.05 (1H, t, $^3J_{H\text{-}H}$ = 9.92 Hz, man.ini), 4.72-3.62 ((2n+1m)H, br, -NCH_3-$\mathbf{CH_2}$-CO- and -CO-**CH**-NH-), 3.50 (14H, br, man.ini), 3.23-3.05 (2mH, br, -$\mathbf{CH_2}$-NH-CO-CF_3), 3.04-2.56 ((3n+2)H, br, -N$\mathbf{CH_3}$- and man.ini), 2.15-0.90 ((6m+12)H, br, -CH-$\mathbf{CH_2}$-$\mathbf{CH_2}$-$\mathbf{CH_2}$-CH_2-NH- and -CO-$\mathbf{CH_3}$ of man.ini).

7.4.4.7 *End Group Labeling of (Man)-PSar$_n$-b-PGlu(OBn)$_m$ with Oregon Green 488*

In a glass vial, 42.06 mg of Man-PSar$_{277}$-b-PGlu(OBn)$_{28}$ were dissolved in 1 mL of DMSO under dry nitrogen atmosphere. 1.2 eq of Oregon Green 488 NHS ester (with respect to the terminal amino group of the polymer) dissolved in DMSO were added via syringe. The solution was protected from light and stirred for 3 days at 40 °C under dry nitrogen atmosphere. After that, the labeled polymer was directly subjected to dialysis against water for 3 days. Subsequent lyophilization yielded 41 mg (yield: 95.6%) of labeled polymer as fluffy, yellow solid.

7.4.4.8 *Selective Deprotection of the Mannose Group of Labeled Man-PSar$_n$-b-PGlu(OBn)$_m$*

30.3 mg of Oregon Green 488-labeled polymer were suspended in 1 mL NaOH(aq) solution adjusted to pH 9. The suspension was stirred for 18 hours at room temperature and subsequently subjected to dialysis against Millipore water for 3 days. To remove traces of free dye remaining from the labeling reaction the lyophilized polymer was further purified by reverse phase HPLC. Subsequent lyophilization yielded 19.04 mg (yield: 63.2%) of selectively deprotected polymer as fluffy, yellow solid.
^{1}H-NMR of Man$_{depr}$-PSar$_n$-b-PGlu(OBn)$_m$ (400 MHz, DMSO-d_6): δ [ppm] = 7.56-7.05 (5mH, br, -C_6H_5), 6.91 (d, $^3J_{H\text{-}H}$ = 7.64 Hz, OG 488), 6.59 (dd, $^3J_{H\text{-}H}$ = 2.37 Hz, $^3J_{H\text{-}H}$ = 11.30 Hz, OG 488), 5.62 (1H, man.ini), 5.23-4.84 (2mH, br, -$\mathbf{CH_2}$-C_6H_5), 4.65-3.67 ((2n+1m+3)H, br, –NCH_3-$\mathbf{CH_2}$-CO- and -CO-**CH**-NH- and man.ini), 3.54-3.47 (14H, br, man.ini), 3.10-2.62 ((3n+2)H, br, -N$\mathbf{CH_3}$- and man.ini), 2.41-1.60 ((4m)H, br, -$\mathbf{CH_2}$-$\mathbf{CH_2}$-COOBn), 1.61-0.98 (br, OG 488), 0.91-0.74 (br, OG 488).

7.4.4.9 *Full Deprotection of Man-PSar$_n$-b-PLys(TFA)$_m$*

In a glass vial, 30 mg of diblock copolymer were dissolved in 1 mL of Methanol. 10 eq of hydrazine hydrate (with respect to acetyl and TFA groups) were added and the solution was stirred for 3 days at room temperature. After that, the deprotected polymer was directly subjected to dialysis, first against $NaHCO_3$(aq), then against millipore water. Subsequent lyophilization yielded the labeled polymer as fluffy, colorless solid. Yield: 81.3%.
^{1}H-NMR of Man$_{depr}$-PSar$_n$-b-PLys$_m$ (400 MHz, D_2O): δ [ppm] =5.50 (1H, d, $^3J_{H\text{-}H}$ = 1.89 Hz, man.ini), 4.58-3.88 ((2n+1m)H, br, -NCH_3-$\mathbf{CH_2}$-CO- and -CO-**CH**-NH-), 3.73-3.46 (14H, br, man.ini), 3.24-2.50 ((3n+2m+2)H, br, -NCH_3- and -$\mathbf{CH_2}$-NH_2 and man.ini), 1.96-1.00 (6mH, br, -CH-$\mathbf{CH_2}$-$\mathbf{CH_2}$-$\mathbf{CH_2}$-CH_2-NH_2).

7.4.4.10 *Formation of Micelles*

8.54 mg of (Man)-PSar$_n$-b-PGlu(OBn)$_m$ were dissolved in 2.2 mL of DMSO. Under constant stirring 7.8 mL of Millipore water were added slowly via a syringe pump (0.5 mL/min). The micelle solution was dialyzed against Millipore water for 3 days. After lyophilization micelle solutions with a final concentration of 2 mg/mL were prepared by dissolving the micelles in the appropriate amount of PBS buffer.

7.4.5 Methods and Protocols - Physicochemical Characterization of Micelles

7.4.5.1 *Characterization of PeptoMicelles by Dynamic Light Scattering*

For dynamic light scattering experiments micelle solutions were prepared with concentrations as described. After transfer to a dust free flow box, all samples were filtered (Millex HV 0.45 µm) into dust free cylindrical scattering cells (Suprasil, 20 mm diameter, Hellma, Mühlheim, Germany). Then, dynamic light scattering (DLS) measurements were performed using a Uniphase He/Ne Laser (l = 632.8 nm, 22 mW), a ALV-SP125 Goniometer, a ALV/High QE APD-Avalanche photo-diode with fibre optical detection, an ALV 5000/E/PCI- correlator and a Lauda RC-6 thermostat unit at 20 °C. Angular dependent measurements of typically 15° steps were carried out in the range 30° $\leq$ q $\leq$ 150°. For data evaluation experimental intensity correlation functions were transformed into amplitude correlation functions applying the Siegert relation extended to include negative values after baseline subtraction by calculation $g_1(t) = SIGN(G2(t)) \cdot SQRT(ABS((G2(t) - A)/A)$. All field correlation functions usually showed monomodal decay and were fitted by a sum of two exponentials $g1(t) = a \cdot exp(-t/b) + c \cdot exp(-t/d)$ to take polydispersity into account. Average apparent diffusion coefficients D_{app} were calculated by applying $q^2 \cdot D_{app} = (a \cdot b - 1 + c \cdot d - 1)/(a + c)$ resulting in an angular-dependent diffusion coefficient D_{app} or reciprocal hydrodynamic radius $\langle 1/R_h \rangle_{app}$, according to formal application of Stokes Einstein law. By extrapolation of $\langle 1/R_h \rangle_{app}$ to $q = 0$ z-average hydrodynamic radii $R_h = \langle 1/Rh \rangle_{z^{-1}}$ were obtained (uncorrected for c-dependency).

7.4.6 Methods and Protocols - Biological Characterization of Micelles

7.4.6.1 *Cell Culture*

DC 2.4 cells[421] were cultivated at 37 °C, 5% CO_2 atmosphere in RPMI medium supplemented with 10% FCS (PAA, Cölbe, Germany), 2 mM L-glutamine (Biochrom AG, Berlin, Germany), 100 U/mL penicillin, 100 µg/mL streptomycin (Gibco, Paisly, UK) and 50 µM β-mercaptoethanol (Roth, Karlsruhe, Germany). Medium was changed regularly.

Bone marrow-derived DCs (BMDCs) were differentiated from bone marrow progenitors of C57BL/6 mice as first described by Scheicher *et al*.[422] and modified by Gisch and coworkers.[423] DC culture medium (IMDM with 5 Vol.% FCS [PAA, Cölbe, Germany], 2 mM L-glutamine [Biochrom AG, Berlin, Germany], 100 U/mL penicillin, 100 µg/mL streptomycin [Gibco, Paisly, UK]) and 50 µM β-mercaptoethanol [Roth, Karlsruhe, Germany], supplemented with 5% of GM-CSF containing cell culture supernatant [Zal *et al*., 1994,[424] a kind gift by Dr. B. Stockinger, MRC National Institute for Medical Research, Mill Hill, London]) was replenished on days 3 and 6 of culture. BM cells were seeded on 100 mm² bacterial dishes (2 x 10^6 cells/10 ml) and cultivated at 37 °C, 10% CO_2 atmosphere. Aliquots of non-adherent and loosely adherent immature BMDCs were harvested on days 6 or 7 of culture and were reseeded (10^6 cells/ml) on wells of six well tissue-culture plates (StarLab, Hamburg, Germany).

7.4.6.2 *Cellular Uptake of Micelles*

On day one, 150.000 DC 2.4 cells or BMDCs in 500 µL of medium were seeded onto a 24 well plate, respectively. The next day, 20 µg of micelles per well were added. After one hour, cells were harvested with PBS EDTA buffer (DC 2.4) or by frequent pipetting (BMDCs). Subsequently, cells were washed two times with PBS EDTA buffer, fixed with PBS buffer containing 0.7% PFA and subjected to FACS analysis.

7.4.6.3 *Determination of Cellular Toxicity of PeptoMicelles in DC 2.4 Cells by MTT Assay*

Cytotoxicity of PeptoMicelles was assessed by MTT assay using the "CellTiter 96® Non-Radioactive Cell Proliferation Assay" kit (Promega, Madison, USA) according to manufacturer's protocol. DC 2.4 cells were seeded onto 96-well culture plates at a concentration of 5×10^4 cells per well. Cells were incubated with 10/50 µg micelles of **P2** in a final volume of 100 µL (hexaplicates) for 24 hours. The next day, 30 µL of MTT substrate solution were added to each well and cells were cultured for another 4 h. Subsequently, 100 µL of "solubilization solution/stop mix" were added to each well. After 1 h, the absorbance at 570 nm was measured.

7.4.6.4 *Blocking Studies with Mannan and Dynasore-OH*

On day one, DC2.4 cells were seeded out as indicated above. The next day, cells were incubated with mannan (0.2 or 2 mg/mL) for 2 hours or with dynasore-OH (20 µM) for 30 minutes. Cells were washed four times with medium and micelles (50 µg per well) or ovalbumine (20 µg per well) were added. After one hour cells were harvested as indicated above, fixed with PBS buffer containing 0.7% PFA and subjected to FACS analysis.

ACKNOWLEDGEMENTS

Philipp Heller and Nicole Mohr contributed equally to this work. The authors would like to thank Prof. Tomas Kirchhausen for kindly providing dynasore-OH. Prof. Manfred Schmidt and Dr. Karl Fischer are gratefully acknowledged for support for particle characterization in solution by means of dynamic light scattering. Furthermore, the authors would like to thank Prof. Rudolf Zentel for stimulating discussions and scientific advice. The authors would like to acknowledge funding from DFG (SFB 1066-1), NMFZ Mainz and MAterials Science IN MainZ (MAINZ).

7.5 SUPPORTING INFORMATION

7.5.1 NMR Spectra

7.5.1.1 *Synthesis of Mannose Initiator*

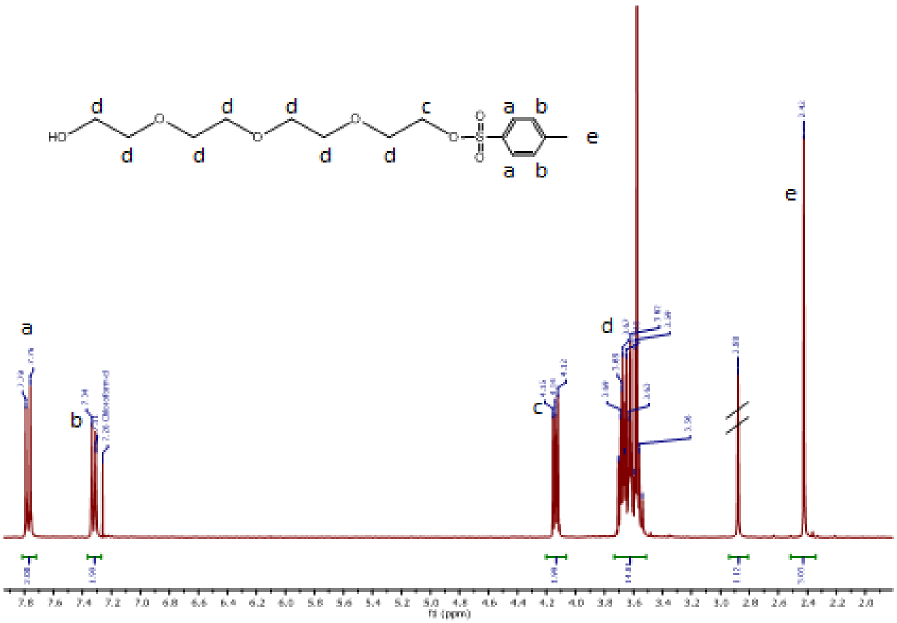

Figure 7.5: ^{1}H-NMR spectrum of tetraethylene glycol monotosylate.

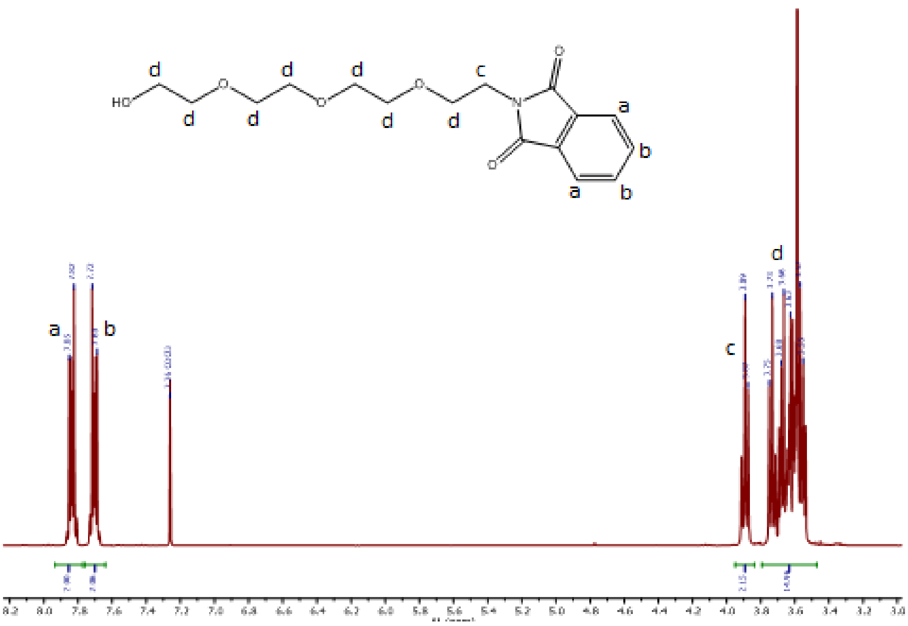

Figure 7.6: ^{1}H-NMR spectrum of *N*-(11-hydroxy-3,6,9-trioxaundecyl)phthalimide.

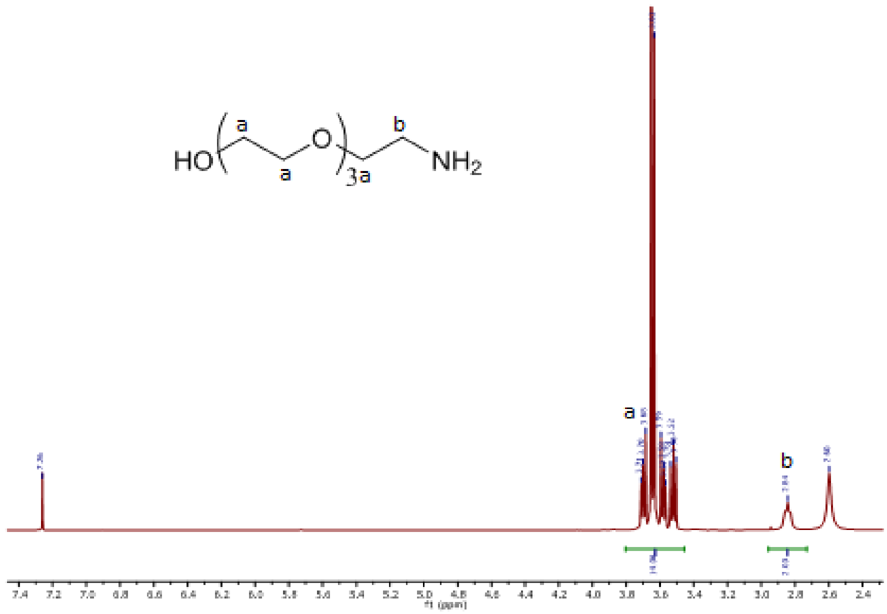

Figure 7.7: ^{1}H-NMR spectrum of 1-amino-11-hydroxy-3,6,9-trioxaundecan.

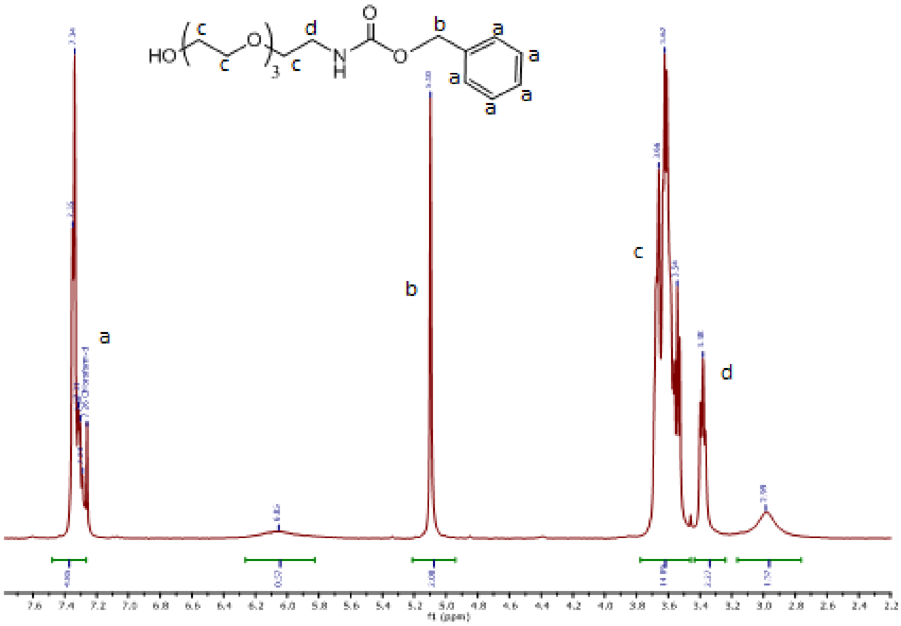

Figure 7.8: ^{1}H-NMR spectrum of 1-(benzoyloxycarbonylamino-11-hydroxy-3,6,9- trioxa) undecan.

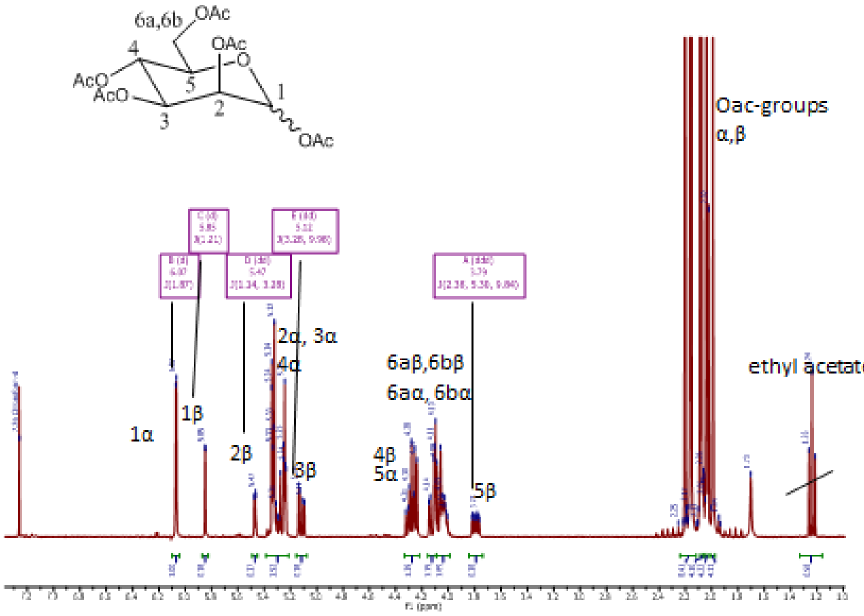

Figure 7.9: ^{1}H-NMR spectrum of 1,2,3,4,6-Penta-*O*-acetyl-D-mannopyranoside.

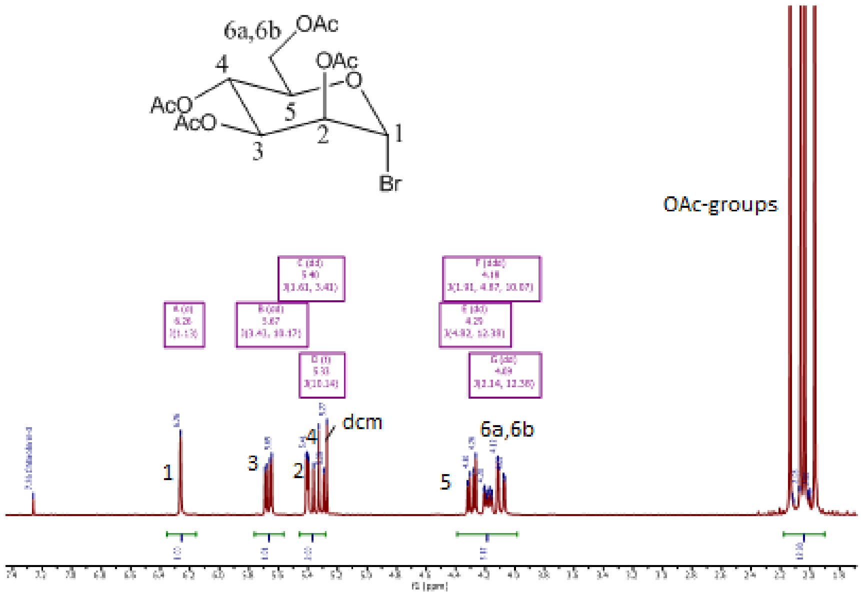

Figure 7.10: ^{1}H-NMR spectrum of 2,3,4,6-Tetra-*O*-acteyl-D-mannopyranosyl bromide.

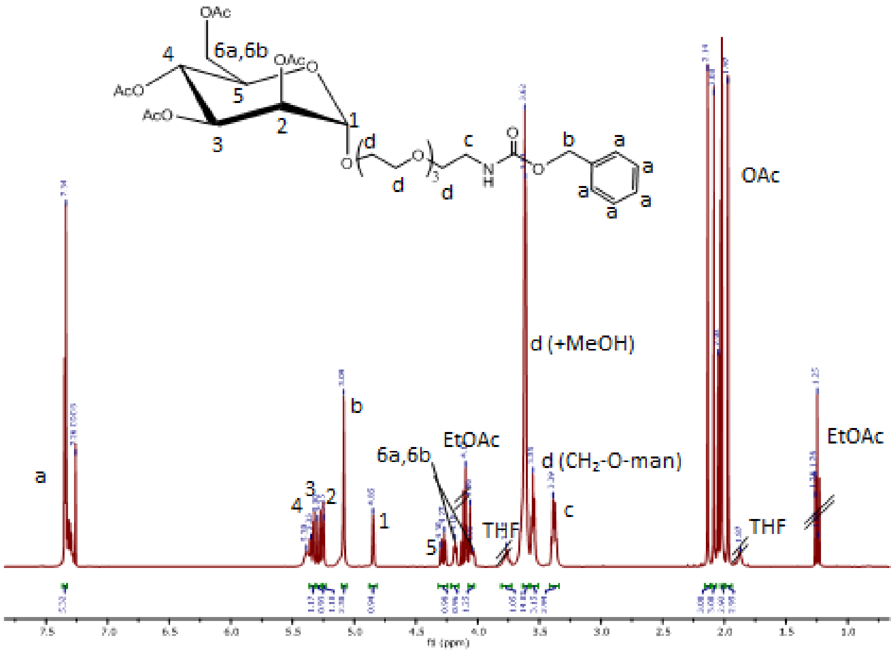

Figure 7.11: ¹H-NMR spectrum of 1-Benzyloxycarbonylamino-3,6,9-trioxaundecan-2,3,4,6-tetra-*O*-acetyl-β-D-mannopyranoside.

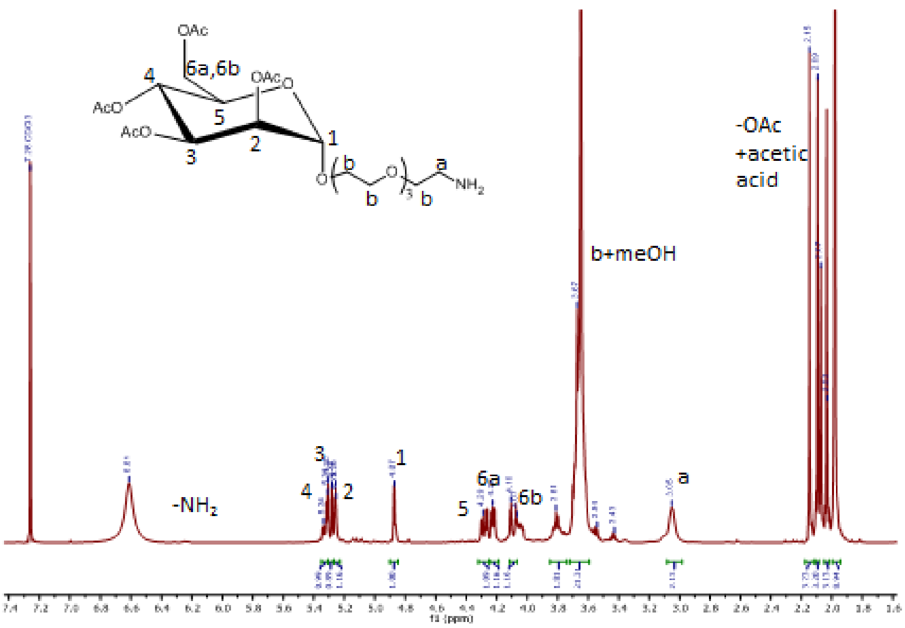

Figure 7.12: ¹H-NMR spectrum of 11-amino-3,6,9-trioxa-undecyl-2,3,4,6-tetra-O-acetyl-O-α-D-mannopyranoside.

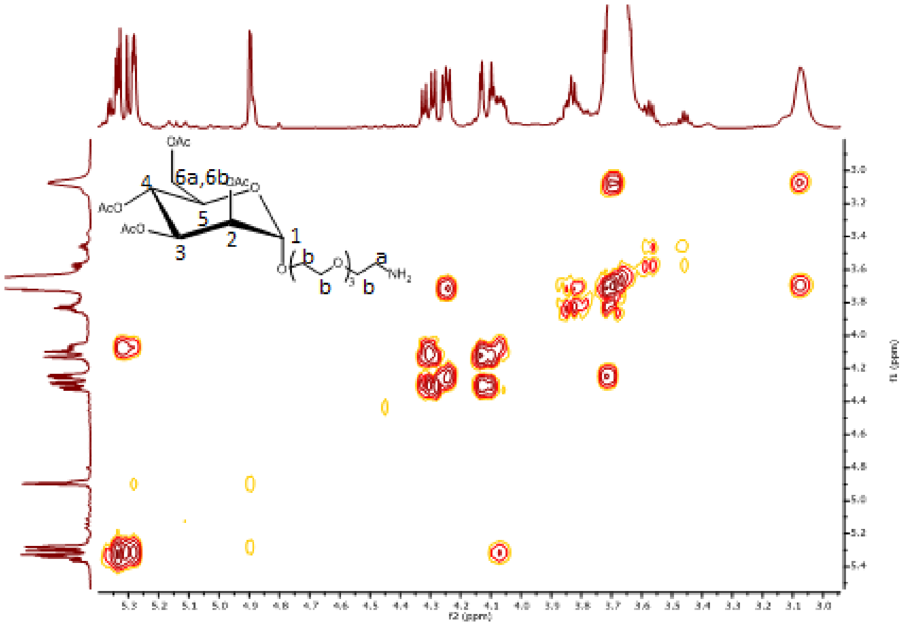

Figure 7.13: ^{1}H-^{1}H-HSQC spectrum of 11-amino-3,6,9-trioxa-undecyl-2,3,4,6-tetra-O-acetyl-O-α-D-mannopyranoside.

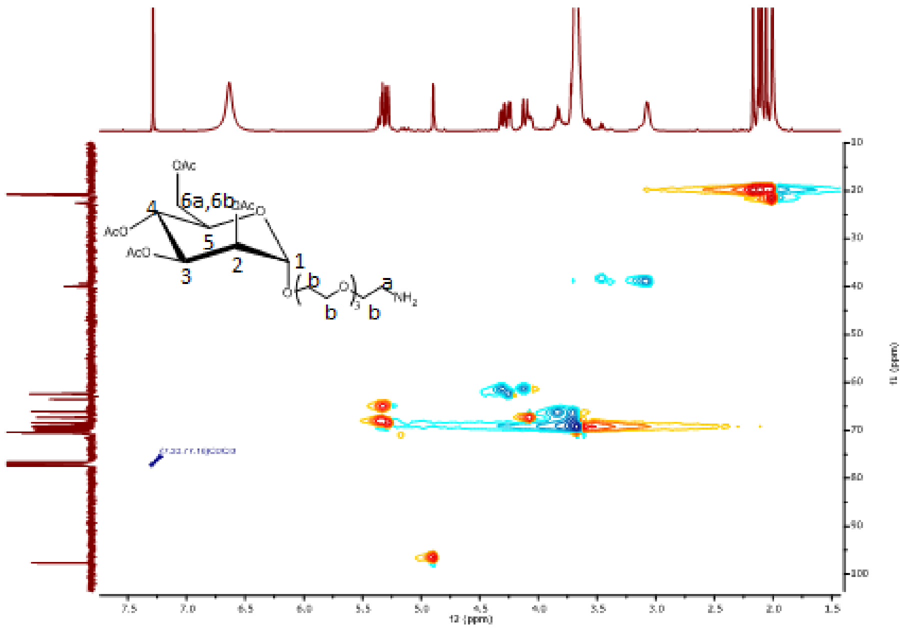

Figure 7.14: ^{1}H-^{13}C-HSQC spectrum of 11-amino-3,6,9-trioxa-undecyl-2,3,4,6-tetra-O-acetyl-O-α-D-mannopyranoside.

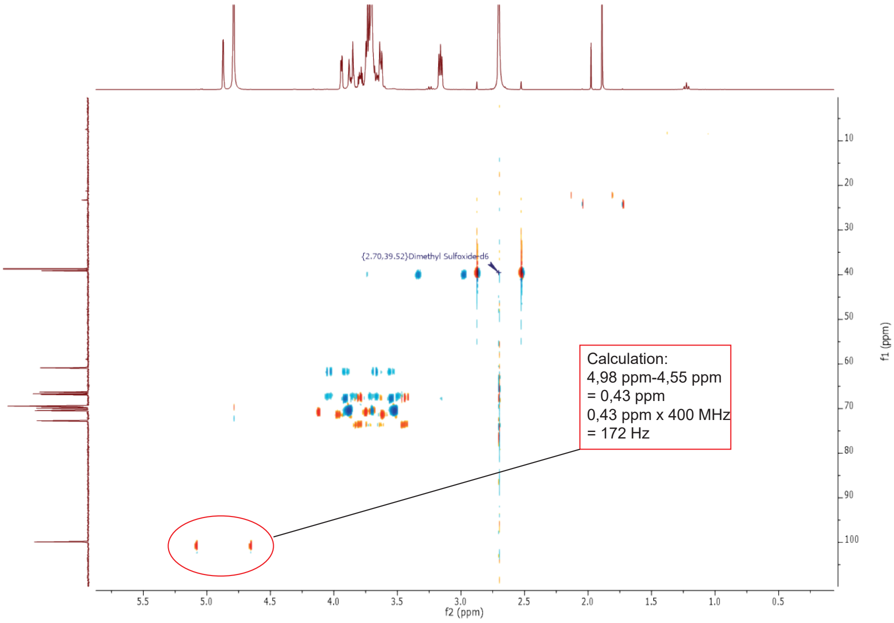

Figure 7.15: Measurement of $^1J_{CH}$ coupling by coupled HSQC spectroscopy. α-mannopyranoside: $^1J_{CH}$ = 170 Hz (equatorial H atom),[425] β-mannopyranoside: $^1J_{CH}$ = 160 Hz (axial H atom).

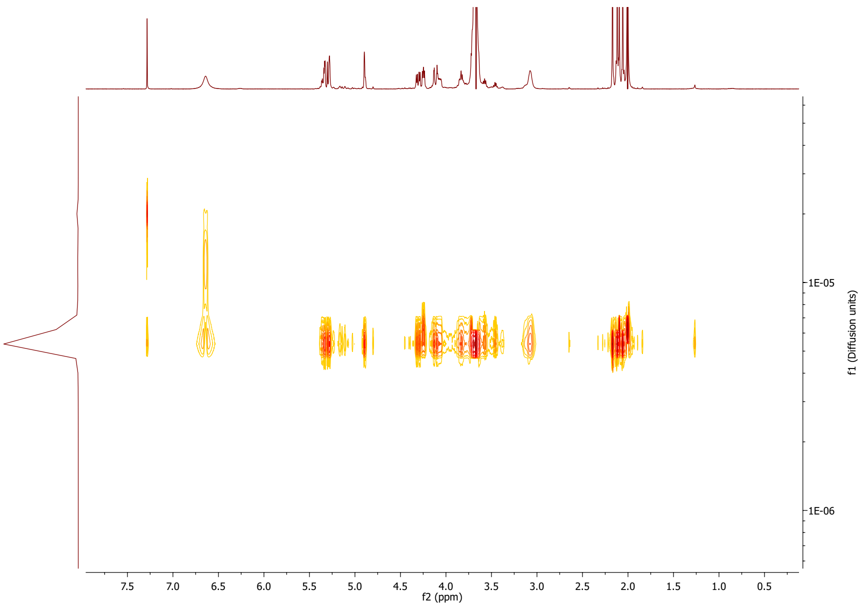

Figure 7.16: DOSY NMR spectrum of 11-amino-3,6,9-trioxa-undecyl-2,3,4,6-tetra-O-acetyl-O-α-D-mannopyranoside.

7.5.1.2 *Synthesis of Polymers*

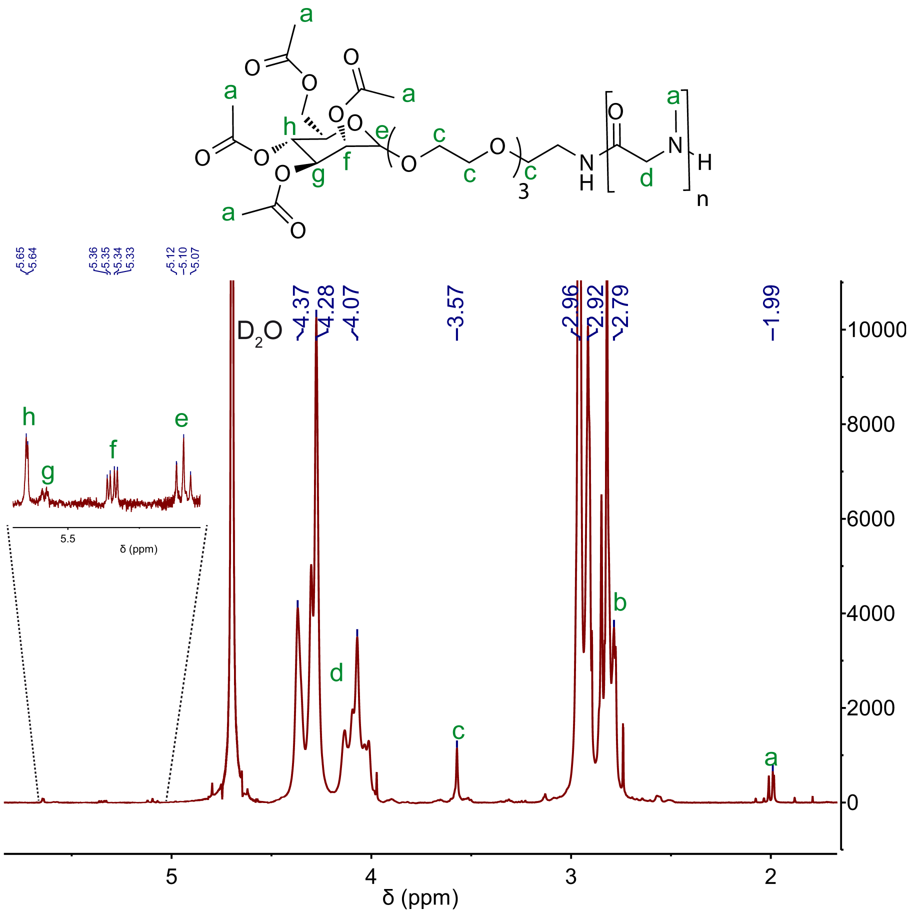

Figure 7.17: ^{1}H-NMR of (Man)-PSar$_n$.

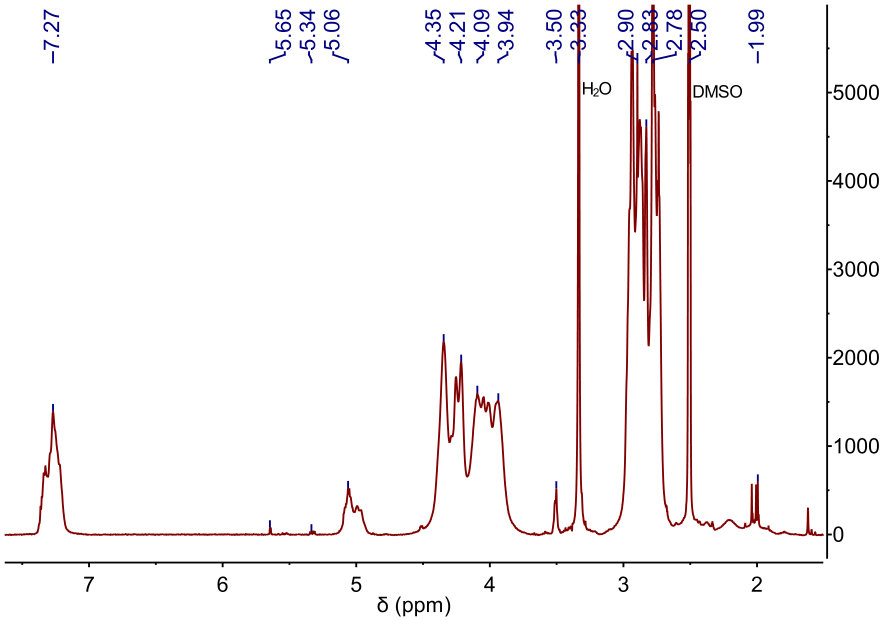

Figure 7.18: ^{1}H-NMR spectrum of (Man)-PSar$_n$-b-PGlu(OBn)$_m$.

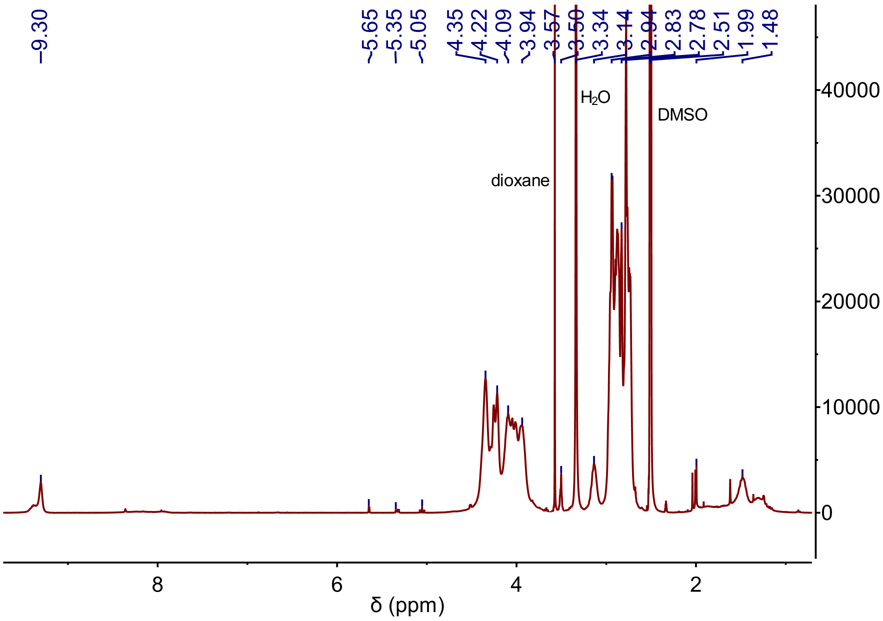

Figure 7.19: ^{1}H-NMR spectrum of (Man)-PSar$_n$-b-PLys(TFA)$_m$.

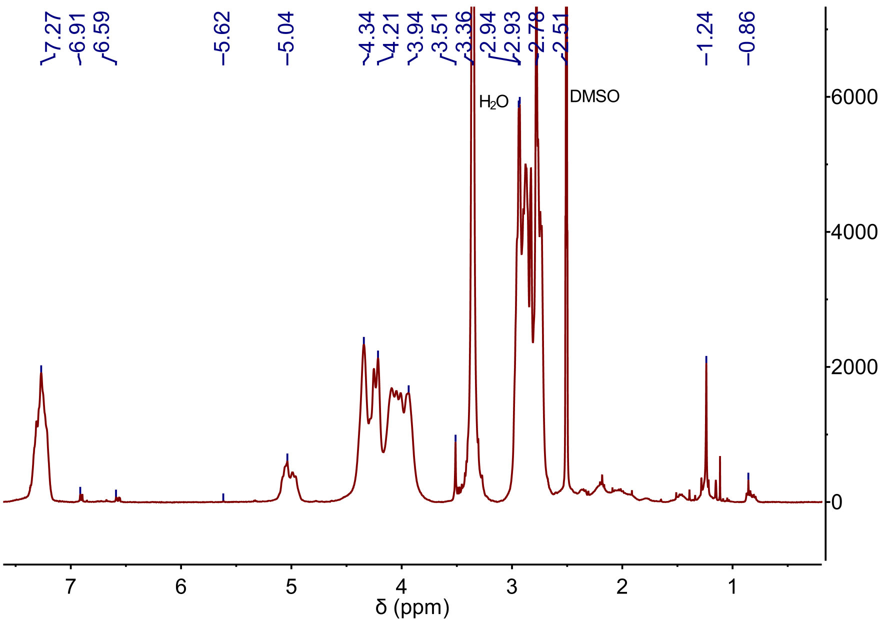

Figure 7.20: ^{1}H-NMR spectrum of OG 488-labeled (Man)-PSar$_n$-b-PGlu(OBn)$_m$with deprotected mannose end group.

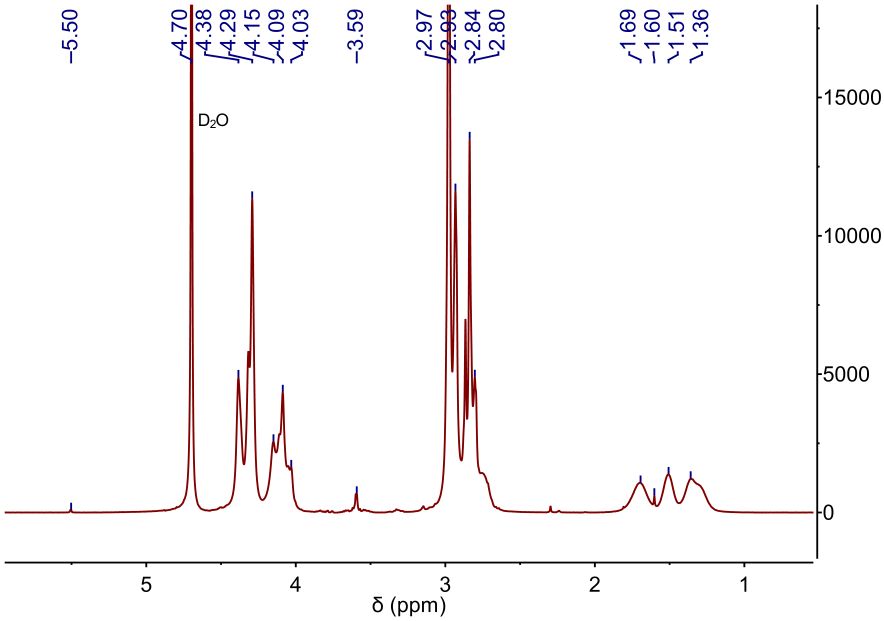

Figure 7.21: ^{1}H-NMR spectrum of (Man)-PSar$_n$-b-PLys.

7.5.2 GPC Plots

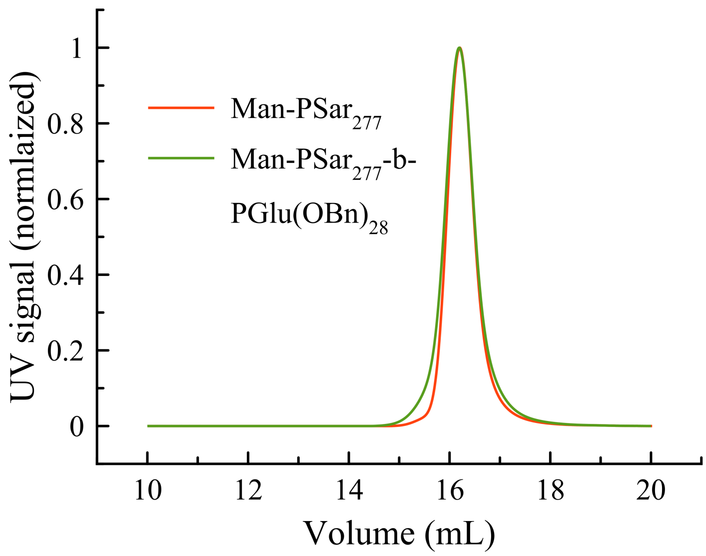

Figure 7.22: HFIP GPC plots from Man-PSar$_{277}$ and Man-PSar$_{277}$-b-PGlu(OBn)$_{28}$ showing the transition from homo to diblock copolymer.

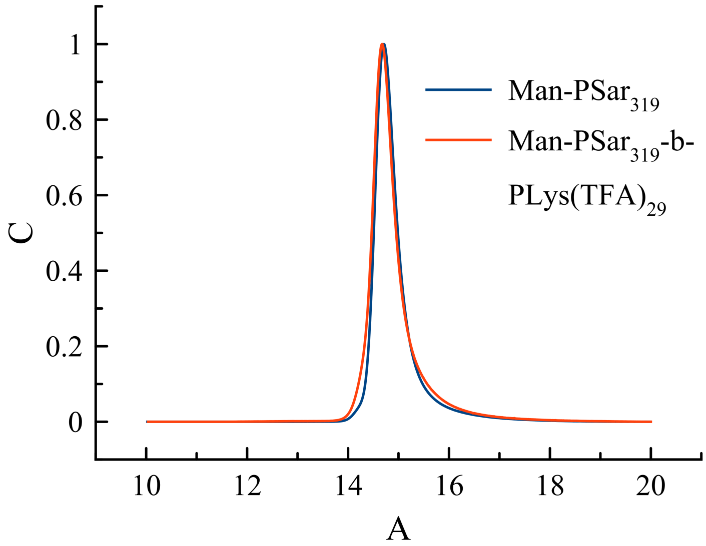

Figure 7.23: HFIP GPC plots from Man-PSar$_{319}$ and Man-PSar$_{319}$-b-PLys(TFA)$_{29}$ showing the transition from homo to diblock copolymer.

7.5.3 HPLC Traces

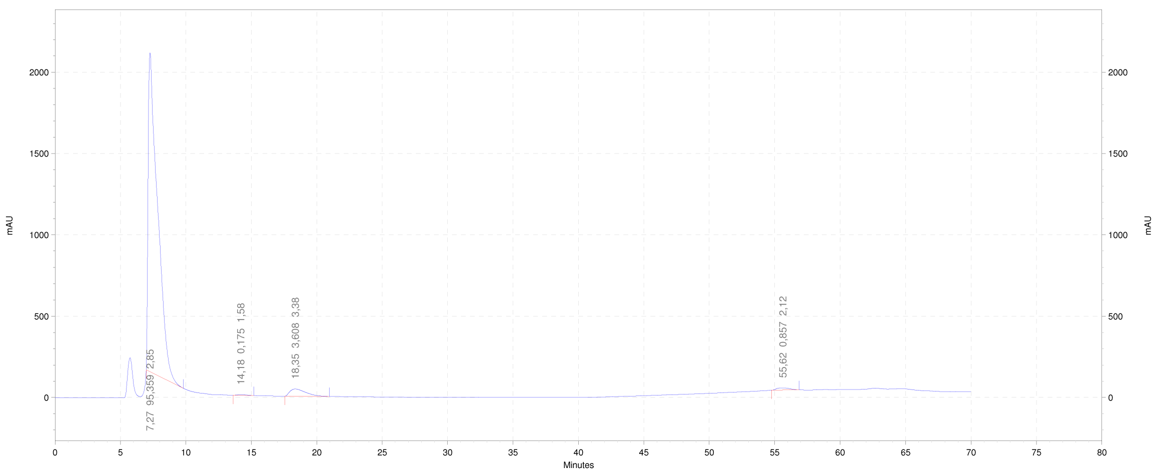

Figure 7.24: HPLC traces of Oregon Green 488-labeled Man-PSar$_{277}$-b-PGlu(OBn)$_{28}$.

7.5.4 Biological Assays

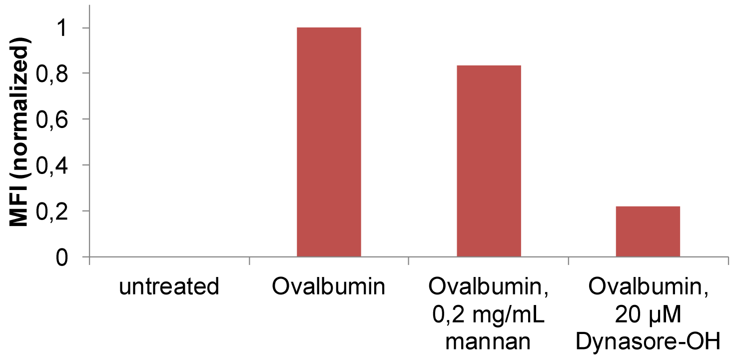

Figure 7.25: Uptake of ovalbumin by untreated DC 2.4 cells or after preincubation with mannan or dynasore-OH, respectively.

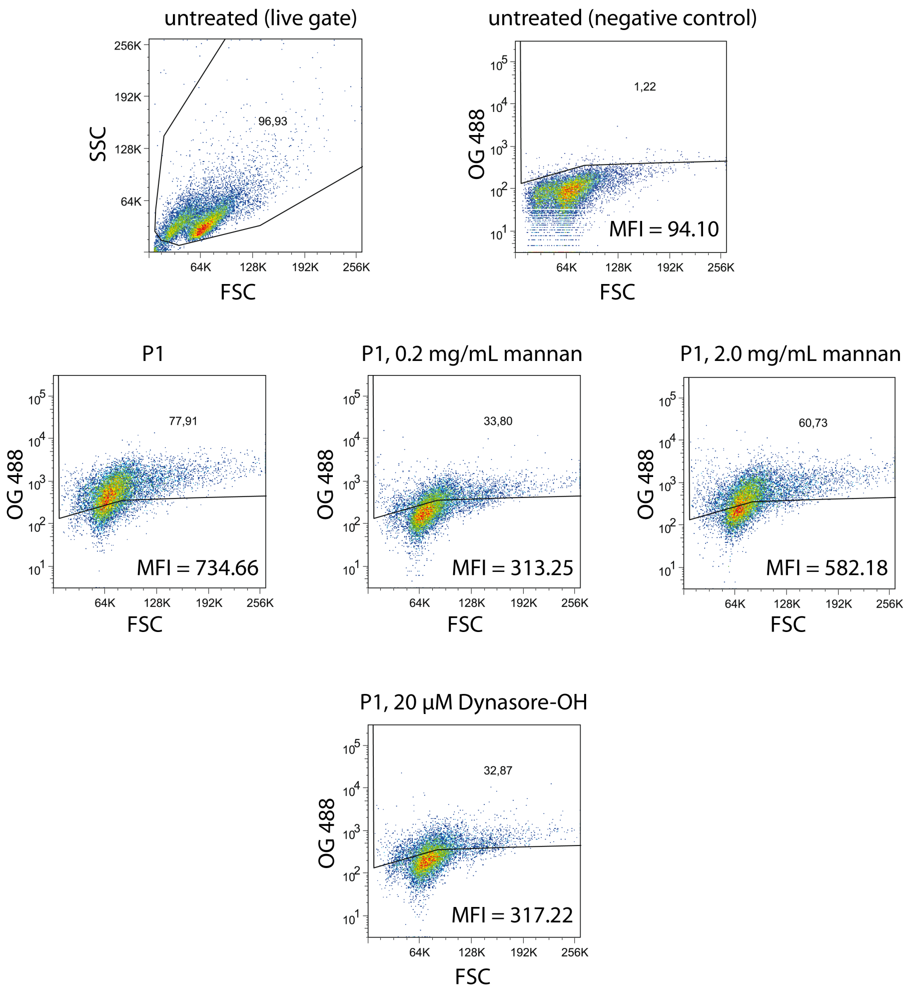

Figure 7.26: Representative dotplots of blocking experiments.

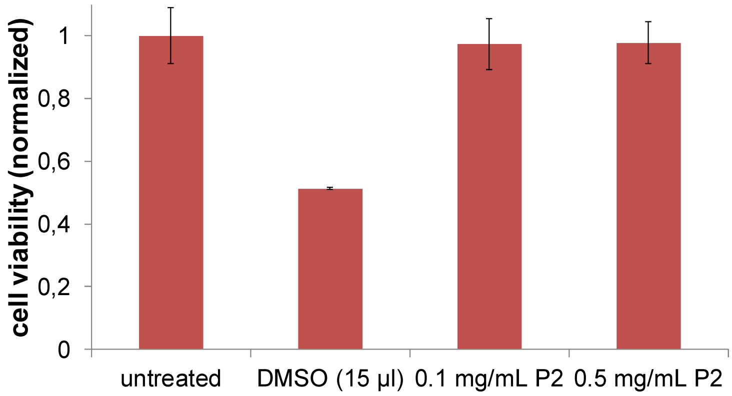

Figure 7.27: MTT assay of DC 2.4 cells after incubation with **P2**.

Part IV

PEPTOPLEXES FROM TRIBLOCK COPOLYPEPT(O)IDES

The following part covers the next stage of PeptoPlex development and the transition from simple diblock-based PeptoPlexes to triblock-based PeptoPlexes, which can be cross-linked by disulfides. At first, in a purely synthetic work the PLys(Boc)-b-PLys(TFA)-b-PSar triblock system with two orthogonal protective groups for the PLys segments was established (Chapter 8). Afterwards, these triblock copolypept(o)ides were utilized as the synthetic fundament for further functionalization with histidine. In a comparative study the connection between the microstructure of histidinylated polymers and the physicochemical and biological properties of corresponding PeptoPlexes (second generation) was investigated (Chapter 9). The triblock copolypept(o)ides also depict the starting point for modification with succinimidyl 3-(2-pyridyldithio)propionate to introduce activated disulfide groups. The combination of disulfide bearing triblock copolypept(o)ides and thiol-containing cross-linkers led to the development of a third generation of PeptoPlexes which can be stabilized covalently (Chapter 10). Furthermore, in a novel assay based on the recruitment of cytosolic galectin-8 to damaged endosomes, the endosomal escape of diblock-based, histidine-modified and cross-linked PeptoPlexes was imaged and qualitatively compared by means of confocal microscopy (Chapter 11).

8 SYNTHESIS AND SEQUENTIAL DEPROTECTION OF TRIBLOCK COPOLYPEPT(O)IDES USING ORTHOGONAL PROTECTIVE GROUP CHEMISTRY

P. Heller, B. Weber, A. Birke, M. Barz, *Macromolecular Rapid Communications*, 2015, **36**, 38-44

ABSTRACT

The synthesis of triblock copolymers based on polysarcosine, poly-*N*-ε-t-butyloxycarbonyl-L-lysine, and poly-*N*-ε-t-trifluoroacetyl-L-lysine by ring-opening polymerization of the corresponding α-amino acid *N*-carboxyanhydrides (NCAs) is described. For the synthesis of *N*-ε-t-butyloxycarbonyl-L-lysine (lysine(Boc)) NCAs, an acid-free method using trimethylsilylchloride/triethylamine as hydrochloric acid (HCl) scavengers is presented. This approach enables the synthesis of lysine(Boc) NCA of high purity (melting point 138.3 °C) in high yields. For triblock copolypept(o)ides, the degree of polymerization (X_n) of the polysarcosine block is varied between 200 and 600; poly-*N*-ε-t-butyloxycarbonyl-L-lysine and poly-*N*-ε-t-trifluoroacetyl-L-lysine blocks are designed to have a X_n in the range of 10-50. The polypeptide-polypeptoid hybrids (polypept(o)ides) can be synthesized with precise control of molecular weight, high end group integrity, and dispersities indices between 1.1 and 1.2. But more importantly, the use of tert-butyloxycarbonyl- and trifluoroacetyl-protecting groups allows the selective, orthogonal deprotection of both blocks, which enables further postpolymerization modification reactions in a block-selective manner. Therefore, the presented synthetic approach provides a versatile pathway to triblock copolypept(o)ides, in which functionalities can be separated in specific blocks.

8.1 INTRODUCTION

First reports on block copolypept(o)ides have already indicated that block copolymers composed of the endogenous amino acids sarcosine (Sar) and glutamic acid,[155, 161] lysine[156] or alanine[162] are a promising platform for the next generation of nano drug delivery systems (nanoDDS). These building blocks enable the generation of core–shell structures with hydrophobic or polyionic core, which can be used to deliver therapeutic agents such as drugs or nucleic acids.[359, 426] Surprisingly, polysarcosine (PSar) was almost completely overlooked as a substitute for PEG in nanoDDS, although it is known to combine properties of polypeptides with the stealth-like properties of PEG (hydrophilic, nonionic, nonimmunogenic, and protein resistant) as already demonstrated by other groups.[361, 362] Additionally, PSar can be polymerized from the corresponding NCA under living conditions as already demonstrated by Sisideo *et al*.,[117] Luxenhofer and co-workers,[121] and other groups.[27, 43, 162, 427, 428] Recently, Luxenhofer and co-workers have additionally reported a reduced stability of PSar to reactive oxygen species (ROS) yielding a more pronounced degradation under oxidative stress.[428]

We previously described the use of PSar in combination with PGlu or PLys to create polypeptide-polypeptoid hybrids (polypept(o)ides) with high end group integrity, precise control of molecular weight, and dispersity indices of around 1.1.[155, 156] These polypept(o)ides are accessible by the sequential ring-opening polymerization of the corresponding α-amino acid *N*-carboxyanhydrides (NCAs).[15, 366, 429–431] In case of lysine, the ε-amine has to be protected during polymerization, otherwise it would interfere during the reaction. Apart from the mere utilization of protective groups for prevention of side reactions during NCA polymerization, the smart combination of orthogonally deprotectable groups within block copolymers is highly desirable. With regard to PLys, this approach allows the selective deprotection of one block, making the ε-amine available for further reactions, while leaving the other block unaffected. It furthermore offers the additional advantage that solubility as well as reactivity of NCAs and polymers are comparable.

Commonly used protective groups for the polymerization of lysine NCA include benzyloxycarbonyl (Z) or trifluoroacetyl (TFA).[36] Thus, it seems reasonable to synthesize PLys(Z)-block-PLys(TFA)-block-PSar triblock copolymers. The deprotection, however, of such triblock copolymers is not trivial. While deprotection conditions for PLys(TFA) are compatible with PSar or polyethylene glycol (PEG), the deprotection of PLys(Z) is difficult to control with respect to PSar integrity. The mixture of HBr with trifluoroacetic acid or glacial acid, which is commonly used for cleavage of the Z group, can degrade either PSar or PEG.[156] Therefore, suitable acid-labile alternatives for the Z group appear preferable, for instance, the tert-butyloxycarbonyl (Boc) group. Surprisingly, the synthesis and application of PLys(Boc) has been reported only in a few publications.[64, 134, 432–434] One reason seems to be that the NCA synthesis is commonly performed after the Fuchs-Farthing method,[13, 14] which utilizes phosgene for ring closure leading to liberation of 2 eq of hydrochloric acid (HCl) per amino acid. Thus, acid-labile-protecting groups appear hardly compatible with the use of phosgene for NCA formation. Nevertheless, Barrett *et al.* reported the synthesis of lysine(Boc) NCAs applying the Fuchs-Farthing method.[434] Because they do not provide melting points and yields, it is difficult to validate this procedure. Iatrou *et al.* performed the ring closure in the presence of Et_3N yielding lysine(Boc) NCA with a yield of 60%.[64] Dygert *et al.* reported the use of AgCN in combination with the Fuchs-Farthing method, which leads to the NCA with the highest melting point reported in literature (136–137 °C).[432] The yields, however, were rather low (51%), which is likely due to extensive recrystallizations to ensure removal of insoluble AgCl. The liberation of HCN gas is also an additional drawback.

Another HCl-free synthesis of NCAs developed by Kricheldorf is hardly recognized. He reported the combination of trimethylsilylchloride/Et_3N for HCl scavenging,[15, 368] which allows a clean water-free synthesis of NCAs in the absence of HCl. Surprisingly, this methodology was not yet applied to lysine(Boc) NCA.

In this work, we report the synthesis of lysine(Boc) NCA by modification of the Kricheldorf method. Furthermore, we want to introduce the combination of PLys(Boc), PLys(TFA), and PSar for the synthesis of orthogonally deprotectable triblock copolypept(o)ides (Fig. 8.1).

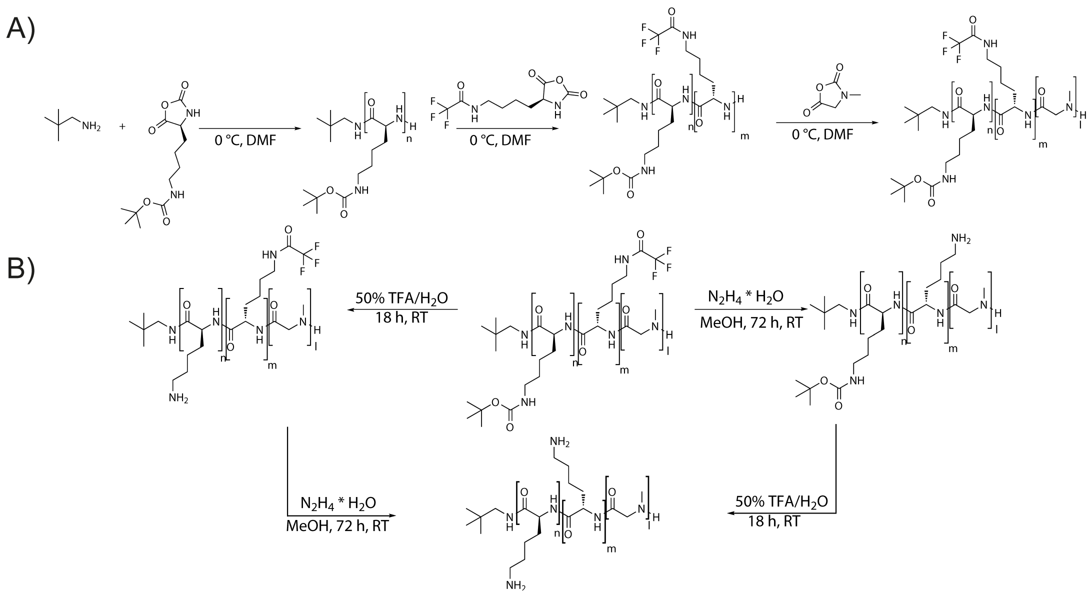

Figure 8.1: (A) Synthesis of PLys(Boc)-PLys(TFA)-PSar triblock copolymers by sequential ring opening polymerization followed by (B) block-specific deprotection of the PLys blocks.

8.2 RESULTS AND DISCUSSION

The synthesis of sarcosine and lysine(TFA) NCAs was reported previously[36, 155] and is analogous to the synthesis of many other NCAs. For lysine(Boc), however, we changed the typical NCA synthesis protocol (for reaction scheme see Subsection 8.4.3) since the acid-labile Boc group is likely to be - at least partially - cleaved by HCl emerging during NCA formation. As proposed by Kricheldorf,[15, 368] we therefore applied trimethylsilyl chloride (TMSCl). In contrast to the original procedure of Kricheldorf, we performed the NCA synthesis in one step instead of consecutive preparation of the silylated amino acid and cyclization. In this way lysine(Boc) NCA can be obtained in good yields (68%) with excellent purity as confirmed by a melting point of 138.3 °C (Lit. 134-137 °C)[432, 435] and ^{1}H-NMR (SI, Fig. 8.4). In general, the use of TMSCl is preferable to methods using an excess of triethylamine or diisopropyl ethylamine, since every trace of free tertiary amine or water (introduced through salt removal by extraction) in the final product can lead to polymerization of the NCA by the activated monomer mechanism (AMM) or initiation by water. Our modification of the Kricheldorf method solves these problems in a very elegant way and facilitates the synthesis of pure lysine(Boc) NCA, since no salts need to be removed.

Although reported in literature, the synthesis of PLys(Boc) homopolymers was carried out to verify that lysine(Boc) NCA can be polymerized in the absence of side reactions. Moreover, we wanted to investigate the effect of chain length on coil to helix transition (SI, Fig. 8.11). Compared with PLys(TFA) and PLys(Z), the change in hydrodynamic radius induced by coil to helix transition is rather small but detectable for PLys(Boc), which additionally supports the geometric interpretation of such effects as reported recently by Huesmann *et al.*[36]

We prepared triblock copolypept(o)ides with different block lengths each time using the first block as macroinitiator. Block ratios were varied systematically creating polypept(o)ides with higher PLys(Boc) or PLys(TFA) content, respectively (Table 8.1).

Table 8.1: Characteristics of different synthesized triblock copolypept(o)ides.

	POLYMER	CALCULATED BLOCK RATIO	BLOCK RATIO[A]	M_N[B]	Đ[B]
P1	PLys(Boc)-PLys(TFA)-PSar	30:30:200	30:33:213	26.6	1.15
P2	PLys(TFA)-PLys(Boc)-PSar	30:30:300	30:33:276	27.5	1.18
P3	PLys(Boc)-PLys(TFA)-PSar	30:30:400	33:34:386	28.1	1.15
P4	PLys(Boc)-PLys(TFA)-PSar	40:30:600	42:35:636	35.8	1.14
P5	PLys(Boc)-PLys(TFA)-PSar	40:30:300	42:28:311	29.4	1.14
P6	PLys(Boc)-PLys(TFA)-PSar	50:10:300	47:13:311	28.6	1.17
P7	PSar-PLys(TFA)-PLys(Boc)	200:20:20	196:18:22	30.8	1.20
P8	PSar-PLys(TFA)-PLys(Boc)	200:30:20	224:30:19	34.0	1.16
P9	PSar-PLys(TFA)-PLys(Boc)	200:30:10	224:36:13	33.0	1.20

[A] as determined by ^{1}H-NMR spectroscopy in DMSO-d_6
[B] kg/mol, as determined by GPC with HFIP as solvent and PMMA standards

Triblock architecture of the synthesized polymers was verified by ^{1}H-NMR spectroscopy, DOSY ^{1}H-NMR spectroscopy and GPC. In general, the desired block length can be obtained with high accuracy as indicated by ^{1}H-NMR. Especially for the first block, the variation between calculated and obtained blocks is 10% and less. Dispersity indices as determined by HFIP GPC are in a range of 1.14 to 1.20 for triblock copolymers. In general, dispersities are lowest for triblock copolymers with a sarcosine block between 300 and 600 units. The long PSar block will largely contribute to the hydrodynamic volume of the polymer and therefore determines its dispersity in hydrodynamic volume. Among triblock copolymers with PSar block lengths from 200 to 400, dispersities are almost identical. In all cases, a slight low-molecular-weight tailing can be observed, since the PLys(Boc) or PLys(TFA) blocks contain polymers in either random coil or helical formation.[36] The triblock copolymers could not be characterized by MALDI TOF measurements neither at protected nor deprotected stage, which is likely related to the elaborated degrees of polymerization. In summary, dispersities of triblock copolypept(o)ides are below 1.2, which is attributed to the fact that the coil to helix transition of polylysine broadens the molecular weight distribution obtained by GPC (Fig 8.2 (C)).

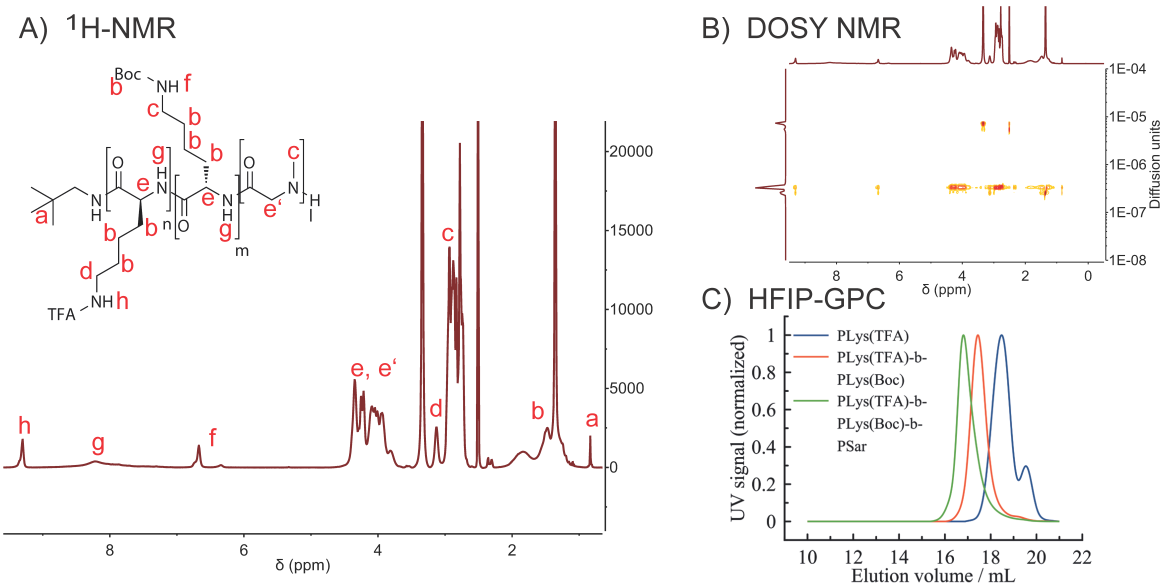

Figure 8.2: Characterization of triblock copolymers (P2). (A) 400 MHz ^{1}H-NMR spectrum in DMSO-d_6, (B) DOSY NMR spectrum in DMSO-d_6 and (C) GPC plots of PLys(TFA)$_{30}$, PLys(TFA)$_{30}$-b-PLys(Boc)$_{33}$ and PLys(TFA)$_{30}$-b-PLys(Boc)$_{33}$-b-PSar$_{276}$ (P2) in HFIP.

Aside from determination of dispersities, GPC also allows monitoring of chain extension of polypept(o)ides from mono- to di- and finally triblock copolymers (Fig 8.2 (C)). In this context, we investigated three different block sequences - PLys(Boc)-b-PLys(TFA)-b-PSar, PLys(TFA)-b-PLys(Boc)-b-PSar, PSar-b-PLys(TFA)-b-PLys(Boc) - and analyzed the concomitant change of hydrodynamic volume, respectively. The GPC traces show chain extension from PLys(TFA) to PLys(TFA)-b-PLys(Boc). Interestingly, for the inverse block sequence the hydrodynamic radius of PLys(Boc)-b-PLys(TFA) was slightly smaller than the radius of PLys(Boc) (SI, Fig. 8.12). In case of starting the polymer synthesis by PSar as first block, the hydrodynamic volume changed only marginally after addition of the lysine blocks due to the predominant share of the PSar block on the total polymer size. Successful chain extension and the absence of homopolymer or diblock copolymer impurities can also be confirmed by DOSY ^{1}H-NMR spectroscopy (Fig 8.2 (B)). Additionally, after full deprotection of triblock copolypept(o)ides, we observed unimodal molecular weight distributions by aqueous GPC (SI, Fig. 8.13).

Besides the synthesis of triblock copolypept(o)ides, the aim of this work is the selective deprotection of each lysine block in the absence of PSar degradation. Therefore, deprotection was adjusted taking two criteria into consideration: (I) quantitative deprotection of the respective block, and (II) no effects on the protective groups of the other block as well as triblock copolymer integrity. Deprotection of PLys(TFA) can be conducted with hydrazine hydrate (10 eq with respect to TFA groups) as reported earlier.[156] Quantitative cleavage of the Boc group can be achieved by dissolving the protected polymers in a 1:1 mixture of H_2O and TFA. Using 50% TFA/H_2O instead of the standard 50% TFA/CH_2Cl_2 known from peptide synthesis allows elimination of liberated t-butyl cations by OH^-, so that no additional cation scavengers need to be added to the reaction mixture.

By investigating the semiprotected polypept(o)ides in ^{1}H-NMR, ^{19}F-NMR, ^{13}C-NMR, and HSQC measurements, completeness of protective group removal and orthogonality of deprotection conditions was investigated. The ^{1}H-NMR signals of the initiator can be related to the ε-amide signals shifted by the Boc- and TFA-protecting groups. Cleavage of one protecting group does not influence the integral of the other amide signal and vice versa (Fig. 8.3 (A)). In ^{19}F-NMR, the TFA-protecting group can be monitored. During the deprotection of the Boc group, the fluorine signal at 75.8 ppm remains untouched, while it completely vanishes during TFA cleavage using hydrazine hydrate (Fig. 8.3 (B)). We obtained the same results either by analyzing the deprotected polymers at constant concentrations or by using an internal standard ($CFCl_3$) for calibration. Consequently, the proton and fluorine signals clearly show that PLys(TFA) is deprotectable without effects on PLys(Boc) and vice versa.

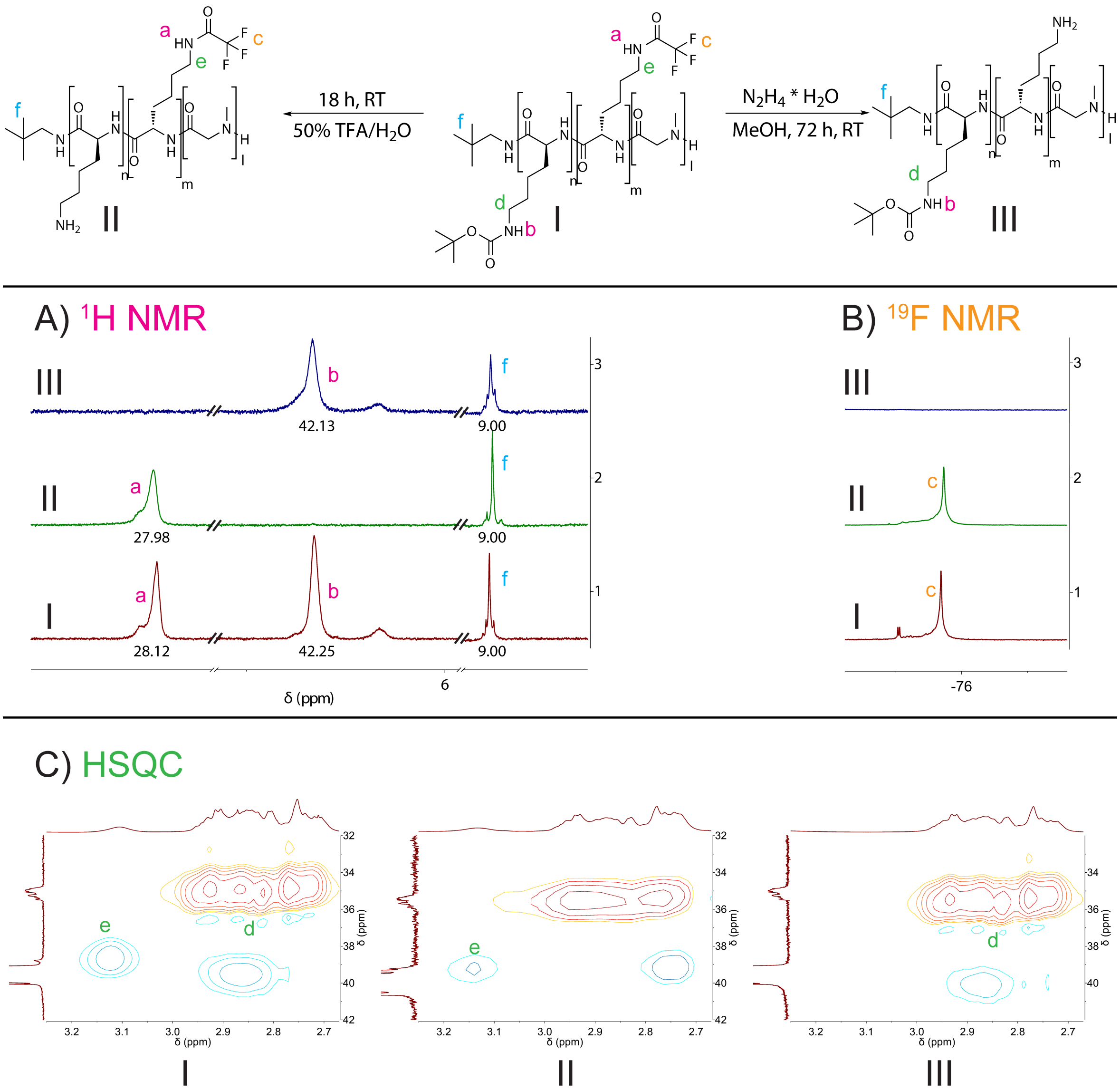

Figure 8.3: Orthogonal deprotection of PLys(Boc)-b-PLys(TFA)-b-PSar monitored by (A) ^{1}H-NMR spectroscopy, (B) ^{19}F-NMR spectroscopy and (C) heteronuclear single quantum coherence (HSQC) measurements.

This is further verified by heteronuclear single quantum coherence (HSQC) measurements before and after protective group removal, in which the chemical shifts between the ε-C and ε-H atoms of the lysine side chain are coupled (Fig. 8.3 (C)). The cross-coupling peaks of ε-C and ε-H atoms of the PLys(Boc) (d) and PLys(TFA) (e) side chains can be seen in the HSQC spectrum of the fully protected triblock copolypept(o)ide (I). After applying the deprotection conditions for the Boc-protecting group, only the cross-coupling peaks of ε-C and ε-H atoms of PLys(Boc) vanish (II). Applying the conditions for TFA removal leads to the disappearance of cross-coupling peaks of ε-C and ε-H atoms of PLys(TFA). We are well aware that HSQC measurements cannot be regarded as being quantitative. However, the selective disappearance of cross-coupling peaks supports the results obtained from ^{1}H-NMR and ^{19}F-NMR experiments. In summary, the NMR experiments demonstrated that both protecting groups display the expected orthogonal reactivity and thus can be used for block-selective deprotection of the triblock copolypept(o)ides. In addition, the reported conditions do not alter the integrity of the polysarcosine block.

Regardless of order, complete deprotection of polypept(o)ides could be achieved by performing the single deprotection steps successively. The now water-soluble polymers can be analyzed by ^{1}H-NMR spectroscopy and water GPC displaying the absence of protecting group-associated signals and unimodal molecular weight distributions (SI, Fig. 8.13). Furthermore, fully deprotected triblock copolypept(o)ides do not differ from their deprotected diblock counterparts of the comparable PSar and PLys block lengths.

8.3 CONCLUSION

Triblock copolypept(o)ides with orthogonally deprotectable lysine blocks have been synthesized and block selective deprotection was ensured. Therefore, this class of triblock copolymers represent a very interesting starting point for further polymer analogous reactions, when the preservation of block architecture is desirable. Additionally, the same synthetic strategy can be applied to PEG-based triblock copolymers, enabling the synthesis of multifunctional triblock copolymers for the next generation of block copolypept(o)ides for drug delivery or gene therapy.

8.4 EXPERIMENTAL SECTION

8.4.1 Materials

DMF was purchased from Acros (99.8%, Extra Dry over Molecular Sieve) dried over BaO and distilled *in vacuo* followed by excessive stirring *in vacuo* to remove traces of dimethylamine. THF and hexane were purchased from Sigma-Aldrich and distilled from sodium. Triethylamine was purchased from Carl Roth and distilled from potassium hydroxide. Other solvents were used as received. Diphosgene and chlorotrimethylsilane were purchased from Alfa Aesar and used as provided. Neopentylamine was purchased from TCI Europe, dried over NaOH and fractionally distilled. Sarcosine was purchased from Sigma-Aldrich, all other amino acids were purchased from ORPEGEN.

8.4.2 Instrumentation

8.4.2.1 *Polymer Characterization*

400 MHz ^{1}H-NMR spectra and ^{19}F NMR spectra were recorded on a Bruker Avance II 400. HSQC and DOSY NMR measurements were performed on a Bruker Avance III HD 400. All spectra were recorded at room temperature and analyzed with MestReNova software. Degrees of polymerization as well as molecular weights were calculated by comparing the integral of the neopentylamine initiator peak either with the integrals of the side chain amide protons (for PLys(Boc) and PLys(TFA)) or with the average of integrals of methyl group and α-protons (for PSar) in the 400 MHz ^{1}H-NMR spectra.

Attenuated total reflectance Fourier transformed infrared (ATR-FTIR) spectroscopy was performed on a FT/IR-4100 (JASCO Corporation) with an ATR sampling accessory (MIRacleTM, Pike Technologies). IR Spectra were analyzed using Spectra Manager 2.0 (JASCO Corporation).

Melting points were determined using a METTLER FP62 (METTLER WAAGEN GMBH).

Hexafluoroisopropanol (HFIP) gel permeation chromatography (GPC) was performed with HFIP containing 3 g/L potassium trifluoroacetate as eluent at 40 °C and a flow rate of 0.8 mL/min. The columns were packed with modified silica (PFG columns; particle size: 7 mm, porosity: 100 and 1000 Å). Polymer was detected with a refractive index detector (G 1362A RID, JASCO) and a UV/Vis Detector (UV-2075 Plus, JASCO). Molecular weights were calculated using a calibration performed with PMMA standards (Polymer Standards Services GmbH) and toluene as internal standard. Elution diagrams were analyzed using WinGPC UniChrome 8.00 (Build 994) software from Polymer Standards Services.

Aqueous gel permeation chromatography was performed in buffered aqueous solution (50 mM sodium chloride, pH 7) as eluent using a Superose 6 10/300 GL column. Polymer was detected with a UV/Vis detector (UV-2077 Plus, JASCO) and a RI-detector (JASCO RI 2031 Plus series). The flow rate was set to 0.4 mL min^{-1}. For calibration protein standards were used. All elution diagrams were evaluated with WinGPC UniChrome 8.00 (Build 994) software from Polymer Standards Services.

8.4.3 Methods and Protocols

8.4.3.1 *Synthesis of N-ε-tert-butyloxycarbonyl-L-Lysine N-Carboxyanhydride*

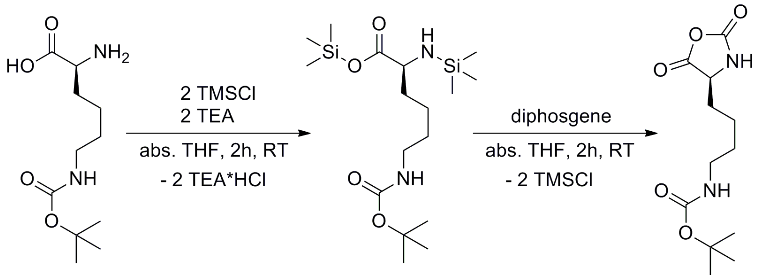

9.8 g (39.8mmol) of *N*-ε-Boc-protected lysine were weighed into a three-neck flask and dried under vacuum for 1 h. The solid was suspended in 300 mL of absolute THF under a steady flow of dry nitrogen. Afterwards, 9.9 ml (79.6 mmol) of absolute trimethylsilylchloride and 11.0 ml (79.6 mmol) of absolute triethylamine were added slowly via syringe. The suspension was stirred for 2 h followed by addition of 4.8 ml (39.8 mmol) of diphosgene, again via syringe. The suspension was mildly refluxed for another 2 h. Overnight, a steady flow of dry nitrogen was lead through the solution into two gas washing bottles filled with aqueous NaOH solution removing TMSCl. The suspension was filtered under dry nitrogen atmosphere to remove the salts of TEA and unconverted amino acid. The filtrate was evaporated under reduced pressure. Subsequently, absolute THF was added to completely dissolve the crude reaction product. The solution was precipitated with absolute hexane and stored at 4 °C for 1 h. The solid was collected by filtration under dry nitrogen atmosphere and washed with hexane. The crude reaction product was then recrystallized twice with absolute THF/hexane. 6.52 g of purified reaction product (23.9 mmol; 68% yield; colorless needles) were transferred into a Schlenk tube and stored at -80 °C. Melting point: 138.3 °C (Lit. 134 - 137° C).[432, 435]

^{1}H-NMR (400 MHz, DMSO-d$_6$): δ [ppm] = 9.07 (1H, s, -**NH**-CO-O-CO-), 6.95-6.34 (1H, br, -**NH**-CO-O-C(CH_3)$_3$), 4.42 (1H, t, $^3J_{H,H}$ = 6.35 Hz, -CO-**CH**-CH2-), 2.90 (2H, q, $^3J_{H,H}$ = 6.03 Hz, -**CH$_2$**-NH-CO-O-C(CH_3)$_3$), 1.79-1.56 (2H, m, -CH-**CH$_2$**-CH$_2$-CH$_2$-CH$_2$-NH-), 1.45-1.12 (13 H, m, -CH-CH$_2$-**CH$_2$-CH$_2$**-CH$_2$-NH- and -NH-CO-O-C(**CH$_3$**)$_3$).

8.4.3.2 *Synthesis of N-ε-Trifluoroacetyl-L-Lysine N-Carboxyanhydride*

12.5 g (51.6 mmol) of *N*-ε-trifluoroacetyl protected lysine and 300 mL of absolute THF were added into a three necked flask equipped with a reflux condenser and a septum under a steady flow of dry nitrogen. The condenser outlet was connected to two gas washing bottles filled with aqueous NaOH, removing excess HCl and phosgene. Then, 5.50 mL (45.6 mmol) of diphosgene were added slowly via syringe and the nitrogen stream was reduced. The colorless suspension was mildly refluxed for 2 h, yielding a cloudy solution. After this, a steady flow of dry nitrogen was lead through the solution overnight. The solution was filtered under dry nitrogen atmosphere. The solvent was evaporated under reduced pressure and absolute THF was added to completely dissolve the crude reaction product. Excess absolute hexane was added to the solution. After 1 h storage at 4 °C, the solid was collected by filtration under dry nitrogen atmosphere and washed with hexane. The crude product was recrystallized twice with absolute THF/Hexane. 10.43 g of the purified product (39,0 mmol; 75% yield; colorless needles, melting point: 101 °C (lit: 92 - 93 °C)[376]) were obtained and stored in a Schlenk tube at -80 °C.
^{1}H-NMR (300 MHz, DMSO-d_6): δ [ppm] = 9.40 (1H, s, -**NH**-CO-CF_3), 9.09 (1H, s, -**NH**-CO-O-CO-), 4.43 (1H, t, ^{3}J H,H = 6.3 Hz, -CO-**CH**-CH_2-), 3.17 (2H, q, ^{3}J H,H = 6.3 Hz, -**CH_2**-NH-), 1.79-1.61 (2H, m, -C_H-**CH_2**-CH_2-CH_2-CH_2-NH-), 1.53-1.46 (2H, quin, $^3J_{H,H}$ = 7.13 Hz, -CH-CH_2-CH_2-**CH2**-CH_2-NH-), 1.42-1.24 (2H, m, -CH-CH_2-**CH_2**-CH_2-CH_2-NH-).

8.4.3.3 *Synthesis of Sarcosine N-Carboxyanhydride*

The Synthesis of sarcosine NCA was adapted from literature and modified.[121] 14.92 g (167.4 mmol) of sarcosine were weighed into a three neck flask and dried in vacuo for 1 h. 300 mL of absolute THF were added under a steady flow of dry nitrogen and 16.2 mL (134 mmol) of diphosgene were added slowly via syringe and the nitrogen stream was reduced. The colorless suspension was mildly refluxed for 3 h yielding a clear solution. Overnight, a steady flow of dry nitrogen was lead through the solution into two gas washing bottles filled with aqueous NaOH solution. The solvent was evaporated under reduced pressure, yielding a brownish oil as crude reaction product. The oil was heated to 50 °C and dried under reduced pressure (20 mbar, then $<10^{-2}$ mbar for 2 h) to obtain an amorphous solid, free of phosgene and HCl. The crude product was redissolved in 40 mL of absoute THF and precipitated with 300 mL of dry hexane. The solution was cooled to -18 °C overnight to complete precipitation. The solid was filtered under dry nitrogen atmosphere and dried under a stream of dry nitrogen for 60 - 90 minutes and afterwards in high vacuum for 2 h in a sublimation apparatus. The crude product was sublimated at 80 - 85 °C and $<1x10^{-2}$ mbar. The product was collected from the sublimation apparatus in a glove box on the same day. The 12.64 g of purified product (110 mmol, 65% yield, colorless crystallites) were stored in a Schlenk tube at -80 °C, only handled in a glove box and used up quickly. Melting point: 102 - 104 °C (lit: 102 - 105 °C).[15, 368]
^{1}H-NMR (300 MHz, $CDCl_3$): δ [ppm] = 4.22 (2H, s, –N(CH_3)-**CH_2**-CO-), 2.86 (3H, s, -CH_3).

8.4.3.4 *Synthesis of Poly(N-ε-t-Butyloxycarbonyl-L-Lysine)*

Under nitrogen counter flow, n eq of lysine(Boc) NCA were transferred into a pre-dried Schlenk tube equipped with a stir bar and dried in high vacuum for 1 h. Then, lysine(Boc) NCA was dissolved in absolute DMF. In a glass vial flooded with nitrogen, 2 eq of neopentylamine were added to 2 mL of dry DMF and mixed. For initiation, 1 mL of the prepared stock solution was directly added to the Schlenk tube via syringe (yielding a reaction solution with 100 mg/mL monomer concentration). The solution was stirred at 0 °C and kept at a constant pressure of 1.25 bar of dry nitrogen via the Schlenk line to prevent impurities

from entering the reaction vessel while allowing CO_2 to escape. Completion of the reaction was confirmed by IR spectroscopy (disappearance of the NCA peaks (1853 and 1786 cm^{-1})). Directly after completion of the reaction the polymer was precipitated to cold ether and centrifuged (4500 rpm at 4 °C for 15 min). After discarding the liquid fraction, new ether was added and the polymer was resuspended using a sonic bath. The suspension was centrifuged again and the procedure was repeated. After DMF removal by the resuspension steps, the polymer was suspended in water and lyophilized to obtain a stiff, porous, colorless solid.
^{1}H-NMR of PLys(Boc)$_{33}$ (400 MHz, DMSO-d$_6$): δ [ppm] = 8.50-7.22 (33H, br, (1n), -**NH**-CO-CH$_2$-), 6.89-6.99 (33H, br, (1n), -**NH**-CO-O-C(CH$_3$)$_3$), 4.46-3.60 (33H, br, (1n), -CO-**CH**-NH-), 3.02-2.72 (67H, br, (2n), -**CH$_2$**-NH-CO-O-C(CH$_3$)$_3$), 2.03-0.97 (483H, br, (15n), -CH-**CH$_2$-CH$_2$-CH$_2$**-CH$_2$-NH- and -NH-CO-O-C(**CH$_3$**)$_3$), 0.84 (9H, br, -CH$_2$-C(**CH$_3$**)$_3$).

synthesis of triblock copolymers In case of intermediate workup of the first block, 1 eq of previously prepared lyophilized hompolymer was transferred into a pre-dried Schlenk tube equipped with a stir bar, dried in high vacuum for 1 h and then dissolved in absolute DMF. In case of no intermediate workup, the homopolymer solution was directly used for further polymerizations. For the second block, m eq of the desired NCA were dissolved in absolute DMF and added to the hompolymer solution via syringe (yielding a reaction solution with 100 mg/mL monomer concentration). The solution was stirred at 0° C and kept at a constant pressure of 0.25 bar of dry nitrogen via the Schlenk line to prevent impurities from entering the reaction vessel while allowing CO_2 to escape. Completion of the reaction was confirmed by IR spectroscopy (disappearance of the NCA peaks (1853 and 1786 cm^{-1})). Directly after completion of the reaction, p eq of the next desired NCA were dissolved in absolute DMF and added to the diblock copolymer via syringe. Again, the solution was stirred at 0° C and kept at a constant pressure of 0.25 bar of dry nitrogen via the Schlenk line. Completion of the reaction was confirmed by IR spectroscopy. The final triblock copolymer was precipitated into cold ether and centrifuged (4500 rpm at 4°C for 15 min). After discarding the liquid fraction, new ether was added and the polymer was resuspended using a sonic bath. The suspension was centrifuged again and the procedure was repeated. After DMF was removed by the resuspension steps the polymer was dissolved in 20% methanol/Millipore water and lyophilized to obtain a fluffy, colorless powder. For different chain lengths and scales yields ranged from 70 to 90%.
^{1}H-NMR of PLys(Boc)$_{42}$-b-PLys(TFA)$_{28}$-PSar$_{311}$ (400 MHz, DMSO-d$_6$): δ [ppm] = 9.47-9.22 (28H (1n), br, -**NH**-CO-CF$_3$), 8.36-8.03 (br, -**NH**-CO-CH$_2$-), 7.01-6.14 (42H (1m), br, -**NH**-CO-O-C(CH$_3$)$_3$), 4.68-3.57 (668H (1n + 1m + 2p), br, -CO-**CH**-NH- and -NCH$_3$-**CH$_2$**-CO-), 3.18-2.60 (1110H (2n + 2m +3p), br, -**CH$_2$**-NH-CO-CF$_3$ and -**CH$_2$**-NH-CO-O-C(CH$_3$)$_3$ and -NCH$_3$-), 2.07-0.96 (653H (6(n + m) + 9m), br, -CH-**CH$_2$-CH$_2$-CH$_2$**-CH$_2$-NH- and -NH-CO-O-C(**CH$_3$**)$_3$), 0.84 (9H, br, -CH2-C(**CH$_3$**)$_3$).

8.4.3.5 *Deprotection of the PLys(TFA) Block*

In a round-bottom flask, the polymer was dissolved in MeOH at a concentration of 30-50 mg/mL and 10 eq of hydrazine hydrate (with regard to the (TFA)-group) were added with an Eppendorf pipette. The solution was stirred for 72 h. Afterwards, the solution was diluted with Millipore water and dialyzed with a Spectra/Por (Roth) membrane with a nominal molecular weight cut-off (NMWCO) of 3500 g/mol for 3-5 days with regular substitution of water and then lyophilized to yield the deprotected polymer as a fluffy, colorless powder.
^{1}H-NMR of PLys(Boc)$_{42}$-b-PLys$_{28}$-PSar$_{311}$ (400 MHz, DMSO-d$_6$): δ [ppm] = 8.88-7.59 (br, -**NH**-CO-CH$_2$-), 6.92-6.23 (42H (1m), br, -**NH**-CO-O-C(CH$_3$)$_3$), 4.87-3.84 ((1n + 1m + 2p),

br, -CO-**CH**-NH- and -NCH_3-**CH_2**-CO-), 3.84-3.13 (br, H_2O), 3.13-2.56 ((2n + 2m +3p), br, -**CH_2**-NH_2 and -**CH_2**-NH-CO-O-$C(CH_3)_3$ and -NCH_3-), 2.12-0.93 ((6(n + m) + 9m), br, -CH-**CH_2-CH_2-CH_2**-CH_2-NH- and -NH-CO-O-C(**CH_3**)$_3$), 0.84 (9H, br, -CH_2-C(**CH_3**)$_3$).

8.4.3.6 *Deprotection of the PLys(Boc) Block*

In a round-bottom flask, 30-50 mg of polymer were dissolved in 50% TFA/H_2O. The solution was stirred for 18 h . Afterwards, the solution was diluted with Millipore water and dialyzed with a Spectra/Por (Roth) membrane with a nominal molecular weight cut-off (NMWCO) of 3500 g/mol - first against $NaHCO_3$(aq), after 2 days against water. Subsequently, the solution was lyophilized to yield the deprotected polymer as a fluffy, colorless powder.
^{1}H-NMR of $PLys_{42}$-b-$PLys(TFA)_{28}$-$PSar_{311}$ (400 MHz, DMSO-d_6): δ [ppm] = 9.73-9.07 (28H (1n), br, -**NH**-CO-CF_3), 8.75-7.61 (br, -**NH**-CO-CH_2-), 5.28-3.29 ((1n + 1m + 2p), br, -CO-**CH**-NH- and -NCH_3-**CH_2**-CO- and H_2O), 3.28-2.63 (991H (2n + 2m +3p), br, -**CH_2**-NH-CO-CF_3 and -**CH_2**-NH_2 and -NCH_3-), 2.26-0.99 (483H (6(n + m)), br, -CH-**CH_2-CH_2-CH_2**-CH_2-NH-), 0.83 (9H, br, -CH_2-C(**CH_3**)$_3$).

ACKNOWLEDGEMENTS

Philipp Heller and Benjamin Weber contributed equally to this work. The manuscript was written through contributions of all authors. All authors have given approval to the final version of the manuscript. The authors acknowledge funding from the DFG 1066–1, COMATT, NMFZ Mainz, and MAterials Science IN MainZ (MAINZ). The authors declare no competing financial interest. The authors thank Dr. Johannes Liermann and Prof. Rudolf Zentel for stimulating discussions and scientific advice.

8.5 SUPPORTING INFORMATION

8.5.1 NMR Spectra

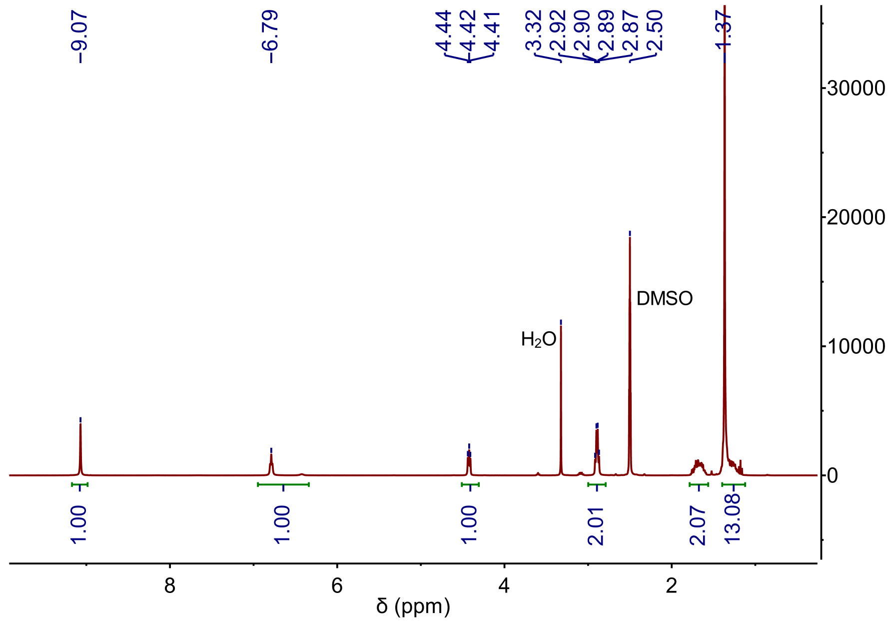

Figure 8.4: ^{1}H-NMR spectrum of *N*-ε-tert-butyloxycarbonyl-L-Lysine *N*-Carboxyanhydride.

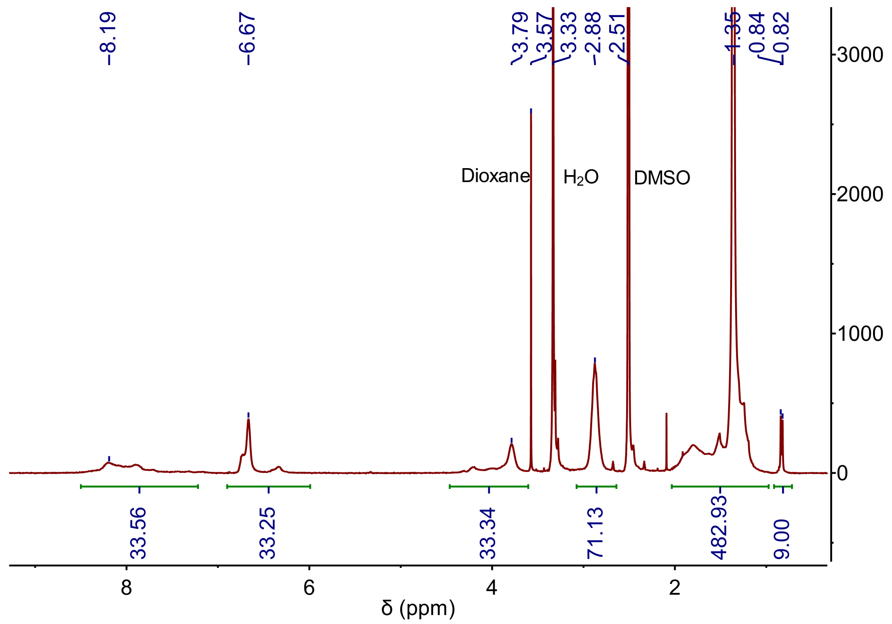

Figure 8.5: ^{1}H-NMR spectrum of PLys(Boc)$_{33}$.

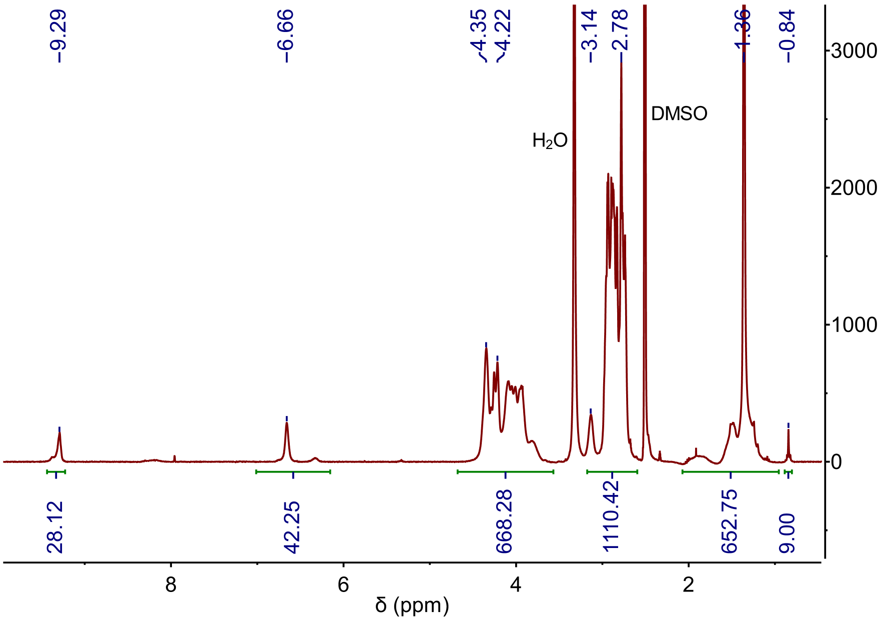

Figure 8.6: ^{1}H-NMR spectrum of PLys(Boc)$_{42}$-b-PLys(TFA)$_{28}$-b-PSar$_{311}$.

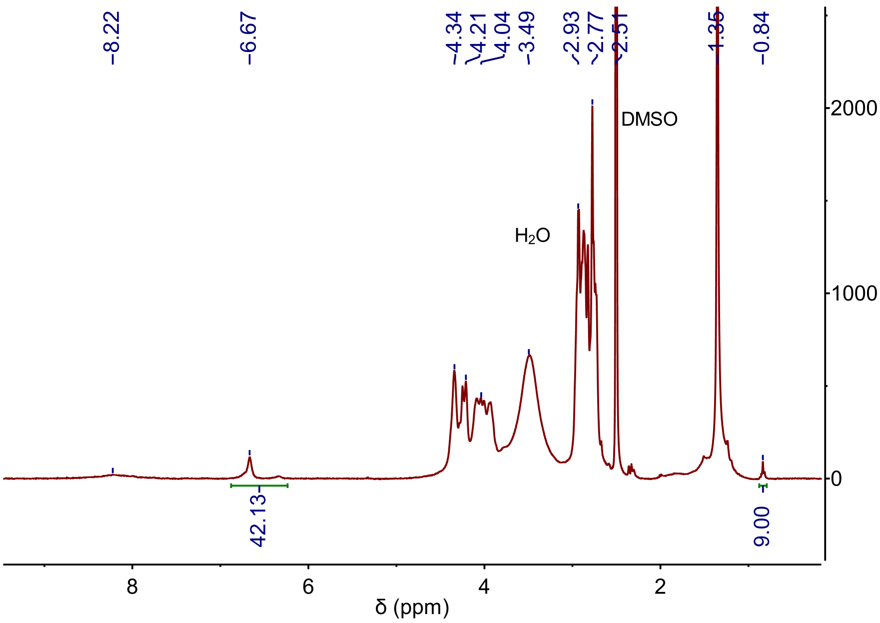

Figure 8.7: ^{1}H-NMR spectrum of PLys(Boc)$_{42}$-b-PLys$_{28}$-b-PSar$_{311}$.

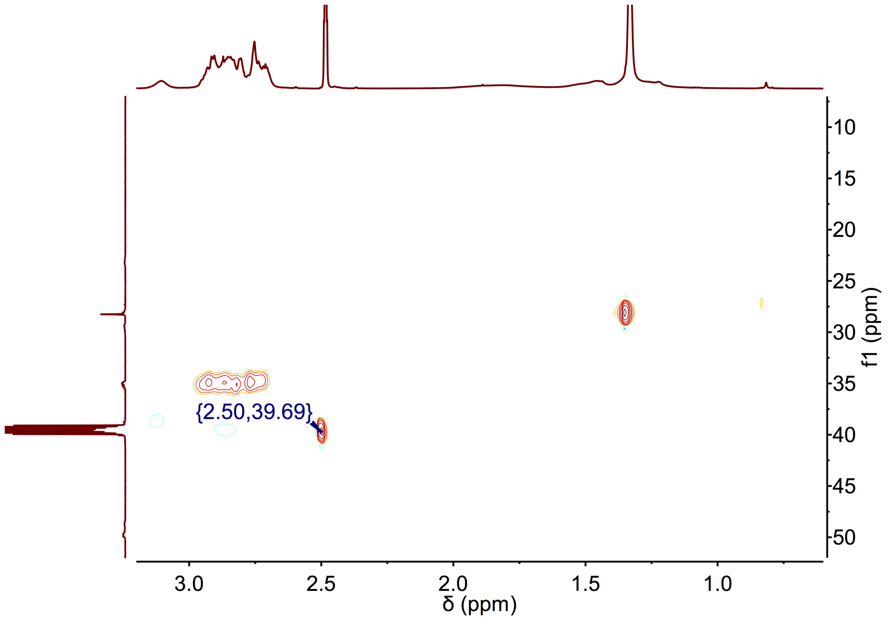

Figure 8.8: Heteronuclear single quantum coherence (HSQC) measurements of PLys(Boc)$_{42}$-b-PLys$_{28}$-b-PSar$_{311}$.

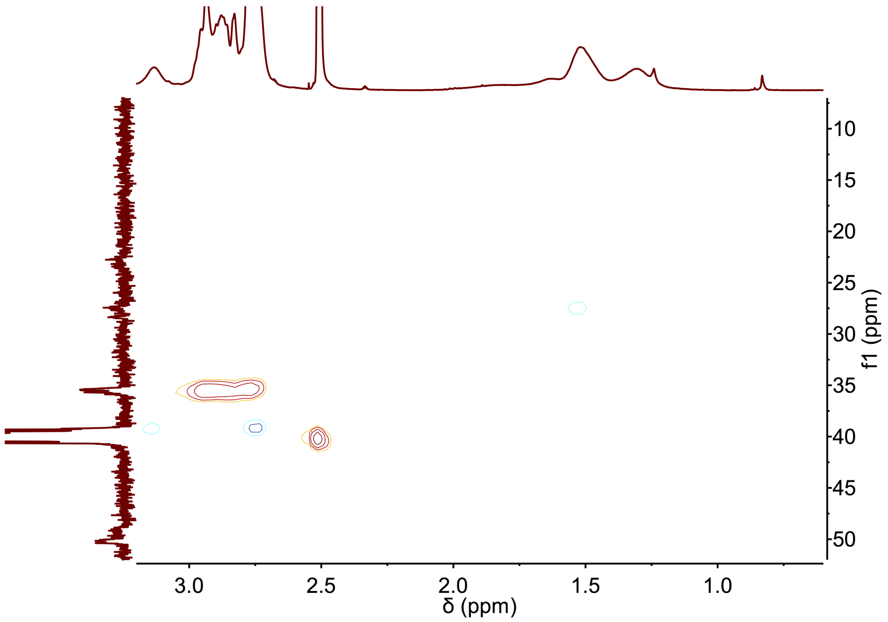

Figure 8.9: Heteronuclear single quantum coherence (HSQC) measurements of PLys$_{42}$-b-PLys$_{28}$-b-PSar$_{311}$.

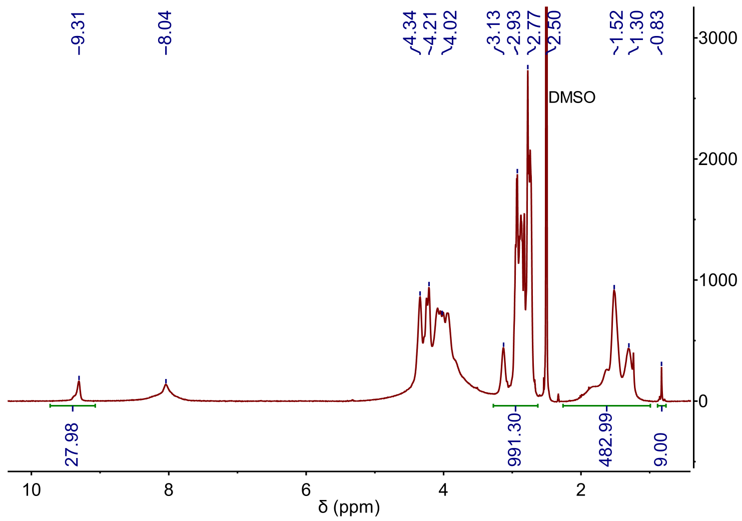

Figure 8.10: ^{1}H-NMR spectrum of $PLys_{42}$-b-$PLys(TFA)_{28}$-b-$PSar_{311}$.

8.5.2 GPC Plots

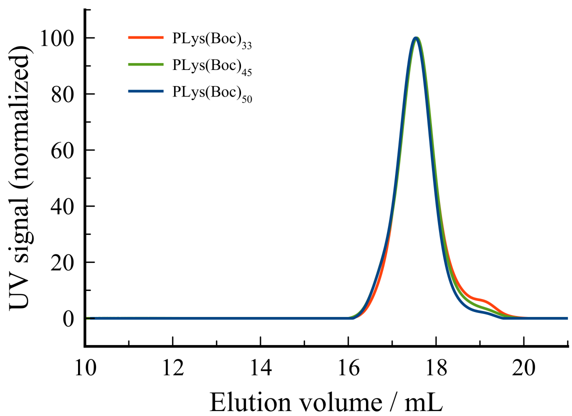

Figure 8.11: HFIP GPC traces of PLys(Boc) with varying chain lengths (36, 45 and 50) showing the transition from random coil to α-helix conformation.

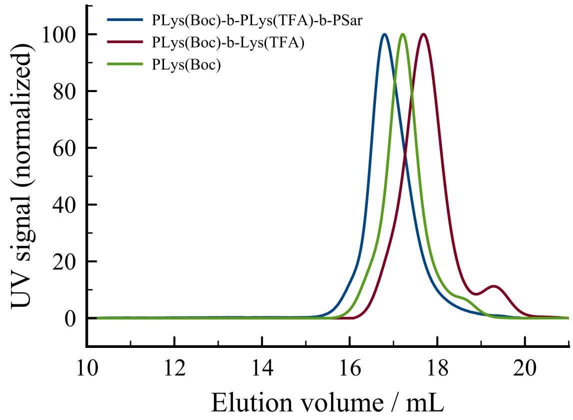

Figure 8.12: HFIP GPC traces of PLys(Boc)$_{47}$, PLys(Boc)$_{47}$-b-PLys(TFA)$_{13}$ and PLys(Boc)$_{47}$-b-PLys(TFA)$_{13}$-PSar$_{311}$ showing the transition from homopolymer to di- and triblock copolymers.

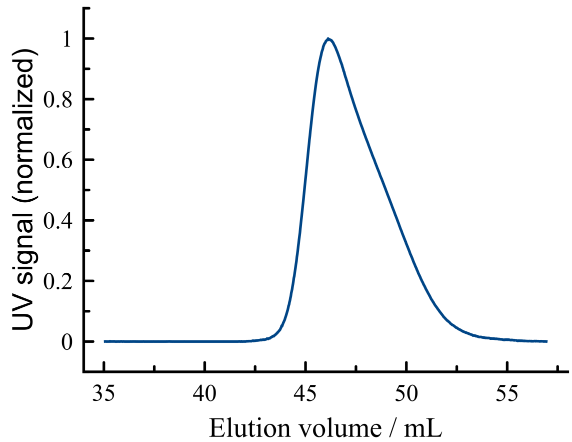

Figure 8.13: Aqueous GPC traces of fully deprotected triblock copolymer (PSar$_{224}$-b-PLys$_{59}$) showing unimodal molecular weight distribution. Interaction of the PLys block with the column material leads to low molecular weight tailing.

9 THE INFLUENCE OF BLOCK IONOMER MICROSTRUCTURE ON POLYPLEX PROPERTIES: CAN SIMULATIONS HELP TO UNDERSTAND DIFFERENCES IN TRANSFECTION EFFICIENCY?

P. Heller, J. Zhou, B.Weber, D. Hobernik, M. Bros, F. Schmid, M. Barz, *Small*, 2017

ABSTRACT

Gene therapies enable therapeutic interventions at gene transcription and translation level, providing enormous potential to improve standards of care for multiple diseases. Non-viral transfection agents and in particular polyplexes based on block ionomers are - besides viral vectors and cationic lipid formulations - among the most promising systems for this purpose. Block ionomers combine a hydrophilic non-charged block, e.g. PEG, with a hydrophilic cationic block. For efficient transfection, however, endosomolytic moietes, e.g imidazoles, are additionally required to facilitate endosomal escape, which raises the general question how to distribute these functionalities within the block copolymer. Combining molecular dynamics simulation with physicochemical and biological characterization, this work aims to provide a first rational for the influence of block ionomer microstructure on polyplex properties, e.g. size and shape and transfection efficiency. Our findings underline that a triblock microstructure is most efficient in compacting pDNA, which reduces polyplex size, enhances stability against degradation by DNase I and thus provides better transfection performance.

9.1 INTRODUCTION

Over the last decades, the increasing knowledge about the function of nucleic acids paved the road for therapeutic interventions at gene transcription and translation level.[5] Most of these interventions known as gene therapy, rely on the transfection of cells, which in the majority of cases requires the use of viral or non-viral vectors to ensure efficient processing of the encoded information.[436] Since viral transduction agents raise concern in terms of immune responses against the viral capsid, the design of non-viral transfection agents is pursued by many researchers worldwide.

In this regard, the use of block ionomers in the synthesis of polyplexes has turned out to be particularly promising, whenever gene therapy of tumors is desired.[222, 437] Block ionomers are block copolymers combining a cationic and a stealth-like block in a single, double hydrophilic block copolymer. They can induce the formation of core-shell polyplexes in which the cationic block complexes the nucleic acid by electrostatic interaction while the hydrophilic stealth-like block, e.g. PEG,[355, 356] PSar,[37, 120] POx,[358] PHPMA,[438, 439] POEGMA[440] or PPE[441] shields the assembly from undesired interactions with blood components and increases its stability towards disintegration. Furthermore, a third functionality is required to enhance transfection efficiency, which are endosomolytic groups as for example the imidazole side chain of histidine.[6, 226, 442] These groups enable endosomal escape by membrane interactions or by the proton sponge effect.[7] Therefore, a rational design of block ionomers requires the combination of cationic/complexing, endosomolytic and shielding groups in one single polymer. Controlled and living polymerization techniques enable polymer chemists to govern the polymer microstructure during the polymerization process itself, providing access to various polymer architectures in which the different functionalities can be arranged into blocks or are deployed randomly. Since nucleic acid condensation by a (block) ionomer in aqueous solution is the key step for polyplex formation, this raises the question on how to distribute these functionalities among a block ionomer in order to optimize polyplex properties. In other words, how does the microstructure of block ionomers influence complexation of plasmid DNA (pDNA) and hence the physicochemical properties and the performance of derived polyplexes.

In this context, Pun and coworkers recently investigated the influence of histidine incorporation and its spatial arrangement on the properties of HPMA-based brush polymers.[442] But in contrast to block copolymer self-assembly,[443–445] our knowledge and mechanistic understanding of microstructure-attributed effects on polyplex formation are still limited. Despite the advance of characterization techniques, a detailed investigation of the internal structure of individual polyplexes remains challenging. Simulation studies can help to bridge this gap and to understand the organization of polyplexes on the molecular level.[208, 328, 446, 447] Unfortunately, all-atom simulations of DNA with thousands of base pairs in solution are still infeasible even with state of the art supercomputers. Therefore, we carry out coarse-grained molecular dynamics simulations to elucidate the connection between the polymer microstructure and polyplex properties.[328, 448, 449] Such simulations also give insight into the underlying assembly mechanism. For example, it is now well recognized that complex formation in strong polyelectrolyte systems is driven by the gain of translational entropy, associated with the release of counter ions, rather than by the gain of enthalpy due to the electrostatic interaction.[208] In a second step, results obtained from simulations are compared with experimental data.

Combining simulation with physicochemical and biological characterization, this work aims to provide a rationale for the influence of block ionomer microstructure on polyplex properties, e.g. size, shape and transfection efficiency. For instance, the size or compactness of polyplexes is of major importance for the stability against extra- and intracellular nucleases, which can immediately degrade pDNA and thereby reduce transfection efficiency substantially.[450, 451]

9.2 RESULTS AND DISCUSSION

Incorporation of endosomolytic moieties, e.g. the imidazole side chain of histidine, into the shielding segment of block ionomers would foster unspecific interactions, which compromises polyplex stability in biological fluids. Therefore, the endosomolytic groups should either be incorporated as a middle block between a hydrophilic stealth-like block and a cationic block or should be distributed randomly within the latter. This premise yields two possible polymer microstructures: a triblock copolymer, in which all functionalities (cationic, endosomolytic, shielding) are separated into three distinct segments or a diblock copolymer in which one segment combines two out of three functionalities. For comparison, a diblock copolymer with a cationic and a shielding segment, but without any endosomolytic functionalities is of interest and can be considered as internal standard.

A coarse-grained model was applied to gain an understanding of the influence of block ionomer microstructure on polyplex formation. In this model pDNA is represented by a semi-flexible ring polymer, which carries negative charges. Its parameters are set according to Ref. [448]. We chose polypept(o)ides as model reagents for non-viral vectors in this study, since their controlled synthesis enables us to regulate the microstructure in the desired fashion.[37, 158] Thus, the complexing, the endosomolytic and the shielding groups are lysine, imidazole (histidine) and sarcosine, repectively. In the simulation these groups are represented by cationic hydrophilic beads, neutral hydrophobic beads, and neutral hydrophilic beads. Every bead represents either two DNA base pairs or two amino acids, hence one bead size corresponds to roughly 0.8 nm. The polypept(o)ides are modelled as fully flexible linear chains. The model and the model parameters are described in detail in the supporting information (SI). Compared to the experimental situation, the DNA rings in the simulations were modelled shorter and more flexible than in reality: The DNA length was chosen 2400 base pairs (1200 beads), which was half of the size in experiments, see below. The persistence length was roughly 6 nm, whereas it is around 50 nm in reality. These deviations were necessary to ensure proper sampling of the complexes in the simulations. We found that it was impossible to equilibrate and statistically sample "DNA" chains of the correct length and stiffness in reasonable simulation times.

The length of the polymers was chosen according to the experiments. All three polymer microstructures have the same number of shielding beads, which was set to 100, corresponding to 200 amino acids. The only difference between the three model polymers is the arrangement of beads representing complexing and endosomolytic groups: (1) The **Diblock** structure contains only complexing beads. (2) The **Triblock** structure combines blocks of complexing and endosomolytic beads. (3) The **Random** structure has randomly distributed complexing and endosomolytic beads. Fig. 9.1 displays a scheme of the three microstructures implemented in the simulation.

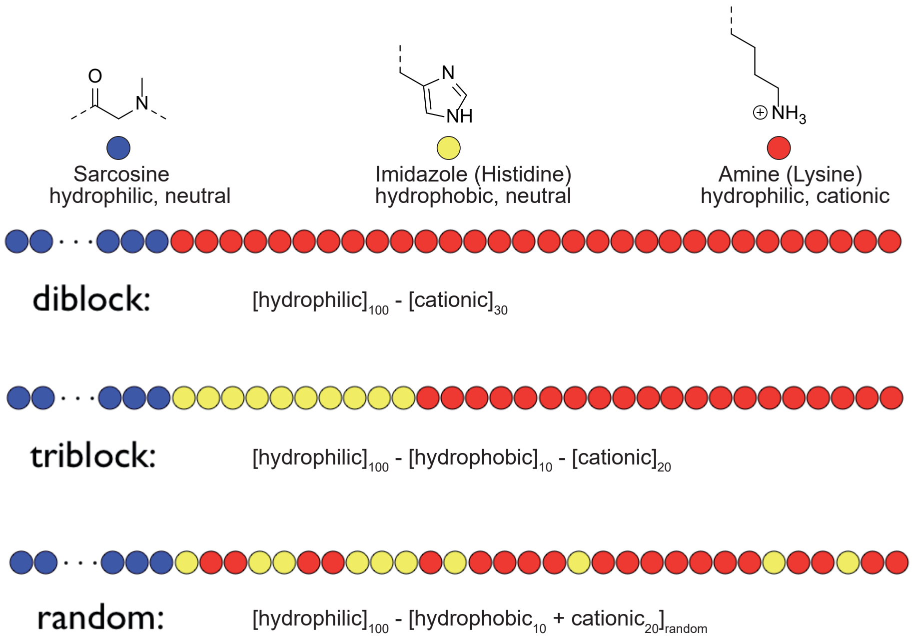

Figure 9.1: Polymer microstructures considered in the simulations.

Small counter-ions are included explicitly in the simulations, but no additional salt ions. This corresponds to the experimental situation during the complex self-assembly (described in SI). As illustrated in Fig. 9.2 (c)-9.2 (e), we observed complexation between pDNA and polymers in the simulations of all three cases. The top figures show an individual complex while the bottom figures display only the core without the shielding beads to provide first structural insights. The complex formation itself is driven on the one hand by the entropy gain related to the counterion release, and on the other hand by the electrostatic attraction between negatively charged pDNA and cationic polymer blocks. The hydrophobic groups mainly influence the complex shape.

The time-averaged hydrodynamic radius and the radius of gyration as well as the size of bare pDNA can be seen in Fig. 9.2 (a), demonstrating that the complex formed by the **Triblock** is only slightly larger than the **Diblock** complex. In both cases, the pDNA was compacted during self-assembly yielding polyplexes which are about a factor of two for hydrodynamic radius (R_h) or three for the radius of gyration (R_g) smaller than the pDNA itself. A closer look at the complex core (Fig. 9.2 (d)) reveals that the hydrophobic groups in the triblock copolymer formed patches on the surface of the core, which are driven by hydrophobic interactions. The complex formed by the **Random** polymer is quite different. It displays the largest radius among the three microstructures and the endosomolytic groups distribute evenly inside the complex core (Fig. 9.2 (e)), indicating that internal segregation cannot take place. Furthermore, one may notice that the error bar of the radius measurement for the random complex is the largest one among the three microstructures, which suggests that the shape of the random complex fluctuates strongly.

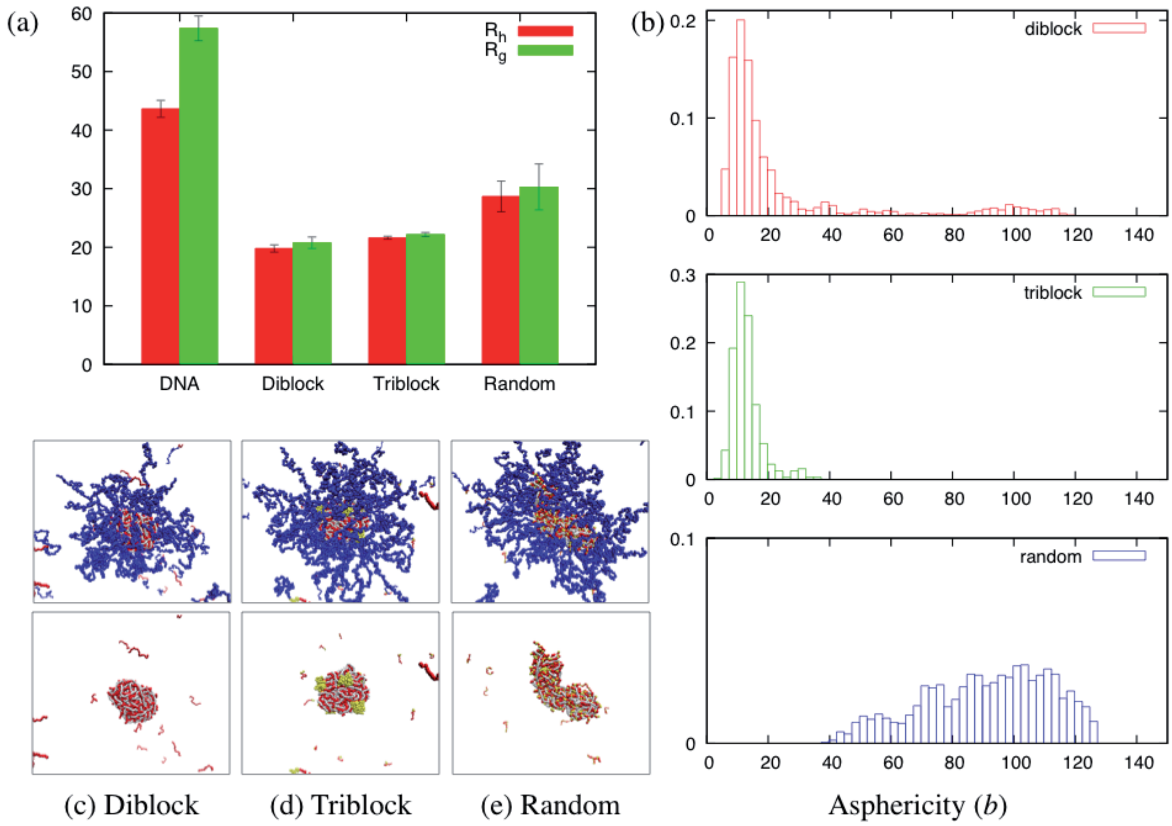

Figure 9.2: Characteristics of the three simulated complexes: (a) Hydrodynamic radius R_h and gyration radius R_g (in simulation units , see SI), also shown are the corresponding values for bare pDNA. (b) Asphericity of the complexes. (c)-(e) Characteristic snapshots of whole complexes (top) and complex core (bottom). Color coding is the same as in Fig. 9.1.

In addition to size, the microstructure of polymers may also influence the shape of polyplexes. To better understand the shape and its fluctuation, we monitored the three eigenvalues λ_i (i = x,y,z) of the gyration tensor of the complex core and computed the asphericity

$$b = \lambda_z - \left(\frac{1}{2}\lambda_y + \lambda_x\right)$$

where λ_z is the maximal eigenvalue. A zero value of the asphericity corresponds to a spherical shape while for a thin rod $b = l^2$ where l is the rod length. Fig. 9.2 (b) illustrates the distribution of the asphericity for the three complex types. Both, the **Diblock** complex and the **Triblock** complex mostly have a well-defined spherical shape with small fluctuations in the asphericity $\left(b \approx R_g/2\right)$. Among these two, the **Triblock** complex has the narrower distribution. In rare instances, the **Diblock** complex adopts elongated conformations with high asphericities up to $b \approx 5R_g$. These conformations are entirely suppressed in the **Triblock** complex, possibly due to the presence of patched hydrophobic groups that may stabilize the spherical conformation. In contrast, **Random** complexes tend to be elongated with asphericities in the range of (1-4)R_g and the asphericity shows a wide distribution, indicating strong shape fluctuations.

To test the theoretical predictions from the simulations, the different polymer microstructures can be synthetically accessed, e.g., by NCA polymerization as previously described by Heller *et al*.[158] Following this approach, di- and triblock copolypept(o)ides of PLys(TFA)-b-PSar or PLys(Boc)-b-PLys(TFA)-b-PSar architecture with narrow molecular weight distributions between 1.11 to 1.19 could be obtained. In an additional step, these polymers can be transferred into the desired PLys-b-PLys(His)-b-PSar and PLys-ran-PLys(His)-b-PSar copolymers. A completely random copolymerization of the corresponding NCAs is probably not possible due to the fact that reactivity and thus copolymerization parameters of lysine and histidine NCAs differ substantially.[15] Deprotection and postpolymerization modification reactions were used as reported in literature (for details on polymer synthesis see Experimental Section and SI). Cleavage of the BOC protective groups was conducted with 50% TFA/H2O. This approach allows the simultaneous deprotection of lysine and imidazole residues. ^{1}H-NMR and diffusion-ordered spectroscopy (DOSY) NMR spectra of imidazole-modified coplypept(o)ides are displayed in the SI. The signals of the aromatic ring protons at 7.57 ppm and 6.80 ppm allow the determination of the amount of imidazole groups per polymer by referring their integral to the initiator proton integral. DOSY NMR spectra show only one diffusing polymer species, respectively, thereby proving the integrity of block copolymers. The properties of the three different polymers are summarized in Table 1, and relate to model polymers used in the simulation setup (Fig. 9.1) according to the applied 2:1 mapping of 2 amino acids onto one simulation bead.

The listed polymers involve one non-modified control (**Diblock**), the triblock copolymer (**Triblock**) and the randomly modified block copolymer (**Random**). Like in the simulations only the spatial arrangement of imidazole groups within the polymer is different.

Table 9.1: Characteristics of synthesized polypept(o)ides.

POLYMER	ARCHITECTURE	CALCULATED BLOCK RATIO	BLOCK RATIO[A]	M_N[B]	Đ[B]	NUMBER OF IMIDAZOLES[C]
Diblock	PLys(TFA)-b-PSar	60:200	55:232	29.0	1.11	0
Triblock	PLys-b-PLys(His)-b-PSar	40:20:200	39:18:225	23.3	1.19	18
Random	PLys-ran-PLys(His)-b-PSar (derived from Diblock)	(40:20):200	(36:19):232	29.0	1.11	19

[A,C] as determined by ^{1}H-NMR spectroscopy
[B] kg/mol, calculated from the GPC of protected precursor polymers with HFIP as solvent and PMMA standards

For a comparison of simulation predictions and experimental data, polyplexes based on pDNA (pEGFP-N1, 4733 base pairs) and the polypept(o)ides were prepared and characterized.

To get a first idea at which N/P ratios (primary amines of polymers to phosphate groups of pDNA) stable complexation of pDNA occurs, gel electrophoresis was performed (SI, Fig. 9.18). **Diblock** and **Triblock** display only marginal differences in their complexation behavior and lead to full pDNA retention around N/P 4-5. In contrast, Random forms less stable polyplexes with pDNA: around a N/P ratio of 6 nearly full pDNA retention is achieved. This pattern can be directly attributed to the varying spatial imidazole arrangement. As the imidazole groups (pK_a = 6.1) are non-charged and thus hydrophobic at neutral pH,[452] the overall cationic charge density of the **Random** polymer is lower than that of the two other polymers which impairs its complexation capacity.

Based on these findings, polyplexes were analyzed by multi-angle dynamic light scattering (DLS). All samples were measured from 30° to 150° at steps of 15°. All auto correlation functions for the **Diblock** and **Triblock**-based polyplexes display a monomodal decay and can be fitted by a double exponential fit taking low polydispersities of polyplexes into account. This results in an angle-dependent diffusion coefficient D_{app} or reciprocal hydrodynamic radius $R_{h,app}^{-1}$, according to formal application of the Stokes Einstein law. By extrapolation of R_h^{-1} to $q = 0$ z-average hydrodynamic radius $R_h = \left\langle R_h^{-1} \right\rangle_{z^{-1}}$ was obtained. For the **Diblock** we determined an average R_h of 51 nm ($\mu_2 = 0.09$), while the **Triblock** forms polyplexes with R_h of 62 nm ($\mu_2 = 0.08$). Both polyplexes display a minor angle dependency of q^2 indicating the formation of spherical nanoparticles with low polydispersity. Also, both polyplex types have a smaller radius than free pDNA, which displayed a R_h of 95 nm (data not shown).

It was, however, not possible to fit correlation functions for the polyplex based on the Random polymer by the sum of two exponentials. In this case, a three exponential fit was necessary. As shown in Fig. 9.3, the autocorrelation function of Random-based polylexes has a second decay at higher correlation times, which corresponds to the presence of larger aggregates of an apparent radius Rh,app(ϑ = 30°) of 186 nm. In contrast to Diblock and Triblock, Random also displayed an angle-dependency, which is neither neglectable nor linear, so that an extrapolation to q = 0 was impossible. This effect can also be attributed to the presence of multi-pDNA aggregates.

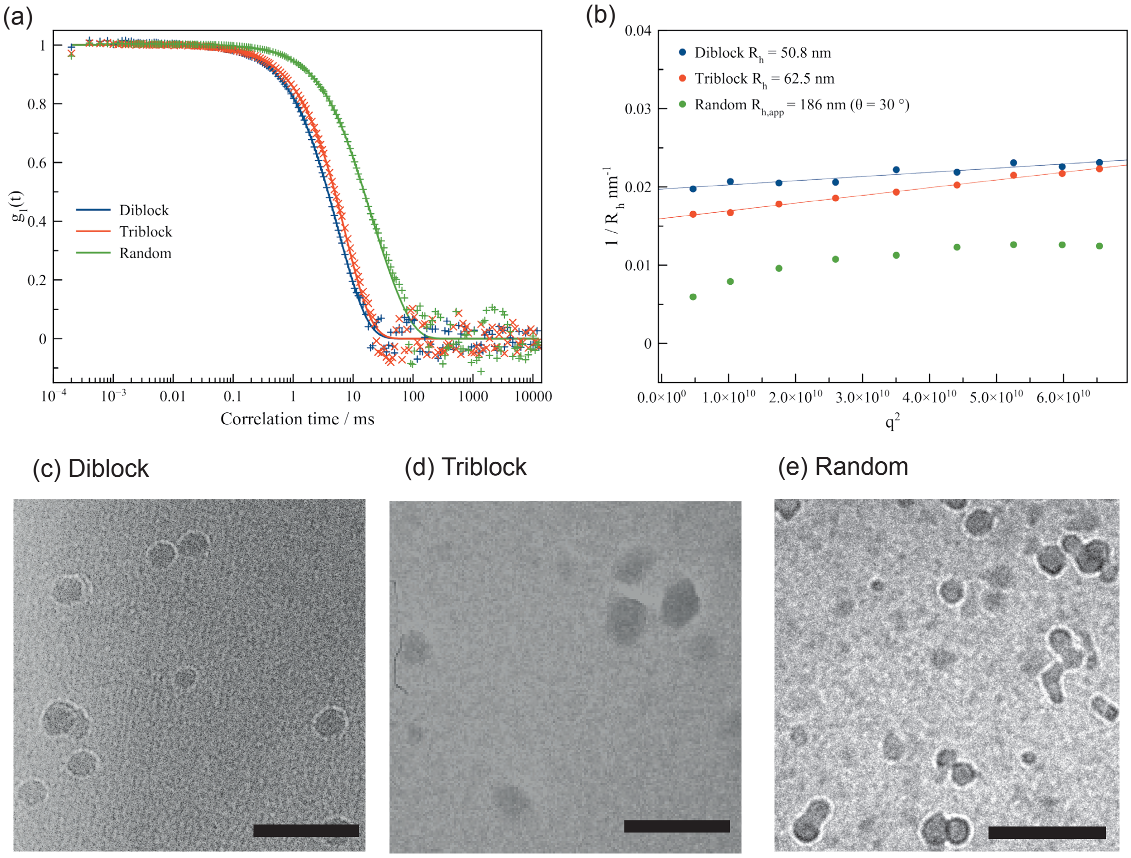

Figure 9.3: Physicochemical characterizationof polyplexes based on **Diblock**, **Triblock** and **Random** polymers by multi angle DLS: (a) Autocorrelation function at scattering angle 30° and (b) scattering angle dependency of $1/R_h$. (c) Representative cryogenic TEM images of polyplexes based on pDNA in aqueous solution (scale bar corresponds to 200 nm).

In the next step, polyplexes based on the different block copolymers were visualized by cryogenic TEM in aqueous solution. Cryo-TEM images for **Diblock** and **Triblock**-based polyplexes displayed similar radii of around 50 to 60 nm and low polydispersity. As already expected from the light scattering experiments, for polyplexes based on the **Random** polymer small single pDNA complexes (R_h = 60-70 nm) coexist with multi-pDNA complexes (Fig. 9.3) reaching a size of several hundred nanometers. Cryogenic TEM images did not show the internal structure suggested by the simulations (Fig. 9.4). The formation of hydrophobic patches for polyplexes based on **Triblock** polymers could not be observed. Possible reasons are the small size of these patches in hand with a minor difference in scattering contrast in comparison to the other blocks.

In summary, multi angle DLS and cryogenic TEM measurements revealed the formation of spherical polyplexes for **Diblocks** and **Triblocks** with similar radii. Polyplexes based on the **Random** polymer tend to form multi-pDNA complexes, which reach R_h of several hundred nanometers.

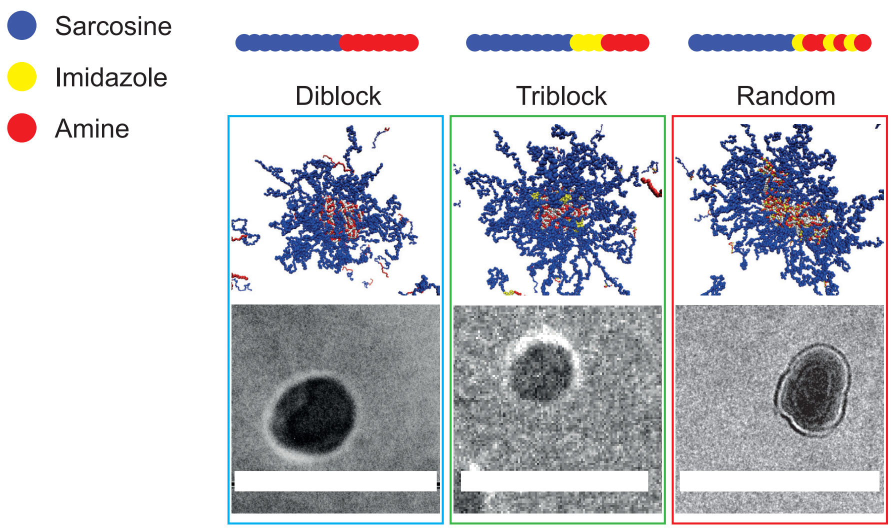

Figure 9.4: Polymer-microstructure related morphology of polyplexes: top) simulation snapshots and bottom) cryogenic TEM pictures of polyplexes based on **Diblock**, **Triblock**, and **Random** polypept(o)ides (scale bar corresponds to 200 nm).

When we relate these findings to the simulations we obtain a qualitative description of the experimental results. In absolute values, the hydrodynamic radii are much smaller in the simulations than in the experiments. Assuming that the simulation unit roughly corresponds to 0.8 nm as discussed above, the factor is about 1/3. This difference reflects the fact that the "DNA" plasmids in the simulations are shorter and more flexible, as discussed above. However, if we use the hydrodynamic radius of the free plasmids as the reference and rescale the sizes of the complex accordingly, the values become comparable: **Diblock** and **Triblock** complexes are of similar radius and roughly have half of the size of the free plasmid ($R_h \approx 0.5 R_{h,free}$ both in simulation and theory, see also Fig. 9.2), the **Triblock** being slightly larger than the **Diblock**-based complex. The **Random**-based single pDNA complexes have a size of $R_h \approx 0.6 - 0.7 R_{h,free}$ in the experiments and $R_h \approx 0.67 R_{h,free}$ in simulations. The formation of multi-pDNA complexes in the case of **Random** could not be observed in the simulations, simply because only one model pDNA was present in the simulation box. Therefore, whenever the simulations indicate poor compaction of pDNA, the formation of aggregates needs to be considered carefully. Nevertheless, we can conclude that the formation of polyplexes containing only single pDNA can be well described by applying the introduced coarse-grained model in the molecular dynamics simulations.

Finally, the influence of polymer microstructure on gene delivery was investigated. Therefore, transfection efficiencies of the three different polyplexes were evaluated in HEK 293T cells using a pDNA encoding for an eGFP (enhanced green fluorescence protein) reporter, measuring eGFP expression by flow cytometry and fluorescence microscopy (Fig. 9.5 (c) and (d)).

Employing mean fluorescence intensity (MFI) as an expression parameter, the highest transfection level was observed for **Triblock**-based polyplexes, which corresponds to around 35% of jetPEI efficiency. In contrast, the **Random**-based polyplexes turned out to be least efficient, with **Diblock**-based polyplexes in between. The same results were obtained from qualitative screening of transfection efficiency by fluorescence microscopy.

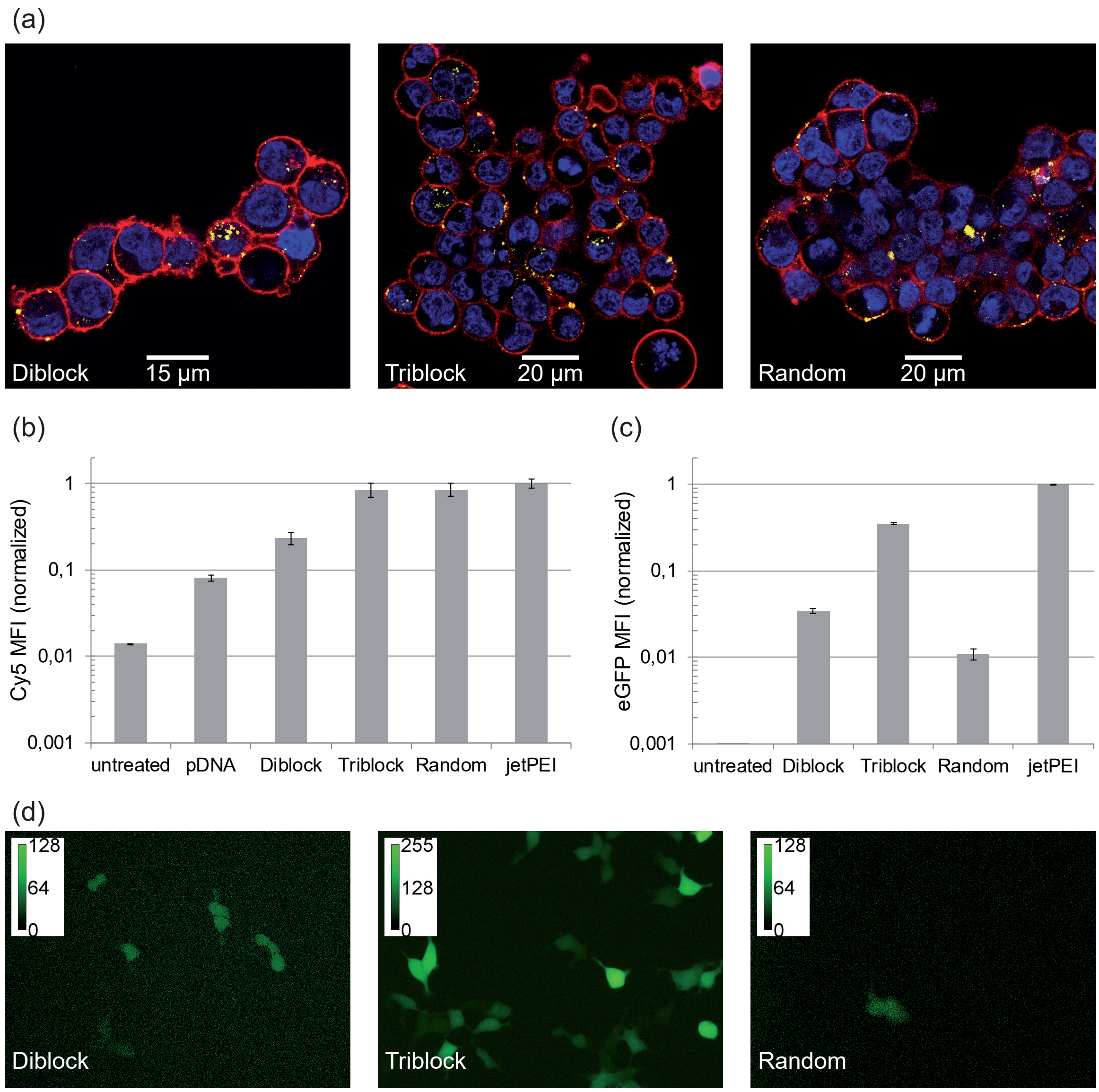

Figure 9.5: Influence of polymer microstructure (**Diblock**, **Triblock** and **Random**) on cell uptake and transfection efficiency of polyplexes: Cellular uptake of **Diblock**, **Triblock** and **Random**-based polyplexes analyzed by (a) confocal microscopy (blue: nucleus, Hoechst; red: cell membrane, Cell Mask; yellow: polyplexes, Cy5) and (b) FACS (n = 3). Transfection efficiency determined by eGFP expression analyzed by (c) FACS (n = 3) and (d) fluorescence microscopy.

Initially, we expected that the integration of imidazole groups into the polymers would increase the transfection efficiency due to the proton sponge effect.[6] While this holds true for the **Triblock**-based system achieving transfection rates in the same order of magnitude as obtained using jetPEI, **Random**-based polyplexes are actually 3.4 times less efficient than the **Diblock** control. Since the amount of imidazole groups is equal for both polymers, the converse transfection results have to be a direct consequence of the diverging polymer microstructure and the resulting altered physicochemical polyplex properties described above. Interestingly, the differences in transfection efficiency are not attributed to differences in cellular uptake. Cells incubated with the three types of polyplexes containing Cy5-labeled pDNA displayed comparable levels of cell-associated and intracellular fluorescence as analyzed by LSCM and flow cytometry (Fig. 9.5 (a) and (b)). Consequently, the polymer microstructure has no significant impact on cellular uptake - in sharp contrast to its effect on transfection efficiency.

We next investigated polyplex stability against degradation by DNase I. Besides cellular uptake, endosomal escape and nuclear import, stability of gene delivery systems against intra- and extracellular nucleases is another bottleneck for cell transfection.[450, 451] In relation to this, Li *et al*. showed that better compaction as realized for example by introduction of hydrophobic moieties enhances polyplex stability against nuclease activity or polyanions, ultimately leading to higher transfection efficiency.[453]

As pointed out beforehand, **Diblock** and **Triblock**-based polyplexes have a more compact structure than **Random**-based ones. Judging from this, we assumed that this may contribute to the observed transfection results. The stability of polyplexes and their ability to protect pDNA from degradation was assessed by gel electrophoresis after their incubation with DNase I as model nuclease. Electrophoresis was performed under high pH conditions with NaKE buffer as introduced by Davis *et al*.[454] in which previously complexed pDNA can be partially released from polyplexes, thereby allowing the visualization of intact or degraded DNA (Fig. 9.6 bottom).

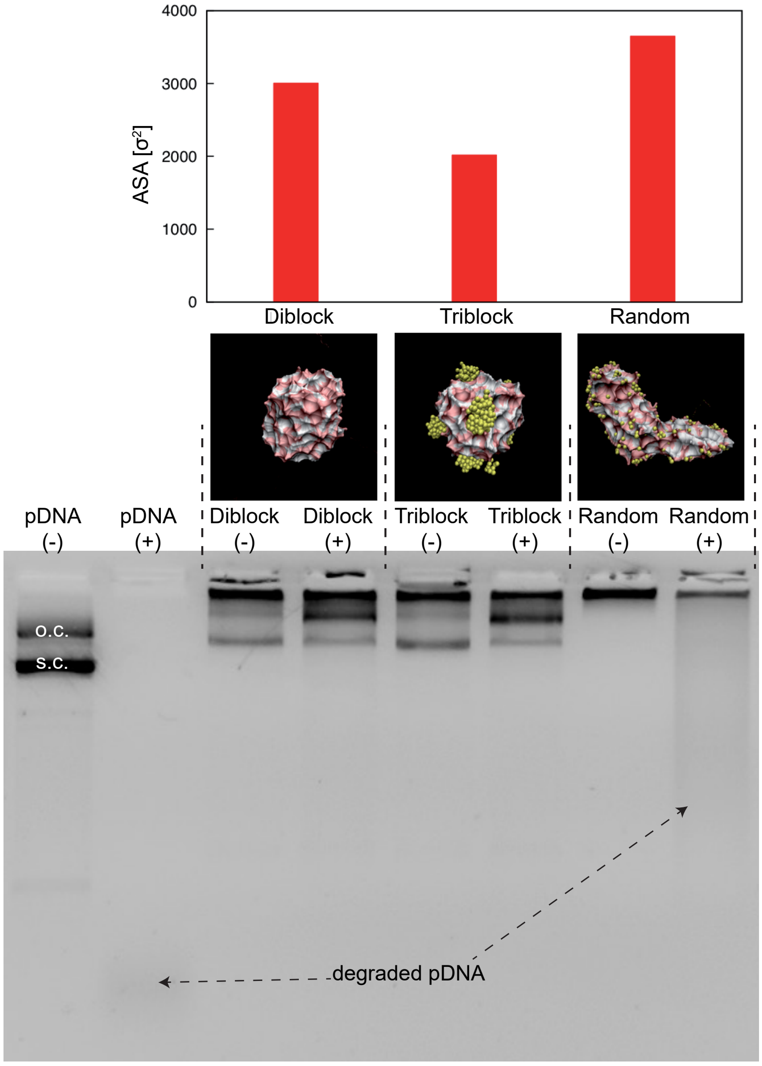

Figure 9.6: *In silico* assessment of accessible surface area (ASA) and experimental determination of stability of polyplexes against DNase I (-: control, +: incubated with DNase I, o.c.: open circle, s.c.: super coiled).

In case of **Diblock** and **Triblock**-based polyplexes, release of intact pDNA adopting open circle and super coiled conformation occured for untreated as well as DNase I-treated samples, suggesting that both polymers were able to protect pDNA against degradation, which proceeded rapidly and completely for uncomplexed pDNA. In case of **Random**-based polyplexes, no pDNA release could be observed for the untreated control, which underlines the formation of large multi-DNA aggregates causing pDNA to remain stuck in the gel even at NaKE buffer conditions.

On the other hand, the DNase I-treated sample displayed a blurred elongated band on the gel, which clearly indicates degradation of pDNA. The degradation products are of higher molecular weight than the degradation products from free pDNA control, which portends that degradation speed is at least reduced. The experiment shows, however, that the **Random** polymer is not capable to protect pDNA against nuclease-mediated degradation to the same extent as Diblock and Triblock polymers. Since the degradation of pDNA is correlated with its accessibility by nucleases, the inferior protection capacities of the **Random** polymer must be related to a less dense packing and shielding of the complexed pDNA. Therefore, we returned to the simulations and determined the accessible surface area (ASA) at the core-shell interface. As visualized in Fig. 9.6, the Diblock-based polyplex has an ASA of 3,006 ± 4, the **Triblock**-based of 2,019 ± 5 and the **Random**-based of 3,651 ± 10 simulation units^2. Since - as discussed above - the complex sizes are not directly comparable in experiments and simulations, we normalized the simulation data with respect to the **Diblock**-based polyplex, which means that the normalized ASA of the **Triblock**-based polyplex is 0.67 and thus by 33% smaller than the ASA of the **Diblock**. This is due to the formation of hydrophobic patches shielding the core additionally. In contrast, the normalized ASA of the **Random**-based polyplex is 1.22, i.e. 22% higher than the one of the **Diblock** and 1.8 times higher compared to the **Triblock**. Considering the hydrodynamic diameter of DNase I of a few nanometers (molecular weight ~ 39 kDa) these slight differences in ASA may already induce the differences in stability against degradation. This in turn gives a reasonable explanation for the transfection results for the different polymers: The **Diblock** polymer can provide adequate shielding of pDNA against nuclease activity, but lacks endosomolytic properties. The **Random** polymer has buffering capacities introduced by imidazole at the expense of inferior DNA complexation and protection capabilities. Only the **Triblock** polymer combines both functionalities, which is reflected by the highest transfection efficiency of all three polymers.

9.3 CONCLUSION

In this work we aimed to gain a first understanding on the influence of polymer microstructure on polyplex formation and transfection efficiency using pDNA. Simulations based on a coarse-grained model indicated that a triblock copolymer is much more efficient in complexing the pDNA than a diblock containing the endosomolytic imidazole moieties randomly distributed among the cationic block. In this respect, only minor differences between triblock and a simple diblock copolymer lacking imidazoles could be detected. In addition, in case of triblock copolymers the simulations indicate the formation of hydrophobic patches that reduce the accessible surface area (ASA) of the core containing the pDNA, which provides a possible explanation for the experimental finding that triblock copolymer-based polyplexes are more efficient in protecting pDNA from degradation. This enhanced polyplex stability along with endosomolytic properties seem to be important parameters determining transfection efficiency, since diblock copolymers containing randomly distributed imidazole units are even less efficient in transfecting HEK 293T cells than diblock copolymers lacking these groups. In conclusion, the conducted studies indicate the potential of simulations to understand parameters determining polyplex size and shape, and underline the importance of polymer microstructure on the final performance of block ionomer-based polyplexes.

9.4 EXPERIMENTAL SECTION

9.4.1 Materials

DMF over molecular sieves was purchased from VWR, dried over BaO and subsequently distilled and degassed *in vacuo*. THF and *n*-hexane were purchased from Sigma-Aldrich and distilled from Na/K. Other solvents were used as received. Diphosgene and chlorotrimethylsilane were purchased from Alfa Aesar and used as provided. Neopentylamine was purchased from TCI Europe, dried over NaOH and fractionally distilled. Sarcosine was purchased from Sigma Aldrich, TFA or BOC protected lysine from ORPEGEN. (Boc)L-His(Boc)-OH*Benzene was purchased from Iris Biotech.

9.4.2 Instrumentation

9.4.2.1 *Polymer Characterization*

400 MHz ^{1}H-NMR spectra and ^{19}F NMR spectra were recorded on a Bruker Avance II 400. HSQC and DOSY NMR measurements were performed on a Bruker Avance III HD 400. All spectra were recorded at room temperature and analyzed with MestReNova software. Degrees of polymerization as well as molecular weights were calculated by comparing the integral of the neopentylamine initiator peak either with the integrals of the side chain amide protons (for PLys(Boc) and PLys(TFA)) or with the average of integrals of methyl group and α-protons (for PSar) in the 400 MHz ^{1}H-NMR spectra. The number of imidazole groups per polymer was calculated by referring the integrals of the aromatic ring protons at 7.57 ppm and 6.80 ppm to the initiator proton integral.

Attenuated total reflectance Fourier transformed infrared (ATR-FTIR) spectroscopy was performed on a FT/IR-4100 (JASCO Corporation) with an ATR sampling accessory (MIRacleTM, Pike Technologies). IR Spectra were analyzed using Spectra Manager 2.0 (JASCO Corporation).

Melting points were determined using a METTLER FP62 (METTLER WAAGEN GMBH).

Hexafluoroisopropanol (HFIP) gel permeation chromatography (GPC) was performed with HFIP containing 3 g/L potassium trifluoroacetate as eluent at 40 °C and a flow rate of 0.8 mL/min. The columns were packed with modified silica (PFG columns; particle size: 7 mm, porosity: 100 and 1000 Å). Polymer was detected with a refractive index detector (G 1362A RID, JASCO) and a UV/Vis Detector (UV-2075 Plus, JASCO). Molecular weights were calculated using a calibration performed with PMMA standards (Polymer Standards Services GmbH) and toluene as internal standard. Elution diagrams were analyzed using WinGPC UniChrome 8.00 (Build 994) software from Polymer Standards Services.

9.4.2.2 *Biological Experiments*

FACS experiments were executed on a FACS Canto II flow cytometer equipped with BD FACS Diva software (both from BD Biosciences, San Diego, CA). Data were analyzed using FlowJo software (FLOWJO, Ashland, OR).

Live cell images were acquired on an inverted confocal microscope TCS SP5 (Leica, Wetzlar, Germany) equiped with an oil-immersion objective (63 magnification; NA 1.4) and a laser set capable of 405 nm/488 nm/561 nm excitation. Images were recorded at 512 x 512 8-bit-pixel resolution with a pinhole of 130 µm and confocal plane depth of 1.0 µm, resulting in a total image size width and height of 246 µm.

Fluorescence images for visualization of eGFP expression were acquired on an inverted fluorescence microscope BX50 (Olympus, Hamburg, Germany) equipped with an oil-immersion objective (UPlanFl 60x/1.25 Oil Iris Ph3) and a mercury lamp with a filter set capable of excitation in red/green and UV range. Images were recorded at 2080 x 1544 3x12 bit resolution (ColorView II Camera; Soft Imaging System, Münster, Germany).

9.4.3 Methods and Protocols - Preparation of PeptoPlexes

9.4.3.1 *Synthesis of Precursor Polymers*

Synthesis of protected precursor diblock or triblock copolypept(o)ides and deprotection of lysine side chains were conducted as reported earlier.[156, 158] See Subsections 5.4.3 and 8.4.3.

9.4.3.2 *Modification of Polymers with Histidine and Cleavage of Boc Groups*

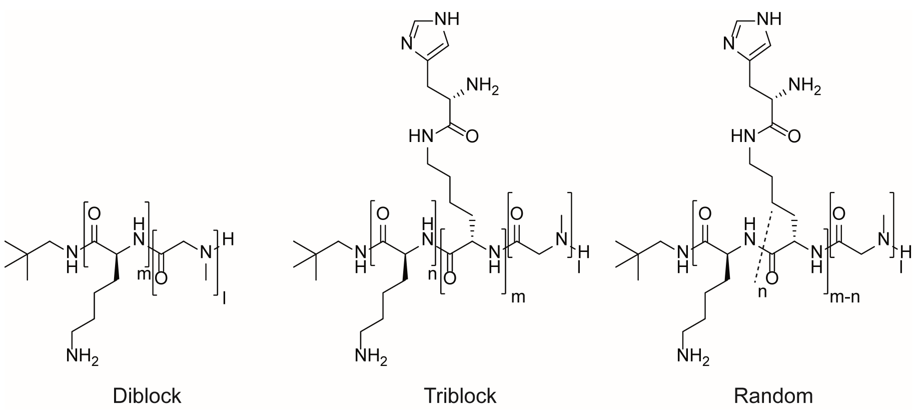

Figure 9.7: Chemical structures of investigated polymers.

For functionalization with imidazole groups a protocol published by Midoux *et al.* was partially adopted.[226] Around 30 mg of diblock or triblock copolypept(o)ides with a deprotected lysine block were dissolved in dry DMF. In parallel, 0.4 eq (with respect to lysine units of diblock copolypept(o)ide) or 1.2 eq (with respect to lysine units of triblock copolypept(o)ide) of (Boc)L-His(Boc)-OH*Benzene were dissolved in dry DMF and reacted for 25 minutes with 5 eq. of 1-ethyl-3-(3-dimethylaminopropyl)carbodiimide*HCl (EDC) and 5 eq. of hydroxybenzotriazole (HOBt) in the presence of 4 droplets of *N,N*-diisopropylethylamine (DIPEA) at room temperature under frequent stirring. Histidine and polymer solutions were combined and stirred for another 72 h at room temperature, away from light. The crude product was precipitated in diethyl ether, centrifuged and washed twice with diethyl ether. For cleavage of BOC groups, the pellet was dissolved in 50% (v/v) trifluoracetic acid/H_2O and the solution stirred for 17 h at room temperature. The reaction mixture was dialyzed with a Spectra/Por (Roth) membrane with a nominal molecular weight cut-off (NMWCO) of 3500 g/mol against an aqueous solution of $NaHCO_3$ for one day, afterwards against pure water. Lyophilization yielded the modified polymers as fluffy, colorless powder.

^{1}H-NMR of imidazole-modified di/triblock copolypept(o)ide (400 MHz, DMSO-d_6): δ [ppm] = 7.78-7.34 (18H (1n His), br, -NH-**CH**=N), 7.00-6.57 (18H (1n His), br, -C=**CH**-NH-), 4.54-3.83 (br, -CO-**CH**-NH- and -NCH_3-**CH_2**-CO-), 3.25-2.55 (br, -**CH_2**-NH-CO-R and -**CH_2**-NH_2 and -N**CH_3**-), 2.03-0.90 (br, -CH-**CH_2-CH_2-CH_2**-CH_2-NH-), 0.80 (9H, br, -CH_2-C(**CH_3**)$_3$).

9.4.3.3 *Plasmid Preparation*

pEGFP-N1 pDNA (Takara/Clontech, Mountain View, USA) was amplified in *E. coli* DH5α and was isolated following standard plasmid preparation protocols (Qiagen, Hilden, Germany).

9.4.3.4 *Labeling of Plasmid DNA*

pEGFP-N1 pDNA was labeled with Cy5 dye using the Label IT® Nucleic Acid Labeling Kit from Mirus Bio (Madison, WI). Absorbance of Cy5-labeled pDNA was measured using a Nanodrop® ND-1000. Labeling density was calculated to be one dye molecule per 151 bases following protocols provided by Mirus.

9.4.3.5 *Formation of PeptoPlexes*

Block copolypept(o)ides were dissolved in sterile water and filtrated (450 nm) to obtain solutions with final concentrations of 1 mg/mL. Polyplexes were prepared by diluting the desired amount of pDNA in sterile water and subsequent addition of polymers at the amounts indicated followed by immediate vortexing for 10 seconds. The obtained polyplex solutions were allowed to stand at room temperature for at least 30 minutes before further use. The concentration with respect to pDNA was kept at 0.02 mg/ml. N to P ratios were calculated by referring the amount of primary amines from the lysine residues to the amount of phosphate groups in the pDNA backbone. Polyplexes of jetPEI (Polyplus-transfection® SA, Strasbourg, France) were formed according to manufacturer's protocol.

9.4.4 Physicochemical Characterization of PeptoPlexes

9.4.4.1 *Characterization of PeptoPlexes by Agarose Gel Electrophoresis*

Gel electrophoresis was performed with a 0.7% agarose gel at 90 V (150 mA) to monitor pDNA complexation at different N/P ratios. Polyplexes were formed using 300 ng of pDNA and the respective amount of polymers. GelRed was used for pDNA and polyplex staining.

9.4.4.2 *Characterization of PeptoPlexes by Dynamic Light Scattering Experiment*

Polyplex solutions with 10 µg of pDNA, N/P 6 were prepared in 300 µl Milli-Q water and subsequently diluted to final volume of 3 mL of PBS. After transfer to a dust free flow box, all samples were filtered (Millex HV 0.45µm) into dust free cylindrical scattering cells (Suprasil, 20 mm diameter, Hellma, Mühlheim, Germany). Dynamic light scattering measurements (DLS) were performed using a Uniphase He/Ne Laser (l=632.8 nm, 22 mW), a ALV-SP125 Goniometer, a ALV/High QE APD-Avalanche photo-diode with fibre optical detection, a ALV 5000/E/PCI-correlator and a Lauda RC-6 thermostat unit at 20 °C. Angular dependent measurements of typically 15° steps were carried out in the range $30° \leq q \leq 150°$. For data evaluation experimental intensity correlation functions were transformed into amplitude correlation functions applying the Siegert relation extended to include negative values after baseline subtraction by calculation $g_1(t) = SIGN(G2(t))$ **.**

$SQRT(ABS((G2(t) - A)/A)$. All field correlation functions usually showed monomodal decay and were fitted by a sum of two exponentials $g1(t) = a \cdot exp(-t/b) + c \cdot exp(-t/d)$ to take polydispersity into account. Average apparent diffusion coefficients D_{app} were calculated by applying $q^2 \cdot D_{app} = (a \cdot b - 1 + c \cdot d - 1)/(a + c)$ resulting in an angular-dependent diffusion coefficient D_{app} or reciprocal hydrodynamic radius $\langle 1/R_h \rangle_{app}$, according to formal application of Stokes Einstein law. By extrapolation of $\langle 1/R_h \rangle_{app}$ to $q = 0$ z-average hydrodynamic radii $R_h = \langle 1/R_h \rangle_{z^{-1}}$ were obtained (uncorrected for c-dependency).

9.4.4.3 *Characterization of PeptoPlexes by Cryogenic Transmission Electron Microscopy*

5 µL of polyplex solutions in Milli-Q water (N/P 6, same concentration as for DLS) were applied to freshly glow-discharged carbon grids with a copper 200 mesh (Quantfoil Micro Tools GmbH). Excess fluid was removed by direct blotting (2.5 s) and the grids were individually plunge-frozen in liquid ethane. Grids were cryotransferred in liquid nitrogen using a Gatan cryoholder (model 626 DH) to a Technai T12 transmission electron microscope equipped with a field emission electron source and operating at 120 kV accelerating voltage. Images were recorded using a TemCam-F416 (TVIPS, Gauting, Germany).

9.4.5 Biological Characterization of PeptoPlexes

9.4.5.1 *Cell Culture*

HEK 293T cells were grown in DMEM, supplemented with 10% FBS, 4 mM L-glutamine, 0.1 µM 2-mercaptoethanol, 100 units x mL^{-1} penicillin, and 100 µg x mL^{-1} streptomycin. Cells were maintained in a 37 °C humidified atmosphere with 5% CO_2 and were handled under sterile conditions.

9.4.5.2 *Determination of Transfection Efficiency by Flow Cytometry and Fluorescence Microscopy*

HEK 293T cells were seeded into wells of 24 well (6 well for Fluorescence Microscopy) cell culture plates (each 1.0 x 10^5 cells in 1 mL). One day later, culture medium was changed and cells were incubated with polyplexes (formed with 5 µg of pDNA, N/P 6) in a final volume of 1.25 mL. The following day, medium was replenished. Two days after the onset of transfection, cells were imaged by Fluorescence Microscopy; or were harvested (PBS/2 mM EDTA) and samples were analyzed by flow cytometry for frequencies of eGFP positive cells.

9.4.5.3 *Determination of Cellular PeptoPlex Binding by Flow Cytometry*

HEK 293T cells were seeded into wells of 48 well cell culture plates (each 0.4 x 10^5 cells in 0.5 mL). One day later, culture medium was changed and cells were incubated for 2 h with polyplexes (formed with 0.5 µg of Cy5-labeled pDNA, N/P 6) in a final volume of 0.125 mL at either 4 °C or 37 °C. Afterwards, cells were harvested (PBS/2 mM EDTA) and samples were analyzed by flow cytometry for frequencies of Cy5-positive cells. To assess intracellular accumulation of polyplexes quantitatively, MFI values obtained for incubation at 4 °C were subtracted from those obtained for incubation at 37 °C.

9.4.5.4 *Analysis of Cellular Uptake by Confocal Laser Scanning Microscopy*

HEK 293T cells were seeded into wells of chambered coverslips (8 well µ-slide; Ibidi Germany) (each 1 x 10^4 cells in 0.1 mL). On the next day, the medium was replaced with OptiMEM, and cells were incubated with polyplexes (formed with 0.5 µg of Cy5-labeled pDNA, N/P 6) for 2 h. Afterwards, cells were washed with PBS and stained with Hoechst (nuclear staining) and Cell Mask (cell membrane) dyes following standard protocols. The 8-well plate was moved to the confocal microscope equipped with a live cell unit. Images were captured with a Leica confocal microscope and analyzed using IMAGEJ software (1.490, NIH Bethesda, MD).

9.4.5.5 *Incubation of PeptoPlexes with DNase I*

Polyplexes were formed with 0.5 µg of pDNA (N/P6). 10 µl of each sample (equal to 200 ng pDNA) were incubated with either 0.2 U (in 10 µl HBSS) of DNAse I or 10 µl of HBSS only, for 30 min at 37 °C. Afterwards, samples were analyzed by agarose gel electrophoresis.

ACKNOWLEDGEMENTS

Philipp Heller, Prof. Jiajia Zhou and Benjamin Weber contributed equally to this work. The authors would like to acknowledge funding from DFG (SFB 1066-1) and the NMFZ Mainz. Computational resources at Johannes Gutenberg University Mainz (MOGON high performance computing center) are gratefully acknowledged. The simulations were carried out using the open source software package ESPResSo.[449] Simulation images were rendered using VMD.[455] The authors also gratefully acknowledge support by the Microscopy Core Facility of the Institute of Molecular Biology (IMB) Mainz. Philip Heller is grateful for support by MAterials Science IN MainZ (MAINZ). The manuscript was written through contributions of all authors. All authors have given approval to the final version of the manuscript.

9.5 SUPPORTING INFORMATION

9.5.1 Simulations

We use the bead-spring model[328] (also see Subsection 4.1.2) to simulate the plasmid DNA (pDNA) and the polypept(o)ides. There are six types of beads in the system:

Table 9.2: Characteristics of beads for simulation.

TYPE	HYDROPHOBICITY	CHARGE	COLOR
DNA	hydrophilic	-1	white
Sarcosine	hydrophilic	0	blue
Imidazole	hydrophobic	0	yellow
Lysine	hydrophilic	+1	red
cation	-	+1	-
anion	-	-1	-

Short-range interactions between different beads are simulated through a Lennard-Jones interaction,

$$V_{LJ}(r) = \begin{cases} 4\varepsilon \left[\left(\frac{\sigma}{r}\right)^{12} - \left(\frac{\sigma}{r}\right)^{6} + c_{\text{shift}} \right] & r < r_{\text{cut}} \\ 0 & \text{otherwise} \end{cases} \tag{9.1}$$

Except between two hydrophobic beads (imidazole), the Lennard-Jones interaction between a pair of beads are chosen to be purely repulsive by setting: $r_{\text{cut}} = \sqrt[6]{2}$ and $c_{\text{shift}} = 1/4$. The interaction potential between two hydrophobic beads has an attractive well, which is modeled by setting $r_{\text{cut}} = 2.5$ and $c_{\text{shift}} \approx 0.00408$. The shift of the energy level is chosen to ensure that the potential is zero at the cutoff.

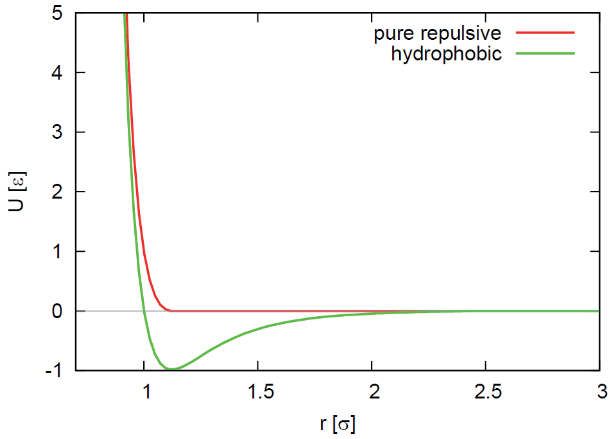

Figure 9.8: Short-range one-bonded interaction between two beads

The beads are connected by harmonic springs to form polymers. The bonded interaction has the form

$$V_{\text{harm}}(r) = \frac{1}{2}K_r\,(r - r_0)^2 \tag{9.2}$$

where r is the distance between two connected beads. The parameters are chosen as $K_r = 5000\varepsilon$ and $r_0 = \sigma$, and chain crossing is prohibited. While the polymers are linear chains and fully flexible, the plasmid DNA are ring polymers and semiflexible. The stiffness of the DNA chain is modeled by a harmonic bond-angle potential,

$$V_{\text{angle}}(\Phi) = \frac{1}{2}K_\Phi\,(\Phi - \Phi_0)^2 \tag{9.3}$$

where Φ is the angle between two adjacent bonds. Following Ref. [328], the parameters are chosen as $K_\Phi = 8\varepsilon$ and $\Phi_0 = \pi$.

The mapping from the real system to our model is about 2:1, hence two monomers are represented by one bead in the simulation. The monomer unit is either one DNA base pare (0.3 nm) or with one amino acid (0.4 nm), hence 1 corresponds to roughly 0.8 nm. In this case, a DNA chain of length 4800 bp corresponds to 2400 beads in the simulation. Unfortunately, we found that it was impossible to equilibrate and statistically sample chains of that size in reasonable simulation times. Therefore, in the simulations, we used a shorter DNA chain containing only 1200 beads. The length of the polypeptides was chosen to match that in the experiments, i.e., the sarcosine blocks contain 100 beads.

We perform Langevin simulations on the complex formation, where water is treated implicitly. The effect of water is represented by a viscous environment that provides friction to the polymer motion, and a dielectric background for the Coulomb interaction. The temperature of the system is set at $k_B T = 1\varepsilon$. The Bjerrum length is chosen as $l_B = 3\sigma$ (taken from Ref. [328]). The friction coefficient for the Langevin thermostat is $\xi = 1.0\tau^{-1}$, where $\tau = \sigma\sqrt{m/\varepsilon}$ is the time unit of the simulation. All simulations are carried out using the open-source package ESPResSo[449]. ESPResSo is using the velocity-Verlet algorithm for the integration, and the time step is 0.01τ.

For all simulations, we used a periodic cubic box of size 200σ. We start the simulation with the DNA in the center of the box, and randomly distributed polymer chains. The number of polymer chains is set such that the number of lysine beads (positively charged) is twice of the DNA beads. A few simulations were conducted where the number of Lysine beads was three times the number of DNA beads. The results did not change significantly. The added monovalent cations and anions can neutralize the DNA and polymer chains separately (i.e., the number of the cations is equal to the charge of DNA, and the number of the anions is equal to the charge of all lysine units). The equilibrium time is 2×10^7 time steps, and the measurement is done every 2000 steps in the following 10^7 time steps. Four runs with independent starting configurations are performed for each parameter setting.

During the simulation, we monitor several quantities of the complex, such as the hydrodynamic radius

$$\frac{1}{R_h} = \frac{1}{N^2}\sum_{i \neq j}\frac{1}{r_{ij}} \tag{9.4}$$

and the gyration tensor

$$S = \frac{1}{N}\sum_{i=1}^{N}\left(r^{(i)} - r_{\text{com}}\right)\left(r^{(j)} - r_{\text{com}}\right) \tag{9.5}$$

where r_{com} is the center-of-mass position. The gyration tensor is a symmetric 3×3 matrix and can be diagonalized by proper rotation

$$S = \begin{matrix} \lambda_x & 0 & 0 \\ 0 & \lambda_y & 0 \\ 0 & 0 & \lambda_z \end{matrix} \tag{9.6}$$

where $\lambda_x \leq \lambda_y \leq \lambda_z$. The radius of gyration is given by

$$R_g^2 = \lambda_x + \lambda_y + \lambda_z \tag{9.7}$$

The shape of the complex can be described by the asphericity

$$b = \lambda_z - \frac{1}{2}\left(\lambda_x + \lambda_y\right) \tag{9.8}$$

which is non-negative number. A zero value corresponds to a spherical shape $\left(\lambda_x = \lambda_y = \lambda_z\right)$, while for a thin rod object $b = l^2$ where l is the rod length.

A few remarks are in order regarding the mapping of simulation units to real units. The mapping can be done based on the size of molecules - this gives the length scale - and the value of the Bjerrum length in water $l_{\text{B,water}} = 0.7\,\text{nm}$ - this gives the scale for the charge unit q. Specifically, the Bjerrum length in the simulation is given by $l_{\text{B}} = (q/e)^2\, l_{\text{B,water}}$ where e is the elementary charge and q the charge. In our case, we have $\sigma \sim 0.8$ nm and $q \sim 2\text{-}3\ e$. With this mapping, one finds that some features of the simulated system do not fully reflect the reality. (I) The linear charge density on the model DNA is much larger than on real DNA (which has two negative charges per base pair). However, this does not really matter since both in the simulations and in real DNA/lysine, the Manning parameter $\xi = Zl_B\lambda$ exceeds one (Z is the valency of counterions, λ the linear charge density on the polyelectrolyte, and in the simulations, we get $\xi = 3$). Therefore, we have strong counterion condensation. This leads to a charge renormalization, such that at some distance from the polyelectrolytes the effective charge corresponds to a Manning parameter about $\xi \sim 1$ (both in theory and simulation). In the simulation model, counterion condensation is accounted for in part by the reduced charge density on the model molecules, and in part by an actual condensation of the explicit ions in the system. (II): Micro-ions are not monovalent, but carry a fractional charge (qe). Apart from the fact that this changes the Debye screening length, it should not affect the results significantly in the Poisson-Boltzmann regime. (III): The DNA is stiffer than the polymers, but still much too flexible compared to real DNA. This is because simulations at higher stiffness required much longer equilibration times and the configuration space could not be sampled properly. (IV): In the simulation model, the peptide molecules and the DNA have the same thickness 1σ, which does not reflect the reality. The thickness of the polypept(o)ides is well represented in the simulations, but the thickness of the DNA is too small (in reality, it is around 3 nm).

9.5.2 Polymer Synthesis

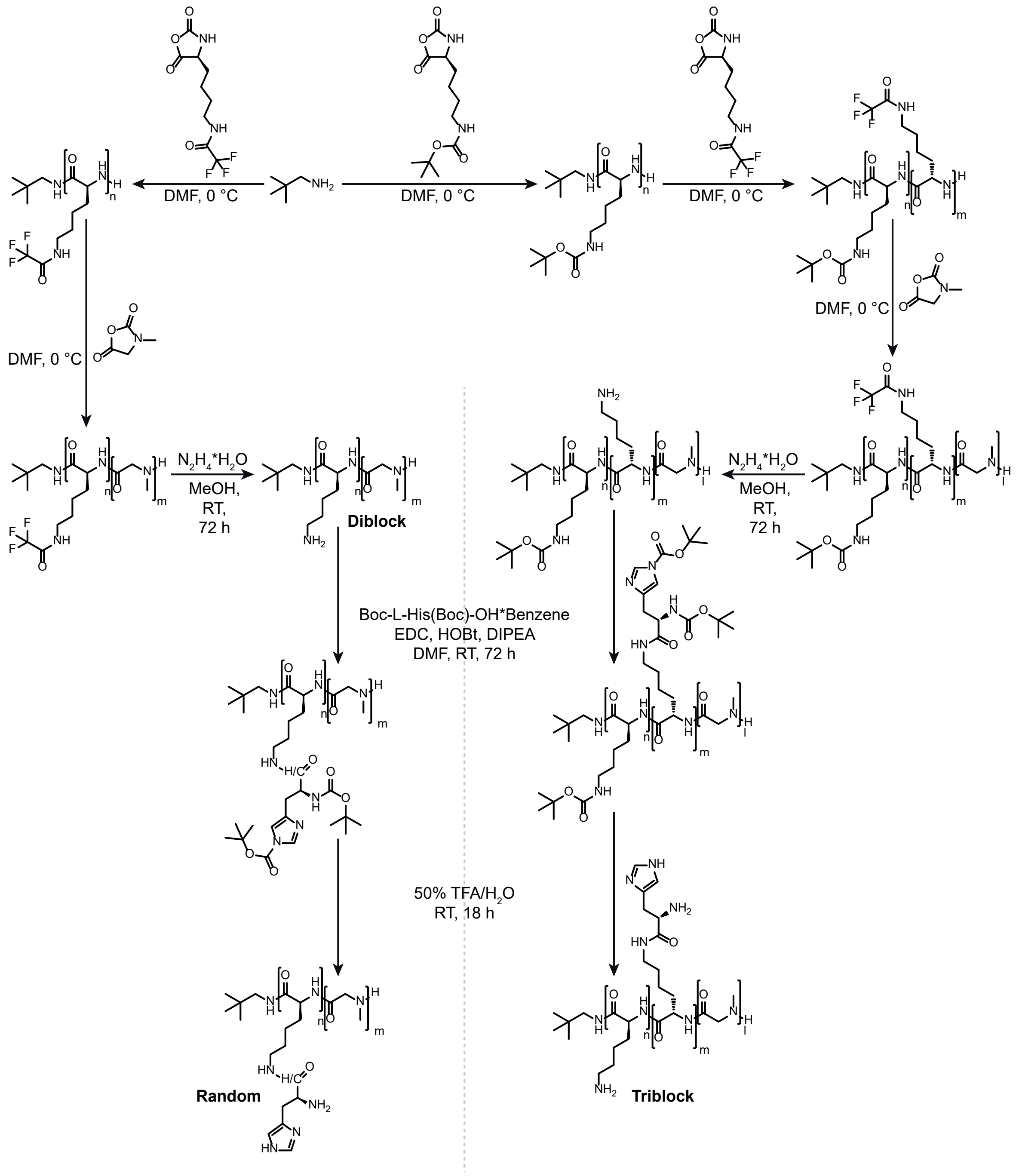

Figure 9.9: Synthetic route towards **Diblock**, **Triblock** and **Random** polymers.

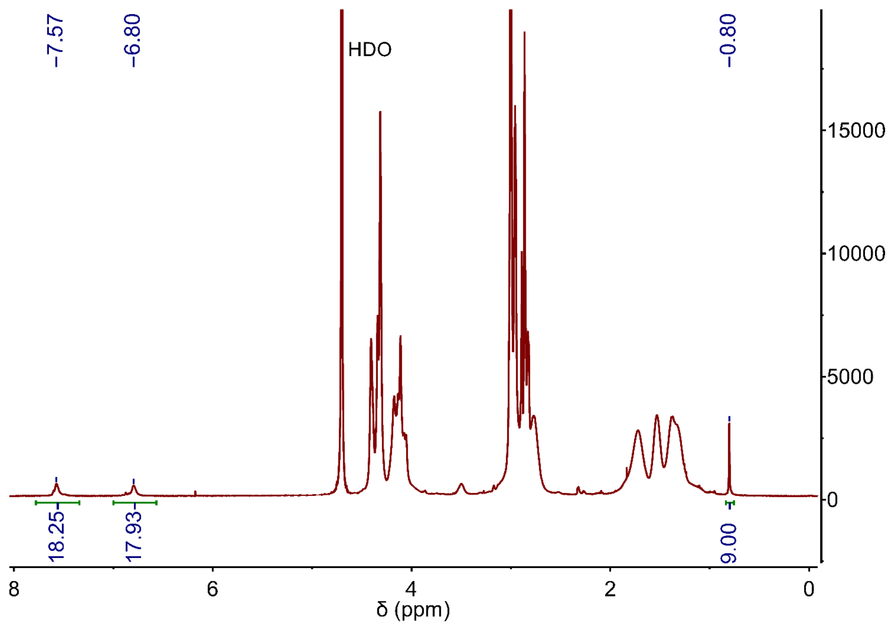

Figure 9.10: ^{1}H-NMR spectrum of homopolymer PLys(Boc)$_{39}$ (block 1 of final **Triblock**).

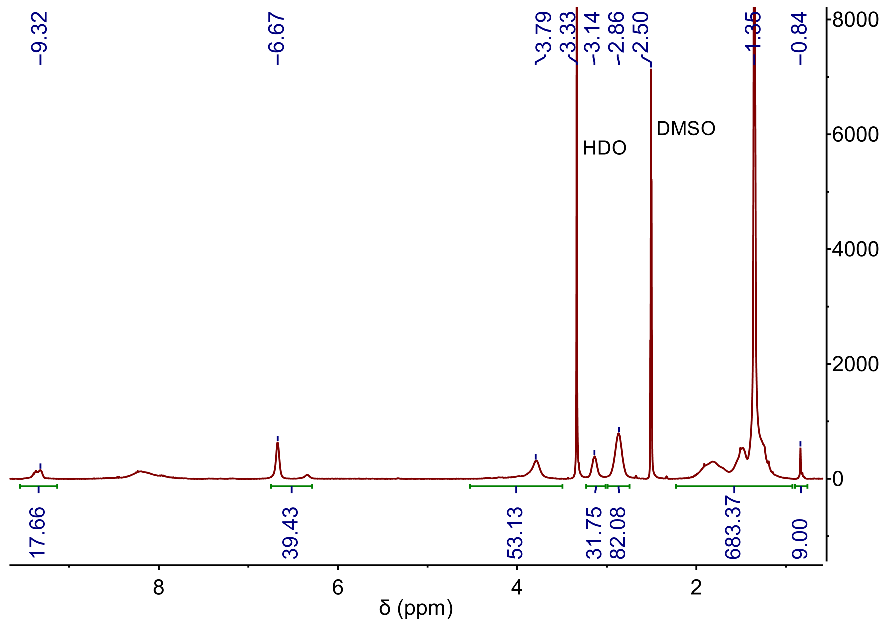

Figure 9.11: ^{1}H-NMR spectrum of diblock copolymer PLys(Boc)$_{39}$-b-PLys(TFA)$_{18}$ (block 1 and 2 of **Triblock**).

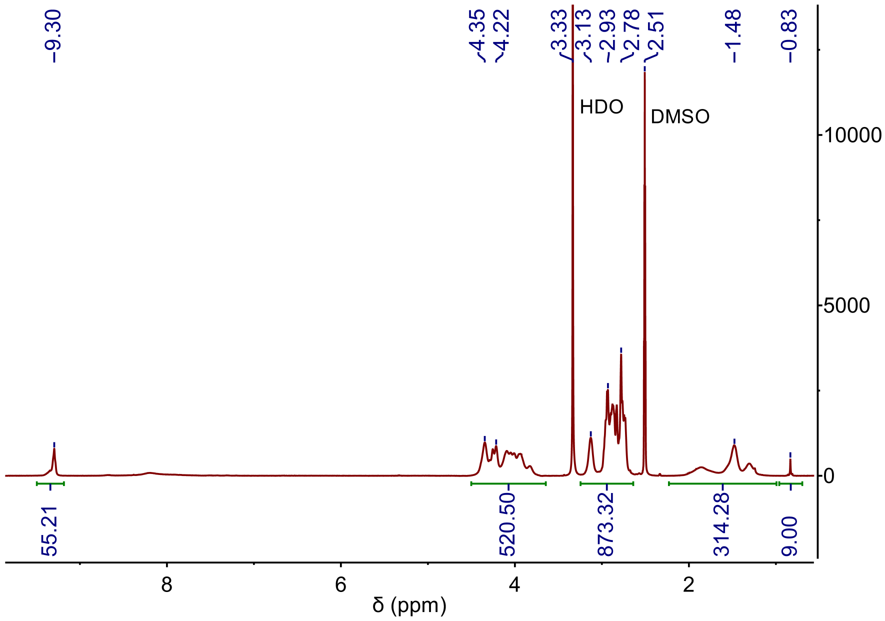

Figure 9.12: ^{1}H-NMR spectrum of diblock copolymer PLys(TFA)$_{55}$-b-PSar$_{232}$ (protected precursor for **Diblock** and **Random**).

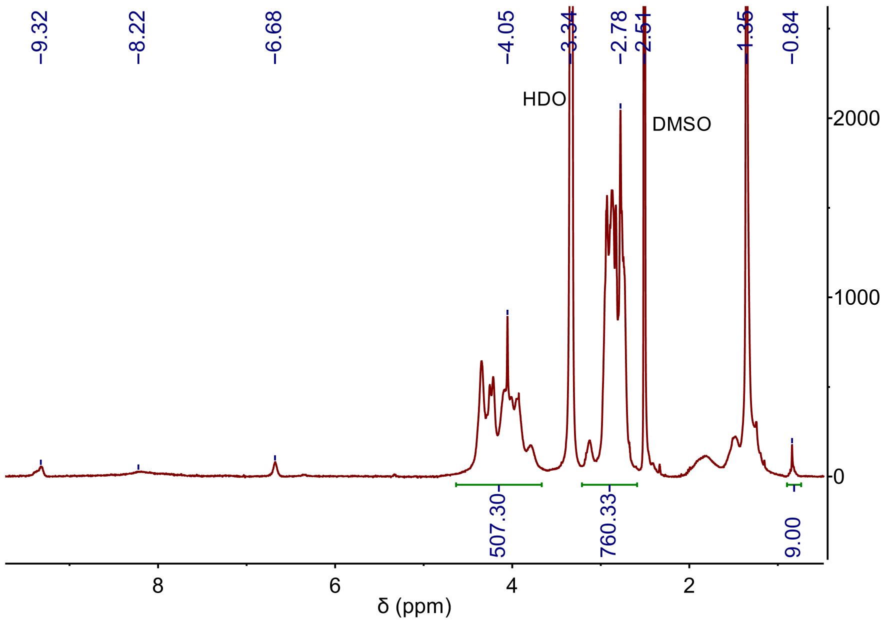

Figure 9.13: ^{1}H-NMR spectrum of triblock copolymer PLys(Boc)$_{39}$-b-PLys(TFA)$_{18}$-b-PSar$_{225}$ (protected precursor for **Triblock**).

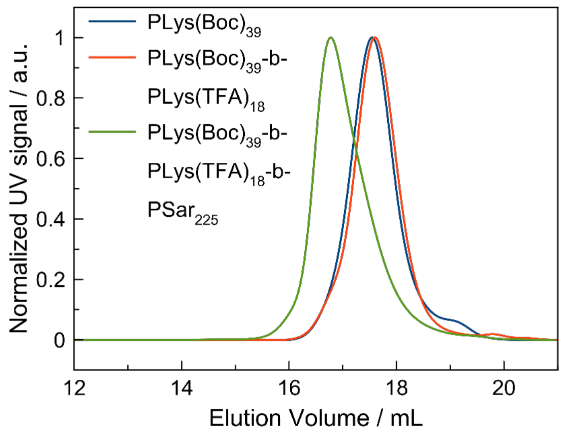

Figure 9.14: HFIP GPC traces of PLys(Boc)$_{39}$, PLys(Boc)$_{39}$-b-PLys(TFA)$_{18}$ and PLys(Boc)$_{39}$-b-PLys(TFA)$_{18}$-PSar$_{225}$ showing the transition from homopolymer to di- and triblock copolymers.

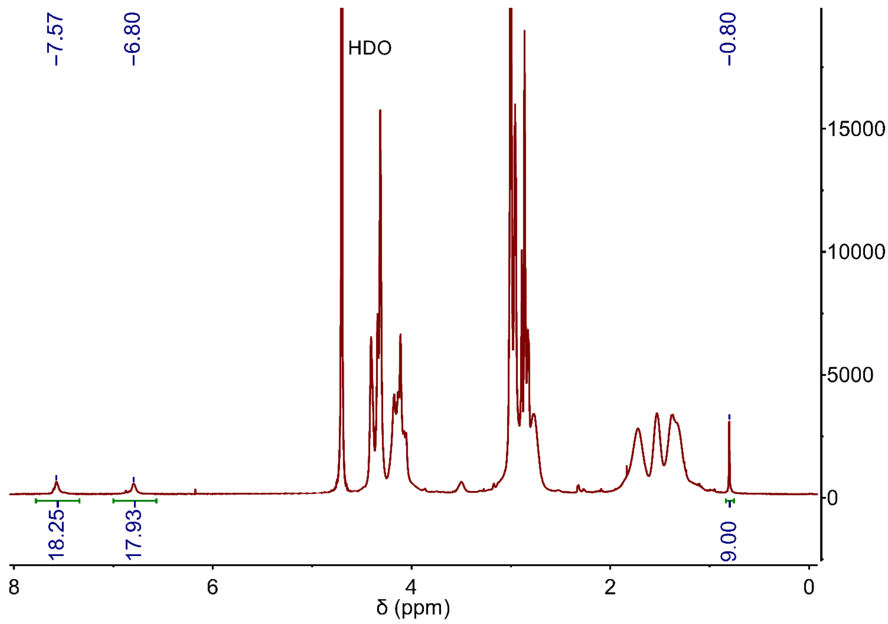

Figure 9.15: Determination of number of imidazole groups per polymer by ^{1}H-NMR, depicted for **Triblock** polymer.

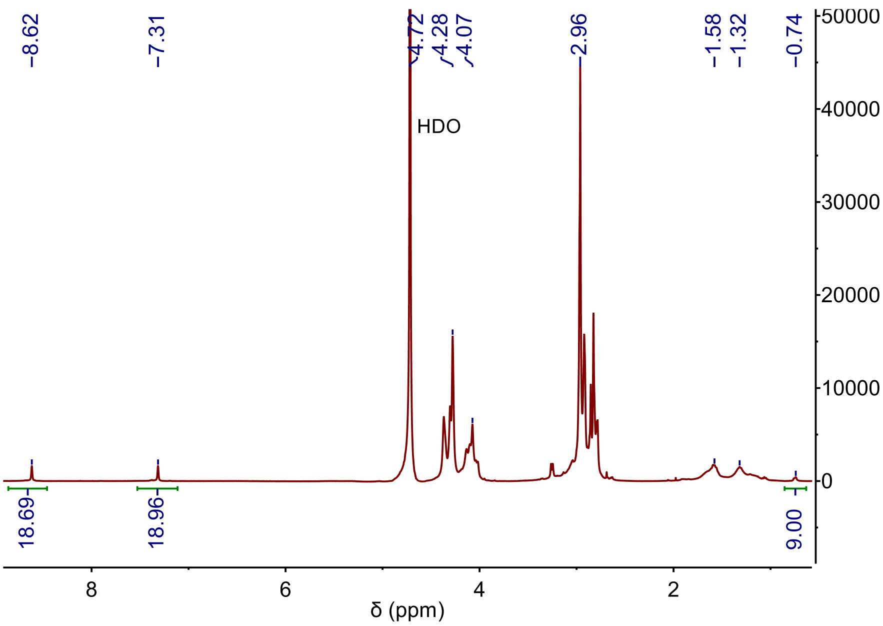

Figure 9.16: Determination of number of imidazole groups per polymer by [1]H-NMR, depicted for **Random** polymer.

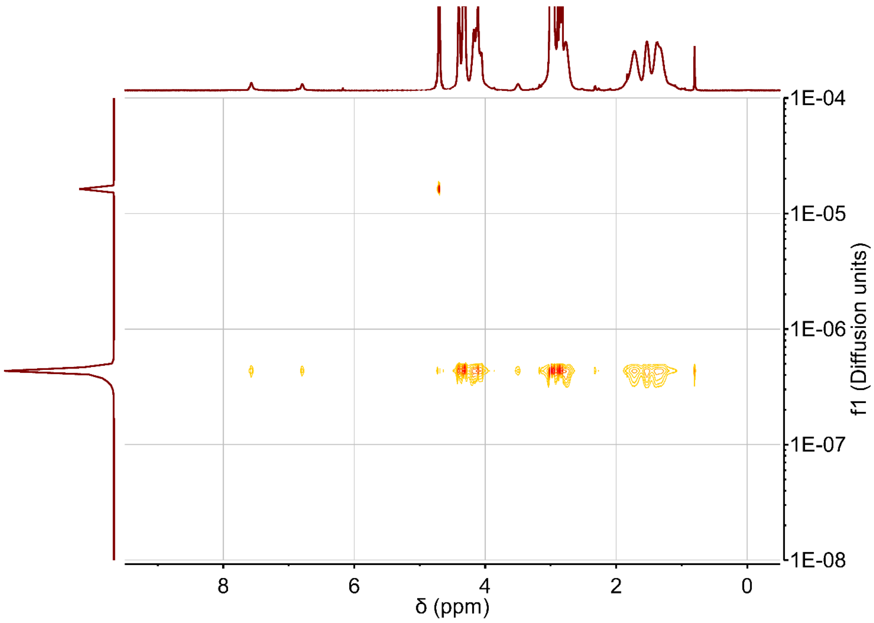

Figure 9.17: DOSY [1]H-NMR showing imidazole-modified triblock copolypept(o)ide as one diffusing polymer species.

9.5.3 Agarose Gel Electrophoresis

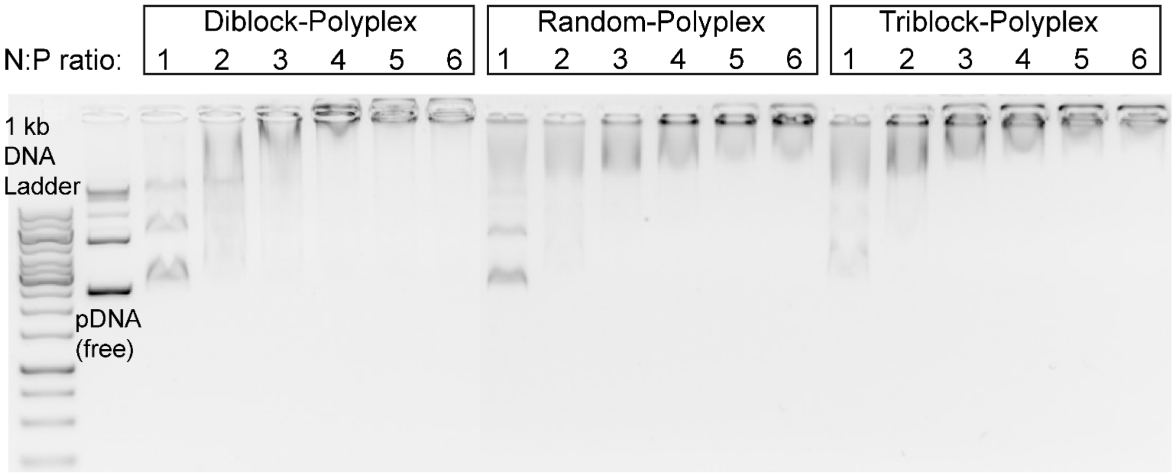

Figure 9.18: Agarose gel eletrophoresis showing complexation behavior of **Diblock**, **Random** and **Triblock** polymers at increasing N/P ratios.

9.5.4 FACS Experiments

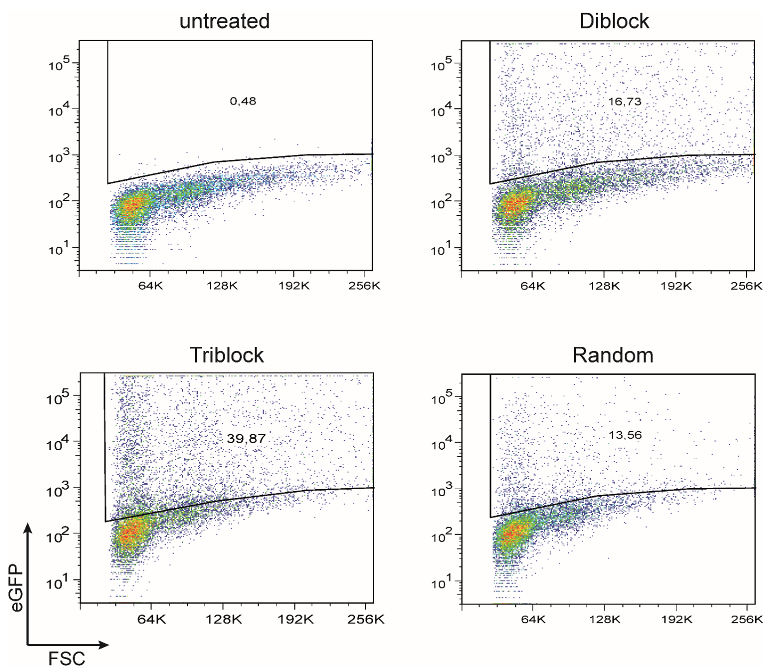

Figure 9.19: Representative dot plots of HEK 293T cells monitored for eGFP expression 24h after transfection with polyplexes.

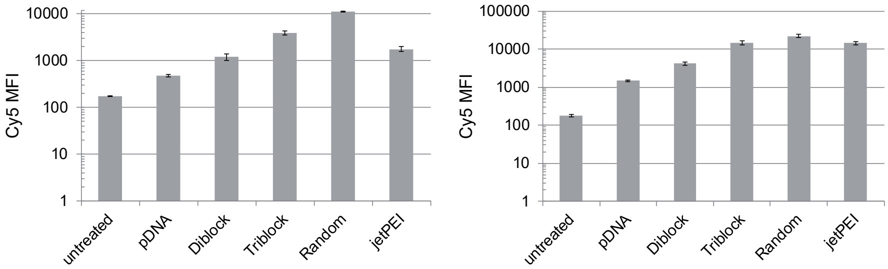

Figure 9.20: Raw MFI values obtained by FACS after incubation of HEK 293T with polyplexes at either 4 °C (left) or 37 °C (right), n = 3.

10 TEAMING REACTIVE TRIBLOCK COPOLYMERS WITH FUNCTIONAL CROSS-LINKERS: A VERSATILE PATHWAY TO DISULFIDE STABILIZED-POLYPLEX LIBRARIES AND THEIR APPLICATION AS PDNA VACCINES

P. Heller, D. Hobernik, U. Lächelt, M. Schinnerer, B. Weber, M. Schmidt, E. Wagner, M. Bros, M. Barz, *submitted*

ABSTRACT

Therapeutic nucleic acids such as pDNA hold great promise for the treatment of multiple diseases. These therapeutic interventions are, however, compromised by the lack of efficient and safe non-viral delivery systems, which guarantee stability during blood circulation together with high transfection efficiency. To provide these desired properties within one system, we propose the use of reactive triblock copolypept(o)ides, which include a stealth-like block for efficient shielding, a hydrophobic block based on reactive disulfides for cross-linking and a cationic block for complexation of pDNA. After the complexation step, bifunctional cross-linkers can be employed to bioreversibly stabilize derived polyplexes by disulfide bond formation and to introduce endosomolytic moieties at the same time. Cross-linked polyplexes show no aggregation in human blood serum. Upon cellular uptake and cleavage of disulfide bonds, the cross-linkers can interact with the endosomal membrane, leading to lysis and efficient endosomal translocation. The approach in principal allows the combination of one polymer with various different cross-linkers and thus enables the fast forward creation of a polyplex library.

Here, we provide a first insight into the potential of this concept and use a screening strategy to identify a lead candidate, which is able to transfect dendritic cells with a model DNA vaccine.

10.1 INTRODUCTION

The implementation of nucleic acids like plasmid DNA (pDNA), mRNA, siRNA and others as a new class of drugs promises to broaden the pharmaceutical repertoire from conventional direct interaction with accessible targets such as proteins and receptors to more sophisticated cellular manipulations via the transcriptional and translational machinery.[5] This strategy provides the opportunity to make formerly "undruggable" therapeutic targets accessible. DNA vaccines in particular provide enormous potential, because in contrast to conventional vaccines, antigen and immune activator can be encoded on one plasmid and thus be combined on DNA level. In addition, the plasmid can contain a cell specific promotor, which prevents transcription in non-target cells.[456]

The transfection of dendritic cells with DNA vaccines, however, is challenging and thus complex demands arise for non-viral vectors.[457] To find and optimize suitable systems, one needs to establish synthetic pathways allowing rapid synthesis and screening of vector compositions. While screening approaches are commonly used for low molecular weight lipid and lipoid formulations,[2, 458] these approaches are more challenging for block ionomer-based complexes (polyplexes) for systemic gene delivery. Various polymeric materials have been examined intensively for gene delivery application.[5] Yet, in most cases optimization steps require the complete synthesis of new polymers,[459–461] which might complicate efficient screening approaches.

Over the last decades, a series of researchers rationalized a chemical design principle for systemic pDNA delivery systems based on polyplexes, which can ensure efficient transfection *in vitro* and even in the more challenging *in vivo* environment.[207, 373, 462, 463] To achieve these properties, core shell structures turned out to be beneficial and thus need to be generated during polyplex formulation.[464] The most common way to gain such structures is the self-assembly of pDNA and block ionomers. Block ionomers are block copolymers combining a neutral, hydrophilic and protein resistant block, e.g. polyethylene glycol (PEG),[220] polyhydroxypropyl methacrylamide (PHPMA)[141, 142] or more recently polysarcosine (PSar),[37, 156] with a cationic block, which provides two functionalities. First, it interacts with the anionic nucleotides, forming a stable complex, thereby condensing the pDNA to a more compact structure, often with a diameter of half or a third of its original size. Second, the cationic block often has endosomolytic properties or is functionalized with endosomolytic groups to facilitate endosomal escape, which is a main hurdle for an efficient transfection of cells.[305] Prominent examples for endosomolytic groups on the one hand include pH buffering secondary and tertiary amines - as found in PEI,[465] histidine[6] and PAMAM[466, 467] - acting through the hypothesized proton sponge effect triggered by the endosomal protonation and through cationic membrane interaction.[305] On the other hand, amphipathic motives, being the key component in many artificial or virus-derived fusogenic peptides, are well known to foster endosomal escape through hydrophobic membrane interaction.[244, 468]

Complementary to these basic prerequisites for transfection, several groups have demonstrated that *in vivo* performance of polyplexes can be improved significantly, if they are additionally stabilized by covalent cross-linking.[235, 463, 469–471] In this respect, cross-linking via disulfide bond formation seems particularly attractive, since it leads to redox-responsive stabilization, as disulfides can be cleaved by elevated concentrations of the natural reducing agent glutathione.[472] As the glutathione concentration differs by a factor of 50-1000[472] between extra- and intracellular environments, Kataoka and co-workers could show that disulfide cross-linking of polyplexes provides stability in extracellular milieu and during blood circulation, while allowing efficient disintegration of polyplexes after cellular uptake.[233, 234, 250] Two different methodologies for the incorporation of disulfide bonds into polyplexes are reported in literature. The first strategy involves reaction of preformed polyplexes with amine-to-amine cross-linking reagents such as dimethyl 3,3'-dithiobispropion- imidate (DTBP)[469, 473] or dithiobis(succinimidyl propionate) (DSP),[474] which already contain a disulfide bond. The second strategy is based on the functionalization of polymers with disulfide or sulfhydryl groups before polyplex formation either by polymerizing thiol-containing monomers[470, 475] or by polymer-analogous reaction,[233] respectively. The latter procedure was performed by Kataoka and co-workers using *N*-succinimidyl 3-(2-pyridyldithio)propionate (SPDP) or 2-iminothiolane (Traut's reagent) to introduce thiols to a poly-L-lysine (PLys) segment of PEG-b-PLys block copolymers.

In conclusion, an ideal polymer for the formation of polyplexes should combine a shielding block based on a stealth-like material, a cationic segment for pDNA complexation, endosomolytic moieties for efficient endosomal translocation and thiols for bioreversible cross-linking. While these requirements seem to create a need for highly complex materials, we here would like to introduce a design concept, which meets the requirements by robust and scalable chemistry and can overcome the aforementioned screening limitations. Our concept is based on the use of reactive triblock copolypept(o)ides, which comprise a hydrophilic polysarcosine block, an activated thiol containing segment for asymmetric disulfide formation and a cationic polylysine block. After polyplex formation between triblock copolypept(o)ides and pDNA, bifunctional cross-linkers containing endosomolytic moieties and two or more thiols can simply be added for the disulfide formation. Thereafter, these endosomolytic cross-linkers provide polyplex stability in extracellular space, while fostering endosomal escape by proton sponge effect or membrane interaction after cellular uptake and being released from the polyplexes upon disulfide cleavage[476–481] (Fig. 10.1).

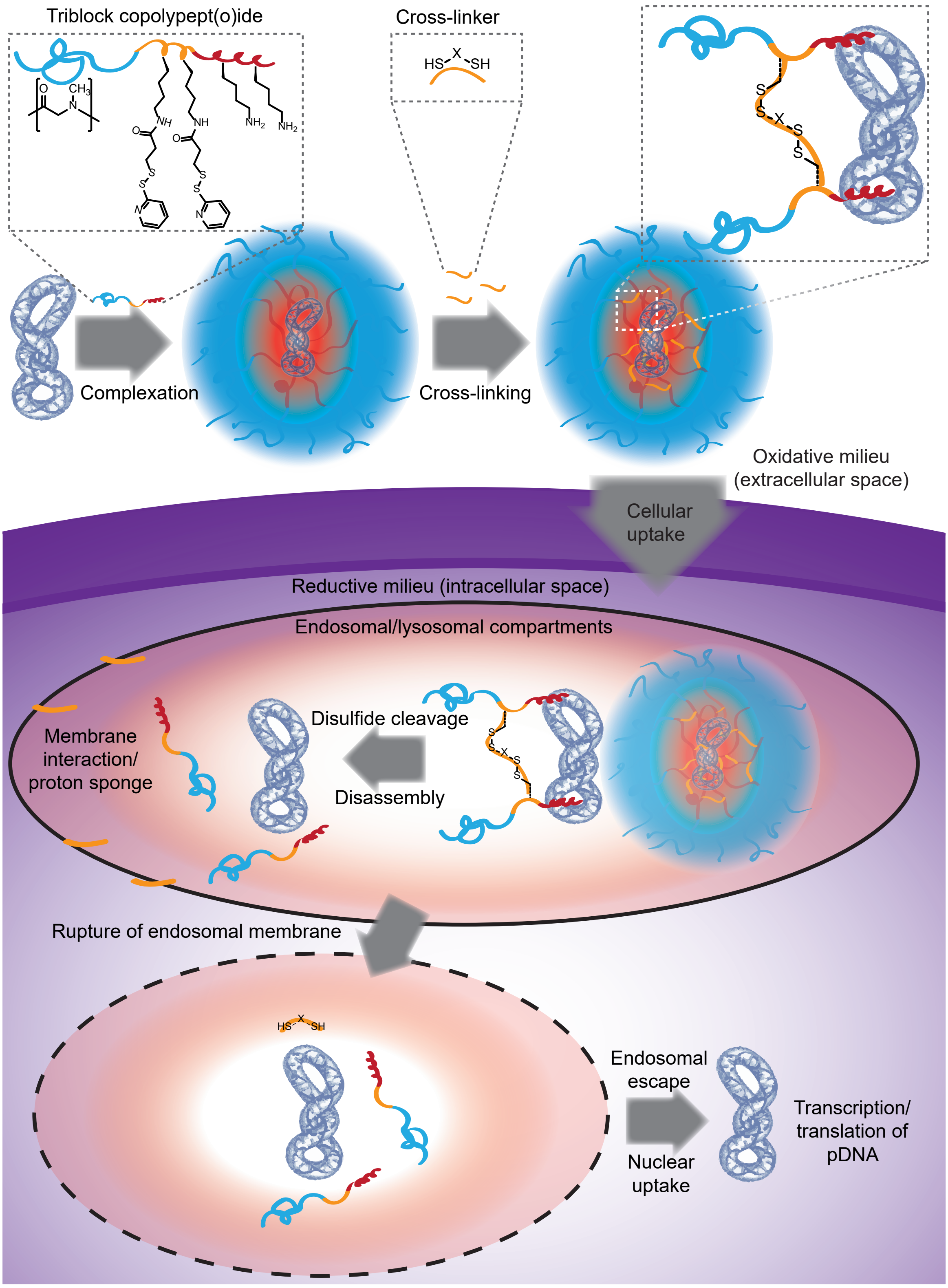

Figure 10.1: Inspired by non-enveloped viruses: The concept of disulfide stabilized polyplexes, in which bifunctional cross-linkers combine bioreversible stabilization via disulfides (extracellular) with endosomolytic properties and reductive destabilization (intracellular).

The versatility of this approach allows control over charge density and degree of cross-linking, but most importantly, it enables the straightforward synthesis of polyplex libraries based on just one single triblock copolymer, which can be combined with an array of different cross-linkers. To validate this novel synthetic concept for cross-linked polyplexes, we report the generation, characterization and evaluation of a polyplex library in search for an efficient non-viral vector for DNA vaccination.

10.2 RESULTS AND DISCUSSION

10.2.1 Rational Synthesis of Cross-linkable Triblock Copolypept(o)ides

Polyplex forming, cross-linkable triblock copolypept(o)ides were obtained from PLys(Boc)-b-PLys(TFA)-PSar precursor polymers (see experimental part and SI). Synthesis and orthogonal deprotection of the latter was reported earlier.[158] By this method, the ε-amine groups of the middle PLys(TFA) segment can be freed selectively making them accessible for block selective modification with succinimidyl 3-(2-pyridyldithio)propionate (SPDP), introducing activated disulfide bonds. The approach yields ionomers of conserved triblock architecture, in which a cross-linkable block in the middle is flanked by a hydrophilic and a cationic segment. As an advantage of the synthetic sequence with two orthogonally protected PLys blocks, the charge densitiy of the cationic, initially Boc-protected, PLys segment is not affected by the SPDP reaction step, which - as previously shown by our group[159] - is important for pDNA complexation capacity. Eventually, charge density and degree of thiol-modification of the triblock copolypept(o)ides can be tuned by variation of block length ratios and remain fixed afterwards.

Considering previous experiments on the impact of PLys-PSar block length ratios on stability and transfection efficiency,[156] we aimed to synthesize a triblock copolypept(o)ide with a cationic segment of 35 lysine units, an equally long cross-linking segment and a hydrophilic segment of 350 sarcosine units (see SI for characterization data).

10.2.2 Effect of Cross-linking

Although polyplexes of pDNA or mRNA with block ionomers are commonly regarded to possess high stability, cross-linking by disulfide formation provides additional stability and thus enhanced circulation times *in vivo*, with the bio-reversible nature of disulfide bonds granting high transfection efficiencies.[234, 463, 469–471]

While *in vivo* effects of enhanced stability of cross-linked polyplexes have been nicely demonstrated by several groups,[234, 463, 469–471] we aimed to understand the underlying effects of cross-linking in more detail *ex vivo*. With blood being the first biological environment a nanoparticle will encounter after intravenous injection, stability in the presence of blood components and prevention of aggregation is of utmost importance. Therefore, we performed dynamic light scattering (DLS) experiments in human blood plasma according to established protocols by Rausch *et al*.[325, 326] This DLS methodology can be used to monitor aggregation of serum components induced by interaction with nanoparticles in general with high sensitivity and may help to understand *in vivo* behavior. Interestingly, it has not yet been applied to polyplexes.

To assess the cross-linking effect, we formed non-cross-linked (**NCPX**) and crosslinked polyplexes (**CPX**) based on triblock copolypept(o)ides and pDNA (p1699) in PBS and added the polyplex solution to human plasma yielding a final plasma concentration of 90 vol%. For both polyplexes (**NCPX** and **CPX**) the autocorrelation functions (ACF) determined by DLS in 90% human plasma are displayed in Fig. 10.2.

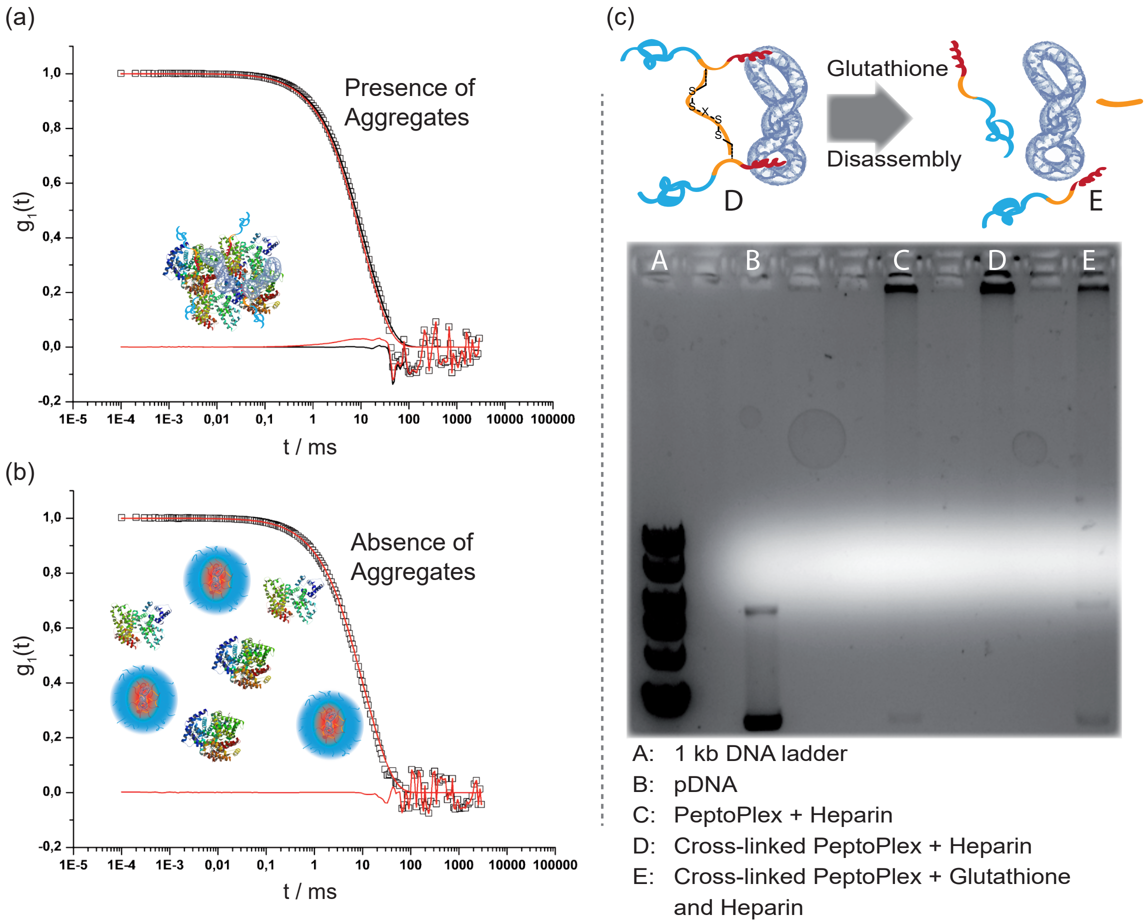

Figure 10.2: Comparison of non-cross-linked (**NCPX**) and cross-linked polyplexes **(CPX**). Characterization of polyplexes by dynamic light scattering in human serum (90% plasma pooled from 6 patients) and 10% PBS demonstrates that (a) non-cross-linked polyplexes form aggregates with plasma proteins as indicated by incongruence of the autocorrelation functions, which take (black) or do not take (red) aggregation into account, while (b) disulfide cross-linked polyplexes do not induce any changes to the aggregation state of serum proteins, (c) schematic depiction of disulfide cleavage and characterization of polyplex stability by gel electrophoresis.

For **NCPX**, the correlation function, which takes aggregation into account (black) and the one that does not (red) are not congruent underlining the formation of aggregates in the presence of human serum. In contrast, for **CPX** both correlation functions are identical. Therefore, it can be concluded that **NCPX** exhibit interaction with serum components and cause aggregate formation, while aggregation is absent for **CPX**.

Besides DLS in human serum, we compared both polyplexes in gel electrophoresis. The stability of cross-linked and non-cross-linked polyplexes in the presence of heparin was analyzed through pDNA staining with ethidium bromide. Due to its polyanionic properties, heparin can interfere with the electrostatic interaction between pDNA and PLys segments within polyplexes. Consequently, in case of **NCPX** incubation with heparin led to partial disintegration, observable by the presence of a free pDNA band in gel electrophoresis (line C). In case of **CPX** no free pDNA could be detected because the additional covalent stabilization prevents heparin-induced disintegration (line D). The reversible character of the disulfide stabilization was verified by treating **CPX** with glutathione (GSH, 10 mM) before addition of heparin, leading to disulfide bond cleavage. Indeed, GSH-treated **CPX** showed the same response to heparin as their non-cross-linked counterparts (line E).

Together with DLS measurements, the results of the heparin displacement assay prove that our cross-linking approach provides additional stabilization independent of electrostatic interactions. At the same time, **CPX** respond to elevated levels of GSH, which ensures that after disulfide cleavage by intracellular levels of GSH, pDNA can still be released at a comparable rate as in the case of **NCPX**.

Consequently, these results give experimental evidence that disulfide cross-linking can be a suitable way to enhance polyplex stability for *in vitro* and *in vivo* application, while intracellular release at GSH concentrations of 10 mM is preserved.

10.2.3 Preparation of Cross-linked Polyplexes Applying Endosomolytic Crosslinkers

To validate the concept, check the versatility and explore combinatorial aspects, we synthesized a small library of polyplexes based on pDNA (p1699), reactive triblock copolypept(o)ide and various bi- to tetradentate cross-linkers bearing terminal cysteines for disulfide formation. These cross-linkers are designed to incorporate endosomolytic sequence defined aminoethylene oligomers into the polyplexes.[461, 482, 483] Their secondary or tertiary amines provide pH buffering capacity as it is the case for prominent transfection agents like PEI[465] or PAMAM.[467] Some of the applied cross-linkers supplemented with a PEG block or without also have already been used as standalone transfection reagents by the group of Wagner.[461, 482–484]

The key step in the formation of **CPX** is the cross-linking reaction after polyplex formation, which stabilizes the polyplex and introduces the aforementioned endosomolytic moieties. The kinetics of the reaction, which is associated with the occurrence of 2-mercaptopyridine as cleavage product, was confirmed for all applied cross-linkers by measuring the absorbance of the thione form at 343 nm in UV-Vis spectroscopy (SI, Fig. 10.13). The cross-linking reaction can be conducted for polymer only as well as for polyplexes without side reactions with nucleobases or other functional groups along the nucleotide. The spectroscopic measurements prove that the pyridylthiol groups on the polymer side chain were readily cleaved and thus well accessible for all cross-linkers despite increasing steric hindrance in the polyplex. The used cross-linkers differ substantially in their architecture. We roughly classify them as low molecular weight (LMW) and high molecular weight (HMW) cross-linkers (Fig. 10.3). For LMW cross-linkers, <1 µg are necessary to saturate all PDP groups in 1 µg of polymer (100% cross-linking). In contrast, for HMW cross-linkers >1 µg are required for 100% cross-linking.

Owing to the diverse architecture, cross-linking protocols for LMW and HMW cross-linkers had to be optimized individually. For LMW cross-linkers, polyplex formation and cross-linking reaction were sharply separated: polyplexes were formed first at a N/P ratio of 4-8, after 30 minutes of incubation cross-linkers were added in a second step. This procedure could not be applied for HMW cross-linkers without increasing the hydrodynamic diameter of polyplexes (data not shown).

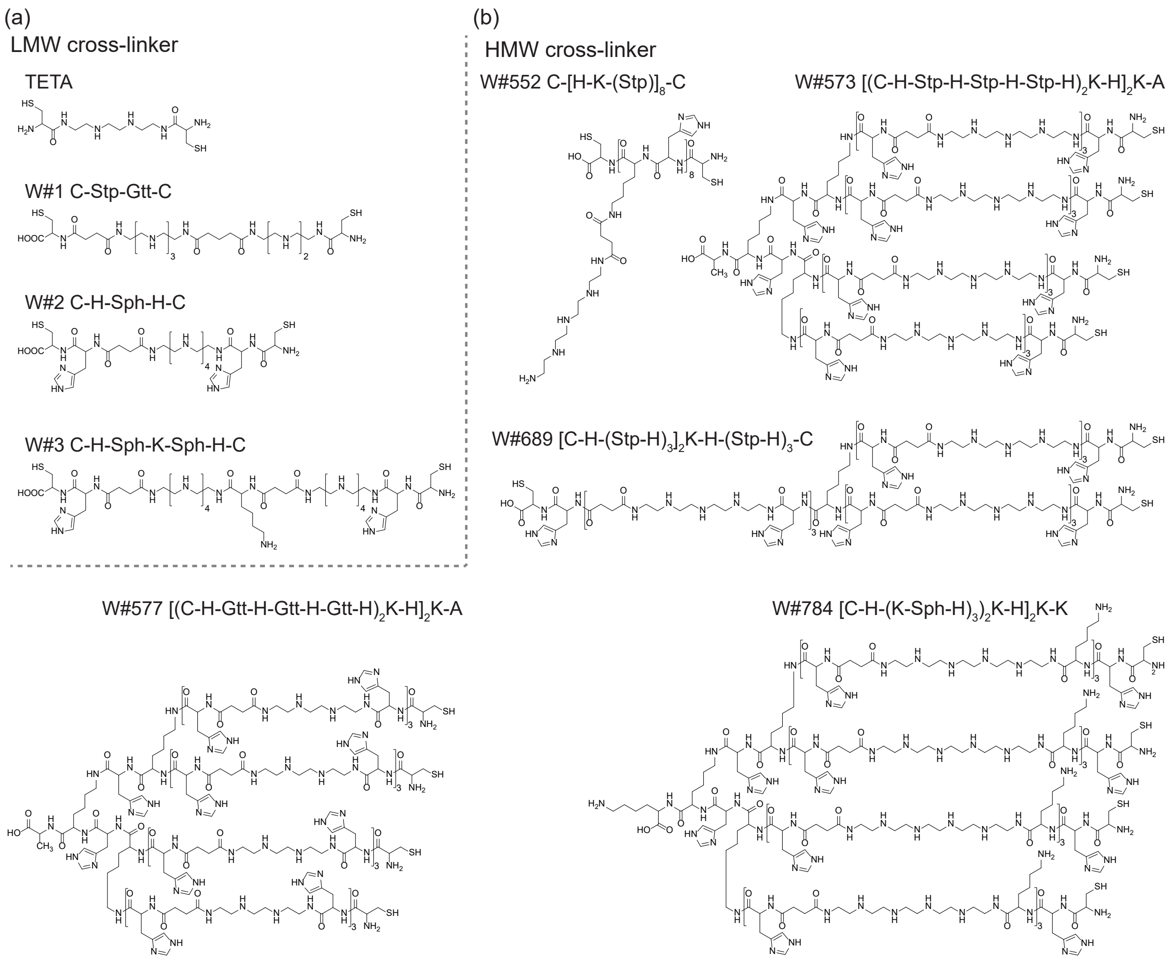

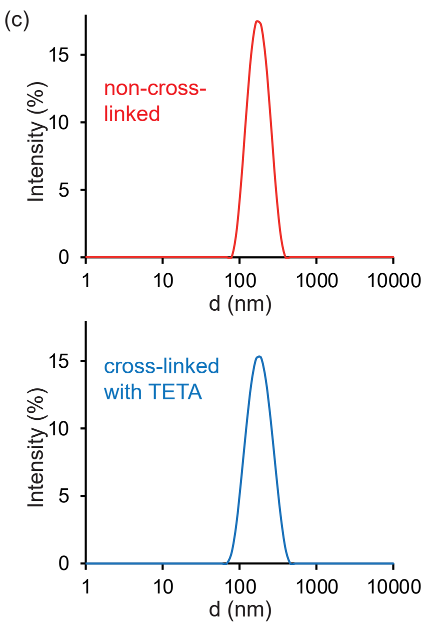

(d)

Cross-linker	N/P ratio (polypept(o)ide)	z-average (d.nm)	PDI
none	8	155.0	0.164
TETA	8	154.8	0.189
W#1	8	134.7	0.246
W#2	8	132.1	0.231
W#3	8	119.9	0.235
none	4	143.5	0.122
W#552	4	107.6	0.209
W#573	4	117.4	0.143
W#577	4	123.4	0.185
W#689	4	120.8	0.198
W#784	4	155.7	0.139

Figure 10.3: Overview on the different classes of cross-linkers. (a) low molecular weight (LMW) cross-linkers and (b) high molecular weight (HMW) cross-linkers, (c) representative dynamic light scattering (detection angle of 173°) characterization of polyplexes before and after cross-linking (TETA cross-linker), (d) average hydrodynamic radius distribution and polydispersity index of polyplexes employing the different classes of cross-linkers at fixed N/P ratios.

Most likely, this is due to their bigger size and steric hindrance interfering with the cross-linking reaction. To overcome this issue, the protocol for polyplex formation and cross-linking was altered. Since HMW cross-linkers are already of comparable size as the PLys segments of one polypept(o)ide chain and introduce many amines contributing to the final N/P ratio, polypept(o)ides were applied at a relatively low N/P ratio of 4 and degree of cross-linking was adjusted to 50%. Moreover, HMW cross-linkers and polypept(o)ides were added to pDNA exactly at the same time during vortexing, meaning that polyplex formation and cross-linking reaction were initiated simultaneously. In this way, hydrodynamic radii of cross-linked polyplexes could be reduced markedly. Interestingly, when applied for LMW cross-linkers, this protocol - i.e. simultaneous addition of polymer and cross-linker to pDNA - again led to an increase of the hydrodynamic diameter and poorly defined polyplexes (data not shown). A possible explanation is the small size and therefore insufficient DNA binding of LMW cross-linkers.

For LMW cross-linkers, hydrodynamic diameters of polyplexes decreased with increasing cross-linker size. At first glance, this observation seems contradictory as the cross-linking reaction with larger cross-linkers might be more and more impaired by steric hindrance. Yet, the larger cross-linkers (especially W#3) contain more cationic groups, which allow better association with the negatively charged pDNA inside the core of pre-formed polyplexes. Apparently, this leads to additional compaction of pDNA being reflected in smaller diameters. In contrast, for HMW cross-linkers hydrodynamic diameters increased from the smaller bidentate structure (W#552) to the larger 3-arm (W#689) or 4-arm (W#573, W#577, W#784) structures. In this case, as all HMW cross-linkers have enough cationic groups to associate efficiently with pDNA, steric hindrance might be the determining factor for size of cross-linked polyplexes, leading to the largest diameter for the largest cross-linker. Following this argumentation, W#552 can be regarded as good compromise between steric and DNA binding properties to get preferably small cross-linked polyplexes.

Eventually, results from light scattering show that final polyplex size can be fine-tuned by combination of the same polymer with different cross-linker architectures.

10.2.4 *In Vitro* Screening of Cross-linked Polyplexes for Transfection Efficiency

Following physicochemical characterization, the polyplex library was next evaluated for transfection efficiency and cytotoxicity in HEK 293T cells to find a lead compound. In general, compared to **NCPX**, **CPX** (cross-linked with TETA) showed a clear improvement of reporter gene expression in luciferase experiments (Fig. 10.4 (a)) as well as in flow cytometry (SI, Fig. 10.15). As can be deduced from luciferase data, it is indeed the cross-linking itself that enhances transfection efficiency. Simple addition of cross-linker to non-cross-linkable polyplexes (derived from PLys-b-PSar diblock copolypept(o)ides) has no beneficial effect. Flow cytometry analysis further shows that **CPX** (with TETA-cross-linker) are able to transfect the majority of the cell population with frequencies of eGFP positive cells coming close to those achieved by the commercial transfection reagent TransfeX^{TM} (71% and 86%). In terms of mean fluorescence intensity (MFI), **CPX** reach up to 57% of TransfeX level, which is remarkable for a core-shell polyplex with stealth-like corona.

At first glance, it might be surprising that transfection efficiency increases after cross-linking. Cross-linking of polyplexes, even if it is reversible, can lead to over-stabilization, impairing pDNA release and resulting in lower transfection levels, as was for example observed by Miyata *et al*.[233] Yet, because in our approach polymer charge density is exactly the same for **NCPX** and **CPX**, the higher transfection efficiency of the latter has to be a direct consequence of the cross-linking process and can be attributed to two synergistic effects:

I) As already suggested by the results of heparin displacement assay and DLS, cross-linked polyplexes feature increased stability but no over-stabilization. An adequate degree of stabilization is advantageous in preventing premature polyplexes dissociation and pDNA degradation - which might be an issue for **NCPX** - while allowing sufficient pDNA release in the intracellular environment.
II) The applied cross-linkers introduce endosomolytic properties (proton sponge effect/membrane interaction) to the polyplexes which gives them an advantage with respect to endosomal escape compared to **NCPX**.

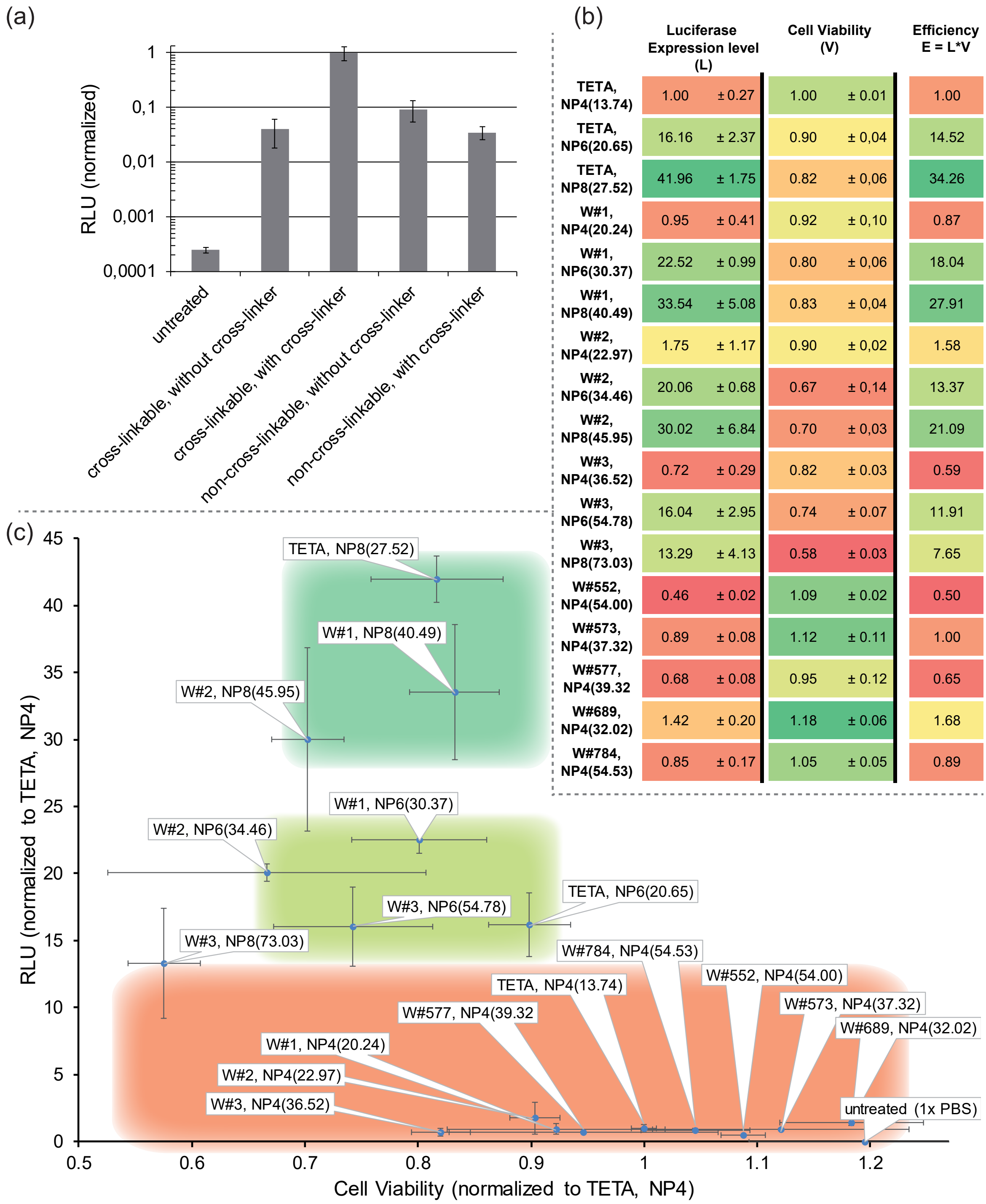

	Luciferase Expression level (L)		Cell Viability (V)		Efficiency E = L*V
TETA, NP4(13.74)	1.00	± 0.27	1.00	± 0.01	1.00
TETA, NP6(20.65)	16.16	± 2.37	0.90	± 0,04	14.52
TETA, NP8(27.52)	41.96	± 1.75	0.82	± 0,06	34.26
W#1, NP4(20.24)	0.95	± 0.41	0.92	± 0,10	0.87
W#1, NP6(30.37)	22.52	± 0.99	0.80	± 0,06	18.04
W#1, NP8(40.49)	33.54	± 5.08	0.83	± 0,04	27.91
W#2, NP4(22.97)	1.75	± 1.17	0.90	± 0,02	1.58
W#2, NP6(34.46)	20.06	± 0.68	0.67	± 0,14	13.37
W#2, NP8(45.95)	30.02	± 6.84	0.70	± 0,03	21.09
W#3, NP4(36.52)	0.72	± 0.29	0.82	± 0.03	0.59
W#3, NP6(54.78)	16.04	± 2.95	0.74	± 0.07	11.91
W#3, NP8(73.03)	13.29	± 4.13	0.58	± 0.03	7.65
W#552, NP4(54.00)	0.46	± 0.02	1.09	± 0.02	0.50
W#573, NP4(37.32)	0.89	± 0.08	1.12	± 0.11	1.00
W#577, NP4(39.32	0.68	± 0.08	0.95	± 0.12	0.65
W#689, NP4(32.02)	1.42	± 0.20	1.18	± 0.06	1.68
W#784, NP4(54.53)	0.85	± 0.17	1.05	± 0.05	0.89

Figure 10.4: *In vitro* screening of different cross-linkers and N/P ratios for transfection efficiency and cytotoxicity in HEK 293T cells. (a) comparison of transfection efficiency of **NCPX** (cross-linkable without cross-linker), **CPX** (cross-linkable with cross-linker), **NCPX** (non-cross-linkable without cross-linker) and **NCPX** (non-cross-linkable with free cross-linker), (b) efficiency level of **CPX** with different cross-linkers as product of relative transfection efficiency and cell viability (data depict the mean ± SED (n = 3) normalized to TETA N/P 4 sample, color code green to red), (c) relative transfection efficiency of different **CPX** plotted against associated cell viability.

As can be seen in Fig. 10.4 (b) and (c), of all tested cross-linkers TETA achieved the highest transfection rate, with the other LMW cross-linkers being in the same range. This leads to the conclusion that at least for LMW cross-linkers the stabilization of polyplexes and the introduction of endosomolytic groups per se is more important than cross-linker architecture. Moreover, a minimum N/P ratio of 6 with respect to the triblock copolypept(o)ide seems to be necessary to achieve significant luciferase expression levels. Compared to LMW cross-linkers, HMW cross-linkers turned out to be much less efficient. One may think, that simply higher N/P ratios with respect to the polypept(o)ide or a higher amount of cross-linker would be necessary to increase transfection efficiency. However, when considering final N/P ratios for **CPX** (shown in brackets in Fig. 10.4 (b) and (c)), taking the contribution from the polypept(o)ide as well as from the cross-linkers into account, it becomes apparent that LMW **CPX** and HMW **CPX** are in the same final N/P range. In other words, HMW and LMW cross-linker introduced a comparable amount of amines to the polyplexes, although the initial N/P ratios and degree of cross-linking differed. Consequently, other explanations for the different performance of LMW and HMW cross-linkers have to be taken into consideration, such as the steric hindrance during polyplex formation, which already has been suggested in the DLS experiments, as well as a lower relative endosomal buffer capacity. The HMW cross-linkers have been designed as standalone transfecting agents, containing both nucleic acid binding and endosomal buffering domains. In this work and the presented cross-linking approach, the PLys block provides sufficient nucleic acid binding properties already without cross-linker as determined by agarose gel electrophoresis. Therefore, introduction of maximal buffer capacity with the cross-linkers, such as in case of TETA, is beneficial for high transfection efficiency, whereas oligomers which also provide charge density for nucleic acid binding exhibit suboptimal balance of pK_a values for this particular purpose.

In addition to transfection efficiency, cytotoxicity is another crucial aspect for non-viral vectors. We therefore plotted relative luciferase expression level against relative cell viability and calculated the product to assess cross-linker efficiency (Fig. 10.4 (b) and (c)). Efficient cross-linkers (high transfection efficiency, low cytotoxicity) are depicted in dark green, with TETA showing the best compromise between both values.

Consequently, **TETA-CPX** was identified as lead candidate and thus chosen for further experiments. In summary, the proposed cross-linking strategy kept covalent stabilization and charge density in the right balance to affect transfection efficiency advantageously and was successfully combined with a screening approach to identify a lead polyplex system.

10.2.5 Detailed Characterization of the Lead Candidate

TETA-CPX was analyzed in more detail by multi angle DLS and cryo-TEM imaging. Polyplexes displayed a hydrodynamic radius of 85 nm and a minor angle dependency, indicating primarily spherical shape. Cryo-TEM images confirmed this observation. The transmission electron microscopy studies revealed an average diameter of around 150 nm. Furthermore, the images indicate the formation of core-shell polyplexes. The pDNA with its higher scattering contrast is surrounded by a shell of polymer with lower scattering density, which is presumably the PSar block (Fig. 10.5).

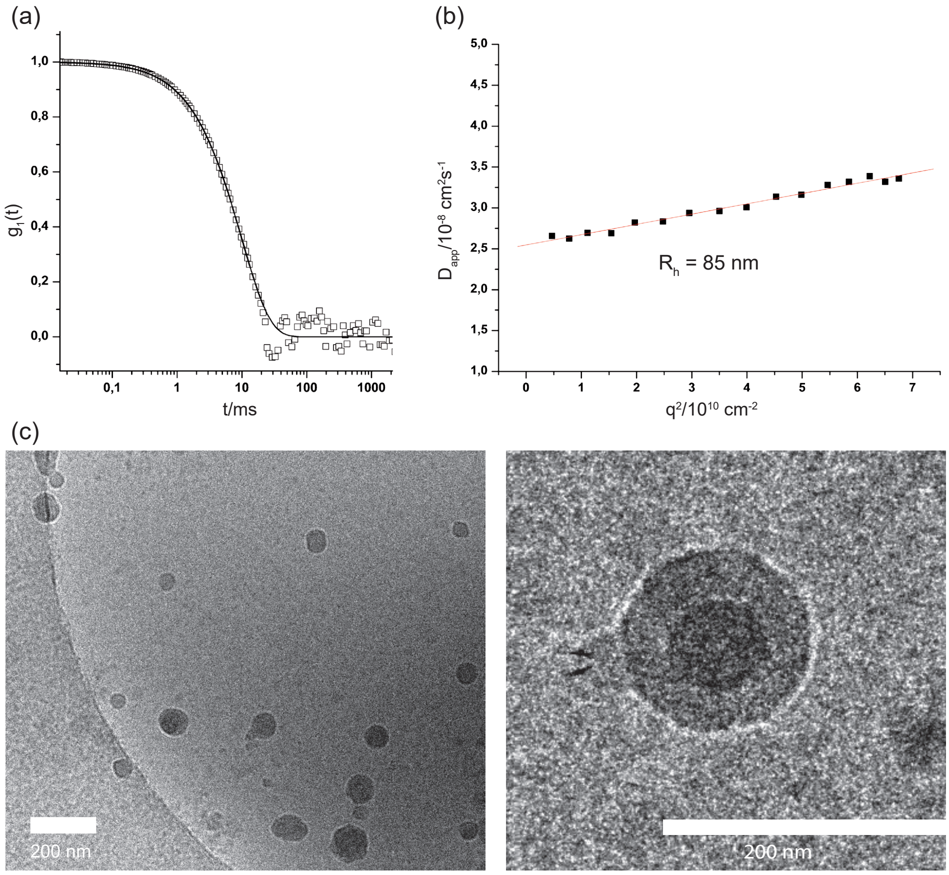

Figure 10.5: Detailed characterization of **TETA-CPX** in solution. Dynamic light scattering studies in PBS buffer: (a) autocorrelation function at 30°, (b) angle dependent scattering vector, (c) cryogenic TEM imaging at different magnifications visualizes polyplexes with core-shell structure (white bars correspond to 200 nm).

Because **TETA-CPX** performed best in the screening for transfection efficiency, exhibited a core-shell structure with a uniform size distribution and did not cause aggregation in blood serum, these polyplexes were subsequently applied as pDNA vaccine formulation for dendritic cell induced T cell stimulation.

10.2.6 Towards pDNA Vaccines

Dendritic cells (DCs) constitute professional antigen presenting cells with the ability to take up, process and present exogenous antigens to T cells.[485] Therefore, DCs are in the focus of the development of immunotherapeutic strategies.[486] In this regard, DNA-based vaccines possess several advantages when compared with conventional protein-based vaccines, including more efficient presentation of antigen via MHC I to induce cytotoxic $CD8^+$ T cells for direct killing of tumor and virus-infected cells,[487] and the possibility to limit vaccine expression to DCs by usage of DC-specific gene promotors as previously shown by Bros and coworkers.[1]

To assess the suitability of **TETA-CPX** to serve as a carrier for a DNA vaccine, we first used confocal microscopy to verify uptake by DCs. Fig. 10.6 (a) clearly shows intracellular localization of **TETA-CPX** containing Cy5-labeled pDNA, thus confirming that DCs as a target can be reached by cross-linked polyplexes.

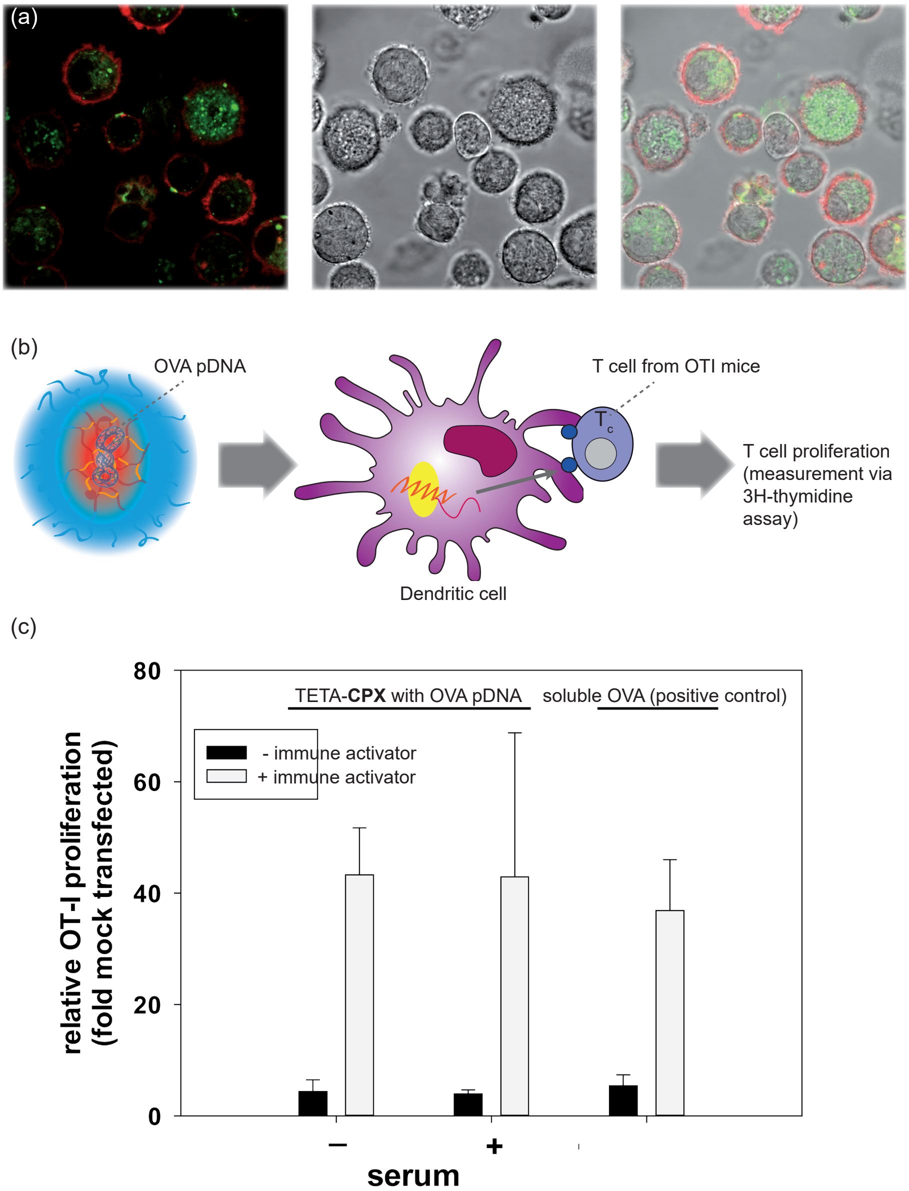

Figure 10.6: Vaccination experiments with **TETA-CPX**. (a) Confocal microscopy images of cross-linked polyplexes containing Cy5-labeled pDNA showing intracellular localization in DCs after 4 h of incubation, left: fluorescence channels, middle: transmitted light channel and right: merged (red = CD11c staining, green = Cy5-labeled pDNA), (b) schematic depiction of proliferation experiments, (c) OT-I T cell proliferation after DC TC co-culture with transfected DC2.4 cells, DC 2.4 were either transfected with 300 ng OVA encoding plasmid DNA using **TETA-CPX** or loaded with 1 mg/ml soluble OVA protein, cells were either stimulated with 100 ng/ml immune activator LPS or left untreated, prior to transfection, polyplexes were partially incubated with native mouse serum 1:1 (v/v) (data show mean ± SED (n = 3)).

Next, DCs were transfected with a model antigen-encoding pDNA, and subsequently used to stimulate antigen-specific T cells (Fig. 10.6 (b)). Namely, DCs (DC2.4 cells) were transfected with ovalbumin (OVA)-encoding pDNA by means of **TETA-CPX** and co-cultured with OVA peptide-responsive $CD8^{+}$ T cells derived from OT-I mice.[488] After 4 days of co-culture, T cell proliferation was analyzed by incorporation of tritium marked thymidine.

DCs loaded with soluble OVA protein were used as control. Fig. 10.6 (c) shows that DC2.4 cells transfected with OVA-encoding pDNA but left unstimulated induced only poor T cell stimulation. This result is in accordance with the general observation that immature DCs rather induce antigen-specific T cell tolerance due to low expression of co-stimulatory molecules.[489] This result indicates that the **TETA-CPX** polyplexes themselves do not exert strong immune-stimulatory effects as, in contrast, reported for other types of gene delivery systems or nano-carriers.[490] Stimulation of transfected DCs with LPS prior to the onset of their co-culture with OT-I T cells yielded strong T cell proliferation. Again this result is in line with the finding that DCs activated for example by TLR ligands up-regulate costimulatory molecules, proinflammatory mediators, and hence induce strong T cell proliferation.[491] In agreement, LPS stimulated DCs that were transfected with OVA encoding pDNA showed 42-fold increase in $CD8^+$ T cell proliferation as compared to mock transfected cells. The extent of $CD8^+$ T cell proliferation induced by pDNA-transfected DCs was at similar level as evoked by DCs loaded with OVA protein.

A crucial aspect of using polyplexes for DNA transfection is their potential use *in vivo*.[492] To assess the compatibility of polyplexes for *in vivo* applications on a functional level, we monitored the transfection efficiency of **TETA-CPX** after exposure to native mouse serum that may interact with the pDNA/polyplex and thereby affect its functional properties as described for other nanoparticles.[493] Therefore, **TETA-CPX** formed with OVA-encoding pDNA were incubated with native mouse serum for 30 minutes at 37 °C at a 1:1 (v:v)-ratio prior to transfection. Apparently, pre-incubation of pDNA/polyplexes with native mouse serum did not influence their transfection efficiency and DCs were still able to induce T cell proliferation (Fig. 10.6 (c)). These findings relate back to the stability of polyplexes in 90% serum as demonstrated by dynamic light scattering experiments before.

Proliferation experiments show that **TETA-CPX** may be a suitable vector for pDNA vaccination for several reasons: I) They are not cytotoxic for DCs at effective concentrations (SI, Fig. 10.16). II) They mediate efficient pDNA transfection. III) They do not bear unspecific immune-modulatory activity allowing control of the level of immune activation. IV) Incubation with native serum has no effect on transfection efficiency. Eventually, **TETA-CPX** seems to be a first step in the development of systemically applicable pDNA vaccines.

10.3 CONCLUSION

In this work we presented a novel synthetic concept, in which disulfide stabilized polyplexes are prepared by a robust, scalable synthetic pathway. The proposed approach utilizes reactive triblock copolypept(o)ides, which can complex pDNA, and endosomolytic cross-linkers to form disulfide cross-linkable polyplexes. The approach moreover allows the fast generation of polyplex libraries based on the combination of one polymer with multiple cross-linkers. The bifunctional cross-linkers do not only provide bioreversible covalent stabilization but also introduce endosomolytic groups to the polyplexes, which are released after cellular uptake. Cross-linked polyplexes show superior stability and transfection efficiency compared to non-cross-linked analogs. Via a screening strategy we were able to identify a lead compound, **TETA-CPX**, which proved successful in the transfection of dendritic cells with a model pDNA vaccine and retained its functionality even in the presence of serum proteins. It therefore depicts a promising candidate for *in vivo* DNA vaccination, which underlines the potential of the presented approach.

10.4 EXPERIMENTAL SECTION

10.4.1 Materials

DMF was purchased from Acros (99.8%, Extra Dry over Molecular Sieve) dried over BaO and distilled *in vacuo* followed by excessive stirring *in vacuo* to remove traces of dimethylamine. THF and *n*-hexane were purchased from Sigma-Aldrich and distilled from sodium. Triethylamine was purchased from Carl Roth and distilled from potassium hydroxide Other solvents were used as received. Diphosgene and chlorotrimethylsilane were purchased from Alfa Aesar and used as provided. Neopentylamine was purchased from TCI Europe, dried over NaOH and fractionally distilled. Sarcosine was purchased from Sigma-Aldrich, all other amino acids were purchased from ORPEGEN. Succinimidyl 3-(2-pyridyldithio)propionate (SPDP) was purchased from ThermoFisher Scientific.

10.4.2 Instrumentation

10.4.2.1 *Polymer Characterization*

400 MHz ^{1}H-NMR spectra and ^{19}F NMR spectra were recorded on a Bruker Avance II 400. HSQC and DOSY NMR measurements were performed on a Bruker Avance III HD 400. All spectra were recorded at room temperature and analyzed with MestReNova software. Degrees of polymerization as well as molecular weights were calculated by comparing the integral of the neopentylamine initiator peak either with the integrals of the side chain amide protons (for PLys(Boc) and PLys(TFA)) or with the average of integrals of methyl group and α-protons (for PSar) in the 400 MHz ^{1}H-NMR spectra.

Attenuated total reflectance Fourier transformed infrared (ATR-FTIR) spectroscopy was performed on a FT/IR-4100 (JASCO Corporation) with an ATR sampling accessory (MIRacleTM, Pike Technologies). IR Spectra were analyzed using Spectra Manager 2.0 (JASCO Corporation).

Melting points were determined using a METTLER FP62 (METTLER WAAGEN GMBH).

Hexafluoroisopropanol (HFIP) gel permeation chromatography (GPC) was performed with HFIP containing 3 g/L potassium trifluoroacetate as eluent at 40 °C and a flow rate of 0.8 mL/min. The columns were packed with modified silica (PFG columns; particle size: 7 mm, porosity: 100 and 1000 Å). Polymer was detected with a refractive index detector (G 1362A RID, JASCO) and a UV/Vis Detector (UV-2075 Plus, JASCO). Molecular weights were calculated using a calibration performed with PMMA standards (Polymer Standards Services GmbH) and toluene as internal standard. Elution diagrams were analyzed using WinGPC UniChrome 8.00 (Build 994) software from Polymer Standards Services.

10.4.2.2 *Biological Experiments*

(3-(4,5-Dimethylthiazol-2-yl)-2,5-diphenyltetrazolium bromide (MTT) assay measurements were performed using a Dynex MRX TC Revelation microtiter plate reader (Dynex Technologies, Chantilly, VA).

Luciferase assay was carried out with a 96 well plate chemoluminescence reader (Centro LB 960; Berthold Technologies, Bad Wildbad, Germany) using Mikrowin 2000 software.

FACS experiments were executed on a FACS Canto II flow cytometer equipped with BD FACS Diva software (both from BD Biosciences, San Diego, CA). Data were analyzed using FlowJo software (FLOWJO, Ashland, OR).

Live cell images were acquired on an inverted confocal microscope TCS SP5 (Leica, Wetzlar, Germany) equiped with an oil-immersion objective (63 magnification; NA 1.4) and a laser set capable of 405 nm/488 nm/561 nm excitation. Images were recorded at 512 x 512 8-bit-pixel resolution with a pinhole of 130 μm and confocal plane depth of 1.0 μm, resulting in a total image size width and height of 246 μm.

10.4.3 Methods and Protocols - Preparation of PeptoPlexes

10.4.3.1 *Synthesis of N-ε-tert-butyloxycarbonyl-L-Lysine N-Carboxyanhydride*

9.8 g (39.8mmol) of *N*-ε-Boc-protected lysine were weighed into a three-neck flask and dried under vacuum for 1 h. The solid was suspended in 300 mL of absolute THF under a steady flow of dry nitrogen. Afterwards, 9.9 ml (79.6 mmol) of absolute trimethylsilylchloride and 11.0 ml (79.6 mmol) of absolute triethylamine were added slowly via syringe. The suspension was stirred for 2 h followed by addition of 4.8 ml (39.8 mmol) of diphosgene, again via syringe. The suspension was mildly refluxed for another 2 h. Overnight, a steady flow of dry nitrogen was lead through the solution into two gas washing bottles filled with aqueous NaOH solution removing TMSCl. The suspension was filtered under dry nitrogen atmosphere to remove the salts of TEA and unconverted amino acid. The filtrate was evaporated under reduced pressure. Subsequently, absolute THF was added to completely dissolve the crude reaction product. The solution was precipitated with absolute hexane and stored at 4 °C for 1 h. The solid was collected by filtration under dry nitrogen atmosphere and washed with hexane. The crude reaction product was then recrystallized twice with absolute THF/hexane. 6.52 g of purified reaction product (23.9 mmol; 68% yield; colorless needles) were transferred into a Schlenk tube and stored at -80 °C. Melting point: 138.3 °C (Lit. 134 - 137° C).[432, 435]
^{1}H-NMR (400 MHz, DMSO-d$_6$): δ [ppm] = 9.07 (1H, s, -**NH**-CO-O-CO-), 6.95-6.34 (1H, br, -**NH**-CO-O-C(CH$_3$)$_3$), 4.42 (1H, t, ^{3}J $_{H,H}$ = 6.35 Hz, -CO-**CH**-CH2-), 2.90 (2H, q, ^{3}J $_{H,H}$ = 6.03 Hz, -**CH$_2$**-NH-CO-O-C(CH$_3$)$_3$), 1.79-1.56 (2H, m, -CH-**CH$_2$**-CH$_2$-CH$_2$-CH$_2$-NH-), 1.45-1.12 (13 H, m, -CH-CH$_2$-**CH$_2$-CH$_2$**-CH$_2$-NH- and -NH-CO-O-C(**CH$_3$**)$_3$).

10.4.3.2 *Synthesis of N-ε-Trifluoroacetyl-L-Lysine N-Carboxyanhydride*

12.5 g (51.6 mmol) of *N*-ε-trifluoroacetyl protected lysine and 300 mL of absolute THF were added into a three necked flask equipped with a reflux condenser and a septum under a steady flow of dry nitrogen. The condenser outlet was connected to two gas washing bottles filled with aqueous NaOH, removing excess HCl and phosgene. Then, 5.50 mL (45.6 mmol) of diphosgene were added slowly via syringe and the nitrogen stream was reduced. The colorless suspension was mildly refluxed for 2 h, yielding a cloudy solution. After this, a steady flow of dry nitrogen was lead through the solution overnight. The solution was filtered under dry nitrogen atmosphere. The solvent was evaporated under reduced pressure and absolute THF was added to completely dissolve the crude reaction product. Excess absolute hexane was added to the solution. After 1 h storage at 4 °C, the solid was collected by filtration under dry nitrogen atmosphere and washed with hexane. The crude product was recrystallized twice with absolute THF/Hexane. 10.43 g of the purified product (39,0 mmol; 75% yield; colorless needles, melting point: 101 °C (lit: 92 - 93 °C)[376]) were obtained and stored in a Schlenk tube at -80 °C.
^{1}H-NMR (300 MHz, DMSO-d$_6$): δ [ppm] = 9.40 (1H, s, -**NH**-CO-CF$_3$), 9.09 (1H, s, -**NH**-CO-O-CO-), 4.43 (1H, t, ^{3}J H,H = 6.3 Hz, -CO-**CH**-CH$_2$-), 3.17 (2H, q, ^{3}J H,H = 6.3 Hz, -**CH$_2$**-NH-), 1.79-1.61 (2H, m, -C$_H$-**CH$_2$**-CH$_2$-CH$_2$-CH$_2$-NH-), 1.53-1.46 (2H, quin, ^{3}J $_{H,H}$ = 7.13 Hz, -CH-CH$_2$-CH$_2$-**CH2**-CH$_2$-NH-), 1.42-1.24 (2H, m, -CH-CH$_2$-**CH$_2$**-CH$_2$-CH$_2$-NH-).

10.4.3.3 *Synthesis of Sarcosine N-Carboxyanhydride*

The Synthesis of sarcosine NCA was adapted from literature and modified.[121] 14.92 g (167.4 mmol) of sarcosine were weighed into a three neck flask and dried in vacuo for 1 h. 300 mL of absolute THF were added under a steady flow of dry nitrogen and 16.2 mL (134 mmol) of diphosgene were added slowly via syringe and the nitrogen stream was reduced. The colorless suspension was mildly refluxed for 3 h yielding a clear solution. Overnight, a steady flow of dry nitrogen was lead through the solution into two gas washing bottles filled with aqueous NaOH solution. The solvent was evaporated under reduced pressure, yielding a brownish oil as crude reaction product. The oil was heated to 50 °C and dried under reduced pressure (20 mbar, then $<10^{-2}$ mbar for 2 h) to obtain an amorphous solid, free of phosgene and HCl. The crude product was redissolved in 40 mL of absoute THF and precipitated with 300 mL of dry hexane. The solution was cooled to -18 °C overnight to complete precipitation. The solid was filtered under dry nitrogen atmosphere and dried under a stream of dry nitrogen for 60 - 90 minutes and afterwards in high vacuum for 2 h in a sublimation apparatus. The crude product was sublimated at 80 - 85 °C and $<1\text{x}10^{-2}$ mbar. The product was collected from the sublimation apparatus in a glove box on the same day. The 12.64 g of purified product (110 mmol, 65% yield, colorless crystallites) were stored in a Schlenk tube at -80 °C, only handled in a glove box and used up quickly. Melting point: 102 - 104 °C (lit: 102 - 105 °C).[15, 368]
^{1}H-NMR (300 MHz, $CDCl_3$): δ [ppm] = 4.22 (2H, s, –N(CH_3)-**CH_2**-CO-), 2.86 (3H, s, -CH_3).

10.4.3.4 *Synthesis of Triblock Copolymers*

Triblock copolypept(o)ides were prepared as reported earlier.[158] Under a steady flow of dry nitrogen, 35 eq of lysine(Boc) NCA were transferred into a pre-dried Schlenk tube equipped with a stir bar and dried under high vacuum for 1 h. Then, lysine(Boc) NCA was dissolved in absolute DMF. In a glass vial flooded with nitrogen, 2 eq of neopentylamine were added to 2 mL of dry DMF and mixed. For polymerization initiation, 1 mL of the prepared stock solution was directly added to the Schlenk tube via syringe (yielding a reaction solution with 100 mg/mL monomer concentration). The solution was stirred at 0 °C and kept at a constant pressure of 1.25 bar of dry nitrogen via the Schlenk line to prevent impurities from entering the reaction vessel while allowing CO_2 to escape. Completion of the reaction was confirmed by IR spectroscopy (disappearance of the NCA peaks (1853 and 1786 cm^{-1})). After completion of the reaction, 35 eq of lysine(TFA) NCA were dissolved in absolute DMF (at a concentration of 100 mg/mL) and added to the homopolymer via syringe. The solution was stirred at 0 °C and kept at a constant pressure of 1.25 bar of dry nitrogen via the Schlenk line. After completion of the reaction (IR spectroscopy), 350 eq sarcosine NCA were dissolved in absolute DMF (at a concentration of 100 mg/mL) and added to the diblock copolymer via syringe. Again, the solution was stirred at 0 °C and kept at a constant pressure of 1.25 bar of dry nitrogen via the Schlenk line. Completion of the reaction was confirmed by IR spectroscopy. The final triblock copolymer was precipitated in ether and centrifuged (4500 rpm at 4 °C for 15 min). After discarding the liquid fraction, fresh ether was added and the polymer was resuspended using a sonic bath. The suspension was centrifuged again and the procedure was repeated. After DMF was removed by the resuspension steps, the polymer was dissolved in 20% methanol/Millipore water and lyophilized to obtain a fluffy, colorless powder.
^{1}H-NMR of PLys(Boc)$_{35}$-b-PLys(TFA)$_{41}$-PSar$_{367}$ (400 MHz, DMSO-d_6): δ [ppm] = 9.47-9.22 (41H (1n), br, -N_εH-CO-CF_3), 8.36-8.03 (br, -CO-$C_\alpha H_2$-**NH**-), 7.01-6.14 (35H (1m), br, -**N_εH**-CO-O-C(CH_3)$_3$), 4.68-3.57 (804H (1n + 1m + 2p), br, -CO-**CH**-NH- and -NCH_3-**CH_2**-CO-), 3.18-2.60 (1262H (2n + 2m + 3p), br, -**CH_2**-N_εH-CO-CF_3 and -**CH_2**-NεH-CO-O-C(CH_3)$_3$ and

-NCH_3-), 2.07-0.96 (712H (6(n + m) + 9m), br, -CH-$\mathbf{CH_2}$-$\mathbf{CH_2}$-$\mathbf{CH_2}$-CH_2-N_εH- and -NH-CO-O-C($\mathbf{CH_3}$)$_3$), 0.84 (9H, br, -CH2-C($\mathbf{CH_3}$)$_3$).

10.4.3.5 *Deprotection of the PLys(TFA) Block*

In a round-bottom flask, the polymer was dissolved in MeOH at a concentration of 30-50 mg/mL and 20 eq of hydrazine hydrate (with regard to the (TFA)-group) were added with an Eppendorf pipette. The solution was stirred for 72 h. Afterwards, the solution was diluted with Millipore water and dialyzed with a Spectra/Por (Roth) membrane with a nominal molecular weight cut-off (NMWCO) of 3500 g/mol for 3-5 days with regular substitution of water and then lyophilized to yield the deprotected polymer as a fluffy, colorless powder.
^{1}H-NMR of PLys(Boc)$_{35}$-b-PLys$_{41}$-PSar$_{367}$ (400 MHz, DMSO-d$_6$): δ [ppm] = 8.88-7.59 (br, -CO-$C_\alpha H_2$-**NH**-), 6.92-6.23 (33H (1m), br, -$\mathbf{N_\varepsilon H}$-CO-O-C(CH_3)$_3$), 4.87-3.65 (808H (1n + 1m + 2p), br, -CO-**CH**-NH- and -NCH_3-$\mathbf{CH_2}$-CO-), 3.09-2.63 (1191H (2n + 2m + 3p), br, -$\mathbf{CH_2}$-$N_\varepsilon H_2$ and -$\mathbf{CH_2}$-N_εH-CO-O-C(CH_3)$_3$ and -NCH_3-), 2.12-0.93 (574H (6(n + m) + 9m), br, -CH-$\mathbf{CH_2}$-$\mathbf{CH_2}$-$\mathbf{CH_2}$-CH_2-N_εH- and -NH-CO-O-C($\mathbf{CH_3}$)$_3$), 0.84 (9H, br,-CH2-C($\mathbf{CH_3}$)$_3$).

10.4.3.6 *Modification with SPDP and Deprotection of the PLys(Boc) Block*

35.6 mg of polymer and 12.4 mg of SPDP (1.25 eq with respect to ε-NH_2 groups) were weighed into a round-bottom flask and immediately dried under high vacuum for 30 minutes. Subsequently, the flask was flushed with argon and the solids dissolved in 1mL of absolute DMF. The solution was stirred at room temperature for 72 h. Afterwards, the polymer was precipitated in ether and centrifuged. The remaining pellet was in dissolved in 50% TFA/H_2O to remove the Boc protecting groups. The solution was stirred for 18 h at room temperature, diluted with Millipore water and dialyzed with a Spectra/Por (Roth) membrane with a nominal molecular weight cut-off (NMWCO) of 3500 g/mol for three days with regular substitution of water (containing 10^{-4} vol% acetic acid). Eventually, the solution was lyophilized to yield the functionalized polymer as a fluffy, colorless powder.
^{1}H-NMR of PLys$_{35}$-b-PLys(PDP)$_{41}$-PSar$_{367}$ (400 MHz, DMSO-d$_6$): δ [ppm] = 8.51-8.32 (36H (1q), br, -N=**CH**-CH=), 8.31-7.88 (br, -CO-$C_\alpha H_2$-**NH**- and -$\mathbf{N_\varepsilon H}$-CO-CH_2-CH_2-S-S-), 7.87-7.59 (75H (2q), br, -S-S-C=**CH-CH**=), 7.34-7.02 (35H (1q), br, -N=CH-**CH**=), 4.84-3.21 ((1n + 1m + 2p), br, -CO-**CH**-NH- and –NCH_3-$\mathbf{CH_2}$-CO- and H_2O), 3.21-2.59 (1141H (2n + 2m + 3p + 4q), br, -$\mathbf{CH_2}$-N_εH-CO-$\mathbf{CH_2}$-$\mathbf{CH_2}$-S-S- and -$\mathbf{CH_2}$-$N_\varepsilon H_2$ and -NCH_3-), 2.22-0.92 (218H (6(n + m)), br, -CH-$\mathbf{CH_2}$-$\mathbf{CH_2}$-$\mathbf{CH_2}$-CH_2-N_εH-), 0.83 (9H, br, -CH_2-C($\mathbf{CH_3}$)$_3$).

10.4.3.7 *Synthesis of W-crosslinkers*

W-crosslinkers (W#1-#3, W#552, W#689, W#573, W#577, W#784) were synthesized using Fmoc-α-amino acids (Iris Biotech, Marktredwitz, Germany) and Fmoc-oligoamino acids (Fmoc-Gtt(Boc$_2$)-OH, Fmoc-Stp(Boc$_3$)-OH, Fmoc-Sph(Boc$_4$)-OH, in house synthesis[494, 495] for conventional Fmoc solid phase peptide synthesis, analog to previously described procedures.[482–484] The general procedure is as follows. Syntheses were conducted in syringe microreactors (Multisyntech, Witten, Germany) using 2-chlorotrityl resins preloaded with the C-terminal amino acid of the peptide sequences as solid support. Coupling steps were carried out using 4 eq Fmoc-α-amino acid or Fmoc-oligoamino acid, 4 eq 1-hydroxybenzotriazole (Sigma-Aldrich, Munich, Germany), 4 eq benzotriazol-1-yloxy-tripyrrolidinophosphonium hexafluorophosphate (Multisyntech, Witten, Germany), 8 eq *N,N*-diisopropylethylamine (Iris Biotech, Marktredwitz, Germany) and a mixture of *N,N*-dimethylformamide (DMF) / dichloromethane (DCM) 1:1 (v/v, 10 mL/g resin) as solvent. Coupling times were 60 minutes at room temperature (W#1-#3, W#689, W#573, W#577) or 12 minutes at 50 °C (W#552, W#784) using a Biotage Syro Wave microwave cavity (Biotage AB, Uppsala, Sweden). Deprotection steps were carried out by 4 times incubation with 20 % piperidine in DMF (v/v, 10 mL/g resin) for 10 minutes at room temperature. After each coupling and deprotection step, the resin was washed 3 times with DMF and 3 times with DCM (10 mL/g resin) followed by a Kaiser test to detect free amino groups.[496] In case of an unexpected result (positive after coupling, negative after deprotection), the last coupling or deprotection step respectively, was repeated. Final cleavage was carried out by incubation with a mixture of trifluoroacetic acid / triisopropylsilane / water 95:2.5:2.5 (v/v/v, 10 mL/g resin) for 90 minutes at room temperature. The cleavage solution was concentrated under a nitrogen stream and the oligomer precipitated by dropping into 50 mL of a precooled mixture of methyl tert-butyl ether/n-hexane 1:1 (v/v). After centrifugation, the supernatant was discarded and the product pellet was dissolved and purified by size exclusion chromatography using a ÄKTApurifier 10 system (GE Healthcare Bio-Sciences AB, Uppsala, Sweden), a Sephadex G10 column. Pooled fractions were snap-frozen and freeze-dried.

10.4.3.8 *Formation of PeptoPlexes*

The SPDP-modified polymer was dissolved in sterile water (with 0.2 vol% acetic acid) to obtain a stock solution with a final concentration of 2 mg/mL. Cross-linkers were dissolved in sterile water (with 0.2 vol% acetic acid) at a concentration of 10-20 mg/mL.Non-cross-linked polyplexes were prepared by diluting the desired amount of plasmid DNA in sterile water, adding polymer as needed and vortexing for 10 seconds. The obtained polyplex solutions were incubated for 30 minutes at room temperature. In case of LMW cross-linking, the desired amount of cross-linker and 10x PBS were added to preformed polyplexes at the same time while vortexing to obtain final solutions of cross-linked polyplexes in 1x PBS. In case of HMW cross-linking, the desired amount of polymer and cross-linker were added to the pDNA at the same time while vortexing, followed by addition of 10x PBS after 30 minutes of incubation at room temperature. The cross-linking reaction was carried out for another 18 h under constant shaking at room temperature. Final concentration of polyplex solutions with respect to pDNA was kept at 0.03-0.05 mg/ml.

Polyplex solutions of TransfeX^{TM} (ATCC, Manassas, Virginia, USA) and plasmid DNA were prepared according to manufacturer's protocol using 3 µl of stock solution per 1 µg of DNA.

10.4.4 Methods and Protocols - Physicochemical Characterization of PeptoPlexes

10.4.4.1 *Characterization of PeptoPlexes by Gel Electrophoresis*

Gel electrophoresis was performed to monitor polyplex formation and stability. For this, 100 ng of pDNA and the desired amount of polymer were premixed at N/P 8 and cross-linked as indicated above. Incubation with 10 mM glutathione was performed for 2 h at 37 °C while shaking. Incubation with 2 mg/mL heparin was performed for 1 h at 37 °C while shaking. Samples were loaded into slots of 0.8% agarose gels and electrophoresis was run at 90 mV. Ethidium bromide was used for plasmid DNA and polyplex staining.

10.4.4.2 *Characterization of PeptoPlexes by Dynamic Light Scattering*

Single-angle dynamic light scattering measurements were performed at 25 °C using a Malvern Zetasizer NanoZS with a 633 nm He/Ne Laser at a fixed scattering angle of 173°. Polyplex solutions were prepared with 2 µg pDNA at varying N/P ratios and varying cross-linkers and diluted to a final volume of 300 µl in 1x PBS before measurement.

For multi-angle DLS and serum DLS, solutions of TETA cross-linked and non-cross-linked polyplexes with 5 µg pDNA at N/P 6 were prepared and subsequently diluted to a final volume of 1.5 mL in 1x PBS. Cylindrical quartz cuvettes (Hellma, Mühlheim, Germany) were cleaned by dust-free distilled acetone and transferred into a dust-free flow box. Polyplex solutions were filtered into these cuvettes through Millex GHP filters, 0.45 µm poresize (Millipore). Then, dynamic light scattering (DLS) measurements were performed on a HeNe Laser (25 mW output power at = 632.8 nm) and on an ALV-CGS 8F SLS/DLS 5022F goniometer with eight simultaneously working ALV 7004 correlators and eight QEAPD avalanche photodiode detectors. The correlation functions of the particles were fitted using a sum of two exponentials from which the initial slope, i.e. the first cumulant Γ, was calculated. The z-average diffusion coefficient D_z was calculated by extrapolating Γ/q^2 for $q = 0$. By formal application of Stokes law, the inverse z-average hydrodynamic radius is $R_h = \langle 1/R_h \rangle_{z^{-1}}$.

To investigate the aggregation behavior of **NCPX** and **TETA-CPX** in human plasma, EDTA-plasma pooled from 6 donors was used. The following mixtures were prepared:

1. plasma: PBS 9:1
2. PBS: **NCPX** solution (c = 0.008 mg/mL) 9:1
3. plasma: **NCPX** solution (c = 0.008 mg/mL) 9:1
4. PBS: **TETA-CPX** solution (c = 0.011 mg/mL) 9:1
5. plasma: **TETA-CPX** solution (c = 0.011 mg/mL) 9:1

The plasma was filtered through a Millex GS 0.22 µm filter and PBS was filtered through a Pall GHP 0.2 m filter. The cuvettes were incubated for 20 min at room temperature before measurement.

If there is no aggregate formation, the determined autocorrelation function of solutions 3 and 5 ($g_1(t)_{mix}$) should be well-fitted by the weighted sum of the fit functions of the autocorrelation functions of the two single components (equation 10.1). In order to fit the plasma autocorrelation function (ACF) three exponentials are needed, reflecting the large size differences of the plasma proteins, whereas for **NCPX** and **CPX** a sum of two exponentials are needed.

$$g_1(t)_{mix} = a_P \cdot g_1(t)_P + a_S \cdot g_1(t)_s \tag{10.1}$$

$g_1(t)_P$ = fit function that describes the measured ACF of the particles in buffer
$g_1(t)_S$ = fit function that describes the measured ACF of the plasma in buffer
a_i = amplitudes

The only variable fit parameters of the correlation function fit of the mixture are the amplitudes a_i whereas all other parameters were kept constant to the values obtained by the fit of the ACF of plasma and particles, respectively. In the case of aggregate formation, a third fit function ($g_1(t)_a$) needs to be added to adequately fit the autocorrelation function of the mixture equation 10.2.

$$g_1(t)_{mix} = a_P \cdot g_1(t)_P + a_S \cdot g_1(t)_s + a_A \cdot g_1(t)_A \tag{10.2}$$

10.4.4.3 *Characterization of PeptoPlexes by Cryogenic Transmission Electron Microscopy*

5 µL of polyplex solution (prepared with 0.5 µg pDNA at N/P 6, TETA-cross-linked) were applied to freshly glow-discharged carbon grids with a copper 200 mesh (Quantfoil Micro

Tools GmbH). Excess fluid was removed by direct blotting (2.5 s) and the grids were individually plunge-frozen in liquid ethane. Grids were cryotransferred in liquid nitrogen using a Gatan cryoholder (model 626 DH) to a Technai T12 transmission electron microscope equipped with a field emission electron source and operating at 120 kV accelerating voltage. Images were recorded using a TemCam-F416 (TVIPS, Gauting, Germany).

10.4.5 Methods and Protocols - Biological Characterization of PeptoPlexes

10.4.5.1 *Cell Culture*

HEK 293T cells were grown in DMEM, supplemented with 10% FBS, 4 mM L-glutamine, 0.1 µM 2-mercaptoethanol, 100 units x mL^{-1} penicillin, and 100 µg x mL^{-1} streptomycin. Cells were maintained in a 37 °C humidified atmosphere with 5% CO_2 and were handled under sterile conditions.

Cells of the mouse DC model cell line DC2.4[421] were grown in IMDM, supplemented with 5% FBS, 2mM L-glutamine, 100 IU x mL^{-1} penicillin, 100 µg x mL^{-1} streptomycin and 50 µM β-mercaptoethanol. Cells were maintained in a 37 °C humidified atmosphere with 10% CO_2 and were handled under sterile conditions.

Bone marrow-derived DCs (BMDCs) were differentiated from bone marrow progenitors of C57BL/6 mice as first described by Scheicher *et al*.[422] and modified by Gisch and coworkers.[423] DC culture medium (IMDM with 5 Vol.% FCS [PAA, Cölbe, Germany], 2 mM L-glutamine [Biochrom AG, Berlin, Germany], 100 U/mL penicillin, 100 µg/mL streptomycin [Gibco, Paisly, UK]) and 50 µM β-mercaptoethanol [Roth, Karlsruhe, Germany], supplemented with 5% of GM-CSF containing cell culture supernatant [Zal *et al*., 1994,[424] a kind gift by Dr. B. Stockinger, MRC National Institute for Medical Research, Mill Hill, London]) was replenished on days 3 and 6 of culture. BM cells were seeded on 100 mm^2 bacterial dishes (2 x 10^6 cells/10 ml) and cultivated at 37 °C, 10% CO_2 atmosphere. Aliquots of non-adherent and loosely adherent immature BMDCs were harvested on days 6 or 7 of culture and were reseeded (10^6 cells/ml) on wells of six well tissue-culture plates (StarLab, Hamburg, Germany).

10.4.5.2 *Determination of Transfection Efficiency of PeptoPlexes in HEK 293T Cells by Flow Cytometry*

To assess transfection efficiencies on single cell level, pEGFP-N1 reporter vector (pEGFP-N1; Takara/Clontech, Mountain View, CA) was used. HEK 293T cells were seeded onto 12 well culture plates (each 0.8 x 10^5 cells in 0.5 mL). One day later, non-cross-linked or TETA cross-linked polyplexes (formed with 2.5 µg pDNA at N/P 8, respectively) were added to each well. After 24 h, medium was changed. 48 h after the onset of transfection, cells were harvested (PBS/2 mM EDTA), and samples were analyzed by flow cytometry for frequencies of eGFP positive cells.

10.4.5.3 *Determination of Transfection Efficiency of PeptoPlexes in HEK 293T Cells by Luciferase Activity*

HEK 293T cells were seeded onto 96 well culture plates (10^4 cells in 100 µL per well) 24 h prior to transfection. Polyplexes formed with 0.3 µg pDNA (pCMV_GFP_2A_click_beetle_luciferase plasmid DNA construct (p1699); DKFZ, Heidelberg, Germany) per well were combined with different cross-linkers and added to the cells in triplicates, respectively. Medium was changed 24 h post transfection. After incubation for 48 h, cells were lysed in Passive Lysis Buffer (PLB; Promega, Madison, CA) and luciferase activity was measured.

Bioluminescence was determined according to the following procedure: addition of 100 µL substrate solution per well, 3 s equilibration, 10 s measurement.

10.4.5.4 *Determination of Cellular Toxicity of PeptoPlexes in HEK 293T Cells and DC2.4 Cells by MTT Assay*

Cytotoxicity of polyplexes was assessed by MTT assay using the "CellTiter 96® Non-Radioactive Cell Proliferation Assay" kit (Promega, Madison, USA) according to manufacturer's protocol. HEK 293T cells or DC2.4 cells were seeded onto 96-well culture plates in triplicates (10^4 cells in 100 µL per well) 24 h prior to transfection. Polyplexes formed with 0.3 µg pDNA (pCMV_GFP_2A_click_beetle_luciferase plasmid DNA construct; DKFZ, Heidelberg, Germany) per well were combined with different cross-linkers and added to the cells in triplicates, respectively. In case of HEK 293T cells, 24 h post transfection 20 µl of MTT substrate solution were added to each well, and cells were incubated for another 2 h. Subsequently, 100 µL of mixed solubilization/stop solution were added to each well. After 1 h, the absorbance at 570 nm was measured. In case of DC 2.4 cells medium was changed 8 h post transfection and cells were incubated for another 40 h before proceeding as described above.

10.4.5.5 *Analysis of Cellular Uptake by Confocal Laser Scanning Microscopy*

Bone marrow derived progenitor cells were cultured in 12 well plates (2 x 10^5 progenitor cells per well) for 7 days in presence of GM-CSF. TETA cross-linked polyplexes formed at N/P 8 with 1 µg Cy5-labeled pDNA (pCMV_GFP_2A_click_beetle_luciferase plasmid DNA construct; DKFZ, Heidelberg, Germany) per well were added to the cells, followed by 4 h of incubation. Cells were washed and incubated with Hoechst 33258 (Sigma-Aldrich, Deisenhofen, Germany) to stain cell nuclei and anti-mouse CD11c PE (clone N418, eBioscience, San Diego, CA) to stain the cell membrane of BMDC. Cells were washed to remove access dye. Samples were measured using a TCS SP5 instrument (Leica, Wetzlar, Germany) and analyzed using IMAGEJ software (1.490, NIH Bethesda, MD).

10.4.5.6 *Isolation of OT-I T Cells from Murine Spleen*

Spleens of OT-I mice were sterically removed and ground through a 40 µm cell-strainer. Cells were then lysed with Gey's solution to remove erythrocytes. After washing with EMEM supplemented with 2% FBS, 100 IU x mL^{-1} penicillin and 100 µg x mL^{-1} streptomycin cells were taken up in IMDM supplemented with 5% FBS, 2 mM L-glutamine, 50 µM β-mercaptoethanol, 100 IU x mL^{-1} penicillin and 100 µg x mL^{-1} streptomycin.

10.4.5.7 *Functional Testing of Transfection Efficiency by T Cell Proliferation Assay*

DC2.4 were seeded onto 96-well culture plates with a cell density of 2,5 x 10^4 in 200 µl 24 h prior to transfection. TETA cross-linked polyplexes were formed at N/P 8 with 0,3 µg of OVA-encoding pDNA per well. Before addition to the cells, one part was incubated with serum 1:1 (v/v). Cells were then transfected in triplicates. Medium was changed 8 h after transfection and cells were cultured for another 40 h. Cells were partially stimulated with 100 ng/mL LPS overnight and medium was changed. Auto-proliferation of DC2.4 was blocked with Mitomycin C for 30 minutes. After repeated washing of the cells, OT-I T cells were added at a concentration of 5 x 10^5 cells in 100 µl. T cells were incubated with DC2.4 cells for 72 h, then 0,75 µCi of tritium marked thymidine were added per well. After further cultivation for 18 h, cell proliferation was assessed using Microbeta TriLux (PerkinElmer, Waltham, MA, USA).

ACKNOWLEDGEMENTS

Philipp Heller and Dominika Hobernik contributed equally to this work. The authors would like to acknowledge funding from DFG (SFB 1066-1) and the NMFZ Mainz. Support by the Microscopy Core Facility of the Institute of Molecular Biology (IMB) Mainz is gratefully acknowledged. Philipp Heller is grateful for support by MAterials Science IN MainZ (MAINZ). The manuscript was written through contributions of all authors. All authors have given approval to the final version of the manuscript.

10.5 SUPPORTING INFORMATION

10.5.1 Polymer Synthesis and Characterization

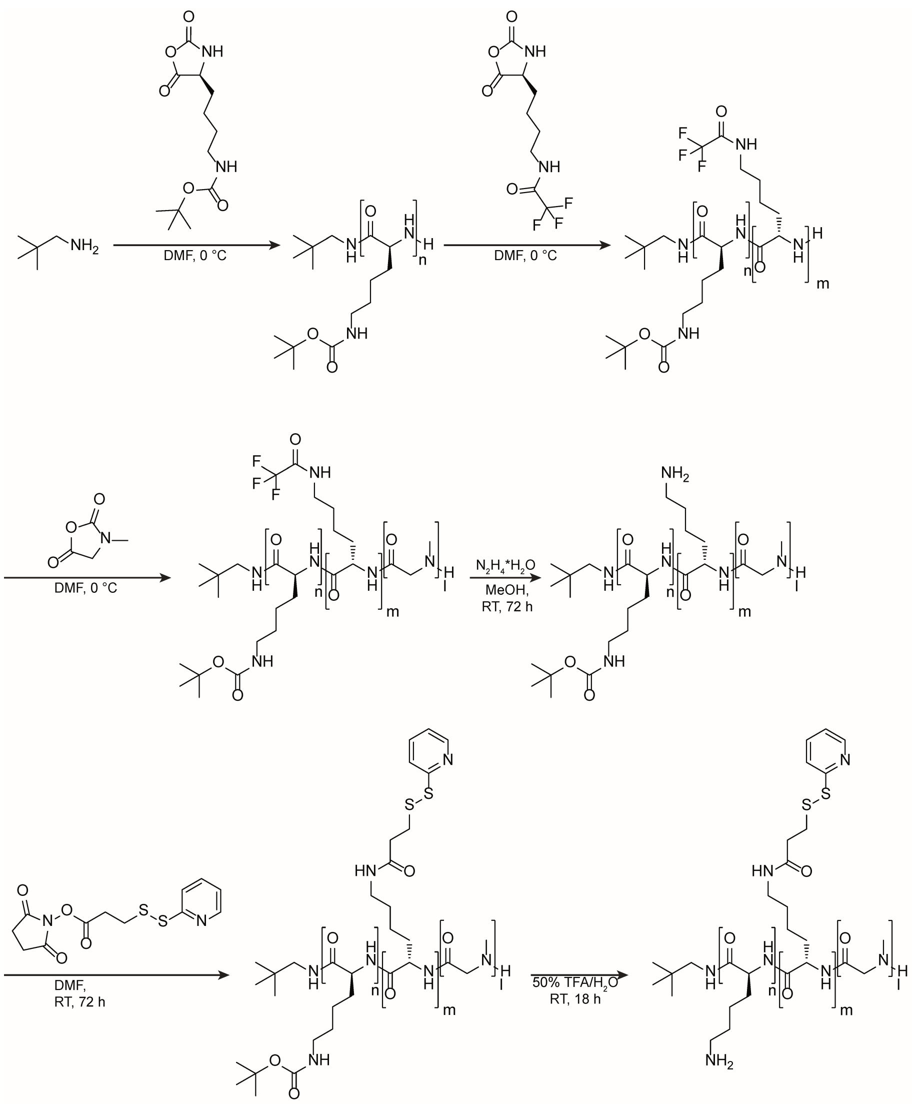

Figure 10.7: Synthetic route towards cross-linkable triblock copolypept(o)ides.

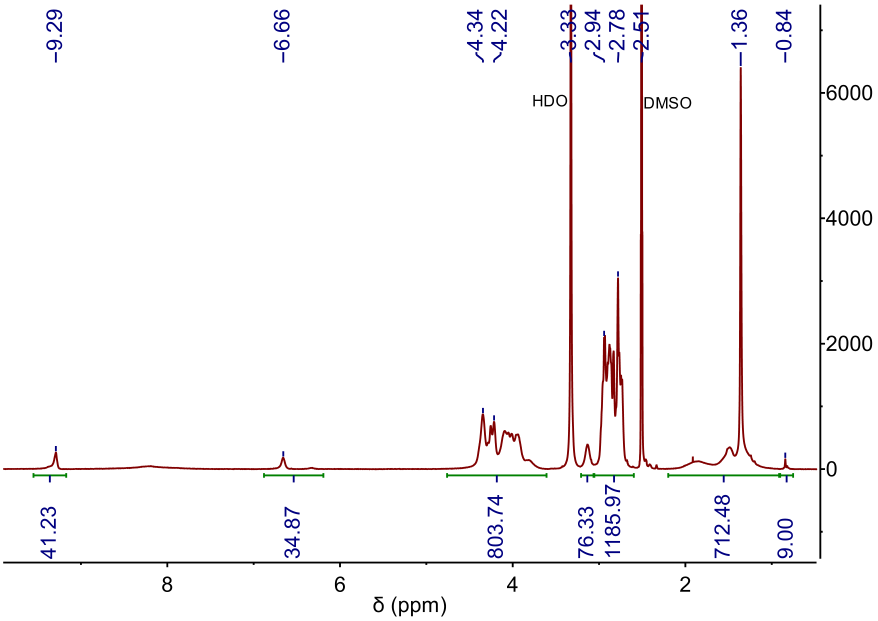

Figure 10.8: ^{1}H-NMR spectrum of protected precursor polymer PLys(Boc)$_{35}$-b-PLys(TFA)$_{41}$-PSar$_{367}$ in DMSO.

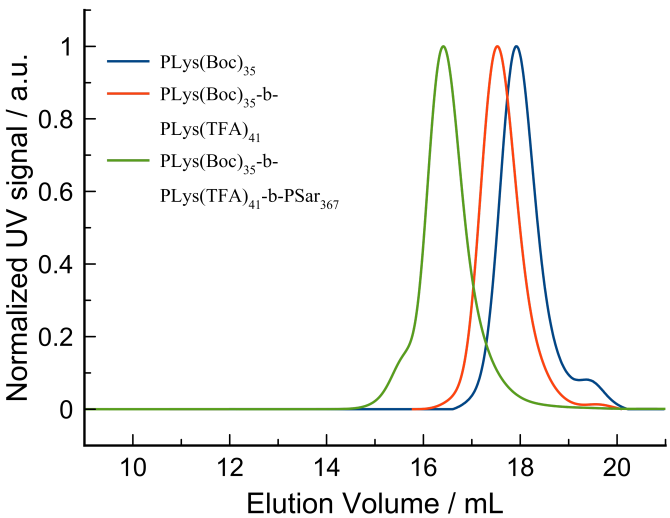

Figure 10.9: HFIP GPC of protected precursor polypept(o)ides showing the transition from homo to triblock copolymers.

Table 10.1: Characterization data of synthesized precursor polypept(o)ides.

POLYMER	ARCHITECTURE	CALCULATED BLOCK RATIO	BLOCK RATIO[A]	M_N[B]	Đ[B]
Triblock	PLys(Boc)-PLys(TFA)-PSar	35:35:350	35:41:367	35.1	1.25
Diblock	PLys(TFA)-PSar	50:250	55:249	29.0	1.20

[A] as determined by ^{1}H-NMR spectroscopy in DMSO-d_6
[B] kg/mol, as determined by GPC with HFIP as solvent and PMMA standards

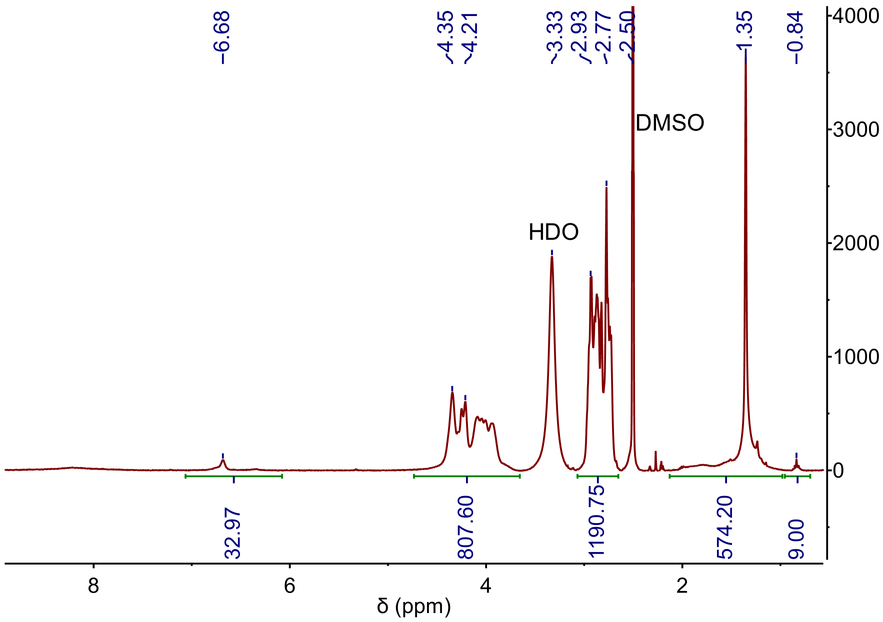

Figure 10.10: ^{1}H-NMR spectrum of $PLys_{35}$-b-$PLys_{41}$-$PSar_{367}$ in DMSO.

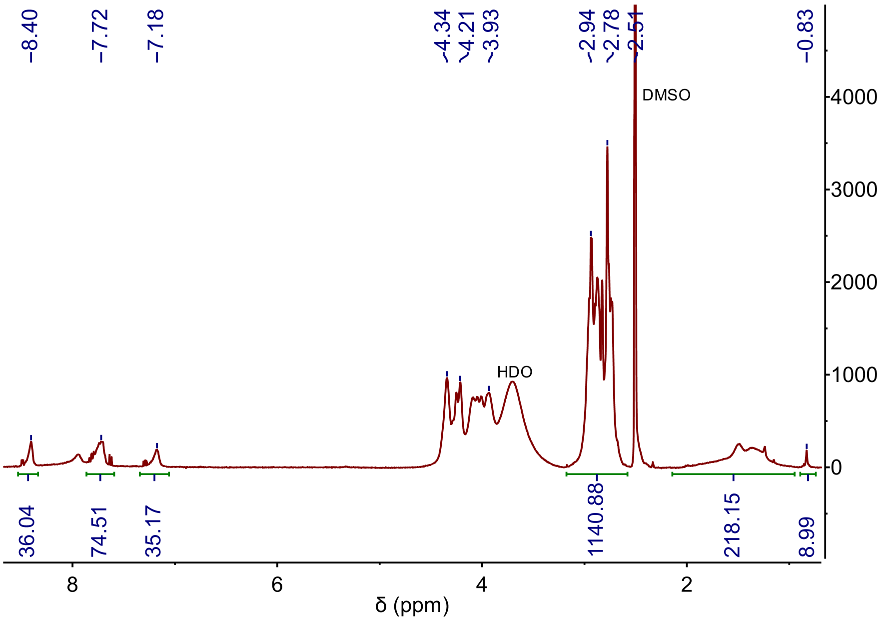

Figure 10.11: ^{1}H-NMR spectrum of PLys$_{35}$-b-PLys(PDP)$_{41}$-PSar$_{367}$ in DMSO.

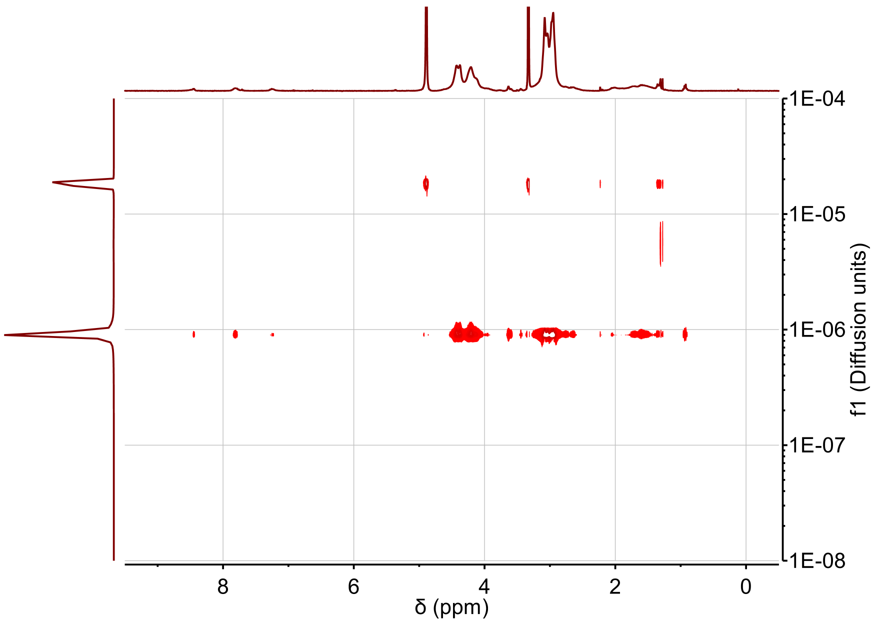

Figure 10.12: DOSY ^{1}H-NMR spectrum of PLys$_{35}$-b-PLys(PDP)$_{41}$-PSar$_{367}$ in MeOD showing only one diffusing polymer species.

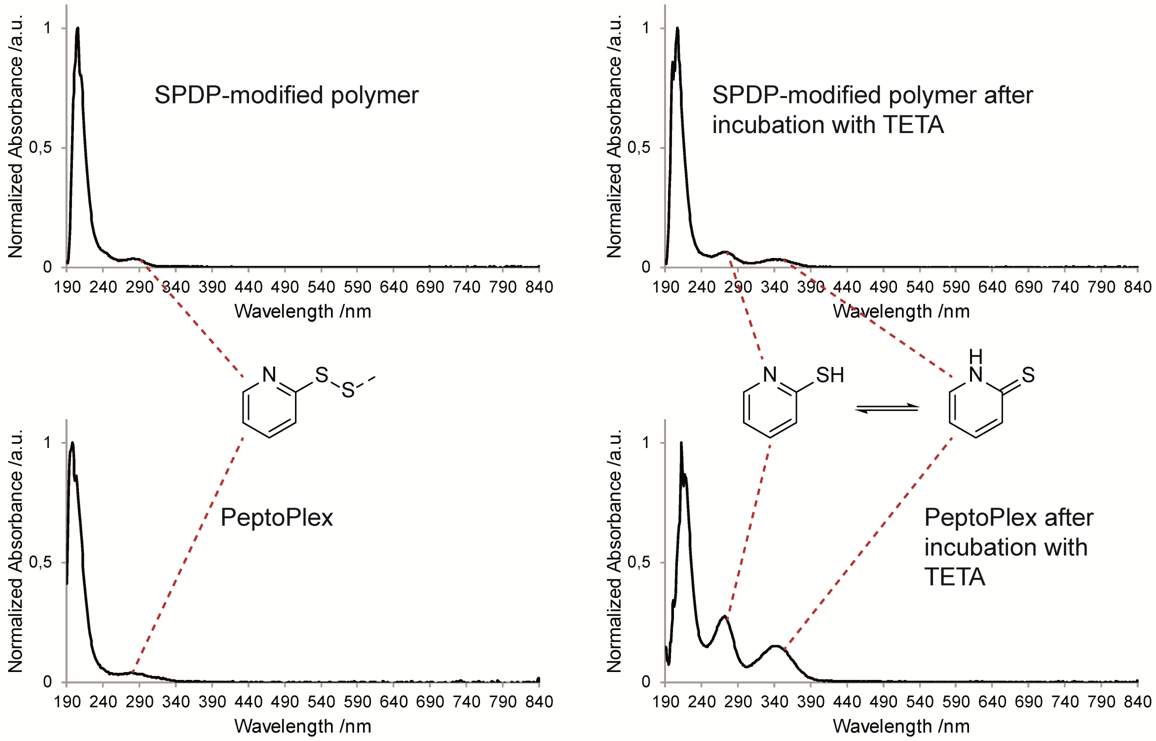

Figure 10.13: UV-Vis spectra proving the cross-linking reaction between PDP groups and TETA on single polymer and polyplex level.

10.5.2 Biological Assays

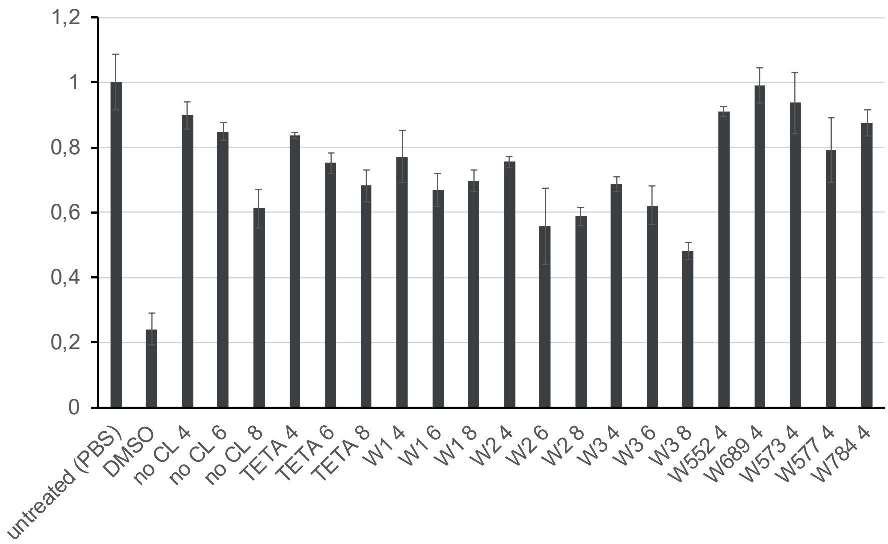

Figure 10.14: Metabolic activity of HEK 293T cells after transfection with cross-linked polyplexes and 24 h of incubation. Applied cross-linkers and N/P ratios are indicated. 10% (v/v) DMSO was added to the cells as positive control. The conversion of MTT to formazan was measured photometrically at 570 nm. Values are normalized to the untreated (PBS) control. Data show the mean ± SEM of triplicates of one experiment.

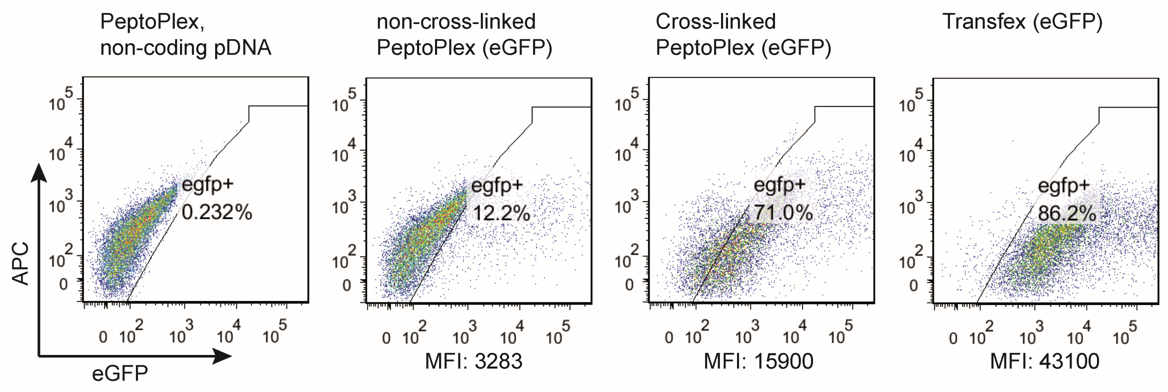

Figure 10.15: Dotplots showing eGFP expression (% postivie cells and MFI) of HEK 293T cells after 48 h of transfection with non-cross-linked or TETA cross-linked polyplexes at N/P 8. Non-coding pDNA was used as negative control, polyplexes obtained from Transfex^{TM} were used as positive control.

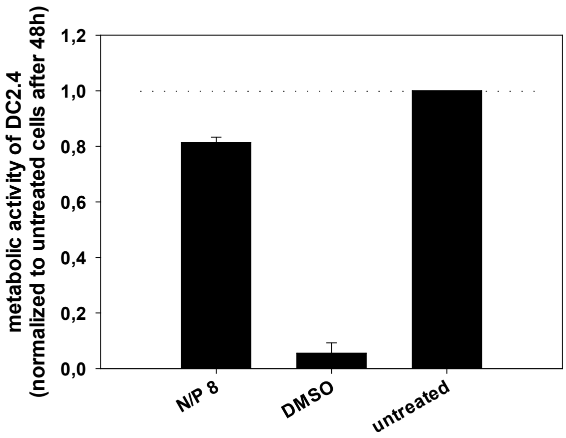

Figure 10.16: Metabolic activity of DC2.4 cells after transfection with **TETA-CPX** at N/P 8 and 48 h of incubation. 10% (v/v) DMSO was added to the cells as positive control. The conversion of MTT to formazan was measured photometrically at 570 nm. Values are normalized to the untreated (PBS) control. Data show the mean ± SEM of triplicates of one experiment.

11 GALECTIN 8-GUIDED IMAGING - VISUALIZING THE ENDOSOMAL ESCAPE OF PEPTOPLEXES

11.1 INTRODUCTION

In the last decades, significant advances in the field of fluorescence microscopy, particularly the development of laser scanning and spinning disc microscopes (see Chapter 4), have paved the road for the elucidation of intracellular processes. In this context, fusion constructs, which link a functional intracellular protein with a fluorescenting protein, represent an essential tool for visualization of such processes.

Apart from cellular uptake and nuclear import, endosomal escape of nucleic acids is one of the main intracellular hurdles for efficient gene delivery. Many non-viral vectors suffer from poor transfection efficiency because after cellular uptake they remain stuck in endosomal and lysosomal compartments where the delivered nucleic acid will eventually be degraded by lysosymal enzymes.[305] So far, endosomal escape of non-viral vectors is a^n inefficient and barely elucidated process. A strategy to image this key step of cell transfection is of major interest and might help to develop new concepts for nucleic acid delivery and to understand the variation in efficiency between different transfection reagents.[497]

Imaging the actual escape event by tracking the labeled nucleic acid/polyplex itself is very difficult, as the dynamic range in fluorescence intensity between nucleic acid densely packed in the endosomes and nucleic acid diffusely distributed in the cytosol is very large. Moreover, it is challenging and requires long-term live cell imaging to catch the exact moment, during which the release into the cytosol occurs. To circumvent this issue, the visualization of endosomal membrane rupture, which goes along with the release of any nanoparticle, represents an indirect way to display endosomal escape. Galectin-8 belongs to a class of cytosolic carbohydrate-sensing proteins which are recruited to damaged endosomes and accumulate there after a bacterial invasion.[498, 499] More specifically, galectin-8 binds to glycans located at the inner side of endosomal membranes, which become exposed to the cytosol upon endosomal membrane damage. A fusion construct combining galectin-8 with the fluorescenting protein mcherry (gal-8-mcherry[499]) was successfully applied as a surrogate for indirect visualization of the endosomal escape of lipoplexes and lipid nanoparticles by staining the damaged endosomal membrane through accumulated fluorescence.[497]

11.2 RESULTS AND DISCUSSION

In an effort to adopt this methodology for qualitative imaging of the endosomal release of different PeptoPlex formulations, HEK 293T cells were transiently transfected with a gal-8-mcherry encoding DNA. Gal-8-mcherry expression of the majority of the cell population was verified by flow cytometry (data not shown). After 48 hours, cells were incubated for another 17 hours with Cy5-labeled PeptoPlexes at a concentration of 1.67 ng/µL with respect to pDNA and imaged using a costum-built spinning disc confocal microscope. Thereby, the first objective was to visualize the endosomal release of PeptoPlexes per se and to verify co-localization between PeptoPlexes and gal-8 in the same endosomal compartments.

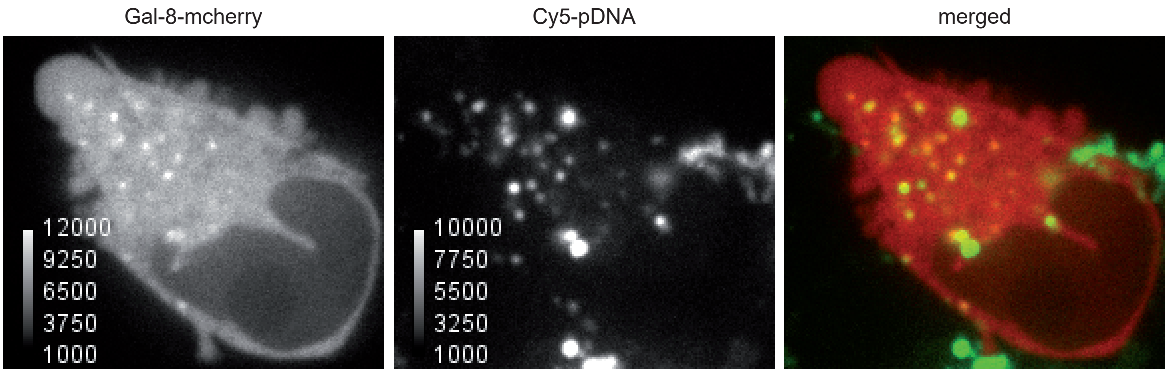

Figure 11.1: Representative imaging of a single gal-8 positive HEK 293T cell after 17 hours of incubation with PeptoPlexes. Left: gal-8-mcherry channel, middle: Cy5-pDNA channel, right: merged.

As shown in Fig. 11.1 non-bound gal-8 is diffusely distributed in the cytosol of cells, providing a clear illustration of the cell body. Damaged endosomes stand out against the background fluorescence due to gal-8-mcherry concentration leading to higher fluorescence intensity in a confined region. The prevailing part of endosomal compartments which contain PeptoPlexes (Cy5 positive) are also positive for gal-8, indicating the membrane damage induced by the PeptoPlexes. Given that HEK 293T cells are fairly susceptible to transfection, the high number of double positive compartments is not surprising. Only a small fraction of PeptoPlex-containing endosomes show no gal-8 binding, while there are no compartments exclusively positive for gal-8. Notably, no gal-8 recruitment to the cell membrane was observed.

In a subsequent step, three different PeptoPlex formulations - **NCPX**, **TETA-CPX** (see Chapter 10) and **Triblock-His-PX** (see chapter 9) - were screened for induction of endosomal membrane damage and release. Unfortunately, as the gal-8 studies were conducted during a research stay in the group of Prof. Kirchhausen prior to the development of the lead PeptoPlex formulation (**L-CPX**) introduced in Chapter 12, the latter could not be included in these experiments. Aiming towards a qualitative readout it is reasonable to assume that the degree of PeptoPlex-mediated membrane damage correlates with the degree of gal-8 recruitment and therefore with fluorescence intensity at the site of gal-8 accumulation. For comparison of the three PeptoPlex formulations fluorescence intensity at selected gal-8 positive endosomes was quantified with imagej software and related to background fluorescence in the surrounding cytosol region (Fig. 11.2).

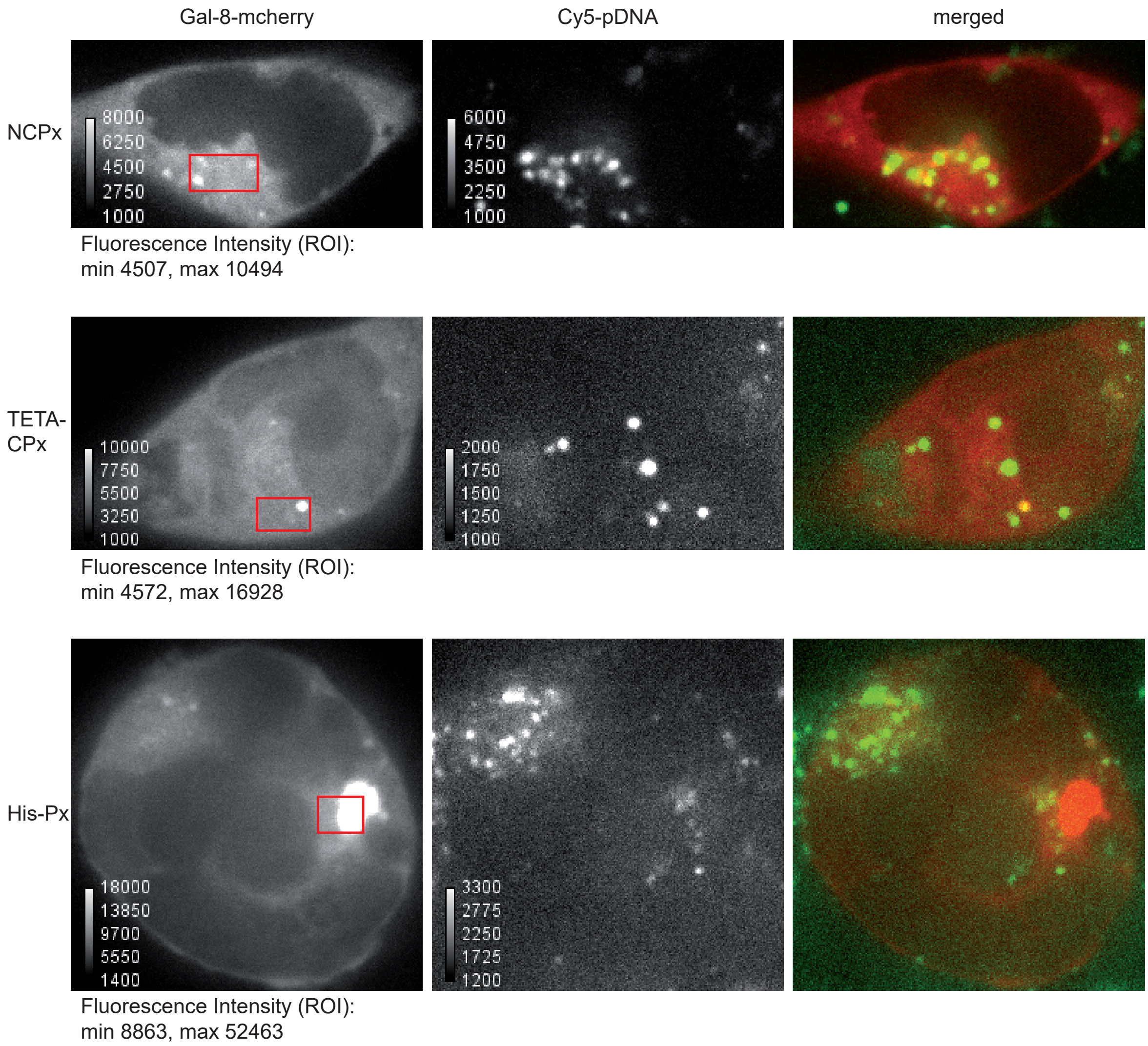

Figure 11.2: Qualitative comparison of gal-8-mcherry-associated fluorescence intensity in region of interest (ROI) for three different PeptoPlex formulations as a measure of induced endosomal membrane damage. ROI is indicated with red square. Left: gal-8-mcherry channel, middle: Cy5-pDNA channel, right: merged.

Of the three formulations, **NCPX** showed the smallest difference between cytosolic fluorescence and endosome-associated fluorescence (min 4507, max 10494, factor 2.3). In case of **TETA-CPX** relative fluorescence intensity at distinct endosomes was slightly higher (min 4572, max 16928, factor 3.7), indicating more gal-8 accumulation. The highest difference was observed for **Triblock-His-PX** (min 8863, max 52463, factor 5.9), probably as a consequence of the most pronounced gal-8 recruitment. Although by far not all His-Px-containing endosomes exhibited fluorescence intensity at this degree, no spots of similar brightness were found for the other two PeptoPlex formulations. The presented results have to be interpreted carefully, since in these experiments cells were only transiently transfected with the gal-8-mcherry construct and therefore gal-8 expression level varies from cell to cell. Nevertheless, as endosome-associated fluorescence intensity was referred to cytosol background levels for each case, a qualitative comparison between the PeptoPlex formulations becomes possible. The observed increased endosomal damage marked by the increased gal-8 recruitment for **Triblock-His-PX** and **TETA-CPX** compared to **NCPX** might be related to the pH buffering properties of histidine (see Chapter 9) and TETA cross-linker (see Chapter 10). The observation is also in line with the higher transfection efficiency of

Triblock-His-PX and **TETA-CPX** in contrast to standard PeptoPlexes (see Chapters 9 and 10), confirming endosomal escape properties as one likely factor.

Eventually, it was demonstrated that gal-8-mcherry provides a suitable option to visualize endosomal damage and escape of PeptoPlexes and has the potential for application in quantitative readouts. The fact that, in principle, gal-8-mcherry can be genetically introduced into various other cell line makes it especially attractive as an imaging tool.

Part V

PEPTOPLEX-BASED ARTIFICIAL VIRUSES

The next part outlines the latest stage of PeptoPlex development. As key step, a cystein-containing virus-inspired fusogenic peptide (LAH4-L1) was applied as functional cross-linker and incorporated into the cross-linkable PeptoPlexes introduced in the previous part. Moreover, PeptoPlexes were furnished with DC-targeting ligands and a nuclear localization signal to enhance the import of pDNA into the nucleus. In this system, the triblock copolypept(o)ides can be regarded as a framework for the attachement of the virus-mimicking functionalities, eventually yielding PeptoPlex-based artificial viruses. The latest generation of PeptoPlexes was succesfully applied for the delivery of pDNA (Chapter 12) and mRNA (Chapter 13) to dendritic cells. Moreover, first in vivo experiments on biodistribution were performed (Chapter 14).

12 TOWARDS A SYNTHETIC NON-ENVELOPED VIRUS: FROM THE TRANSFECTION OF DENDRITIC CELLS TO PDNA VACCINES FOR SYSTEMIC APPLICATION

P. Heller, D. Hobernik, B. Weber, M. Schinnerer, M. Bros, M. Barz, *to be submitted*

12.1 INTRODUCTION

The development of vectors for *in vivo*[500] or *ex vivo*[501] gene therapy has fascinated researchers in various fields. While synthetic biology aims to improve the properties of viral vectors and virus like particles by genetic methods, e.g. directed evolution,[502] chemists develop lipid[503] or polymer[5] based non-viral transfection agents, i.e. liposomes, lipoplexes or polyplexes.

The combination of both research branches, however, tries to unite aspects of both areas by teaming virus derived/inspired peptides with polymeric material to augment transfection efficiency through enhancing cellular uptake, endosomal escape or nuclear translocation.[215, 216, 462, 504]

As key aspect of their superior efficacy, viruses, and in particular non-enveloped viruses, combine stability in the extracellular space with pH or redox triggered disintegration after receptor mediated endocytosis.[504] During the disintegration process distinct proteins of the viral capsid are exposed mediating endosomal escape by membrane destabilization.[504] After translocation into the cytosol, other specialized viral proteins (nuclear localization sequences) enable nuclear import and insertion of the genetic code into the genome of the host cell.[504] Yet, although the utilization of viruses and virus like particles in the context of gene therapy has reached a level of enormous sophistication, it still faces several hurdles like limited packaging capacity and safety concerns.[5] Non-viral vectors may be a suitable tool to overcome these limitations but often suffer from inferior transfection efficiency or unfavorable biodistribution after intravenous injection. Therefore, tuning non-viral vectors with key viral structures, which are elementary for the intracellular trafficking of viruses, constitutes a rational approach to overcome the individual drawbacks of both types of vectors.[5, 504]

Among the possible applications of gene therapy, DNA vaccines seem particularly promising. This concept relies on the expression and presentation of encoded antigens by dendritic cells, which can subsequently induce T cell-based immune repsonses.[505] As T-cell recruitment by dendritic cells is a naturally efficient process, succesful initiation of an immune response requires < 100 activated dendritic cells per lymph node.[339] Moreover, because dendritic cells are phagocytic and i.a. reside in the spleen, they are a readily accessible target for systemic nanoparticle-based immunotherapies, as has been demonstrated recently for the example of mRNA vaccines.[2, 506] What sets DNA vaccination apart from conventional peptide-based formulations is efficient presentation of antigen via MHC I to $CD8^+$ T cells by all subpopulations of dendritic cells, since DNA-encoded transgenes are expressed like endogenous genes. In contrast, peptide antigens internalized by dendritic cells are predominantly presented via MHC II. Only the $CD8^+$ dendritic cell subpopulation mediates MHC I presentation of exogenous antigens, known as cross presentation. Furthermore, to induce T cell responses, dendritic cells must be activated by adjuvants that engage danger receptors. Therefore, peptide-based vaccine formulations contain immunostimulatory molecules of a different material. DNA vaccines, in contrast, may encode multiple antigens and contain immunostimulatory CpG-rich motifs outside of the expression cassette that serve as adjuvants. From delivery perspective, an optimized carrier system for a DNA vaccine would be universally compatible with any antigen, which can be encoded on nucleic acid level.

In an effort to develop such an optimized system for the functional transfection of dendritic cells with a pDNA encoded antigen, we herein propose a novel concept, which aims to follow the above mentioned paradigm by combining synthetic, polymeric elements with virus-inspired components. The synthesis of such a polyplex-based artificial virus appears to be an exciting task itself. Orienting on natural non-enveloped viruses one may disect the requirements for a synthetic pDNA vaccine applicable for systemic vaccination into five parts:

- Compaction and stabilization of pDNA within a stimuli-responsive core shell structure.
- Efficient shielding of the pDNA by a stealth like corona to avoid aggregation through contact with serum proteins or complement activation.
- Efficient binding to specific transmembrane receptors of target cells.
- Incorporation of moieties for endosomal escape and nuclear entry, which are exposed upon cellular uptake.

12.2 RESULTS AND DISCUSSION

The synthetic framework for all these different functionalities is provided by triblock copolypept(o)ides (Fig. 12.1 (a)), which we have introduced recently.[158, 159] They include a hydrophilic polysarcosine (PSar) block for shielding against aggregation, a middle hydrophobic block based on reactive disulfides (PLys(PDP)) for bioreversible cross-linking and a cationic polylysine (PLys) block for complexation of pDNA. These multifunctional block ionomers are derived from PLys(Boc)-b-PLys(TFA)-PSar precursor polymers, which are obtainable with low dispersity by NCA polymerization (<1.2, SI, Fig. 12.5 and 12.6 for characterization) and can be deprotected orthogonally as reported earlier.[158] By this method, the ε-amine groups of the middle PLys(TFA) segment can be freed selectively making them accessible for block selective modification with succinimidyl 3-(2-pyridyldithio)propionate (SPDP), introducing activated disulfide bonds. Successive deprotection of the PLys(Boc) block yields the final block composition described above. Eventually, charge density and degree of thiol-modification of the triblock copolypept(o)ides can be tuned by variation of block length ratios and remain fixed afterwards. Furthermore, ω chain ends of the polymers can be functionalized with targeting ligands such as mannose, trimannose or aDEC205 antibody to increase cellular uptake of the final vaccine by dendritic cell populations (Fig. 12.1 (b)).

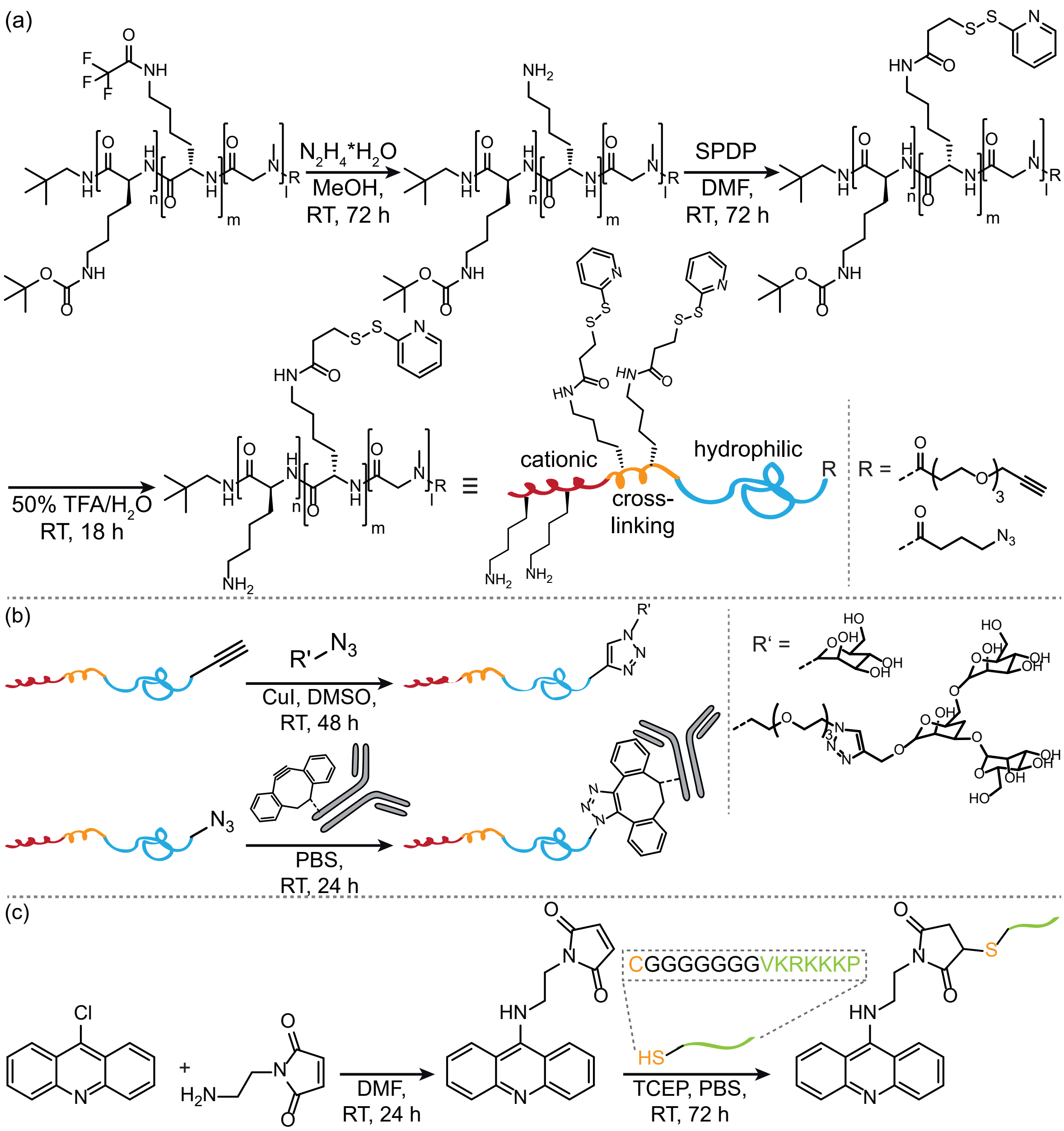

Figure 12.1: Synthetic elements for PeptoPlex-based artificial virus. (a) Sequential deprotection and modification of triblock copolypept(o)ides with SPDP. (b) Attachment of ligands via click chemistry. (c) Synthesis of NLS intercalator conjugate (NLS-9AA).

Incorporation of fusogenic virus-inspired peptides for enhanced endosomal escape is conducted on polyplex level by reaction between cysteins within the peptide sequence on the one hand and reactive disulfides of the middle polymer block on the other. Besides allowing the incorporation of the peptides, the disulfide formation results in redox-responsive cross-linking of the polyplexes, as shown by us and others,[233, 479] being sensitive to the transition from an oxidative milieu (extracellular space) to reductive environments (intracellular space) after uptake by antigen-presenting cells.. We chose C5HTat5HC and LAH4-L1 as two different types of endosomolytic peptides for incorporation into the polyplexes by disulfide cross-linking. Both peptides have been used as standalone transfection reagents. The hydrophilic C5HTat5HC was introduced by Lo and Wang as a more potent derivative of the cell-penetrating peptide HIV Tat and already contains terminal cysteins.[507] Its supposed mechanism of action for endosomal escape is interaction of the cationic arginine and histidine residues with negative moieties of the membrane and/or the hypothesized proton sponge effect. In contrast, amphipathic LAH4-L1, developed by Bechinger and co-workers,[8] contains histidine as well as hydrophobic domains which mediate membrane destabilization by insertion and a pH-dependent switch from transmembrane to in-plane orientation. To make LAH4-L1 compatible for our synthetic approach, the two peripheral alanines within the original peptide sequence were replaced by cysteins (in the following indicated as CLAH4-L1C).

Finally, to augment the import of pDNA into the cell nucleus, the SV40 large T antigen nuclear localization signal (NLS)[508] is exploited. In case of dendritic cells, this procedure is especially important, as they are largely non-dividing. Non-dividing cells do not break down the nuclear membrane like dividing cells do during mitosis. A permanently intact nuclear membrane represents a great obstacle for nuclear localization of pDNA, since passive diffusion across the membrane or through nuclear pores is not possible for large biomolecules. Several groups have shown that transfection levels can be elevated by employing NLS sequences which hijack the natural nuclear transport machinery through binding to importins.[509] NLS sequences thereby were either attached to pDNA[510–513] or to a non-viral vector.[352, 514, 515] We chose intercalation as method to attach the NLS sequence directly to the pDNA.[516, 517] This strategy seems advantageous since a covalent linkage could impair bioactivity of pDNA, whereas electrostatic interaction as mere driving force for binding would set the NLS sequence in competition with the triblock copolypept(o)ides, which also rely on ionic attraction for complexation of the pDNA. As recommended by prior investigations from Parelkar *et al.*,[518] the intercalator is installed at the valine end of the NLS sequence. For linkage, the peptide is provided with a C-terminal cysteine separated by a glycine spacer whose length was adjusted according to theoretical considerations by Cohen and Granek.[519] Covalent joining with the intercalating agent 9-chloroacridine was realized via a two step process involving thiol maleimide coupling as decisive reaction (Fig. 12.1 (c)), yielding NLS-9-aminoacridine (NLS-9AA) as confirmed by SEC and NMR (SI Fig. 12.9 and 12.10).

Binding of NLS-9AA to pDNA was verified by gel electrophoresis (Fig. 12.3 (a)). The usual nucleic acid staining reagents (e.g. ethidium bromide) were omitted in this experiment. In this way, only the fluorescence of the aromatic acridine system is detected, visualizing the pDNA as single band and proving the association of both components. For formation of preferably small polyplexes, pDNA was first loaded with NLS-9AA. As shown by Cai *et al.*, spatial distribution of NLS within a polyplex has a crucial impact on transfection efficiency.[520] Hence, adding NLS-9AA first ensures that it is situated in the core of the final polyplex and remains attached to the pDNA during intracellular trafficking, until nuclear import. The next steps involved the addition of the cysteine-modified fusogenic peptides and at last the polypept(o)ide at a N/P ratio of 4 (Fig. 12.2).

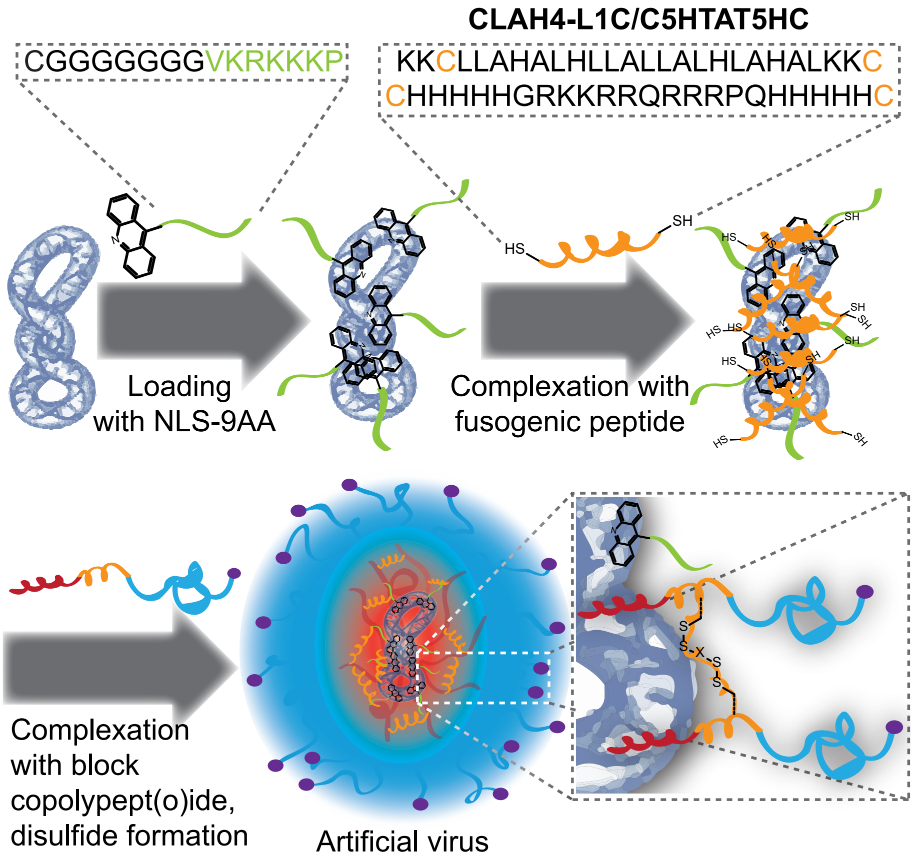

Figure 12.2: Formation of PeptoPlex-based artificial viruses.

All components were added under constant mixing. Especially in the case of LAH4-L1, which yields very large polyplexes when used as standalone reagent (SI, Fig. 12.12), the protocol for polyplex formation had to be optimized in interative steps (SI, Fig. 12.11) to eventually obtain reasonably small cross-linked polyplexes with incorporated CLAH4-L1C and NLS-9AA (in the following termed as **L-CPX**). In this respect, the sequence in which the single components are added to the pDNA has a decisive impact on final polyplex size. Moreover, loading of pDNA with NLS-9AA further decreased polyplex size, presumably because of pre-complexation of the plasmid before addition of the other components (SI, Fig. 12.11).

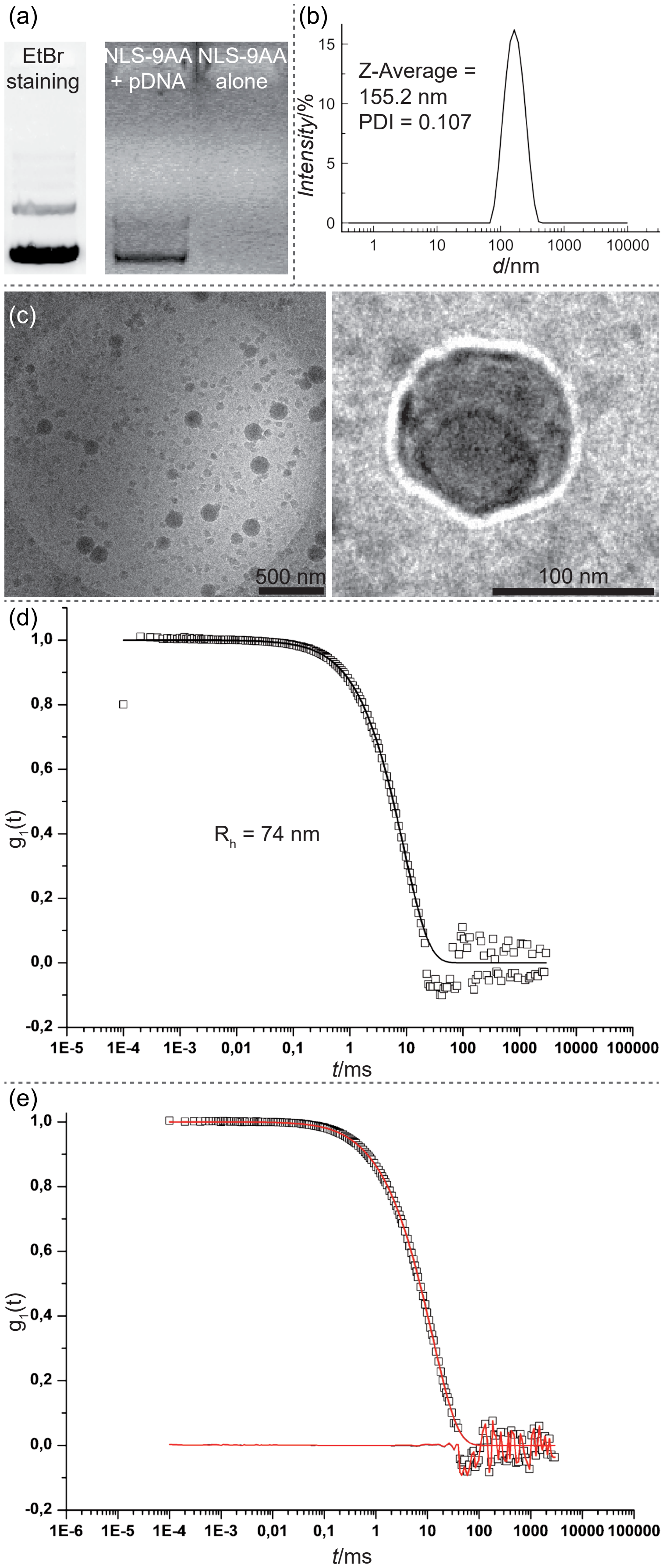

Figure 12.3: Physicochemical characterization of polyplexes. (a) Gel electrophoresis of pDNA either stained with ethidium bromide (left) or NLS-9AA (right), confirming association of both components. (b) Size distribution of **L-CPX** as determined by single-angle DLS. (c) Cryo-TEM images of **L-CPX** in overview (left) and close-up (right), revealing core-shell structure. (d) Multi-angle DLS of **L-CPX** in PBS and (e), in 90% human plasma, proving the absence of aggregation.

For the optimized **L-CPX** formulation, a diameter of around 150 nm and a narrow size distribution were determined by cryo-TEM as well as single- and multi-angle dynamic light scattering (DLS) (Fig. 12.3 (b,c,d)). Cryo-TEM furthermore indicated the formation of core-shell polyplexes. As can bee seen in the closeup (Fig. 12.3 (c)), the pDNA with its higher scattering contrast is surrounded by a shell of polymer with lower scattering density, which is presumably the PSar block.

To assess stability of **L-CPX** in the presence of blood proteins, DLS in human serum was performed according to established protocols by Rausch *et al*.[325, 326] The correlogram shows that the autocorrelation function which takes aggregation into account and the one that does not are perfectly congruent. Thus, it can be concluded that **L-CPX** are stable in serum and do not cause considerable aggregation of plasma proteins. In addition, **L-CPX** do not trigger any activation of the complement system, as was verified by screening of human C5a concentration through ELISA in serum after exposure to **L-CPX** (SI, Fig. 12.16).

After the optimized formulation protocol was established, providing small polyplexes with serum stability, we next evaluated their transfection capacity. Initially, the performance of polyplexes cross-linked with either CLAH4-L1C (**L-CPX**) or C5HTat5HC (**T-CPX**) was compared in the dendritic cell-like cell line DC2.4 by luciferase assay (SI, Fig. 12.13). CLAH4-L1C turned out to be much more efficient than C5HTat5HC when used as cross-linker, with **L-CPX** reaching transfection levels of jetPEI. This could be due to the different endosomal escape mechanisms of the both peptides described above. Considering this observation, one may argument that, at least in dendritic cells and in our experimental system, an endosomal escape agent which exerts membrane destabilization by insertion is more efficient than a reagent relying on cationic interaction or on the proton sponge effect. Consequently, for all following experiments, CLAH4-L1C was the cross-linker of choice.

Next, the impact of the dendritic cell targeting ligands mannose and of NLS-9AA incorporation on transfection efficiency of **L-CPX** were examined (SI, Fig. 12.14). Luciferase assay in DC2.4 cells revealed a clear beneficial influence of both components, with the effect of mannose being more pronounced than that of NLS-9AA. In addition, simultaneous furnishing of **L-CPX** with mannose and NLS-9AA yielded a synergistic effect. Transfection efficiency of the mannosylated polyplex (**M-L-CPX**) with incorporated NLS-9AA exceeded that of **L-CPX** by an order of magnitude. As suggested by FACS experiments with Cy5-labeled pDNA, the positive impact of mannose is founded on increased cellular binding of mannosylated polyplexes to dendritic cells (Fig. 12.4 (b)), which also has been demonstrated for many other particles.[157, 389] In this context, one should note that uptake of non-mannosylated polyplexes was smaller than that of free pDNA, possibly owing to the shielding effect of the PSar corona. Supplementary to flow cytometry, confocal microscopy verified intracellular localization of **L-CPX** and **M-L-CPX** (Fig. 12.4 (a)). Apart from mannose, trimannose was also tested as targeting ligand, but did not exhibit a beneficial effect compared to mannose (data not shown).

After identification of **M-L-CPX** as lead formulation, we next assessed its transfection efficiency on primary bone marrow-derived dendritic cells (BMDCs) (Fig. 12.4 (c)). In luciferase assay, **M-L-CPX** reached transfection levels of standalone LAH4-L1 polyplexes (LAH4-L1-PX), one of the most efficient transfection agents known, and surpassed jetPEI by a factor of 6, underlining the validity of the screening experiments in DC2.4 cells conducted before.

These positive results encouraged us to test gene delivery capacity of **L-CPX** and **M-L-CPX** with NLS-9AA on a more functional level. Therefore, ovalbumin (OVA) encoding pDNA was applied as model DNA vaccine and delivered to BMDCs by means of **L-CPX** and **M-L-CPX**. Cells transfected with both formulations and incubated under activating conditions (SI for protocol) were able to induce OVA-dependent $CD8^+$ T cell proliferation during co-culture, as assessed by ^{3}H-thymidine assay. In contrast, untreated BMDCs or cells treated with jetPEI/OVA-pDNA polyplexes were not able to stimulate CD8$^+$ T cells to proliferate. The outcome shows that only for **L-CPX** and **M-L-CPX** transfection efficiencies in BMDCs are high enough to induce sufficient intracellular production and accumulation of OVA to exceed the threshold for T cell activation.

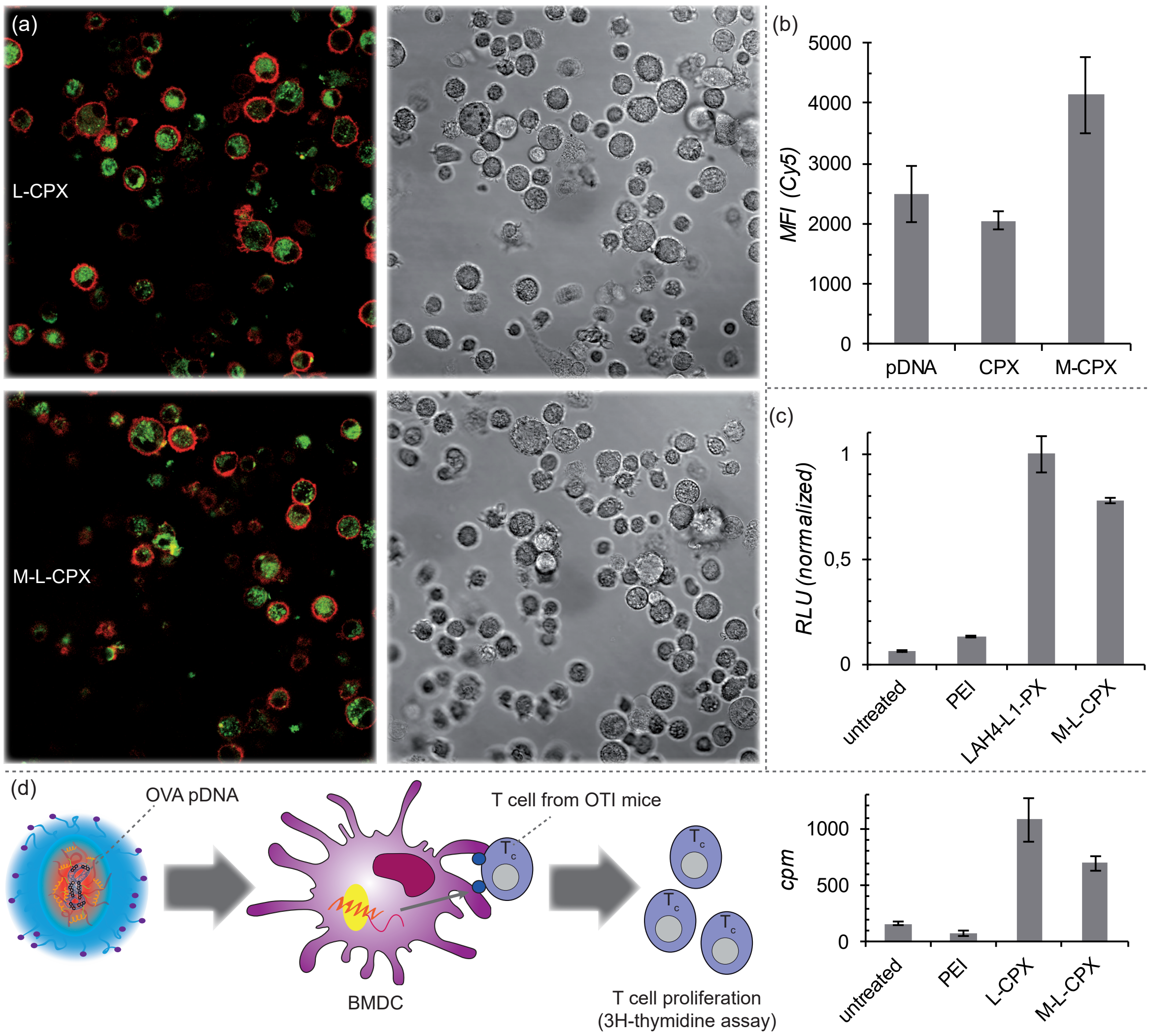

Figure 12.4: Biological evaluation of polyplexes. (a) Confocal microscopy images confirming intracellular localization of **L-CPX** and **M-L-CPX** (red: CD11c$^+$ staining, green: Cy5-labeled pDNA). (b) MFI-related cellular uptake levels of free pDNA, **CPX** and **M-CPX** in CD11c$^+$ cells as determined by flow cytometry (mean ± sd, n = 2). (c) Transfection efficiency of **M-L-CPX** in comparison to LAH4-L1 and PEI, as assessed by luciferase assay in BMDCs (mean ± sd, n = 3). (d) Transfection of BMDCs with OVA encoding pDNA as model DNA vaccine and measurement of subsequent T cell proliferation by ^{3}H-thymidine assay (mean ± sd, n = 3).

Keeping in mind that BMDCs are largely non-dividing and therefore intrinsically difficult to transfect, the fact that our polyplex formulations work not only on reporter but also on functional level underlines the suitability of these systems to serve as non-viral vectors for pDNA vaccination. In contrast to standalone LAH4-L1, cross-linked polyplexes are much smaller and combine adequate transfection efficiency in target cells with stability in human serum and low cytotoxicity and complement activation (SI, Fig. 12.15 and 12.16). These properties make the presented polyplexes promising candidates for further development of DNA vaccines for systemic application.

12.3 EXPERIMENTAL SECTION

12.3.1 Materials

DMF was purchased from Acros (99.8%, Extra Dry over Molecular Sieve) dried over BaO and distilled *in vacuo* followed by excessive stirring *in vacuo* to remove traces of dimethylamine. THF and *n*-hexane were purchased from Sigma-Aldrich and distilled from sodium. Triethylamine was purchased from Carl Roth and distilled from potassium hydroxide Other solvents were used as received. Diphosgene and chlorotrimethylsilane were purchased from Alfa Aesar and used as provided. Neopentylamine was purchased from TCI Europe, dried over NaOH and fractionally distilled. Sarcosine was purchased from Sigma-Aldrich, all other amino acids were purchased from ORPEGEN. Succinimidyl 3-(2-pyridyldithio)propionate (SPDP) was purchased from ThermoFisher Scientific. Alkyne-PEG_3-NHS ester was obtained from Conju Probe. 9-Chloroacridine was purchased from Sigma-Aldrich. 1-(Aminoethyl)maleimide hydrochloride was purchased from Fluorochem. Mannopyranosyl azide was obtained from LC Scientific Inc. Peptides were purchased from LifeTein LLC.

12.3.2 Instrumentation

12.3.2.1 *Polymer Characterization*

400 MHz ^{1}H-NMR spectra and ^{19}F NMR spectra were recorded on a Bruker Avance II 400. HSQC and DOSY NMR measurements were performed on a Bruker Avance III HD 400. All spectra were recorded at room temperature and analyzed with MestReNova software. Degrees of polymerization as well as molecular weights were calculated by comparing the integral of the neopentylamine initiator peak either with the integrals of the side chain amide protons (for PLys(Boc) and PLys(TFA)) or with the average of integrals of methyl group and α-protons (for PSar) in the 400 MHz ^{1}H-NMR spectra.

Attenuated total reflectance Fourier transformed infrared (ATR-FTIR) spectroscopy was performed on a FT/IR-4100 (JASCO Corporation) with an ATR sampling accessory (MIRacleTM, Pike Technologies). IR Spectra were analyzed using Spectra Manager 2.0 (JASCO Corporation).

Melting points were determined using a METTLER FP62 (METTLER WAAGEN GMBH).

Hexafluoroisopropanol (HFIP) gel permeation chromatography (GPC) was performed with HFIP containing 3 g/L potassium trifluoroacetate as eluent at 40 °C and a flow rate of 0.8 mL/min. The columns were packed with modified silica (PFG columns; particle size: 7 mm, porosity: 100 and 1000 Å). Polymer was detected with a refractive index detector (G 1362A RID, JASCO) and a UV/Vis Detector (UV-2075 Plus, JASCO). Molecular weights were calculated using a calibration performed with PMMA standards (Polymer Standards Services GmbH) and toluene as internal standard. Elution diagrams were analyzed using WinGPC UniChrome 8.00 (Build 994) software from Polymer Standards Services.

Preparative reverse phase-HPLC was performed with a Knauer HPLC-System (Berlin, Germany), consisting of two HPLC pumps (Smartline 1000), an UV/Vis-detector (Smartline 2500), a RI-detector (Smartline 2400) and a Phenomenex (Torrance, U.S.A.) Luna-column (10 µm, C18(2), 100 A, 250 × 30 mm^2) run at a flow of 10.0 mL/min and loaded with a 2 mL injection loop. The system was operated and samples analyzed with D-7000 HPLC-System-Manager software (version 4.1). For the preparative run a gradient from 100% acetonitrile to 100% water over 60 min was utilized. The UV/Vis-detector was set to a wavelength of 399 nm.

12.3.2.2 *Biological Experiments*

3-(4,5-Dimethylthiazol-2-yl)-2,5-diphenyltetrazolium bromide (MTT) assay measurements were performed using a Dynex MRX TC Revelation microtiter plate reader (Dynex Technologies, Chantilly, VA).

Luciferase assay was carried out with a 96 well plate chemoluminescence reader (Centro LB 960; Berthold Technologies, Bad Wildbad, Germany) using Mikrowin 2000 software.

FACS experiments were executed on a FACS Canto II flow cytometer equipped with BD FACS Diva software (both from BD Biosciences, San Diego, CA). Data were analyzed using FlowJo software (FLOWJO, Ashland, OR).

Live cell images were acquired on an inverted confocal microscope TCS SP5 (Leica, Wetzlar, Germany) equiped with an oil-immersion objective (63 magnification; NA 1.4) and a laser set capable of 405 nm/488 nm/561 nm excitation. Images were recorded at 512 x 512 8-bit-pixel resolution with a pinhole of 130 μm and confocal plane depth of 1.0 μm, resulting in a total image size width and height of 246 μm.

12.3.3 Methods and Protocols - Preparation of PeptoPlexes

12.3.3.1 *Synthesis of N-ε-tert-butyloxycarbonyl-L-Lysine N-Carboxyanhydride*

9.8 g (39.8mmol) of *N*-ε-Boc-protected lysine were weighed into a three-neck flask and dried under vacuum for 1 h. The solid was suspended in 300 mL of absolute THF under a steady flow of dry nitrogen. Afterwards, 9.9 ml (79.6 mmol) of absolute trimethylsilylchloride and 11.0 ml (79.6 mmol) of absolute triethylamine were added slowly via syringe. The suspension was stirred for 2 h followed by addition of 4.8 ml (39.8 mmol) of diphosgene, again via syringe. The suspension was mildly refluxed for another 2 h. Overnight, a steady flow of dry nitrogen was lead through the solution into two gas washing bottles filled with aqueous NaOH solution removing TMSCl. The suspension was filtered under dry nitrogen atmosphere to remove the salts of TEA and unconverted amino acid. The filtrate was evaporated under reduced pressure. Subsequently, absolute THF was added to completely dissolve the crude reaction product. The solution was precipitated with absolute hexane and stored at 4 °C for 1 h. The solid was collected by filtration under dry nitrogen atmosphere and washed with hexane. The crude reaction product was then recrystallized twice with absolute THF/hexane. 6.52 g of purified reaction product (23.9 mmol; 68% yield; colorless needles) were transferred into a Schlenk tube and stored at -80 °C. Melting point: 138.3 °C (Lit. 134 - 137° C).[432, 435]
^{1}H-NMR (400 MHz, DMSO-d_6): δ [ppm] = 9.07 (1H, s, -**NH**-CO-O-CO-), 6.95-6.34 (1H, br, -**NH**-CO-O-C(CH_3)$_3$), 4.42 (1H, t, $^3J_{H,H}$ = 6.35 Hz, -CO-**CH**-CH2-), 2.90 (2H, q, $^3J_{H,H}$ = 6.03 Hz, -**CH_2**-NH-CO-O-C(CH_3)$_3$), 1.79-1.56 (2H, m, -CH-**CH_2**-CH_2-CH_2-CH_2-NH-), 1.45-1.12 (13 H, m, -CH-CH_2-**CH_2-CH_2**-CH_2-NH- and -NH-CO-O-C(**CH_3**)$_3$).

12.3.3.2 *Synthesis of N-ε-Trifluoroacetyl-L-Lysine N-Carboxyanhydride*

12.5 g (51.6 mmol) of *N*-ε-trifluoroacetyl protected lysine and 300 mL of absolute THF were added into a three necked flask equipped with a reflux condenser and a septum under a steady flow of dry nitrogen. The condenser outlet was connected to two gas washing bottles filled with aqueous NaOH, removing excess HCl and phosgene. Then, 5.50 mL (45.6 mmol) of diphosgene were added slowly via syringe and the nitrogen stream was reduced. The colorless suspension was mildly refluxed for 2 h, yielding a cloudy solution. After this, a steady flow of dry nitrogen was lead through the solution overnight. The solution was filtered under dry nitrogen atmosphere. The solvent was evaporated under

reduced pressure and absolute THF was added to completely dissolve the crude reaction product. Excess absolute hexane was added to the solution. After 1 h storage at 4 °C, the solid was collected by filtration under dry nitrogen atmosphere and washed with hexane. The crude product was recrystallized twice with absolute THF/Hexane. 10.43 g of the purified product (39,0 mmol; 75% yield; colorless needles, melting point: 101 °C (lit: 92 - 93 °C)[376]) were obtained and stored in a Schlenk tube at -80 °C.
^{1}H-NMR (300 MHz, DMSO-d_6): δ [ppm] = 9.40 (1H, s, -**NH**-CO-CF_3), 9.09 (1H, s, -**NH**-CO-O-CO-), 4.43 (1H, t, ^3J H,H = 6.3 Hz, -CO-**CH**-CH_2-), 3.17 (2H, q, ^3J H,H = 6.3 Hz, -**CH_2**-NH-), 1.79-1.61 (2H, m, -C_H-**CH_2**-CH_2-CH_2-CH_2-NH-), 1.53-1.46 (2H, quin, $^3J_{H,H}$ = 7.13 Hz, -CH-CH_2-CH_2-**CH2**-CH_2-NH-), 1.42-1.24 (2H, m, -CH-CH_2-**CH_2**-CH_2-CH_2-NH-).

12.3.3.3 *Synthesis of Sarcosine N-Carboxyanhydride*

The Synthesis of sarcosine NCA was adapted from literature and modified.[121] 14.92 g (167.4 mmol) of sarcosine were weighed into a three neck flask and dried in vacuo for 1 h. 300 mL of absolute THF were added under a steady flow of dry nitrogen and 16.2 mL (134 mmol) of diphosgene were added slowly via syringe and the nitrogen stream was reduced. The colorless suspension was mildly refluxed for 3 h yielding a clear solution. Overnight, a steady flow of dry nitrogen was lead through the solution into two gas washing bottles filled with aqueous NaOH solution. The solvent was evaporated under reduced pressure, yielding a brownish oil as crude reaction product. The oil was heated to 50 °C and dried under reduced pressure (20 mbar, then $<10^{-2}$ mbar for 2 h) to obtain an amorphous solid, free of phosgene and HCl. The crude product was redissolved in 40 mL of absoute THF and precipitated with 300 mL of dry hexane. The solution was cooled to -18 °C overnight to complete precipitation. The solid was filtered under dry nitrogen atmosphere and dried under a stream of dry nitrogen for 60 - 90 minutes and afterwards in high vacuum for 2 h in a sublimation apparatus. The crude product was sublimated at 80 - 85 °C and $<1\text{x}10^{-2}$ mbar. The product was collected from the sublimation apparatus in a glove box on the same day. The 12.64 g of purified product (110 mmol, 65% yield, colorless crystallites) were stored in a Schlenk tube at -80 °C, only handled in a glove box and used up quickly. Melting point: 102 - 104 °C (lit: 102 - 105 °C).[15, 368]
^{1}H-NMR (300 MHz, $CDCl_3$): δ [ppm] = 4.22 (2H, s, –N(CH_3)-**CH_2**-CO-), 2.86 (3H, s, -CH_3).

12.3.3.4 *Synthesis of Triblock Copolymers*

Triblock copolypept(o)ides were prepared as reported earlier.[158] Under a steady flow of dry nitrogen, 35 eq of lysine(Boc) NCA were transferred into a pre-dried Schlenk tube equipped with a stir bar and dried under high vacuum for 1 h. Then, lysine(Boc) NCA was dissolved in absolute DMF. In a glass vial flooded with nitrogen, 2 eq of neopentylamine were added to 2 mL of dry DMF and mixed. For polymerization initiation, 1 mL of the prepared stock solution was directly added to the Schlenk tube via syringe (yielding a reaction solution with 100 mg/mL monomer concentration). The solution was stirred at 0 °C and kept at a constant pressure of 1.25 bar of dry nitrogen via the Schlenk line to prevent impurities from entering the reaction vessel while allowing CO_2 to escape. Completion of the reaction was confirmed by IR spectroscopy (disappearance of the NCA peaks (1853 and 1786 cm^{-1})). After completion of the reaction, 35 eq of lysine(TFA) NCA were dissolved in absolute DMF (at a concentration of 100 mg/mL) and added to the homopolymer via syringe. The solution was stirred at 0 °C and kept at a constant pressure of 1.25 bar of dry nitrogen via the Schlenk line. After completion of the reaction (IR spectroscopy), 300 eq sarcosine NCA were dissolved in absolute DMF (at a concentration of 100 mg/mL) and added to the diblock copolymer via syringe. Again, the solution was stirred at 0 °C and

kept at a constant pressure of 1.25 bar of dry nitrogen via the Schlenk line. Completion of the reaction was confirmed by IR spectroscopy. For end group capping and functionalization with azide or alkyne groups, 3 eq *N,N*-diisopropylethylamine (with respect to terminal amine of polymer) and 3 eq of either γ-azido butyric acid pentafluorophenyl ester or alkyne-PEG_3-NHS ester were added to the polymer solution after completion of the polymerization reaction. Following 72 h of stirring at room temperature, the final triblock copolymer was precipitated in ether and centrifuged (4500 rpm at 4 °C for 15 min). After discarding the liquid fraction, fresh ether was added and the polymer was resuspended using a sonic bath. The suspension was centrifuged again and the procedure was repeated. After DMF was removed by the resuspension steps, the polymer was dissolved in 20% methanol/Millipore water and lyophilized to obtain a fluffy, colorless powder.
^{1}H-NMR of $PLys(Boc)_{35}$-b-$PLys(TFA)_{40}$-$PSar_{276}$ (400 MHz, DMSO-d_6): δ [ppm] = 9.47-9.22 (40H (1n), br, -N_εH-CO-CF_3), 8.36-8.03 (br, -CO-$C_\alpha H_2$-**NH**-), 7.01-6.14 (35H (1m), br, -**N_εH**-CO-O-C$(CH_3)_3$), 4.68-3.57 (626H (1n + 1m + 2p), br, -CO-**CH**-NH- and -NCH_3-**CH_2**-CO-), 3.18-2.60 (1514H (2n + 2m + 3p), br, -**CH_2**-N_εH-CO-CF_3 and -**CH_2**-NεH-CO-O-C$(CH_3)_3$ and -NCH_3-), 2.07-0.96 (604H (6(n + m) + 9m), br, -CH-**CH_2-CH_2-CH_2**-CH_2-N_εH- and -NH-CO-O-C(**CH_3**$)_3$), 0.84 (9H, br, -CH2-C(**CH_3**$)_3$).

12.3.3.5 *Deprotection of the PLys(TFA) Block*

In a round-bottom flask, the polymer was dissolved in MeOH at a concentration of 30-50 mg/mL and 20 eq of hydrazine hydrate (with regard to the (TFA)-group) were added with an Eppendorf pipette. The solution was stirred for 72 h. Afterwards, the solution was diluted with Millipore water and dialyzed with a Spectra/Por (Roth) membrane with a nominal molecular weight cut-off (NMWCO) of 3500 g/mol for 3-5 days with regular substitution of water and then lyophilized to yield the deprotected polymer as a fluffy, colorless powder.
^{1}H-NMR of $PLys(Boc)_{35}$-b-$PLys_{40}$-$PSar_{276}$ (400 MHz, DMSO-d_6): δ [ppm] = 8.88-7.59 (br, -CO-$C_\alpha H_2$-**NH**-), 6.92-6.23 ((1m), br, -**N_εH**-CO-O-C$(CH_3)_3$), 4.87-3.65 ((1n + 1m + 2p), br, -CO-**CH**-NH- and -NCH_3-**CH_2**-CO-), 3.09-2.63 ((2n + 2m + 3p), br, -**CH_2**-$N_\varepsilon H_2$ and -**CH_2**-N_εH-CO-O-C$(CH_3)_3$ and -NCH_3-), 2.12-0.93 ((6(n + m) + 9m), br, -CH-**CH_2-CH_2-CH_2**-CH_2-N_εH- and -NH-CO-O-C(**CH_3**$)_3$), 0.84 (9H, br,-CH2-C(**CH_3**$)_3$).

12.3.3.6 *Modification with SPDP and Deprotection of the PLys(Boc) Block*

35.6 mg of polymer and 12.4 mg of SPDP (1.25 eq with respect to ε-NH_2 groups) were weighed into a round-bottom flask and immediately dried under high vacuum for 30 minutes. Subsequently, the flask was flushed with argon and the solids dissolved in 1mL of absolute DMF. The solution was stirred at room temperature for 72 h. Afterwards, the polymer was precipitated in ether and centrifuged. The remaining pellet was in dissolved in 50% TFA/H_2O to remove the Boc protecting groups. The solution was stirred for 18 h at room temperature, diluted with Millipore water and dialyzed with a Spectra/Por (Roth) membrane with a nominal molecular weight cut-off (NMWCO) of 3500 g/mol for three days with regular substitution of water (containing 10^{-4} vol% acetic acid). Eventually, the solution was lyophilized to yield the functionalized polymer as a fluffy, colorless powder.
^{1}H-NMR of $PLys_{35}$-b-$PLys(PDP)_{40}$-$PSar_{276}$ (400 MHz, DMSO-d_6): δ [ppm] = 8.51-8.32 (20H (1q), br, -N=**CH**-CH=), 8.31-7.88 (br, -CO-$C_\alpha H_2$-**NH**- and -**N_εH**-CO-CH_2-CH_2-S-S-), 7.87-7.59 (44H (2q), br, -S-S-C=**CH-CH**=), 7.34-7.02 (21H (1q), br, -N=CH-**CH**=), 4.84-3.21 ((1n + 1m + 2p), br, -CO-**CH**-NH- and –NCH_3-**CH_2**-CO- and H_2O), 3.21-2.59 ((2n + 2m + 3p + 4q), br, -**CH_2**-N_εH-CO-**CH_2-CH_2**-S-S- and -**CH_2**-$N_\varepsilon H_2$ and -NCH_3-), 2.22-0.92 ((6(n + m)), br, -CH-**CH_2-CH_2-CH_2**-CH_2-N_εH-), 0.84 (9H, br, -CH_2-C(**CH_3**$)_3$).

12.3.3.7 *Functionalization of Polymers with Mannose/Trimannose*

The protocol for click reaction was partially adopted from Turner *et al.*[521] 15 mg of polymer (1 eq), 2 eq of azide-linked mannose or trimannose (synthesized and kindly provided by Jens Langhanki) and 0.1 eq CuI were weighed into a Schlenk tube and dissolved in freeze-pumped, dry DMSO under argon atmosphere. After 24 h of stirring at 40 °C, the polymer was dialyzed with a Spectra/Por (Roth) membrane with a nominal molecular weight cut-off (NMWCO) of 1000 g/mol for 3 - 5 days with regular substitution of water (containing 10^{-4} vol% acetic acid). After liophilization, a fluffy, colorless powder was obtained. Fig. 12.8 shows the ^{1}H-NMR spectrum of mannosylated PSar as model polymer.
^{1}H-NMR of Mannose-PSar$_{200}$ (400 MHz, D_2O): δ [ppm] = 7.96 (0.51H, s, triazole-H), 6.00 (0.37H, s, α-H of mannose), 4.16-3.93 (200H, br, -NCH_3-**CH_2**-CO-), 3.56-3.52 (3.40H, dd, mannose-H), 3.47-3.43 (3.31H, dd, mannose-H), 3.22-2.49 (316 H, br, -NCH_3-).

12.3.3.8 *Preparation of NLS-9-aminoacridine Conjugate (NLS-9AA)*

a) synthesis of 1-(2-(acridin-9-ylamino)ethyl)-1*h*-pyrrole-2,5-dione 128 mg (0.599 mmol) of 9-Chloroacridine and 84 mg (0.599 mmol) of 1-(aminoethyl)maleimid were weighed into a round bottom flask and dissolved in 2 ml of dry DMF. After 24 h of stirring at room temperature, the precipitate was collected by filtration and washed with DMF. The crude product was dissolved in water and non-converted educts were extracted with toluol using a separating funnel. After liophi-lization, 120 mg of the final product were obtained as yellow solid.
^{1}H-NMR of 1-(2-(acridin-9-ylamino)ethyl)-1*H*-pyrrole-2,5-dione (400 MHz, D_2O): δ [ppm] = 7.85 (2H, d, $^3J_{H-H}$ = 9 Hz, Ar-H), 7.69 (2H, t, J = 8 Hz, Ar-H), 7.31 (4H, $^3J_{H-H}$ = 8 Hz, Ar-H), 6.53 (2H, s, -CO-**CH=CH**-CO-), 3.96 (2H, t, $^3J_{H-H}$ = 5 Hz, -NH-CH_2-**CH_2**-N-$(CO)_2$), 3.83 (1H, t, $^3J_{H-H}$ = 5 Hz, -NH_2^+-CH_2-**CH_2**-N-$(CO)_2$), 3.69 (2H, t, $^3J_{H-H}$ = 5 Hz, -NH-**CH_2**-), 3.18 (1H, t, $^3J_{H-H}$ = 5 Hz, -NH_2^+-**CH_2**-).

b) conjugation with nls sequence The SV40 large T cell antigen NLS sequence, modified with a glycine spacer and a terminal cysteine (amino acid sequence: PKKKRKVGGGGGGGC) was linked to the intercalator 1-(2-(Acridin-9-ylamino)ethyl)-1*H*-pyrrole-2,5-dione via thiol maleimide reaction. 3.4 mg ($1.08 \cdot 10^{-5}$ mol) of the intercalator, 5 mg ($3.61 \cdot 10^{-6}$ mol) of peptide and 31.2 mg ($1.09 \cdot 10^{-4}$ mol) of TCEP were weighed into a round bottom flask and dissolved in degassed PBS. After 72 h of stirring at room temperature, the crude product was purified with HPLC (gradient: 100% acetonitrile to 100% water over 60 min). Lyophilization yielded 3.1 mg of NLS-9AA as fluffy, yellow powder.

12.3.3.9 *Formation of PeptoPlexes (optimized protocol)*

The SPDP-modified polymer was dissolved in sterile water (with 0.2 vol% acetic acid) to obtain a stock solution with a final concentration of 4 mg/mL. CLAH4-L1C and C5HTat5HC peptides were dissolved in degassed, sterile water (with 0.2 vol% acetic acid) at a concentration of 10 mg/mL. NLS-9AA was dissolved in sterile water at a concentration of 2 µg/mL.

Polyplex formation and cross-linking protocol was adjusted by varying different parameters (SI, Fig. 12.11) resulting in the following optimized procedure: As first step of polyplex formation, pDNA was loaded with NLS-9AA by diluting the former in sterile water and adding the latter while vortexing for 10 seconds (14 NLS molecules per plasmid, c(NLS-9AA) = 0.4 µM). After 20 minutes of incubation at room temperature, CLAH4-L1C or C5HTat5HC were added to the pDNA (at amounts to saturate 50-100% of SPDP groups in the final polyplex) while vortexing for 10 seconds. After 10 minutes of incubation at room temperature, triblock copolypept(o)ide was added to the mixture at N/P 4 while vortexing for 10 seconds. The polyplex solution was incubated for 30 minutes at room temperature before addition of 10x PBS to obtain a final 1x PBS solution. In case of functionalization with aDEC205 (see Section 14.1), DBCO-modified antibody dissolved in PBS (kindly provided by Meike Schinnerer) was added to the final polyplex solution. The cross-linking (and click) reaction were carried out for another 18 h under constant shaking at room temperature. Final concentration of polyplex solutions with respect to pDNA was kept at 0.03-0.05 mg/ml.

Polyplex solutions of pDNA and LAH4-L1 were prepared at a weight ratio of 1:10 by simply mixing both components while vortexing. Polyplex solutions of jetPEI (Polyplus-transfection, Strasbourg, France) and pDNA were prepared according to manufacturer's protocol using 1.5 µl of stock solution per 1 µg of DNA.

12.3.4 Methods and Protocols - Physicochemical Characterization of PeptoPlexes

12.3.4.1 *Characterization of Polyplexes by Gel Electrophoresis*

Gel electrophoresis was performed to confirm association of pDNA and NLS-9AA. For this, 500 ng of pDNA were loaded with $2.22 \cdot 10^{-9}$ mol NLS-9AA as indicated below or left untreated. Samples were loaded into slots of 0.7% agarose gels and electrophoresis was run at 90 mV. For the untreated sample, ethidium bromide was used for staining.

12.3.4.2 *Characterization of Polyplexes by Dynamic Light Scattering*

Single-angle dynamic light scattering measurements were performed at 25 °C using a Malvern Zetasizer NanoZS with a 633 nm He/Ne Laser at a fixed scattering angle of 173°. Polyplex solutions were prepared with 2 µg pDNA at N/P 4 according to indicated protocols and diluted to a final volume of 300 µl in 1x PBS before measurement.

For multi-angle DLS and serum DLS, solutions of cross-linked polyplexes with 5 µg pDNA at N/P 4 were prepared and subsequently diluted to a final volume of 1.5 mL in 1x PBS. Cylindrical quartz cuvettes (Hellma, Mühlheim, Germany) were cleaned by dust-free distilled acetone and transferred into a dust-free flow box. Polyplex solutions were filtered into these cuvettes through Millex GHP filters, 0.45 µm poresize (Millipore). Then, dynamic light scattering (DLS) measurements were performed on a HeNe Laser (25 mW output power at = 632.8 nm) and on an ALV-CGS 8F SLS/DLS 5022F goniometer with eight simultaneously working ALV 7004 correlators and eight QEAPD avalanche photodiode detectors. The correlation functions of the particles were fitted using a sum of two exponentials from which the initial slope, i.e. the first cumulant Γ, was calculated. The z-average diffusion coefficient D_z was calculated by extrapolating Γ/q^2 for q = 0. By formal application of Stokes law, the inverse z-average hydrodynamic radius is $R_h = \langle 1/R_h \rangle_{z^{-1}}$.

To investigate the aggregation behavior of **L-CPX** in human plasma, EDTA-plasma pooled from 6 donors was used. The following mix-tures were prepared:

1. plasma: PBS 9:1
2. PBS: **L-CPX** solution (c = 0.092 mg/mL) 9:1
3. plasma: **L-CPX** solution (c = 0.092 mg/mL) 9:1

The plasma was filtered through a Millex GS 0.22 µm filter and PBS was filtered through a Pall GHP 0.2 m filter. The cuvettes were incubated for 20 min at room temperature before measurement.

If there is no aggregate formation, the determined autocorrelation function of solutions 3 and 5 ($g_1(t)_{mix}$) should be well-fitted by the weighted sum of the fit functions of the autocorrelation functions of the two single components (equation 12.1). In order to fit the plasma autocorrelation function (ACF) three exponentials are needed, reflecting the large size differences of the plasma proteins, whereas for **NCPX** and **CPX** a sum of two exponentials are needed.

$$g_1(t)_{mix} = a_P \cdot g_1(t)_P + a_S \cdot g_1(t)_s \tag{12.1}$$

$g_1(t)_P$ = fit function that describes the measured ACF of the particles in buffer
$g_1(t)_S$ = fit function that describes the measured ACF of the plasma in buffer
a_i = amplitudes
The only variable fit parameters of the correlation function fit of the mixture are the amplitudes a_i whereas all other parameters were kept constant to the values obtained by the fit of the ACF of plasma and particles, respectively. In the case of aggregate formation, a third fit function ($g_1(t)_a$) needs to be added to adequately fit the autocorrelation function of the mixture equation 12.2.

$$g_1(t)_{mix} = a_P \cdot g_1(t)_P + a_S \cdot g_1(t)_s + a_A \cdot g_1(t)_A \tag{12.2}$$

12.3.4.3 *Characterization of Polyplexes by Cryogenic Transmission Electron Microscopy*

5 µL of polyplex solution (prepared with 0.5 µg pDNA at N/P 4, cross-linked with CLAH4-L1C) in 1x PBS were applied to freshly glow-discharged carbon grids with a copper 200 mesh (Quantfoil Micro Tools GmbH). Excess fluid was removed by direct blotting (2.5 s) and the grids were individually plunge-frozen in liquid ethane. Grids were cryotransferred in liquid nitrogen using a Gatan cryoholder (model 626 DH) to a Technai T12 transmission electron microscope equipped with a field emission electron source and operating at 120 kV accelerating voltage. Images were recorded using a TemCam-F416 (TVIPS, Gauting, Germany).

12.3.5 Methods and Protocols - Biological Characterization of PeptoPlexes

12.3.5.1 *Cell Culture*

HEK 293T cells were grown in DMEM, supplemented with 10% FBS, 4 mM L-glutamine, 0.1 µM 2-mercaptoethanol, 100 units x mL^{-1} penicillin, and 100 µg x mL^{-1} streptomycin. Cells were maintained in a 37 °C humidified atmosphere with 5% CO_2 and were handled under sterile conditions.

Cells of the mouse DC model cell line DC2.4[421] were grown in IMDM, supplemented with 5% FBS, 2mM L-glutamine, 100 IU x mL^{-1} penicillin, 100 µg x mL^{-1} streptomycin and 50 µM β-mercaptoethanol. Cells were maintained in a 37 °C humidified atmosphere with 10% CO_2 and were handled under sterile conditions.

Bone marrow-derived DCs (BMDCs) were differentiated from bone marrow progenitors of C57BL/6 mice as first described by Scheicher *et al.*[422] and modified by Gisch and co-workers.[423] DC culture medium (IMDM with 5 Vol.% FCS [PAA, Cölbe, Germany], 2 mM L-glutamine [Biochrom AG, Berlin, Germany], 100 U/mL penicillin, 100 µg/mL streptomycin [Gibco, Paisly, UK]) and 50 µM β-mercaptoethanol [Roth, Karlsruhe, Germany], supplemented with 5% of GM-CSF containing cell culture supernatant [Zal *et al.*, 1994,[424] a kind gift by Dr. B. Stockinger, MRC National Institute for Medical Research, Mill Hill, London]) was replenished on days 3 and 6 of culture. BM cells were seeded on 100 mm^2 bacterial dishes (2 x 10^6 cells/10 ml) and cultivated at 37 °C, 10% CO_2 atmosphere. Aliquots of non-adherent and loosely adherent immature BMDCs were harvested on days 6 or 7 of culture and were reseeded (10^6 cells/ml) on wells of six well tissue-culture plates (StarLab, Hamburg, Germany).

12.3.5.2 *Determination of PeptoPlexes Uptake by Flow Cytometry*

BMDCs were cultured in 12 well plates (2 x 10^5 progenitor cells per well) for 7 days in presence of GM-CSF. TETA cross-linked (mannosylated) polyplexes formed at N/P 8 with 1 µg Cy5-labeled pDNA (pCMV_GFP_2A_click_beetle_luciferase plasmid DNA construct; DKFZ, Heidelberg, Germany) per well were added to the cells, followed by 4 h of incubation. Cells were harvested, washed with PBS and incubated with anti-mouse CD11c PE (clone N418, eBiosciece, San Diego, CA) to stain the cell membrane of BMDCs. Cells were washed with PBS to remove excess dye. Samples were analyzed by flow cytometry for frequencies of Cy5 positive cells.

12.3.5.3 *Determination of Transfection Efficiency of PeptoPlexes in DC 2.4 Cells or BMDCs by Luciferase Activity*

DC 2.4 cells were seeded onto 96 well culture plates (10^4 cells in 100 µL per well) 24 h prior to transfection. BMDCs were seeded onto 96 well plates (2,5 x 10^5 progenitor cells in 100 µL per well) 24 h prior to transfection. Polyplexes formed with 0.3 µg pDNA (pCMV_GFP_2A_click_beetle_luciferase plasmid DNA construct (p1699); DKFZ, Heidelberg, Germany) per well were added to the cells in triplicates, respectively. Medium was changed 24 h post transfection. After incubation for 48 h, cells were lysed in Passive Lysis Buffer (PLB; Promega, Madison, CA) and luciferase activity was determined.

12.3.5.4 *Determination of Cellular Toxicity of PeptoPlexes in HEK 293T Cells by MTT Assay*

Cytotoxicity of polyplexes was assessed by MTT assay using the "CellTiter 96® Non-Radioactive Cell Proliferation Assay" kit (Promega, Madison, USA) according to manufacturer's protocol. HEK 293T cells were seeded onto 96-well culture plates in triplicates (10^4 cells in 100 µL per well) 24 h prior to transfection. **L-CPX** formed with 0.3 µg pDNA (pCMV_GFP_2A_click_beetle_luciferase plasmid DNA construct; DKFZ, Heidelberg, Germany) per well were added to the cells in triplicates, respectively. 24 h post transfection 20 µl of MTT substrate solution were added to each well, and cells were incubated for another 2 h. Subsequently, 100 µL of mixed solubilization/stop solution were added to each well. After 1 h, the absorbance at 570 nm was measured.

12.3.5.5 *Determination of Complement Activation of PeptoPlexes by C5a ELISA*

166.7 µl of human serum were incubated for 1 h at 37 °C with 33.3 µl of polyplex solution formed with 1 µg pDNA (pCMV_GFP_2A_click_beetle_luciferase plasmid DNA construct; DKFZ, Heidelberg, Germany). ELISA to determine levels of human complement factor C5a after incubation was conducted according to manufacturer's protocol.

12.3.5.6 *Analysis of Cellular Uptake by Confocal Laser Scanning Microscopy*

BMDCs were cultured in 12 well plates (2 x 10^5 progenitor cells in 1 mL per well) for 7 days in presence of GM-CSF. CLAH4-L1C cross-linked polyplexes formed at N/P 4 with 1 µg Cy5-labeled pDNA (pCMV_GFP_2A_click_beetle_luciferase plasmid DNA construct; DKFZ, Heidelberg, Germany) per well were added to the cells, followed by 4 h of incubation. Cells were washed and incubated with Hoechst 33258 (Sigma-Aldrich, Deisenhofen, Germany) to stain cell nuclei and anti-mouse CD11c PE (clone N418, eBiosciece, San Diego, CA) to stain the cell membrane of BMDC. Cells were washed to remove access dye. Samples were measured using a TCS SP5 instrument (Leica, Wetzlar, Germany) and analysed using IMAGEJ software (1.490, NIH Bethesda, MD).

12.3.5.7 *Isolation of OT-I T Cells from Murine Spleen*

Spleens of OT-I mice were sterically removed and ground through a 40 µm cell-strainer. Cells were then lysed with Gey's solution to remove erythrocytes. After washing with EMEM supplemented with 2% FBS, 100 IU x mL^{-1} penicillin and 100 µg x mL^{-1} streptomycin cells were taken up in IMDM supplemented with 5% FBS, 2 mM L-glutamine, 50 µM β-mercaptoethanol, 100 IU x mL^{-1} penicillin and 100 µg x mL^{-1} streptomycin.

12.3.5.8 *Functional Testing of Transfection Efficiency by T Cell Proliferation Assay*

BMDCs were cultured in 12 well plates (2 x 105 progenitor cells in 1 mL per well) for 7 days in presence of GM-CSF. Polyplexes formed with 3 µg pDNA (sOVA plasmid) per well were added to the cells. Medium was changed 8 h after transfection and cells were cultured for another 40 h. Cells were partially stimulated with 100 ng/mL LPS overnight and medium was changed. After repeated washing of the cells, OT-I T cells were added at a concentration of $5x10^5$ cells in 100 µl. T cells were incubated with BMDCs for 72 h, then 0,75 µCi of tritium marked thymidine were added per well. After further cultivation for 18 h, cell proliferatin was assessed using Microbeta TriLux (PerkinElmer, Waltham, MA, USA).

12.4 SUPPORTING INFORMATION

12.4.1 Polymer Synthesis and Characterization

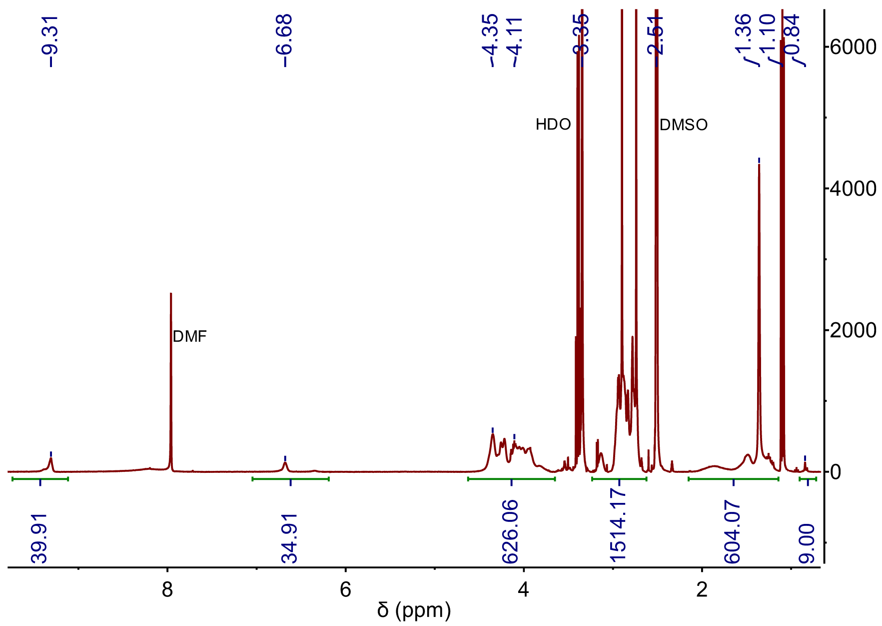

Figure 12.5: ^{1}H-NMR spectrum of protected precursor polymer PLys(Boc)$_{35}$-b-PLys(TFA)$_{40}$-PSar$_{276}$ in DMSO.

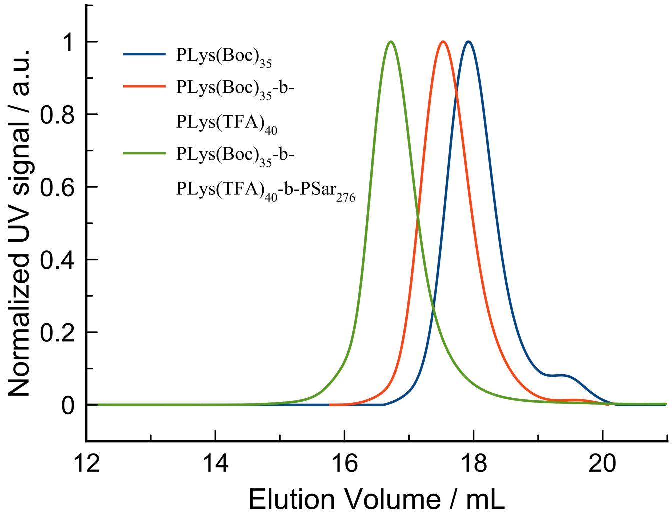

Figure 12.6: HFIP GPC of protected precursor polypept(o)ides showing the transition from homo to triblock copolymers. PDI (GPC) of triblock = 1.19, M_n (GPC) of triblock = 32.3 kgmol^{-1}.

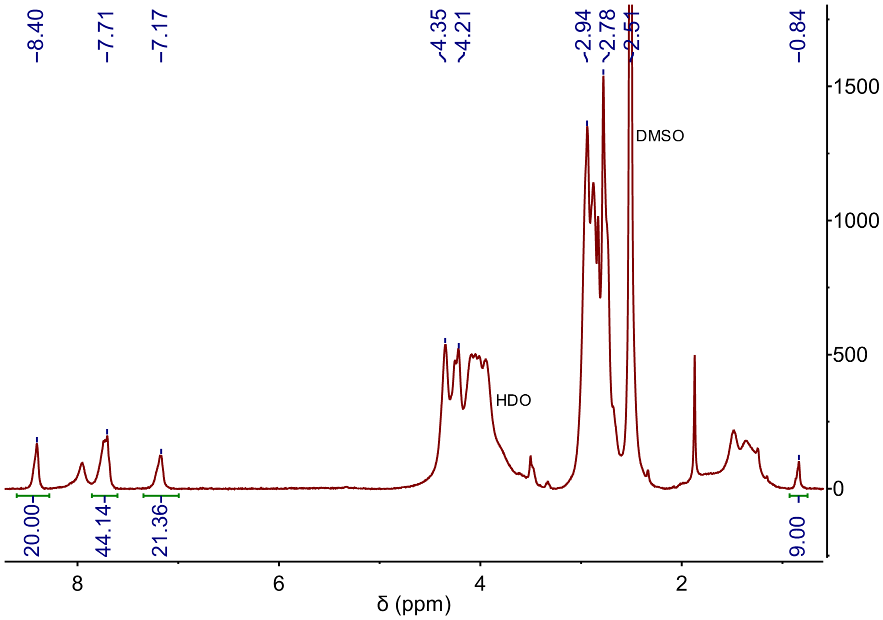

Figure 12.7: ^{1}H-NMR spectrum of $PLys_{35}$-b-$PLys(PDP)_{40}$-$PSar_{276}$ in DMSO.

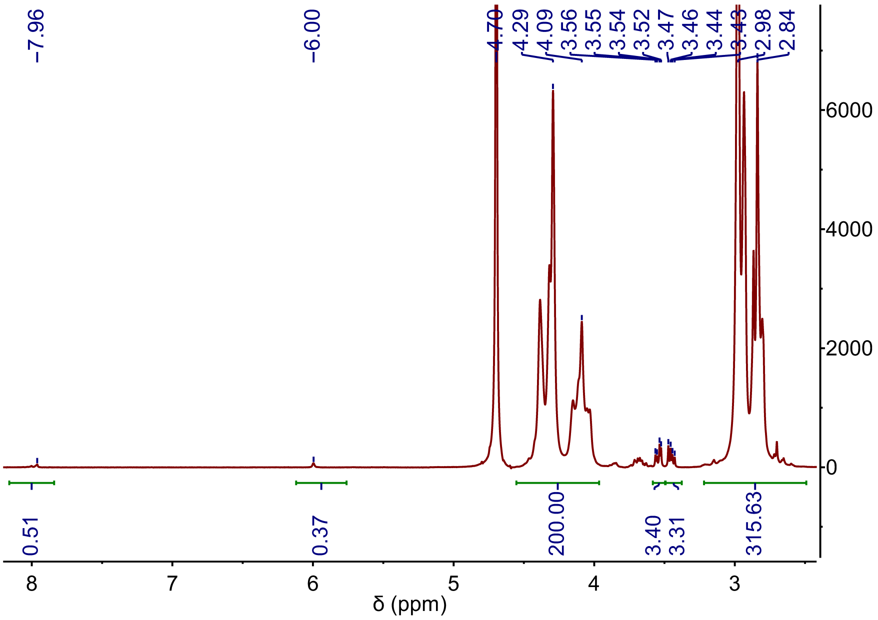

Figure 12.8: ^{1}H-NMR spectrum of Mannose-PSar$_{200}$ in D_2O.

12.4.2 NLS-9AA Synthesis and Characterization

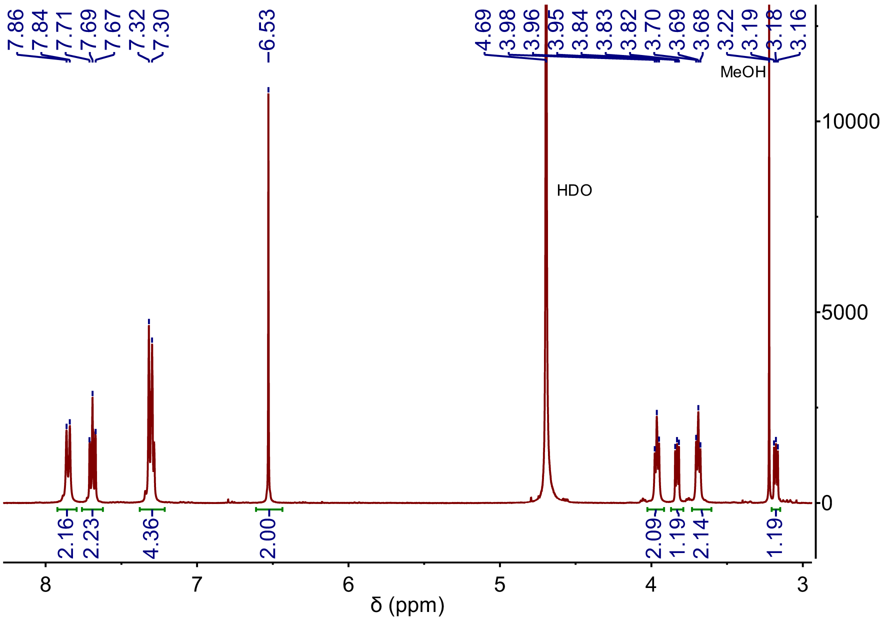

Figure 12.9: ^{1}H-NMR spectrum of 1-(2-(acridin-9-ylamino)ethyl)-1*H*-pyrrole-2,5-dione in D_2O.

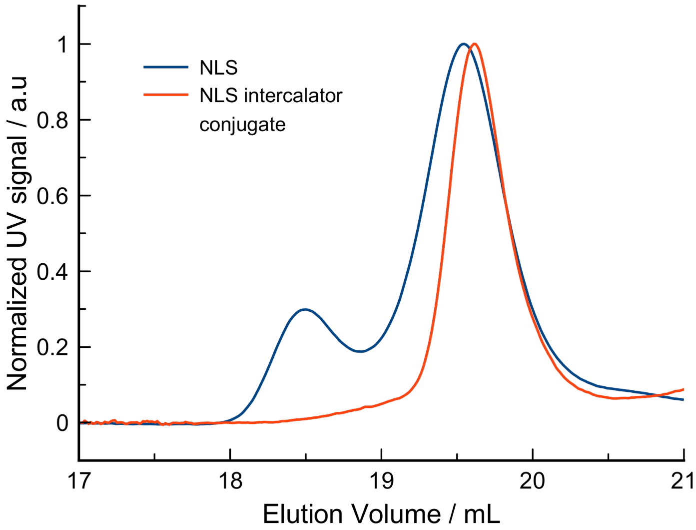

Figure 12.10: HFIP GPC traces showing terminal cysteine containing NLS sequence before (partially oxidized to dimers) and after reaction with 1-(2-(acridin-9-ylamino)ethyl)-1*H*-pyrrole-2,5-dione.

12.4.3 Optimization of Polyplex Formation Protocol

12.4.3.1 *Tested Formulation Protocols*

1. Polyplexes with pDNA and the triblock polypept(o)ide were formed first, CLAH4-L1C was added afterwards. Result: Formation of large polydisperse aggregates, presumably due to impaired pDNA complexation and inter-particle cross-linking.

2. Polyplexes with pDNA and the triblock polypept(o)ide were formed first and partially (50%) cross-linked with TETA (see Chapter 10) to increase stability, CLAH4-L1C was added afterwards. Result: Formation of large polydisperse aggregates, presumably due to impaired pDNA complexation and inter-particle cross-linking.

3. Triblock copolypept(o)ide and CLAH4-L1C were added simultaneously to pDNA in PBS, i.e. complexation and disulfide formation start in parallel. Result: Formation of large polydisperse aggregates (yet slightly smaller than in case 1 and 2), presumably due to impaired pDNA complexation and inter-particle cross-linking.

4. Triblock copolypept(o)ide and CLAH4-L1C were added simultaneously to pDNA in H_2O (0.2 vol% acetic acid), i.e. disulfide formation proceeds slower than in PBS due to acidic pH. After 30 minutes, salt concentration and pH was adjusted to PBS condition by adding the appropiate amount of 10x PBS. Result: Formation of significantly smaller polyplexes with lower dispersity (z-average d = 194.1 nm, PdI = 0.208) than in previous cases.

5. CLAH4-L1C was added first to pDNA in (0.2 vol% acetic acid), polypept(o)ide was added afterwards followed by buffer switch to PBS. Formation of significantly smaller polyplexes (z-average d = 204.3 nm, PdI = 0.117) than in previous cases. Dispersity of polyplexes is significantly smaller compared to case 4.

6. pDNA was loaded with NLS-9AA. CLAH4-L1C was added next, followed by addition of polypept(o)ide and buffer switch to PBS. Result: Formation of smallest polyplexes (z-average d = 204.3 nm, PdI = 0.117).

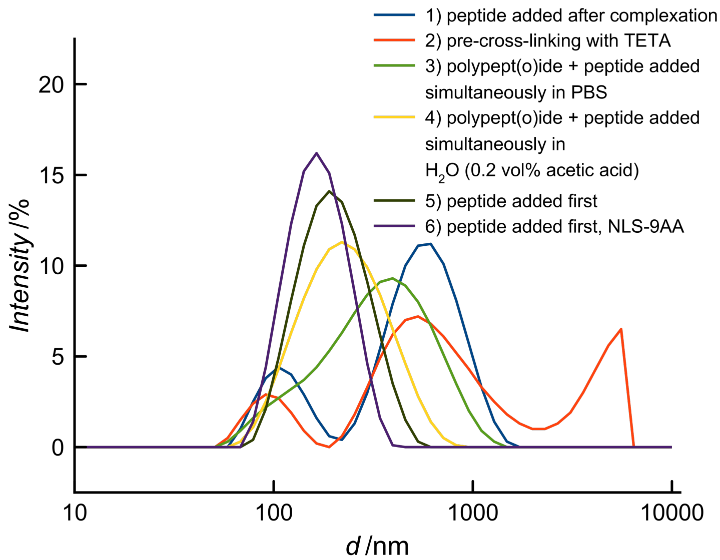

Figure 12.11: Size comparison of polyplexes with incorporated CLAH4-L1C cross-linker resulting from different formulation protocols by single angle DLS.

Conclusion: Protocols 5 or 6, respectively, were adapted for all following preparations of peptide cross-linked polyplexes.

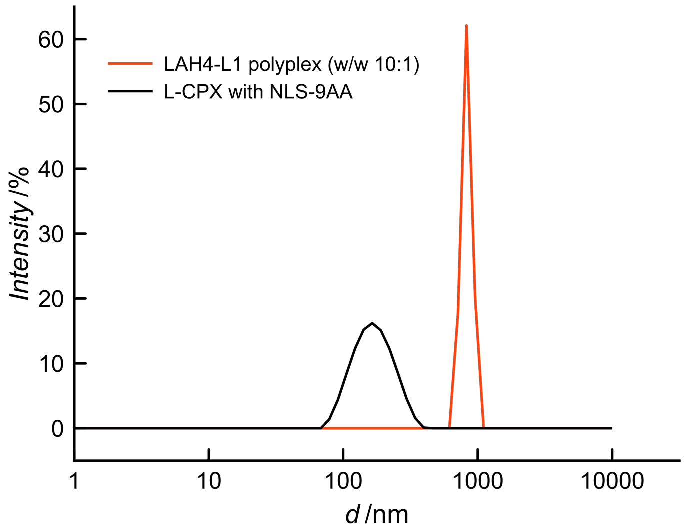

Figure 12.12: Comparison of size of LAH4-L1-based polyplexes (w/w 10:1) and L-CPX with NLS-9AA (optimized formulation protocol) by single angle DLS.

12.4.4 Biological Assays

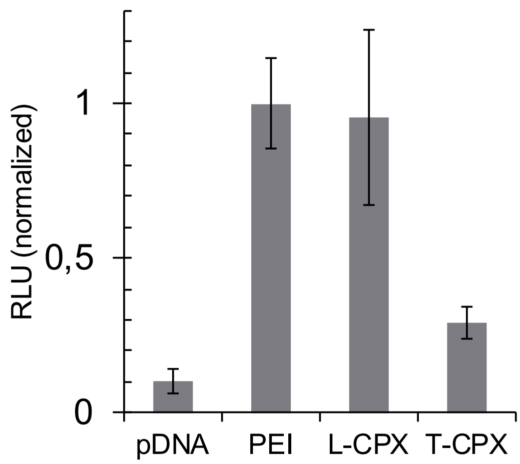

Figure 12.13: Transection efficiency as determined by luciferase assay for **L-CPX** and **T-CPX** in DC2.4 cells compared to jetPEI (data show mean ± sd, n = 3).

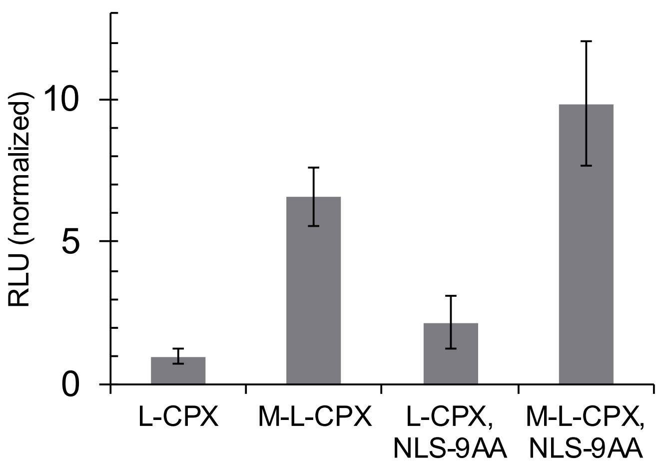

Figure 12.14: Transection efficiency as determined by luciferase assay for **L-CPX** with or without mannose and NLS-9AA in DC2.4 cells (data show mean ± sd, n = 3).

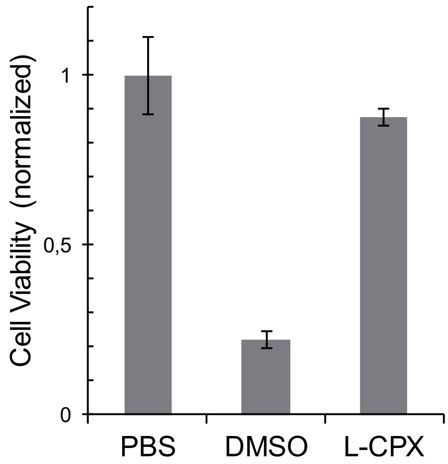

Figure 12.15: Cell viability as determined by MTT assay for **L-CPX** in HEK 293T cells compared to PBS and DMSO controls (data show mean ± sd, n = 3).

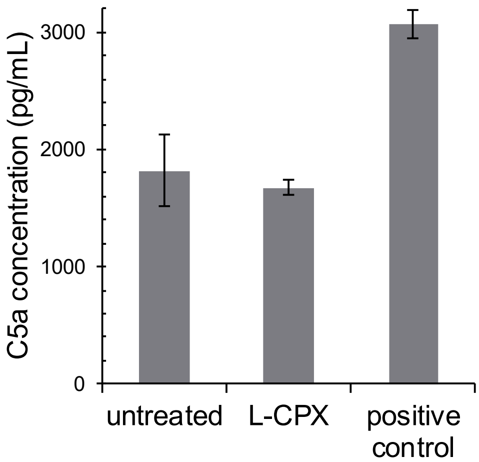

Figure 12.16: C5a concentration in human serum as determined by ELISA for **L-CPX** compared to untreated and positive control (data show mean ± sd, n = 2).

13 PEPTOPLEXES FOR MESSENGER RNA DELIVERY

13.1 INTRODUCTION

Since a few years, *in vitro* transcribed (IVT) mRNA has been rediscovered as a promising class of drugs within the field of nucleic acid therapy. Progress in overcoming intrinsic challenges of therapeutic mRNA, particularly related to stability, translational efficacy and immunogenicity, provide the basis for an array of potential applications, such as vaccination, immunotherapy, replacement of protein-based therapeutics and genome engineering.[522] For instance, just recently BioNTech has managed to translate individualized mRNA-based vaccines against cancer into clinics.[2, 3, 506] In this particular case, administration of mRNA *in vivo* was realized through formulation with different neutral and cationic lipids (lipoplexes). Targeting of antigen-presenting cell populations in the spleen could solely be achieved by varying physicochemical parameters of the lipoplexes, i.e. size and net charge, without the need for specific ligands.[2] The mRNA-lipoplexes developed by BioNTech for mRNA vaccination are between 200 and 400 nm in diameter. However, other potential, more elaborate applications of IVTmRNA, for example *in vivo* lymphocyte activation or reprogramming, will require smaller particles as well as ligand-mediated, active targeting, since these cells exhibit very low endocytose activity, in sharp contrast to antigen-presenting cells.

In this context, a collaboration with BioNTech led to the evaluation of the polypept(o)ides developed in this work as carriers for mRNA delivery. Since the experiments with mRNA only started in the last third of the PhD, the optimized cross-linked formulations with mannose or trimannose as ligands (see Chapters 10 and 12) were already available for this purpose. To establish a first proof of concept, pDNA was replaced with mRNA and targeted as well as non-targeted mRNA-PeptoPlexes were applied for the transfection of dendritic cells.

13.2 RESULTS AND DISCUSSION

In contrast to pDNA, mRNA only has to get into the cytoplasm to exert its biological effects. Hence, the implementation of a NLS sequence for delivery is not required. On the other hand, mRNA has a linear, single-stranded structure providing a smaller and more flexible template for polymer binding than a typical plasmid. Derived polyplexes, which are held together only by electrostatic interaction, should thus be less stable against plasma proteins than comparable pDNA complexes. Overall, RNA is far less robust than DNA and much more susceptible to nuclease attack and premature degradation, which makes additional stabilization of polyplexes, as achievable by disulfide cross-linking, a vital requisite to improve protection of the enclosed cargo. Nevertheless, similar to the protocol for pDNA PeptoPlexes, mRNA PeptoPlexes were formed by simply adding polymers to the mRNA during vortexing (Fig. 13.1).

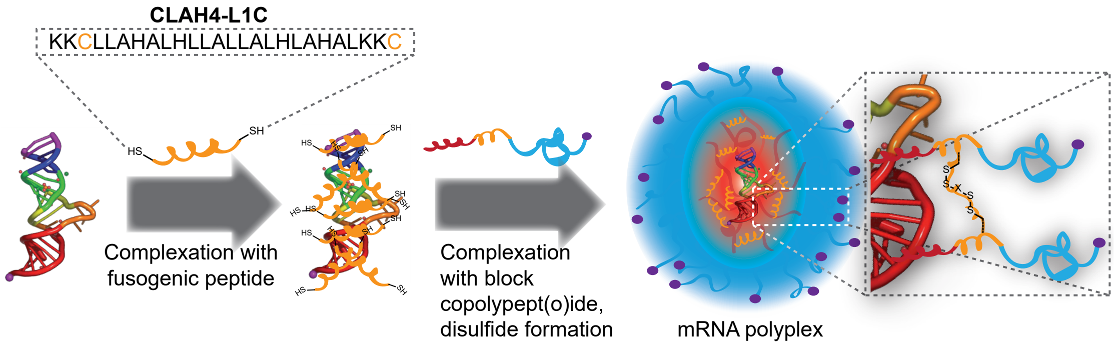

Figure 13.1: Formation of mRNA PeptoPlexes.

Complexation could be achieved with the same polymers as for pDNA (see Chapter 12, Fig. 12.1), while disulfide cross-linking was realized by adding cross-linker before (in case of CLAH4-L1C) or after (in case of TETA) complexation.

Initially, mRNA PeptoPlexes were characterized by gel electrophoresis, dynamic light scattering (DLS) and Cryo-TEM imaging (Fig. 13.2).

In contrast to pDNA, complete retardation of mRNA in agarose gel was already observed at N/P 0.5 (Fig. 13.2 (a)). This is due to the much smaller size and the linear structure of mRNA which favor complexation by a cationic polymer chain. Compared to the pDNA-PeptoPlexes discussed in Chapter 12, mRNA-PeptoPlexes are smaller in diameter, which again is a consequence of the smaller size of mRNA. They are also much smaller than the mRNA-lipoplexes developed by BioNTech (200-400 nm[2]). According to single- and multi-angle DLS, mRNA-PeptoPlexes cross-linked with CLAH4-L1C (**L-CmRPX**) have a hydrodynamic diameter of around 120 nm (Fig 13.2 (b, d)) with a size distribution a bit broader than for comparable pDNA PeptoPlexes. Cryo-TEM imaging revealed spherical structures with a slightly smaller diameter of about 100 nm Fig 13.2 (c)).

Next, TETA cross-linked and non-cross-linked PeptoPlexes were compared for their aggregation behavior in 90% human plasma by means of DLS (Fig. 13.2 (e)). As in the case of pDNA, non-cross-linked PeptoPlexes led to aggregation of plasma proteins, visualized by the incongruence of autocorrelation functions which take (black) or do not take (red) aggregation into account (also see Chapter 4). In contrast, for cross-linked PeptoPlexes both autocorrelation functions are identical indicating absence of aggregates. Results prove, that disulfide cross-linking like for pDNA represents an appropriate strategy to stabilize mRNA PeptoPlexes against interaction with plasma proteins.

Following physicochemical characterization, **L-CmRPX** optionally functionalized with mannose (M) or trimannose (TriM) were evaluated for transfection efficiency and cytotoxicity *in vitro* in BMDCs and human dendritic cells.

In murine BMDCs, transfection efficiency of mannose or trimannose decorated PeptoPlexes, as determined by luciferase assay, was more than doubled compared to the unmodified control, being only slightly beneath PEI level (Fig. 13.3 (a)). In human DCs, we first investigated the effect of serum on transfection efficiency of **L-CmRPX** (Fig. 13.3 (b), left). Despite stabilization by disulfide cross-linking, **L-CmRPX** performed better in serum-free medium (OptiMEM) than in serum supplemented with 10% FCS. As aggregation with serum proteins was ruled out by DLS, other factors like altered cellular uptake levels in presence or absence of serum proteins might be an explanation. However, one should note that **L-CmRPX**-mediated transfection of BMDCs, even when performed in full medium, was significantly higher than that of PEI in serum-free medium, underlining the efficacy of CLAH4-L1C cross-linked PeptoPlexes. With respect to effects of (tri)mannose modification on transfection efficiency of polyplexes, in human BMDCs the same discrepancy

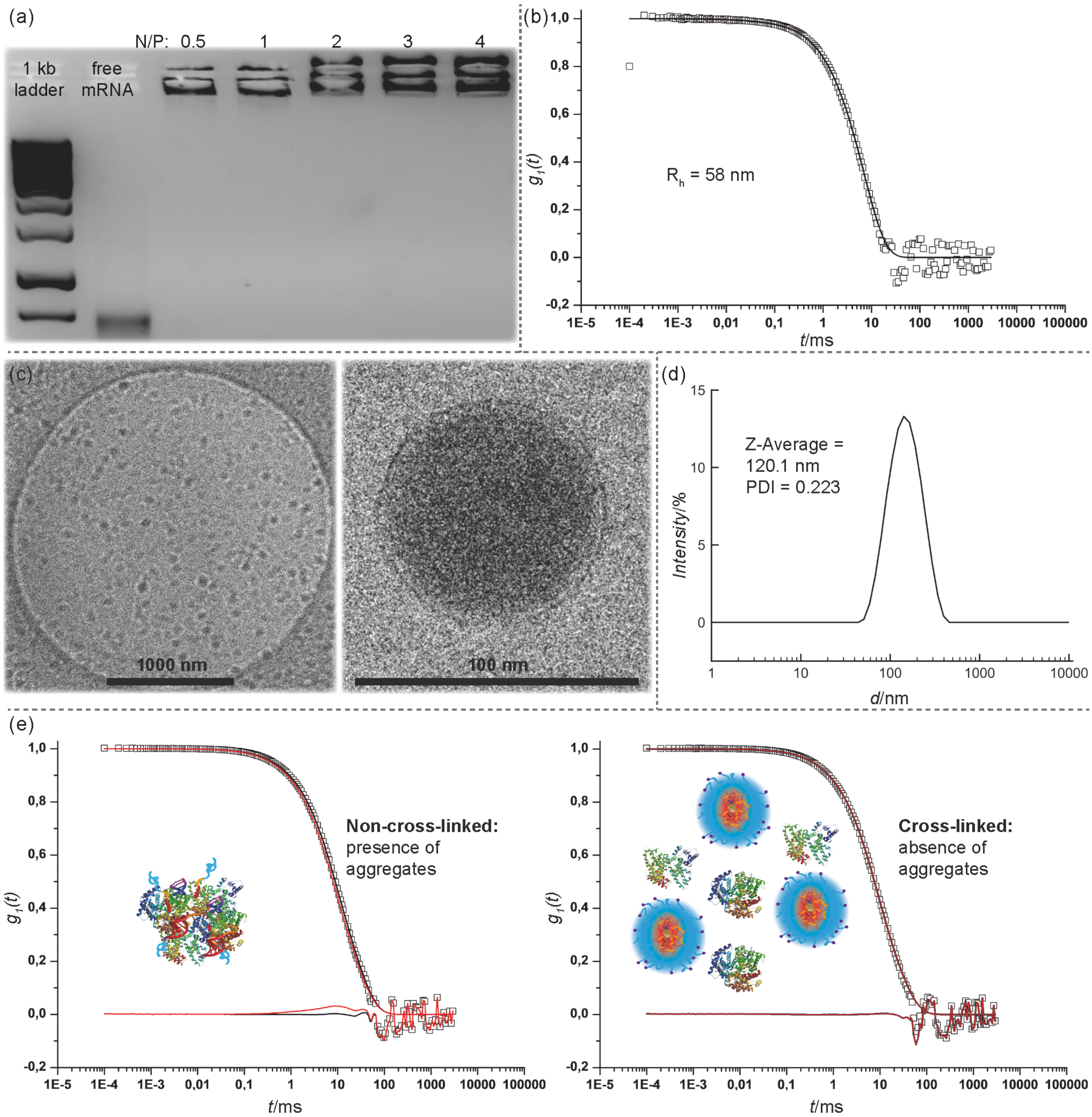

Figure 13.2: Physicochemical characterization of mRNA polyplexes. (a) Gel electrophoresis with free mRNA and polyplexes formed at various N/P ratios. (b) Autocorrelation function from multi-angle DLS. (c) CryoTEM imaging in overview (left) and close-up (right). (d) Size distribution as determined by single-angle DLS. (e) Left: DLS of non-cross-linked polyplexes in 90% human plasma showing presence of aggregates as indicated by incongruence of autocorrelation functions which take (black) or do not take (red) aggregation into account. Right: DLS of cross-linked polyplexes in 90% human plasma showing absence of aggregates, as indicated by congruence of both autocorrelation functions.

as in murine BMDCs between **L-CmRPX** on the one hand and **M-L-CmRPX** and **TriM-L-CmRPX** on the other was observed. But additionally, trimannose compared favorably with mannose (Fig. 13.3 (b)) with **TriM-L-CmRPX** being three times more efficient than **L-CmRPX**. Considering possible cytotoxicity, no negative effects of L-CmRPX on cell viability were observed at concentrations relevant for transfection (Fig. 13.3 (c)). PEI also showed no detectable cytotoxicity. Yet, it has to be considered that PEI polyplexes were applied in a 5-times lower concentration with respect to the amount of mRNA than **L-CmRPX**, as cytotoxicity of PEI does not allow higher concentrations.

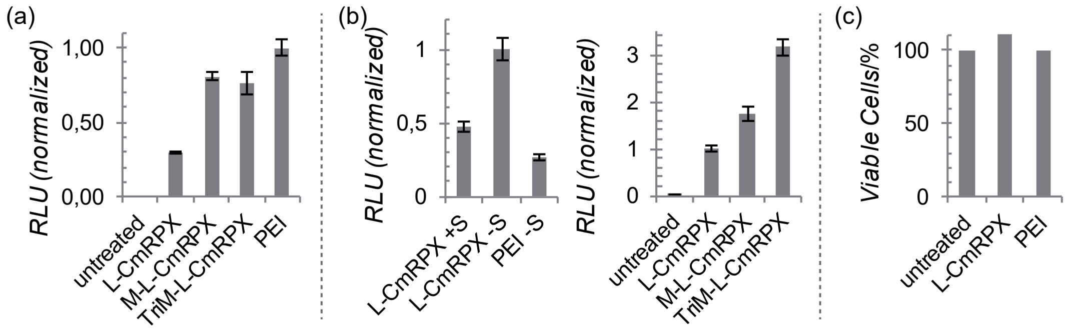

Figure 13.3: *In vitro* characterization of mRNA polyplexes cross-linked with CLAH4-L1C and decorated with mannose (M) or trimannose (TriM) by luciferase and XTT assay. (a) Transfection efficiency in murine BMDCs (mean ± sd, n = 3). (b) Transfection efficiency in human BMDCs in dependence of serum (S) and surface decoration (mean ± sd, n = 3). (c) Viability of human BMDCs after incubation with polyplexes at transfection concentrations.

Overall, *in vitro* experiments show that mRNA polyplexes with CLAH4-L1C cross-linker are potent vectors for delivery of mRNA into dendritic cells. Moreover, efficacy of these systems is increasable by active targeting strategies involving modification with mannose or trimannose. As stated above, active targeting will become increasingly relevant for immunotherapeutic interventions when moving from dendritic cells to other immune cell populations. In this context, obtained results provide a proof of concept that mRNA-PeptoPlexes constitute a suitable platform for targeted delivery of mRNA.

13.3 EXPERIMENTAL SECTION

13.3.1 Materials

See Subsection 12.3.1.

13.3.2 Instrumentation

13.3.2.1 *Polymer Characterization*

See Subsection 12.3.2.

13.3.2.2 *Biological Experiments*

See Subsection 12.3.2.

13.3.3 Methods and Protocols - Preparation of PeptoPlexes

13.3.3.1 *Synthesis of Precursor Polymers*

See Subsections 12.3.3.

13.3.3.2 *Modification with SPDP and Deprotection of the PLys(Boc) Block*

See Subsection 12.3.3.

13.3.3.3 *Functionalization of Polymers with Mannose/Trimannose*

See Subsection 12.3.3.

13.3.3.4 *Formation of PeptoPlexes (optimized protocol)*

The SPDP-modified polymer was dissolved in sterile, RNase free water (with 0.2 vol% acetic acid) to obtain a stock solution with a final concentration of 4 mg/mL. CLAH4-L1C was dissolved in degassed, sterile water (with 0.2 vol% acetic acid) at a concentration of 10 mg/mL.

mRNA polyplex formation and cross-linking protocol was adopted from the optimized protocols for TETA cross-linked pDNA polyplexes (see Subsection 10.4.3) or peptide cross-linked pDNA polyplexes (see Subsection (12.3.3)): As first step of polyplex formation, CLAH4-L1C was added to the mRNA (at amounts to saturate 50% of SPDP groups in the final polyplex) while vortexing for 10 seconds. After 10 minutes of incubation at room temperature, triblock copolypept(o)ide was added to the mixture at N/P 4 (if not indicated otherwise) while vortexing for 10 seconds. The polyplex solution was incubated for 30 minutes at room temperature before addition of RNase free 10x PBS to obtain a final 1x PBS solution. The cross-linking reaction was carried out for another 18 h under constant shaking at room temperature. Final concentration of polyplex solutions with respect to mRNA was kept at 0.03-0.05 mg/ml.

Polyplex solutions of jetPEI (Polyplus-transfection, Strasbourg, France) and mRNA were prepared according to manufacturer's protocol using 1.5 µl of stock solution per 1 µg of DNA.

13.3.4 Methods and Protocols - Physicochemical Characterization of PeptoPlexes

13.3.4.1 *Characterization of PeptoPlexes by Gel Electrophoresis*

Gel electrophoresis was performed to monitor polyplex formation. For this, 500 ng of mRNA and the desired amount of polymer were premixed as indicated above and were loaded into slots of 0.7% agarose gels (90 V, 150 mA). GelRed was used for mRNA and PeptoPlex staining.

13.3.4.2 *Characterization of PeptoPlexes by Dynamic Light Scattering*

Single-angle dynamic light scattering measurements were performed at 25 °C using a Malvern Zetasizer NanoZS with a 633 nm He/Ne Laser at a fixed scattering angle of 173°. Polyplex solutions (**L-CmRPX**) were prepared with 2 µg mRNA at N/P 4 according to indicated protocols and diluted to a final volume of 300 µl in 1x PBS before measurement.

For multi-angle DLS and serum DLS, solutions of TETA cross-linked polyplexes (**TETA-CmRPX**) with 5 µg mRNA at N/P 4 were prepared and subsequently diluted to a final volume of 1.5 mL in 1x PBS. Measurements were performed by Meike Schinnerer.

To investigate the aggregation behavior of **TETA-CmRPX** in human plasma, EDTA-plasma pooled from 6 probands was used. The following mixtures were prepared:

1. plasma: PBS 9:1
2. PBS: **TETA-CmRPX** solution (c = 0.076 mg/mL) 9:1
3. plasma: **TETA-CmRPX** solution (c = 0.076 mg/mL) 9:1

For instrumental specifications and measurement protocol see Subsection 10.4.4.

13.3.4.3 *Characterization of Polyplexes by Cryogenic Transmission Electron Microscopy*

Cryo-TEM imaging was performed by Benjamin Weber. 5 µL of polyplex solution (prepared with 0.5 µg mRNA at N/P 4, cross-linked with CLAH4-L1C) in 1x PBS were used. For instrumental specifications and measurement protocol see Subsection 12.3.4.

13.3.5 Methods and Protocols - Biological Characterization of PeptoPlexes

13.3.5.1 *Cell Culture*

Human dendritic cells were generated from progenitor cells obtained from pooled donor blood (cells were cultured at BioNTech). For BMDC generation and culture see Subsection 12.3.5.

13.3.5.2 *Determination of Transfection Efficiency of PeptoPlexes in BMDCs by Luciferase Activity*

BMDCs were seeded onto 96 well plates (2,5 x 10^5 progenitor cells in 100 µL per well) 24 h prior to transfection. PeptoPlexes formed with 0.5 µg mRNA or jetPEI polyplexes formed with 0.1 µg mRna (D2 Cap mRNA 293, BioNTech, Mainz, Germany) per well were added to the cells in triplicates, respectively. After incubation for 24 h, cells were lysed in Passive Lysis Buffer (PLB; Promega, Madison, CA) and luciferase activity was determined.

13.3.5.3 *Determination of Transfection Efficiency of PeptoPlexes in Human Dendritic Cells by Luciferase Activity*

Experiments were conducted by BioNTech. Human DCs were seeded onto 96 well plates (2,0 x 10^5 progenitor cells in 40 µL per well). PeptoPlexes formed with 0.25 µg mRNA or jetPEI polyplexes formed with 0.05 µg mRNA (D2 Cap mRNA 293, BioNTech, Mainz, Germany) per well were added to the cells in triplicates, respectively. Cells were centrifuged at 300 g for 4 minutes. After incubation for 20 h, cells were lysed and luciferase activity was determined.

13.3.5.4 *Determination of Cellular Toxicity of PeptoPlexes in in Human Dendritic Cells by XTT Assay*

Experiments were conducted by BioNTech. Human DCs were seeded onto 96 well plates and incubated for 20 h with PeptoPlexes or jetPEI polyplexes as described above. Subsequently, XTT substrate solution was added to the cells and absorbance was measured after 2 h.

14 FURTHER EXPERIMENTS AND PERSPECTIVES

14.1 MODIFICATION OF PEPTOPLEXES WITH ANTI-DEC205

Complementary to mannose/trimannose targeting (see Chapters 12 and 13), first experiments were conducted involving functionalization of PeptoPlexes with a DEC205 antibody (aDEC205) as targeting ligand. The DEC205 receptor is expressed at high levels by subsets of dendritic cells including the splenic $CD8^+$ population[523] and therefore represents a suitable surface structure for antibody targeting. Linkage of aDEC205 was realized by copper-free click reaction between terminal azide-containing PLys-b-PLys(PDP)-b-PSar triblock copolypept(o)ide (for synthetic protocol see Subsection 12.3.3) and DBCO-modified antibody as last step after formation of cross-linked PeptoPlexes (see Chapter 12, Fig. 12.1 (b) and Subsection 12.3.3). In a preceding experiment, the presence of the azide in the polymer was verified by reaction with a DBCO-carboxyrhodamine conjugate. HFIP GPC with the UV detector set to the absorption maximum of carboxyrhodamine (501 nm) demonstrated the successful linkage of polymer and dye in comparison to a negative control (polymer only) (Fig. 14.1 (a)). Apparently, as visible in GPC the reaction conditions (H_2O as solvent, constant shaking for 17 hours at room temperature) led to partial aggregation of the parent polymer. Most likely, this aggregation is triggered by partial cleavage of the side chain pyridyldithiol (PDP) groups through the amines of the PLys block.

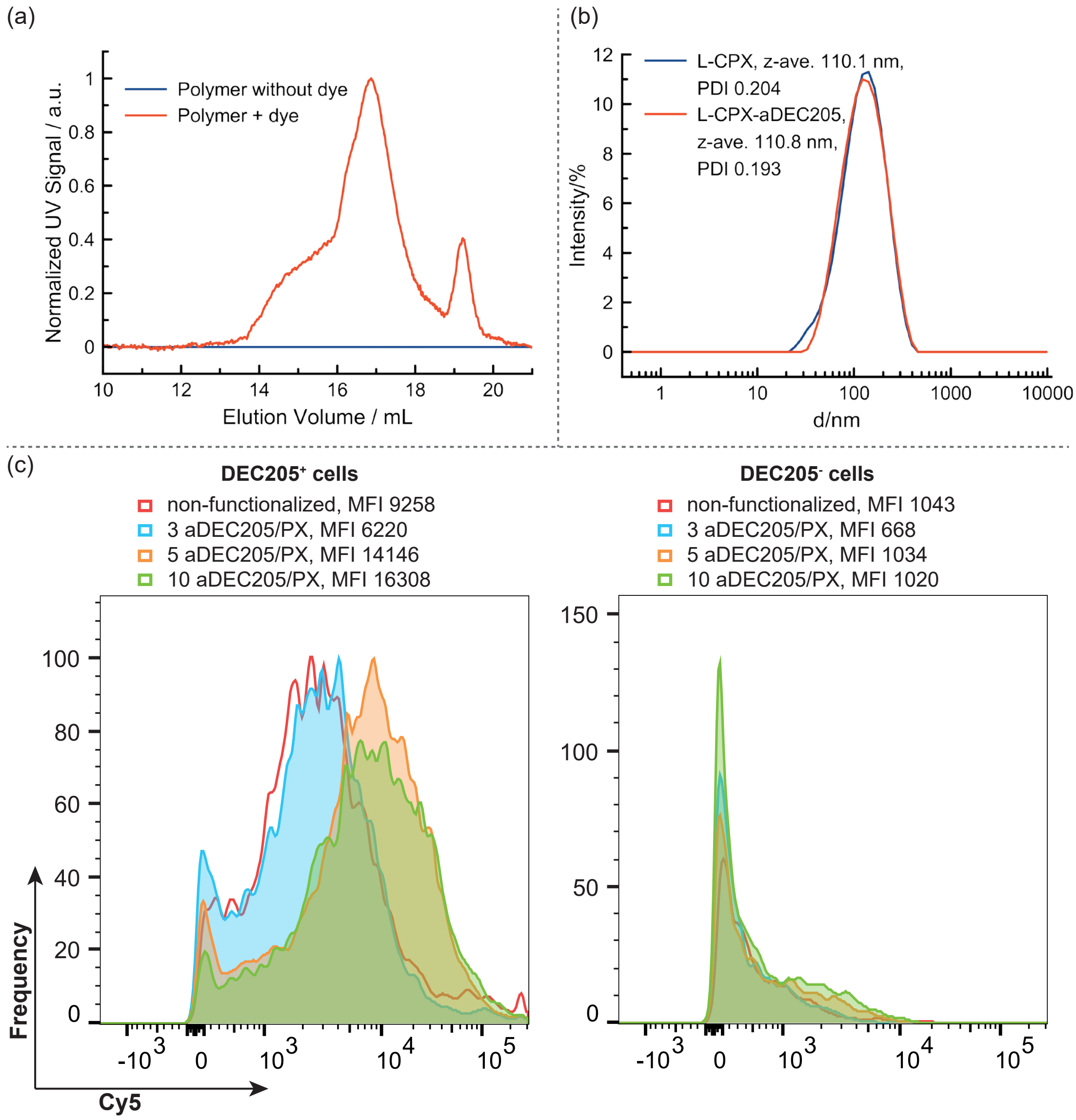

Figure 14.1: Modification of PeptoPlexes with aDEC205. (a) HFIP GPC traces of polymer reacted with DBCO-carboxyrhodamine vs unmodified polymer (UV detector set to 501 nm) as proof for the terminal azide group. (b) Size distribution of unmodified **L-CPX** vs aDEC205-modified **L-CPX** at 5 mAB/PX as determined by single angle DLS. (c) Cellular uptake of **L-CPX** as a function of aDEC205-modification in DEC205^{+} (left) and DEC205^{-} (right) cells.

The click reaction between cross-linked PeptoPlexes (**L-CPX**, see Chapter 12) and aDEC205 was conducted for 17 hours at room temperature under constant shaking. The ratio of antibody to PeptoPlex (mAB/PX) was adjusted to 3, 5 or 10 aDEC205 per PeptoPlex. PeptoPlexes fabricated with a mAB/PX ratio of up to 5 did not show a significant size difference compared to their non-functionalized counterparts (Fig. 14.1 (b)). This result is expectable due to the much larger hydrodynamic diameter of a single PeptoPlex compared to an antibody.

Subsequently, aDEC205-modified **L-CPX** were investigated for their cellular uptake by BMDCs. Cells were incubated for 4 hours with modified or unmodified PeptoPlexes containing Cy5-labeled pDNA (concentration with respect to pDNA: 0.5 µg/mL per well) and then subjected to FACS measurements. For analysis, cells were counterstained with another DEC205 antibody to discriminate between DEC205 receptor positive and negative cells. As indicated by the population shift in the histogram and with regard to MFI, a slight but significant increase of uptake in DEC205$^+$ cells was observed for **L-CPX** formulated at 5 or 10 mAB/PX, while a ratio of 3 did not enhance uptake compared to non-modified control (Fig. 14.1 (c)). In this context, one has to keep in mind that BMDCs intrinsically have a very high phagocytose, endocytose and macropinocytose activity. Thus, especially *in vitro* unspecific uptake of particles always contibutes to overall uptake levels. This explains why the difference between background uptake levels of non-functionalized **L-CPX** and targeted PeptoPlexes is not more pronounced. Yet, in contrast to DEC205$^+$ cells, DEC205$^-$ cells did not show any difference in uptake levels regardless of modification. This outcome clearly indicates that aDEC205-modification of **L-CPX** increases cellular uptake in a receptor-specific manner and represents a valuable alternative to mannose and trimannose targeting for future *in vitro* and *in vivo* experiments.

14.2 FIRST *in vivo* EXPERIMENTS

After successfully demonstrating the functionality of PeptoPlexes for *in vitro* transfection of BMDCs, their biodistribution in mice after intraveneous injection in the tail vein was investigated in a preliminary experiment. For this, **L-CPX** was formed with a 1:1 mixture of Cy5-labeled and non-labeled pDNA (5 µg in total, formulated in 100 µl PBS), allowing quantitative measurement of fluorescence at organ, tissue and single cell level by IVIS imaging and flow cytometry, respectively. Main objective of this experiment was to verify if the fluorescence signal of the applied amount of labeled pDNA was sufficient for assessing biodistribution of PetoPlexes and if the administered PeptoPlex dose was tolerated by the mice. The fluorescence signal from the labeled pDNA turned out to be strong enough and after 24 hours IVIS imaging revealed a primary accumulation of **L-CPX** in liver and spleen, and smaller fractions detected in the lungs and kidneys (Fig. 14.2 (a)).

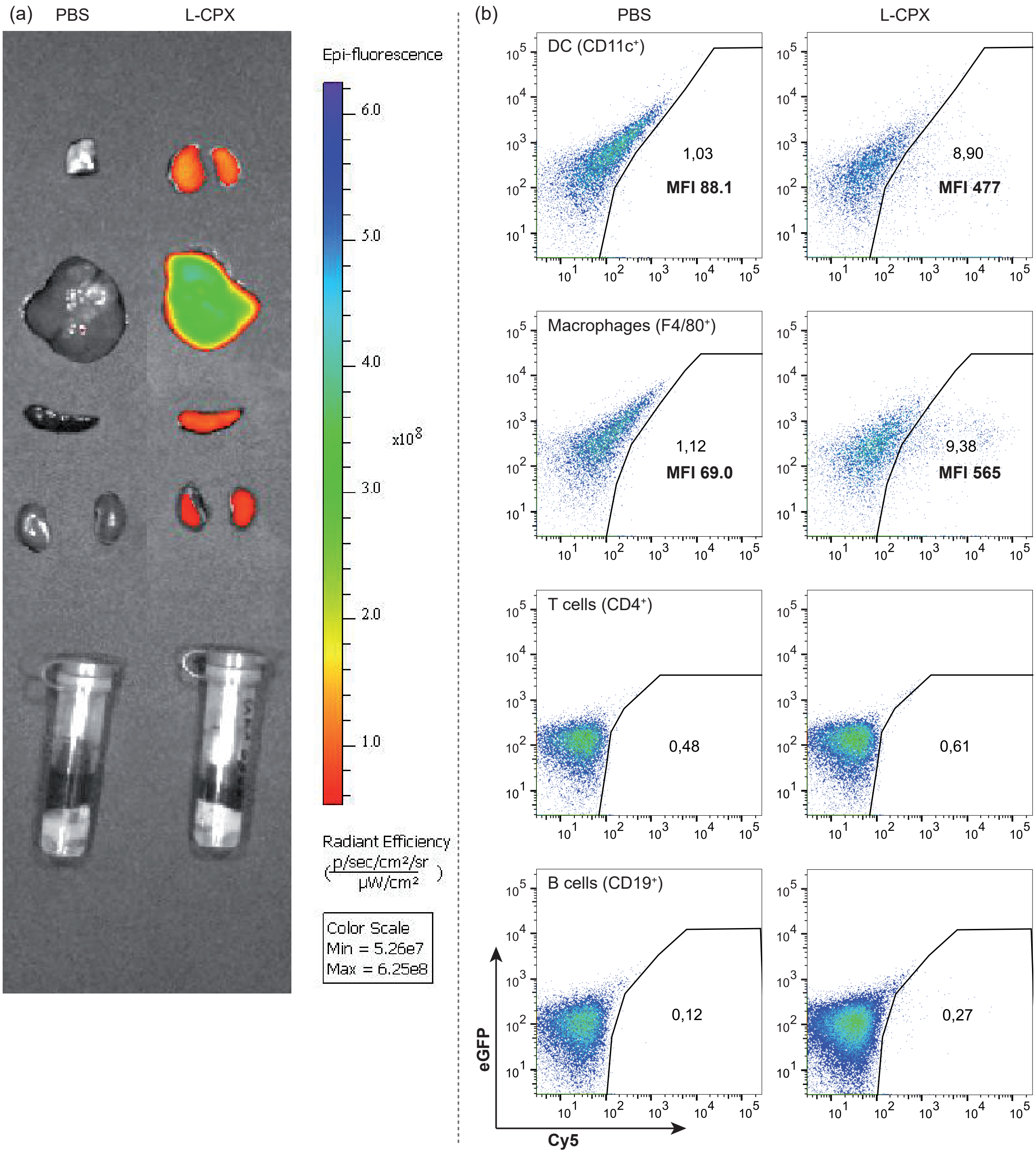

Figure 14.2: Biodistribution of **L-CPX** in mice. (a) *Ex vivo* organ IVIS imaging. (b) Uptake in spleen cell populations as determined by flow cytometry.

In general, the accumulation of nanoparticles in liver and spleen is not surprising because these two organs play an important role in filtering the blood from all kinds of foreign substances. Moreover, as the spleen is a major component of the immune system and harbors large populations of lymphocytes and monocytes including DC subsets, accumulation of the PeptoPlexes in this organ is desirable. The additional fluorescence signal in the lungs and kidneys might be ascribed to the strong perfusion of the lungs on the one hand and partial renal excretion of disassembled PeptoPlexes or free dye on the other hand. However, since this experiment was conducted as a preliminary trial with only two mice, further trials are necessary to substantiate the observation. FACS analysis of spleen cells revealed a primary association of **L-CPX** with macrophages and DCs. No binding to or uptake in T cells and B cells was detected (Fig. 14.2 (b)). Again, this result is equally expectable and desirable, since macrophages and DCs are the main phagocytic and antigen-presenting cell types. With regard to the percentage of Cy5-positive cells, around 9% of the total spleen macrophage and DC population could be reached by **L-CPX**, respectively. The Cy5-positive populations were significantly shifted compared to Cy5-negative cells. Eventually, the fact that a substantial fraction of DCs could be reached *in vivo* with **L-CPX** despite the rather small injected dose, is a promising outcome suggesting further experiments with reporter genes.

Parallel to the *in vivo* experiments with pDNA-based PeptoPlexes, the mRNA analog **L-CmRPX** (see Chapter 13) loaded with 10 µg luciferase coding mRNA and formulated in 100 µl PBS was injected into mice for subsequent *in vivo* screening of luciferase expression as well as *ex vivo* organ imaging after 6 hours (Fig. 14.3 left and right) and 24 hours (data not shown).

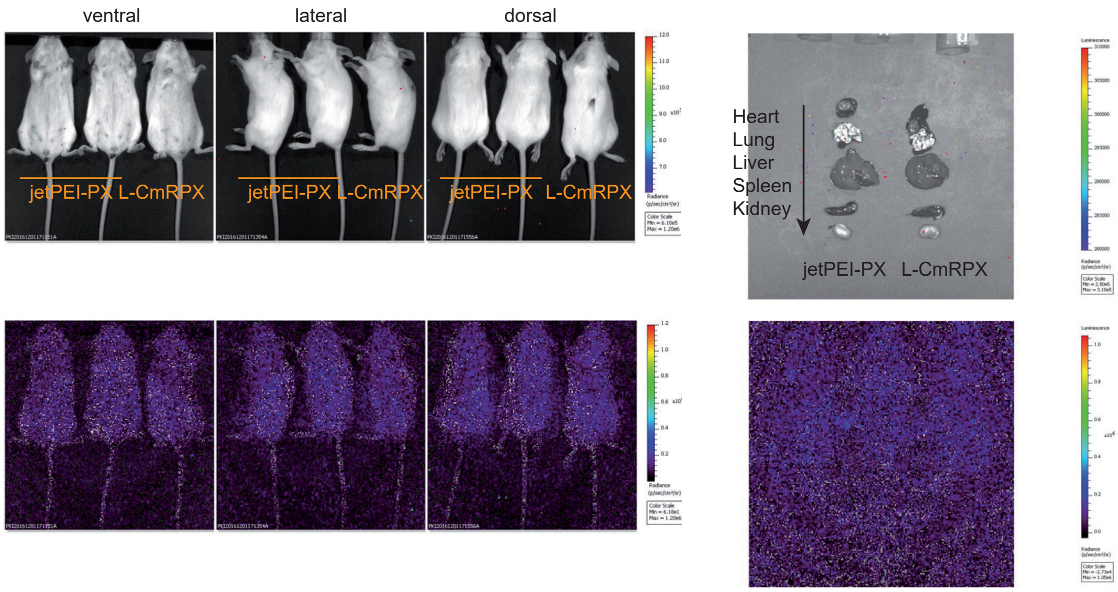

Figure 14.3: *In vivo* screening of luciferase expression (left) and *ex vivo* organ imaging (right) after systemic injection of jetPEI-PX and **L-CmRPX** into mice.

However, despite the good *in vitro* results (see Chapter 13), no luciferase signal was detected *in vivo*. The negative outcome may be attributed either to insufficient stability of **L-CmRPX** *in vivo* or more likely to insufficient targeting of DCs or a too low dose injected to generate a luciferase signal of adequate intensity for detection. As the above described *in vivo* experiment with pDNA-based PeptoPlexes revealed, around 9% of the DC and macrophage populations residing in the spleen were reached by **L-CPX**. Under the assumption that the mRNA analogue **L-CmRPX** reaches a comparable fraction of DCs and macrophages, luciferase accumulation below the detection limit at the dose injected could well be the case. Further experiments with the actively targeted PeptoPlex formulations (mannose, trimannose, aDEC205) and higher doses are therefore necessary to rule out one of the described possibilities.

Part VI

SUMMARY AND OUTLOOK

15 | SUMMARY

The aim of this thesis was to establish a new class of non-viral vectors, based on polypept(o)-ides as underlying material, which are able to mediate the delivery of nucleic acid vaccines into dendritic cells. To reach this goal, efforts started with the synthesis of simple PLys-b-PSar diblock copolymers and eventually led to the deployment of complex artificial viruses built of cross-linkable triblock copolypept(o)ides, virus-inspired peptides and different targeting ligands. Intermediate milestones were the development of mannose-targeted PeptoMicelles, triblock copolypept(o)ides with orthogonal protective groups, the synthesis of histidinylated polymers and the realization of a cross-linking strategy based on disulfides and bifunctional cross-linkers.

In the first experiments on PLys-b-PSar polymers, two different protective groups for the PLys block were tested for their compatibility with block copolypept(o)ide synthesis. Compared to the Cbz group, deprotection conditions for the TFA group were found to be more reconcilable with PSar. The synthesized polypeptides were capable to form PeptoPlexes with pDNA and basic structure-property relationships were revealed. A block length of 30-50 for PLys and of 200-300 for PSar turned out to be best suited for the formation of PeptoPlexes with adequate stability, transfection efficiency and cytotoxicity. DLS as well as TIRF microscopy suggested that PeptoPlexes contain one pDNA molecule in average.

Cellular uptake of polyplexes is the first step of transfection. Since dendritic cells express different types of mannose receptors, this carbohydrate was investigated as a possible targeting ligand by employing micelles as model platform for uptake experiments. Beforehand, a mannose derivate was applied as functional initiator for the synthesis of amphiphilic PSar-b-PGlu(OBn) polymers, which self-assembled into multivalent PeptoMicelles. Mannosylated micelles exhibited enhanced uptake in DC2.4 cells as well as in BMDCs. This proof of principle paved the way for the later functionalization of PeptoPlexes with mannose and other targeting ligands.

After cellular uptake, endosomal escape of polyplexes is the second important step of transfection. As the PLys-b-PSar system lacks any endosomolytic functionality, the polymers had to be augmented with another segment which later could be furnished with endosomolytic as well as cross-linkable moieties. The synthetic groundwork for this was laid by creating PLys(Boc)-b-PLys(TFA)-b-PSar triblock copolypept(o)ides. The necessary synthesis of lysine(Boc) NCA as a new monomer was realized by substituting the conventional Fuchs-Farthing method for NCA synthesis with an acid-free strategy exploiting trimethylsilylchloride/triethylamine as hydrochloric acid (HCl) scavengers. Subsequently, an assortment of triblock copolypept(o)ides with varying block lenghts was synthesized and the orthogonality of the Boc and the TFA groups was demonstrated by NMR spectroscopy.

In a successive simulation-guided study, diblock copolypept(o)ides as well as triblock copolypept(o)ides were modified with histidine as endosomolytic agent. From the two possible polymer microstructures - **Triblock** and **Random** - the triblock architecture turned out to be superior in terms of physicochemical properties as well as transfection efficiency of corresponding PeptoPlexes. Complexes obtained from the triblock structure were smaller and offered better protection of the enclosed pDNA against nuclease activity.

Thus, the triblock architecture was also chosen as basis for the generation of cross-linkable PeptoPlexes. To obtain the required disulfide-containing polymers from PLys(Boc)-b-PLys(TFA)-b-PSar precursors, histidine was substituted with succinimidyl 3-(2-pyridyldithio)propionate (SPDP) in an otherwise similar reaction sequence compared to the one used for histidinylation. Initially, the newly developed disulfide-containing polymers were combined with various bifunctional cross-linkers, which aside from thiols also contained endosomolytic motives, namely histidine or oligo(ethlyneimine). As verified by DLS in human plasma, disulfide cross-linked PeptoPlexes exhibited increased stability against plasma proteins opposed to their non-cross-linked counterparts. A screening approach yielded TETA as most efficient cross-linker in terms of transfection efficiency and cytotoxicity of corresponding PeptoPlexes. **TETA-CPX** was the first PeptoPlex formulation to be successfully employed for the transfection of dendritic cells (DC2.4) with a model pDNA vaccine.

Nevertheless, in the following TETA was swapped for a cystein-containing version of the virus-inspired amphipathic peptide LAH4-L1 as an even more efficient cross-linker. Besides, the resulting PeptoPlexes were further endowed with targeting ligands (mannose, trimannose, aDEC205) and an intercalator-linked nuclear localization sequence (NLS-9AA), thereby being able to mimick key viral functions. The NLS sequence eventually addresses the last obstacle for transfection, i.e. the nuclear import of pDNA.

The optimized PeptoPlex formulations (**L-CPX**) were effectively applied for the transfection of primary dendritic cells with pDNA as well as mRNA. Transfection was verified by luciferase assay and also on functional level by a T cell proliferation assay. In addition, like **TETA-CPX** the virus-mimicking PeptoPlexes were stable in human plasma and did not activate the complement system. First *in vivo* experiments with non-targeted pDNA-PeptoPlexes indicate a favorable biodistribution of **L-CPX** with primary accumulation in liver and spleen and uptake in macrophages and dendritic cells. In a parallel experiment with mRNA-PeptoPlexes, the systemic injection of **L-mRCPX** containing luciferase coding mRNA did not yield a detectable luciferase signal so far.

Already *in vitro* transfection of primary, i.e. non-dividing, cells is non-trivial and represents a challenging task at which many transfection reagents fail. Nevertheless, the latest generation of PeptoPlexes is able to transfect primary dendritic cells. In conclusion, the proof of principle for PeptoPlex-mediated nucleic acid vaccine delivery was successfully demonstrated in this work and the developed PeptoPlexes are now on the brink of further *in vivo* experiments.

16 OUTLOOK

Initially, further development of the polypept(o)ide-based non-viral vectors will take place on polymer synthesis level. With regard to the monomers constituting the triblock copolypept(o)ides, the recently established *S*-ethylsulfonyl-L-homocysteine NCA represents an interesting possible surrogate for the PLys(PDP) segment, which introduces activated disulfide moieties already during NCA polymerization. In this way, cross-linkable triblock copoly- pept(o)ides bearing activated disulfides can be obtained directly by successive polymerization of sarcosine NCA, homocysteine NCA and lysine(Boc) NCA obliterating the need for post polymerization modifications except for the deprotection of the PLys(Boc) segment.

With the successful transfection of dendritic cells the main goal of this work has been reached. However, transfection of primary cells is still a rather inefficient process with potential for optimization. The huge advantage of the modular design principle of the developed cross-linkable PeptoPlexes is that individual components can be varied independently from the other building blocks. On cellular uptake level, in this work, the proof of concept for targeted PeptoPlexes was achieved with ligands which were chosen to address surface structures on dendritic cells. However, with other possible applications for PeptoPlexes such as mRNA-guided *in vivo* reprogramming of T cells or NK cells in sight, active targeting might become increasingly relevant due to the much lower endocytic activity of these cell types. Suitable ligands for targeting T cells include interleukin 2, specific antibodies or cystine-knot peptides, which should be installable on PeptoPlexes in a similar fashion like aDEC205.

Considering possible cross-linkers as alternative to LAH4-L1, other virus-inspired fusogenic peptides such as KALA,[524] GALA[525] or mellitin[526] might be of interest for incorporation into the PeptoPlexes. Synthetic lipids and oligomers with optimized pK_a values or with hydrophobic motives which can mimick the endosomal escape mechanism of fusogenic peptides also represent a promising substitute. To directly assess the endosomolytic performance of cross-linkers, the galectin-8 assay reported in this work provides a novel valuable tool supplementary to the conventional measurement of transfection efficiency by luciferase or GFP expression.

In addition to new cross-linkers, it is certainly worth exploring NLS sequences alternative to the SV40 derived peptide tested in this work, because efficiency of different sequenes in catalyzing nuclear import might vary. Mutliple other NLS sequences, i.a. derived from nucleoplasmin, c-Myc or EGL-13 proteins, have been identified in recent years[527] which in principle should all be compatible with the intercalation approach described herein.

Finally, with respect to the already established PeptoPlex systems, further *in vivo* experiments in particular with targeted formulations are necessary. These include an extended analysis of biodistribution with radio- or fluorescent-labeled PeptoPlexes. Labels thereby should be attached to pDNA and mRNA as well as to polymers. In a subsequent step, assessment of PeptoPlex-mediated *in vivo* transfection, first on reporter gene level and second on functional level, has to be conducted. If *in vivo* transfection activity is evidenced, PeptoPlexes loaded with a mRNA or pDNA vaccine can eventually be tested in a tumor model.

On a more fundamental level, an intriguing project would be the tracking of the optimized virus-mimicking PeptoPlex formulations through the different stages of cell transfection in live-cell imaging by means of confocal microscopy.

Part VII

APPENDIX

LIST OF FIGURES

LIST OF TABLES

ACRONYMS

9-AA	9-aminoacridine
AMM	activated monomer mechanism
BMDC	bone marrow-derived dendritic cell
CD	circular dichroism
CLSM	confocal laser scanning microscope
CPX	cross-linked PeptoPlex
cryo-TEM	cryogenic transmission electron microscopy
Cys	cysteine
DC	dendritic cell
DLS	dynamic light scattering
DMF	dimethyl formamide
DMSO	dimethyl sulfoxide
DNA	deoxyribonucleic acid
Glu	glutamate
Glu(OBn)	γ-benzyl-L-glutamate
GPC	gel permeation chromatography
HFIP	hexafluoro isopropanol
His	histidine
IR	infrared
Lys	lysine
Lys(Boc)	*N*-ε-tert-butyloxycarbonyl-L-lysine
Lys(TFA)	*N*-ε-trifluoroacetyl-L-lysine
Lys(Z)	*N*-ε-benzyloxycarbonyl-L-lysine
mRNA	messenger ribonucleic acid
NAM	normal amine mechanism
NCA	α-amino acid-*N*-carboxy anhydride
NCPX	non-cross-linked PeptoPlex
NLS	nuclear localization signal
NMR	nuclear magnetic resonance
PBS	phosphate buffered saline
pDNA	plasmid deoxyribonucleic acid
PEG	poly(ethylene glycol)
PMMA	poly(methyl methacrylate)
POx	poly(oxazoline)
RI	refractive index
ROP	ring-opening polymerization

Sar	sarcosine
SPDP	succinimidyl 3-(2-pyridyldithio)propionate
TFA	trifluoro acetic acid
THF	tetrahydrofurane
UV	ultra violett

BIBLIOGRAPHY

[1] Sudowe, S.; Dominitzki, S.; Montermann, E.; Bros, M.; Grabbe, S.; Reske-Kunz, A. B. *Immunology* **2009**, *128*, e193–205.

[2] Kranz, L. M. et al. *Nature* **2016**, *534*, 396–401.

[3] Grabbe, S.; Haas, H.; Diken, M.; Kranz, L. M.; Langguth, P.; Sahin, U. *Nanomedicine (Lond).* **2016**, *11*, 2723–2734.

[4] Mullard, A. *Nat. Rev. Drug Discov.* **2016**, *15*, 663–665.

[5] Lächelt, U.; Wagner, E. *Chem. Rev.* **2015**, *115*, 11043–11078.

[6] Midoux, P.; Pichon, C.; Yaouanc, J. J.; Jaffrès, P. A. *Br. J. Pharmacol.* **2009**, *157*, 166–178.

[7] Behr, J. *Int. J. Chem.* **1997**, *2*, 34–36.

[8] Kichler, A.; Leborgne, C.; März, J.; Danos, O.; Bechinger, B. *Proc. Natl. Acad. Sci. U. S. A.* **2003**, *100*, 1564–8.

[9] Deng, C.; Wu, J.; Cheng, R.; Meng, F.; Klok, H. A.; Zhong, Z. *Prog. Polym. Sci.* **2014**, *39*, 330–364.

[10] Leuchs, H. *Ber. Dtsch. Chem. Ges.* **1906**, *39*, 857–861.

[11] Leuchs, H.; Manasse, W. *Ber. Dtsch. Chem. Ges.* **1907**, *40*, 3235–3249.

[12] Leuchs, H.; Geiger, W. *Ber. Dtsch. Chem. Ges.* **1908**, *41*, 1721–1726.

[13] Fuchs, F. *Ber. Dtsch. Chem. Ges.* **1922**, *55*, 2943–2943.

[14] Farthing, A. C.; Reynolds, R. J. W. *Nature* **1950**, *165*, 647–647.

[15] Kricheldorf, H. R. *α-Aminoacid-N-Carboxy-Anhydrides and Related Heterocycles: Syntheses, Properties, Peptide Synthesis, Polymerization.*; Springer: Berlin-Heidelberg-New York, 1987.

[16] Yu, M.; Nowak, A. P.; Deming, T. J.; Pochan, D. J. *J. Am. Chem. Soc.* **1999**, *121*, 12210–12211.

[17] Curtius, T.; Sieber, W. *Ber. Dtsch. Chem. Ges.* **1921**, *54*, 1430–1437.

[18] Curtius, T.; Sieber, W. *Ber. Dtsch. Chem. Ges.* **1922**, *55*, 1543–1558.

[19] Curtius, T.; Hochschwender, K.; Meier, H.; Lehmann, W.; Benckiser, A.; Schenck, M.; Wirbatz, W.; Gaier, J.; Mühlhäusser, W. *J. Prakt. Chem.* **1930**, *125*, 211–302.

[20] Wessely, F. *Z. Physiol. Chem.* **1925**, *146*, 72–90.

[21] Wessely, F.; Sigmund, F. *Z. Physiol. Chem.* **1926**, *159*, 102–119.

[22] Deming, T. J. *Nature* **1997**, *390*, 386–389.

[23] Deming, T. J. *J. Am. Chem. Soc.* **1998**, *120*, 4240–4241.

[24] Kricheldorf, H. R. *Angew. Chemie - Int. Ed.* **2006**, *45*, 5752–5784.

[25] Hadjichristidis, N.; Iatrou, H.; Pitsikalis, M.; Sakellariou, G. *Chem. Rev.* **2009**, *109*, 5528–5578.

[26] Lu, H.; Cheng, J. *J. Am. Chem. Soc.* **2007**, *129*, 14114–14115.

[27] Dimitrov, I.; Schlaad, H. *Chem. Commun. (Camb).* **2003**, 2944–2945.

[28] Aliferis, T.; Iatrou, H.; Hadjichristidis, N. *Biomacromolecules* **2004**, *5*, 1653–1656.

[29] Vayaboury, W.; Giani, O.; Cottet, H.; Deratani, A.; Schue, F. *Macromol. Rapid Commun.* **2004**, *25*, 1221–1224.

[30] Habraken, G. J. M.; Wilsens, K. H. R. M.; Koning, C. E.; Heise, A. *Polym. Chem.* **2011**, *2*, 1322.

[31] Zhao, W.; Gnanou, Y.; Hadjichristidis, N. *Polym. Chem.* **2015**, *6*, 6193–6201.

[32] Scholz, C.; Vayaboury, W. CONTROLLED MOLECULAR WEIGHT AMINO ACID POLYMERS HAVING FUNCTIONALIZABLE BACKBONES AND END GROUPS AND PROCESSES FOR PREPARING THE SAME. 2008.

[33] Zou, J.; Fan, J.; He, X.; Zhang, S.; Wang, H.; Wooley, K. L. *Macromolecules* **2013**, *46*, 4223–4226.

[34] Conejos-Sánchez, I.; Duro-Castano, A.; Birke, A.; Barz, M.; Vicent, M. J. *Polym. Chem.* **2013**, *4*, 3182.

[35] Gibson, M. I.; Cameron, N. R. *J. Polym. Sci. Part A Polym. Chem.* **2009**, *47*, 2882–2891.

[36] Huesmann, D.; Birke, A.; Klinker, K.; Türk, S.; Räder, H. J.; Barz, M. *Macromolecules* **2014**, *47*, 928–936.

[37] Klinker, K.; Barz, M. *Macromol. Rapid Commun.* **2015**, *36*, 1943–1957.

[38] Deming, T. J. *J. Polym. Sci., Part A Polym. Chem.* **2000**, *38*, 3011–3018.

[39] Lu, H.; Cheng, J. *J. Am. Chem. Soc.* **2008**, *130*, 12562–12563.

[40] Chan, B. A.; Xuan, S.; Horton, M.; Zhang, D. *Macromolecules* **2016**, *49*, 2002–2012.

[41] Zhang, X.; Oddon, M.; Giani, O.; Monge, S.; Robin, J. J. *Macromolecules* **2010**, *43*, 2654–2656.

[42] Li, A.; Lu, L.; Li, X.; He, L.; Do, C.; Garno, J. C.; Zhang, D. *Macromolecules* **2016**, *49*, 1163–1171.

[43] Guo, L.; Zhang, D. *J. Am. Chem. Soc.* **2009**, *131*, 18072–18074.

[44] Guo, L.; Li, J.; Brown, Z.; Ghale, K.; Zhang, D. *Pept. Sci.* **2011**, *96*, 596–603.

[45] Lahasky, S. H.; Serem, W. K.; Guo, L.; Garno, J. C.; Zhang, D. *Macromolecules* **2011**, *44*, 9063–9074.

[46] Stukenkemper, T. et al. *Polym. Chem.* **2017**, *8*, 828–832.

[47] Habraken, G. J. M.; Koning, C. E.; Heise, A. *J. Polym. Sci. Part A Polym. Chem.* **2009**, *47*, 6883–6893.

[48] Zhang, X.; Li, J.; Li, W.; Zhang, A. *Biomacromolecules* **2007**, *8*, 3557–3567.

[49] Knoop, R. J. I.; Habraken, G. J. M.; Gogibus, N.; Steig, S.; Menzel, H.; Koning, C. E.; Heise, A. *J. Polym. Sci. Part A Polym. Chem.* **2008**, *46*, 3068–3077.

[50] Agut, W.; Brûlet, A.; Schatz, C.; Taton, D.; Lecommandoux, S. *Langmuir* **2010**, *26*, 10546–10554.

[51] Johnson, R. P.; Uthaman, S.; John, J. V.; Lee, H. R.; Lee, S. J.; Park, H.; Park, I. K.; Suh, H.; Kim, I. *ACS Appl. Mater. Interfaces* **2015**, *7*, 21770–21779.

[52] Fu, L.; Sun, C.; Yan, L. *ACS Appl. Mater. Interfaces* **2015**, *7*, 2104–2115.

[53] Liu, L.; Fu, L.; Jing, T.; Ruan, Z.; Yan, L. *ACS Appl. Mater. Interfaces* **2016**, *8*, 8980–8990.

[54] Schatz, C.; Louguet, S.; Meins, J. F. L.; Lecommandoux, S. *Angew. Chemie - Int. Ed.* **2009**, *48*, 2572–2575.

[55] Kumar Upadhyay, K.; Le Meins, J. F.; Misra, A.; Voisin, P.; Bouchaud, V.; Ibarboure, E.; Schatz, C.; Lecommandoux, S. *Biomacromolecules* **2009**, *10*, 2802–2808.

[56] Agut, W.; Agnaou, R.; Lecommandoux, S.; Taton, D. *Macromol. Rapid Commun.* **2008**, *29*, 1147–1155.

[57] Klinker, K.; Holm, R.; Heller, P.; Barz, M. *Polym. Chem.* **2015**, *6*, 4612–4623.

[58] Ray, J. G.; Ly, J. T.; Savin, D. A. *Polym. Chem.* **2011**, *2*, 1536.

[59] Han, S. S.; Li, Z. Y.; Zhu, J. Y.; Han, K.; Zeng, Z. Y.; Hong, W.; Li, W. X.; Jia, H. Z.; Liu, Y.; Zhuo, R. X.; Zhang, X. Z. *Small* **2015**, *11*, 2543–2554.

[60] Kar, M.; Tiwari, N.; Tiwari, M.; Lahiri, M.; Gupta, S. S. *Part. Part. Syst. Charact.* **2013**, *30*, 166–179.

[61] Holm, R.; Klinker, K.; Weber, B.; Barz, M. *Macromol. Rapid Commun.* **2015**, *36*, 2083–2091.

[62] Bae, Y.; Kataoka, K. *Adv. Drug Deliv. Rev.* **2009**, *61*, 768–784.

[63] Ulkoski, D.; Meister, A.; Busse, K.; Kressler, J.; Scholz, C. *COLLOID Polym. Sci.* **2015**, *293*, 2147–2155.

[64] Iatrou, H.; Dimas, K.; Gkikas, M.; Tsimblouli, C.; Sofianopoulou, S. *Macromol. Biosci.* **2014**, *14*, 1222–1238.

[65] Thornton, P. D.; Billah, S. M. R.; Cameron, N. R. *Macromol. Rapid Commun.* **2013**, *34*, 257–262.

[66] Fetsch, C.; Luxenhofer, R. *Macromol. Rapid Commun.* **2012**, *33*, 1708–1713.

[67] Pan, S.; Wang, C.; Zeng, X.; Wen, Y.; Wu, H.; Feng, M. *Int. J. Pharm.* **2011**, *420*, 206–215.

[68] Sulistio, A.; Gurr, P. A.; Blencowe, A.; Qiao, G. G. *Aust. J. Chem.* **2012**, *65*, 978–984.

[69] Byrne, M.; Thornton, P. D.; Cryan, S.-A.; Heise, A. *Polym. Chem.* **2012**, *3*, 2825.

[70] Duro-Castano, A.; England, R. M.; Razola, D.; Romero, E.; Oteo-Vives, M.; Morcillo, M. A.; Vicent, M. J. *Mol. Pharm.* **2015**, *12*, 3639–3649.

[71] Holm, R.; Weber, B.; Heller, P.; Klinker, K.; Westmeier, D.; Docter, D.; Stauber, R. H.; Barz, M. *Macromol. Biosci.* **2017**, 1600514.

[72] Wibowo, S. H.; Sulistio, A.; Wong, E. H. H.; Blencowe, A.; Qiao, G. G. *Chem. Commun. (Camb).* **2014**, *50*, 4971–88.

[73] Shen, Y.; Li, Z.; Klok, H. A. *Chinese J. Polym. Sci. (English Ed.* **2015**, *33*, 931–946.

[74] Borase, T.; Heise, A. *Adv. Mater.* **2016**, 5725–5731.

[75] Blout, E. R.; de Lozé, C.; Bloom, S. M.; Fasman, G. D. *J Am Chem Soc* **1960**, *82*, 3787–3789.

[76] Bloom, S. M.; Fasman, G. D.; de Loze, C.; Blout, E. R. *J. Am. Chem. Soc.* **1962**, *84*, 458–463.

[77] Blout, E.; Idelson, M. *J. Am. Chem. Soc.* **1956**, *78*, 497–498.

[78] Inoue, K.; Baden, N.; Terazima, M. *J. Phys. Chem. B* **2005**, *109*, 22623–8.

[79] Lu, H.; Wang, J.; Bai, Y.; Lang, J. W.; Liu, S.; Lin, Y.; Cheng, J. *Nat. Commun.* **2011**, *2*, 206–209.

[80] Engler, A. C.; Lee, H. I.; Hammond, P. T. *Angew. Chemie - Int. Ed.* **2009**, *48*, 9334–9338.

[81] Barz, M.; Duro-Castano, A.; Vicent, M. J. *Polym. Chem.* **2013**, *4*, 2989.

[82] Li, C.; Yu, D. F.; Newman, R. A.; Cabral, F.; Stephens, L. C.; Hunter, N.; Milas, L.; Wallace, S. *Cancer Res.* **1998**, *58*, 2404–2409.

[83] Singer, J. W.; Baker, B.; De Vries, P.; Kumar, A.; Shaffer, S.; Vawter, E.; Bolton, M.; Garzone, P. *Adv. Exp. Med. Biol.*; 2003; Vol. 519; pp 81–99.

[84] Singer, J. W. Paclitaxel poliglumex (XYOTAXTM, CT-2103): A macromolecular taxane. J. Control. Release. 2005; pp 120–126.

[85] Marchal, S.; Hor, A. E.; Millard, M.; Gillon, V.; Bezdetnaya, L. *Drugs* **2015**, *75*, 1601–1611.

[86] Conejos-Sánchez, I.; Cardoso, I.; Oteo-Vives, M.; Romero-Sanz, E.; Paul, A.; Sauri, A. R.; Morcillo, M. A.; Saraiva, M. J.; Vicent, M. J. *J. Control. Release* **2015**, *198*, 80–90.

[87] Ucero, Á. C.; Berzal, S.; Ocaña-Salceda, C.; Sancho, M.; Orzáez, M.; Messeguer, A.; Ruiz-Ortega, M.; Egido, J.; Vicent, M. J.; Ortiz, A.; Ramos, A. M. *PLoS One* **2013**, *8*.

[88] Talelli, M.; Vicent, M. J. *Biomacromolecules* **2014**, *15*, 4168–4177.

[89] Gabrielson, N. P.; Lu, H.; Yin, L.; Li, D.; Wang, F.; Cheng, J. *Angew. Chemie - Int. Ed.* **2012**, *51*, 1143–1147.

[90] Zhang, R.; Song, Z.; Yin, L.; Zheng, N.; Tang, H.; Lu, H.; Gabrielson, N. P.; Lin, Y.; Kim, K.; Cheng, J. *Wiley Interdiscip. Rev. Nanomedicine Nanobiotechnology* **2015**, *7*, 98–110.

[91] Engler, A. C.; Shukla, A.; Puranam, S.; Buss, H. G.; Jreige, N.; Hammond, P. T. *Biomacromolecules* **2011**, *12*, 1666–1674.

[92] Xiong, M.; Lee, M. W.; Mansbach, R. A.; Song, Z.; Bao, Y.; Peek, R. M.; Yao, C.; Chen, L.-F.; Ferguson, A. L.; Wong, G. C. L.; Cheng, J. *Proc. Natl. Acad. Sci.* **2015**, *112*, 201507893.

[93] Oelker, A. M.; Morey, S. M.; Griffith, L. G.; Hammond, P. T. *Soft Matter* **2012**, *42*, 10887–10895.

[94] Ahrens, C. C.; Welch, M. E.; Griffith, L. G.; Hammond, P. T. *Biomacromolecules* **2015**, *16*, 3774–3783.

[95] Tang, H.; Zhang, D. *J. Polym. Sci. Part A Polym. Chem.* **2013**, *51*, 4489–4497.

[96] Yakovlev, I.; Deming, T. J. *J. Am. Chem. Soc.* **2015**, *137*, 4078–4081.

[97] Kramer, J. R.; Deming, T. J. *J. Am. Chem. Soc.* **2012**, *134*, 4112–4115.

[98] Kramer, J. R.; Deming, T. J. *Biomacromolecules* **2012**, *13*, 1719–1723.

[99] Kramer, J. R.; Deming, T. J. *Chem. Commun. (Camb).* **2013**, *49*, 5144–5146.

[100] Kramer, J. R.; Deming, T. J. *J. Am. Chem. Soc.* **2014**, *136*, 5547–5550.

[101] Gharakhanian, E. G.; Deming, T. J. *Chem. Commun. (Camb).* **2016**, *52*, 5336–9.

[102] Rodriguez, A. R.; Kramer, J. R.; Deming, T. J. *Biomacromolecules* **2013**, *14*, 3610–3614.

[103] Wu, X.; Zhou, L.; Su, Y.; Dong, C.-M. *Polym. Chem.* **2015**, *6*, 6857–6869.

[104] Liu, G.; Dong, C. M. *Biomacromolecules* **2012**, *13*, 1573–1583.

[105] Wu, X.; Zhou, L.; Su, Y.; Dong, C.-M. *J. Mater. Chem. B* **2016**, *4*, 2142–2152.

[106] Schäfer, O.; Huesmann, D.; Muhl, C.; Barz, M. *Chem. - A Eur. J.* **2016**, 18085–18091.

[107] Patchornik, A.; Berger, A.; Katchalski, E. *J. Am. Chem. Soc.* **1957**, *79*, 5227–5230.

[108] Iatrou, H.; Bilalis, P.; Mavrogiorgis, D.; Karatzas, A.; Skoulas, D.; Fotinogiannopoulou, G. *Polym. Chem.* **2014**, 6256–6278.

[109] Kricheldorf, H. R.; Von Lossow, C.; Schwarz, G. *Macromol. Chem. Phys.* **2004**, *205*, 918–924.

[110] Uchida, S.; Hayakawa, K.; Ogata, T.; Tanaka, S.; Kataoka, K.; Itaka, K. *Biomaterials* **2016**, *109*, 1–11.

[111] Shoulders, M. D.; Raines, R. T. *Annu. Rev. Biochem.* **2009**, *78*, 929–58.

[112] Fillon, Y. A.; Anderson, J. P.; Chmielewski, J. *J. Am. Chem. Soc.* **2005**, *127*, 11798–11803.

[113] Gulin, O. P.; Rabanal, F.; Giralt, E. *Org. Lett.* **2006**, *8*, 5385–5388.

[114] Gkikas, M.; Iatrou, H.; Thomaidis, N. S.; Alexandridis, P.; Hadjichristidis, N. *Biomacromolecules* **2011**, *12*, 2396–2406.

[115] Graf, R.; Spiess, H. W.; Floudas, G.; Butt, H.-J.; Gkikas, M.; Iatrou, H. *Macromolecules* **2012**, *45*, 9326–9332.

[116] Martin, C.; Lebrun, A.; Martinez, J.; Cavelier, F. *J. Polym. Sci. Part A Polym. Chem.* **2013**, *51*, 3103–3109.

[117] Sisido, M.; Imanishi, Y.; Higashimura, T. *Macromol. Chem. Phys.* **1977**, *178*, 3107–3114.

[118] Aoi, K.; Hatanaka, T.; Tsutsumiuchi, K.; Okada, M.; Imae, T. *Macromol. Rapid Commun.* **1999**, *20*, 378–382.

[119] Secker, C.; Brosnan, S. M.; Luxenhofer, R.; Schlaad, H. *Macromol. Biosci.* **2015**, *15*, 881–891.

[120] Gangloff, N.; Ulbricht, J.; Lorson, T.; Schlaad, H.; Luxenhofer, R. *Chem. Rev.* **2016**, *116*, 1753–1802.

[121] Fetsch, C.; Grossmann, A.; Holz, L.; Nawroth, J. F.; Luxenhofer, R. *Macromolecules* **2011**, *44*, 6746–6758.

[122] Fetsch, C.; Luxenhofer, R. *Polymers (Basel).* **2013**, *5*, 112–127.

[123] Kricheldorf, H. R.; Von Lossow, C.; Schwarz, G. *Macromolecules* **2005**, *38*, 5513–5518.

[124] Kricheldorf, H. R.; Lossow, C. V.; Schwarz, G. *Macromol. Chem. Phys.* **2005**, *206*, 282–290.

[125] Kricheldorf, H. R.; Lossow, C. V.; Lomadze, N.; Schwarz, G. *J. Polym. Sci. Part A Polym. Chem.* **2008**, *46*, 4012–4020.

[126] Kricheldorf, H. R.; Von Lossow, C.; Schwarz, G. *J. Polym. Sci. Part A Polym. Chem.* **2006**, *44*, 4680–4695.

[127] Lee, C. U.; Li, A.; Ghale, K.; Zhang, D. *Macromolecules* **2013**, *46*, 8213–8223.

[128] Politakos, N.; Liontos, G.; Kortaberria, G.; Messman, J. M.; Calvo, J.; Moya, S. E.; Mays, J. W.; Avgeropoulos, A. *J. Polym. Sci. Part A Polym. Chem.* **2015**, *53*, 393–404.

[129] Habraken, G. J. M.; Heise, A.; Thornton, P. D. *Macromol Rapid Commun* **2011**, *33*, 272–286.

[130] Douy, A.; Gallot, B. *Polymer (Guildf).* **1987**, *28*, 147–154.

[131] Sisido, M.; Okamoto, A.; Egusa, S.; Imanishi, Y. *Polym. J.* **1985**, *17*, 1253–1261.

[132] Aoi, K.; Tsutsumiuchi, K.; Okada, M. *Macromolecules* **1994**, *27*, 875–877.

[133] Lavilla, C.; Byrne, M.; Heise, A. *Macromolecules* **2016**, *49*, 2942–2947.

[134] Iatrou, H.; Frielinghaus, H.; Hanski, S.; Ferderigos, N.; Ruokolainen, J.; Ikkala, O.; Richter, D.; Mays, J.; Hadjichristidis, N. *Biomacromolecules* **2007**, *8*, 2173–2181.

[135] Deming, T. J. *Soft Matter* **2005**, *1*, 28.

[136] Stukenkemper, T.; Dose, A.; Gonzalez, M. C.; Groenen, A. J. J.; Hehir, S.; Andres-Guerrero, V.; Vanrell, R. H.; Cameron, N. R. *Macromol. Biosci.* **2014**, *15*, 138–145.

[137] Nishiyama, N.; Kataoka, K. *Adv. Polym. Sci.* **2006**, *193*, 67–101.

[138] Obeid, R.; Scholz, C. *Biomacromolecules* **2011**, *12*, 3797–3804.

[139] Osawa, S.; Osada, K.; Hiki, S.; Dirisala, A.; Ishii, T.; Kataoka, K. *Biomacromolecules* **2016**, *17*, 354–361.

[140] Upadhyay, K. K.; Bhatt, A. N.; Mishra, A. K.; Dwarakanath, B. S.; Jain, S.; Schatz, C.; Le Meins, J. F.; Farooque, A.; Chandraiah, G.; Jain, A. K.; Misra, A.; Lecommandoux, S. *Biomaterials* **2010**, *31*, 2882–2892.

[141] Tappertzhofen, K.; Weiser, F.; Montermann, E.; Reske-Kunz, A.; Bros, M.; Zentel, R. *Macromol. Biosci.* **2015**, *15*, 1159–1173.

[142] Tappertzhofen, K.; Beck, S.; Montermann, E.; Huesmann, D.; Barz, M.; Koynov, K.; Bros, M.; Zentel, R. *Macromol. Biosci.* **2016**, *16*, 106–120.

[143] Nowak, A. P.; Breedveld, V.; Pakstis, L.; Ozbas, B.; Pine, D. J.; Pochan, D.; Deming, T. J. *Nature* **2002**, *417*, 424–428.

[144] Breedveld, V.; Nowak, A. P.; Sato, J.; Deming, T. J.; Pine, D. J. *Macromolecules* **2004**, *37*, 3943–3953.

[145] Li, Z.; Deming, T. J. *Soft Matter* **2010**, *6*, 2546.

[146] Zhang, S.; Anderson, M. A.; Ao, Y.; Khakh, B. S.; Fan, J.; Deming, T. J.; Sofroniew, M. V. *Biomaterials* **2014**, *35*, 1989–2000.

[147] Gkikas, M.; Haataja, J. S.; Ruokolainen, J.; Iatrou, H.; Houbenov, N. *Biomacromolecules* **2015**, *16*, 3686–3693.

[148] KWON, G. S.; KATAOKA, K. *Adv. Drug Deliv. Rev.* **1995**, *16*, 295–309.

[149] Kudo, S.; Nagasaki, Y. *Macromol. Rapid Commun.* **2015**, *36*, 1916–1922.

[150] Quadir, M. A.; Morton, S. W.; Deng, Z. J.; Shopsowitz, K. E.; Murphy, R. P.; Epps, T. H.; Hammond, P. T. *Mol. Pharm.* **2014**, *11*, 2420–2430.

[151] Yen, J.; Zhang, Y.; Gabrielson, N. P.; Yin, L.; Guan, L.; Chaudhury, I.; Lu, H.; Wang, F.; Cheng, J. *Biomater. Sci.* **2013**, *1*, 719–727.

[152] Obeid, R.; Armstrong, T.; Peng, X.; Busse, K.; Kressler, J.; Scholz, C. *J. Polym. Sci. Part A Polym. Chem.* **2014**, *52*, 248–257.

[153] Sun, J.; Černoch, P.; Völkel, A.; Wei, Y.; Ruokolainen, J.; Schlaad, H. *Macromolecules* **2016**, *49*, 5494–5501.

[154] Huesmann, D.; Sevenich, A.; Weber, B.; Barz, M. *Polym. (United Kingdom)* **2015**, *67*, 240–248.

[155] Birke, A.; Huesmann, D.; Kelsch, A.; Weilbächer, M.; Xie, J.; Bros, M.; Bopp, T.; Becker, C.; Landfester, K.; Barz, M. *Biomacromolecules* **2014**, *15*, 548–557.

[156] Heller, P.; Birke, A.; Huesmann, D.; Weber, B.; Fischer, K.; Reske-Kunz, A.; Bros, M.; Barz, M. *Macromol. Biosci.* **2014**, *14*, 1380–1395.

[157] Heller, P.; Mohr, N.; Birke, A.; Weber, B.; Reske-Kunz, A.; Bros, M.; Barz, M. *Macromol. Biosci.* **2015**, *15*, 63–73.

[158] Heller, P.; Weber, B.; Birke, A.; Barz, M. *Macromol. Rapid Commun.* **2015**, *36*, 38–44.

[159] Heller, P.; Zhou, J.; Weber, B.; Hobernik, D.; Bros, M.; Schmid, F.; Barz, M. *Small* **2017**, 1603694.

[160] Kidchob, T.; Kimura, S.; Imanishi, Y. *J. Control. Release* **1996**, *40*, 285–291.

[161] Kidchob, T.; Kimura, S.; Imanishi, Y. *J. Control. Release* **1998**, *50*, 205–214.

[162] Kidchob, T.; Kimura, S.; Imanishi, Y. *J. Control. Release* **1998**, *51*, 241–248.

[163] Kanzaki, T.; Horikawa, Y.; Makino, A.; Sugiyama, J.; Kimura, S. *Macromol. Biosci.* **2008**, *8*, 1026–1033.

[164] Hara, E.; Ueda, M.; Kim, C. J.; Makino, A.; Hara, I.; Ozeki, E.; Kimura, S. *J. Pept. Sci.* **2014**, *20*, 570–577.

[165] Makino, A.; Yamahara, R.; Ozeki, E.; Kimura, S. *Chem. Lett.* **2007**, *36*, 1220–1221.

[166] Yamamoto, F.; Yamahara, R.; Makino, A.; Kurihara, K.; Tsukada, H.; Hara, E.; Hara, I.; Kizaka-Kondoh, S.; Ohkubo, Y.; Ozeki, E.; Kimura, S. *Nucl. Med. Biol.* **2013**, *40*, 387–394.

[167] Makino, A.; Hara, E.; Hara, I.; Ozeki, E.; Kimura, S. *Langmuir* **2014**, *30*, 669–74.

[168] Krannig, K. S.; Sun, J.; Schlaad, H. *Biomacromolecules* **2014**, *15*, 978–984.

[169] Kramer, J. R.; Deming, T. J. *Polym. Chem.* **2014**, *5*, 671–682.

[170] Deming, T. J. *Chem. Rev.* **2016**, *116*, 786–808.

[171] Dong, C. M.; Sun, X. L.; Faucher, K. M.; Apkarian, R. P.; Chaikof, E. L. *Biomacromolecules* **2004**, *5*, 224–231.

[172] Dong, C.-M.; Faucher, K. M.; Chaikof, E. L. *J. Polym. Sci. Part A Polym. Chem.* **2004**, *42*, 5754–5765.

[173] Huang, C.-J.; Chang, F.-C. *Macromolecules* **2008**, *41*, 7041–7052.

[174] He, C.; Zhao, C.; Chen, X.; Guo, Z.; Zhuang, X.; Jing, X. *Macromol. Rapid Commun.* **2008**, *29*, 490–497.

[175] Zhao, C.; Zhuang, X.; He, C.; Chen, X.; Jing, X. *Macromol. Rapid Commun.* **2008**, *29*, 1810–1816.

[176] Rao, J.; Luo, Z.; Ge, Z.; Liu, H.; Liu, S. *Biomacromolecules* **2007**, *8*, 3871–3878.

[177] Lee, C. U.; Lu, L.; Chen, J.; Garno, J. C.; Zhang, D. *ACS Macro Lett.* **2013**, *2*, 436–440.

[178] Li, A.; Zhang, D. *Biomacromolecules* **2016**, *17*, 852–861.

[179] Xuan, S.; Lee, C. U.; Chen, C.; Doyle, A. B.; Zhang, Y.; Guo, L.; John, V. T.; Hayes, D.; Zhang, D. *Chem. Mater.* **2016**, *28*, 727–737.

[180] Gangloff, N.; Fetsch, C.; Luxenhofer, R. *Macromol. Rapid Commun.* **2013**, *34*, 997–1001.

[181] Fetsch, C.; Flecks, S.; Gieseler, D.; Marschelke, C.; Ulbricht, J.; van Pée, K.-H.; Luxenhofer, R. *Macromol. Chem. Phys.* **2015**, *216*, 547–560.

[182] Fetsch, C.; Gaitzsch, J.; Messager, L.; Battaglia, G.; Luxenhofer, R. *Sci. Rep.* **2016**, *6*, 33491.

[183] Higuchi, M.; Takizawa, A.; Kinoshita, T.; Tsujita, Y.; Okochi, K. *Macromolecules* **1990**, *23*, 361–365.

[184] Minoura, N.; Higuchi, M.; Kinoshita, T. *Mater. Sci. Eng. C* **1997**, *4*, 249–254.

[185] Zheng, N.; Song, Z.; Liu, Y.; Zhang, R.; Zhang, R.; Yao, C.; Uckun, F. M.; Yin, L.; Cheng, J. *J. Control. Release* **2015**, *205*, 231–239.

[186] Zelzer, M.; Heise, A. *Polym. Chem.* **2013**, *4*, 3896.

[187] Dmitrovic, V.; Habraken, G. J. M.; Hendrix, M. M. R. M.; Habraken, W. J. E. M.; Heise, A.; de With, G.; Sommerdijk, N. A. J. M. *Polymers (Basel).* **2012**, *4*, 1195–1210.

[188] Yu, H.; Tang, Z.; Zhang, D.; Song, W.; Duan, T.; Gu, J.; Chen, X. *Macromol. Biosci.* **2015**, *15*, 829–838.

[189] Farina, C.; Weber, M. S.; Meinl, E.; Wekerle, H.; Hohlfeld, R. *Lancet Neurol.* **2005**, *4*, 567–575.

[190] Yin, L.; Tang, H.; Kim, K. H.; Zheng, N.; Song, Z.; Gabrielson, N. P.; Lu, H.; Cheng, J. *Angew. Chemie - Int. Ed.* **2013**, *52*, 9182–9186.

[191] Vacogne, C. D.; Brosnan, S. M.; Masic, A.; Schlaad, H. *Polym. Chem.* **2015**, *6*, 5040–5052.

[192] Cao, J.; Hu, P.; Lu, L.; Chan, B. A.; Luo, B.-H.; Zhang, D. *Polym. Chem.* **2015**, *6*, 1226–1229.

[193] Lahasky, S. H.; Lu, L.; Huberty, W. a.; Cao, J.; Guo, L.; Garno, J. C.; Zhang, D. *Polym. Chem.* **2014**, *5*, 1418.

[194] Reyes, F. T.; Guo, L.; Hedgepeth, J. W.; Zhang, D.; Kelland, M. A. *Energy and Fuels* **2014**, *28*, 6889–6896.

[195] Dietz, V. E.; Fery, N.; Hamann, K. *Angew. Makromol. Chemie* **1974**, *35*, 115–129.

[196] Wang, J.; Gibson, M. I.; Barbey, R.; Xiao, S. J.; Klok, H. A. *Macromol. Rapid Commun.* **2009**, *30*, 845–850.

[197] Shen, Y.; Desseaux, S.; Aden, B.; Lokitz, B. S.; Kilbey, S. M.; Li, Z.; Klok, H. A. *Macromolecules* **2015**, *48*, 2399–2406.

[198] Schneider, M.; Fetsch, C.; Amin, I.; Jordan, R.; Luxenhofer, R. *Langmuir* **2013**, *29*, 6983–6988.

[199] Schneider, M.; Tang, Z.; Richter, M.; Marschelke, C.; Förster, P.; Wegener, E.; Amin, I.; Zimmermann, H.; Scharnweber, D.; Braun, H. G.; Luxenhofer, R.; Jordan, R. *Macromol. Biosci.* **2016**, *16*, 75–81.

[200] Lu, L.; Lahasky, S. H.; Zhang, D.; Garno, J. C. *ACS Appl. Mater. Interfaces* **2016**, *8*, 4014–4022.

[201] Fokina, A.; Klinker, K.; Braun, L.; Jeong, B. G.; Bae, W. K.; Barz, M.; Zentel, R. *Macromolecules* **2016**, *49*, 3663–3671.

[202] Gkikas, M.; Das, B. P.; Tsianou, M.; Iatrou, H.; Sakellariou, G. *Eur. Polym. J.* **2013**, *49*, 3095–3103.

[203] Hörtz, C.; Birke, A.; Kaps, L.; Decker, S.; Wächtersbach, E.; Fischer, K.; Schuppan, D.; Barz, M.; Schmidt, M. *Macromolecules* **2015**, *48*, 2074–2086.

[204] He, C.; Zhao, C.; Guo, X.; Guo, Z.; Chen, X.; Zhuang, X.; Liu, S.; Jing, X. *J. Polym. Sci. Part A Polym. Chem.* **2008**, *46*, 4140–4150.

[205] Yin, L.; Song, Z.; Kim, K. H.; Zheng, N.; Tang, H.; Lu, H.; Gabrielson, N.; Cheng, J. *Biomaterials* **2013**, *34*, 2340–2349.

[206] Marciel, A. B.; Chung, E. J.; Brettmann, B. K.; Leon, L. *Adv. Colloid Interface Sci.* **2016**,

[207] Scholz, C.; Wagner, E. *J. Control. Release* **2012**, *161*, 554–565.

[208] Ou, Z.; Muthukumar, M. *J. Chem. Phys.* **2006**, *124*, 154902.

[209] Männistö, M.; Vanderkerken, S.; Toncheva, V.; Elomaa, M.; Ruponen, M.; Schacht, E.; Urtti, A. *J. Control. Release* **2002**, *83*, 169–182.

[210] Warrant, R. W.; Kim, S. H. *Nature* **1978**, *271*, 130–135.

[211] Meyer, M.; Philipp, A.; Oskuee, R.; Schmidt, C.; Wagner, E. *J. Am. Chem. Soc.* **2008**, *130*, 3272–3273.

[212] Leng, M.; Felsenfeld, G. *Proc. Natl. Acad. Sci. U. S. A.* **1966**, *56*, 1325–32.

[213] Wu, G. Y.; Wu, C. H. *J. Biol. Chem.* **1987**, *262*, 4429–4432.

[214] Wagner, E.; Zenke, M.; Cotten, M.; Beug, H.; Birnstiel, M. *Proc. Natl. Acad. Sci. U. S. A.* **1990**, *87*, 3410–4.

[215] Wagner, E.; Zatloukal, K.; Cotten, M.; Kirlappos, H.; Mechtler, K.; Curiel, D. T.; Birnstiel, M. L. *Proc. Natl. Acad. Sci. U. S. A.* **1992**, *89*, 6099–6103.

[216] Wagner, E.; Plank, C.; Zatloukal, K.; Cotten, M.; Birnstiel, M. L. *Proc. Natl. Acad. Sci. U. S. A.* **1992**, *89*, 7934–7938.

[217] Zauner, W.; Ogris, M.; Wagner, E. *Adv. Drug Deliv. Rev.* **1998**, *30*, 97–113.

[218] Katayose, S.; Kataoka, K. *Adv. Biomater. Biomed. Eng. Drug Deliv. Syst.*; Springer Japan: Tokyo, 1996; pp 319–320.

[219] Kataoka, K.; Togawa, H.; Harada, A.; Yasugi, K.; Matsumoto, T.; Katayose, S. *Macromolecules* **1996**, *29*, 8556–8557.

[220] Katayose, S.; Kataoka, K. *Bioconjug. Chem.* **1997**, *8*, 702–707.

[221] Katayose, S.; Kataoka, K. *J. Pharm. Sci.* **1998**, *87*, 160–163.

[222] Harada-Shiba, M.; Yamauchi, K.; Harada, A.; Takamisawa, I.; Shimokado, K.; Kataoka, K. *Gene Ther.* **2002**, *9*, 407–414.

[223] Itaka, K.; Yamauchi, K.; Harada, A.; Nakamura, K.; Kawaguchi, H.; Kataoka, K. *Biomaterials* **2003**, *24*, 4495–4506.

[224] Katakura, H.; Harada, A.; Kataoka, K.; Furusho, M.; Tanaka, F.; Wada, H.; Ikenaka, K. *J. Gene Med.* **2004**, *6*, 471–477.

[225] Erbacher, P.; Bousser, M. T.; Raimond, J.; Monsigny, M.; Midoux, P.; Roche, A. C. *Hum. Gene Ther.* **1996**, *7*, 721–9.

[226] Midoux, P.; Monsigny, M. *Bioconjug. Chem.* **1999**, *10*, 406–411.

[227] Fajac, I.; Allo, J. C.; Souil, E.; Merten, M.; Pichon, C.; Figarella, C.; Monsigny, M.; Briand, P.; Midoux, P. *J. Gene Med.* **2000**, *2*, 368–378.

[228] Okuda, T.; Sugiyama, A.; Niidome, T.; Aoyagi, H. *Biomaterials* **2004**, *25*, 537–544.

[229] Kadlecova, Z.; Rajendra, Y.; Matasci, M.; Hacker, D.; Baldi, L.; Wurm, F. M.; Klok, H. A. *Macromol. Biosci.* **2012**, *12*, 794–804.

[230] Kadlecova, Z.; Baldi, L.; Hacker, D.; Wurm, F. M.; Klok, H. A. *Biomacromolecules* **2012**, *13*, 3127–3137.

[231] Kadlecova, Z.; Rajendra, Y.; Matasci, M.; Baldi, L.; Hacker, D. L.; Wurm, F. M.; Klok, H. A. *J. Control. Release* **2013**, *169*, 276–288.

[232] Kakizawa, Y.; Harada, A.; Kataoka, K. *Biomacromolecules* **2001**, *2*, 491–497.

[233] Miyata, K.; Kakizawa, Y.; Nishiyama, N.; Harada, A.; Yamasaki, Y.; Koyama, H.; Kataoka, K. *J. Am. Chem. Soc.* **2004**, *126*, 2355–61.

[234] Vachutinsky, Y.; Oba, M.; Miyata, K.; Hiki, S.; Kano, M. R.; Nishiyama, N.; Koyama, H.; Miyazono, K.; Kataoka, K. *J. Control. Release* **2011**, *149*, 51–57.

[235] Dirisala, A.; Osada, K.; Chen, Q.; Tockary, T. A.; Machitani, K.; Osawa, S.; Liu, X.; Ishii, T.; Miyata, K.; Oba, M.; Uchida, S.; Itaka, K.; Kataoka, K. *Biomaterials* **2014**, *35*, 5359–5368.

[236] Kim, H. J.; Kim, A.; Miyata, K.; Kataoka, K. *Adv. Drug Deliv. Rev.* **2016**, *104*, 61–77.

[237] Christie, R. J.; Matsumoto, Y.; Miyata, K.; Nomoto, T.; Fukushima, S.; Osada, K.; Halnaut, J.; Pittella, F.; Kim, H. J.; Nishiyama, N.; Kataoka, K. *ACS Nano* **2012**, *6*, 5174–5189.

[238] Nishida, H. et al. *J. Control. Release* **2015**, *231*, 29–37.

[239] Oe, Y.; Christie, R. J.; Naito, M.; Low, S. A.; Fukushima, S.; Toh, K.; Miura, Y.; Matsumoto, Y.; Nishiyama, N.; Miyata, K.; Kataoka, K. *Biomaterials* **2014**, *35*, 7887–7895.

[240] Yi, Y.; Kim, H. J.; Mi, P.; Zheng, M.; Takemoto, H.; Toh, K.; Kim, B. S.; Hayashi, K.; Naito, M.; Matsumoto, Y.; Miyata, K.; Kataoka, K. *J. Control. Release* **2016**,

[241] Itaka, K.; Kanayama, N.; Nishiyama, N.; Jang, W. D.; Yamasaki, Y.; Nakamura, K.; Kawaguchi, H.; Kataoka, K. *J. Am. Chem. Soc.* **2004**, *126*, 13612–13613.

[242] Kanayama, N.; Fukushima, S.; Nishiyama, N.; Itaka, K.; Jang, W. D.; Miyata, K.; Yamasaki, Y.; il Chung, U.; Kataoka, K. *ChemMedChem* **2006**, *1*, 439–444.

[243] Ge, Z.; Chen, Q.; Osada, K.; Liu, X.; Tockary, T. A.; Uchida, S.; Dirisala, A.; Ishii, T.; Nomoto, T.; Toh, K.; Matsumoto, Y.; Oba, M.; Kano, M. R.; Itaka, K.; Kataoka, K. *Biomaterials* **2014**, *35*, 3416–3426.

[244] Chen, Q.; Osada, K.; Ge, Z.; Uchida, S.; Tockary, T. A.; Dirisala, A.; Matsui, A.; Toh, K.; Takeda, K. M.; Liu, X.; Nomoto, T.; Ishii, T.; Oba, M.; Matsumoto, Y.; Kataoka, K. *Biomaterials* **2017**, *113*, 253–265.

[245] Uchida, S.; Kinoh, H.; Ishii, T.; Matsui, A.; Tockary, T. A.; Takeda, K. M.; Uchida, H.; Osada, K.; Itaka, K.; Kataoka, K. *Biomaterials* **2016**, *82*, 221–228.

[246] Uchida, H.; Itaka, K.; Uchida, S.; Ishii, T.; Suma, T.; Miyata, K.; Oba, M.; Nishiyama, N.; Kataoka, K. *J. Am. Chem. Soc.* **2016**, *138*, 1478–1481.

[247] Aini, H.; Itaka, K.; Fujisawa, A.; Uchida, H.; Uchida, S.; Fukushima, S.; Kataoka, K.; Saito, T.; Chung, U.-i.; Ohba, S. *Sci. Rep.* **2016**, *6*, 18743.

[248] Lin, C. Y.; Perche, F.; Ikegami, M.; Uchida, S.; Kataoka, K.; Itaka, K. *J. Control. Release* **2016**, *235*, 268–275.

[249] Tangsangasaksri, M.; Takemoto, H.; Naito, M.; Maeda, Y.; Sueyoshi, D.; Kim, H. J.; Miura, Y.; Ahn, J.; Azuma, R.; Nishiyama, N.; Miyata, K.; Kataoka, K. *Biomacromolecules* **2016**, *17*, 246–255.

[250] Sanjoh, M.; Miyata, K.; Christie, R. J.; Ishii, T.; Maeda, Y.; Pittella, F.; Hiki, S.; Nishiyama, N.; Kataoka, K. *Biomacromolecules* **2012**, *13*, 3641–3649.

[251] Zhang, R.; Zheng, N.; Song, Z.; Yin, L.; Cheng, J. *Biomaterials* **2014**, *35*, 3443–3454.

[252] He, H.; Zheng, N.; Song, Z.; Kim, K. H.; Yao, C.; Zhang, R.; Zhang, C.; Huang, Y.; Uckun, F. M.; Cheng, J.; Zhang, Y.; Yin, L. *ACS Nano* **2016**, *10*, 1859–1870.

[253] Nishiyama, N.; Matsumura, Y.; Kataoka, K. Development of polymeric micelles for targeting intractable cancers. 2016.

[254] Stapleton, S.; Milosevic, M.; Allen, C.; Zheng, J.; Dunne, M.; Yeung, I.; Jaffray, D. A. *PLoS One* **2013**, *8*, e81157.

[255] Lammers, T.; Aime, S.; Hennink, W. E.; Storm, G.; Kiessling, F. *Acc. Chem. Res.* **2011**, *44*, 1029–1038.

[256] Cabral, H.; Nishiyama, N.; Kataoka, K. *Acc. Chem. Res.* **2011**, *44*, 999–1008.

[257] Kaida, S.; Cabral, H.; Kumagai, M.; Kishimura, A.; Terada, Y.; Sekino, M.; Aoki, I.; Nishiyama, N.; Tani, T.; Kataoka, K. *Cancer Res.* **2010**, *70*, 7031–7041.

[258] Mi, P.; Cabral, H.; Kokuryo, D.; Rafi, M.; Terada, Y.; Aoki, I.; Saga, T.; Takehiko, I.; Nishiyama, N.; Kataoka, K. *Biomaterials* **2013**, *34*, 492–500.

[259] Mi, P.; Kokuryo, D.; Cabral, H.; Kumagai, M.; Nomoto, T.; Aoki, I.; Terada, Y.; Kishimura, A.; Nishiyama, N.; Kataoka, K. *J. Control. Release* **2014**, *174*, 63–71.

[260] Mi, P.; Dewi, N.; Yanagie, H.; Kokuryo, D.; Suzuki, M.; Sakurai, Y.; Li, Y.; Aoki, I.; Ono, K.; Takahashi, H.; Cabral, H.; Nishiyama, N.; Kataoka, K. *ACS Nano* **2015**, *9*, 5913–5921.

[261] Miura, Y.; Tsuji, A. B.; Sugyo, A.; Sudo, H.; Aoki, I.; Inubushi, M.; Yashiro, M.; Hirakawa, K.; Cabral, H.; Nishiyama, N.; Saga, T.; Kataoka, K. *ACS Biomater. Sci. Eng.* **2015**, *1*, 1067–1076.

[262] Imai, Y.; Kaneko, E.; Asano, T.; Kumagai, M.; Ai, M.; Kawakami, A.; Kataoka, K.; Shimokado, K. *J Atheroscler Thromb* **2007**, *14*, 65–71.

[263] Kumagai, M.; Imai, Y.; Nakamura, T.; Yamasaki, Y.; Sekino, M.; Ueno, S.; Hanaoka, K.; Kikuchi, K.; Nagano, T.; Kaneko, E.; Shimokado, K.; Kataoka, K. *Colloids Surfaces B Biointerfaces* **2007**, *56*, 174–181.

[264] Kumagai, M.; Kano, M. R.; Morishita, Y.; Ota, M.; Imai, Y.; Nishiyama, N.; Sekino, M.; Ueno, S.; Miyazono, K.; Kataoka, K. *J. Control. Release* **2009**, *140*, 306–311.

[265] Kawamura, W.; Miura, Y.; Kokuryo, D.; Toh, K.; Yamada, N.; Nomoto, T.; Matsumoto, Y.; Sueyoshi, D.; Liu, X.; Aoki, I.; Kano, M. R.; Nishiyama, N.; Saga, T.; Kishimura, A.; Kataoka, K. *Sci. Technol. Adv. Mater.* **2016**, *16*, 035004.

[266] Fujita, Y.; Taguchi, H. *Chem. Cent. J.* **2011**, *5*, 1–8.

[267] Vogel, F. R. *Ann. N. Y. Acad. Sci.* **1995**, *754*, 153–160.

[268] Heller, P.; Huesmann, D.; Scherer, M.; Barz, M. In *Mol. Vaccines From Prophyl. to Ther. - Vol. 2*; Giese, M., Ed.; Springer: Vienna/New York, 2014; pp 643–671.

[269] Irvine, D. J.; Hanson, M. C.; Rakhra, K.; Tokatlian, T. *Chem. Rev.* **2015**, *115*, 11109–11146.

[270] Barnier Quer, C.; Robson Marsden, H.; Romeijn, S.; Zope, H.; Kros, A.; Jiskoot, W. *Polym. Chem.* **2011**, *2*, 1482.

[271] Vogel, F. R. *Ann. NY Acad. Sci.* **1995**, *754*, 153–160.

[272] Petrovsky, N.; Aguilar, J. C. *Immunol. Cell Biol.* **2004**, *82*, 488–496.

[273] Panyam, J.; Labhasetwar, V. *Adv. Drug Deliv. Rev.* **2003**, *55*, 329–347.

[274] Lee, Y.-R. Y.-H.; Im, S.-A.; Yang, I.-H.; Ahn, G. W.; Kim, K.; Lee, C.-K. *Arch. Pharmacal Res.* **2010**, *33*, 1859–1866.

[275] Stone, G. W.; Barzee, S.; Snarsky, V.; Santucci, C.; Tran, B.; Langer, R.; Zugates, G. T.; Anderson, D. G.; Kornbluth, R. S. *PLoS One* **2009**, *4*, e7334.

[276] Kasturi, S. P. et al. *Nature* **2011**, *470*, 543–547.

[277] Malyala, P.; O'Hagan, D. T.; Singh, M. *Adv. Drug Deliv. Rev.* **2009**, *61*, 218–225.

[278] O'Hagan, D. T.; Singh, M.; Ulmer, J. B. *Methods* **2006**, *40*, 10–19.

[279] Sherman, M. R.; Williams, L. D.; Saifer, M. G. P.; French, J. A.; Kwak, L. W.; Oppenheim, J. J. *ACS Symp. Ser. Vol. 680* **1997**, 155–169.

[280] Alexis, F.; Pridgen, E.; Molnar, L. K.; Farokhzad, O. C. *Mol. Pharm.* **2008**, *5*, 505–515.

[281] Yang, Y.; Huang, C.-T.; Huang, X.; Pardoll, D. M. *Nat. Immunol.* **2004**, *5*, 508–515.

[282] Galloway, A. L.; Murphy, A.; DeSimone, J. M.; Di, J.; Herrmann, J. P.; Hunter, M. E.; Kindig, J. P.; Malinoski, F. J.; Rumley, M. a.; Stoltz, D. M.; Templeman, T. S.; Hubby, B. *Nanomedicine Nanotechnology, Biol. Med.* **2013**, *9*, 523–531.

[283] Demento, S. L.; Bonafé, N.; Cui, W.; Kaech, S. M.; Caplan, M. J.; Fikrig, E.; Ledizet, M.; Fahmy, T. M. *J. Immunol.* **2010**, *185*, 2989–2997.

[284] Tyagi, R. K.; Garg, N. K.; Sahu, T. *J. Control. Release* **2012**, *162*, 242–254.

[285] Brandt, E. R.; Sriprakash, K. S.; Hobb, R. I.; Hayman, W. a.; Zeng, W.; Batzloff, M. R.; Jackson, D. C.; Good, M. F. *Nat. Med.* **2000**, *6*, 455–9.

[286] Feng, L.; Qi, X. R.; Zhou, X. J.; Maitani, Y.; Cong Wang, S.; Jiang, Y.; Nagai, T. *J. Control. Release* **2006**, *112*, 35–42.

[287] Pejawar-Gaddy, S.; Rajawat, Y.; Hilioti, Z.; Xue, J.; Gaddy, D. F.; Finn, O. J.; Viscidi, R. P.; Bossis, I. *Cancer Immunol. Immunother.* **2010**, *59*, 1685–1696.

[288] Sundgren, A.; Barchi, J. J. *Carbohydr. Res.* **2008**, *343*, 1594–1604.

[289] Monzavi-Karbassi, B.; Pashov, A.; Jousheghany, F.; Artaud, C.; Kieber-Emmons, T. *Int. J. Mol. Med.* **2006**, *17*, 1045–1052.

[290] Reddy, S. T.; Swartz, M. A.; Hubbell, J. A. *Trends Immunol.* **2006**, *27*, 573–579.

[291] Demento, S. L.; Eisenbarth, S. C.; Foellmer, H. G.; Platt, C.; Caplan, M. J.; Mark Saltzman, W.; Mellman, I.; Ledizet, M.; Fikrig, E.; Flavell, R. a.; Fahmy, T. M. *Vaccine* **2009**, *27*, 3013–3021.

[292] Hamdy, S.; Molavi, O.; Ma, Z.; Haddadi, A.; Alshamsan, A.; Gobti, Z.; Elhasi, S.; Samuel, J.; Lavasanifar, A. *Vaccine* **2008**, *26*, 5046–5057.

[293] Barton, G. M.; Medzhitov, R. *Curr. Opin. Immunol.* **2002**, *14*, 380–383.

[294] Akagi, T.; Baba, M.; Akashi, M. *Adv. Polym. Sci.* **2011**, 31–64.

[295] Lee, T. Y.; Kim, Y. H.; Yoon, S. W.; Choi, J. C.; Yang, J. M.; Kim, C. J.; Schiller, J. T.; Sung, M. H.; Poo, H. *Cancer Immunol. Immunother.* **2009**, *58*, 1781–1794.

[296] Yoshida, M.; Babensee, J. E. *J. Biomed. Mater. Res. - Part A* **2004**, *71*, 45–54.

[297] Tamayo, I.; Irache, J. M.; Mansilla, C.; Ochoa-Repáraz, J.; Lasarte, J. J.; Gamazo, C. *Clin. Vaccine Immunol.* **2010**, *17*, 1356–1362.

[298] Copland, M.; Baird, M.; Rades, T.; McKenzie, J.; Becker, B.; Reck, F.; Tyler, P.; Davies, N. *Vaccine* **2003**, *21*, 883–890.

[299] Matsusaki, M.; Larsson, K.; Akagi, T.; Lindstedt, M.; Akashi, M.; Borrebaeck, C. a. K. *Nano Lett.* **2005**, *5*, 2168–2173.

[300] Kwon, Y. J.; Standley, S. M.; Goh, S. L.; Fréchet, J. M. J. *J. Control. Release* **2005**, *105*, 199–212.

[301] Sun, H.; Pollock, K. G. J.; Brewer, J. M. *Vaccine* **2003**, *21*, 849–855.

[302] Moon, H. J.; Lee, J. S.; Talactac, M. R.; Chowdhury, M. Y. E.; Kim, J. H.; Park, M. E.; Choi, Y. K.; Sung, M. H.; Kim, C. J. *Vet. Microbiol.* **2012**, *160*, 277–289.

[303] Geall, A. J. et al. *Proc. Natl. Acad. Sci. U. S. A.* **2012**, *109*, 14604–9.

[304] van den Berg, J. H.; Oosterhuis, K.; Hennink, W. E.; Storm, G.; van der Aa, L. J.; Engbersen, J. F. J.; Haanen, J. B. a. G.; Beijnen, J. H.; Schumacher, T. N.; Nuijen, B. *J. Control. Release* **2010**, *141*, 234–240.

[305] Varkouhi, A. K.; Scholte, M.; Storm, G.; Haisma, H. J. *J. Control. Release* **2011**, *151*, 220–228.

[306] Krieg, A. M. *Annu. Rev. Immunol.* **2002**, *20*, 709–760.

[307] Joshi, M. D.; Unger, W. J.; Storm, G.; van Kooyk, Y.; Mastrobattista, E. *J. Control. Release* **2012**, *161*, 25–37.

[308] White, K. L.; Rades, T.; Furneaux, R. H.; Tyler, P. C.; Hook, S. *J. Pharm. Pharmacol.* **2006**, *58*, 729–737.

[309] Copland, M. J.; Baird, M. a.; Rades, T.; McKenzie, J. L.; Becker, B.; Reck, F.; Tyler, P. C.; Davies, N. M. *Vaccine* **2003**, *21*, 883–890.

[310] Arigita, C.; Bevaart, L.; Everse, L. A.; Koning, G. A.; Hennink, W. E.; Crommelin, D. J. A.; van de Winkel, J. G. J.; van Vugt, M. J.; Kersten, G. F. A.; Jiskoot, W. *Infect. Immun.* **2003**, *71*, 5210–5218.

[311] Espuelas, S.; Haller, P.; Schuber, F.; Frisch, B. *Bioorg. Med. Chem. Lett.* **2003**, *13*, 2557–2560.

[312] Espuelas, S.; Thumann, C.; Heurtault, B.; Schuber, F.; Frisch, B. *Bioconjug. Chem.* **2008**, *19*, 2385–2393.

[313] Sheng, K.-C.; Kalkanidis, M.; Pouniotis, D. S.; Esparon, S.; Tang, C. K.; Apostolopoulos, V.; Pietersz, G. A. *Eur. J. Immunol.* **2008**, *38*, 424–436.

[314] Chenevier, P.; Grandjean, C.; Loing, E.; Malingue, F.; Angyalosi, G.; Gras-Masse, H.; Roux, D.; Melnyk, O.; Bourel-Bonnet, L. *Chem. Commun.* **2002**, 2446–2447.

[315] Saraogi, G. K.; Sharma, B.; Joshi, B.; Gupta, P.; Gupta, U. D.; Jain, N. K.; Agrawal, G. P. *J. Drug Target.* **2011**, *19*, 219–227.

[316] Brandhonneur, N.; Chevanne, F.; Vié, V.; Frisch, B.; Primault, R.; Le Potier, M. F.; Le Corre, P. *Eur. J. Pharm. Sci.* **2009**, *36*, 474–485.

[317] Hamdy, S.; Haddadi, A.; Shayeganpour, A.; Samuel, J.; Lavasanifar, A. *Pharm. Res.* **2011**, *28*, 2288–2301.

[318] Raghuwanshi, D.; Mishra, V.; Suresh, M. R.; Kaur, K. *Vaccine* **2012**, *30*, 7292–7299.

[319] Fehr, T.; Skrastina, D.; Pumpens, P.; Zinkernagel, R. M. *Proc. Natl. Acad. Sci. U. S. A.* **1998**, *95*, 9477–81.

[320] Brin??s, R. P.; Sundgren, A.; Sahoo, P.; Morey, S.; Rittenhouse-Olson, K.; Wilding, G. E.; Deng, W.; Barchi, J. J. *Bioconjug. Chem.* **2012**, *23*, 1513–1523.

[321] Hoffmann-R??der, A.; Kaiser, A.; Wagner, S.; Gaidzik, N.; Kowalczyk, D.; Westerlind, U.; Gerlitzki, B.; Schmitt, E.; Kunz, H. *Angew. Chemie - Int. Ed.* **2010**, *49*, 8498–8503.

[322] Gaidzik, N.; Kaiser, A.; Kowalczyk, D.; Westerlind, U.; Gerlitzki, B.; Sinn, H. P.; Schmitt, E.; Kunz, H. *Angew. Chemie - Int. Ed.* **2011**, *50*, 9977–9981.

[323] Cai, H.; Huang, Z. H.; Shi, L.; Sun, Z. Y.; Zhao, Y. F.; Kunz, H.; Li, Y. M. *Angew. Chemie - Int. Ed.* **2012**, *51*, 1719–1723.

[324] Wolfgang Schärtl, *Light Scattering from Polymer Solutions and Nanoparticle*; Springer Laboratory; Springer: Berlin, Heidelberg, 2007; p 199.

[325] Rausch, K.; Reuter, A.; Fischer, K.; Schmidt, M. *Biomacromolecules* **2010**, *11*, 2836–2839.

[326] Fischer, K.; Schmidt, M. *Biomaterials* **2016**, *98*, 79–91.

[327] Shaw, D. E.; Maragakis, P.; Lindorff-Larsen, K.; Piana, S.; Dror, R. O.; Eastwood, M. P.; Bank, J. A.; Jumper, J. M.; Salmon, J. K.; Shan, Y.; Wriggers, W. *Science* **2010**, *330*, 341–6.

[328] Stevens, M. J.; Kremer, K. *J. Chem. Phys.* **1995**, *103*, 1669.

[329] Rouse, P. E. *J. Chem. Phys.* **1953**, *21*, 1272.

[330] Gould, S. J.; Subramani, S. *Anal. Biochem.* **1988**, *175*, 5–13.

[331] Mosmann, T. *J. Immunol. Methods* **1983**, *65*, 55–63.

[332] Chen, Q.; Osada, K.; Ishii, T.; Oba, M.; Uchida, S.; Tockary, T. A.; Endo, T.; Ge, Z.; Kinoh, H.; Kano, M. R.; Itaka, K.; Kataoka, K. *Biomaterials* **2012**, *33*, 4722–4730.

[333] Maguire, A. M. et al. *N. Engl. J. Med.* **2008**, *358*, 2240–8.

[334] Cartier, N.; Aubourg, P. *Brain Pathol.* **2010**, *20*, 857–862.

[335] LeWitt, P. A. et al. *Lancet Neurol.* **2011**, *10*, 309–319.

[336] Fischer, A.; Hacein-Bey Abina, S.; Cavazzana-Calvo, M. *Nat. Immunol.* **2010**, *11*, 457–460.

[337] Ji, W.; Panus, D.; Palumbo, R. N.; Tang, R.; Wang, C. *Biomacromolecules* **2011**, *12*, 4373–4385.

[338] Moulin, V.; Morgan, M. E.; Eleveld-Trancikova, D.; Haanen, J. B. A. G.; Wielders, E.; Looman, M. W. G.; Janssen, R. A. J.; Figdor, C. G.; Jansen, B. J. H.; Adema, G. J. *Cancer Gene Ther.* **2012**, *19*, 303–311.

[339] Celli, S.; Day, M.; Müller, A. J.; Molina-Paris, C.; Lythe, G.; Bousso, P. *Blood* **2012**, *120*, 3945–3948.

[340] Irvine, A. S.; Trinder, P. K.; Laughton, D. L.; Ketteringham, H.; McDermott, R. H.; Reid, S. C.; Haines, A. M.; Amir, A.; Husain, R.; Doshi, R.; Young, L. S.; Mountain, A. *Nat. Biotechnol.* **2000**, *18*, 1273–1278.

[341] Wang, C.; Ge, Q.; Ting, D.; Nguyen, D.; Shen, H.-R.; Chen, J.; Eisen, H. N.; Heller, J.; Langer, R.; Putnam, D. *Nat. Mater.* **2004**, *3*, 190–6.

[342] Robinson, H. L.; Pertmer, T. M. *Adv. Virus Res.* **2000**, *55*, 1–74.

[343] Yue, Y.; Wu, C. *Biomater. Sci.* **2013**, *1*, 152–170.

[344] Hunter, A. C. *Adv. Drug Deliv. Rev.* **2006**, *58*, 1523–1531.

[345] Moghimi, S. M.; Symonds, P.; Murray, J. C.; Hunter, a. C.; Debska, G.; Szewczyk, A. *Mol. Ther.* **2005**, *11*, 990–995.

[346] Nayak, S.; Herzog, R. W. *Gene Ther.* **2010**, *17*, 295–304.

[347] Martin, I.; Dohmen, C.; Mas-Moruno, C.; Troiber, C.; Kos, P.; Schaffert, D.; Lächelt, U.; Teixidó, M.; Günther, M.; Kessler, H.; Giralt, E.; Wagner, E. *Org. Biomol. Chem.* **2012**, *10*, 3258.

[348] Miyata, K.; Nishiyama, N.; Kataoka, K. *Chem. Soc. Rev.* **2012**, *41*, 2562–2574.

[349] Zhang, Y.; Zheng, M.; Kissel, T.; Agarwal, S. *Biomacromolecules* **2012**, *13*, 313–322.

[350] Ogris, M.; Brunner, S.; Schüller, S.; Kircheis, R.; Wagner, E. *Gene Ther.* **1999**, *6*, 595–605.

[351] Nguyen, H.-K.; Lemieux, P.; Vinogradov, S. V.; Gebhart, C. L.; Guerin, N.; Paradis, G.; Bronich, T. K.; Alakhov, V. Y.; Kabanov, A. V. *Gene Ther.* **2000**, *7*, 126–138.

[352] Parelkar, S. S.; Chan-Seng, D.; Emrick, T. *Biomaterials* **2011**, *32*, 2432–2444.

[353] Emi, N.; Kidoaki, S.; Yoshikawa, K.; Saito, H. *Biochem. Biophys. Res. Commun.* **1997**, *231*, 421–424.

[354] Tockary, T. A.; Osada, K.; Chen, Q.; MacHitani, K.; Dirisala, A.; Uchida, S.; Nomoto, T.; Toh, K.; Matsumoto, Y.; Itaka, K.; Nitta, K.; Nagayama, K.; Kataoka, K. *Macromolecules* **2013**, *46*, 6585–6592.

[355] Uchida, S.; Itaka, K.; Chen, Q.; Osada, K.; Ishii, T.; Shibata, M.-A.; Harada-Shiba, M.; Kataoka, K. *Mol. Ther.* **2012**, *20*, 1196–203.

[356] Nie, Y.; Günther, M.; Gu, Z.; Wagner, E. *Biomaterials* **2011**, *32*, 858–869.

[357] Lutz, J.-F.; Hoth, A. *Macromolecules* **2006**, *39*, 893–896.

[358] Hoogenboom, R. *Angew. Chemie - Int. Ed.* **2009**, *48*, 7978–7994.

[359] Barz, M.; Luxenhofer, R.; Zentel, R.; Vicent, M. J. *Polym. Chem.* **2011**, *2*, 1900–1918.

[360] He, Y.; Cheng, G.; Xie, L.; Nie, Y.; He, B.; Gu, Z. *Biomaterials* **2013**, *34*, 1235–1245.

[361] Zhou, M.; Liu, H.; Venkiteshwaran, A.; Kilduff, J.; Anderson, D. G.; Langer, R.; Belfort, G. *J. Mater. Chem.* **2011**, *21*, 693.

[362] Ostuni, E.; Chapman, R. G.; Holmlin, R. E.; Takayama, S.; Whitesides, G. M. *Langmuir* **2001**, *17*, 5605–5620.

[363] Makino, A.; Kizaka-Kondoh, S.; Yamahara, R.; Hara, I.; Kanzaki, T.; Ozeki, E.; Hiraoka, M.; Kimura, S. *Biomaterials* **2009**, *30*, 5156–5160.

[364] Sun, J.; Zuckermann, R. N. *ACS Nano* **2013**, *7*, 4715–4732.

[365] Petersen, H.; Fechner, P. M.; Martin, A. L.; Kunath, K.; Stolnik, S.; Roberts, C. J.; Fischer, D.; Davies, M. C.; Kissel, T. *Bioconjug. Chem.* **2002**, *13*, 845–854.

[366] Deming, T. J. *Adv. Mater.* **1997**, *9*, 299–311.

[367] Oya, M.; Katakai, R.; Nakai, H.; Iwakura, Y. *Chem. Lett.* **1973**, 1143–1144.

[368] Kricheldorf, H. R. *Chem. Ber.* **1971**, *104*, 87–91.

[369] Wuts, P.; Greene, T. *Greene's protective groups in organic synthesis*; John Wiley & Sons, 2007; pp 152–163.

[370] Naito, M.; Ishii, T.; Matsumoto, A.; Miyata, K.; Miyahara, Y.; Kataoka, K. *Angew. Chemie - Int. Ed.* **2012**, *51*, 10751–10755.

[371] Rodríguez-Hernández, J.; Gatti, M.; Klok, H. A. *Biomacromolecules* **2003**, *4*, 249–258.

[372] Mizrahi, A.; Czerniak, A.; Levy, T.; Amiur, S.; Gallula, J.; Matouk, I.; Abu-lail, R.; Sorin, V.; Birman, T.; de Groot, N.; Hochberg, A.; Ohana, P. *J. Transl. Med.* **2009**, *7*, 69.

[373] Christie, R. J.; Nishiyama, N.; Kataoka, K. *Endocrinology* **2010**, *151*, 466–473.

[374] Vermes, I.; Haanen, C.; Steffens-Nakken, H.; Reutelingsperger, C. *J. Immunol. Methods* **1995**, *184*, 39–51.

[375] Smeets, N. M. B.; Van Der Weide, P. L. J.; Meuldijk, J.; Vekemans, J. A. J. M.; Hulshof, L. A. *Org. Process Res. Dev.* **2005**, *9*, 757–763.

[376] Cherevin, M. S.; Gulevich, T. G.; Popova, L. A.; Zubreichuk, Z. P.; Knizhnikov, V. a. *Russ. J. Org. Chem.* **2007**, *43*, 1427–1431.

[377] Lai, E.; Zanten, J. H. V. *Biophys. J.* **2001**, *80*, 864–873.

[378] Zhao, H.; Li, Y.; Hu, Y. *Clin. Proteomics* **2014**, *11*, 21.

[379] Sparks, M. A.; Williams, K. W.; Whitesides, G. M. *J Med Chem* **1993**, *36*, 778–783.

[380] Mammen, M.; Dahmann, G.; Whitesides, G. M. *J. Med. Chem* **1996**, *38*, 4179–4190.

[381] Qian, X.; Metallo, S. J.; Choi, I. S.; Wu, H.; Liang, M. N.; Whitesides, G. M. *Anal. Chem.* **2002**, *74*, 1805–1810.

[382] Papp, I.; Dernedde, J.; Enders, S.; Riese, S. B.; Shiao, T. C.; Roy, R.; Haag, R. *ChemBioChem* **2011**, *12*, 1075–1083.

[383] Ponader, D.; Wojcik, F.; Beceren-Braun, F.; Dernedde, J.; Hartmann, L. *Biomacromolecules* **2012**, *13*, 1845–1852.

[384] Ponader, D.; Maffre, P.; Aretz, J.; Pussak, D.; Ninnemann, N. M.; Schmidt, S.; Seeberger, P. H.; Rademacher, C.; Nienhaus, G. U.; Hartmann, L. *J. Am. Chem. Soc.* **2014**, *136*, 2008–2016.

[385] Bonduelle, C.; Lecommandoux, S. *Biomacromolecules* **2013**, *14*, 2973–2983.

[386] Lundquist, J. J.; Toone, E. J. *Chem. Rev.* **2002**, *102*, 555–78.

[387] Qian, Z. M.; Li, H.; Sun, H.; Ho, K. *Pharmacol. Rev.* **2002**, *54*, 561–87.

[388] Li, H.; Qian, Z. M. *Med. Res. Rev.* **2002**, *22*, 225–250.

[389] Irache, J. M.; Salman, H. H.; Gamazo, C.; Espuelas, S. *Expert Opin. Drug Deliv.* **2008**, *5*, 703–724.

[390] Cureton, D. K.; Massol, R. H.; Saffarian, S.; Kirchhausen, T. L.; Whelan, S. P. J. *PLoS Pathog.* **2009**, *5*, e1000394.

[391] Pelkmans, L.; Kartenbeck, J.; Helenius, A. *Nat. Cell Biol.* **2001**, *3*, 473–483.

[392] Joshi, M. M. D.; Unger, W. W. J.; Storm, G.; van Kooyk, Y.; Mastrobattista, E. *J. Control. Release* **2012**, *161*, 25–37.

[393] Arigita, C.; Kersten, G. F. A.; Hazendonk, T.; Hennink, W. E.; Crommelin, D. J. A.; Jiskoot, W. *Vaccine* **2003**, *21*, 950–960.

[394] Shimizu, Y.; Yamakami, K.; Gomi, T.; Nakata, M.; Asanuma, H.; Tadakuma, T.; Kojima, N. *Bioorganic Med. Chem.* **2003**, *11*, 1191–1195.

[395] White, K.; Rades, T.; Kearns, P.; Toth, I.; Hook, S. *Pharm. Res.* **2006**, *23*, 1473–1481.

[396] Chono, S.; Tanino, T.; Seki, T.; Morimoto, K. *J. Control. Release* **2008**, *127*, 50–8.

[397] Sinha, J.; Mukhopadhyay, S.; Das, N.; Basu, M. K. *Drug Deliv.* **2000**, *7*, 209–13.

[398] Mitra, M.; Mandal, A. K.; Chatterjee, T. K.; Das, N. *J. Drug Target.* **2005**, *13*, 285–93.

[399] Brinkhuis, R. P. R. P.; Rutjes, F. P. J. T.; van Hest, J. C. M. *Polym. Chem.* **2011**, *2*, 1449.

[400] Hrkach, J. et al. *Sci. Transl. Med.* **2012**, *4*, 128ra39–128ra39.

[401] He, L.; Szameit, K.; Zhao, H.; Hahn, U.; Theato, P. *Biomacromolecules* **2014**, *15*, 3197–3205.

[402] Gauthier, M.; Gibson, M.; Klok, H.-A. *Angew. Chemie Int. Ed.* **2009**, *48*, 48–58.

[403] Krannig, K.-S.; Huang, J.; Heise, A.; Schlaad, H. *Polym. Chem.* **2013**, *4*, 3981.

[404] Krannig, K. S.; Doriti, A.; Schlaad, H. *Macromolecules* **2014**, *47*, 2536–2539.

[405] Huang, J.; Heise, A. *Chem. Soc. Rev.* **2013**, *42*, 7373–90.

[406] Huang, J.; Bonduelle, C.; Thévenot, J.; Lecommandoux, S.; Heise, A. *J. Am. Chem. Soc.* **2012**, *134*, 119–122.

[407] Wei, Q.; Becherer, T.; Angioletti-Uberti, S.; Dzubiella, J.; Wischke, C.; Neffe, A. T.; Lendlein, A.; Ballauff, M.; Haag, R. *Angew. Chemie - Int. Ed.* **2014**, *53*, 8004–8031.

[408] Weis, W. I.; Drickamer, K.; Hendrickson, W. a. *Nature* **1992**, *360*, 127–134.

[409] Rejman, J.; Oberle, V.; Zuhorn, I. S.; Hoekstra, D. *Biochem. J.* **2004**, *377*, 159–69.

[410] Cui, Z.; Han, S. J.; Huang, L. *Pharm. Res.* **2004**, *21*, 1018–1025.

[411] Hattori, Y.; Kawakami, S.; Lu, Y.; Nakamura, K.; Yamashita, F.; Hashida, M. *J. Gene Med.* **2006**, *8*, 824–834.

[412] Cui, L.; Cohen, J. a.; Broaders, K. E.; Beaudette, T. T.; Fréchet, J. M. J. *Bioconjug. Chem.* **2011**, *22*, 949–957.

[413] Sun, X.; Chen, S.; Han, J.; Zhang, Z. *Int. J. Nanomedicine* **2012**, *7*, 2929–2942.

[414] Perche, F.; Gosset, D.; Mével, M.; Miramon, M.-L.; Yaouanc, J.-J.; Pichon, C.; Benvegnu, T.; Jaffrès, P.-A.; Midoux, P. *J. Drug Target.* **2011**, *19*, 315–25.

[415] Macia, E.; Ehrlich, M.; Massol, R.; Boucrot, E.; Brunner, C.; Kirchhausen, T. *Dev. Cell* **2006**, *10*, 839–850.

[416] Burgdorf, S.; Lukacs-Kornek, V.; Kurts, C. *J. Immunol.* **2006**, *176*, 6770–6776.

[417] Gazi, U.; Martinez-Pomares, L. *Immunobiology* **2009**, *214*, 554–561.

[418] Stahl, P.; Schlesinger, P. H.; Sigardson, E.; Rodman, J. S.; Lee, Y. C. *Cell* **1980**, *19*, 207–215.

[419] Xie, H.; Braha, O.; Gu, L. Q.; Cheley, S.; Bayley, H. *Chem. Biol.* **2005**, *12*, 109–210.

[420] Nóbrega, C.; Vázquez, J. T. *Tetrahedron Asymmetry* **2003**, *14*, 2793–2801.

[421] Shen, Z.; Reznikoff, G.; Dranoff, G.; Rock, K. L. *J. Immunol.* **1997**, *158*, 2723–30.

[422] Scheicher, C.; Mehlig, M.; Zecher, R.; Reske, K. *J. Immunol. Methods* **1992**, *154*, 253–264.

[423] Gisch, K.; Gehrke, N.; Bros, M.; Priesmeyer, C.; Knop, J.; Reske-Kunz, A. B.; Sudowe, S. *Int. Arch. Allergy Immunol.* **2007**, *144*, 183–196.

[424] Zal, T.; Volkmann, A.; Stockinger, B. *J. Exp. Med.* **1994**, *180*, 2089–2099.

[425] Guenther, W.; Kunz, H. *Carbohydr. Res.* **1992**, *228*, 217–241.

[426] Cabral, H.; Kataoka, K. *J. Control. Release* **2014**,

[427] Kricheldorf, H. R.; Bösinger, K. *Makromol. Chemie* **1976**, *177*, 1243–1258.

[428] Ulbricht, J.; Jordan, R.; Luxenhofer, R. *Biomaterials* **2014**, *35*, 4848–4861.

[429] Hadjichristidis, N.; Iatrou, H.; Pitsikalis, M.; Sakellariou, G. *Chem. Rev.* **2009**, *109*, 5528–5578.

[430] Cheng, J.; Deming, T. J. *Top. Curr. Chem.* **2012**, *310*, 1–26.

[431] Lu, H.; Wang, J.; Song, Z.; Yin, L.; Zhang, Y.; Tang, H.; Tu, C.; Lin, Y.; Cheng, J. *Chem. Commun.* **2014**, *50*, 139–155.

[432] Dygert, M. K.; Taylor, G. T.; Cardinaux, F.; Scheraga, H. A. *Macromolecules* **1976**, *9*, 794–801.

[433] Li, J.; Wang, T.; Wu, D.; Zhang, X.; Yan, J.; Du, S.; Guo, Y.; Wang, J.; Zhang, A. *Biomacromolecules* **2008**, *9*, 2670–2676.

[434] Barrett, S. E. et al. *J. Control. Release* **2014**, *183*, 124–137.

[435] Plante, L. T.; Crawford, E. J.; Friedkin, M. *J. Med. Chem.* **1976**, *19*, 1295–1299.

[436] Naldini, L. *Nature* **2015**, *526*, 351–360.

[437] Itaka, K.; Kataoka, K. *Curr. Gene Ther.* **2011**, *11*, 457–65.

[438] Chu, T. W.; Feng, J.; Yang, J.; Kopeček, J. *J. Control. Release* **2015**, *220*, 608–616.

[439] Nuhn, L.; Barz, M.; Zentel, R. *Macromol. Biosci.* **2014**, *14*, 607–618.

[440] Lutz, J.; Hoth, A. *Macromolecules* **2006**, *39*, 893–896.

[441] Steinbach, T.; Wurm, F. R. *Angew. Chemie - Int. Ed.* **2015**, *54*, 6098–6108.

[442] Shi, J.; Schellinger, J. G.; Johnson, R. N.; Choi, J. L.; Chou, B.; Anghel, E. L.; Pun, S. H. *Biomacromolecules* **2013**, *14*, 1961–1970.

[443] Mai, Y.; Eisenberg, A. *Chem. Soc. Rev.* **2012**, *41*, 5969.

[444] Gröschel, A. H.; Schacher, F. H.; Schmalz, H.; Borisov, O. V.; Zhulina, E. B.; Walther, A.; Müller, A. H. *Nat. Commun.* **2012**, *3*, 710–719.

[445] Betthausen, E.; Hanske, C.; Müller, M.; Fery, A.; Schacher, F. H.; Müller, A. H. E.; Pochan, D. J. *Macromolecules* **2014**, *47*, 1672–1683.

[446] Peng, B.; Muthukumar, M. *J. Chem. Phys.* **2015**, *143*, 243133.

[447] Zhou, J.; Barz, M.; Schmid, F. *J. Chem. Phys.* **2016**, *144*, 164902.

[448] Jiang, X.; Qu, W.; Pan, D.; Ren, Y.; Williford, J. M.; Cui, H.; Luijten, E.; Mao, H. Q. *Adv. Mater.* **2013**, *25*, 227–232.

[449] Limbach, H. J.; Arnold, A.; Mann, B. A.; Holm, C. *Comput. Phys. Commun.* **2006**, *174*, 704–727.

[450] Rattan, R.; Vaidyanathan, S.; Wu, G. S. H.; Shakya, A.; Orr, B. G.; Banaszak Holl, M. M. *Mol. Pharm.* **2013**, *10*, 3013–3022.

[451] Rattan, R.; Bielinska, A. U.; Banaszak Holl, M. M. *J. Gene Med.* **2014**, *16*, 75–83.

[452] Hansen, A. L.; Kay, L. E. *Proc. Natl. Acad. Sci.* **2014**, *111*, E1705–E1712.

[453] Li, J.; Chen, Q.; Zha, Z.; Li, H.; Toh, K.; Dirisala, A.; Matsumoto, Y.; Osada, K.; Kataoka, K.; Ge, Z. *J. Control. Release* **2015**, *209*, 77–87.

[454] Hill, I. R.; Garnett, M. C.; Bignotti, F.; Davis, S. S. *Anal. Biochem.* **2001**, *291*, 62–8.

[455] Humphrey, W.; Dalke, A.; Schulten, K. *J. Mol. Graph.* **1996**, *14*, 33–38.

[456] Höhn, Y.; Sudowe, S.; Reske-Kunz, A. B. *Methods Mol. Biol.* **2013**, *940*, 199–213.

[457] Nguyen, D. N.; Green, J. J.; Chan, J. M.; Langer, R.; Anderson, D. G. *Adv. Mater.* **2009**, *21*, 847–867.

[458] Akinc, A. et al. *Nat. Biotechnol.* **2008**, *26*, 561–9.

[459] Anderson, D. G.; Lynn, D. M.; Langer, R. *Angew. Chemie - Int. Ed.* **2003**, *42*, 3153–3158.

[460] Favretto, M. E.; Krieg, A.; Schubert, S.; Schubert, U. S.; Brock, R. *J. Control. Release* **2015**, *209*, 1–11.

[461] He, D.; Müller, K.; Krhac Levacic, A.; Kos, P.; Lächelt, U.; Wagner, E. *Bioconjug. Chem.* **2016**, *27*, 647–659.

[462] Cheng, Y.; Yumul, R. C.; Pun, S. H. *Angew. Chemie - Int. Ed.* **2016**, *55*, 12013–12017.

[463] Neu, M.; Germershaus, O.; Mao, S.; Voigt, K. H.; Behe, M.; Kissel, T. *J. Control. Release* **2007**, *118*, 370–380.

[464] Nomoto, T.; Matsumoto, Y.; Miyata, K.; Oba, M.; Fukushima, S.; Nishiyama, N.; Yamasoba, T.; Kataoka, K. *J. Control. Release* **2011**, *151*, 104–109.

[465] Boussif, O.; Lezoualc'h, F.; Zanta, M. A.; Mergny, M. D.; Scherman, D.; Demeneix, B.; Behr, J. P. *Proc. Natl. Acad. Sci. U. S. A.* **1995**, *92*, 7297–301.

[466] Haensler, J.; Szoka, F. C. *Bioconjug. Chem.* **1993**, *4*, 372–379.

[467] Lin, C.; Engbersen, J. F. J. *J. Control. Release* **2008**, *132*, 267–272.

[468] Copolovici, D. M.; Langel, K.; Eriste, E.; Langel, l. *ACS Nano* **2014**, *8*, 1972–1994.

[469] Oupický, D.; Carlisle, R. C.; Seymour, L. W. *Gene Ther.* **2001**, *8*, 713–724.

[470] Piao, J.-G.; Yan, J.-J.; Wang, M.-Z.; Wu, D.-C.; You, Y.-Z. *Biomater. Sci.* **2014**, *2*, 390.

[471] Russ, V.; Frohlich, T.; Li, Y.; Halama, A.; Ogris, M.; Wagner, E. *J. Gene Med.* **2010**, *12*, 180–193.

[472] Meister, A.; Anderson, M. E. *Annu. Rev. Biochem.* **1983**, *52*, 711–760.

[473] Trubetskoy, V. S.; Loomis, A.; Slattum, P. M.; Hagstrom, J. E.; Budker, V. G.; Wolf, J. a. *Bioconjug. Chem.* **1999**, *10*, 624–628.

[474] Neu, M.; Sitterberg, J.; Bakowsky, U.; Kissel, T. *Biomacromolecules* **2006**, *7*, 3428–3438.

[475] Novo, L.; Van Gaal, E. V. B.; Mastrobattista, E.; Van Nostrum, C. F.; Hennink, W. E. *J. Control. Release* **2013**, *169*, 246–256.

[476] Arunachalam, B.; Phan, U. T.; Geuze, H. J.; Cresswell, P. *Pnas* **2000**, *97*, 745–750.

[477] Bauhuber, S.; Hozsa, C.; Breunig, M.; Göpferich, A. *Adv. Mater.* **2009**, *21*, 3286–3306.

[478] Go, Y. M.; Jones, D. P. *Biochim. Biophys. Acta - Gen. Subj.* **2008**, *1780*, 1273–1290.

[479] Klein, P. M.; Wagner, E. *Antioxid. Redox Signal.* **2014**, *21*, 804–17.

[480] Wu, C.; Belenda, C.; Leroux, J. C.; Gauthier, M. A. *Chem. - A Eur. J.* **2011**, *17*, 10064–10070.

[481] Yang, J.; Chen, H.; Vlahov, I. R.; Cheng, J.-X.; Low, P. S. *Proc. Natl. Acad. Sci. U. S. A.* **2006**, *103*, 13872–13877.

[482] Schaffert, D.; Troiber, C.; Salcher, E. E.; Fröhlich, T.; Martin, I.; Badgujar, N.; Dohmen, C.; Edinger, D.; Kläger, R.; Maiwald, G.; Farkasova, K.; Seeber, S.; Jahn-Hofmann, K.; Hadwiger, P.; Wagner, E. *Angew. Chemie - Int. Ed.* **2011**, *50*, 8986–8989.

[483] Scholz, C.; Kos, P.; Wagner, E. *Bioconjug. Chem.* **2014**, *25*, 251–261.

[484] Lächelt, U.; Kos, P.; Mickler, F. M.; Herrmann, A.; Salcher, E. E.; Rödl, W.; Badgujar, N.; Bräuchle, C.; Wagner, E. *Nanomedicine Nanotechnology, Biol. Med.* **2014**, *10*, 35–44.

[485] Melief, C. J. M.; van Hall, T.; Arens, R.; Ossendorp, F.; van der Burg, S. H. *J. Clin. Invest.* **2015**, *125*, 3401–12.

[486] Amoozgar, Z.; Goldberg, M. S. *Adv. Drug Deliv. Rev.* **2015**, *91*, 38–51.

[487] Melief, C. J. M. *Clin. Cancer Res.* **2013**, *19*, 4295–4296.

[488] Clarke, S. R. K.; Barnden, M.; Kurts, C.; Carbone, F. R.; Miller, J. F.; Heath, W. R. *Immunol. Cell Biol.* **2000**, *78*, 110–117.

[489] Morel, P. A.; Turner, M. S. *Immunol. Res.* **2011**, *50*, 124–9.

[490] Park, J.; Babensee, J. E. *Acta Biomater.* **2012**, *8*, 3606–17.

[491] Steinman, R. M. *Annu. Rev. Immunol.* **2012**, *30*, 1–22.

[492] Farris, E.; Brown, D. M.; Ramer-Tait, A. E.; Pannier, A. K. *Exp. Biol. Med. (Maywood).* **2016**,

[493] Ritz, S.; Schöttler, S.; Kotman, N.; Baier, G.; Musyanovych, A.; Kuharev, J.; Landfester, K.; Schild, H.; Jahn, O.; Tenzer, S.; Mailänder, V. *Biomacromolecules* **2015**, *16*, 1311–21.

[494] Salcher, E. E.; Kos, P.; Fröhlich, T.; Badgujar, N.; Scheible, M.; Wagner, E. *J. Control. Release* **2012**, *164*, 380–386.

[495] Schaffert, D.; Badgujar, N.; Wagner, E. *Org. Lett.* **2011**, *13*, 1586–1589.

[496] Kaiser, E.; Colescott, R.; Bossinger, C.; Cook, P. *Anal. Biochem.* **1970**, *34*, 595–598.

[497] Wittrup, A.; Ai, A.; Liu, X.; Hamar, P.; Trifonova, R.; Charisse, K.; Manoharan, M.; Kirchhausen, T.; Lieberman, J. *Nat. Biotechnol.* **2015**, *33*, 1–9.

[498] Paz, I.; Sachse, M.; Dupont, N.; Mounier, J.; Cederfur, C.; Enninga, J.; Leffler, H.; Poirier, F.; Prevost, M. C.; Lafont, F.; Sansonetti, P. *Cell. Microbiol.* **2010**, *12*, 530–544.

[499] Thurston, T. L. M.; Wandel, M. P.; von Muhlinen, N.; Foeglein, A.; Randow, F. *Nature* **2012**, *482*, 414–418.

[500] Yin, H.; Kanasty, R. L.; Eltoukhy, A. A.; Vegas, A. J.; Dorkin, R. J.; Anderson, D. G. *Nat Rev Genet* **2014**, *15*, 541–555.

[501] Naldini, L. *Nat. Rev. Genet.* **2011**, *12*, 301–15.

[502] Powell, S. K.; Khan, N.; Parker, C. L.; Samulski, R. J.; Matsushima, G.; Gray, S. J.; McCown, T. J. *Gene Ther.* **2016**, *23*, 1–8.

[503] Zhao, Y.; Huang, L. *Adv. Genet.* **2014**, *88*, 13–36.

[504] Ni, R.; Zhou, J.; Hossain, N.; Chau, Y. *Adv. Drug Deliv. Rev.* **2016**, *106*, 3–26.

[505] Ferraro, B.; Morrow, M. P.; Hutnick, N. A.; Shin, T. H.; Lucke, C. E.; Weiner, D. B. *Clin. Infect. Dis.* **2011**, *53*, 296–302.

[506] Kreiter, S.; Vormehr, M.; van de Roemer, N.; Diken, M.; Löwer, M.; Diekmann, J.; Boegel, S.; Schrörs, B.; Vascotto, F.; Castle, J. C.; Tadmor, A. D.; Schoenberger, S. P.; Huber, C.; Türeci, Ö.; Sahin, U. *Nature* **2015**, *520*, 692–696.

[507] Lo, S. L.; Wang, S. *Biomaterials* **2008**, *29*, 2408–2414.

[508] Collas, P.; Husebye, H.; Aleström, P. *Transgenic Res.* **1996**, *5*, 451–8.

[509] Escriou, V.; Carri??re, M.; Scherman, D.; Wils, P. NLS bioconjugates for targeting therapeutic genes to the nucleus. 2003; http://www.ncbi.nlm.nih.gov/pubmed/12564982.

[510] Ludtke, J. J.; Zhang, G.; Sebestyén, M. G.; Wolff, J. A. *J. Cell Sci.* **1999**, *112*, 2033–2041.

[511] Zanta, M. a.; Belguise-Valladier, P.; Behr, J. P. *Proc. Natl. Acad. Sci. U. S. A.* **1999**, *96*, 91–6.

[512] Ciolina, C.; Byk, G.; Blanche, F.; Thuillier, V.; Scherman, D.; Wils, P. *Bioconjug. Chem.* **1999**, *10*, 49–55.

[513] Neves, C.; Byk, G.; Scherman, D.; Wils, P. *FEBS Lett.* **1999**, *453*, 41–45.

[514] Nakamura, T.; Moriguchi, R.; Kogure, K.; Minoura, A.; Masuda, T.; Akita, H.; Kato, K.; Hamada, H.; Ueno, M.; Futaki, S.; Harashima, H. *Biol. Pharm. Bull.* **2006**, *29*, 1290–3.

[515] Xu, Y.; Liang, W.; Qiu, Y.; Cespi, M.; Palmieri, G. F.; Mason, A. J.; Lam, J. K. W. *Mol. Pharm.* **2016**, *13*, 3141–3152.

[516] Shiraishi, T.; Hamzavi, R.; Nielsen, P. E. *Bioconjug. Chem.* **2005**, *16*, 1112–1116.

[517] Yoo, H. S.; Jeong, S. Y. *Eur. J. Pharm. Biopharm.* **2007**, *66*, 28–33.

[518] Parelkar, S. S.; Letteri, R.; Chan-Seng, D.; Zolochevska, O.; Ellis, J.; Figueiredo, M.; Emrick, T. *Biomacromolecules* **2014**, *15*, 1328–1336.

[519] Cohen, O.; Granek, R. *Nano Lett.* **2014**, *14*, 2515–2521.

[520] Cai, X.; Dong, H.; Ma, J.; Zhu, H.; Wu, W.; Chu, M.; Li, Y.; Shi, D. *J. Mater. Chem. B* **2013**, *1*, 1712–1721.

[521] Turner, D. M.; Tom, C. T. M. B.; Renslo, A. R. *ACS Comb. Sci.* **2014**, *16*, 661–664.

[522] Sahin, U.; Karikó, K.; Türeci, Ö. *Nat. Rev. Drug Discov.* **2014**, *13*, 759–80.

[523] Shrimpton, R. E.; Butler, M.; Morel, A. S.; Eren, E.; Hue, S. S.; Ritter, M. A. *Mol. Immunol.* **2009**, *46*, 1229–1239.

[524] Wyman, T. B.; Nicol, F.; Zelphati, O.; Scaria, P. V.; Plank, C.; Szoka, F. C. *Biochemistry* **1997**, *36*, 3008–3017.

[525] Li, W.; Nicol, F.; Szoka, F. C. *Adv. Drug Deliv. Rev.* **2004**, *56*, 967–985.

[526] Dempsey, C. E. *Biochim. Biophys. Acta - Rev. Biomembr.* **1990**, *1031*, 143–161.

[527] Ray, M.; Tang, R.; Jiang, Z.; Rotello, V. M. *Bioconjug Chem* **2015**, *26*, 1004–1007.

DECLARATION

I hereby declare that I wrote the dissertation submitted without any unauthorized external assistance and used only sources acknowledged in the work. All textual passages which are appropriated verbatim or paraphrased from published and unpublished texts as well as all information obtained from oral sources are duly indicated and listed in accordance with bibliographical rules. In carrying out this research, I complied with the rules of standard scientific practice as formulated in the statutes of Johannes Gutenberg University Mainz to insure standard scientific practice.

Mainz, März 2017

Philipp Heller

COLOPHON

This document was typeset using the typographical look-and-feel `classicthesis` developed by André Miede. The style was inspired by Robert Bringhurst's seminal book on typography *"The Elements of Typographic Style"*. `classicthesis` is available for both LaTeX and LyX:

https://bitbucket.org/amiede/classicthesis/

Final Version as of May 24, 2017 (`classicthesis` version 4.2).